Design, Synthesis, and Application of a Nucleophilic Octahedral Stereogenic-Only-at-Metal Iridium(III) Catalyst

Dissertation

zur Erlangung
des Doktorgrades
der Naturwissenschaften
(Dr. rer. nat.)

vorgelegt von

M.Sc.
Thomas Josef Cruchter

aus Trier

dem
Fachbereich Chemie
der Philipps-Universität
Marburg / Lahn

2018

Original document stored on the publication server of the
Philipps University of Marburg
(German: Philipps-Universität Marburg)

http://archiv.ub.uni-marburg.de

Except where specified by copyright notices in square brackets,
this work and its contents are licensed under a

Creative Commons Attribution-ShareAlike 4.0 International License

(CC BY-SA 4.0)

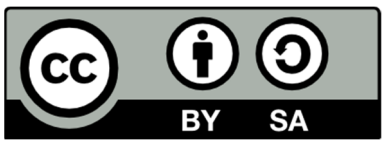

https://creativecommons.org/licenses/by-sa/4.0/

All content not licensed under the said Creative Commons licence, i.e., content that is explicitely marked with a copyright notice in square brackets, is all rights reserved, and you must request permission from the copyright owner to use this material.

Danksagung

Mein besonderer Dank gilt zunächst Herrn Prof. Dr. Eric Meggers für die Möglichkeit meine Promotion in seinem Arbeitskreis durchführen zu können. Ich möchte mich an dieser Stelle ausdrücklich für die sehr interessante und offene Aufgabenstellung bedanken, die es mir ermöglicht hat viele eigene Ideen einbringen und umsetzen zu können. Das wiederum hat es mir ermöglicht entscheidende Erfahrungen im eigenständigen wissenschaftlichen Arbeiten zu sammeln, meinen wissenschaftlichen Verstand zu schärfen und meine Vorgehensweise zur Lösung wissenschaftlicher Fragestellungen weiterzuentwickeln. – *Vielen Dank !*

Bei Herrn Prof. Dr. Armin Geyer bedanke ich mich herzlich für die Übernahme des Zweitgutachtens der vorliegenden Arbeit. Und bei Herrn Prof. Dr. Jörg Sundermeyer bedanke ich mich herzlich für die Bereitschaft der Prüfungskommission beizuwohnen. – *Vielen Dank !*

Besonderer Dank geht an meinen Kooperationspartner Michael G. Medvedev vom 'A. N. Nesmeyanov Institute of Organoelement Compounds RAS' (Moskau) und vom 'N. D. Zelinsky Institute of Organic Chemistry RAS' (Moskau) für die von ihm durchgeführten quantenmechanischen Berechnungen der vorliegenden Arbeit und für die professionelle, effiziente und exzellente Zusammenarbeit. In diesem Zusammenhang möchte ich mich auch ausdrücklich bei Dr. Vladimir A. Larionov und Dr. Alexander F. Smolyakov für die Herstellung des Kontaktes zu M. G. M. bedanken. – *Большое спасибо !*

Stellvertretend für M. G. M. möchte ich mich bei der Staatlichen Lomonossow-Universität Moskau bedanken für die zur Verfügung gestellte Rechenzeit auf dem 'IBM Blue Gene/P' Supercomputer der 'Faculty of Computational Mathematics and Cybernetics' sowie für die zur Verfügung gestellte Rechenzeit auf dem 'Lomonosov' Supercomputer des 'Moscow University Supercomputing Center'. Stellvertretend für M. G. M. möchte ich mich außerdem beim Rechenzentrum des 'NRC «Kurchatov Institute»' bedanken für die zur Verfügung gestellte Rechenzeit auf dem 'HPC2' Supercomputer. – *Большое спасибо !*

Ich danke den Mitarbeitern der NMR-Abteilung des Fachbereichs Chemie für die zügige und kompetente Messung der benötigten NMR-Handmessungen und für den praktisch jederzeit reibungslosen Ablauf der automatisierten NMR-Messungen.

Den Mitarbeitern der Abteilung für Massenspektrometrie und Elementaranalytik des Fachbereichs Chemie danke ich für die zügige und jederzeit zuverlässige Messung der abgegeben MS-Proben.

Mein besonderer Dank gilt den Mitarbeitern der Abteilung für Kristallstrukturanalyse des Fachbereichs Chemie für die zügige und professionelle Messung meiner abgegebenen Kristalle und für die Lösung meiner Kristallstrukturen. Hierbei möchte ich mich besonders dafür bedanken, dass von mir dringend benötigte Messungen vorgezogen werden konnten.

Ich bedanke mich besonders bei Thomas Mietke und Dr. Vladimir A. Larionov für die konstruktive und professionelle Zusammenarbeit bei verschiedenen Projekten (siehe Publikationsliste am Ende der vorliegenden Dissertation) und danke beiden darüber hinaus für die wertvollen fachlichen Diskussionen ohne die die vorliegende Arbeit wahrscheinlich weit weniger erfolgreich ausgefallen wäre. – *Vielen Dank !* / *Большое спасибо !*

Ich bedanke mich bei allen Mitgliedern des AK Meggers, des AK Vázquez und des AK Höbenreich für eine angenehme und konstruktive Zusammenarbeit.

Ich danke meinen Bachelorstudenten Svilena Draganova und Tobias Schwarz sowie meinen Vertiefungsstudenten Maximilian Fritz und Franziska Nousch für ihre Beiträge zur vorliegenden Arbeit. Darüber hinaus danke ich meinen Studenten aus dem OC-FPR und dem OC-MPR, die durch ihre Synthesestufen zu dieser Arbeit beigetragen haben.

Dr. Melanie Helms möchte ich für eine angenehme und gute Boxenpartnerschaft danken.

Ich bedanke mich bei Dr. Melanie Helms, Dr. Elisabeth Martin, Dr. Markus Dörr, Dr. Vladimir A. Larionov, Dr. Wei Zuo und Thomas Mietke ausdrücklich für das Korrekturlesen von Teilen der vorliegenden Arbeit. – *Vielen Dank !* / *Большое спасибо !* / *唔該晒 !*

Bei Ina Pinnschmidt, Andrea Tschirch und Dr. Lilu Zhang bedanke ich mich für ihre unkomplizierte und schnelle Hilfe in allen organisatorischen Fragen.

Bei Liesel und Helmut Chable möchte ich mich herzlich für ihre großzügige Unterstützung bedanken. – *Vielen Dank !*

Großer Dank gebührt meinen Eltern und Großeltern, die mich zu jeder Zeit nicht nur in den Jahren meines Studiums liebevoll in jeder Hinsicht und Lebenslage unterstützt haben und ohne deren Unterstützung mein Studium und meine Promotion nicht möglich gewesen wären. – *Vielen Dank !*

Von ganzem Herzen danke ich meiner Frau Shigeko für ihre unbegrenzte moralische Unterstützung und Geduld während meiner Promotion und darüber hinaus.
–どうもありがとうございました！

Für Meine Familie

Die Ergebnisse der vorliegenden Dissertation entstanden zwischen November 2013 und Juni 2017 am Fachbereich Chemie der Philipps-Universität Marburg in der Arbeitsgruppe Meggers unter der Betreuung von Prof. Dr. Eric Meggers.

Vom Fachbereich Chemie der Philipps-Universität Marburg (Hochschulkennziffer: 1180)

als Dissertation am 16.03.2018 angenommen.

Erstgutachter: Prof. Dr. Eric Meggers
Zweitgutachter: Prof. Dr. Armin Geyer

Tag der mündlichen Prüfung: 22.03.2018

Teile der in dieser Dissertation vorgestellten Forschungsergebnisse wurden bereits vorab publiziert in den folgenden Peer-Review-Artikeln:

[4] *Asymmetric Nucleophilic Catalysis with an Octahedral Chiral-at-Metal Iridium(III) Complex*
T. Cruchter, M. G. Medvedev, X. Shen, T. Mietke, K. Harms, M. Marsch, E. Meggers
ACS Catal. **2017**, *7*, 5152–5162 (*Research Article*).

- Highlight in *Synfacts* (M. Lautens, I. Franzoni, *Synfacts* **2017**, *13*, 0945).
- Hauptpublikation zur vorliegenden Dissertation.

[3] *Suzuki Cross-Coupling for Post-Complexation Derivatization of Non-Racemic Bis-Cyclometalated Iridium(III) Complexes*
T. Mietke, T. Cruchter, E. Winterling, M. Tripp, K. Harms, E. Meggers
Chem. Eur. J. **2017**, *23*, 1–10 (*Full Paper*).

- Artikel als Teil einer Sonderausgabe von *Chem. Eur. J.* anlässlich des 150-jährigen Bestehens der GDCh.

[2] *Polymer-Supported Chiral-at-Metal Lewis Acid Catalysts*
V. A. Larionov, T. Cruchter, T. Mietke, E. Meggers
Organometallics **2017**, *36*, 1457–1460 (*Communication*).

[1] *Metal-Templated Design: Enantioselective Hydrogen-Bond-Driven Catalysis Requiring Only Parts-per-Million Catalyst Loading*
W. Xu, M. Arieno, H. Löw, K. Huang, X. Xie, T. Cruchter, Q. Ma, J. Xi, B. Huang, O. Wiest, L. Gong, E. Meggers
J. Am. Chem. Soc. **2016**, *138*, 8774–8780 (*Article*).

Die vollständige Publikationsliste des Autors der vorliegenden Dissertation, die auch jene Publikationen enthält, welche keinen unmittelbaren Bezug zu den in dieser Dissertation vorgestellten Forschungsergebnissen haben, findet sich am Ende der vorliegenden Arbeit.

Kurzdarstellung

***Hauptthema (Kapitel 2.)*:** Die Entwicklung, Synthese und Anwendung eines vielseitigen chiralen nukleophilen Iridium(III)-Katalysators, welcher als einziges Chiralitätselement ein stereogenes oktaedrisches Metallzentrum besitzt ('stereogenic-only-at-metal'), wird vorgestellt. Der entwickelte Katalysator verfügt neben zwei maßgeschneiderten bidentaten cyclometallierten Phenylbenzoxazol-Liganden über einen bidentaten deprotonierten 7-Chloro-3*H*-imidazo[4,5-*h*]chinolin-Liganden, welcher als nukleophiles katalytisch aktives Zentrum fungiert.

Zunächst wurden 28 verschiedene 'stereogenic-only-at-metal' Iridium(III)-Komplexe synthetisiert, diese evaluiert und schließlich der leistungsfähigste Komplex ausgewählt. In diesem Zusammenhang wurde dargelegt, dass es sich bei dem ausgewähltem Komplex zunächst um die protonierte, katalytisch inaktive Präkatalysatorform des eigentlichen Katalysators handelte.

Es konnte gezeigt werden, dass der entwickelte 'stereogenic-only-at-metal' Komplex als effizienter Katalysator für die asymmetrische Steglich-Umlagerung von *O*-acylierten Azlactonen (bis zu 96% ee, bis zu 99% Ausbeute), die asymmetrische Black-Umlagerung von *O*-acylierten Benzofuranonen (bis zu 94% ee, bis zu 99% Ausbeute) und für die asymmetrische Addition von 2-Cyanopyrrol an Arylalkylketene (bis zu 95% ee, bis zu 99% Ausbeute) dient.

Einblicke in den Mechanismus der Steglich- und Black-Umlagerungen mit dem entwickelten Katalysator, insbesondere in Hinblick auf die Art und Weise der Enantioinduktion, konnten erlangt werden mit Hilfe einer Kristallstruktur des Katalysators, mit Hilfe einer Kristallstruktur eines Katalyseintermediat-Analogons in Kombination mit DFT-unterstützer Analyse der Zugänglichkeit des katalytisch aktiven Zentrums sowie mit Hilfe der expliziten quantenmechanischen Modellierung des stereogenen Schrittes einer exemplarischen Black-Umlagerung mit einem leicht vereinfachten Modell des entwickelten Katalysators. Die entsprechenden theoretischen Berechnungen wurden in enger Zusammenarbeit geplant und abgestimmt mit und durchgeführt von Kooperationspartner Michael G. Medvedev.

***Nebenthema (Kapitel 3.)*:** Nebenthema der vorliegenden Dissertation ist die versuchte Entwicklung eines kooperativen bifunktionalen 'stereogenic-only-at-metal' Enamin/Wasserstoffbrückenbindungs-Katalysators, der als Katalysator für die asymmetrische Michael-Addition von enolisierbaren Aldehyden und / oder Ketonen an Nitroalkene und / oder Nitroacrylate angedacht war.

Ein synthetischer Zugang zu den angedachten Katalysatoren konnte erfolgreich etabliert werden, jedoch führten Stabilitätsprobleme mit den Komplexen sowie unbefriedigende Katalyseergebnisse schließlich zum Abbruch des Projektes. Dessen ungeachtet konnten wichtige Erkenntnisse in Bezug auf die Synthese Amin-funktionalisierter bis-cyclometallierter Iridium(III)-Komplexe sowie C_2-symmetrischer bis-cyclometallierter Bispyrazol-Iridium(III)-Komplexe erlangt werden, welche bereits zu erfolgreich abgeschlossenen Projekten des AK Meggers beigetragen haben und daher auch für zukünftige Projekte wieder relevant werden könnten.

Abstract

***Main Topic (Chapter 2.)*:** The design, synthesis, and application of a versatile chiral nucleophilic iridium(III) catalyst, which features a stereogenic octahedral metal center as its exclusive element of chirality ('stereogenic-only-at-metal'), is presented. The devised catalyst features two custom-tailored bidentate cyclometalated phenylbenzoxazole ligands as well as a bidentate deprotonated 7-chloro-3*H*-imidazo[4,5-*h*]quinoline ligand, which serves as the catalyst's nucleophilic catalytically active site.

At first, 28 different stereogenic-only-at-metal iridium(III) complexes were synthesized, evaluated, and the best-performing complex eventually selected. In this regard, it was revealed that the selected catalyst candidate was in fact the protonated precatalytic form of the actual catalyst.

Next, it could be demonstrated that the developed stereogenic-only-at-metal complex serves as an efficient catalyst for the asymmetric Steglich rearrangement of *O*-acylated azlactones (up to 96% ee, up to 99% yield), for the asymmetric Black rearrangement of *O*-acylated benzofuranones (up to 94% ee, up to 99% yield), and for the asymmetric addition of 2-cyanopyrrole to aryl alkyl ketenes (up to 95% ee, up to 99% yield).

Insights into the mechanism of the Steglich and the Black rearrangements with the developed stereogenic-only-at-metal catalyst, in particular into the catalyst's manner of enantioinduction, could be gained with a crystal structure of the active catalyst, with a crystal structure of a catalysis intermediate analog in combination with a DFT-assisted active site accessibility analysis, and with the explicit quantum chemical modeling of the stereogenic step of a showcase Black rearrangement with a slightly simplified model of the devised catalyst. The respective theoretical calculations were planned and coordinated in close collaboration with and performed by cooperation partner Michael G. Medvedev.

***Secondary Topic (Chapter 3.)*:** Secondary topic of the present thesis is the attempted development of a cooperative bifunctional stereogenic-only-at-metal enamine/hydrogen-bonding catalyst, which was intended to catalyze Michael additions of enolizable aldehydes and / or ketones to nitroalkenes and / or nitroacrylates.

A synthetic access to the envisioned catalysts could be successfully established, however, stability problems with the complexes as well as unsatisfactory catalysis results ultimately led to the termination of this project. In spite of that, important knowledge could be attained regarding the synthesis of amine-functionalized bis-cyclometalated iridium(III) complexes and C_2-symmetric bis-cyclometalated bispyrazole iridium(III) complexes, which has already contributed to successfully accomplished projects from the Meggers group and which may accordingly be helpful for future projects.

Table of Contents

Design, Synthesis, and Application of a Nucleophilic Octahedral Stereogenic-Only-at-Metal Iridium(III) Catalyst

1. Theoretical Background

1.1 Nucleophilic Catalysis and Lewis Base Catalysis – Definition of Terms

The terms 'nucleophilic catalysis' and 'Lewis base catalysis' are often used synonymously in the literature.[1–4] In other cases, a much wider field in catalysis is referred to by the term 'Lewis base catalysis' than by the term 'nucleophilic catalysis', which can be misleading and confusing.[5,6] In the present thesis, the terms 'nucleophilic catalysis' and 'nucleophilic catalyst' exclusively refer – by definition – to catalysts and catalysis in which a catalyst with a nucleophilic / Lewis basic lone pair activates a substrate by an initial $n \rightarrow \pi^*$ (most common), $n \rightarrow \sigma^*$ (less common), or $n \rightarrow n^*$ (less common) interaction[5] and where the resultant catalyst-substrate adduct then reacts *without any structural changes of the catalyst-attached entity that are caused by the nature of the catalyst itself under transfer of this entity* and under catalyst regeneration. Reactions, in which the *catalyst-attached entity undergoes structural changes that are caused by the nature of the catalyst itself before the resultant entity is transferred* under catalyst regeneration, such as reactions that are catalyzed via enamine or iminium ion formation by secondary amines,[7,8] or NHC-catalyzed umpolung reactions via Breslow-type intermediates with aldehydes and imines,[9] are <u>not</u> included in the hereby given definition of 'nucleophilic catalysis' / 'nucleophilic catalyst' and are beyond the scope of the herein discussed reactions.[5,6,10] In contrast, those reactions are explicitely included in the very general definition of 'Lewis base catalysis' given by Denmark, Beutner, and Vedejs.[5,6]

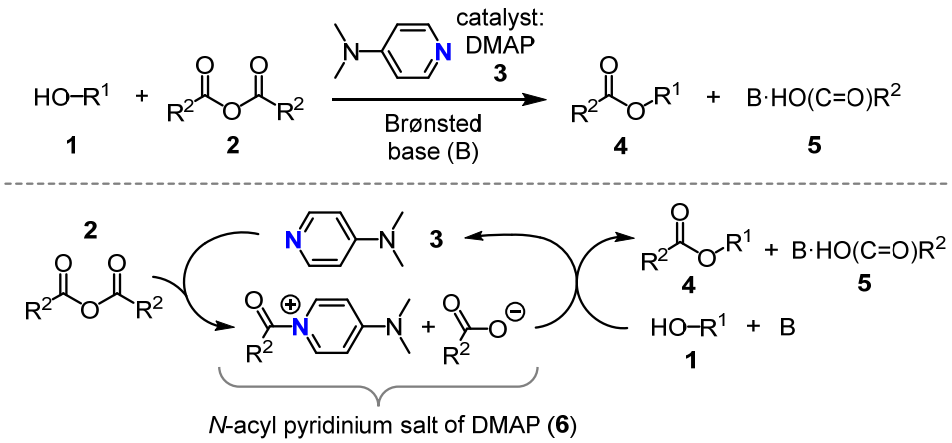

Scheme 1. "Archetypical" nucleophile-catalyzed reaction: Acylation of an alcohol (**1**) with an anhydride (**2**) catalyzed by 4-dimethylaminopyridine (DMAP; **3**). A Brønsted base (B) is added to prevent accumulation of acid $R^2(C{=}O)OH$.

A simple example for a reaction which follows the above given definition of nucleophilic catalysis is depicted in Scheme 1, which shows the acylation of an alcohol (**1**) with an an-

hydride (**2**) as acylating reagent and which is catalyzed by "archetypical" nucleophilic catalyst 4-dimethylaminopyridine (**3**; DMAP).[11]

1.2 Asymmetric Nucleophilic Catalysis – Overview

Over the past twenty years, since the introduction of the first "chiral DMAP" reagent by Vedejs and Chen in 1996 (**38**; see Figure 2),[12] a significant amount of work has been carried out by research groups all over the world in developing highly active and at the same time highly selective nucleophilic catalysts capable of various asymmetric transformations, such as (dynamic) kinetic resolutions of racemic compounds (see Scheme 2) and desymmetrizations of meso compounds,[13–20] Steglich-type acyl migration reactions (see Scheme 3),[3,20,22–25] reactions of ketenes with various substrates (see Scheme 4),[26,27] and others.[28]

An example for a kinetic resolution (KR) with a chiral nucleophilic catalyst and at the same time an example for a dynamic kinetic resolution (DKR) with the same chiral catalyst are shown in Scheme 2.

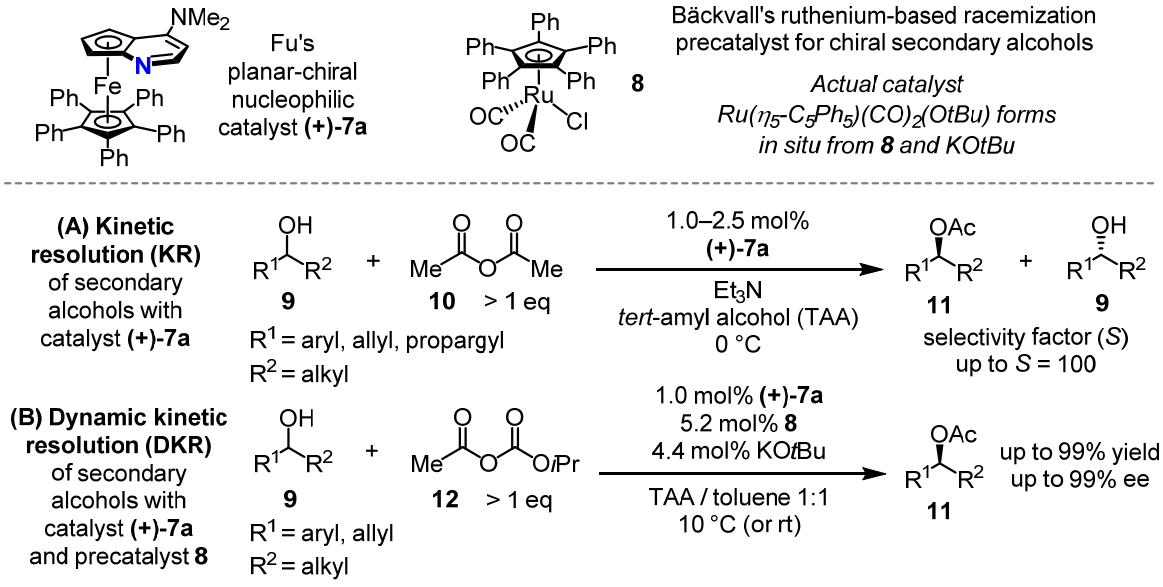

Scheme 2. Kinetic resolution (KR) with Fu's planar-chiral nucleophilic catalyst **(+)-7a** versus dynamic kinetic resolution (DKR) with a combination of **(+)-7a** and Bäckvall's alcohol racemization precatalyst **8**.[13e,f,29]

Fu and co-workers initially employed planar-chiral catalyst **(+)-7a** in the kinetic resolution of secondary alcohols (**9**) with acetic anhydride (**10**) as acylation reagent (Scheme 2).[13e,f] Although they could achieve resolutions with excellent selectivity factors of up to $S = 100$ (a definition for S is given in the next paragraph), this approach comes with the limitation that at least 50% of starting material **9** or of product **11** are lost in case there is no further use for them. Later on, Fu and co-workers were able to get around this shortcoming by the combination of nucleophilic acylation catalyst **(+)-7a** with Bäckvall's racemization pre-

catalyst **8**,[29] which racemizes secondary alcohols **9** in the presence of KO*t*Bu under appropriate reaction conditions.[13e,f,29] With mixed anhydride **12**, which serves as a substitute for acetic anhydride (**10**), the combination of catalyst **(+)-7a** and precatalyst **8** accordingly resulted in an elegant dynamic kinetic resolution of secondary alcohols (**9**) giving the acylated products (**11**) in up to 99% yield and up to 99% ee (Scheme 2).[13e,f]

At this point, it is necessary to explain the selectivity factor *S*: This factor is a highly useful parameter which allows direct comparisons of kinetic resolutions which have been stopped at different conversion levels.[28e,30] The selectivity factor *S* can be interpreted as the quotient of the rate constants of the fast reacting starting material enantiomer (k_{fast} in Eq. 1) and the slow reacting starting material enantiomer (k_{slow} in Eq. 1).[28e] In contrast, direct comparisons of kinetic resolutions by means of ee values alone are only feasible in case the resolutions have been stopped at (almost) identical conversion levels. As a rule of thumb, kinetic resolutions start to become synthetically useful when they provide selectivity factors of $S \geq 10$.[28e] In cases with $S \geq 10$ but $S < 50$ kinetic resolutions have to be stopped at conversion levels of (much) more than 50% in order to obtain a sufficiently enriched starting material while the ee of the product remains low and synthetically less useful.[28e] Kinetic resolutions with $S > 50$ provide both a highly enriched starting material and a highly enriched product at around 50% conversion.[28e] The selectivity factor *S* of a kinetic resolution can be directly calculated from the ee values of the unconsumed starting material **S** and the formed product **P** at any conversion (*C*) according to Kagan's equation (Eq. 1).[28e,30]

$$C = \frac{\text{ee } \mathbf{S}}{\text{ee } \mathbf{S} + \text{ee } \mathbf{P}} 100 \qquad S = \frac{ln[1 - C(1 + \text{ee } \mathbf{P})]}{ln[1 - C(1 - \text{ee } \mathbf{P})]} \qquad S = \frac{k_{fast}}{k_{slow}} \qquad \text{(Eq. 1)}$$

An example for a Steglich-type acyl migration reaction, i.e., an intramolecular stereogenic acyl migration or rearrangement,[21] is shown in Scheme 3, which shows the Steglich rearrangement of achiral *O*-acylated azlactone **13a** with Fu's planar-chiral catalyst **(−)-7b** to chiral *C*-acylated azlactone **14a**.[22a] In the depicted mechanism, the nitrogen atom of the fused pyrrolidinopyridine moiety of **(–)-7b** first attacks the carbonate moiety of **13a**, which goes along with the formation of *N*-acylated cation **15a-A** and its associated enolate counteranion **15a-B**, which together constitute *N*-acyl pyridinium salt **15a**.[22a] Enolate **15a-B** then reacts with *N*-acylated cation **15a-A** under stereogenic C-C bond formation which stereoselectively provides *C*-acylated azlactone **14a** under regeneration of catalyst **(–)-7b**.[22a]

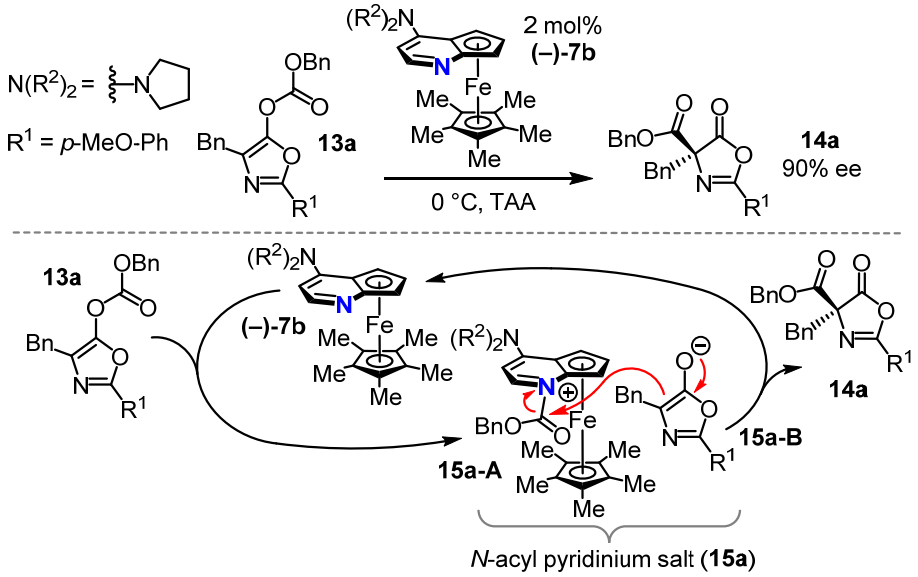

Scheme 3. Steglich rearrangement of *O*-acylated azlactone **13a** to *C*-acylated azlactone **14a** with Fu's planar-chiral nucleophilic catalyst **(–)-7b**.[22a]

An example for chiral nucleophilic catalysis with ketenes as substrates is shown in Scheme 4, which shows the formal [2+2]-cycloaddition between aryl alkyl ketenes (**16**) and *N*-Boc-protected imines (**17**) giving *N*-Boc-protected *β*-lactams (**19**) from Ye and co-workers (the authors denote the reaction as a 'Staudinger reaction').[27a] The reaction is catalyzed by chiral *N*-heterocyclic carbene (NHC) **(*S*)-20**, which is formed *in situ* by deprotonation of imidazolium salt **(*S*)-18** with cesium carbonate as Brønsted base.[27a]

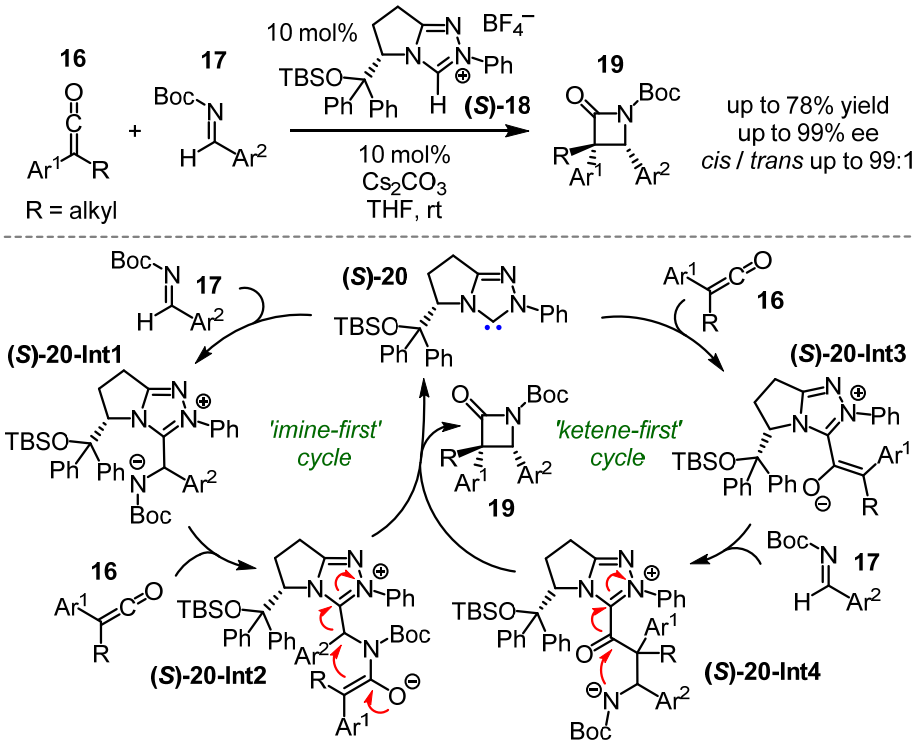

Scheme 4. Asymmetric formal [2+2]-cycloaddition between ketenes (**16**) and *N*-Boc-protected imines (**17**) giving *N*-Boc-protected *β*-lactams (**19**) catalyzed by NHC catalyst **(*S*)-20** from Ye and co-workers. Curved arrows are only drawn for the final step of each of both cycles.[27a]

For the reaction from Scheme 4 two catalytic pathways are plausible:[26f,27a]

- An 'imine-first' cycle[26f] in which NHC catalyst **(*S*)-20** first attacks the imine substrate (**17**) and where the resulting catalyst-substrate adduct **(*S*)-20-Int1** subsequently attacks the ketene substrate (**16**).
- Or a 'ketene-first' cycle[26f] in which NHC catalyst **(*S*)-20** first attacks the ketene substrate (**16**) and where the resulting catalyst-substrate adduct **(*S*)-20-Int3** subsequently attacks the imine substrate (**17**).

In both cases resulting intermediates **(*S*)-20-Int2** ('imine-first' cycle) and **(*S*)-20-Int4** ('ketene-first' cycle) fragment to the desired *β*-lactam (**19**) and NHC catalyst **(*S*)-20**.[26f,27a]

The so far developed chiral nucleophilic catalysts rely in large part on *N*-nucleophiles (Figure 1, A) and here in particular on 4-dimethylaminopyridine (DMAP; **3**) or on closely related 4-pyrrolidinopyridine (PPY) as their catalytically active entities due to their high intrinsic activity (Figure 1, A.1).[1,2,4−6,11,13−17,20,22−25,28,31]
However, powerful non-DMAP-type *N*-based nucleophilic catalysts have been developed as well, which rely on amidines (Figure 1, A.2),[15,20] isothioureas (Figure 1, A.3),[4,16,20,24] imidazoles (Figure 1, A.4),[17,25] and aliphatic (di-)amines (Figure 1, A.5).[32,33]
There are also notable examples for nucleophilic catalysts which do not rely on *N*-nucleophiles, they rely on *O*-nucleophiles (Figure 1, B),[3,18] *P*-nucleophiles (phosphines; Figure 1, C),[19] *C*-nucleophiles (NHCs; Figure 1, D),[26,27] and others.[28]

Generally speaking, the introduction of a steering stereocenter in proximity to a catalyst's active site represents a straightforward approach to achieve enantiocontrol in an asymmetric transformation. However, as steering stereocenters often comprise sterically demanding moieties, this may go along with significant loss of catalytic activity, as it is the case for chiral acylation reagent **38** (see Figure 2) from Vedejs and Chen, which has to be employed in its *N*-acylated form in stoichiometric amounts.[12] Hence, from the standpoint of catalytic activity, it is desirable to have a remote stereocenter, but this, on the other hand, may be detrimental for an efficient enantioinduction.[14a,d,23a,b,g,24,25a] This phenomenon has aptly been called the *'selectivity-reactivity dilemma'* by Fuji et al.[14a] and is also encountered for systems which are not entirely planar, such as catalyst **40** (Figure 2), although it is less pronounced there.[4,15,25a] With regard to nucleophilic catalysts, several interesting strategies have been devised to circumvent low catalytic activity when aiming for high selectivity, including strategies that go beyond "classic" tetrahedral carbon stereocenters as stereogenic elements. Selected examples for such catalysts are presented in the next paragraphs.

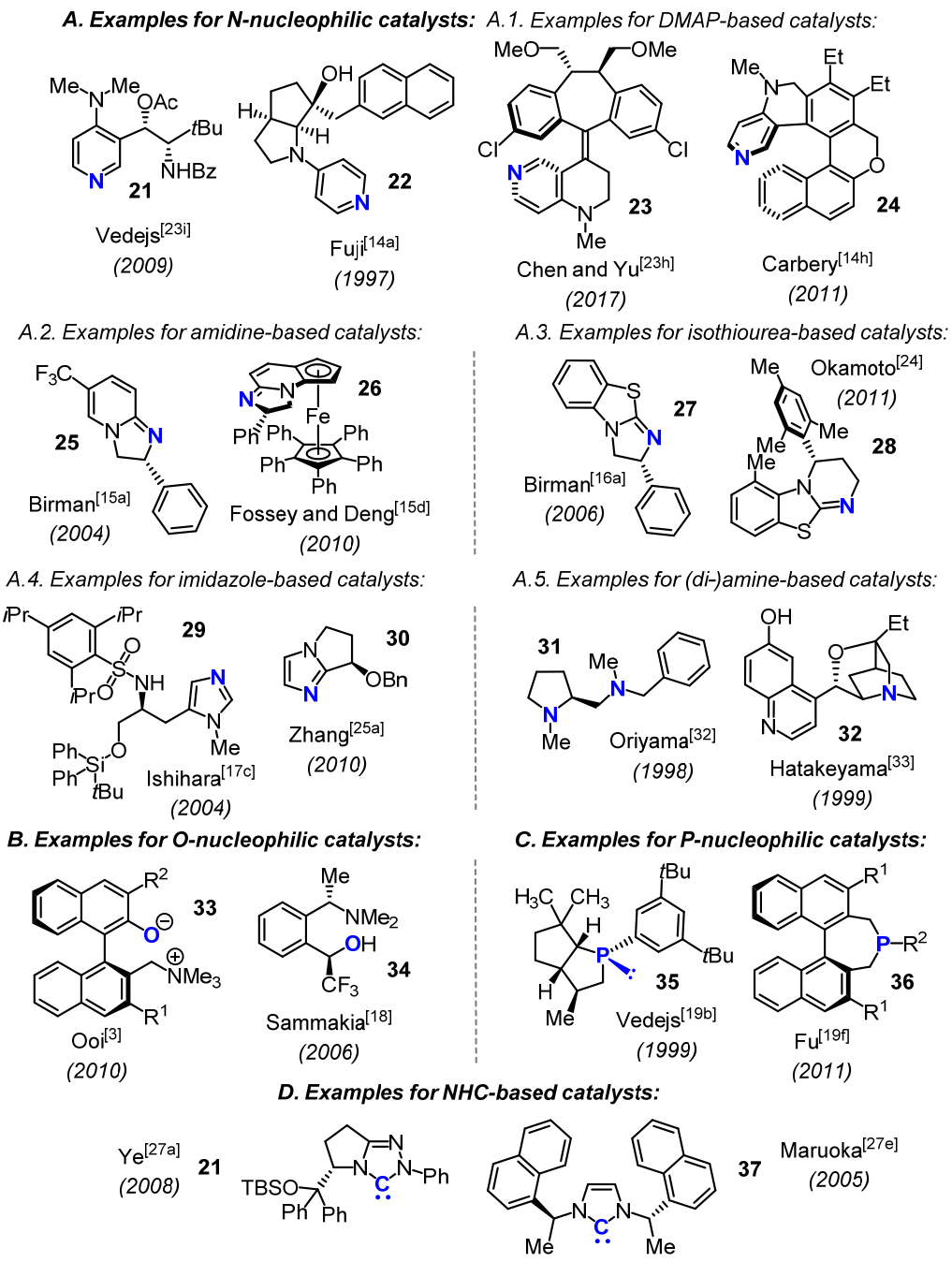

Figure 1. Examples for nucleophilic catalysts relying on different nucleophilic entities.

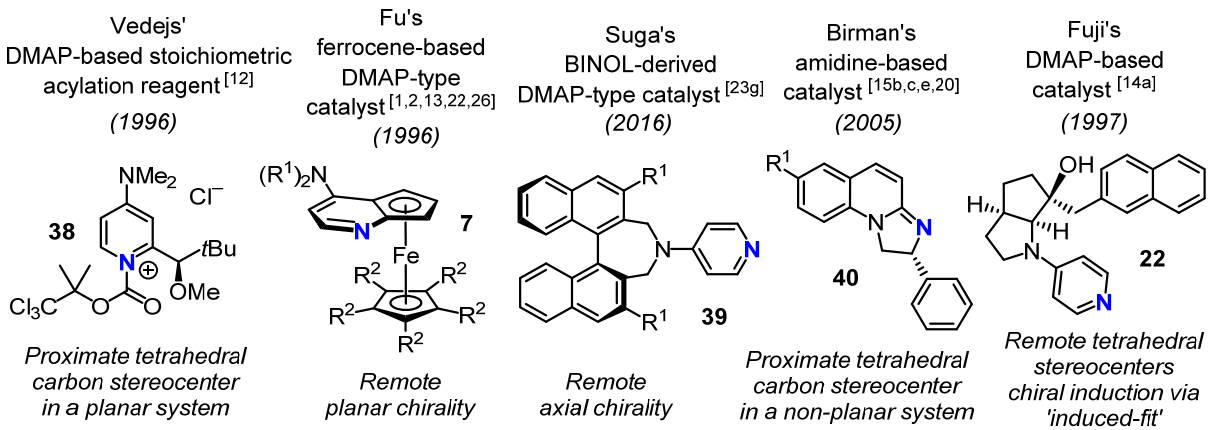

Figure 2. Vedejs' asymmetric acylation reagent (**38**) and four chiral nucleophilic catalysts (**7**,**39**,**40**,**22**) relying on different scaffolds and elements of chirality.

In 1996, shortly after Vedejs' and Chen's seminal publication about stoichiometric acylation reagent **38**,[12] Fu and co-workers introduced planar-chiral ferrocene-fused DMAP derivatives as chiral nucleophilic catalysts (**7**, Figure 2; see also **7a** and **7b** in Schemes 2 and 3),[13a] which have, up to date, been demonstrated to efficiently catalyze a broad array of asymmetric transformations and also been extended to analogous ruthenocyl-fused derivatives.[31] Due to their unrivaled versatility,[1,2,13,22,26] Fu's ferrocene-fused DMAP derivatives (**7**) have emerged as a reference standard in asymmetric nucleophilic catalysis.[15d,34a] Meanwhile, the concept of creating planar-chiral nucleophilic catalysts by ferrocene fusion has been extended by others to non-DMAP-type catalysts, such as NHC- and amidine-based systems (see for example catalyst **26** from Fossey and Deng in Figure 1).[15d,35]

Another interesting and early example for a nucleophilic catalyst developed with the intention to circumvent the *'selectivity-reactivity dilemma'* [14a] is Fuji's catalyst **22** from 1997 (Scheme 5).[14a] Although relying on "classic" tetrahedral carbon stereocenters, in catalyst **22** the stereoinformation is apparently too far away from the nucleophilic nitrogen to efficiently control the stereochemical outcome of an asymmetric transformation. However, catalyst **22** was found to be able to give moderate to fair results in kinetic resolutions of chiral secondary alcohols, selectivity factors in the range $S \sim 5–10$ were found.[14a]

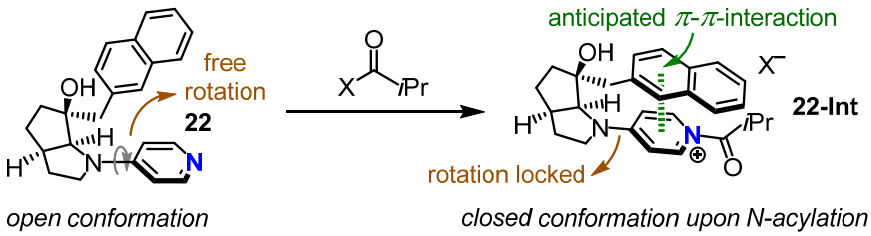

Scheme 5. Fuji's catalyst **22** adapts a closed conformation upon *N*-acylation (**22-Int**), probably due to a favorable π-π-interaction, which explains why catalyst **22** is able to discriminate between both enantiomers of chiral secondary alcohols.[14a]

Fuji and co-workers revealed that catalyst **22** adapts a closed conformation upon *N*-acylation, probably due to a favorable π-π-interaction (**22-Int**, Scheme 5), which explains why the catalyst is able to discriminate between both enantiomers of chiral secondary alcohols.[14a]

In contrast to that, Ooi and co-workers developed axial-chiral BINOL-derived *O*-nucleophilic ammonium betaines **33** (Figure 1), which they employed as highly selective catalysts in Steglich rearrangements of *O*-acylated azlactones.[3]

And quite recently, Suga and co-workers reported about axial-chiral BINOL-derived DMAP-type catalyst **39** (Figure 2), which they employed as a catalyst in Steglich-type rearrangements of *O*-acylated oxindoles, in kinetic resolutions of alcohols, and in desymmetrizations of diols.[23g]

Carbery and co-workers developed helicenoidal DMAP derivative **24** (Figure 1), which they employed as a catalyst in kinetic resolutions of alcohols.[14h,i]

In this context, it is worth of mentioning that Suginome and co-workers have very recently (2017) reported an "elongated version" of a helical-chiral nucleophilic catalyst (Figure 3).[36]

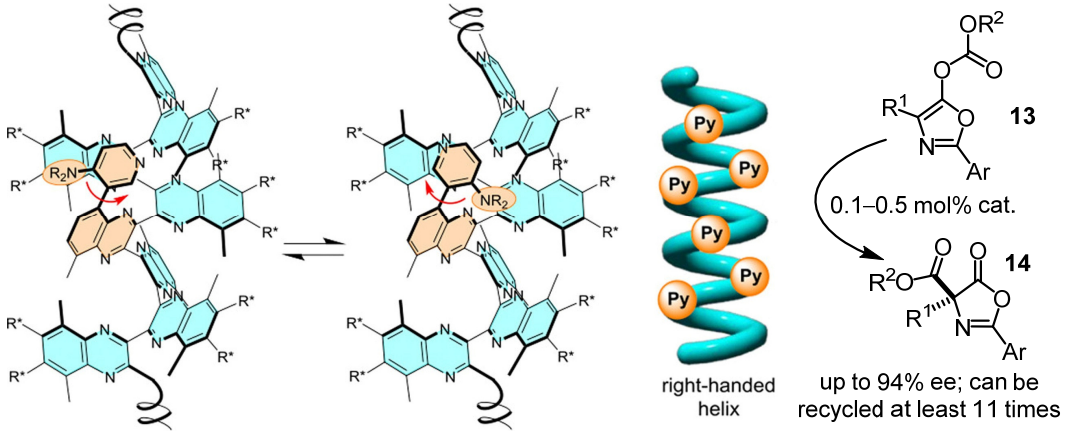

Figure 3. DMAP-functionalized single-handed polymeric poly(quinoxaline-2,3-diyl) chains from Suginome and co-workers.[36] [Figure of the helix reproduced and adapted with permission from ref. 36. Copyright © 2017, American Chemical Society]

Suginome and co-workers attached DMAP (**3**) via its 3-position to single-handed polymeric poly(quinoxaline-2,3-diyl) chains and demonstrated that the resulting polymer chains serve as suitable catalysts for asymmetric Steglich rearrangements of *O*-acylated azlactones (**13** → **14**, Figure 3).[36] An interesting aspect of this chiral nucleophilic chains is the fact that the aryl-aryl bond between DMAP and the polymeric backbone is not fixed but automatically adapts the energetically favored rotamer which is dictated by the helical backbone (Figure 3).[36]

A nucleophilic catalyst which is also worth mentioning in the context of helical-chiral catalysts is photo- and thermally switchable catalyst **23**, which has also very recently been reported (2017) by Chen, Yu, and co-workers (Scheme 6).

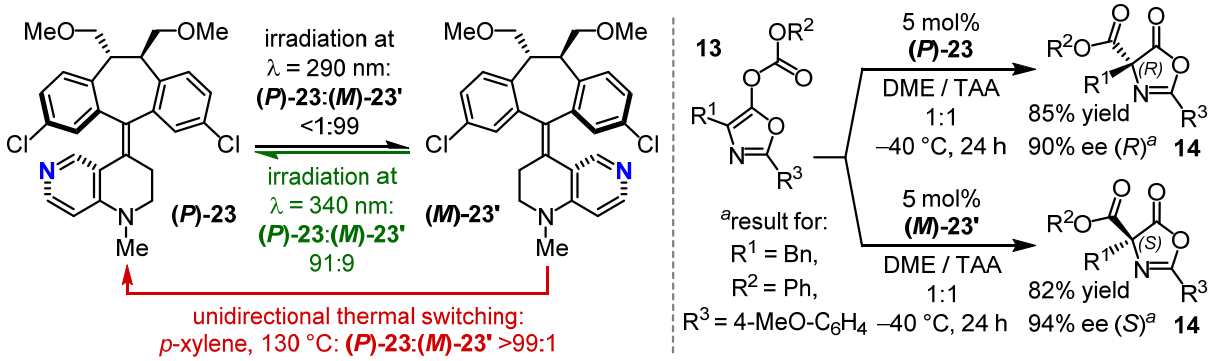

Scheme 6. Photo- and thermally switchable helical-chiral catalysts (***P*)-23** and (***M*)-23'** from Chen, Yu, and co-workers.[23h] Note that (***P*)-23** and (***M*)-23'** are diastereomers or pseudoenantiomers as they feature two tetrahedral carbon stereocenters in their seven-membered rings.

Catalyst **23** allows an enantiodivergent Steglich rearrangement of *O*-acylated azlactones (**13** → **14**) with a single catalyst:[23h] By irradiation with UV-light at λ = 290 nm, catalyst **23** switches to pseudoenantiomer **(*M*)-23'** in a **(*P*)-23** / **(*M*)-23'** ratio of up to <1:99. In contrast, by irradiation with UV-light at a longer wavelength, namely at λ = 340 nm, an inverse **(*P*)-23** / **(*M*)-23'** ratio of up to 91:9 is provided. Alternatively, catalyst **23** can be stirred at 130 °C in *p*-xylene in the absence of UV-light, which then provides catalyst **(*P*)-23** virtually pure in a **(*P*)-23** / **(*M*)-23'** ratio of up to >99:1.[23h] While **(*P*)-23** provides **14a** in 90% ee with respect to the *R*-enantiomer, **(*M*)-23'** provides **14a** in 94% ee with respect to the *S*-enantiomer (Scheme 6).[23h]

In the previous paragraphs, selected examples for chiral nucleophilic catalysts relying on different scaffolds and elements of chirality have been presented and some discussed in detail. Another type of chiral scaffold which could be made use of to develop chiral nucleophilic catalysts is represented by octahedral metal complexes which feature a metal stereocenter. For such complexes the term *'chiral-at-metal'* has been coined and for those complexes which feature a stereogenic metal center as their exclusive element of chirality, i.e., with all coordinating ligands being achiral, the more restricting term *'chiral-only-at-metal'* has been introduced.[37–40] However, both terms are somewhat imprecise as 'chirality' is rather a property of an object as a whole.[40] For this reason, the alternative terms *'stereogenic-at-metal'* and *'stereogenic-only-at-metal'*, which rather point at the metal center as the origin of the chirality of such complexes, are used throughout this thesis.[40] Coming back to nucleophilic catalysis, the merger of an entity capable of nucleophilic catalysis and a stereogenic-only-at-metal complex fragment, offers a possibility to design a potentially powerful chiral nucleophilic catalyst (Figure 4).

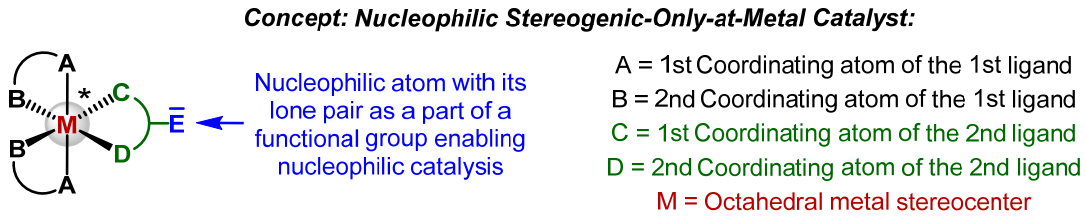

Figure 4. Basic concept for a chiral nucleophilic octahedral stereogenic-only-at-metal catalyst.

In chapter 2., it will be demonstrated that a powerful chiral nucleophilic stereogenic-only-at-metal catalyst could indeed be developed based on this concept. But first, chapters 1.3 and 1.4 will provide a brief summary about the history of stereogenic-at-metal complexes in general and an overview of the so far developed stereogenic-at-metal catalysts from the Meggers laboratory and other research laboratories.

1.3 Stereogenic-at-Metal Catalysts – Introduction and Results from Other Research Groups

In 1899, Swiss chemist and later Nobel Laureate Alfred Werner postulated in a publication about the constitution of cobalt(III) complexes that the formation of an octahedral complex with two identical bidentate ligands, such as ethylenediamine (en), should entail the existence of two enantiomers, provided that both ligands and the two remaining monodentate ligands, or a third bidentate ligand, constitute the *cis*-isomer of the respective complex (i.e., *cis*-[M(en)2XY] *or* *cis*-[M(en)2X^Y]) and not the achiral *trans*-isomer (Figure 5).[41,42] Nowadays, both resulting enantiomers are denoted as Λ- and Δ-enantiomer, depending on whether they represent a left-handed propeller (Λ) or a right-handed propeller (Δ).[40]

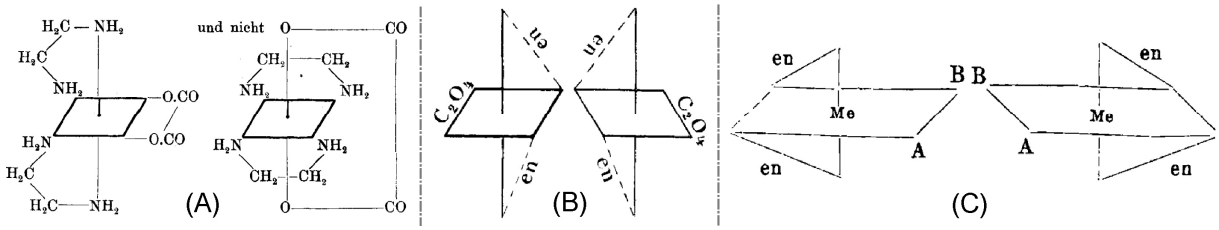

Figure 5. Original figures from Werner's publications from 1899 (A, B)[41] and from 1911 (C):[43] (A) Werner anticipated that $[Co(en)_2(C_2O_4)]^+$ would most probably exist as *cis*-isomer (left) and not as *trans*-isomer (right) due to spatial constraints.[41] (B) He correctly recognized that *cis*-$[Co(en)_2(C_2O_4)]^+$ is chiral and accordingly exists as two enantiomers.[41] (C) He also correctly recognized that the same is the case for complexes of type *cis*-[M(en)2AB] or *cis*-[M(en)2A^B].[43] [Reproduced and adapted with permission from refs. 41, 43. Copyright © Wiley-VCH Verlag GmbH & Co. KGaA]

In his 1899 publication, Werner mentions first though unsuccessful attempts to separate such racemic complex mixtures.[41,44] It took him and his co-workers twelve additional years until they eventually reported the successful separation and characterization of the at that time still postulated complex enantiomers (see Scheme 7).[43,45]

In his 1911 publication, Werner then describes the separation of the Λ- and Δ-configured complex cations of *cis*-$[Co(en)_2(NH_3)Cl]Cl_2$ and *cis*-$[Co(en)_2(NH_3)Br](NO_3)_2$.[43] The work-flow for the separation of the chiral complex cations of *cis*-$[Co(en)_2(NH_3)Cl]Cl_2$ (***rac*-41**) is depicted in detail in Scheme 7. Werner and co-workers achieved the synthesis of enantiopure salts **Λ-44** and **Δ-44** from ***rac*-41** via replacement of the achiral non-coordinated halide anions by chiral (*R*)-3-bromocamphor-8-sulfonate with silver (*R*)-3-bromocamphor-8-sulfonate (**(*R*)-42**), subsequent separation of the resulting diastereomeric salts **Λ-(*R*)-43** and **Δ-(*R*)-43** via fractional crystallization, and finally replacement of (*R*)-3-bromocamphor-8-sulfonate by bromide anions giving salts **Λ-44** and **Δ-44**.[43] As expected for enantiomers, identical absolute specific rotation values with opposite leading signs were found for both salts.[43] The obtained enantiomeric salts were found to be configurationally stable and did not show any signs of racemization, not even in boiling water or after prolonged standing.[43,45]

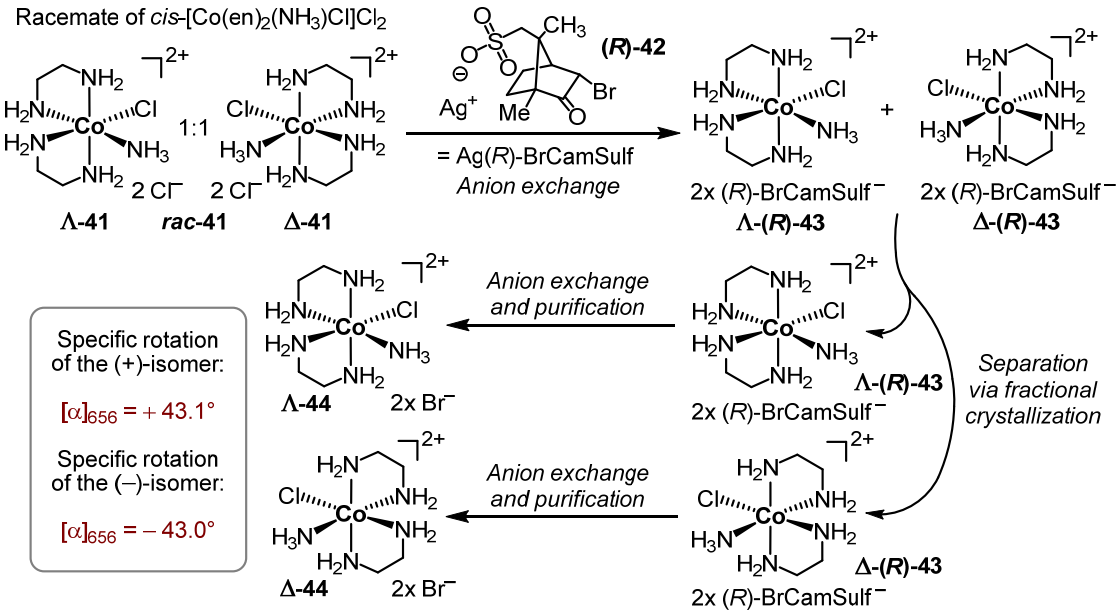

Scheme 7. Synthesis of enantiopure **Λ-44** and **Δ-44** from Werner and co-workers from 1911.[43] In this context, it is worth mentioning that Werner's co-worker V. L. King in 1942 recalled that it took him some 2000 fractional crystallization attempts until he eventually utilized silver (*R*)-3-bromocamphor-8-sulfonate (**(*R*)-42**), which then allowed the above depicted successful separation via fractional crystallization.[45]

In consideration of what was achieved by Werner and his co-workers more than 100 years ago with regard to stereogenic-only-at-metal Co(III) complexes, it is surprising that it was not until 2003 that the first research group started to intentionally use stereogenic-only-at-metal complexes as catalysts for asymmetric transformations.[37a]

In 2003, Fontecave and co-workers reported about stereogenic-only-at-metal Ru(II) complex **Λ/Δ-45**, which they used as a catalyst for the asymmetric oxidation of sulfides (**47**) to chiral sulfoxides (**48**; Scheme 8).[37a] In order to obtain enantiopure **Λ-45** from ***rac*-45**, Fontecave and co-workers first selectively precipitated the Δ-configured complex cation of ***rac*-45** by the addition of (*n*-Bu$_3$)NH·Λ-TRISPHAT as Λ-TRISPHAT$^-$ salt **Δ-(2Λ)-46** (Scheme 8, Step I). Next, they selectively precipitated enantiopure **Λ-45** from the remaining solution by the addition of diethyl ether (Scheme 8, Step II).[37a]

When Fontecave and co-workers added 2 mol% of complex **Λ-45** to a solution of sulfide **47** and hydrogen peroxide in MeOH, desired sulfoxide **48** was produced with 18% ee (*S*). With 2 mol% of **Δ-(2Λ)-46** desired sulfoxide **48** was also produced with 18% ee (*R*), which indicated that the two chiral Λ-TRISPHAT$^-$ counteranions did not have any influence on the enantioselectivity of the reaction **47** → **48**. This finding was reaffirmed with a control experiment by Fontecave and co-workers in which they employed 2 mol% ***rac*-45** in the presence of 4 eq of (*n*-Bu$_3$)NH·Λ-TRISPHAT, which provided **48** completely racemic (Scheme 8).[37a]

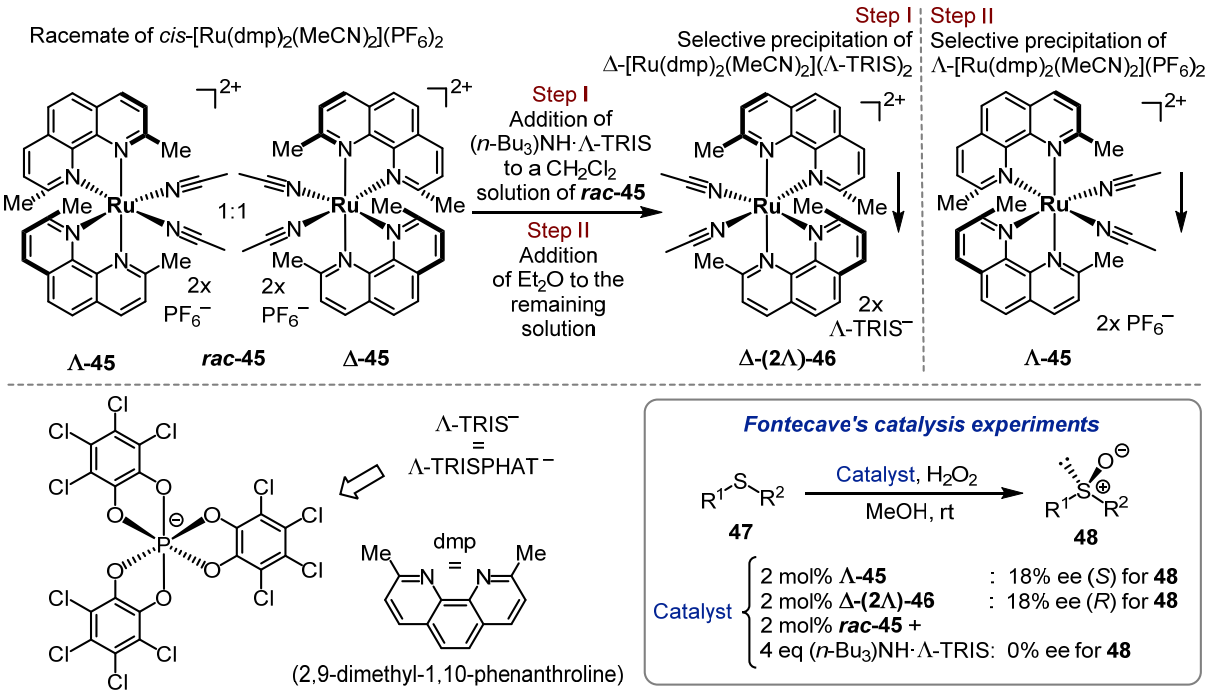

Scheme 8. Early use of a stereogenic-only-at-metal catalyst in an asymmetric reaction from Fontecave and co-workers.[37a] Catalyst **Λ-45** catalyzes the oxidation of sulfides (**47**) to chiral sulfoxides (**48**) with H_2O_2 as oxidant.[37a] In order to obtain **Λ-45**, Fontecave and co-workers first precipitated the Δ-enantiomer of ***rac*-45** by the addition of (*n*-Bu_3)NH·Λ-TRISPHAT as **Δ-(2Λ)-46** (Step I) and obtained then pure **Λ-45** from the remaining solution by Et_2O-induced precipitation of **Λ-45** (Step II).[37a]

Even though the enantioselectivities for the sulfoxides (**48**) are low and far from synthetically useful, Fontecave and co-workers demonstrated with this proof-of-principle study that stereogenic-only-at-metal complexes are suited as scaffolds for the design of chiral catalysts.

One year later in 2004, Belokon and co-workers reported about salicylimine-based cobaltate(III) complex **Λ-(*R*,*R*)-49**, which they used as a catalyst for the cyanosilylation of benzaldehyde (**50**) with trimethylsilyl cyanide to give the corresponding *O*-silylated cyanohydrin (**51**) in up to 77% ee (Scheme 9).[46]

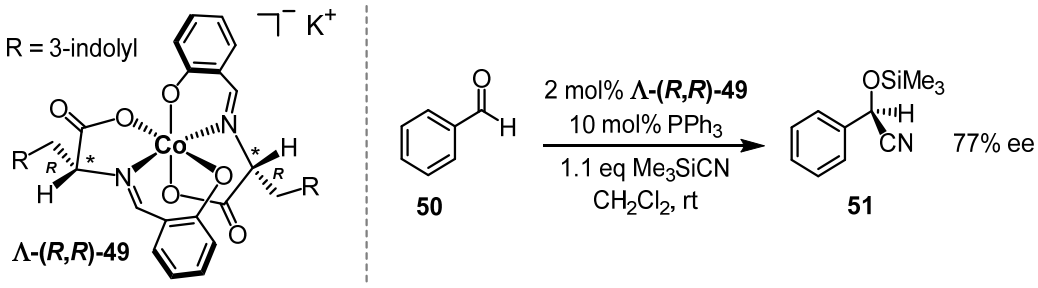

Scheme 9. Belokon's stereogenic-at-metal complex **Λ-(*R*,*R*)-49** catalyzes the cyanosilylation of benzaldehyde (**50**) with trimethylsilyl cyanide to give the corresponding *O*-silylated cyanohydrin (**51**) in up to 77% ee.[46]

However, this catalytic system turned out to be very sensitive to variations of the reaction parameters: Exchange of the potassium countercation for other cations, such as Na^+, Li^+, Cs^+,

inversion of the cobalt stereocenter (=**Δ-(*R*,*R*)-49**), and omission or replacement of co-catalyst PPh_3, resulted all in a dramatic or even in a total loss of enantioselectivity.[46]

It is worth noting that **Λ-(*R*,*R*)-49** represents a stereogenic-at-metal catalyst but *not* a stereogenic-*only*-at-metal catalyst due to the presence of one carbon-centered stereocenter in each of its identical tridentate ligands. Such a catalyst design entails the advantage that the Λ- and Δ-configured catalysts are diastereomers, which allows a straightforward resolution, for example via chromatography or via fractional crystallization.[46,47] In particular cases, spatial constraints may even completely prevent the formation of the second diastereomer (e.g., in case of Ohkuma's catalyst **Λ-(*S*, *S*, *S*)-67** from Scheme 13).[48]

In 2007, Fontecave and co-workers reported about dinuclear chiral bis-ruthenium complex **Λ-52**, which consists of a Λ-configured octahedral ruthenium(II) fragment containing the stereoinformation of the dinuclear complex and a ruthenium(II) half-sandwich fragment serving as the complex's catalytically active site (Scheme 10).[37b] The half-sandwich fragment of **Λ-52** catalyzes the asymmetric transfer hydrogenation of ketones (**53**) with sodium formate to give chiral secondary alcohols (**54**).[37b] Though the concept is interesting, only low enantioselectivities of not more than 26% ee could be achieved (Scheme 10).[37b]

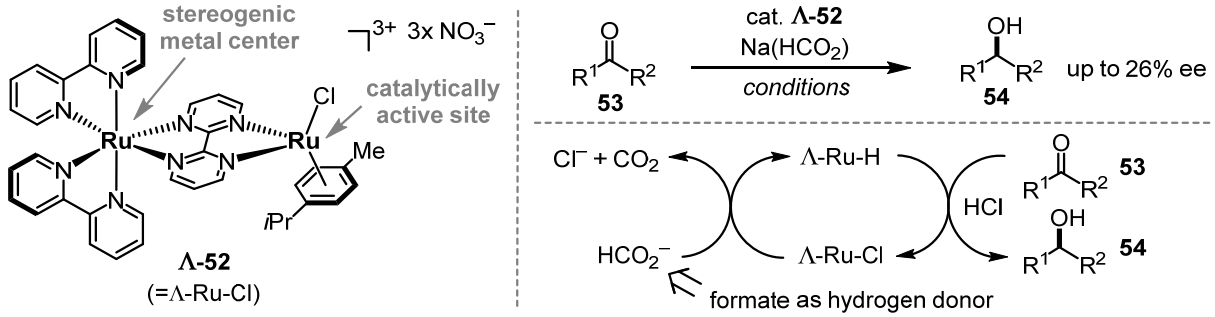

Scheme 10. Fontecave's dinuclear transfer hydrogenation catalyst **Λ-52**.[37b] Both ruthenium complex fragments fulfill different tasks: The octahedral chiral-only-at-metal fragment comprises the dinuclear complex's chiral information while the half-sandwich fragment serves as the dinuclear complex's catalytically active site.[37b]

One year later in 2008, Gladysz and co-workers used chiral Co(III) tris(ethylenediamine) complex **Λ-57** as a catalyst for the asymmetric Michael addition of dimethyl malonate (**56**) to cylopentenone (**55**), which provided addition product **58** in up to 33% ee (Scheme 11).[49] In this context, it is worth noting that Werner had already reported the isolation of enantiopure complexes Λ-$[Co(en)_3]X_3$ with $X^- = Br^-$, Cl^-, NO_3^- in 1912,[50] one year after his seminal publication from 1911 (see Scheme 7).[43] Surprisingly, such Co(III) tris(ethylenediamine) complexes or related complexes had never been applied or reported before as chiral catalysts, which may be attributed to their very low solubility in organic solvents.[49] Gladysz and co-workers addressed this issue in case of **Λ-57** by the substitution of the hard anions $X^- = Br^-$,

Cl^-, NO_3^- for the soft anion $X^- = BArF_{24}^-$ (tetrakis[3,5-bis(trifluoromethyl)phenyl]borate),[51] which renders the $[Co(en)_3]^{3+}$ complex cation as $BArF_{24}^-$ salt soluble in a range of common organic solvents (Scheme 11).[49]

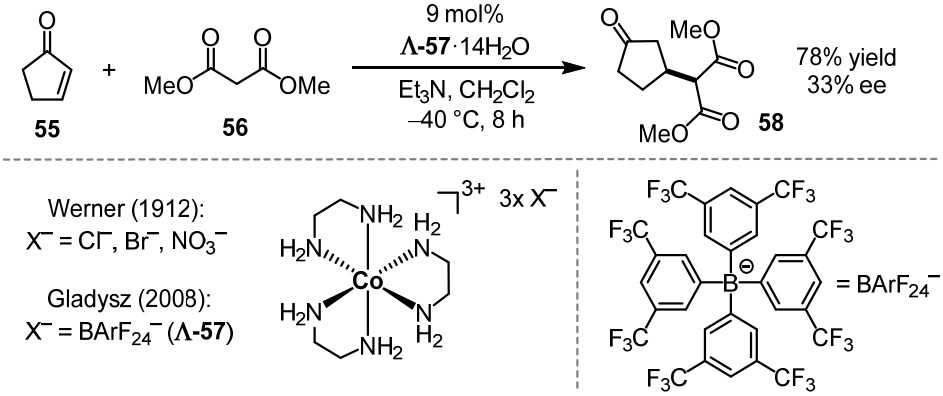

Scheme 11. Gladysz and co-workers replaced in Werner's complex Λ-$[Co(en)_3]X_3$[50] the hard anions chloride, bromide, and nitrate by the soft anion $BArF_{24}^-$ resulting in Λ-$[Co(en)_3](BArF_{24})_3$ (**Λ-57**), which is well soluble in a range of common organic solvents.[49] As a proof-of-principle, **Λ-57** was used in form of its tetradecahydrate as a catalyst for the asymmetric addition of dimethyl malonate (**56**) to cyclopentenone (**55**), which provided conjugate addition product **58** in up to 33% ee.[49]

As Co(III) tris(ethylenediamine) complexes are coordinatively inert under the applied conditions, Gladysz and co-workers assume that the reaction is catalyzed via hydrogen-bonding catalysis in the ligand sphere without direct participation of the cobalt center.[49]

In 2015 and 2016, Gladysz and co-workers presented catalysts **Λ-(2*S*,2*S*,2*S*)-59** and **Λ-(*S*)-60**, which can be considered as '2nd generation catalysts' of catalyst **Λ-57** (Scheme 12).[52–54] **Λ-(2*S*,2*S*,2*S*)-59** differs from **Λ-57** in that respect that the achiral ethylenediamine ligands of **Λ-57** are replaced by chiral (*S*,*S*)-1,2-diphenylethylenediamine ligands.[52] **Λ-(2*S*,2*S*,2*S*)-59** showed excellent performance as a catalyst for the Michael addition of malonates (**61**) to nitroalkenes (**62**)[52] and for the Michael addition of 1,3-dicarbonyl compounds (**64**) to di-*tert*-butyl azodicarboxylate (**65**)[53] giving the corresponding products **63** and **66** in up to 98% ee and in up to >99% ee, respectively (Scheme 12).[52,53] A much more subtle change with respect to catalyst **Λ-57** was made in case of **Λ-(*S*)-60**: Gladysz and co-workers formally replaced here only one ethylenediamine ligand of **Λ-57** by an ethylenediamine ligand bearing a 3-(dimethylamino)propyl residue featuring *S*-configuration at the junction point.[54] **Λ-(*S*)-60** showed, similar to catalyst **Λ-(2*S*,2*S*,2*S*)-59**, excellent performance as a catalyst for the Michael addition of malonates (**61**) to nitroalkenes (**62**) giving the corresponding products **63** with up to 99% ee (Scheme 12).[54]

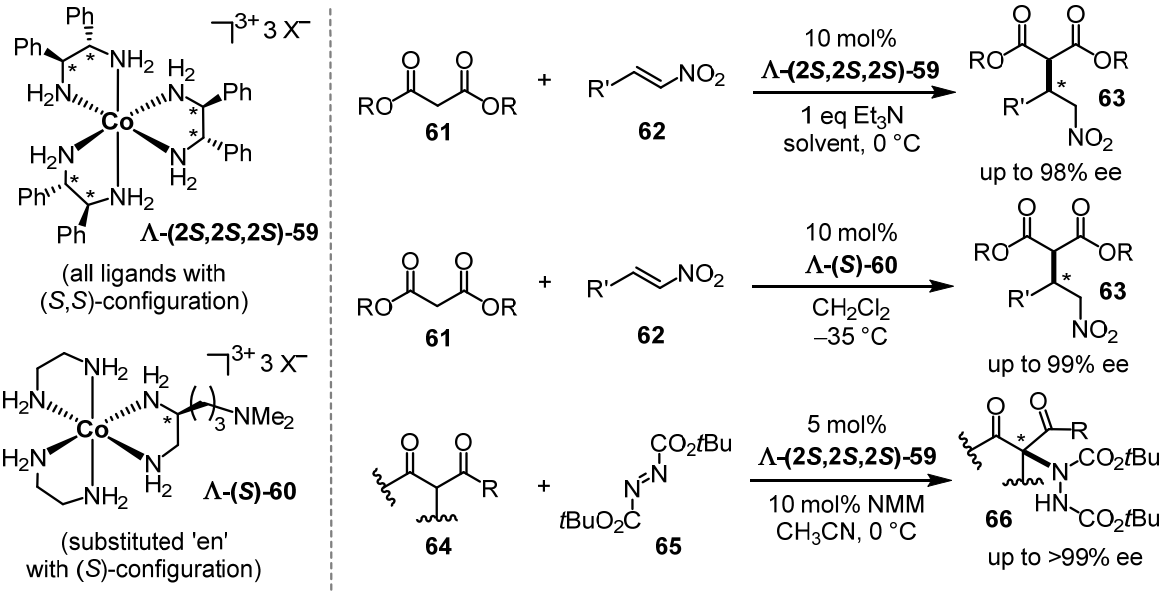

Scheme 12. Gladysz's '2nd generation catalysts' **Λ-(2*S*,2*S*,2*S*)-59**[52,53] and **Λ-(*S*)-60**[54] and their application as catalysts for the Michael addition of malonates (**61**) to nitroalkenes (**62**)[52,54] and for the Michael addition of 1,3-dicarbonyl compounds (**64**) to di-*tert*-butyl azodicarboxylate (**65**).[53]

In 2008, Ohkuma and co-workers reported that Ru(II) complex **Λ-(*S*,*S*,*S*)-67**, which features two *S*-configured phenylglycinate ligands (phgly) and one *S*-configured BINAP ligand, is an excellent catalyst for the asymmetric cyanosilylation of aldehydes (**68** → **69**) in combination with lithium carbonate as additive (Scheme 13, A).[48]

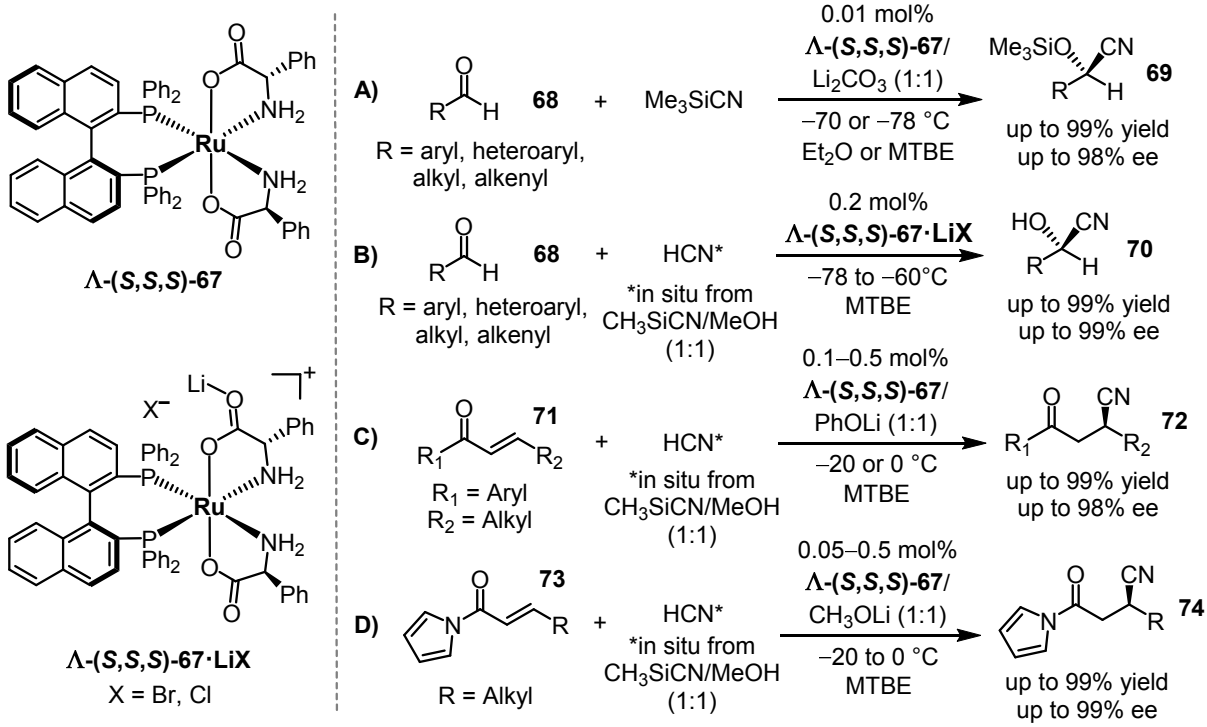

Scheme 13. Ohkuma's catalyst **Λ-(*S*,*S*,*S*)-67** is, as lithium salt **Λ-(*S*,*S*,*S*)-67·LiX** or in combination with a lithium salt, a powerful catalyst for the asymmetric cyanosilylation of aldehydes (**68** → **69**; A),[48] the asymmetric hydrocyanation of aldehydes (**68** → **70**; B),[56] the asymmetric conjugate hydrocyanation of *α,β*-unsaturated ketones (**71** → **72**; C),[57] and the related asymmetric conjugate hydrocyanation of *α,β*-unsaturated *N*-acyl pyrroles (**73** → **74**; D).[58]

Ohkuma and co-workers initially thought that the obtained complex was *trans*-[Ru(phgly)$_2$(BINAP)],[55] which would render the complex "non-stereogenic-at-metal". However, a crystal structure in a follow-up publication revealed that it was rather *cis*-[Ru(phgly)$_2$(BINAP)] and this crystal structure also revealed that the metal center is Λ-configured (see also Figure 5 in this context).[56] Accordingly, the entire stereochemical designation of the *cis*-complex is Λ-(*S*,*S*,*S*)-[Ru(phgly)$_2$(BINAP)] (i.e., **Λ-(*S*,*S*,*S*)-67**).

Apart from the asymmetric cyanosilylation of aldehydes (**68** → **69**; Scheme 13, A),[48] catalyst **Λ-(*S*,*S*,*S*)-67** was identified – as lithium salt **Λ-(*S*,*S*,*S*)-67·LiX** or in combination with a lithium salt – as a powerful catalyst for the asymmetric hydrocyanation of aldehydes (**68** → **70**; Scheme 13, B),[56] for the asymmetric conjugate hydrocyanation of *α*,*β*-unsaturated ketones (**71** → **72**; Scheme 13, C),[57] and for the related asymmetric conjugate hydrocyanation of *α*,*β*-unsaturated *N*-acyl pyrroles (**73** → **74**; Scheme 13, D).[58]

In 2013, Belokon and co-workers reported about salicylimine-based cobalt(III) complex **Λ-(2*R*,2*R*)-75** (Scheme 14), which can be considered as a strongly modified derivative of **Λ-(*R*,*R*)-49** from Scheme 9.[59] Due to the formal replacement of two cobalt-coordinating carboxylates for two cobalt-coordinating amines, complex **Λ-(2*R*,2*R*)-75** is, in contrast to **Λ-(*R*,*R*)-49**, positively charged. **Λ-(2*R*,2*R*)-75** was found to be a powerful catalyst for the enantioselective *α*-alkylation of O'Donnell's substrate **76**[60] with alkyl halides (**77**) to give the corresponding *α*-alkylated products **78** with up to 92% ee (Scheme 14), which can be used as precursors for the synthesis of (non-)natural amino acids.[59,60]

One year later, Belokon and co-workers reported that **Λ-(2*R*,2*R*)-75** also efficiently catalyzes the enantioselective Michael addition of O'Donnell's substrate **76** to EWG-activated alkenes (**79**; EWG: electron-withdrawing group) to give the corresponding *α*-alkylated products **80** with up to 96% ee (Scheme 14).[61]

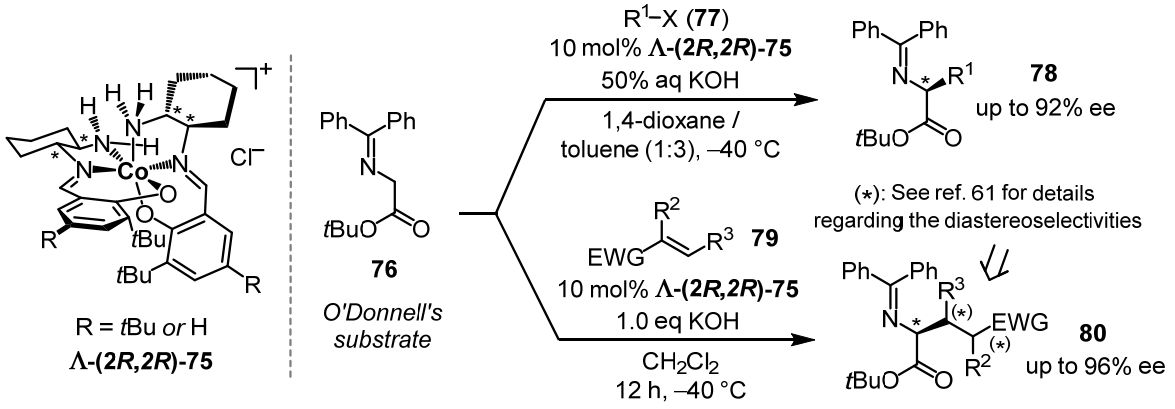

Scheme 14. Belokon's salicylimine-based cobalt(III) complex **Λ-(2*R*,2*R*)-75** serves as an efficient catalyst for the asymmetric *α*-alkylation of O'Donnell's substrate **76**[60] with alkyl halides (**77**)[59] and for the asymmetric Michael addition of O'Donnell's substrate **76** to EWG-activated alkenes (**79**).[61]

Finally, Figure 6 shows an overview of the stereogenic-at-metal catalysts which have been discussed in chapter 1.3. With regard to the main topic of the present thesis – the design, synthesis, and application of a nucleophilic octahedral stereogenic-only-at-metal catalyst – it is striking that apparently none of these stereogenic-at-metal or stereogenic-only-at-metal catalysts acts as a nucleophilic catalyst.

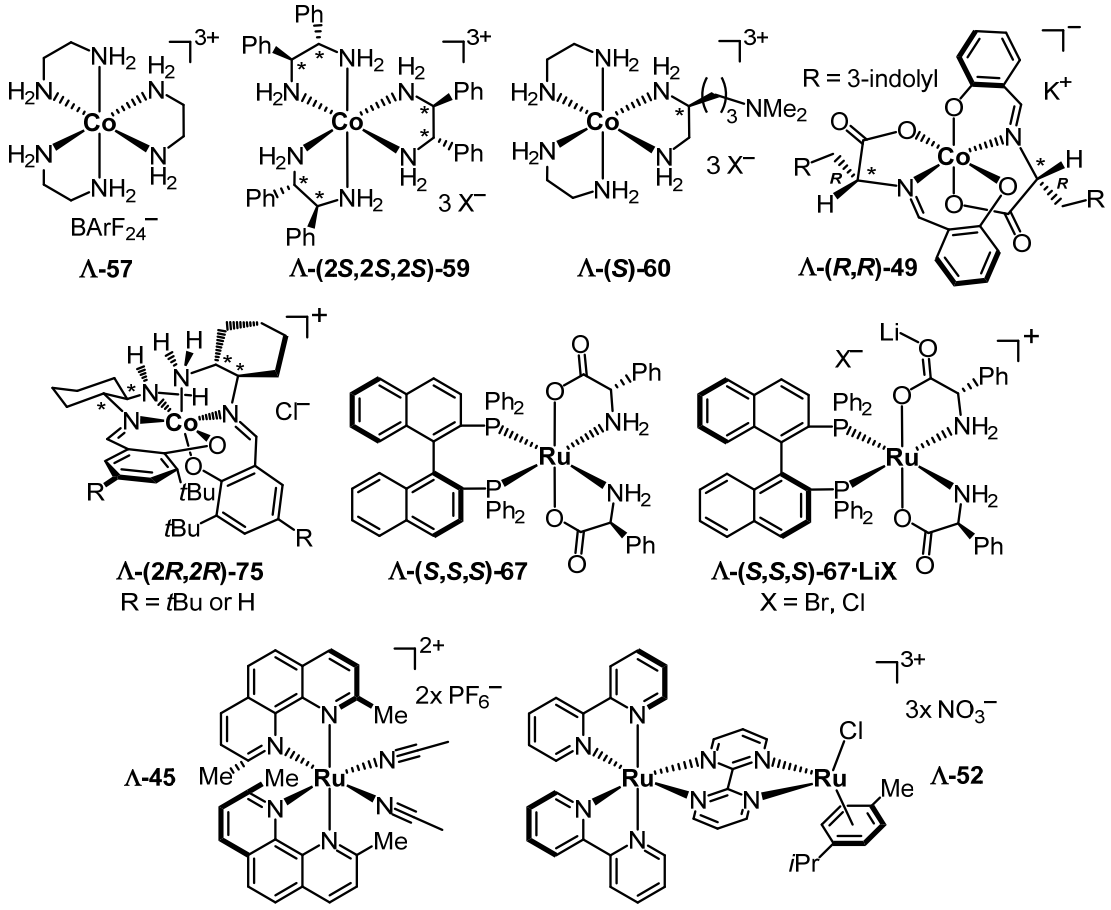

Figure 6. Overview of the stereogenic-at-metal catalysts which have been discussed in chapter 1.3.

1.4 Stereogenic-at-Metal Catalysts – Contributions from the Meggers Laboratory

In 2013, Meggers and co-workers reported about Ir(III)-based stereogenic-only-at-metal complex **Λ-81**, which serves as an efficient catalyst for the asymmetric transfer hydrogenation of *β*,*β*-disubstituted nitroalkenes (**82**) with Hantzsch ester **83** as hydride donor (Scheme 15).[38a]

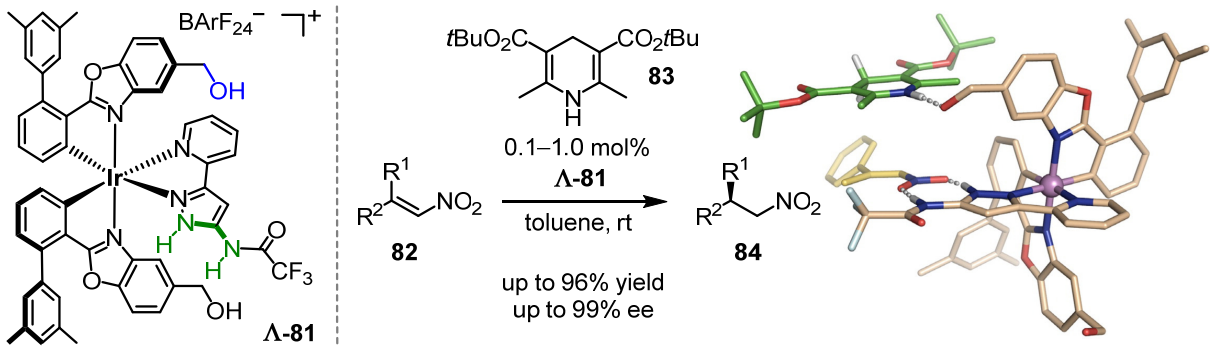

Scheme 15. Stereogenic-only-at-metal complex **Λ-81** from Meggers and co-workers serves as an efficient bifunctional cooperative catalyst for the asymmetric transfer hydrogenation of *β*,*β*-disubstituted nitroalkenes (**82**) to *β*-chiral nitroalkanes (**84**) with Hantzsch ester **83** as hydride donor.[38a] Mechanistic details are provided in the text. The model on the right side has been taken from ref. 38a [Model reproduced with permission from ref. 38a. Copyright © 2013, American Chemical Society]

As depicted in Scheme 15, it is supposed that **Λ-81** acts as a bifunctional cooperative catalyst: While the bidentate 5-amino-3-(2-pyridyl)-1*H*-pyrazole ligand is supposed to activate and spatially align a nitroalkene (**82**) by double hydrogen-bonding (structure highlighted in green), a hydroxymethyl group located at one of both cyclometalated phenylbenzoxazole ligands (structure highlighted in blue) is supposed to activate and to align Hantzsch ester **83** via single hydrogen-bonding. Accordingly, both activated substrates **82** and **83** are perfectly aligned in the resulting ternary complex to react with each other.[38a] At this point, it is worth noting that the catalytic entity of the bidentate 5-amino-3-(2-pyridyl)-1*H*-pyrazole ligand basically mimics the catalytic entity of well-established thiourea-based hydrogen-bonding organocatalysts.[38a,62] As depicted in Scheme 15, 0.1–1.0 mol% of **Λ-81** were found to be sufficient to provide the desired *β*-chiral nitroalkanes (**84**) in yields of up to 96% and with enantioselectivities of up to 99%. Noteworthy, the introduction of both 3,5-dimethylphenyl substituents in **Λ-81** was found to enhance both the selectivity and activity of the catalyst in case of reaction **82** + **83** → **84**.[38a]

In the same year, Meggers and co-workers also reported about catalyst **Λ-85**, which was developed based on catalyst **Λ-81** as a catalyst for the asymmetric Friedel–Crafts alkylation of indoles (**87**) with *α*-substituted *β*-nitroacrylates (**86**) as substrates (Scheme 16).[38b] Catalyst **Λ-85** differs from catalyst **Λ-81** in that respect that the hydroxymethyl groups of **Λ-81** are replaced by carboxamide groups and that the 3,5-dimethylphenyl groups are replaced by

N-carbazolyl groups (Scheme 16). These two modifications improved both the catalyst's activity and enantioselectivity in case of reaction **86** + **87** → **88** compared to catalyst **Λ-81**.[38b]

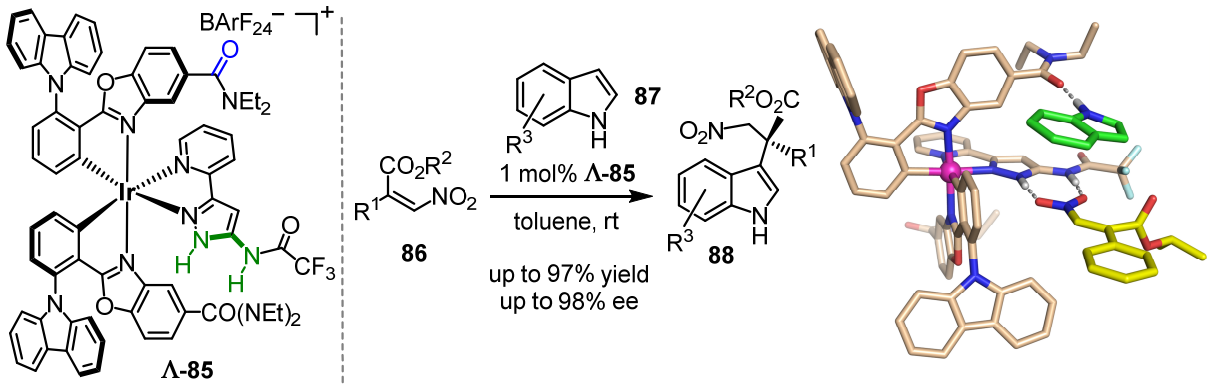

Scheme 16. Stereogenic-only-at-metal catalyst **Λ-85** from Meggers and co-workers serves as an efficient bifunctional cooperative catalyst for the asymmetric Friedel–Crafts alkylation of indoles (**87**) with *α*-substituted *β*-nitroacrylates (**86**).[38b] The model on the right side has been taken from ref. 38b [Model reproduced with permission from ref. 38b. Copyright © Wiley-VCH Verlag GmbH & Co. KGaA]

Catalyst **Λ-85** was found to give Friedel–Crafts alkylation products **88**, which feature an all-carbon quaternary stereocenter, with a loading of just 1 mol% of **Λ-85** in up to 97% yield and with up to 98% ee (Scheme 16).[38b] In analogy to the transfer hydrogenations with **Λ-81** from Scheme 15, **Λ-85** is supposed to activate and align the nitroacrylates (**86**) by double hydrogen-bonding and the indoles (**87**) via single hydrogen-bonding (Scheme 16).[38b]

In 2016, Meggers and co-workers reported about catalyst **Λ-89** (Scheme 17), which can be regarded as a significantly improved version of catalyst **Λ-81** for the already mentioned transfer hydrogenation of *β*,*β*-disubstituted nitroalkenes (**82**) to *β*-chiral nitroalkanes (**84**; see Scheme 15).[38a,63]

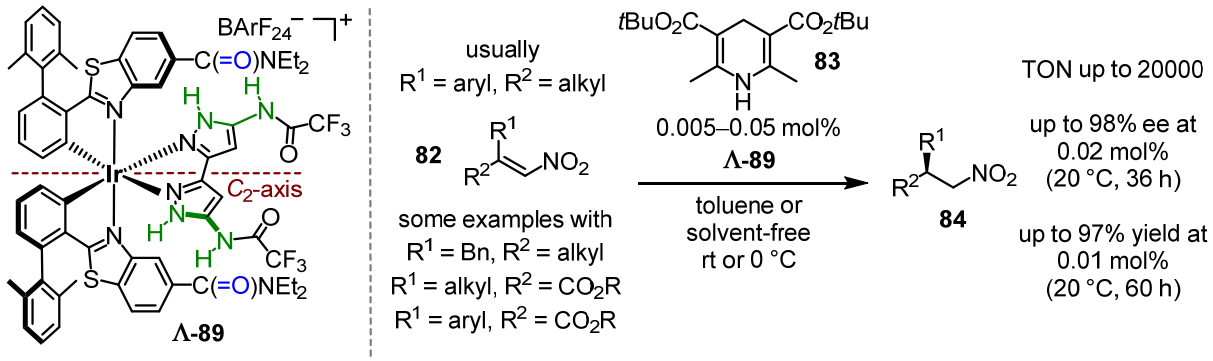

Scheme 17. C_2-symmetric catalyst **Λ-89** from Meggers and co-workers serves as an extraordinarily efficient catalyst for the asymmetric reduction of *β*,*β*-disubstituted nitroalkenes (**82**) to *β*-chiral nitroalkanes (**84**) with Hantzsch ester **83** as hydrogen donor.[63] Loadings of just 0.005–0.05 mol% of **Λ-89** (which corresponds in case of full turnovers to turnover numbers (TONs) of up to 20000) were found to be sufficient to provide desired products **84** with excellent yields and enantioselectivities.[63]

At the start of the development of catalyst **Λ-89**, Meggers and co-workers discovered that complex **Λ-85** (see Scheme 16) was a better catalyst in terms of selectivity and activity for the reaction **82** + **83** → **84** compared to initially used complex **Λ-81** (see Scheme 15). Hence, complex **Λ-85** became the new catalyst platform for further developments.[38a,63] Further improvements in terms of activity and selectivity were then achieved 1.) via replacement of the *N*-carbazolyl substituents for 2,6-dimethylphenyl substituents, 2.) via replacement of the cyclometalated phenylbenzoxazole ligands for phenylbenzothiazole ligands, and 3.) via replacement of the dissymmetric pyridylpyrazole ligand for a symmetric bispyrazole ligand.[63] The latter modification renders the complex C_2-symmetric. As a consequence, **Λ-89** features two indistinguishable catalytic sites capable of bifunctional cooperative hydrogen-bonding catalysis.[63]

Catalyst **Λ-89** was found to be extraordinarily effective, giving the desired *β*-chiral nitroalkanes (**84**) within short reaction times in very good to excellent yields and enantioselectivities with loadings of just 0.005–0.05 mol% of **Λ-89** (Scheme 17).[63]

In the same year, Meggers and co-workers reported about catalyst **Λ-(*R*,*R*)-90** (Scheme 18), which can be regarded as a significantly improved version of catalyst **Λ-85** for the already mentioned Friedel–Crafts alkylation of indoles (**87**) with *α*-substituted *β*-nitroacrylates (**86**; see Scheme 16).[64] In case of catalyst **Λ-(*R*,*R*)-90**, exchange of the *N*-carbazolyl groups of **Λ-85** for 2,6-dimethylphenyl groups was found to be detrimental for the reaction **86** + **87** → **88** and hence the *N*-carbazolyl groups were retained (compare with **Λ-89** from Scheme 17 and see the previous paragraphs).[64]

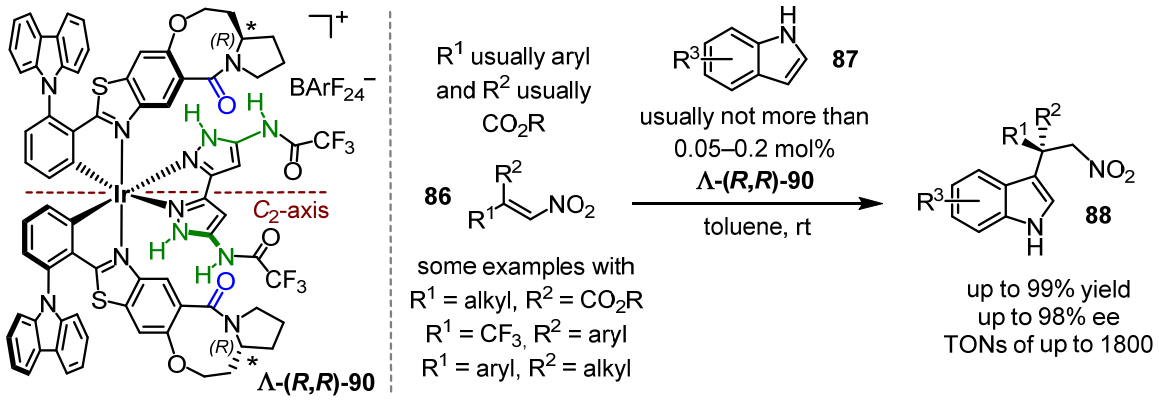

Scheme 18. C_2-symmetric catalyst **Λ-(*R*,*R*)-90** from Meggers and co-workers serves as an extraordinarily efficient catalyst for the asymmetric Friedel–Crafts alkylation of indoles (**87**) with *α*-substituted *β*-nitroacrylates (**86**).[64] 0.05–0.2 mol% of **Λ-(*R*,*R*)-90** were found to be sufficient to provide desired products **88** in good to excellent yields and enantioselectivities.[64]

As in case of catalyst **Λ-89**, 1.) replacement of the dissymmetric pyridylpyrazole ligand by the corresponding symmetric bispyrazole ligand and 2.) replacement of the phenylbenzoxazole ligands by phenylbenzothiazole ligands both significantly contributed in improving the

catalyst.[64] However, catalyst **Λ-(*R*,*R*)-90** exhibits an additional feature which distinguishes it from catalyst **Λ-89** in addition to that: Meggers and co-workers recognized that the catalytically relevant carboxamide moieties in catalysts **Λ-85** and **Λ-89** rotate around their C_{aryl}–CO-bond. In contrast, only a narrow window of the dihedral angle between the benzoxazole plane and the plane of the carbonyl group permits effective cooperative catalysis.[64] Hence, it was anticipated that a conformational fixation of the carboxamide moiety would result in a perfect alignment of this group for cooperative catalysis, which would enhance the catalyst at least in terms of activity. And indeed, replacement of the *N*,*N*-diethylcarboxamide moieties by proline-derived fused eight-membered lactam moieties, giving final catalyst **Λ-(*R*,*R*)-90** (Scheme 18), not only significantly increased the activity of the catalyst but also the enantioselectivity.[64] Interestingly and in accordance with the supposed mechanism, **Λ-(*R*,*R*)-90**'s diastereomer **Δ-(*R*,*R*)-90** is virtually inactive as its fixed carboxamides are misaligned for cooperative catalysis.[64]

The sophisticated structure of **Λ-(*R*,*R*)-90** results in a high catalytic efficiency, which allows it provide products **88**, which feature an all-carbon quaternary stereocenter, with excellent yields of up to 99% and with enantioselectivities of up to 98% with catalyst loadings of just 0.05–0.2 mol% of **Λ-(*R*,*R*)-90** (Scheme 18).[64]

The so far presented stereogenic-at-metal catalysts from the Meggers group – **Λ-81**, **Λ-85**, **Λ-89**, and **Λ-(*R*,*R*)-90** – operate all as bifunctional cooperative catalysts which achieve their asymmetric transformations by the combination of 1.) activating an *α*,*β*-unsaturated nitro compound as Michael acceptor with the catalysts acting as double hydrogen-bond donors and 2.) by simultaneously activating another substrate with the catalysts acting as single hydrogen-bond acceptors.

Meggers and co-workers reasoned that deprotonation of the amidopyrazole ligand in catalysts **Λ-81** and **Λ-85**, electronic fine-tuning of the resulting deprotonated amidopyrazolato ligand, and appropriate decoration of the catalyst's cyclometalated ligands could result in a powerful metal-templated Brønsted base catalyst.[65,66] And indeed, starting from catalyst **Λ-81**, catalysts **Λ-91** and **Λ-92** were developed, which serve as cooperative bifunctional Brønsted base catalysts (Scheme 19).[66]

Catalyst **Λ-91** was found to be an efficient catalyst for the asymmetric Michael addition of thiols (**94**) to *α*,*β*-unsaturated *N*-pyrazolylamides (**93**) to give products **95** in up to 98% yield and with up to 97% ee with 0.02–1.0 mol% of catalyst **Λ-91**.[66] Catalyst **Λ-92** was found to be an efficient catalyst for the asymmetric *aza*-Henry reaction between monosubstituted nitromethanes (**96**) and *N*-Boc-protected imines (**97**; Scheme 19) to give desired products **98** in up to 98% yield and with up to 98% ee with just 0.25–0.75 mol% of **Λ-92** (Scheme 19).[66]

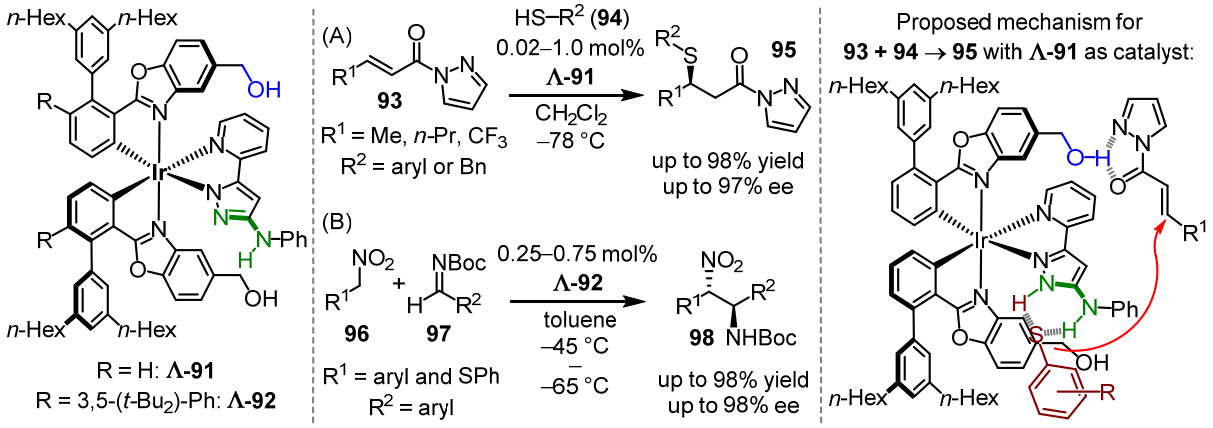

Scheme 19. Brønsted base catalysts **Λ-91** and **Λ-92** from Meggers and co-workers.[66] Catalyst **Λ-91** serves as an efficient catalyst for the Michael addition of thiols (**94**) to *α,β*-unsaturated *N*-pyrazolylamides (**93**) and catalyst **Λ-92** serves as an efficient catalyst for the *aza*-Henry reaction between monosubstituted nitromethanes (**96**) and *N*-Boc-protected imines (**97**).[66] The proposed mechanism for the reaction **93** + **94** → **95** with catalyst **Λ-91** is depicted on the right side.[66]

The proposed mechanism for the reaction **93** + **94** → **95** with **Λ-91** as catalyst is depicted on the right side of Scheme 19 and is as follows: Thiols (**94**) are supposed to be activated by proton transfer to the pyrazolato ligand with the resulting thiolate being bound to the resulting aminopyrazole ligand via two hydrogen bonds.[66] The benzoxazole-attached hydroxymethyl moiety is supposed to activate and align *α,β*-unsaturated *N*-pyrazolylamides (**93**) via a three-center hydrogen bond (Scheme 19).[66] In contrast to catalyst **Λ-81** from Scheme 15, the hydroxymethyl group does not act as a hydrogen-bond acceptor but as a hydrogen-bond donor.[66]

In case of the *aza*-Henry reaction (**96** + **97** → **98**), catalyst **Λ-91** only showed a good performance when 10 mol% were employed and the selectivity dropped significantly when lower loadings were used.[66] Introduction of 3,5-bis(*tert*-butyl)phenyl substituents next to the 3,5-bis(*n*-hexyl)phenyl substituents of **Λ-91** giving catalyst **Λ-92** solved this problem: **Λ-92** provides *aza*-Henry reaction products **98** with just 0.25–0.75 mol% loading of **Λ-92** in yields of up to 98% and with enantioselectivities of up to 98% ee (Scheme 19).[66]

The proposed mechanism for the reaction **96** + **97** → **98** with **Λ-92** as catalyst is as follows: The aminopyrazolato ligand of **Λ-92** is supposed to deprotonate nitromethanes (**96**) and the resulting nitronates are supposed to be bound to the resulting aminopyrazole ligand by double hydrogen-bonding, which resembles the mode of action of catalysts **Λ-81**, **Λ-85**, **Λ-89**, and **Λ-(*R*,*R*)-90** with regard to *α,β*-unsaturated nitro compounds (see Schemes 15–18).[66] The *N*-Boc imines (**97**), on the other hand, are then assumed to be activated via single hydrogen-bonding between the Boc group's carbonyl group and the hydroxymethyl group of catalyst **Λ-92** with the hydroxymethyl group acting as hydrogen-bond donor.[66]

The so far presented stereogenic-at-metal catalysts from the Meggers laboratory essentially all rely on a primary double hydrogen-bonding donor motif enabling ligand-sphere-mediated 'organocatalysis' acting in cooperation with a secondary single hydrogen-bonding donor or hydrogen-bonding acceptor motif.

In 2014, Meggers and co-workers presented catalyst **Λ-99**, which does, in contrast, not rely on such a primary double hydrogen-bonding donor motif (Scheme 20).[67] Catalyst **Λ-99** was found to be an efficient catalyst for the asymmetric *α*-amination, or rather *α*-hydrazination,[68] of enolizable aldehydes (**100**) with azodicarboxylates (**101**).[67]

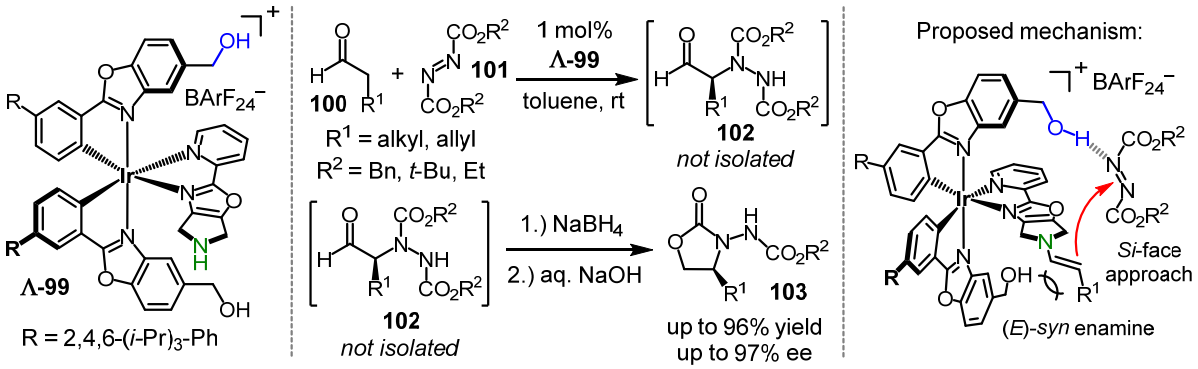

Scheme 20. Complex **Λ-99** from Meggers and co-workers serves as an efficient bifunctional cooperative enamine/hydrogen-bonding catalyst for the *α*-amination, or rather *α*-hydrazination,[68] of enolizable aldehydes (**100**) with azodicarboxylates (**101**).[67] The proposed mechanism is shown on the right side and explained in detail in the text.

As depicted in Scheme 20, catalyst **Λ-99** is supposed to operate as a bifunctional cooperative enamine/hydrogen-bonding catalyst.[67] At first, **Λ-99** activates an enolizable aldehyde (**100**) via enamine formation. The benzoxazole-attached hydroxymethyl group of **Λ-99** then activates an azodicarboxylate (**101**) via single hydrogen-bonding, which triggers the conjugate addition reaction with the underlying enamine.[67] Next, the resultant iminium species hydrolyzes (note that water is formed upon enamine formation), which gives chiral *α*-hydrazino aldehydes (**102**) as primary products.[67] As these products (**102**) are prone towards racemization, they were usually *in situ* reduced to the corresponding alcohols and cylized to the depicted oxazolidinones (**103**). Catalyst **Λ-99** was found to give oxazolidinone products **103** in up to 96% yield and with up to 97% ee with 1 mol% of catalyst **Λ-99** (Scheme 20).[67]

All of the so far presented stereogenic-at-metal catalysts from the Meggers group essentially operate as metal-templated 'organocatalysts', i.e., without direct participation of the metal center apart from its electronic influence and its structural role as a "glue" for the participating ligands. On the contrary, in 2014 Meggers and co-workers reported about stereogenic-only-at-metal catalyst **Λ-104**, which strongly differs from the previously

discussed catalysts by the fact that the metal center is here directly involved in the catalytic cycle (Scheme 21).[69] Complex **Λ-104** does not bear a third kinetically-inert bidentate ligand but two kinetically labile monodentate acetonitrile ligands.[69] Originally, catalyst **Λ-104** was developed as a catalyst for the enantioselective Friedel–Crafts alkylation of indoles (**87**) with *α,β*-unsaturated 2-acyl imidazoles (**105**) as electrophiles (Scheme 21).[69]

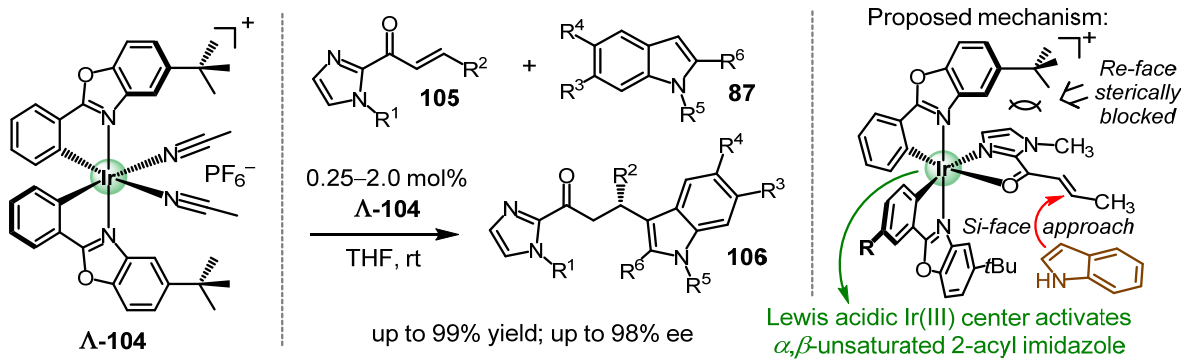

Scheme 21. Lewis acidic stereogenic-only-at-metal catalyst **Λ-104** from Meggers and co-workers.[69] Catalyst **Λ-104** was originally developed as a catalyst for the enantioselective Friedel–Crafts alkylation of indoles (**87**) with *α,β*-unsaturated 2-acyl imidazoles (**105**) as electrophiles.[69] The proposed mechanism is shown on the right side and explained in detail in the text.

As depicted in Scheme 21, *α,β*-unsaturated 2-acyl imidazoles (**105**) are supposed to coordinate to the Lewis acidic Ir(III) center of **Λ-104** as bidentate ligands replacing both kinetically labile acetonitrile ligands. Coordination to the Lewis acidic Ir(III) center increases the electrophilicity of the *α,β*-unsaturated 2-acyl imidazoles (**105**) to such an extent that indole derivatives (**87**) are able to react with coordinated **105** in a Friedel–Crafts reaction.[69] One of both present benzoxazole-attached *tert*-butyl substituents is crucial for the enantioselectivity as it completely blocks one prochiral face of coordinated **105**.[69]

For catalyst **Λ-104**, loadings of just 0.25–2.0 mol% of **Λ-104** were found to be sufficient to provide Friedel–Crafts alkylation products **106** in yields of up to 99% and with up to 98% ee (Scheme 21).[69] Strikingly and although the coordination number varies in the course of the catalytic cycle, the metal-located stereoinformation is completely retained and no racemization occurs under the reaction conditions.[69] Meanwhile, a polymer-supported version of catalyst **Λ-104** has been developed, which did not even show any signs of racemization after 15 cycles with **105** + **87** → **106** as catalyzed reaction.[70]

Since the aforementioned publication from 2014, catalyst **Λ-104** and derivatives thereof have proven to be extraordinarily versatile Lewis acidic catalysts for a broad range of asymmetric transformations, and that both with and without the participation of photocatalysis.[40,47,69–72] A discussion about all the reactions which have been established since 2014 with Lewis acidic stereogenic-at-metal bisacetonitrile complexes of type **Λ-104** would

go far beyond the scope of this introduction.[40,47,69–72] Therefore, only an assortment of examples will be presented in the subsequent paragraphs.

Also in 2014, Meggers and co-workers demonstrated with a groundbreaking publication in *Nature* that catalysts of type **Λ-104** are also powerful asymmetric visible-light photoredox catalysts (Scheme 22).[71a]

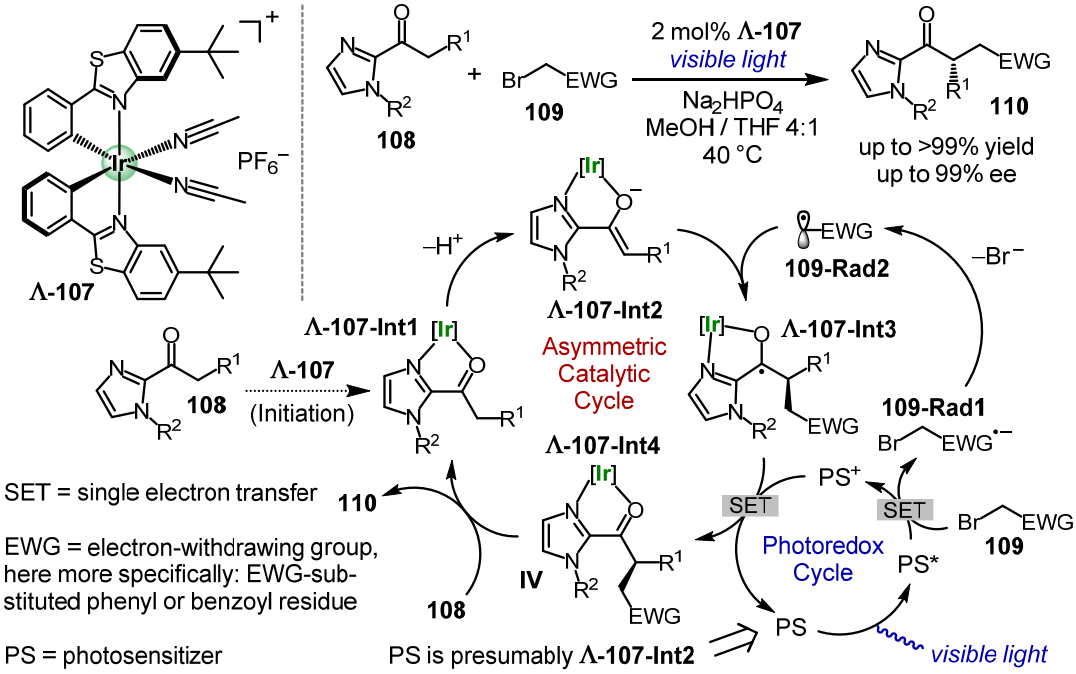

Scheme 22. Visible-light-driven asymmetric *α*-alkylation of 2-acyl imidazoles (**108**) with acceptor-substituted benzyl bromides and phenacyl bromides (**109**) catalyzed by **Λ-107**.[71a] The depicted mechanism is described in detail in the text below.[71a]

While previously established "traditional" asymmetric photoredox systems rely on a dual-catalyst approach with a photocatalyst / photosensitizer being responsible for substrate activation by visible light and a chiral catalyst being responsible for asymmetric induction,[73] the photoredox catalysts of type **Λ-104** are a merger of both: they are photosensitizer and chiral catalyst in one molecule.[71a] The first asymmetric visible-light-driven photoredox reaction which was established with such a catalyst and reported in the aforementioned *Nature* publication, is the asymmetric *α*-alkylation of 2-acyl imidazoles (**108**) with acceptor-substituted benzyl bromides and phenacyl bromides (**109**), which is shown in Scheme 22.[71a] Although benzoxazole-based complex **Λ-104** (see Scheme 21) was found to be a suitable catalyst for the visible-light-driven reaction **108** + **109** → **110**, its benzothiazole congener **Λ-107** was found to be a superior catalyst in terms of yield and enantioselectivity, giving the desired *α*-alkylated products (**110**) in up to >99% yield and with up to 99% ee with just 2 mol% of catalyst **Λ-107** (Scheme 22).[71a]

The proposed mechanism for the reaction is depicted in Scheme 22: In analogy to the Friedel–Crafts alkylation from Scheme 21, 2-acyl imidazole (**108**) first replaces both acetonitrile ligands of **Λ-107** and coordinates to the iridium(III) center in a bidendate fashion, which results in intermediate **Λ-107-Int1**.[71a] Weak Brønsted base Na_2HPO_4 next helps to form the corresponding enolate complex **Λ-107-Int2**.[71a] The next step is assumed to be the stereogenic reaction between photo-reductively generated electrophilic radical **109-Rad2** and nucleophilic enolate complex **Λ-107-Int2**, which results in the formation of Ir(III)-coordinated ketyl radical **Λ-107-Int3**.[71a] Electrophilic radical **109-Rad2** is assumed to be formed by fragmentation of radical anion **109-Rad1**, which is formed from **109** via single electron transfer (SET) with the photoexcited photosensitizer PS* as reductant.[71a] According to mechanistic experiments, the effective photosensitizing species is most presumably enolate complex **Λ-107-Int2**.[71a] Ketyl radical **Λ-107-Int3** is next assumed to regenerate the oxidized photosensitizer PS^+ via SET which results in the formation of Ir(III)-coordinated product **Λ-107-Int4** and regenerated photosensitizer PS. Product **110** is finally released from **Λ-107-Int4** and the released stereogenic-at-metal Ir(III) complex fragment can start a new catalytic cycle with 2-acyl imidazole (**108**; Scheme 22).[71a] Although mechanistic experiments strongly support this mechanism, alternative pathways or at least their contribution to the overall reaction, such as the contribution of a radical–chain pathway or a radical–radical recombination pathway, cannot be entirely ruled out.[71a]

Based on archetypical catalysts **Λ-104** and **Λ-107**, other Lewis acidic bis-cyclometalated stereogenic-at-metal complexes based on Ir(III), Rh(III), and Ru(II) have been developed in the Meggers laboratory in recent years, from which an assortment is presented in Figure 7.

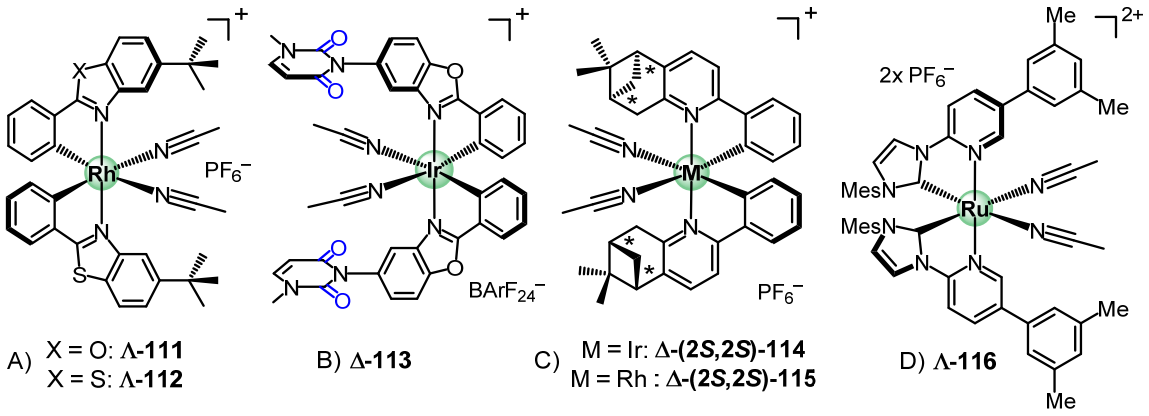

Figure 7. Lewis acidic stereogenic-at-metal catalysts from the Meggers laboratory which have been developed on the basis of catalysts **Λ-104** and **Λ-107**: A) Congeneric Rh(III) catalysts **Λ-111**[71b] and **Λ-112**.[71m] B) 1-Methylpyrimidine-2,4(1*H*,3*H*)-dione-substituted Ir(III) catalyst **Δ-113**.[71r] C) 2-Phenyl-5,6-(*S*,*S*)-pinenopyridine-cyclometalated Ir(III) catalyst **Δ-(2*S*,2*S*)-114** and its Rh(III) congener **Δ-(2*S*,2*S*)-115**.[47] D) Ru(II)-based catalyst **Λ-116**, which features two pyridyl-substituted *N*-heterocyclic carbenes as cyclometalating ligands.[71b2]

In the following paragraphs, selected applications for the catalysts from Figure 7 are presented.

A recent application for Rh(III)-based catalyst **Λ-111** is the visible-light-driven asymmetric *β*-amination of *α*,*β*-unsaturated 2-acyl imidazoles (**105**) via proton-coupled electron transfer (PCET) with *N*-aryl carbamates (**117**) as amination reagents (Scheme 23).[71v] In contrast to the reaction from Scheme 22, an iridium(III)-based photosensitizer (**118**) is added here and the role of Rh(III) complex **Λ-111** is limited to facilitate the one-electron reduction of the coordinated *α*,*β*-unsaturated 2-acyl imidazole and to control the stereochemical outcome of the radical–radical coupling process.[71v] Interestingly, replacement of benzoxazole-based Rh(III) catalyst **Λ-111** by benzoxazole-based Ir(III) catalyst **Λ-104** or benzothiazole-based Rh(III) catalyst **Λ-112** both resulted in a sluggish reaction.[71v] Products **120** could be obtained in up to 99% yield and with up to 99% ee with 5 mol% of catalyst **Λ-111** in combination with 2 mol% of photosensitizer **118** (Scheme 23).[71v]

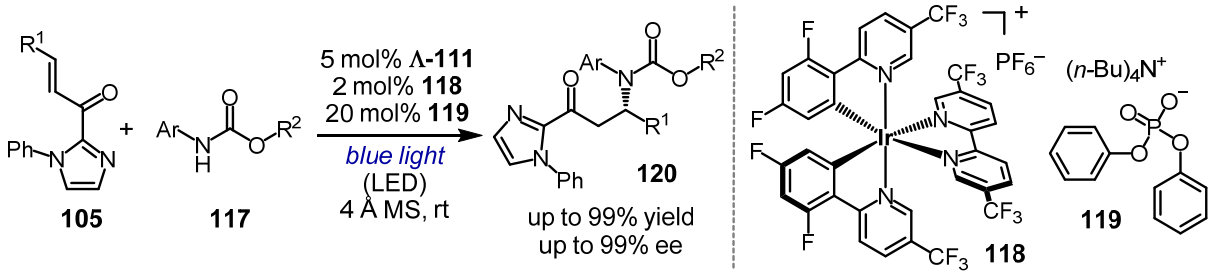

Scheme 23. Visible-light-driven asymmetric *β*-amination of *α*,*β*-unsaturated 2-acyl imidazoles (**105**) with *N*-aryl carbamates (**117**) via PCET with stereogenic-only-at-metal catalyst **Λ-111** and photosensitizer **118**.[71v]

A very recent application for related benzothiazole-based Rh(III) catalyst **Λ-112** is the asymmetric visible-light-driven intermolecular [2+2]-cycloaddition between *α*,*β*-unsaturated 2-acylimidazoles, 2-acylpyrazoles, *N*-acylpyridines (**121**) and alkenes (**122**; Scheme 24).[71w]

The proposed mechanism for this reaction is depicted in Scheme 24. It is expected that an *α*,*β*-unsaturated compound (**121**) at first coordinates to the Rh(III) center and that the resulting intermediate **Λ-112-Int1** is then excited from the electronic ground state (S_0 state) to the lowest excited singlet state (S_1 state → **Λ-112-Int1-S$_1$**) upon irradiation with blue visible light.[71w] **Λ-112-Int1-S$_1$** is assumed to next undergo an intersystem crossing (ISC) so that the intermediate is then in the lowest excited triplet state (T_1 state → **Λ-112-Int1-T$_1$**). In **Λ-112-Int1-T$_1$**, the two highest occupied molecular orbital electrons (HOMO electrons), which are the electrons of the conjugated double bond of **Λ-112-Int1-T$_1$**, have the same spin and hence behave as 1,2-biradicals.[71w,74] This allows **Λ-112-Int1-T$_1$** to react with alkene **122** stepwise via biradical intermediate **Λ-112-Int2** to intermediate **Λ-112-Int3**, which then releases product **123** to start a new catalytic cycle with substrate **121**.[71w]

With 0.5–4 mol% of catalyst **Λ-112**, desired products **123** could be obtained with 91–99% ee and with d.r. values of 6:1–20:1 (Scheme 24).[71w]

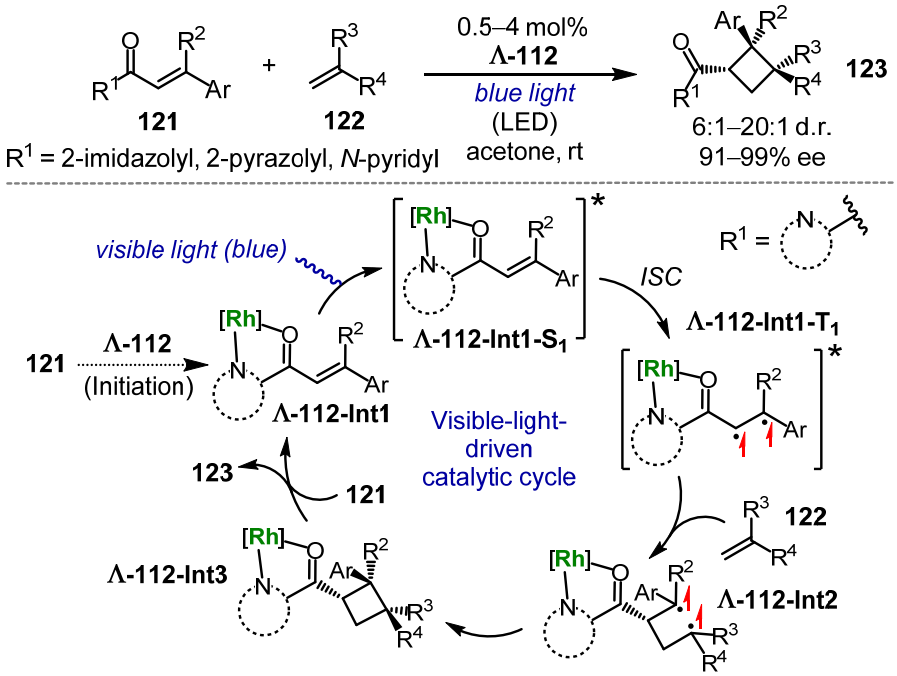

Scheme 24. Asymmetric visible-light-driven intermolecular [2+2]-cycloaddition between *α,β*-unsaturated 2-acylimidazoles, 2-acylpyrazoles, *N*-acylpyridines (**121**) and alkenes (**122**) catalyzed by **Λ-112**. The proposed mechanism is described in detail in the text.[71w]

The next catalyst from Figure 7, catalyst **Δ-113**, can be regarded as a merger of catalyst **Λ-104** (see Scheme 21) and catalyst **Λ-85** (see Scheme 16) or catalyst **Λ-89** (Scheme 17): The *tert*-butyl groups of catalyst **Λ-104** are formally replaced in **Δ-113** by 1-methylpyrimidine-2,4(1*H*,3*H*)-dione moieties, which render this Lewis acidic catalyst bifunctional as it is able to interact with approaching (indole) substrates via these moieties as hydrogen-bond acceptor, just like **Λ-85** and **Λ-89** via their carboxamide moieties.[71r] Complex **Δ-113** was found to be a powerful catalyst for the asymmetric Friedel–Crafts C2-alkylation of 3-substituted indoles (**124**) with *α,β*-unsaturated 2-acylimidazoles (**105**; Scheme 25).[71r]

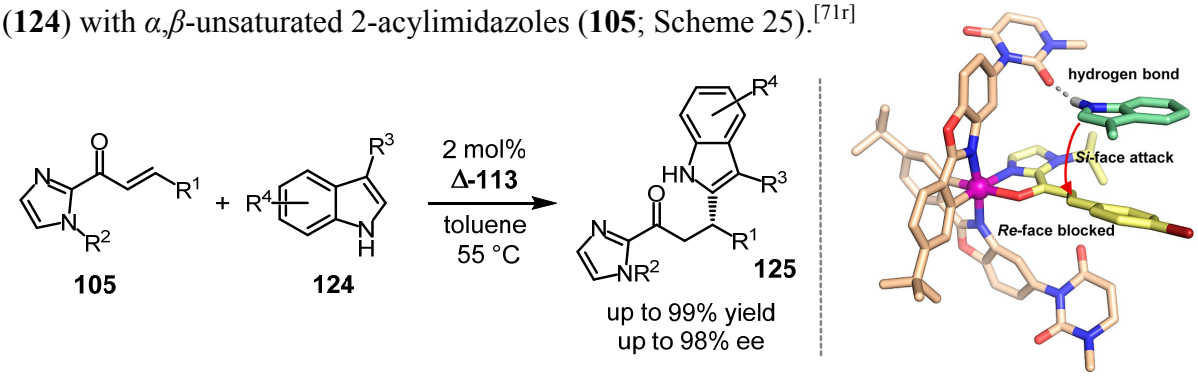

Scheme 25. Asymmetric Friedel–Crafts C2-alkylation of 3-substituted indoles (**124**) with *α,β*-unsaturated 2-acylimidazoles (**105**) catalyzed by **Δ-113**.[71r] The model on the right side shows the proposed mechanism and has been taken from ref. 71r. [Model reproduced with permission from ref. 71r. Copyright © 2017, American Chemical Society]

The proposed mechanism for the reaction **105** + **124** → **125** with **Δ-113** as catalyst is depicted on the right side of Scheme 25: While coordination of the *α,β*-unsaturated 2-acylimidazole (**105**) to the Ir(III) center increases its electrophilicity as a Michael acceptor, the approaching indole (**124**) becomes activated via single hydrogen-bonding with one of **Δ-113**'s 1-methylpyrimidine-2,4(1*H*,3*H*)-dione moieties acting as hydrogen-bond acceptor. In contrast, the remaining 1-methylpyrimidine-2,4(1*H*,3*H*)-dione moiety acts as a passive volume and blocks the *Re*-face of the coordinated *α,β*-unsaturated 2-acylimidazole.[71r]

As depicted in Scheme 25, 2 mol% of catalyst **Δ-113** were able to provide the desired C2-alkylated indoles (**125**) in up to 99% yield and with up to 98% ee.[71r]

The next catalysts from Figure 7, Ir(III) catalyst **Δ-(2*S*,2*S*)-114** and its Rh(III) congener **Δ-(2*S*,2*S*)-115**, feature pinene-derived cyclometalated phenylpyridine ligands instead of cyclometalated phenylbenzoxazole or phenylbenzothiazole ligands.[47] **Δ-(2*S*,2*S*)-115** was identified as an efficient catalyst for the asymmetric alkynylation of 2-trifluoroacetyl imidazoles (**126**) with aryl- and alkylacetylenes (**127**) to give the corresponding alkynylated products **128** with 3−6 mol% of **Δ-(2*S*,2*S*)-115** in up to 99% yield and with up to >99% ee (Scheme 26).[47]

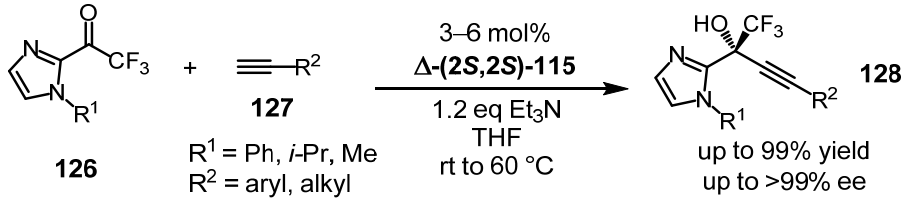

Scheme 26. Asymmetric alkynylation of 2-trifluoroacetyl imidazoles (**126**) with aryl- and alkylacetylenes (**127**) catalyzed by **Δ-(2*S*,2*S*)-115**.[47]

As Λ- and Δ-configured stereogenic-at-metal complexes **Λ-(2*S*,2*S*)-115** and **Δ-(2*S*,2*S*)-115** are diastereomers, just like **Λ-(*R*,*R*)-90** and **Δ-(*R*,*R*)-90** from Scheme 18,[64] they are directly separable via conventional silica gel flash chromatography.[47] It is worth noting and in sharp contrast to catalyst **Λ-(*R*,*R*)-90**, where the "mismatched" diastereomer **Δ-(*R*,*R*)-90** is virtually inactive,[64] that both catalysts **Λ-(2*S*,2*S*)-115** and **Δ-(2*S*,2*S*)-115** almost showed identical catalytic activity and enantioselectivity (with inverse *R*/*S* ratios) as catalysts for reaction **126** + **127** → **128**.[47] **Δ-(2*S*,2*S*)-115**'s Ir(III) congener **Δ-(2*S*,2*S*)-114** was found to be catalytically less active and drastically less enantioselective for this reaction.[47]

The last catalyst from Figure 7 and this chapter, stereogenic-only-at-metal Ru(II) catalyst **Λ-116**, features two pyridyl-substituted *N*-heterocyclic carbenes as cyclometalating ligands and has very recently been devised and identified as a highly active and enantioselective catalyst for the asymmetric alkynylation of trifluoromethyl ketones (**129**) with terminal alkynes (**127**; Scheme 27).[71b2]

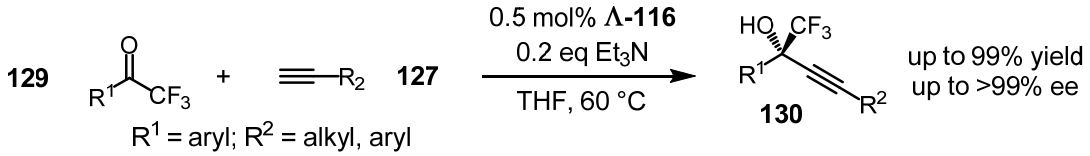

Scheme 27. Asymmetric alkynylation of trifluoromethyl ketones (**129**) with aryl- and alkylacetylenes (**127**) catalyzed by **Λ-116**.[71b2]

With just 0.5 mol% of catalyst **Λ-116**, alkynylated products **130** were provided in up to 99% yield and with up to >99% ee (Scheme 27).[71b2] Interestingly, benzothiazole-based Ir(III) catalyst **Δ-107** (see Scheme 22) and benzothiazole-based Rh(III) catalyst **Δ-112** (see Figure 7) were both found to be much less catalytically active in this reaction than catalyst **Λ-116** under identical reaction conditions.[71b2]

Finally, Figure 8 shows an overview of the stereogenic-at-metal catalysts from the Meggers laboratory which have been discussed in chapter 1.4.

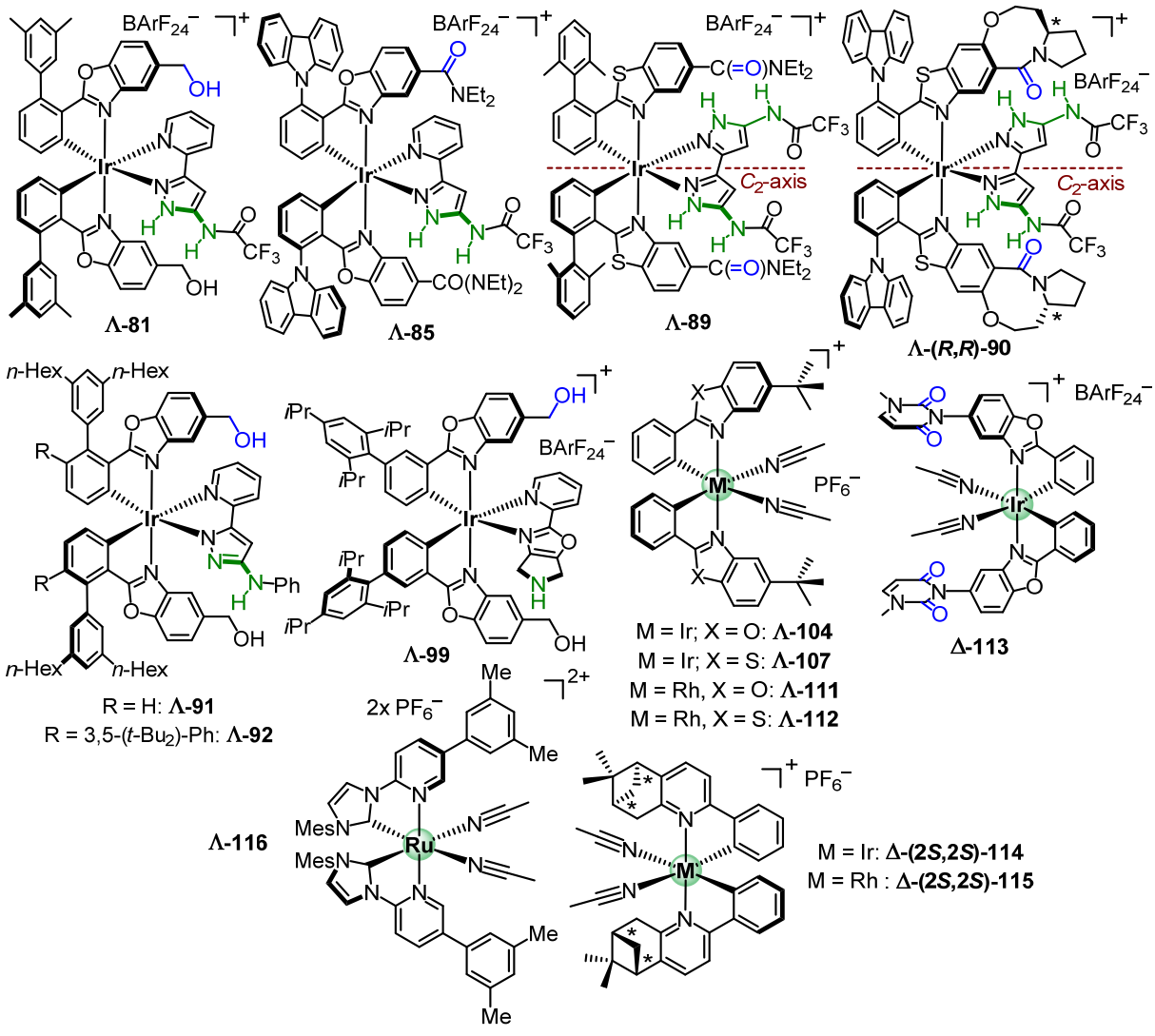

Figure 8. Overview of the stereogenic-at-metal catalysts from the Meggers laboratory which have been discussed in chapter 1.4.

In summary, the complexes which have been discussed in chapter 1.4 rely on the following motifs / moieties that allow them to operate as powerful asymmetric stereogenic-at-metal catalysts and in part as bifunctional catalysts by synergistic combinations of them:

- Complexes **Λ-81**,[38a] **Λ-85**,[38b] **Λ-89**,[63] **Λ-(*R*,*R*)-90**,[64] **Λ-91**,[66] and **Λ-92**[66] feature thiourea-mimicking double hydrogen-bonding motifs,[62] which are implemented via amidopyrazole / aminopyrazolato moieties. In case of **Λ-91** and **Λ-92**,[66] these motifs form *in situ* in the course of the Brønsted base catalysis cycles (see Schemes 15–19).
- Complexes **Λ-81**,[38a] **Λ-85**,[38b] **Λ-89**,[63] **Λ-(*R*,*R*)-90**,[64] **Λ-91**,[66] **Λ-92**,[66] **Λ-99**,[67] and **Δ-113**[71r] feature single hydrogen-bonding donor or acceptor motifs, which are implemented via hydroxymethyl groups acting as single hydrogen-bond acceptors (see Scheme 15; **Λ-81**) or donors (see Schemes 19 and 20; **Λ-91**, **Λ-92** and **Λ-99**) and via carboxamide or urea moieties acting as single hydrogen-bond acceptors (see Schemes 16–18 and 25; **Λ-85**, **Λ-89**, **Λ-(*R*,*R*)-90**, and **Δ-113**).
- Stereogenic-only-at-metal Complex **Λ-99**[67] features a bidentate ligand which comprises a cyclic secondary amine, which allows this complex to perform asymmetric enamine catalysis (see Scheme 20).
- Complexes **Λ-104**,[69] **Λ-107**,[71a] **Λ-111**,[71b] **Λ-112**,[71m] **Δ-113**,[71r] **Λ-116**,[71b2] **Δ-(2*S*,2*S*)-114**,[47] and **Δ-(2*S*,2*S*)-115**[47] all represent, with regard to both acetonitrile ligands, kinetically labile yet configurationally stable octahedral stereogenic-at-metal complexes which feature two vicinal coordination sites enabling Lewis acid catalysis.
- The latter feature / motif has successfully been combined with photocatalysis. Two cases can be distinguished here: a.) Asymmetric visible-light-driven catalysis where the stereogenic-at-metal Lewis acid catalyst *itself* or an *in situ formed derivative thereof* acts as photoactive species. Examples are the reaction from Scheme 22[71a] with catalyst **Λ-107** and the reaction from Scheme 24 with catalyst **Λ-112**.[71w] b.) And asymmetric visible-light-driven catalysis where an *additional* photosensitizer is added and where the stereogenic-at-metal catalyst is not or at least not significantly contributing as a photoactive species. An example for the latter case is the reaction from Scheme 23 with catalyst **Λ-111**.[71v]

With respect to the main topic of the present thesis, it is again striking that apparently none of the catalysts from chapter 1.4 acts as a nucleophilic catalyst, which has been, as a reminder, also concluded for the stereogenic-at-metal catalysts from other laboratories from chapter 1.3. In a broader sense, catalyst **Λ-99**[67] can be referred to as a 'nucleophilic catalyst' as its

secondary amine attacks an enolizable aldehyde in a nucleophilic fashion to form an intermediate enamine (see Scheme 20). However, as explained in chapter 1.1, catalysts and reactions which involve enamine or iminium ion formation should be clearly distinguished from "classic" nucleophilic catalysts such as DMAP as they catalyze different reactions.[5,6,10] This becomes apparent when considering that DMAP and other "classic" nucleophilic catalysts are often employed as acyl transfer catalysts (see chapter 1.2 for examples). In contrast, **Λ-99** is most probably not able to act as an acyl transfer catalyst: Acylation would result in the formation of a non-conjugated amide, which is obviously a 'thermodynamic pit' rendering acyl transfer catalysis with **Λ-99** unfeasible.

2. Design, Synthesis, and Application of a Nucleophilic Octahedral Stereogenic-Only-at-Metal Iridium(III) Catalyst

2.1 Aim of the Research Project

In chapter 1.1 of the present thesis the concept of *nucleophilic catalysis* has been introduced and in chapter 1.2 different examples for *nucleophilic catalysts* relying on different catalytically active entities and on different elements of chirality have been presented. In chapters 1.3 and 1.4, *stereogenic-at-metal catalysts* from the Meggers laboratory and from other research laboratories have been presented, discussed, and summarized in Figures 6 and 8.

Examination of chapters 1.3 and 1.4 and Figures 6 and 8 reveals that apparently no *nucleophilic stereogenic-at-metal catalyst* has been presented so far. And indeed, at the time when this project was started there had been no report about such a catalyst, which would allow to perform asymmetric nucleophile-catalyzed reactions like those from chapter 1.2, such as stereogenic acyl transfer reactions. As a result, it was envisioned to design a *nucleophilic stereogenic-only-at-metal catalyst*, which would complement the family of stereogenic-at-metal catalysts that are currently developed in the Meggers laboratory.[40,72]

2.2 Preliminary Research Results from Former Members of the Meggers Laboratory

2.2.1 Preliminary Research Results from Zhijie Lin

Efforts to design a nucleophilic stereogenic-only-at-metal catalyst can be traced back in the Meggers laboratory to the year 2013 and before.[75a] At that time, former PhD student Zhijie Lin (Z. L.) attempted to design a nucleophilic stereogenic-at-metal catalyst by means of the attachment of DMAP and PPY moieties to bidentate *N*,*N*-coordinating ligands of bis-heteroleptic bis-cyclometalated Ir(III) complexes (Figure 9).[75a]

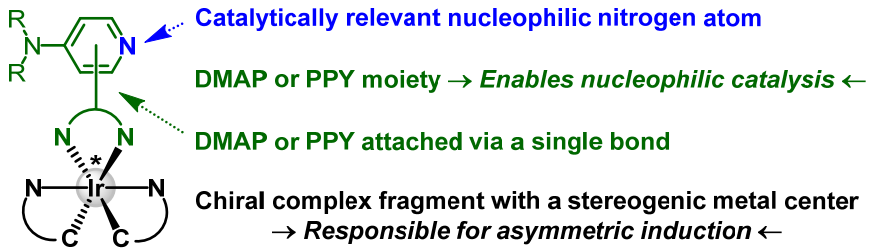

Figure 9. Zhijie Lin's initial layout for a DMAP-type octahedral nucleophilic stereogenic-at-metal Ir(III) catalyst.[75a] C^N represents a bidentate cyclometalated[75b] *C*,*N*-coordinating ligand and N^N a non-cyclometalated[75b] bidentate *N*,*N*-coordinating ligand.

Altogether, Z. L. synthesized 16 different stereogenic-at-metal complexes of the type depicted in Figure 9 by combinations of ten different cyclometalating[75b] ligands C^N and nine different DMAP- and PPY-functionalized non-cyclometalating[75b] ligands N^N.[75a] Z. L. then tested the obtained stereogenic-at-metal complexes as catalysts in kinetic resolutions of

various racemic alcohols with different acetic anhydrides as resolving agents.[75a] Despite Z. L.'s efforts, only selectivity factors of usually $S \leq 3$ and of $S = 3.7$ in one single case could be achieved. The experiment with $S = 3.7$ is depicted in Scheme 28 (catalyst: **Λ-Z1**; identifier **Z** refers to Z. L.). Due to the overall less encouraging results, the nucleophilic stereogenic-at-metal catalyst project was eventually discontinued by Z. L.[75a]

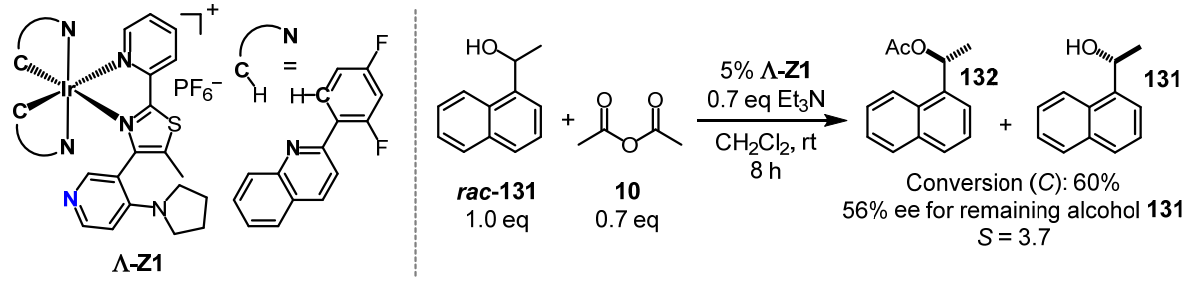

Scheme 28. Z. L.'s kinetic resolution of *rac*-1-(1-naphthyl)ethanol (***rac*-131**) with acetic anhydride (**10**) as resolving agent and **Λ-Z1** as nucleophilic catalyst.[75a] This conditions provided a selectivity factor of $S = 3.7$, which represents the best result of all of the kinetic resolutions which were performed by Z. L.[75a]

New impetus to this project was given shortly after Z. L.'s time as a PhD student in 2013 / 2014 by the development of stereogenic-at-metal complexes **Λ-81** and **Λ-85** as bifunctional cooperative hydrogen-bonding catalysts (see chapter 1.4, Schemes 15 and 16)[38] and, moreover, by the development of **Λ-91** and **Λ-92** as structurally related Brønsted base catalysts (see chapter 1.4, Scheme 19).[66] The primary catalytic motifs / moieties of these catalysts, which are a double hydrogen-bonding motif / an aminopyrazole moiety, are embedded in the non-cyclometalated ligand's plane, and not, in contrast to Z. L.'s layout, tagged to the non-cyclometalated ligand via a (biarylic) single bond (see Figure 9 and Scheme 28).[38,66,75a] This embedding of the catalytically active motif / moiety comes with the advantage that its spatial orientation is clearly defined and constrained, which renders it easier to improve a given catalyst on a rational basis. Moreover, such a layout offers the opportunity to place the catalytically active moiety / motif closer to the stereogenic metal center, which is, in principle, beneficial for an efficient enantioinduction.

It was considered difficult to embed DMAP or PPY in the plane of the non-cyclometalated ligand without having its nucleophilic nitrogen pointing too far away from the catalyst's metal center, which would render it challenging to achieve enantioinduction, and without having it pointing to a sterically crowded area, which would result in low catalytic activity. On this account, it was reasoned – inspired by chiral amidine-,[15,20] isothiourea,[4,16,20,24] and imidazole-based[17,25] nucleophilic catalysts reported by Birman and others – to install a 3*H*-imidazo[4,5-*h*]quinoline ligand as bidentate non-cyclometalated ligand, which was expected to constitute the catalyst's nucleophilic site after *in situ* or *ex situ* deprotonation of the initially

formed inactive HX salt (Figure 10). As will be demonstrated in chapter 2.3, this novel catalyst layout proved to be highly capable.

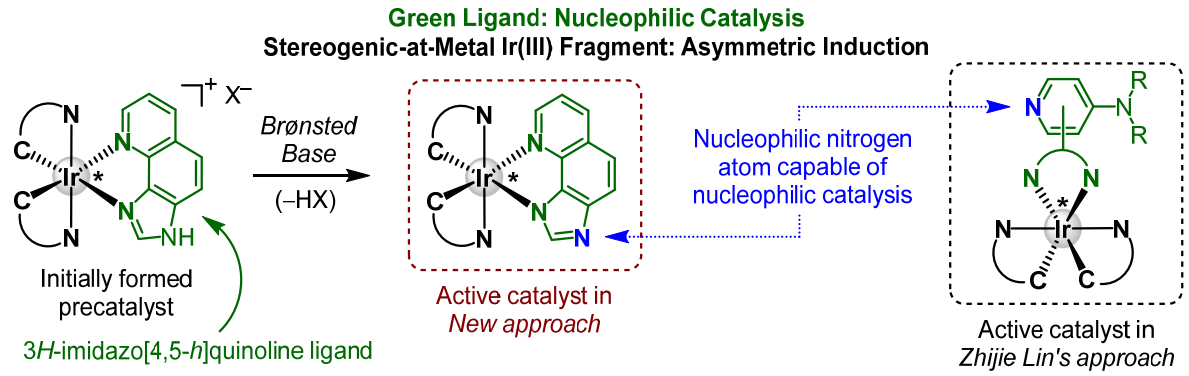

Figure 10. Novel layout for a nucleophilic octahedral stereogenic-at-metal Ir(III) catalyst with a deprotonated 3*H*-imidazo[4,5-*h*]quinoline ligand serving as the catalyst's active site. Zhijie Lins's initial layout from Figure 9 is depicted on the right side for a direct comparison. C^N represents a cyclometalated bidentate *C*,*N*-coordinating ligand and N^N a non-cyclometalated bidentate *N*,*N*-coordinating ligand.[75]

2.2.2 Preliminary Research Results from Xiaodong Shen

In 2013, former PhD student Xiaodong Shen (X. S.) initiated the development of a nucleophilic stereogenic-only-at-metal catalyst relying on the catalyst layout depicted in Figure 10.[76] As a start, X. S. synthesized Ir(III) complexes **Λ-X1**– **Λ-X8** (identifier **X** refers to X. S.), which all rely on two phenylbenzoxazoles as cyclometalated ligands and a non-cyclometalated 3*H*-imidazo[4,5-*h*]quinoline ligand as scheduled catalytically relevant ligand (Figure 11).[76]

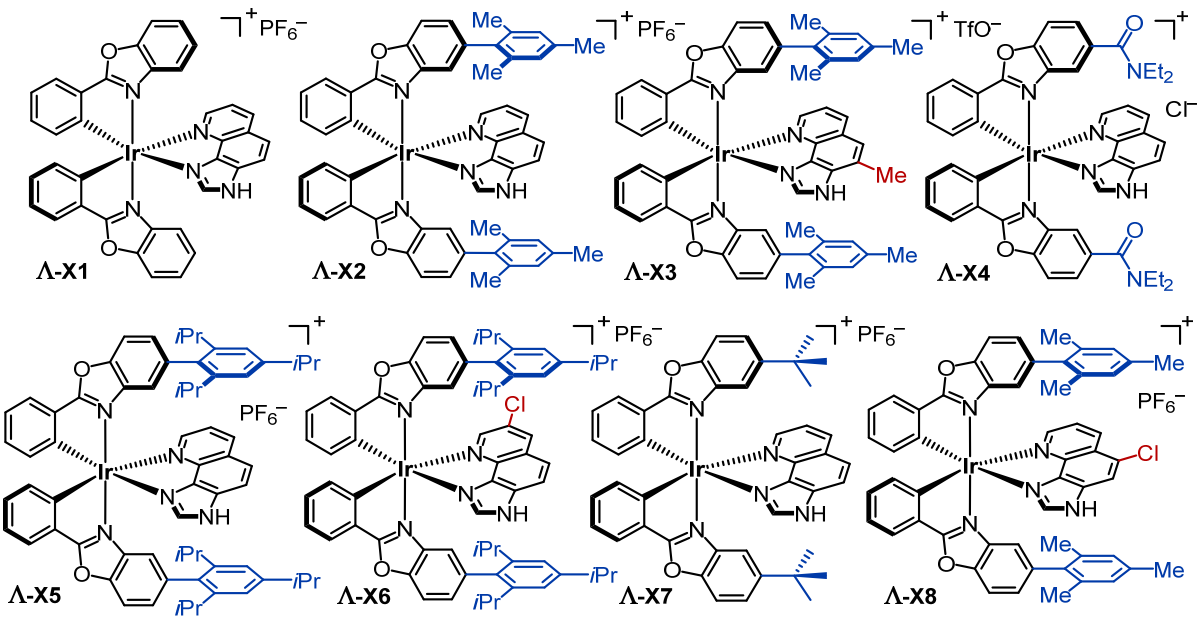

Figure 11. Complexes **Λ-X1**–**Λ-X8** were synthesized by X. S. as nucleophilic stereogenic-only-at-metal catalyst candidates. They all feature a 3*H*-imidazo[4,5-*h*]quinoline ligand as scheduled catalytically relevant ligand.[76]

For reasons of clarity, complex **Λ-X1** is regarded as parent structure and modifications with respect to **Λ-X1** are highlighted in blue in case of the cyclometalated ligands and in red in case of the non-cyclometalated ligand (see Figure 11; the counteranions are not regarded).

Next, complexes **Λ-X1**–**Λ-X8** were screened by X. S. as catalysts in the kinetic resolution of *rac*-1-(1-naphthyl)ethanol (***rac*-131**) with acetic anhydride (**10**) as resolving agent, the results of this screening are summarized in Table 1.[76] For all entries, the conversion values *C* and the selectivity factors *S* were calculated according to Kagan's equation[28e,30] (see chapter 1.2, Eq. 1) from the ee values of remaining alcohol **131** and produced ester **132**.

As can be seen from Table 1, most of the complexes of the small library **Λ-X1**–**Λ-X8** displayed high catalytic activity under the applied reaction conditions and some complexes also provided moderately encouraging selectivity factors of up to $S = 4.0$.[76]

Table 1. Kinetic resolution of *rac*-1-(1-naphthyl)ethanol (***rac*-131**) with acetic anhydride (**10**) as resolving agent and complexes **Λ-X1**–**Λ-X8** as catalysts. Experiments performed by X. S.[76]

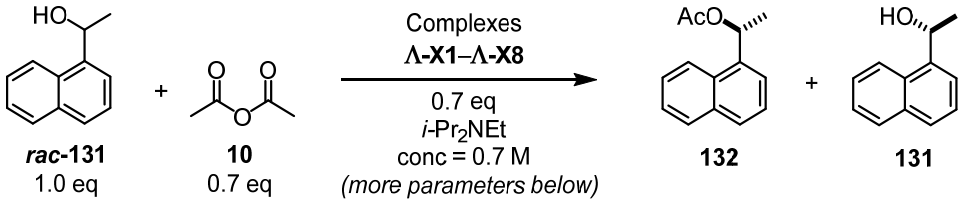

entry	complex	complex loading (mol%)	*t* (°C)	solvent	time	*C*[a] (%)	ee of **131**[b] (%)	*S*[a]
1	**Λ-X2**	2	rt	CH_2Cl_2	50 min	70	35	1.81
2	**Λ-X2**	0.2	rt	CH_2Cl_2	50 min	65.5	31	1.84
3	**Λ-X2**	0.2	rt	TAA	50 min	65	50	2.70
4	**Λ-X2**	0.2	0	TAA	50 min	54.5	51	4.00
5	**Λ-X2**	0.2	−78	toluene	24 h	n.d.[c]	n.d.[c]	n.d.[c]
6	**Λ-X2**	1	−78	toluene	19 h	n.d.[c]	n.d.[c]	n.d.[c]
7	**Λ-X2**	1	−40	toluene	6 h	53	33	2.46
8	**Λ-X2**[d]	1	0	TAA	2 h	68	60	3.08
9	**Λ-X3**	2	rt	TAA	n.d.[c]	n.d.[c]	n.d.[c]	n.d.[c]
10	**Λ-X1**	0.2	0	TAA	4 h	47	5	1.17
11	**Λ-X4**	5	rt	CH_2Cl_2	2 h	60	20	1.55
12	**Λ-X5**	0.2	0	TAA	2 h	56	45	3.16
13	**Λ-X5**	0.2	0	$CHCl_3$	2 h	50	36	2.95
14	**Λ-X6**	0.2	0	TAA	1 h	50	38	3.16
15	**Λ-X6**	0.2	0	TAA	3 h	62	51	3.03
16	**Λ-X7**	0.2	rt	TAA	3 h	57	27	1.92
17	**Λ-X7**	0.2	rt	TAA	4 h	60	29	1.90
18	**Λ-X8**	0.2	0	TAA	2 h	39	12	1.63
19	**Λ-X8**	0.2	0	TAA	7 h	60	23	1.66
20	–[e]	–[e]	20	TAA	n.d.[c]	n.d.[c]	n.d.[c]	n.d.[c]

[a]Calculated according to Kagan's equation (Eq. 1 from chapter 1.2).[28e,30] [b]Ee values of **131** and **132** determined from the crude product mixtures by chiral HPLC analysis. [c]No significant conversion observed, values not determined (n.d.). [d]Reisolated complex was used. [e]No complex added; this experiment was performed to rule out a significant racemic background reaction.

Based on the results from Table 1, the following conclusions were drawn:

- Most of complexes **Λ-X1**–**Λ-X8** are, in combination with *i*-Pr_2NEt and under the applied reaction conditions, highly active catalysts, at least for that particular reaction.
- The introduction of bulky substituents in the 5-position of the cyclometalated phenylbenzoxazole ligands appears to be crucial for a significant enantiodiscrimination, which becomes clear when comparing the result for **Λ-X1** ($S \sim 1$) with the results for all other complexes which provided a significant turnover ($S > 1$ or even $S >> 1$).
- The introduction of bulky *aryl* substituents in the 5-positions of the cyclometalated phenylbenzoxazole ligands (**Λ-X2**, **Λ-X3**, **Λ-X5**, **Λ-X6**) appears to be superior to the introduction of bulky *aliphatic* substituents (**Λ-X4**, **Λ-X7**). Admittedly, the results for **Λ-X8** do not follow this "rule".
- The 4-position of the 3*H*-imidazo[4,5-*h*]quinoline ligand must remain unoccupied to maintain a high catalytic activity (**Λ-X3**). This is logical as the *N*-acylation of the catalyst would otherwise suffer from emerging 1,3-allylic strain. However, modifications at other positions of that ligand appear to be feasible (see **Λ-X6** and **Λ-X8**).
- From the four screened solvents CH_2Cl_2, $CHCl_3$, toluene, and *tert*-amyl alcohol (TAA), solvent TAA gave the best results in terms of selectivity.
- From all screened complexes (**Λ-X1**–**Λ-X8**), complex **Λ-X2** provided the most encouraging result (Table 1, entry 4).

With complex **Λ-X2** as the most promising complex so far and the conditions from Table 1 and TAA as solvent, X. S. then shortly studied the kinetic resolution of ***rac*-131** with bulkier anhydrides, namely isobutyric anhydride (**133**) and pivalic anhydride (**135**), and the kinetic resolution of *rac*-2,2-dimethyl-1-phenyl-1-propanol (***rac*-137**) with acetic anhydride (**10**; Scheme 29).[76]

The kinetic resolution of ***rac*-131** with isobutyric anhydride (**133**) proceeded smoothly but without satisfying enantioselectivity and the kinetic resolution of ***rac*-131** with pivalic anhydride (**135**) was found to be very sluggish and resulted in virtually no conversion after 24 h even though 2 mol% of **Λ-X2** were employed. The kinetic resolution of ***rac*-137** with acetic anhydride (**10**) proceeded smoothly but also without satisfying enantioselectivity (Scheme 29; compare with Table 1, entries 1–8).[76]

Accordingly, the most promising result in terms of catalytic activity and enantioselectivity was still the one from Table 1, entry 4 with alcohol ***rac*-131**, acetic anhydride (**10**) as

resolving agent, and complex **Λ-X2**. At that point, all experiments related to kinetic resolutions of racemic alcohols were discontinued by X. S.[76]

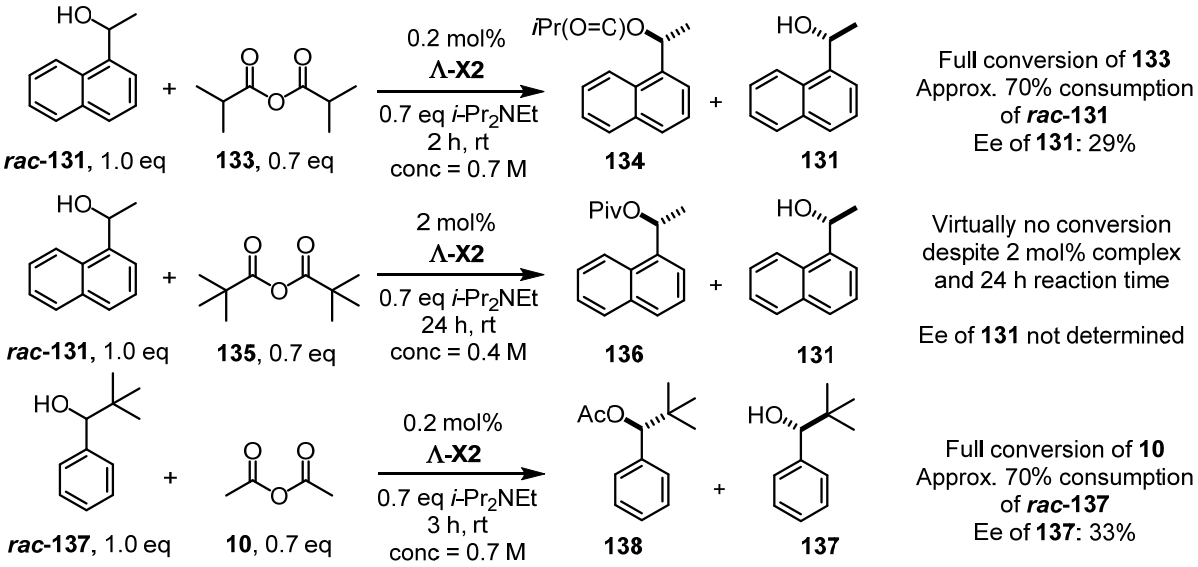

Scheme 29. Kinetic resolutions of *rac*-1-(1-naphthyl)ethanol (***rac*-131**) with isobutyric anhydride (**133**) and pivalic anhydride (**135**) and kinetic resolution of *rac*-2,2-dimethyl-1-phenyl-1-propanol (***rac*-137**) with acetic anhydride (**10**). Experiments performed by X. S.[76]

2.3 Results and Discussion

2.3.1 Catalyst Development and Kinetic Resolution of Racemic Alcohols

When the nucleophilic stereogenic-at-metal catalyst project was taken over from X. S. in September 2014, the results from Table 1 and additional balls-and-sticks modeling with complexes of the type depicted in Figure 10 still prompted us to expect that appropriate modifications of the catalyst's structure could eventually result in a good or even excellent catalyst for the kinetic resolution of racemic alcohols or for other asymmetric nucleophile-catalyzed transformations.

On these grounds, complexes **Λ-T1**–**Λ-T13** were synthesized in order to evaluate them as nucleophilic stereogenic-at-metal catalyst candidates (Figure 12; identifier **T** refers to T. C.).

Complexes **Λ-T1**–**Λ-T13** were, like all stereogenic-at-metal Ir(III) complexes from chapter 2., prepared via two different routes which are schematically depicted in Scheme 30.

For both routes, the respective phenylbenzoxazole (X = O) and phenylbenzothiazole (X = S) ligands to be cyclometalated are prepared beforehand, which are then reacted with $IrCl_3 \cdot 3H_2O$ in 2-ethoxyethanol to the corresponding iridium(III) dimers $[Ir^{III}(C\hat{}N)_2(\mu\text{-}Cl)]_2$ according to a modified version of Nonoyama's procedure (Scheme 30, A).[77]

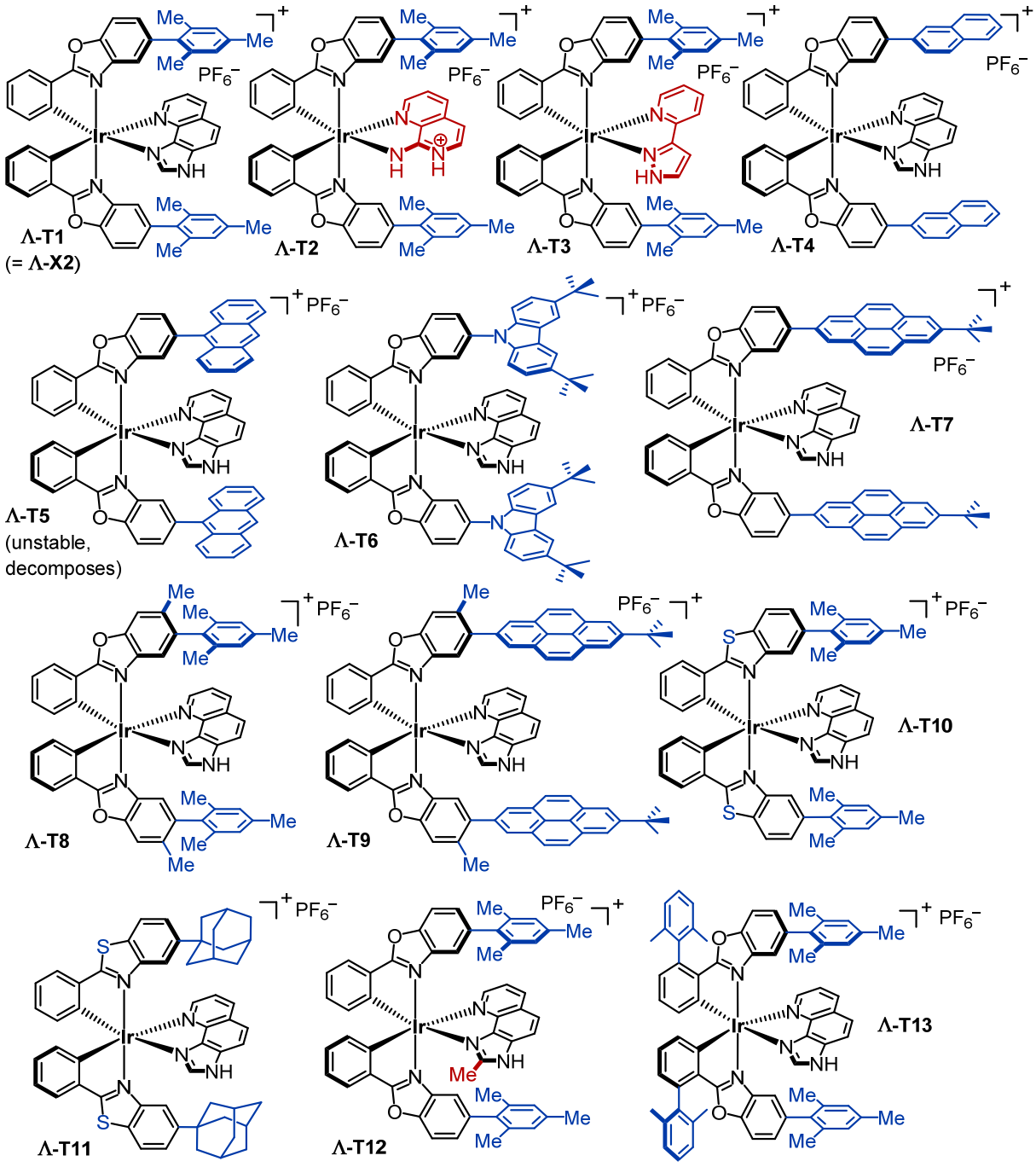

Figure 12. Complexes **Λ-T1**−**Λ-T13** were synthesized as stereogenic-at-metal nucleophilic catalyst candidates. Structural modifications with respect to the cyclometalated ligand of **Λ-X1** (see chapter 2.2.2, Figure 11) are highlighted in blue and modifications with respect to the non-cyclometalated ligand of **Λ-X1** are highlighted in red. **Λ-T1**−**Λ-T13** were synthesized according to the two synthesis routes from Scheme 30 (synthetic details for each complex are provided in the experimental section).

Route I differs from Route II as follows: In case of Route I, the phenylbenzoxazole and phenylbenzothiazole ligands to be cyclometalated already contain the substituent R^1 (aryl or alkyl) which is later incorporated in the final complex. In case of Route II, the ligands feature a triflate group (T) at that position which is later on utilized to introduce aryl substituents in a post-complexation approach via Suzuki-Miyaura cross-couplings (see Scheme 30, C2).[78]

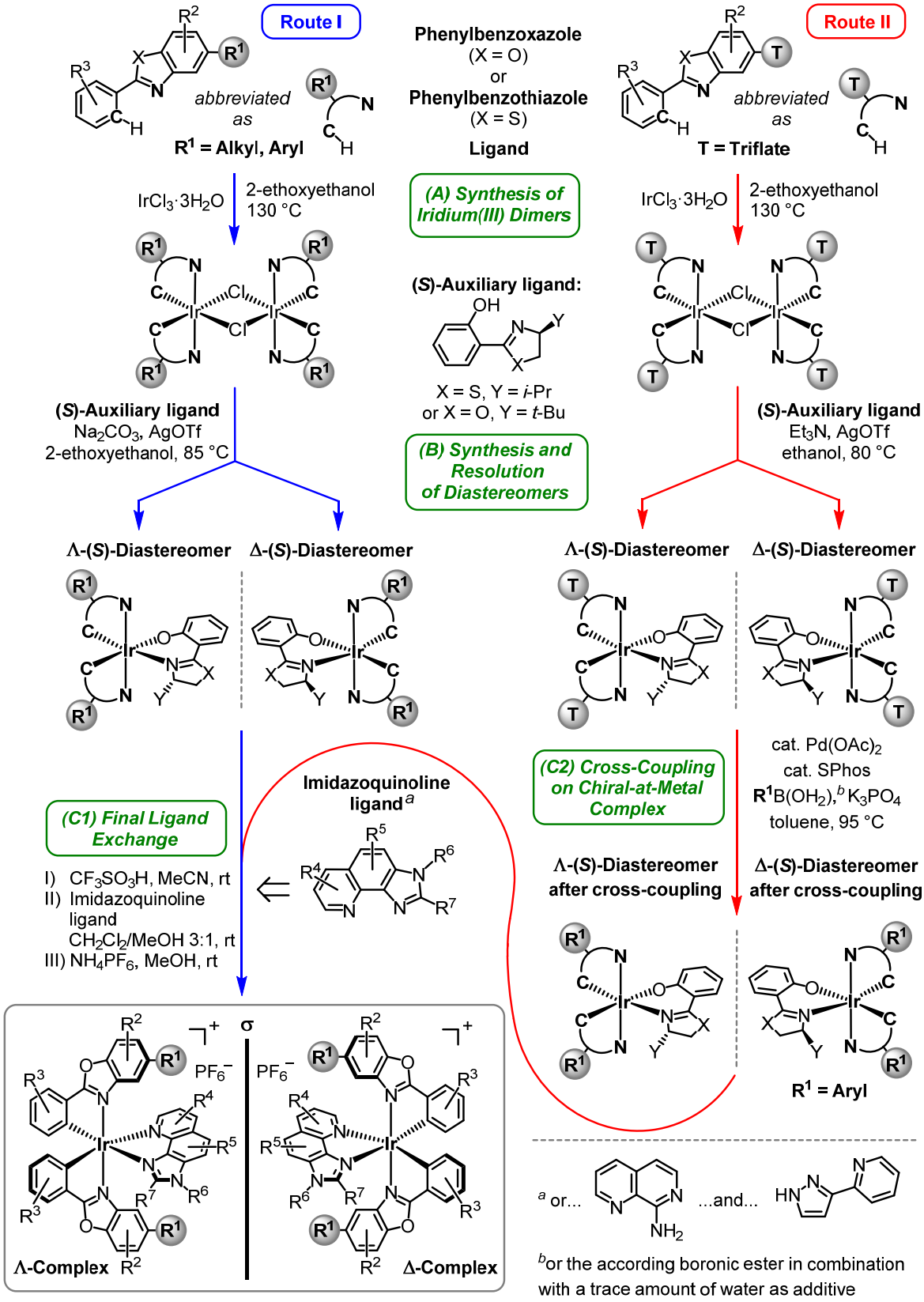

Scheme 30. General synthesis routes (Route I and II) for complexes **Λ/Δ-T1**−**Λ/Δ-T28** from chapter 2. Details for the synthesis of each complex are provided in the experimental section.

In case of both routes the initially obtained iridium(III) dimers $[Ir^{III}(C\hat{}N)_2(\mu\text{-}Cl)]_2$ (Scheme 30, A) are at first cleaved with a bidentate chiral auxiliary ligand to give chromato-

graphically separable pairs of Λ-(*S*)- and Δ-(*S*)-configured diastereomers (Scheme 30, B).[79] Preferably, *i*Pr-substituted (*S*)-salicylthiazoline (X = S, Y = *i*Pr)[71d] is used as chiral auxiliary ligand as it usually provides diastereomers which are stable towards silica gel chromatography and, moreover, readily separable.[79] However, in some cases the resulting diastereomers were found to be hardly separable. In such cases *t*Bu-substituted (*S*)-salicyloxazoline (X = O, Y = *t*Bu)[80] is used as an alternative auxiliary ligand. The according diastereomers are usually less stable towards prolonged silica gel chromatography but usually provide diastereomers which feature an excellent separability.[79]

Next, the auxiliary ligands of the separated diastereopure Λ-(*S*)- and Δ-(*S*)-configured complexes are cleaved off with triflic acid in acetonitrile to give intermediate enantiopure Λ- and Δ-configured bisacetonitrile complexes (not shown). After short column purification of these bisacetonitrile intermediates, both semi-labile monodentate acetonitrile ligands are replaced by the final bidentate 3*H*-imidazo[4,5-*h*]quinoline ligands to give the desired enantiopure Λ- and Δ-configured complexes (Scheme 30, C1).[81,82] In particular cases, either a 1,7-naphthyridin-8-amine ligand or a 2-(1*H*-pyrazol-3-yl)pyridine ligand were installed as final ligands instead of 3*H*-imidazo[4,5-*h*]quinoline (see Figure 12).

In case of Route II, the separated diastereopure Λ-(*S*)- and Δ-(*S*)-configured auxiliary complexes are at first subjected to Suzuki-Miyaura cross-couplings to install the desired aryl functionality at the 5-position of their cyclometalated phenylbenzoxazole or phenylbenzothiazole ligands (Scheme 30, C2).[78] At this point, it is worth mentioning that the utilized post-complexation cross-coupling procedure, which has been devised by PhD student Thomas Mietke in the Meggers laboratory, has been proven to not affect the configuration of the Ir(III) stereocenter.[78] After this cross-coupling step, the auxiliary ligands are, just as in case of Route I, cleaved off with triflic acid in acetonitrile to give intermediate enantiopure Λ- and Δ-configured bisacetonitrile complexes (not shown), which are, after short-column purification, reacted to the desired Λ- and Δ-configured 3*H*-imidazo[4,5-*h*]quinoline-functionalized complexes (Scheme 30, C1).[81,82]

Coming back to the complex library depicted in Figure 12, complexes **Λ-T1**−**Λ-T13** were prepared to be evaluated for the following reasons:

- Complex **Λ-T1** is identical with complex **Λ-X2** and was prepared to reconfirm the results from X. S. and to ensure reproducibility of the previous experimental results.
- Complexes **Λ-T2** and **Λ-T3** featured with a 1,7-naphthyridin-8-amine ligand and a 2-(1*H*-pyrazol-3-yl)pyridine ligand potential alternatives to 3*H*-imidazo[4,5-*h*]quinoline.

- Complexes **Λ-T4**−**Λ-T7**, **Λ-T9**, and **Λ-T11** featured untested moieties at the 5-position of their cyclometalated phenylbenzoxazole ligands (**Λ-T4**−**Λ-T7**, **Λ-T9**) and phenylbenzothiazole ligands (**Λ-T11**; compare with **Λ-X1**−**Λ-X8**).
- Complexes **Λ-T8** and **Λ-T9** both featured additional methyl groups at the 6-positions of their cyclometalated phenylbenzoxazole ligands. These modifications were expected to (further) constrain the rotational freedom of the aryl substituents at the neighboring 5-positions.
- Complexes **Λ-T10** and **Λ-T11** featured cyclometalated phenyl*benzothiazole* ligands instead of phenyl*benzoxazole* ligands.
- Complex **Λ-T12** was prepared to evaluate the influence of the introduction of a methyl group at the methylene bridge between both nitrogen atoms of the 3*H*-imidazo[4,5-*h*]quinoline ligand's fused imidazole.
- And finally, complex **Λ-T13** was prepared to study the influence of the introduction of additional aryl substituents at the *ortho*-positions of the phenylbenzoxazoles' phenyl rings. For previously established kinetically-inert stereogenic-at-metal catalysts from the Meggers laboratory, the latter modification had been found to be highly beneficial (for example in case of catalyst **Λ-81**; see chapter 1.4 for further details).[38a]

Next, complexes **Λ-T1**−**Λ-T13** were screened as catalysts in the kinetic resolution of *rac*-1-(1-naphthyl)ethanol (***rac*-131**) with acetic anhydride (**10**) as resolving agent. The results of this screening are summarized in Table 2.

Table 2. Kinetic resolution of *rac*-1-(1-naphthyl)ethanol (***rac*-131**) with acetic anhydride (**10**) as resolving agent and complexes **Λ-T1**–**Λ-T13**.[a]

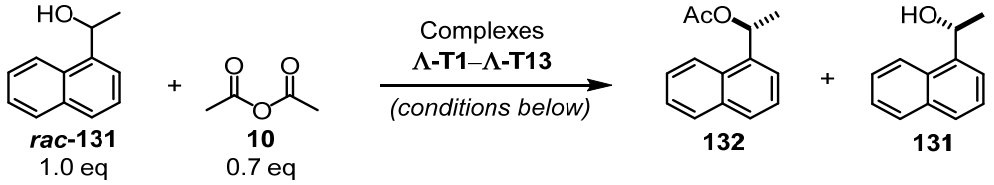

entry	Complex	complex loading (mol%)	*t* (°C)	solvent	time (min)	*C*[b] (%)	ee of **131**[c] (%)	*S*[b]
1[d]	**Λ-T1 (≙Λ-X2)**	0.2	0	TAA	50 / 100	45 / 62	30 / 49	2.92 / 2.89
2[d]	**Λ-T1 (≙Λ-X2)**	0.2	0	TAA	50 / 110	48 / 65	36 / 56	3.22 / 3.15
3	**Λ-T2**	1	0	TAA	50 / 100	~25 / ~50	< 3 / < 3	~1.0 / ~1.0
4[e]	***rac*-T3**	0.5	rt	TAA	125	trace[f]	–[f]	–[f]
5	**Λ-T4**	0.2	0	TAA	50 / 110	11 / 37	3 / 11	1.65 / 1.64
6[g]	**Λ-T5**	–[g]	–[g]	–[g]	–[g]	–[g]	–[g]	–[g]
7	**Λ-T6**	0.2	0	TAA	50 / 100	19 / 37	13 / 30	3.80 / 3.92
8	**Λ-T7**	0.3	0	TAA	50 / 100	22 / 48	8 / 22	1.99 / 1.97
9[d]	**Λ-T8**	0.3	0	TAA	50 / 100	53 / 60	42 / 51	3.21 / 3.19
10[d]	**Λ-T8**	0.3	0	TAA	50 / 100	55 / 65	43 / 56	3.06 / 3.05
11	**Λ-T9**	0.3	0	TAA	50 / 100	22 / 45	10 / 25	2.35 / 2.36
12	**Λ-T9**	0.6	0	TAA	50 / 100	28 / 56	14 / 34	2.35 / 2.35
13	**Λ-T10**	0.6	0	TAA	50 / 100	31 / 45	14 / 22	2.16 / 2.14
14	**Λ-T10**	1.8	0	TAA	50 / 100	51 / 60	26 / 33	2.11 / 2.08
15	**Λ-T11**	0.3	0	TAA	50 / 100	10 / 21	6 / 13	3.11 / 3.35
16	**Λ-T12**	0.6	0	TAA	50 / 100	32 / 53	19 / 38	2.84 / 2.86
17	**Λ-T13**	0.6	0	TAA	50 / 100	69 / 69	51 / 52	2.49 / 2.49
18	**Λ-T13**	0.3	0	TAA	50 / 100	63 / 67	44 / 49	2.52 / 2.51
19	**Λ-T13**	0.1	0	TAA	50 / 100	45 / 59	28 / 41	2.62 / 2.56

[a]Standard reaction conditions: Substrate ***rac*-131** (1.0 eq; 200−400 µmol), 0.7 eq **10**, and 0.7 eq *i*-Pr_2NEt with catalysts **Λ-T1**−**Λ-T13** in the indicated solvent at conc = 0.7 M at the indicated temperature. [b]Calculated according to Kagan's equation (see Eq. 1 from chapter 1.2).[28e,30] [c]Enantioselectivities of **131** and **132** determined from crude product mixtures by chiral HPLC analysis (Chiralpak IB (5 µm, 25 cm x 4.6 mm); *n*-hexane/*i*-PrOH 90:10, λ = 254 nm, flow = 0.5 mL/min, *t* (column) = 40 °C: **132**: t_R = 7.7 min and 8.3 min; **131**: t_R = 11.8 min and 14.2 min). [d]Two different freshly prepared batches of catalysts were used. [e]1.1 eq Ac_2O and 1.1 eq *i*-Pr_2NEt were added. [f]Direct comparison with a reference batch without any complex indicated that the trace formation of **132** exclusively originated from the uncatalyzed racemic background reaction. [g]Not tested, **Λ-T5** was found to be unstable, see explanations in text.

Based on the results from Table 2, the following conclusions were drawn:

- First of all, the experiments with complex **Λ-T1** confirmed the results which had been obtained by X. S. with **Λ-X2** (**Λ-T1** ≙ **Λ-X2**), though a slightly lower selectivity factor was found under identical reaction conditions (Table 2, entry 2: **Λ-T1**: *S* = 3.2 vs. Table 1, entry 4: **Λ-X2**: *S* = 4.0).
- Complex **Λ-T2** with 1,7-naphthyridin-8-amine as scheduled catalytic ligand showed indeed significant catalytic activity under the applied reaction conditions but failed to achieve any enantiodiscrimination (Table 2, entry 3).
- In case of catalyst **Λ-T3** with 2-(1*H*-pyrazol-3-yl)pyridine as scheduled catalytic ligand, only racemic catalyst ***rac*-T3** was evaluated, which showed no catalytic activity at all under the applied reaction conditions (entry 4).

- Compound **Λ-T5** was prepared via Route II from Scheme 30. However, **Λ-T5** could not be obtained pure and slowly decomposed in solution. On the contrary, all other complexes from the library **Λ-T1**−**Λ-T13** were found to be stable. Consequently, **Λ-T5** was not tested (entry 6).
- None of the remaining complexes **Λ-T4** and **Λ-T6**−**Λ-T13** could significantly improve the selectivity of the resolution. They provided, similar to complexes **Λ-X1**−**Λ-X8** screened by X. S. (see chapter 2.2.2, Figure 11 and Table 1), only *S*-factors ranging between $S = 1.6$ (entry 5) and $S = 3.9$ (entry 7), which is far-off from an *S*-factor of $S \sim 10$, which is considered as the lower limit for a synthetically useful kinetic resolution (see chapter 1.2).[28e]

Due to the overall lack of a clear and significant structure–selectivity relationship, giving no real hint how to modify the catalyst in order to improve its selectivity, and due to the so far overall disappointing selectivity factors, it was decided at this point to discontinue all experiments related to kinetic resolutions of alcohols and to shift the focus on asymmetric stereogenic acyl transfer reactions.

2.3.2 Steglich Rearrangement of *O*-Acylated Azlactones and Catalyst Development

Having the 13 complexes **Λ-T1**−**Λ-T13** in stock (see chapter 2.3.1, Figure 12), it was anticipated that there should be other nucleophile-catalyzed reactions which would better match some of these complexes in terms of their enantioinduction abilities and where, moreover, their quite different substitution patterns would have a more pronounced influence than in the kinetic resolutions from chapter 2.3.1. The latter was regarded as important as a clear structure–selectivity relationship would give hints how to modify the complex in order to obtain the best catalyst possible in terms of selectivity.

First, the focus was set on stereogenic Steglich rearrangements of *O*-acylated azlactones (**13**) to *C*-acylated azlactones (**14**),[21] which had also very shortly been examined by X. S. with complex **Λ-X6**.[76] The results of X. S.'s short examination are summarized in Table 3. Even though X. S. had only tested single substrate **13a** with 2 mol% of **Λ-X6** under non-optimized conditions, he could observe full conversion of **13a** to **14a** after 15 h at rt and found for product **14a** promising 59% ee (Table 3, entry 1).[76] This result indicated that there could be still a lot of room for improvements with respect to the catalyst's structure, the reaction conditions, and the employed azlactone substrates (**13**).

Table 3. Short examination of the Steglich rearrangement **13a → 14a** with complex **Λ-X6**. Experiments performed by X. S.[76]

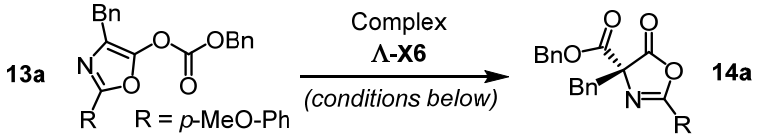

entry	loading of **Λ-X6** (mol%)	solvent	conc (mol/L)	*t* (°C)	time (h)	ee of **14a**[a] (%)	conv
1[b]	2	CH_2Cl_2	0.15	rt	15	59	full[b]
2[b]	1	CH_2Cl_2	0.15	rt	24	53	full[b]
3	0	CH_2Cl_2	0.15	0	24	– [c]	– [c]

[a]Enantioselectivities determined from crude product mixtures by chiral HPLC analysis. [b]**Important:** It was later revealed that the catalyst is only active in case there is a Brønsted base present leading to *in situ* deprotonation of actually inactive complex **Λ-X6** (see Table 4 and the associated explanations). Hence, in cases of entries 1 and 2 there must have either been a trace of Brønsted base present in the reaction mixture or the added catalyst **Λ-X6** must have been (partly) deprotonated when it was added to the reaction mixture. [c]No conversion found.

It is striking that X. S. did *not* add a Brønsted base in case of all three reactions (reaffirmed in a personal dialogue with X. S.),[76] which was regarded as remarkable as complex **Λ-X6** should be catalytically inactive in the absence of a Brønsted base (see chapter 2.2.1, Figure 10 for an illustration). Accordingly, it was at first investigated whether the reaction **13a → 14a** could actually take place with complexes of type **Λ-X6** in the absence of a Brønsted base or not. The results of this investigation are summarized in Table 4. Note that structurally related complex **Λ-T1** was used instead of complex **Λ-X6**.

Table 4. Influence of the (non-)presence of a Brønsted base on the reaction **13a → 14a** with complex **Λ-T1**.

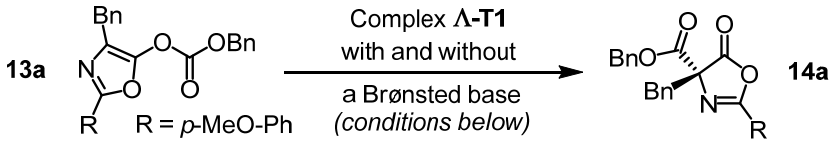

entry	complex	complex loading (mol%)	base	base loading (mol%)	*t* (°C)	solvent	conc (mol/L)	time (h)	ee of **14a**[a] (%)	conv[b]
1	**Λ-T1**	2	no base	–	rt	CH_2Cl_2	0.15	15	– [c]	– [c]
2	***rac*-T1**	10	no base	–	rt	CH_2Cl_2	0.26	12 / 43	– [c] / – [c]	– [c] / – [c]
3	**Λ-T1**	10	*i*Pr_2NEt	20	rt	CH_2Cl_2	0.26	12 / 23	41[d] / 39[d]	~½ / full
4	**Λ-T1**	3	Cs_2CO_3	6	rt	CH_2Cl_2	0.26	17	40	full
5	**no cat.**	–	Cs_2CO_3	20	rt	CH_2Cl_2	0.26	13	– [c]	– [c]

[a]Enantioselectivities determined from crude product mixtures by chiral HPLC analysis. [b]Approximate conversion determined by a combination of TLC and HPLC analysis. [c]No conversion found. [d]Old HPLC column used giving an imperfect peak separation with an uncertainty of about ±1%.

As can be seen from Table 4, complete absence of a Brønsted base resulted in complete catalytic inactivity (entries 1 and 2). X. S. successfully used *i*-Pr_2NEt as base additive in combination with 3*H*-imidazo[4,5-*h*]quinoline-based complexes in the kinetic resolution of racemic alcohols (see chapter 2.2.2, Table 1) and this results were confirmed by experiments

which are part of this thesis (see chapter 2.3.1, Table 2). *i*-Pr$_2$NEt was primarily added in that case to scavenge the acid which is formed in the course of the acylation process. However, it fulfills a second function, it deprotonates the 3*H*-imidazo[4,5-*h*]quinoline-based complexes, which is crucial to enable catalysis by the according deprotonated complexes.

For this reason, *i*-Pr$_2$NEt was added to a mixture of **13a** and **Λ-T1**, which indeed resulted in a clean conversion to **14a** (Table 4, entry 3). Accordingly, there must have either been a trace of a Brønsted base present in the reaction mixture in case of X. S.'s experiments or catalyst **Λ-X6** must have been (partially) deprotonated when it was added (see Table 3).

However, the reaction rates were low with *i*-Pr$_2$NEt as additive and high catalyst loadings were necessary to achieve full conversion within an acceptable reaction time (Table 4, entry 3). For this reason, alternative base additives were screened: Cs_2CO_3, Na_2CO_3, Li_2CO_3, Na(OAc), $Na_2(HPO_4)$, and DBU. From all screened additives, Cs_2CO_3 was identified as the most suitable one as it triggered a rapid rearrangement **13a** → **14a** requiring only a low loading of **Λ-T1** and a small amount of base additive compared to *i*-Pr$_2$NEt. Moreover, it did not negatively influence the selectivity of the reaction and triggered no racemic background reaction (Table 4, entries 3−5). Apart from DBU, which was found to be almost as effective as Cs_2CO_3 but triggered side reactions, all other screened bases were less effective and so Cs_2CO_3 was eventually selected as the base additive of choice.

From here on, the inactive HX salts of 3*H*-imidazo[4,5-*h*]quinoline-based complexes will be referred to as *precatalysts* and their deprotonated, catalytically active forms as *catalysts* and the latter marked with an apostrophe. Accordingly, the catalytically active form of HX salt **Λ-T1** is referred to as **Λ-T1'** (Scheme 31).

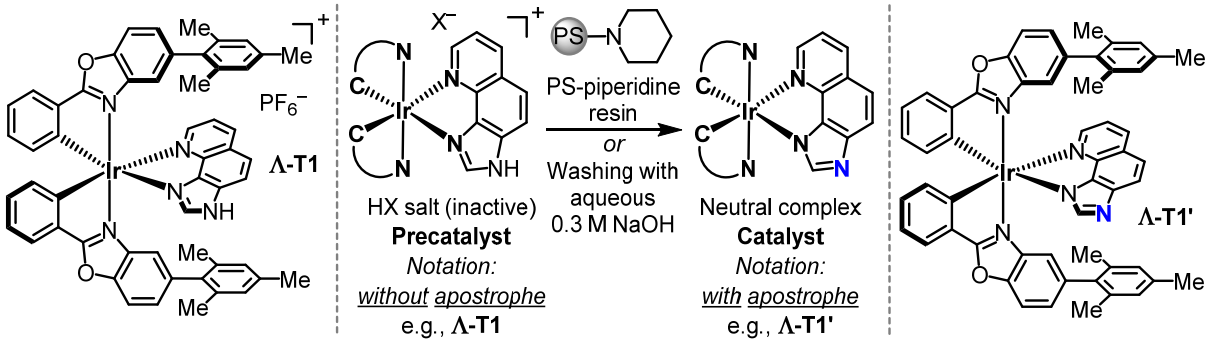

Scheme 31. Deprotonation of 3*H*-imidazo[4,5-*h*]quinoline-based iridium(III) complexes with piperidinomethylated polystyrene beads[83] or by washing with aqueous 0.3 M NaOH. Precatalyst **Λ-T1** and catalyst **Λ-T1'** are depicted as arbitrary examples for an illustration.

Later on, it was revealed that deprotonated 3*H*-imidazo[4,5-*h*]quinoline-based complexes of type **Λ-T1'** are easily accessible in analytically pure form by passing a concentrated solution of the respective precatalysts (e.g., **Λ-T1**) through a short plug of piperidinomethylated poly-

styrene resin beads[83] or, alternatively, by washing them with aqueous 0.3 M NaOH (Scheme 31; details in the experimental section). As the active catalysts of type **Λ-T1'** were found to be highly bench-stable, the active catalysts were later on prepared *ex situ* by default and employed without the need for an additional base additive (see for example Table 10).

Having revealed that Brønsted base addition is a prerequisite to trigger the rearrangement **13a → 14a** when 3*H*-imidazo[4,5-*h*]quinoline-based precatalysts are used and that Cs_2CO_3 is the Brønsted base additive of choice under the applied conditions (see Table 4), now selected precatalysts from the library **Λ-T1**–**Λ-T13** were screened to identify the best match for the reaction **13a → 14a**. The results are summarized in Table 5.

It is worth mentioning that the rearrangement **13a → 14a** proceeded "spot-to-spot". Accordingly, enantioselectivity improvement and retention of a high reaction rate were the primary goals of this screening.

Table 5. Screening of selected precatalysts from precatalyst library **Λ-T1**–**Λ-T13** in the reaction **13a → 14a**.

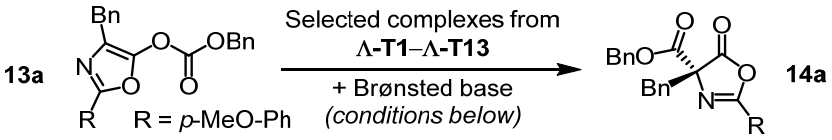

entry	precatalyst	precatalyst loading (mol%)	base	base loading (mol%)	*t* (°C)	solvent	conc (mol/L)	time (h)	ee of **14a**[a] (%)	conv[b]
1	**Λ-T1**	10	*i*Pr$_2$NEt	20	rt	CH_2Cl_2	0.26	12 / 23	41[c] / 39[c]	~½ / full
2	**Λ-T1**	3	Cs_2CO_3	6	rt	CH_2Cl_2	0.26	17	40	full
3	**Λ-T6**	10	*i*Pr$_2$NEt	20	rt	CH_2Cl_2	0.26	12 / 23	10[c] / 10[c]	~½ / full
4	**Λ-T7**	10	*i*Pr$_2$NEt	20	rt	CH_2Cl_2	0.26	12	22[c]	full
5	**Λ-T8**	3	Cs_2CO_3	6	rt	CH_2Cl_2	0.26	11 / 17	44 / 43	~¾ / full
6	**Λ-T8**	3	Cs_2CO_3	6	0	CH_2Cl_2	0.26	16	52	full
7	**Λ-T10**	3	Cs_2CO_3	6	rt	CH_2Cl_2	0.26	11 / 17	10 / 9	~¾ / full
8	**Λ-T11**	3	Cs_2CO_3	6	0	CH_2Cl_2	0.26	16	37	full
9	**Λ-T12**	3	Cs_2CO_3	6	rt	CH_2Cl_2	0.26	11 / 17	54 / 52	~½ / ~¾
10[d]	**Λ-X6**[d]	2	?[e]	?[e]	rt	CH_2Cl_2	0.15	15	59	full
11	**Λ-T13**	10	*i*Pr$_2$NEt	20	rt	CH_2Cl_2	0.26	12 / 23	69[c] / 68[c]	~½ / full
12	**Λ-T13**	3	Cs_2CO_3	6	rt	CH_2Cl_2	0.26	10	68	full
13	**Λ-T13**	3	Cs_2CO_3	6	0	CH_2Cl_2	0.26	10 / 17	76 / 76	~¾ / full

[a]Enantioselectivities determined from crude product mixtures by chiral HPLC analysis. [b]Approximate conversion determined by a combination of TLC and HPLC analysis. [c]Old HPLC column used giving an imperfect peak separation with an uncertainty of about ±1%. [d]Experiment performed by X. S.,[76] result copied for clarity from Table 3. [e]See remark '*b*' from Table 3.

With precatalyst **Λ-T1** as a reference, the following conclusions were drawn from Table 5:

- Larger or more extended aryl substituents than the 2,4,6-trimethylphenyl substituents of **Λ-T1** not necessarily resulted in a better enantioselectivity: Even though the 3,6-di-*tert*-butylcarbazole substituents of **Λ-T6** and the 2-(*tert*-butyl)pyrenyl substituents of **Λ-T7** extend over a larger area, both precatalysts **Λ-T6** and **Λ-T7** were found to be less selective than **Λ-T1** in the reaction **13a → 14a** (see entries 1–4).

- However, replacement of the 2,4,6-tri*methyl*phenyl substituents (**Λ-T1**) by 2,4,6-tri*iso-propyl*phenyl substituents and chlorine introduction at the 7-position of the 3*H*-imidazo-[4,5-*h*]quinoline ligand (**Λ-X6**) − which of both was of higher importance was unclear at that point − had a strongly positive effect on the selectivity of the studied reaction (see entries 1, 2 and 10 for **Λ-T1** and **Λ-X6**).
- Introduction of methyl substituents at the 6-positions of the phenylbenzoxazole ligands did slightly improve the selectivity of the studied reaction (**Λ-T8**). But not to an extent which justified the more complicated synthesis (see entries 1, 2, 5 and 6 for **Λ-T1** with **Λ-T8**).
- Replacement of the phenyl*benzoxazole* ligands (**Λ-T1**) by phenyl*benzothiazole* (**Λ-T10)** ligands resulted in a significant drop of the enantioselectivity (see entries 2 and 7). Also phenyl*benzothiazole*-based complex **Λ-T11** featuring 1-adamantyl substituents could not convince in terms of enantioselectivity (see entries 2 and 8).
- Introduction of a methyl substituent at the methylene bridge between both nitrogen atoms of the 3*H*-imidazo[4,5-*h*]quinoline ligand's fused imidazole improved the selectivity of the studied reaction but came along with a significant reduction of catalytic activity (see entries 2 and 9 for **Λ-T1** and **Λ-T12**).
- Lowering of the temperature from rt to 0 °C significantly improved the selectivity and still allowed short reaction times (entries 5 and 6 as well as entries 12 and 13).
- Attachment of 2,6-dimethylphenyl substituents at the *ortho*-positions of the phenylbenz-oxazoles' phenyl rings had a strongly positive effect on the enantioselectivity of the studied reaction (compare entries 2, 12, 13 for **Λ-T1** and **Λ-T13**).

  This finding was quite remarkable as simple balls-and-sticks modeling had misleadingly indicated that aryl substituents at these positions would be too far away. However, an X-ray structure of a catalysis intermediate analog (see chapter 2.3.8, Figure 21), an X-ray-based and DFT-assisted molecular surface modeling (see chapter 2.3.8, Figures 22 and 23), and an explicit quantum chemical modeling of the stereogenic step of an intramolecular acyl migration reaction (see chapter 2.3.8, Figures 25 and 26) later clearly visualized the importance of one of both 2,6-dimethylphenyl substituents.
- The overall best result was achieved with precatalyst **Λ-T13**, which was able to provide product **14a** in 76% ee under the conditions from entry 13.

Inspired by the insights from this screening and in particular the finding that the introduction of sterically demanding aryl groups at the *ortho*-positions of the phenylbenzoxazoles' phenyl rings had a strongly positive effect (**Λ-T1** vs. **Λ-T13**), complexes **Λ-T14**–**Λ-T16** (Figure 13) were synthesized next to test them in the reaction **13a** → **14a**.

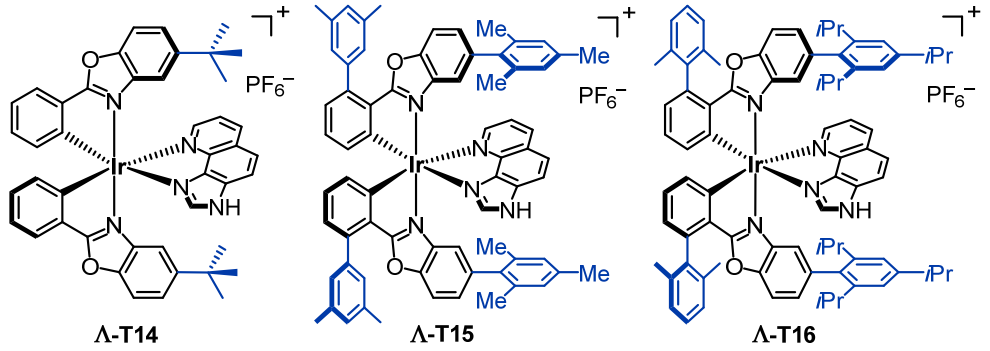

Figure 13. Complexes **Λ-T14**–**Λ-T16** were prepared as precatalyst candidates for the Steglich rearrangement of *O*-acylated azlactones (**13a** → **14a**). Structural modifications with respect to the cyclometalated ligand of **Λ-X1** (see chapter 2.2.2, Figure 11) are highlighted in blue.

The three complexes **Λ-T14**–**Λ-T16** were prepared with the following intentions:

- Complex **Λ-T14** was prepared to evaluate, by comparison with the results for **Λ-T1**, whether bulky *aliphatic* substituents in the 5-position of the phenylbenzoxazole ligands would be less or more favorable than *aryl* substituents. In this regard, only 1-adamantyl-substituted **Λ-11** had been tested so far (see Table 5), which is benzothiazole-based and thus only directly comparable with benzothiazole-based **Λ-10** but not with the other complexes that are benzoxazole-based.
- Complex **Λ-T15** was prepared to evaluate whether the positive influence of the introduction of the 2,6-dimethylphenyl substituents in case of **Λ-T13** was general or restricted to that particular substituents.
- Complex **Λ-T16** was prepared for the following reasons:

  a.) Experiments from Table 5 had revealed that 2,4,6-tri*isopropyl*phenyl- *and* chlorine-substituted **Λ-X6** performs much better than 2,4,6-tri*methyl*phenyl-substituted **Λ-T1** lacking the chlorine substituent at its 3*H*-imidazo[4,5-*h*]quinoline ligand (entries 2 and 10).

  b.) Furthermore, introduction of 2,6-dimethylphenyl substituents at the *ortho*-positions of the phenylbenzoxazoles' phenyl rings had proved to be highly beneficial (compare entries 1 and 2 with entries 11–13 for **Λ-T1** and **Λ-T13**).

  It was anticipated that **Λ-X6**'s chlorine substituent would only have a minor influence on the enantioselectivity of the studied reaction and that, in contrast, the installation of 2,4,6-tri*isopropyl*phenyl substituents at the 5-positions of the phenylbenzoxazoles (→A), *and* the simultaneous attachment of 2,6-dimethylphenyl substituents at the *ortho*-positions of the phenylbenzoxazoles' phenyl rings (→B) would result in a synergistically improved highly selective complex (**Λ-T16**).

After preparation of complexes **Λ-T14**–**Λ-T16**, they were screened in the reaction **13a** → **14a**. The results of this screening are summarized in Table 6.

Table 6. Screening of precatalysts **Λ-T14**–**Λ-T16** in the reaction **13a** → **14a**.

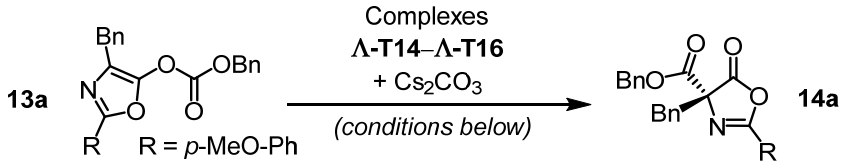

entry	complex	complex loading (mol%)	Cs_2CO_3 loading (mol%)	*t* (°C)	solvent	conc (mol/L)	time (h)	ee of **14a**[a] (%)	conv[b]
1	**Λ-T14**	3	6	rt	CH_2Cl_2	0.26	20	20	full
2[c]	**Λ-T1**	3	6	rt	CH_2Cl_2	0.26	17	40	full
3	**Λ-T15**	3	6	rt	CH_2Cl_2	0.26	11	64	full
4[c]	**Λ-T13**	3	6	rt	CH_2Cl_2	0.26	10	68	full
5	**Λ-T16**	3	6	rt	CH_2Cl_2	0.26	10	81	full

[a]Enantioselectivities determined from crude product mixtures by chiral HPLC analysis. [b]Approximate conversion determined by a combination of TLC and HPLC analysis. [c]Results for **Λ-T1** and **Λ-T13** copied from Table 5 for clarity and direct comparisons.

With precatalyst **Λ-T1** as a reference, the following conclusions were drawn from Table 6:

- *Tert*-butyl-substituted **Λ-T14** performed significantly worse than 2,4,6-trimethylphenyl-substituted **Λ-T1** (compare entries 1 and 2) and, moreover, than the majority of all the complexes with aryl substituents at the 5-positions of their benzoxazoles (compare also with the results from Table 5).
- 3,4-Dimethylphenyl-substituted complex **Λ-T15** almost reached the performance of 2,6-dimethylphenyl-substituted complex **Λ-T13**, which indicated that the introduction of other substituents than 2,6-dimethylphenyl at the *ortho*-positions of the phenylbenzoxazoles' phenyl rings had a positive influence on the enantioselectivity as well (see entries 3 and 4).
- Complex **Λ-T16**, which had been designed with the anticipation of a strongly synergistic effect originating from the simultaneous presence of 2,4,6-triisopropylphenyl substituents *and* 2,6-dimethylphenyl substituents, indeed proved as the most selective complex so far and provided product **14a** with respectable 81% ee (entry 13).

With the insights from both screenings from Tables 5 and 6, complexes **Λ-T17**–**Λ-T28** were prepared next (Figure 14).

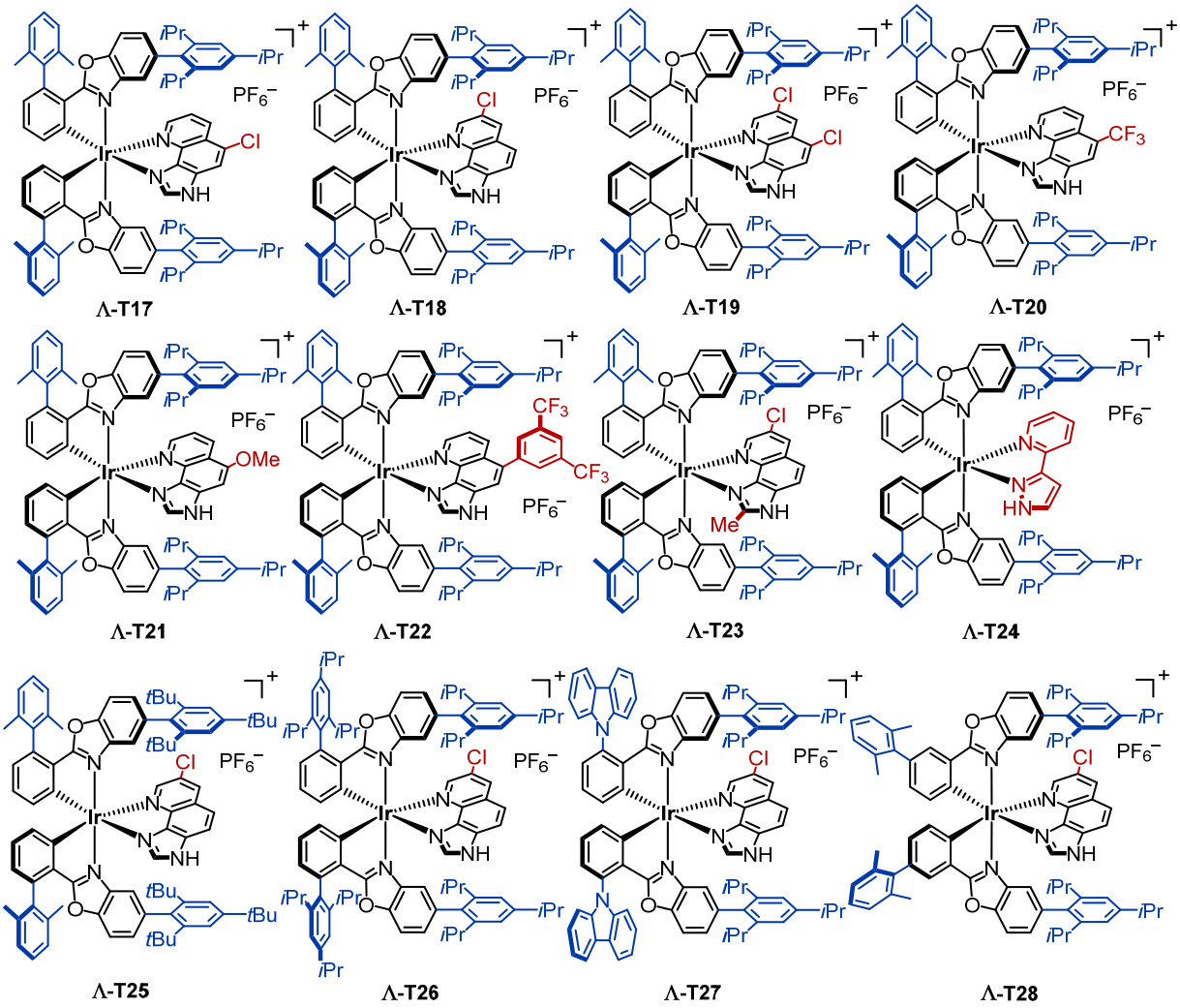

Figure 14. Complexes **Λ-T17**–**Λ-T28** were prepared as precatalyst candidates for the Steglich rearrangement of *O*-acylated azlactones (**13a** → **14a**). Structural modifications with respect to the cyclometalated ligand of **Λ-X1** (see chapter 2.2.2, Figure 11) are highlighted in blue and modifications with respect to the non-cyclometalated ligand of **Λ-X1** are highlighted in red.

Complexes **Λ-T17**–**Λ-T28** were prepared to address the following points:

- Complexes **Λ-T17**–**Λ-T23** were prepared to evaluate different substitution patterns of the key 3*H*-imidazo[4,5-*h*]quinoline ligand.
- Complex **Λ-T24** was prepared to evaluate the replacement of the 3*H*-imidazo[4,5-*h*]quinoline ligand by a 2-(1*H*-pyrazol-3-yl)pyridine ligand.
- Since 2,4,6-tri*isopropyl*phenyl-substituted **Λ-T16** had proven superior compared to 2,4,6-tri*methyl*-phenyl-substituted **Λ-T13** (see Table 6, entries 4 and 5), 2,4,6-tri*tertbutyl*-phenyl-substituted **Λ-T25** was prepared as a logical consequence.
- Since the introduction of 2,6-dimethylphenyl (**Λ-T13**) and 3,4-dimethylphenyl (**Λ-T15**) substituents at the *ortho*-positions of the phenylbenzoxazoles' phenyl rings had proven highly beneficial, complexes **Λ-T26** and **Λ-T27** featuring 2,4,6-triisopropylphenyl and *N*-carbazolyl substitutents at these positions were prepared as a logical consequence.

- Complex **Λ-T28** was prepared to evaluate the shift of the 2,6-dimethylphenyl substituents from the *ortho*-positions of the phenylbenzoxazoles' phenyl rings to the according *meta*-positions. This modification was inspired by the highly selective cooperative enamine/hydrogen-bonding catalyst presented in chapter 1.4 (**Λ-99**; see Scheme 20).[67]

After preparation of complexes **Λ-T17**–**Λ-T28**, the complexes were screened in the Steglich rearrangement **13a** → **14a**. The results of this screening are summarized in Table 7.

Table 7. Screening of precatalysts **Λ-T17**–**Λ-T18** in the reaction **13a** → **14a**.

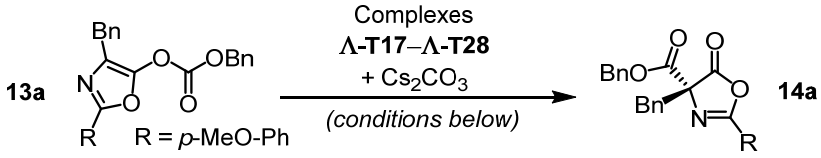

entry	complex	complex loading (mol%)	Cs_2CO_3 loading (mol%)	*t* (°C)	solvent	conc (mol/L)	time (h)	ee of **14a** (%)[a]	conv[b]
1[c]	**Λ-T16**	3	6	rt	CH_2Cl_2	0.26	10	81	full
2	**Λ-T17**	3	6	rt	CH_2Cl_2	0.26	10	84	full
3	**Λ-T17**	3	6	0	CH_2Cl_2	0.26	10	88	full
4	**Λ-T18**	3	6	rt	CH_2Cl_2	0.26	10	85	full
5	**Λ-T18**	3	6	0	CH_2Cl_2	0.26	10	88	full
6	**Λ-T18**	0.2	3	0	CH_2Cl_2	1.0	12	88	full
7	**Λ-T18**	0.2	3	0	EtOAc	1.0	12	88	full
8	**Λ-T19**	0.2	3	0	CH_2Cl_2	1.0	12	88	full
9	**Λ-T20**	0.2	3	0	CH_2Cl_2	1.0	12	88	full
10	**Λ-T21**	0.5	3	0	EtOAc	0.5	12	78	full
11	**Λ-T22**	0.2	3	0	CH_2Cl_2	1.0	12	82	full
12	**Λ-T23**	2	6	0	CH_2Cl_2	1.0	14	n.d.	low
							41	n.d.	low
13	**Λ-T23**	2	6	rt	CH_2Cl_2	1.0	9	81	full
14	***rac*-T24**	0.5	3	rt	CH_2Cl_2	1.0	12	–[d]	–[d]
15	**Λ-T25**	0.5	3	0	EtOAc	0.5	12	84	full
16	**Λ-T26**	0.2	3	0	CH_2Cl_2	1.0	10	n.d.	low
							22	n.d.	low
							35	n.d.	low
17	**Λ-T26**	2	6	0	CH_2Cl_2	1.0	9	n.d.	low
							21	65	full
18	**Λ-T27**	0.2	3	0	CH_2Cl_2	1.0	10	73	full
19	**Λ-T28**	0.2	3	0	CH_2Cl_2	1.0	15	53	full

[a]Enantioselectivities determined from crude product mixtures by chiral HPLC analysis. [b]Approximate conversion determined by a combination of TLC and HPLC analysis. [c]Result for **Λ-T16** copied from Table 6 for clarity and direct comparisons. [d]No conversion found.

The following conclusions were drawn from the results from Table 7:

- Evaluation of different 3*H*-imidazo[4,5-*h*]quinoline ligands (**Λ-T17**−**Λ-T23**): Introduction of a chlorine substituent at the 5-position of the 3*H*-imidazo[4,5-*h*]quinoline ligand (**Λ-T17**), introduction of a chlorine substituent at the 7-position of this ligand (**Λ-T18**), introduction of two chlorine substituents at both the 5-position and the 7-position of this ligand (**Λ-T19**), and introduction of a trifluoromethyl substituent at the 5-position of this

ligand (**Λ-T20**) resulted virtually all in the same enhancement in comparison to non-substituted complex **Λ-T16** (see entries 2−9). As the preparation of the 7-chloro-3*H*-imidazo[4,5-*h*]quinoline ligand is the most straightforward one of all four required 3*H*-imidazo[4,5-*h*]quinoline ligands, **Λ-T18** was chosen as new benchmark and reference complex.

- It is worth noting that the loading of benchmark precatalyst **Λ-T18** could be lowered from 3 mol% to 0.2 mol% and the Cs_2CO_3 loading lowered from 6 mol% to 3 mol% without a drop in selectivity (in both cases 88% ee) and while still maintaining a short reaction time of just 12 h (see entries 5 and 6). Moreover, replacement of solvent CH_2Cl_2 by EtOAc did not show any effect in terms of enantioselectivity (entries 6 and 7).
- In contrast, the introduction of a methoxy substituent at the 5-position of the 3*H*-imidazo[4,5-*h*]quinoline ligand resulted in less selective complex (**Λ-T21**) and the introduction of a 3,5-bis(trifluoromethyl)phenyl substituent at the same position (**Λ-T22**) in a similarly selective complex as non-substituted complex **Λ-T16** (entries 1, 10, 11).
- In case of complex **Λ-T1**, the installation of a methyl group at the methylene bridge between both nitrogen atoms of the fused imidazole of the 3*H*-imidazo[4,5-*h*]quinoline ligand (**Λ-T12**) had resulted in an improved enantioselectivity for the reaction **13a** → **14a**, albeit at the cost of catalytic activity (see Table 5, entries 2 and 9). A similar finding was expected for complex **Λ-T23**. Complex **Λ-T23** was indeed found to be significantly less active than **Λ-T18** (see Table 7, compare entries 5, 6 and 12, 13) but was, unexpectedly, also found to be less selective than **Λ-T18** (Table 7, entries 4 and 13).
- No conversion at all was found with complex ***rac*-T24** (entry 14). This finding is in accordance with the result obtained for ***rac*-T3** with respect to the kinetic resolution of *rac*-1-(1-naphthyl)ethanol (chapter 2.3.1; Table 2, entry 4). Both findings underline that the 2-(1*H*-pyrazol-3-yl)pyridine ligand is apparently not suited for the development of a nucleophilic stereogenic-at-metal catalyst.
- Replacement of the 2,4,6-tri*methyl*phenyl groups of **Λ-T13** by 2,4,6-tri*isopropyl*phenyl group had provided with complex **Λ-T16** a significantly improved precatalyst (see Table 6, entries 4 and 5). A similar finding was expected for 2,4,6-tri*tertbutyl*phenyl-substituted complex **Λ-T25** with regard to **Λ-T18**. Surprisingly, the opposite was the case: **Λ-T25** proved to be slightly less enantioselective than complex **Λ-18**. (Table 7, entries 7 and 15).
- Introduction of 2,6-dimethylphenyl substituents (**Λ-T13**, **Λ-T15**) and 3,5-dimethylphenyl substituents (**Λ-T16**) at the *ortho*-positions of the phenylbenzoxazoles' phenyl rings had both resulted in a significantly enhanced selectivity of the studied reaction (see Table 6, entries 3–5 and Table 7, entry 1). Accordingly, it was expected that **Λ-T26** and / or **Λ-T27**

could provide even better results. However, 2,4,6-triisopropylphenyl-substituted **Λ-T26** (Table 7, entries 16, 17) and *N*-carbazolyl-substituted **Λ-T27** (entry 18) were both found to be less selective than complex **Λ-T18**. Moreover, 2,4,6-triisopropylphenyl-substituted **Λ-T26** showed a significantly decreased activity (see entries 5, 6 vs. entries 16, 17).

- Finally, complex **Λ-T28** was evaluated where the 2,6-dimethylphenyl substituents of **Λ-T18** are formally shifted from the *ortho*-positions of the phenylbenzoxazoles' phenyl rings to the according *meta*-positions. This complex showed a significantly lower enantioselectivity than complex **Λ-T18** (see entries 6 and 19).

In short, **Λ-T18** was identified as new benchmark precatalyst: With just 0.2 mol% of **Λ-T18** in combination with 3 mol% of Cs_2CO_3 in CH_2Cl_2 or EtOAc as solvent (conc = 1.0 M), Steglich rearrangement product **14a** was smoothly provided with this system with respectable 88% ee at a reaction temperature of 0 °C and after a reaction time of 12 h (entries 6 and 7).

Noticing that the complex structure optimization had somewhat reached a "dead point" and having already spent a considerable amount of time on the synthesis of complex library **Λ-T1**–**Λ-T28**, precatalyst **Λ-T18** was, based on the previous screenings (Tables 5–7), eventually selected as the final complex of choice for the Steglich rearrangement of *O*-acylated azlactones to *C*-acylated azlactones (**13** → **14**).

The detailed synthesis route for enantiomeric precatalysts **Λ-** and **Δ-T18** and enantiomeric catalysts **Λ-** and **Δ-T18'** is shown in Scheme 32 below and is based on general synthesis Route I from Scheme 30. Enantiopurities of >99% ee were found for both enantiomeric catalysts **Λ-** and **Δ-T18'** by chiral HPLC analysis and the absolute configurations of the enantiomeric complexes were assigned by CD spectroscopy (details are provided in the experimental section). Figure 15 shows the CD spectra of enantiomeric precatalysts **Λ-** and **Δ-T18** (left side) and the chiral HPLC traces of catalysts ***rac*-**, **Λ-**, and **Δ-T18'** (right side). Figure 16 shows the three-dimensional structure of active catalyst **Λ-T18'** from two different perspectives. The structure from Figure 16 was deduced from a crystal structure which was obtained for racemic catalyst ***rac*-T18'** (details are provided in the experimental section).

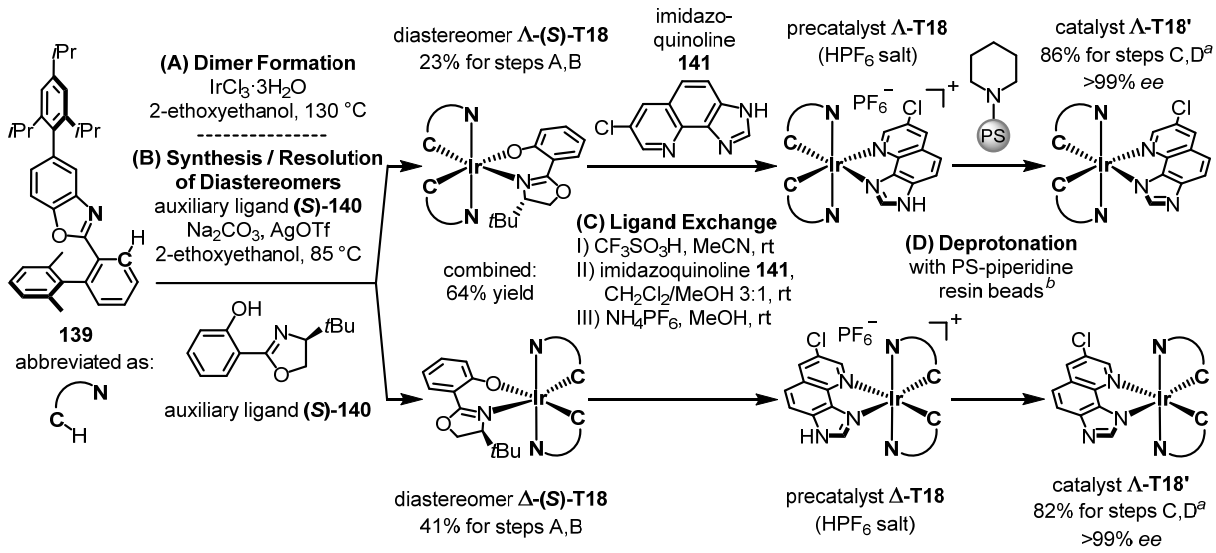

Scheme 32. Synthesis of precatalyst **Λ/Δ-T18** and catalyst **Λ/Δ-T18'** starting from phenylbenzoxazole **139** and $IrCl_3 \cdot 3H_2O$. The here depicted synthesis scheme is based on general synthesis Route I from Scheme 30. Details are provided in the experimental section. [a]Yield of deprotonation step D: 99%. [b]Alternatively, wash a CH_2Cl_2 solution of **Λ/Δ-T18** with aqueous 0.3 M NaOH and water. [Reproduced and adapted with permission from ref. 84. Copyright © 2017, American Chemical Society]

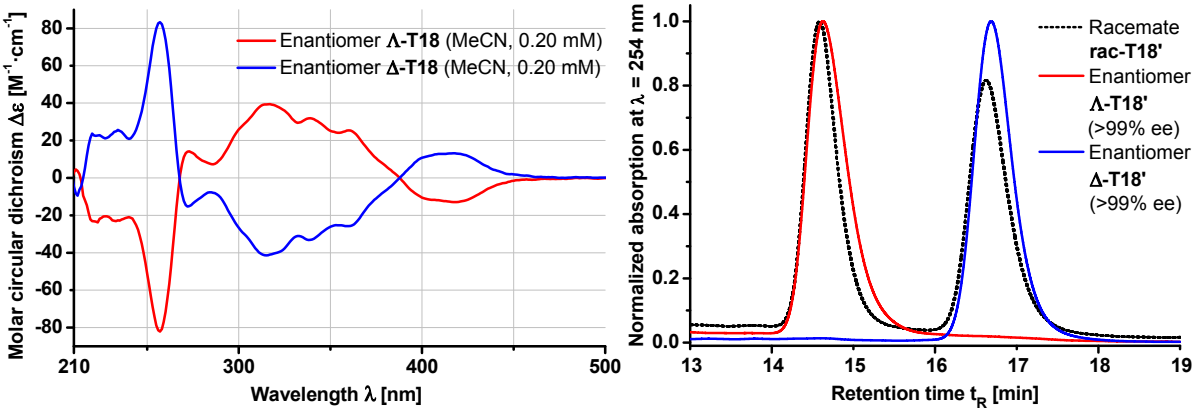

Figure 15. *Left*: CD spectra of enantiomeric precatalysts **Λ-** and **Δ-T18**. *Right*: Superposition of absorption-normalized excerpts of the HPLC traces of catalysts ***rac*-**, **Λ-**, and **Δ-T18'**. Experimental details are provided in the experimental section. [Reproduced and adapted with permission from ref. 84. Copyright © 2017, American Chemical Society]

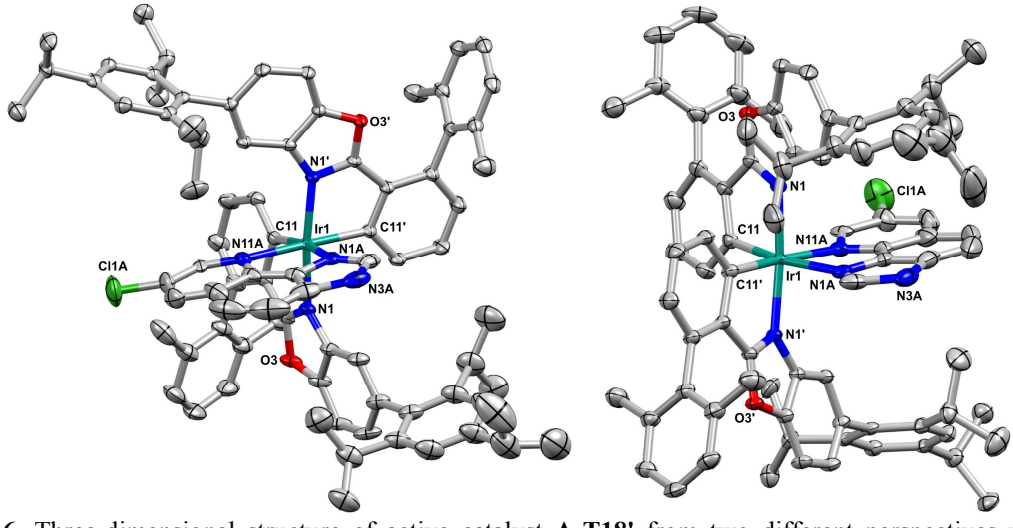

Figure 16. Three-dimensional structure of active catalyst **Λ-T18'** from two different perspectives with 50% probability of thermal ellipsoids.[85] Three-dimensional structures deduced from the crystal structure obtained for ***rac*-T18'**. Cocrystallized solvent molecules and positional disorder are omitted for clarity.

The high catalytic activity of **Λ-T18** in combination with Cs_2CO_3 (see Table 7, entries 6 and 7) foreshadowed that further enantioselectivity improvements could be achievable by lowering of the temperature and / or by variations of other reaction parameters.

As a start, a solvent screening was performed at 0 °C with **Λ-T18** for the reaction **13a** → **14a**. The results of this screening are summarized in Table 8.

Table 8. Steglich rearrangement **13a** → **14a**. Solvent screening with complex **Λ-T18** at 0 °C.

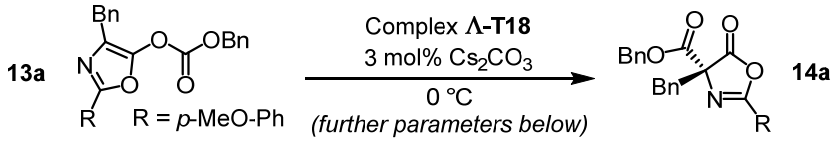

entry	catalyst loading (mol%)	solvent	conc (mol/L)	time (h)	ee of **14a**[a] (%)	conv[b] (%)
1	0.2	CH_2Cl_2	1.0	12	88	full
2	0.2	toluene	1.0	12	82	full
3	0.2	THF	1.0	12	88	full
4	0.2	$CHCl_3$	1.0	12	86	full
5	0.2	EtOAc	1.0	12	88	full
6	0.2	TAA	1.0	12	n.d.	trace[c]
7	0.5	TAA	0.25	12	62	<50%[c]
8	0.2	MTBE	1.0	12	88	full[d]
9	0.2	1,4-dioxane[e]	1.0	12	82	full
12	0.5	acetone	0.5	12	87	<50%
13	0.5	DMF	0.5	12	87	<90%
14	0.5	MeCN	0.5	12	n.d.	trace
15	0.5	*i*-PrOH	0.25	12	64	full
16	0.5	DMPU	0.5	12	85	<90%
17	0.6	NMP	0.5	12	86	<90%
18	0.5	$C_6CH_5NO_2$	0.5	12	n.d.	trace
19	0.5	C_6H_5Cl	0.5	12	77	full
20	0.5	CH_3NO_2	0.5	12	n.d.	trace
21	0.5	DME	0.5	12	86	full
22	0.5	C_6H_5Cl	0.5	12	77	full
23	0.5	CPME	0.5	12	82	~50%
24	0.5	THP	0.5	12	74	>90%
25	0.5	α-Me-THF	0.5	12	85	full
26	0.6	EtOAc / C_6F_{14} 8:1	0.5	12	87	full
27	0.5	CPME / C_6F_{14} 8:1	0.5	12	85	full

[a]Enantioselectivities determined from crude product mixtures by chiral HPLC analysis. [b]Approximate conversion determined by a combination of TLC and HPLC analysis. [c]TAA: Very low solubility of **13a** under these conditions prevented full conversion. [d]MTBE: Full and clean conversion but solubility of **13a** critically low in MTBE. [e]1,4-Dioxane: Reaction performed at rt (mp of 1,4-dioxane approx. 10 °C).

The solvent screening from Table 8 revealed that CH_2Cl_2, THF, and EtOAc all worked equally well for the reaction **13a** → **14a** at 0 °C in terms of enantioselectivity and activity. Moreover, no side products were observed with these solvents and the short reaction time of 12 h in all three cases indicated that the reaction temperature could be further decreased.

Accordingly, CH_2Cl_2, THF, and EtOAc were then screened at –20 °C and at –30 °C (Table 9). At a temperature of –20 °C, THF and EtOAc both outperformed CH_2Cl_2 in terms of enantio-

selectivity and particularly in terms of activity (entries 1–3). THF and EtOAc, which were both head-to-head at –20 °C, were next evaluated at –30 °C (entries 4 and 5). While an acceptable catalytic activity was maintained in case of EtOAc with full conversion after 66 h, the catalytic activity dropped dramatically in case of THF and only ~25% conversion were found after 53 h. In case of the reaction with EtOAc which was performed at –30 °C (entry 5), product **14a** could be isolated by short-column chromatography in excellent 95% yield and with respectable 93% ee (entry 5). As a result, EtOAc was chosen as the solvent of choice for Steglich rearrangements of *O*-acylated azlactones (**13** → **14**).

Table 9. Steglich rearrangement **13a** → **14a**. Solvent screening with complex **Λ-T18** at –20 °C and –30 °C.

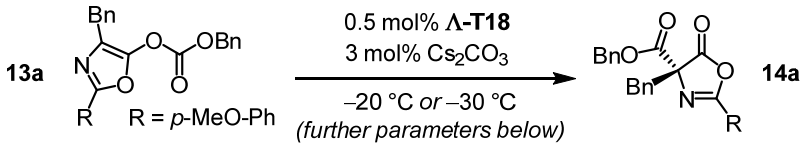

entry	solvent	*t* (°C)	conc (mol/L)	time (h)	ee of **14a**[a] (%)	conv[b]
1	CH_2Cl_2	–20	0.5	48	87	~½
2	THF	–20	0.5	48	90	full
3	EtOAc	–20	0.5	48	90	full
4	THF	–30	0.65	53	n.d.	~¼
5	EtOAc	–30	0.65	53 / 66	92 / 93 (93[c])	>95% / full

[a]Enantioselectivities determined from crude product mixtures by chiral HPLC analysis. [b]Approximate conversion determined by a combination of TLC and HPLC analysis. [c]Ee of isolated product **14a**.

Next, the scope of the Steglich rearrangement (**13** → **14**) was investigated. For this reason, nine *O*-acylated azlactones **13a–i** including test substrate **13a** were prepared (Figure 17), used as substrates with precatalyst **Λ/Δ-T18** *or* catalyst **Λ/Δ-T18'**, and resulting products **14a–i** isolated and their ee values and yields determined. The results of this study are summarized in Table 10.

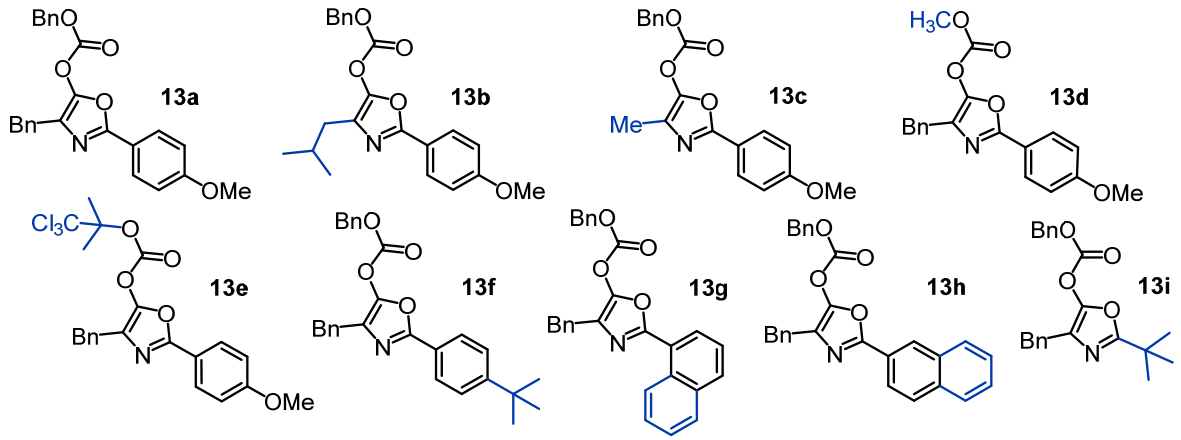

Figure 17. *O*-Acylated azlactones **13a–i** were prepared and screened as substrates in the Steglich rearrangement (**13** → **14**) with precatalyst **Λ/Δ-T18** / catalyst **Λ/Δ-T18'** (see Table 10). Modifications with respect to compound **13a** are highlighted in blue.

Table 10. Scope: Steglich rearrangement of *O*-acylated azlactones (**13** → **14**).[a]

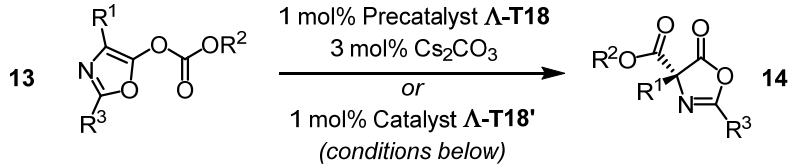

entry	*t* (°C)	time (h)	R^1	R^2	R^3	yield (%)[b]	ee (%)[b]	product
1[c,d]	0	12	Bn	Bn	*p*-MeO-Ph	97	88	**14a** (*R*)
2[c,d]	0	12	*i*Bu	Bn	*p*-MeO-Ph	91	70	**14b** (*R*)
3[c,d]	0	12	Me	Bn	*p*-MeO-Ph	80	45	**14c** (*R*)
4[c]	−30	72	Bn	Bn	*p*-MeO-Ph	95	93	**14a** (*R*)
5	−30	72	Bn	Me	*p*-MeO-Ph	68	88	**14d** (*R*)
6	−30	72	Bn	$C(CH_3)_2CCl_3$	*p*-MeO-Ph	99	90	**14e** (*R*)
7	−30	72	Bn	Bn	*p*-(*t*Bu)-Ph	89	91	**14f** (*R*)
8	−30	72	Bn	Bn	1-Naphtyl	88	91	**14g** (*R*)
9	−30	72	Bn	Bn	2-Naphtyl	90	95	**14h** (*R*)
10[e,f]	−30	72	Bn	Bn	2-Naphtyl	94	94	**14h** (*R*)
11[e]	−30	72	Bn	Bn	*p*-MeO-Ph	97	93	**14a** (*R*)
12[e,f]	−30	72	Bn	Bn	*p*-MeO-Ph	93	93	**14a** (*R*)
13[e,g]	−30	72	Bn	Bn	*t*Bu	91	96	***ent*-14i** (*S*)[g]
14[e,g,h]	−30	72	Bn	Bn	*t*Bu	90	96	***ent*-14i** (*S*)[g]

[a]Standard reaction conditions: substrate **13** (1.0 eq; approx. 90 µmol) with precatalyst **Λ-T18** (1 mol%) and Cs_2CO_3 (3 mol%) in EtOAc (conc = 0.65 M) at the indicated temperature. [b]Isolated yields; enantioselectivities determined from isolated products by chiral HPLC analysis. [c]0.5 mol% of catalyst were used. [d]conc = 0.5 M. [e]Active catalyst **T18'** was used instead of precatalyst **T18** (no addition of Cs_2CO_3). [f]Scaled-up reactions, entry 10: 400 mg (919 µmol) of substrate **13h**; entry 12: 381 mg (917 µmol) of substrate **13a**. [g]Δ-configured catalyst **Δ-T18'** used (major product: *S*-configuration). [h]CD_2Cl_2 solution of **Δ-T18'** left standing for 7 d at 25 °C before usage.

With 0.5 mol% of precatalyst **Λ-T18** in the presence of 3 mol% Cs_2CO_3 at 0 °C, substrate **13a** provided product **14a** in 88% ee and was isolated in 97% yield after 12 h (Table 10, entry 1). Substrate **13b** with R^1 = *i*-Bu instead of R^1 = Bn provided product **14b** in 70% ee and was isolated in 91% yield after 12 h (entry 2). Substrate **13c** with R^1 = Me provided product **14c** in 45% ee and was isolated in 80% yield after 12 h (entry 3).

For substrate **13a** being the best performing substrate so far, the temperature was then lowered to –30 °C and the reaction time prolonged to 72 h, which pushed the ee of product **14a** from 88% to 93% and product **14a** was isolated in 95% yield (entry 4).

While 0.5 mol% of precatalyst **Λ-T18** were used for substrates **13a–c** from entries 1–4, the precatalyst loading (and later the catalyst loading: see entries 10–14) was increased for all following reactions which were screened at –30 °C to 1 mol% in order to ensure complete conversion within 72 h.

With substrate **13d** residue R^2 = Bn was now exchanged for R^2 = Me and product **14d** obtained in 88% ee and isolated in 68% yield (entry 5). Substrate **13e** with $R^2 = C(CH_3)_2CCl_3$ provided product **14e** in 90% ee with 99% yield (entry 6).

Finally, variations of the third residue R^3 were screened (entries 7–9, 11, 13). The best results were obtained here with substrate **13h** with R^3 = 2-naphtyl, which provided product **14h** in 95% ee and with 90% yield (entry 9), and substrate **13i** with R^3 = *t*-Bu, which provided product ***ent*-14i** in 96% ee and with 91% yield (entry 13; note that the Δ-configured complex was used in the latter case instead of the usually used Λ-complex). Importantly, the reactions from entries 11 and 13 had been, in contrast to all other discussed reactions so far, performed with active catalyst **Λ/Δ-T18'** in the absence of Cs_2CO_3. Beforehand, it had been recognized that both methods − use of HPF_6 salt **Λ/Δ-T18** in combination with Cs_2CO_3 *or* use of active catalyst **Λ/Δ-T18'** alone − had led to identical results, which is visible from entries 4 and 11.
In order to study the catalyst's stability in solution, a CH_2Cl_2 solution of catalyst **Δ-T18'** was left standing for 7 d at 25 °C before usage, which then provided product ***ent*-14i** with the same selectivity and yield as freshly prepared catalyst **Δ-T18'** (entry 14, compare with entry 13; details in the experimental section). In this context, it is worth mentioning that neither any decomposition nor any racemization of precatalysts **Λ/Δ-T18** and catalysts **Λ/Δ-T18'** was observed when they were stored as solvent-free solids for ≥ 6 months at 4 °C under standard atmospheric conditions (details are provided in the experimental section).
Exemplarily, two reactions with substrates **13a** and **13h** were scaled up by a factor of ten (~1 mmol scale) and similar yields and basically identical selectivities for products **14a** and **14h** obtained as for the corresponding standard scale examples (see entries 10 and 12, compare with entries 9 and 11).

There are no results shown in Table 10 for substrates **13b** and **13c** at –30 °C for the following reasons: Substrate **13b** had been revealed to require much higher catalyst loadings *or* a much longer reaction time than 72 h at already –20 °C to reach completion (1 mol% **Λ-T18**, 3 mol% Cs_2CO_3, conc = 0.65 M of **13b**, t = –20 °C, solvent: EtOAc; about ⅔ conversion after 72 h and a crude ee of 75% for **14b**). And in case of substrate **13c**, a preliminary experiment at −20 °C had revealed that temperature lowering was unable to push the ee of product **14c** in a useful height (same conditions as for **13b** at –20 °C; full conversion found after 72 h with 46% crude ee for product **14c**). As a consequence, no further efforts were put in both "mismatched" substrates **13b** and **13c**.

Noteworthy, all Steglich rearrangements **13** → **14** presented in Table 10 (and in this work in general) were set up under normal atmosphere without any special precautions against moisture and oxygen. *C*-Acylated azlactones **14** which were synthesized with Λ-configured (pre-)catalyst **Λ-T18** / **Λ-T18'** were unambiguously assigned as *R*-configured. Stereochemical assignment details are provided in the experimental section of this work.

As explained above, precatalytic HPF_6 salt **Λ/Δ-T18** in combination with Cs_2CO_3 *and* active catalyst **Λ/Δ-T18'** alone both gave identical results in case of the investigated Steglich rearrangements (**13** → **14**). As a consequence, all reactions discussed from now on were performed with catalyst **Λ/Δ-T18'** instead with precatalyst **Λ/Δ-T18** and Cs_2CO_3 as additive.

2.3.3 Black Rearrangement of *O*-Acylated Benzofuranones

Having demonstrated that **Λ/Δ-T18'** is a powerful stereogenic-at-metal catalyst for the Steglich rearrangement of *O*-acylated azlactones (**13**) to *C*-acylated azlactones (**14**; chapter 2.3.2, see Table 10), the objective was now to ascertain whether **Λ/Δ-T18'** would be a suitable catalyst for other asymmetric reactions.

For this reason, the related Black rearrangement[86] of *O*-acylated benzofuranones (**142**) to *C*-acylated benzofuranones (**143**) was investigated next. As a start, substrates **142a** and **142b** were synthesized and tested with catalyst **Λ-T18'**. The results of this initial screening are summarized in Table 11.

Table 11. Initial screening of *O*-acylated benzofuranones **142a** and **142b** with catalyst **Λ-T18'**.

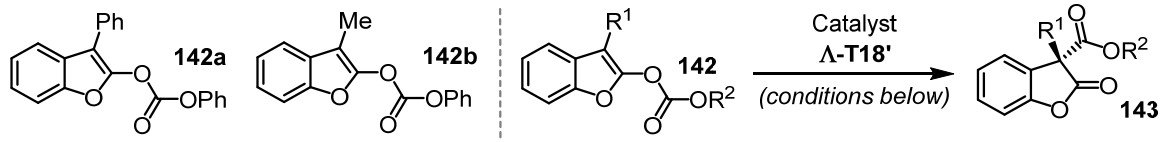

entry	substrate	loading **Λ-T18'** (mol%)	*t* (°C)	solvent	conc (mol/L)	time (h)	ee **143** (%)[a]	conv[b]
1	**142a**	1	rt	CH_2Cl_2	0.5	11	26 (**143a**)	full
2	**142a**	1	rt	THF	0.5	11	29 (**143a**)	full
3	**142b**	1	rt	CH_2Cl_2	0.5	11	67 (**143b**)	full
4	**142b**	1	rt	THF	0.5	11	73 (**143b**)	full

[a]Enantioselectivities determined from crude product mixtures by chiral HPLC analysis. [b]Approximate conversion determined by a combination of TLC and HPLC analysis.

With **142a** in CH_2Cl_2, 1 mol% of **Λ-T18'**, rt as reaction temperature, and a concentration of conc = 0.5 M full conversion was found after 11 h and product **143a** provided with 26% ee (entry 1), which did not significantly improve when THF was used as solvent (29% ee; entry 2). However, when substrate **142b** was tested under identical conditions, product **143b** was provided with promising 67% ee in CH_2Cl_2 as solvent (entry 3) and with 73% ee in THF as solvent (entry 4). As a result, substrate **142b** was declared as benchmark substrate and a conditions screening was carried out to improve the enantiomeric excess of product **142b**. The results of this screening are summarized in Table 12.

At first, additional solvents were screened (Table 12, entries 1−8). TAA, the only alcohol of this panel of eight solvents, provided product **143b** with 88% ee and thus with the best

selectivity by far. Moreover, product **143b** could be isolated in excellent 98% yield from this reaction via short-column chromatography (entry 8).

Table 12. Conditions screening for the Black rearrangement **142a** → **143b** with catalyst **Λ-T18'**.

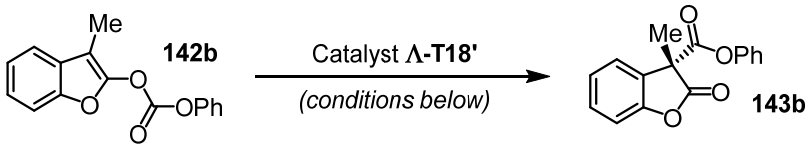

entry	*t* (°C)	solvent	conc (mol/L)	time (h)	ee **143b**[a] (%)	yield (%)	conv[b]
1	rt	CH_2Cl_2	0.5	11	67	n.d.	full
2	rt	THF	0.5	11	73	n.d.	full
3	rt	Et_2O	0.5	12	73	n.d.	full
4	rt	EtOAc	0.5	12	71	n.d.	full
5	rt	toluene	0.5	12	75	n.d.	full
6	rt	CPME	0.5	12	74	n.d.	full
7	rt	MTBE	0.5	12	76	n.d.	full
8	rt	TAA[c]	0.5	13	88[d]	98	full
9	0	TAA[c]	0.3	10	91[d]	99	full
10	0	isopropanol[e]	0.3	10	87	n.d.	full
11	0	2-ethoxyethanol[e]	0.3	10	86	n.d.	full
12	0	DMF	0.3	10	74	n.d.	full
13	−30	MTBE	0.6	13	86	n.d.	full
14	−30	CPME	0.6	13	86	n.d.	full
15	−30	toluene	0.6	13	86	n.d.	full
16	−30	THF	0.6	13	82	n.d.	full
17	−30	EtOAc	0.6	13	81	n.d.	full
18	−15	TAA / MTBE 10:1	0.4	15	92	n.d.	incomplete
19	−15	TAA / CPME 10:1	0.4	15	92[d]	99	full
20	−15	TAA / toluene 10:1	0.4	15	92[d]	99	full
21	−30	TAA / toluene 2:1	0.2	48 (20)	93[d]	98	full (20 h: ⅔)
22	−30	TAA / CPME 1:1	0.2	48 (20)	93[d]	99	full (20 h: ~90%)
23	−30	TAA / CPME 2:1	0.2	48 (20)	94[d]	99	full (20 h: >90%)

[a]Enantioselectivities determined from crude product mixtures by chiral HPLC analysis. [b]Approximate conversion determined by a combination of TLC and HPLC analysis. [c]Mp (TAA): −12 °C.[87] [d]Ee determined from isolated product. [e]Formation of side products observed.

Further improvement could be achieved by reduction of the temperature to 0 °C, which then provided **143b** with 91% ee and in 99% isolated yield after only 10 h (entry 9). It is worth noting that the concentration of **142a** was lowered for this experiment due to the low solubility of substrate **142a** in alcohols including TAA.

Encouraged by these results, other protic solvents were screened at 0 °C (entries 10−12). However, other alcohols such as isopropanol (entry 10) were found to be less selective than TAA and promoted the formation of side products (entries 10 and 11). DMF did not promote the formation of side products, but gave product **143b** with less selectivity then the screened alcohols (entry 12, compare with entries 9−11).

As TAA provided a clean reaction, high enantioselectivity, and high catalytic activity, it was considered to further lower the temperature to improve the enantioselectivity. However,

TAA's high melting point of −12 °C precluded that.[87] As a solution, it was intended to overcompensate the lower intrinsic selectivity of other screened solvents, namely MTBE, CPME, toluene, THF, or EtOAc, by a drastically reduced reaction temperature. However, this failed and TAA still provided **143b** with a higher selectivity at rt than the other solvents at −30 °C (compare entry 8 with entries 13−17).

As a result, it was decided to screen solvent mixtures in which co-solvent TAA would be – figuratively speaking – in charge of maintaining a high ee while a second solvent would be in charge of keeping TAA and the substrate in solution at very low temperatures. At first, 10:1 mixtures of TAA and others solvents were screened at −15 °C (entries 18−20). All three reactions provided product **143b** with slightly improved 92% ee (compare with entry 9) and two reactions had run to completion within 15 h, which indicated that further improvements could be achievable by further lowering of the temperature.

Accordingly, further experiments were performed at a reduced temperature of −30 °C. Prior to this, experiments had indicated that changes of the solvent mixture ratios would be required to keep TAA and the substrate in solution at −30 °C and that a decrease of the concentration of **142a** would be, moreover, necessary as well. For this reason, a 1:1 and a 2:1 mixture of TAA / CPME (entries 21 and 22) as well as a 2:1 mixture of TAA / toluene (entry 23) were used at a concentration of conc = 0.2 M for the experiments at −30 °C. From these three experiments, the 1:1 TAA / CPME experiment gave the best result in terms of selectivity and activity: >90% conversion was found here after 20 h and full conversion after 48 h providing product **143b** in 99% isolated yield and with 94% ee (entry 23, compare with entries 21 and 22). As a result, the conditions from entry 23 were defined as conditions of choice for Black rearrangements (**142** → **143**) with catalyst **Λ-T18'** at temperatures < 0 °C and the conditions from entry 9 as conditions of choice for Black rearrangements with catalyst **Λ-T18'** at temperatures ≥ 0 °C.

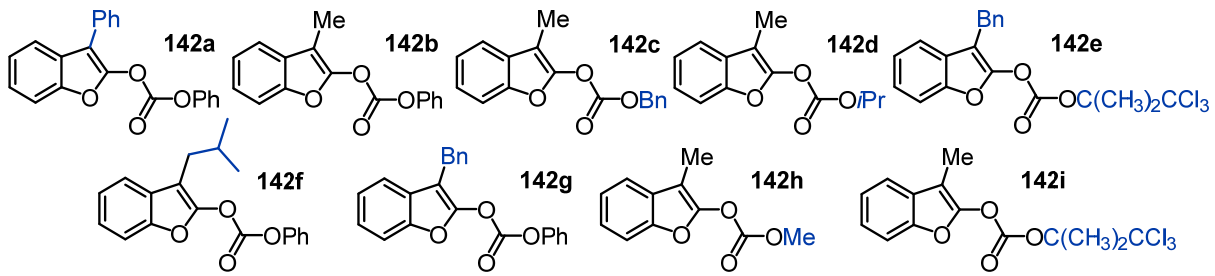

Figure 18. *O*-Acylated benzofuranones **142a−i** were synthesized and screened as substrates in the Black rearrangement (**142** → **143**) with catalyst **Λ/Δ-T18'** (see Table 13). Modifications with respect to compound **142b** are highlighted in blue.

Next, the scope of the Black rearrangement was investigated. For this reason, nine *O*-acylated benzofuranones **142a–i** including probe substrates **142a** and **142b** were prepared (Figure 18),

used as substrates with catalyst **Λ/Δ-T18'**, and resulting products **143a–i** isolated and their ee values and yields determined. The results of this study are summarized in Table 13.

Table 13. Scope: Black rearrangement of *O*-acylated benzofuranones (**142** → **143**).[a]

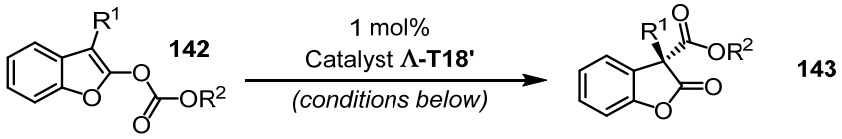

entry	*t* (°C)	time (h)	R^1	R^2	yield (%)[b]	ee (%)[b]	product
1[c,d]	0	18 h	Ph	Ph	n.d.[c]	30	**143a** (*R*)
2[d]	0	10 h	Me	Ph	99	91	**143b** (*R*)
3[d]	0	18 h	Me	Bn	99	80	**143c** (*R*)
4[d,e]	0	48 h	Me	*i*-Pr	98	82	**143d** (*R*)
5[d]	0	20 h	Bn	$C(CH_3)_2CCl_3$	98	89	**143e** (*S*)[j]
6	−15	48 h	Me	Ph	98	92	**143b** (*R*)
7	−15	48 h	*i*Bu	Ph	99	90	**143f** (*R*)
8	−15	48 h	Bn	Ph	99	91	**143g** (*R*)
9	−30	48 h	Me	Ph	99	94	**143b** (*R*)
10[f]	−30	48 h	Me	Ph	99	94	***ent*-143b** (*S*)[f]
11	−30	48 h	Me	Me	93	70	**143h** (*R*)
12	−30	48 h	Me	$C(CH_3)_2CCl_3$	99	93	**143i** (*S*)[j]
13[g]	−30	48 h	Me	$C(CH_3)_2CCl_3$	99	93	**143i** (*S*)[j]
14[g]	−30	48 h	Me	Ph	99 (73[h])	92 (98[h])	**143b** (*R*)
15[i]	−30	48 h	Me	Ph	99	93	**143b** (*R*)

[a]Standard reaction conditions: substrate **142** (1.0 eq; 70−90 µmol) with catalyst **Λ-T18'** (1 mol%) in TAA/CPME 2:1 (conc = 0.2 M) at the indicated temperature. [b]Isolated yields; enantioselectivities determined from isolated products by chiral HPLC analysis (except entry 1: ee of **143a** from crude mixture). [c]Not determined (n.d.), incomplete after 18 h; ~50% conv acc. to TLC. [d]Solvent: TAA, conc = 0.3 M. [e]2 mol% catalyst used. [f]Δ-configured catalyst used. [g]Scaled-up reactions, entry 13: 252 mg (717 µmol) of substrate **142i**; entry 14: 830 mg (3.09 mmol) of substrate **142b**. [h]Yield and ee after recrystallization from methanol. [i]Recovered catalyst used (>99% ee; recovered from entry 14). [j]No inversion of the stereocenter, product is *S*-configured due to higher priority of the exocyclic acyl fragment compared to the endocyclic one in this particular case.[88]

At first, substrate **142a** with R^1, R^2 = Ph was tested at 0 °C in TAA in the presence of 1 mol% of **Λ-T18'** (entry 1). Only 50% conversion and 30% ee were found for product **143a** after 18 h. However, when with substrate **142b** residue R^1 = Ph was replaced by R^1 = Me, full conversion was found after just 10 h under identical conditions and corresponding product **143b** could be isolated in 91% ee (entry 2). Next, migrating acyl group R^2 = Ph was replaced with substrate **142c** by R^2 = Bn (entry 3) and with substrate **142d** by R^2 = *i*-Pr (entry 4). This modifications resulted in a decreased selectivity for both products, for product **143c** 80% ee were found and for product **143d** 82% ee. Moreover, in case of substrate **142d** a higher catalyst loading of 2 mol% was necessary to achieve full conversion within 48 h. Substrate **142e** with R^1 = Bn and R^2 = $C(CH_3)_2CCl_3$ provided product **143e** in 89% ee (entry 5).

For **142b**, being the best performing substrate so far, the temperature was now lowered to −15 °C, the solvent switched from TAA to TAA/CPME 2:1, and the reaction time increased to 48 h. This pushed the ee for product **143b** to 92% (entry 6). Under these conditions,

substrates **142f** with R^1 = *i*-Bu (entry 7) and **142g** with R^1 = Bn (entry 8) were tested as well, which provided products **143f** and **143g** with 90% ee and 91% ee, respectively. Next, the temperature was further lowered from −15 °C to −30 °C under otherwise identical reaction conditions. This improved the selectivity for product **143b** from 92% ee to 94% ee (entry 9). With enantiomeric catalyst **Δ-T18'**, substrate **142b** provided product ***ent*-143b** also in 94% ee as expected (entry 10; inverted *R*/*S* ratio). Under identical reaction conditions, two substrates with different acyl groups R^2 were tested: While substrate **142h** with small R^2 = Me provided product **143h** with only moderate 70% ee (entry 11), substrate **142i** with bulky R^2 = $C(CH_3)_2CCl_3$ provided product **143i** with 93% ee (entry 12) and hence with virtually the same selectivity as product **143b** (compare with entries 9 and 10). **142b** and **142i** were exemplarily used as substrates in two scaled-up reactions: substrate **142i** (0.72 mmol; entry 13) provided product **143i** with identical and substrate **142b** (3.1 mmol; entry 14) product **143b** with slightly diminished enantioselectivity compared to the standard scale examples (compare with entries 9 and 12). Noteworthy, the ee of product **143b** from the scaled-up reaction (entry 14) could be pushed to 98% by one round of recrystallization from methanol while maintaining an acceptable yield of 73% (details in the experimental section). Importantly, catalyst **Λ-T18'** could be recovered from this scaled-up experiment (entry 14) in 94% yield with >99% ee (procedure and details in the experimental section) and was then used again in a standard scale reaction with substrate **142b**, which virtually provided the same result as freshly prepared catalyst **Λ-T18'** (93% ee for **143b**, entry 15).

Just like the Steglich rearrangements from Table 10 (chapter 2.3.2), all Black rearrangements from Table 13 were set up under normal atmosphere without any special precautions against moisture and oxygen.

It is worth noting that basically all Black rearrangement products **143** from Table 13 could be isolated in virtually quantitative yields (93−99% yield) apart from product **143a**.

The *C*-acylated benzofuranones (**143**) which were synthesized with Λ-configured catalyst **Λ-T18'** were unambiguously assigned as *R*-configured, except from products **143e** and **143i**, which are *S*-configured due to the higher priority of their exocyclic acyl groups compared to their endocyclic acyl groups.[88] Stereochemical assignment details for the *C*-acylated benzofuranones (**143**) are provided in the experimental section of this work. With respect to that, an X-ray structure of enantiomer **(*S*)-143i** could be obtained from the batch of product **143i** from Table 13, entry 13 (93% ee), which is depicted in Figure 19. Apart from optical rotation data, this X-ray structure served to assign the absolute configuration of products **143**.

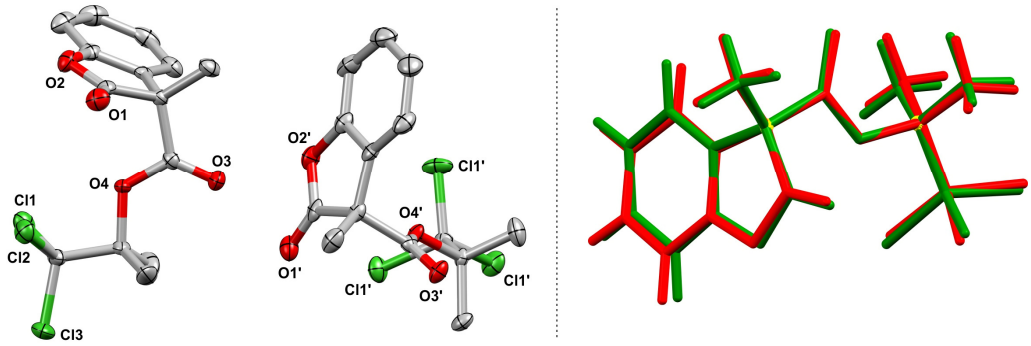

Figure 19. *Left:* Structure of both symmetry-independent molecules **(*S*)-143i** in the asymmetric unit with 60% probability of thermal ellipsoids.[85] *Right*: Molecular overlay of the two symmetry-independent molecules.

It is apparent that some substrates from Table 13 are not shown for temperatures lower than 0 °C (**142a,c,d,e**) or lower than −15 °C (**142f,g**). The reasons for that are as follows:
In case of **142a** and **142d**, it would have been necessary to significantly increase the catalyst loading to achieve full conversion within 48 h or to use significantly longer reaction times. In case of **142c**, a reaction had been performed at −30 °C which had reached ~80−90% conversion after 48 h and full conversion after 72 h. But unexpectedly, **143c** was provided there with a decreased selectivity of 77% ee compared to the 80% ee (Table 13, entry 3) which had been obtained at 0 °C (solvent: TAA/CPME 2:1, conc = 0.2 M of **142c**, 1 mol% **Λ-T18'**). In case of **142f** and **142g**, it would have been again necessary to increase the catalyst loading to achieve full conversion within 48 h at −30 °C or to use significantly longer reaction times. And in case of substrate **142e**, lower temperatures were not evaluated as **142e** had simply been prepared at the end of the project to have with product **143e** a product with a known specific rotation in conjunction with a reliably determined absolute configuration.[22b]

2.3.4 Intermolecular *C*-Acylation of Silyl Ketene Acetals

Next, the asymmetric intermolecular *C*-acylation of silyl ketene acetals (**145**) with different anhydrides (**144**) was investigated.[89] For this reason, four silyl ketene acetals **145a–d** were prepared at first (Scheme 33).

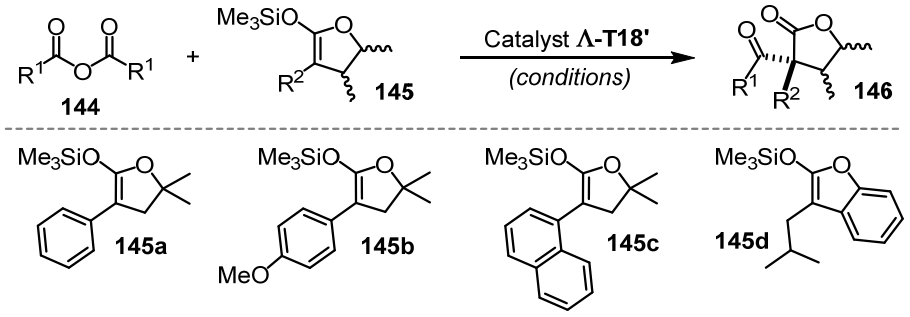

Scheme 33. Intermolecular *C*-acylation of silyl ketene acetals (**145**) with different anhydrides (**144**) as acylating agents and **Λ-T18'** as catalyst.

Next, **145a–d** were screened under different conditions and with different anhydrides (**144a−d**) with **Λ-T18'** as catalyst. The conditions and results of this screening are summarized in Table 14.

Table 14. Screening of silyl ketene acetals **145a–d** with anhydrides **144a–d** and **Λ-T18'** as catalyst.

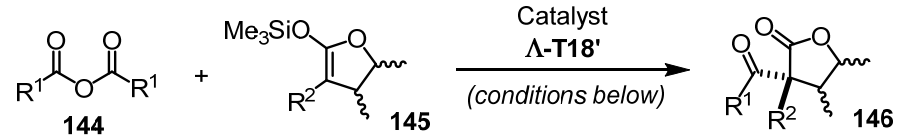

entry	silyl ketene acetal (**145**)	anhydride (**144**) (R^1)	eq of **144**	**Λ-T18'** (mol%)	solvent	conc (mM)	*t* (°C)	time (h)	yield (%)[a]	ee **146** (%)[a]
1	**145a**	R^1 = Me (**144a**)	1.3	3	CH_2Cl_2	80	rt	36	91	17 (**146aa**)
2	**145b**	R^1 = Me (**144a**)	1.2	3	CH_2Cl_2	80	rt	36	88	29 (**146ba**)
3	**145c**	R^1 = Me (**144a**)	1.4	3	CH_2Cl_2	80	rt	36	95	18 (**146ca**)
4	**145b**	R^1 = Me (**144a**)	1.2	3	THF	80	rt	36	85	< 5 (**146ba**)
5	**145b**	R^1 = Me (**144a**)	1.2	3	toluene	80	rt	36	44[b]	6 (**146ba**)
6	**145b**	R^1 = Ph (**144b**)	1.3	3	CH_2Cl_2	80	rt	46	88	27 (**146bb**)
7	**145b**	R^1 = *i*-Pr (**144c**)	1.3	3	CH_2Cl_2	80	rt	46	88	16 (**146bc**)
8	**145b**	R^1 = Bn (**144d**)	1.3	3	CH_2Cl_2	80	rt	46	48[c]	< 5[c] (**146bd**)
9	**145d**	R^1 = Me (**144a**)	1.2	3	CH_2Cl_2	80	rt	43	37[d]	66 (**146da**)

[a]Isolated yields; enantioselectivities determined from isolated products by chiral HPLC analysis. [b]Reason for low yield not further investigated. [c]Significant side-product formation observed (possibly due to the enolizability of anhydride **144d**). [d]Low yield could be traced back to incomplete conversion of substrate **145d** (isolated product contained ~30% of the hydrolysis product of silyl ketene acetal **145d**).

First, silyl ketene acetals **145a–c** were screened with 3 mol% of **Λ-T18'** at rt in CH_2Cl_2 as solvent at conc = 80 mM and with acetic anhydride (**144a**) as acylating agent (Table 14, entries 1–3). These conditions as well as substrates **145a–c** were inspired by a previous work from Fu and co-workers dealing with the reaction **144** + **145** → **146**.[89] After a reaction time of 36 h, products **146aa**, **146ba**, and **146ca** were isolated in promising yields of 88–95%

(entries 1–3). However, the enantioselectivities were low and the best selectivity was provided for product **146ba** with 29% ee (entry 2).

In order to test whether other solvents would be able to improve the selectivity, THF and toluene were evaluated as solvents with **145b** as substrate (entries 4 and 5). Although the reaction in THF provided product **146ba** with 85% yield, **146ba** was virtually obtained racemic with < 5% ee (entry 4). A similar result in terms of selectivity was obtained with toluene as solvent, which provided **146ba** with 6% ee (entry 5).

So far, only acetic anhydride (**144a**) had been employed as acylation agent (entries 1–5). For this reason, benzoic anhydride (**144b**, entry 6), isobutyric anhydride (**144c**, entry 7), and phenylacetic anhydride (**144d**, entry 8) were evaluated with **145b** as substrate. Although desired products **146bb**, **146bc**, and **146bd** were formed and could be isolated, the enantioselectivity could not be improved (entries 6–8).

Finally, benzofuranone-based silyl ketene acetal **145d** was evaluated (entry 9). Synthesis and evaluation of **145d** were inspired by the good results which had previously been obtained with the Black rearrangement of *O*-acylated benzofuranones (**142** → **143**; see chapter 2.3.3, Table 13) and there in particular with Me-substituted **142b**. And indeed, benzofuranone-based silyl ketene acetal **145d**, whose structure significantly differs from the structures of the other silyl ketene acetals **145a–c**, provided desired product **146da** with encouraging 66% ee (entry 9). Although this final result was promising, experiments with silyl ketene acetals (**145**) were discontinued at this point.

In summary, the screening from Table 14 indicates that **Λ-T18'** might be a suitable catalyst for the reaction **144** + **145** → **146** provided that further steps are taken: Although substrates **145a–c** did not match catalyst **Λ-T18'** in terms of enantioinduction (entries 1–8), benzofuranone-based silyl ketene acetal **145d** gave, in contrast, product **146da** with encouraging 66% ee under non-optimized conditions (entry 9). Accordingly, silyl ketene acetals which are structurally similar to **145d** seem to have, in combination with additional conditions screenings, a good chance to result in a highly enantioselective transformation **144** + **145** → **146** with **Λ-T18'** as catalyst.

2.3.5 Steglich-Type Rearrangements of *O*-Acylated Oxindoles

Once again, attention was turned to asymmetric intramolecular $O \rightarrow C$ acyl migration reactions (see chapters 2.3.2 and 2.3.3), now to Steglich-type rearrangements of *O*-acylated oxindoles to chiral *C*-acylated oxindoles. For this purpose, substrates **147a–b**,[90] **149a–b**,[23f] and **151**[22b] were prepared (Scheme 34). These substrates differ structurally from the benzofuranone substrates from chapter 2.3.3 (**142**) by the fact that their benzofused heteroaromatic 5-membered ring contains a substituted nitrogen atom instead of an oxygen atom.

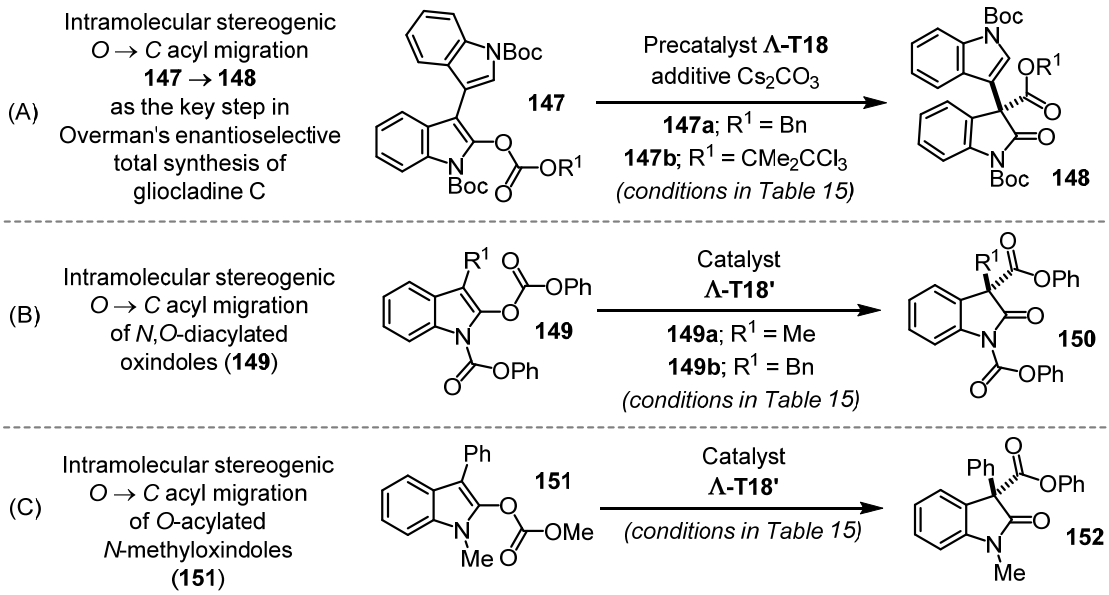

Scheme 34. *O*-Acylated oxindoles as substrates for Steglich-type rearrangements to their chiral *C*-acylated analogues with precatalyst **Λ-T18** / catalyst **Λ-T18'**: (A) Gliocladine C precursors **147a–b**,[90] (B) *N,O*-diacylated oxindoles **149a–b**,[23f] (C) *O*-acylated *N*-methyloxindole **151**.[22b]

Next, the reactions depicted in Scheme 34 were screened with catalyst **Λ-T18'** / precatalyst **Λ-T18**. The conditions and the results of this screening are summarized in Table 15.

Table 15. Screening of *O*-acylated oxindole substrates **147a–b**, **149 a–b**, and **151** with precatalyst **Λ-T18** and addititve Cs_2CO_3 (substrates **147a–b**) *or* catalyst **Λ-T18'** (substrates **149a–b** and **151**).

entry	substrate	complex	complex loading (mol%)	Cs_2CO_3 (mol%)	solvent	conc (M)	*t* (°C)	time (h)	yield (%)[a]	ee product (%)[a]	conv[b]
1	**147a**	**Λ-T18**	0.5	3	EtOAc	0.5	0	18	–	–	no conv
2	**147b**	**Λ-T18**	0.5	3	EtOAc	0.5	0	18	–	–	no conv
3	**147a**	**Λ-T18**	0.5	3	EtOAc	0.5	50	72	n.d.	n.d.	trace[c]
4	**147b**	**Λ-T18**	0.5	3	EtOAc	0.5	50	72	n.d.	n.d.	trace[c]
5	**147b**	**Λ-T18**	5	15	THF	0.5	40	48	–	n.d.	< 50%[c]
								130	16[c]	28 (**148b**)	full[c]
6	**149a**	**Λ-T18'**	2	–	THF	0.4	rt	12	–	n.d.	80–90%
								48	98	< 5 (**150a**)	full
7	**149b**	**Λ-T18'**	2	–	THF	0.4	rt	12	–	n.d.	~50%
								48	96	59 (**150b**)	full
8	**151**	**Λ-T18'**	5	–	CH_2Cl_2	0.5	35	11	n.d.	< 5[d] (**152**)	full

[a]Isolated yields; enantioselectivities determined from isolated products by chiral HPLC analysis. [b]Determined by a combination of TLC and HPLC analysis. [c]Formation of large amounts of side-products. [d]Determined from crude mixture, product not isolated.

As a start, *O*-acylated *N*-Boc-protected oxindoles **147a–b** were tested (Table 15, entries 1–5) from which **147b** serves as substrate of the stereogenic key step **147b → 148b** in Overman's enantioselective total synthesis of (+)-gliocladine C.[90] Most likely, substrate **147a** could also be used for this purpose.[90] With 0.5 mol% of precatalyst **Λ-T18** in the presence of 3 mol% Cs_2CO_3 at conc = 0.5 M and at rt, no conversion was found in case of both substrates after 18 h (entries 1 and 2). Consequently, the temperature was then increased to 50 °C (entries 3 and 4). After 72 h at 50 °C, trace amounts of products **148a** and **148b** were found but also considerable amounts of side products. A final experiment was performed with substrate **147b** with a 10-fold increased loading of **Λ-T18** and a 5-fold increased loading of Cs_2CO_3, a slightly decreased temperature of 40 °C with the intention to reduce side product formation, and with THF as solvent (entry 5). However, after 48 h there was < 50% conversion and a considerable amount of side products. After a total reaction time of 130 h, the reaction had reached full conversion but desired **148b** could only be isolated in low 16% yield and with 28% ee.

Next, *N*,*O*-diacylated oxindoles **149a–b** were screened (entries 6 and 7). With 2 mol% of catalyst **Λ-T18'** in THF at conc = 0.4 M and at rt, about 80–90% conversion was found in case of **149a** after 12 h and full conversion after 48 h. *N*,*C*-diacylated product **150a** could be isolated in excellent 98% yield but was basically racemic with < 5% ee (entry 6). With low expectations, substrate **149b** was tested under the same conditions. In this case, about 50% conversion was found after 12 h and full conversion after 48 h. Product **150b** could be isolated in excellent 96% yield and, contrary to the expectations, with encouraging 59% ee (entry 7).

Finally, *O*-acylated *N*-methyloxindole **151** was tested with 5 mol% of catalyst **Λ-T18'** in CH_2Cl_2 at conc = 0.5 M and at a temperature of 35 °C (entry 8). Full and clean conversion was found here after 11 h. However, chiral HPLC analysis of the crude product mixture indicated a virtually racemic conversion with < 5% ee for product **152**. As a result, no efforts were made to isolate **152**.

At that point, all experiments with asymmetric intramolecular acyl migrations were stopped as highly promising results with ketenes as substrates were obtained at the same time, which were given a higher priority (see chapters 2.3.6 and 2.3.7).

The results from Table 15 were interpreted as follows:

- Gliocladine C precursors **147a–b** are no suitable substrates for **Λ-T18'** (entries 1–5). The synthetic protocol from Overman and co-workers yet indicates that substrates **147a–b** intrinsically require a comparatively high catalyst loading.[90] However, the extraordinarily

low activity of substrates **147a–b** in the presence of catalyst **Λ-T18'** hints at a deeper lying problem: Modeling with **Λ-T18'** suggests that the enolates which are formed in the course of the reaction **147** → **148** (see chapter 2.3.8, Figure 23) are hardly able to attack the *N*-acylated catalysis intermediates due to steric clashes with **Λ-T18'** 's expanded framework, which manifests in a highly sluggish reaction.

- In case of *N*,*O*-diacylated oxindoles **149a–b**, the experiment with **149a** was less promising (entry 6) as product **150a** was provided almost racemic (< 5% ee). In contrast, substrate **149b** provided **150b** in encouraging 59% ee. Given that just 2 mol% of **Λ-T18'** were used and that **150b** was isolated in 96% yield, there seems to be a realistic chance that reaction **149** → **150** can be developed into a highly enantioselective reaction with **Λ-T18'** as catalyst by the evaluation of more *N*,*O*-diacylated oxindoles (**149**) and a systematic reaction conditions screening and optimization.
- The result for *O*-acylated *N*-methyloxindole **151** is not promising for further experiments as < 5% ee were found for product **152** (entry 8). However, it should be considered that phenyl-substituted **151** is structurally very similar to phenyl-substituted benzofuranone substrate **142a**, which was clearly identified as a "mismatched" substrate for catalyst **Λ-T18'** (see chapter 2.3.3, Table 13, entry 1). In order to draw a final conclusion here, more experiments should be performed with *O*-acylated *N*-methyloxindoles (**151**) which bear *aliphatic* substituents at their 3-positions.

2.3.6 Asymmetric Reactions with Aryl Alkyl Ketenes as Substrates

Having demonstrated that stereogenic-only-at-metal catalyst **Λ/Δ-T18'** is capable of catalyzing asymmetric acyl transfer reactions (chapters 2.3.2–2.3.5) and this partly with very high and competitive levels of activity and selectivity, as demonstrated for the Steglich rearrangement of *O*-acylated azlactones (see chapter 2.3.2) and for the related Black rearrangement of *O*-acylated benzofuranones (see chapter 2.3.3), it was now investigated whether **Λ/Δ-T18'** would be a suitable catalyst for a different type of asymmetric reaction. And so, the focus was shifted on asymmetric nucleophile-catalyzed reactions between aryl alkyl ketenes (**153**) and various reaction partners (Scheme 35).

At this point, it is worth mentioning that all reactions with aryl alkyl ketenes (**153**) were, in contrast to the acyl transfer reactions from chapters 2.3.1–2.3.5, performed under strict exclusion of moisture and oxygen due to the sensitive nature of ketenes.[91,92]

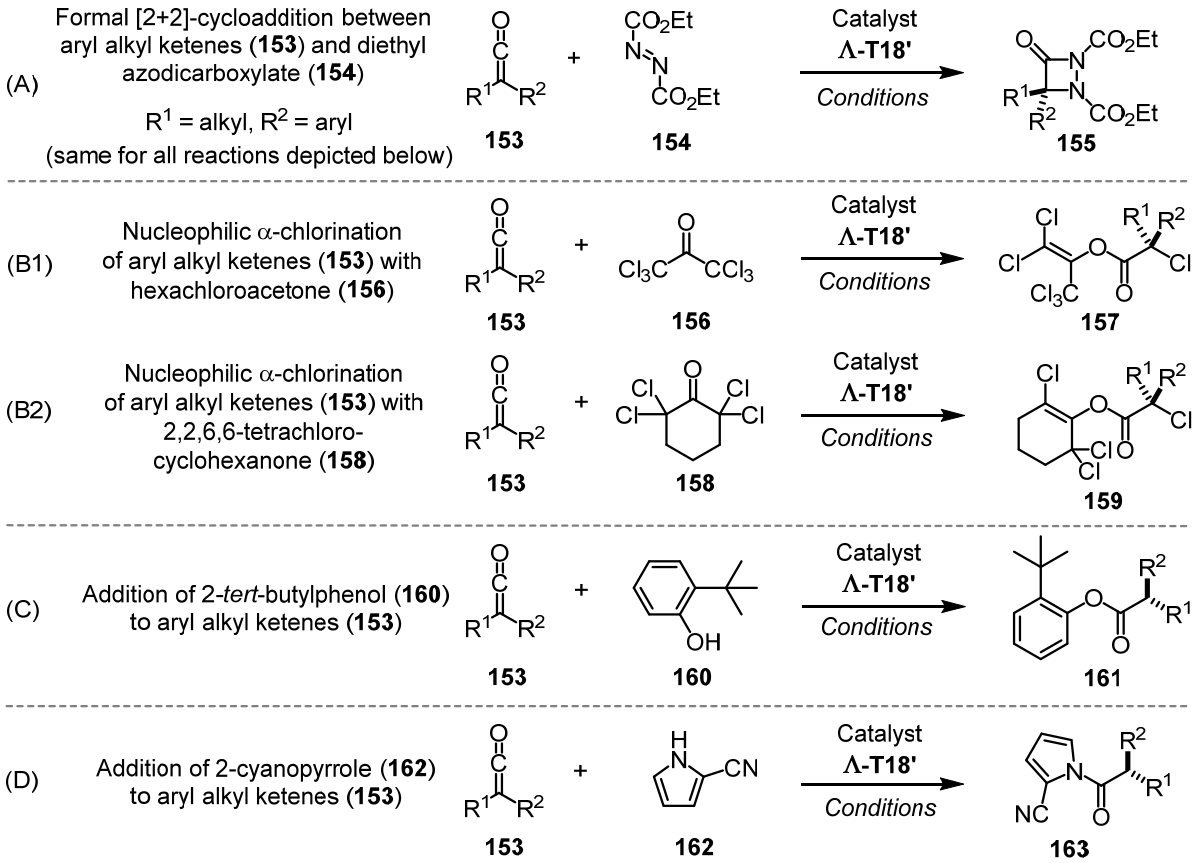

Scheme 35. Investigation of different reactions between aryl alkyl ketenes (**153**) and various reaction partners with **Λ-T18'** as scheduled catalyst: (A) Formal [2+2]-cycloaddition between aryl alkyl ketenes (**153**) and diethyl azodicarboxylate (**154**);[26j] (B) Nucleophilic *α*-chlorination of aryl alkyl ketenes (**153**) with (B1) hexachloroacetone (**156**) and (B2) 2,2,6,6-tetrachlorocyclohexanone (**158**) as chlorinating agents;[26h,27c] (C) Addition of 2-*tert*-butylphenol (**160**) to aryl alkyl ketenes (**153**);[26e] (D) Addition of 2-cyanopyrrole (**162**) to aryl alkyl ketenes (**153**).[26c]

Because of the somewhat laborious synthesis of pure aryl alkyl ketenes (**153**)[91] and their limited shelf life,[91,92] the reactions from Scheme 35 were at first only investigated with one

single probe ketene, namely with phenyl ethyl ketene (**153a** with R^1 = Ph, R^2 = Et). The conditions and the results of the reaction screening are summarized in Table 16.

Table 16. Reaction screening with phenyl ethyl ketene (**153a**) and **Λ-T18'**.

entry	ketene (identifier)	reaction partner	eq reaction partner	**Λ-T18'** (mol%)	solvent	conc (mM)	*t* (°C)	time (h)	yield (%)[a]	ee (product) (%)[a]	conv[b]
1	**153a** (A)	**154**	1.07	3	CH_2Cl_2	14	rt	6	–[c]	n.d.	full[c]
								25	12[c]	64 (**155a**)	full[c]
2	**153a** (B1)	**156**	1.20	3	toluene	17	–78	1	94	9 (**157a**)	full
3	**153a** (B2)	**158**	1.20	3	toluene	18	–78	1	–[d]	–	–[d]
4	**153a** (B2)	**158**	1.20	3	toluene	18	–30	37	–[d]	–	–[d]
							rt	85	–[d]	–	–[d]
5	**153a** (C)	**160**	1.04	3	toluene	12	rt	2.5	63	13 (**161a**)	full
6	**153a** (D)	**162**	2.00	2	toluene	12	rt	5.5	92	86 (**163a**)	full

[a]Isolated yields; enantioselectivities determined from isolated products by chiral HPLC analysis. [b]Determined by a combination of TLC and HPLC analysis. [c]Formation of one major side product observed. [d]Ketene **153a** consumed but reaction partner **158** unconsumed, no formation of product **159** observed.

At first, the formal [2+2]-cycloaddition between aryl alkyl ketenes (**153**) and diethyl azodicarboxylate (**154**; DEAD) was investigated (Scheme 35, A).[26j] This reaction was investigated at first for the following reason: According to the experimental records of former PhD student Xiaodong Shen, phenyl ethyl ketene (**153a**) reacted with DEAD (**154**) in the presence of complex **Λ-X2** (see chapter 2.2.2, Figure 11) and base additive Et_3N to desired cycloproduct **155a** with 45% ee under the following conditions: 3 mol% **Λ-X2**; 3 mol% Et_3N; solvent: CH_2Cl_2; conc = 50 mM; *t* = rt; reaction time: 2.5 h.[76] However, **155a**'s enantiomeric excess had only been determined from the crude product mixture and neither had the conversion been determined nor had product **155a** been isolated.[76] And so, the same reaction was performed with 3 mol% of catalyst **Λ-T18'** and 1.07 eq of DEAD (**154**) at conc = 14 mM at rt in CH_2Cl_2 (Table 16, entry 1). Full conversion was found after 6 h. However, TLC analysis indicated that **155a** had not been formed as major product but another unidentified side-product (*remark*: the crude product mixture was compared with an authentic racemic sample of **155a**). The reaction was left running for a total of 25 h, which caused no alteration of the TLC pattern and desired cycloaddition product **155a** was eventually isolated in 12% yield with 64% ee. Noteworthy, an additional experiment was performed at –25 °C (data not included in Table 16), but also this modification was not able to suppress the formation of the undesired side-product, which was not characterized.

Next, the nucleophilic *α*-chlorination of aryl alkyl ketenes (**153**) with hexachloroacetone (**156**) and 2,2,6,6-tetrachlorocyclohexanone (**158**) as chlorinating agents was investigated (Scheme 35, B1 and B2).[26h,27c] With 3 mol% of catalyst **Λ-T18'**, 1.20 eq of **156**, conc = 17 mM, a reaction temperature of –78 °C, and toluene as solvent, phenyl ethyl ketene

(**153a**) provided desired product **157a** after a reaction time of 1 h in excellent 94% yield but only with 9% ee. (entry 2). Assuming that 2,2,6,6-tetrachlorocyclohexanone (**158**) would give a better result,[26h] phenyl ethyl ketene (**153a**) was subjected to the same reaction conditions but with **158** as chlorinating agent (entry 3). In this case, no formation of desired **159a** was indicated after 1 h (*remark*: the crude product mixture was compared with an authentic racemic sample of **159a**). As this was an unexpected result,[26h] the reaction was repeated under the same conditions but with an increased temperature of –30 °C (entry 4). Again, no indication for any formation of **159a** was found after 37 h reaction at –30 °C, which did not change when the mixture was left stirring for another 48 h at rt (entry 4).

Finally, the asymmetric addition of 2-*tert*-butylphenol (**160**) to aryl alkyl ketenes (**153**) giving *α*-chiral esters (**161**) (Scheme 35, C)[26e] and the asymmetric addition of 2-cyanopyrrole (**162**) to aryl alkyl ketenes (**153**) giving *α*-chiral amides (**163**; Scheme 35, D)[26c] were investigated.

With 3 mol% of catalyst **Λ-T18'**, 1.04 eq 2-*tert*-butylphenol (**160**), conc = 12 mM, toluene as solvent, rt as temperature, and a reaction time of 2.5 h, *α*-chiral ester **161a** could be isolated in promising 63% yield but with disappointing 13% ee (entry 5).

In contrast, with 3 mol% of catalyst **Λ-T18'**, 2.00 eq 2-cyanopyrrole (**162**), conc = 12 mM, toluene as solvent, rt as temperature, and a reaction time of 5.5 h, *α*-chiral amide **163a** could be isolated in highly encouraging 92% yield with 86% ee (entry 6).

Since the reaction between phenyl ethyl ketene (**153a**) and 2-cyanopyrrole (**162**) was the most promising one from all the reactions from Scheme 35 and Table 16 by far, it was decided to focus deeper on that reaction (see chapter 2.3.7).

It is worth noting that also other NH-heterocycles than 2-cyanopyrrole (**162**) were tested as reaction partners for **153a** under the conditions from Table 16, entry 6: namely 2-acetyl-pyrrole, pyrrole, indole, and carbazole.[26c] In case of all these NH-heterocycles, only traces of the according amides were found after 2 d reaction time. And so it was decided to stay with 2-cyanopyrrole (**162**) as reaction partner.

2.3.7 Asymmetric Addition of 2-Cyanopyrrole to Aryl Alkyl Ketenes

The asymmetric addition of 2-cyanopyrrole (**162**) to aryl alkyl ketenes (**153**) giving *α*-chiral amides (**163**) had proven a match for catalyst **Λ-T18'** (chapter 2.3.6): In a first non-optimized attempt, *α*-chiral amide **163a** had been obtained with 2 mol% of **Λ-T18'** from phenyl ethyl ketene (**153a**) and 2-cyanopyrrole (**162**) in encouraging 92% yield with 86% ee (see chapter 2.3.6, Table 16, entry 6).

On these grounds, it was decided to further focus on this reaction. First, a solvent screening was performed, the results of this screening are summarized in Table 17.

Table 17. Reaction conditions screening for the reaction **153a + 162 → 163a** with **Λ-T18'**.

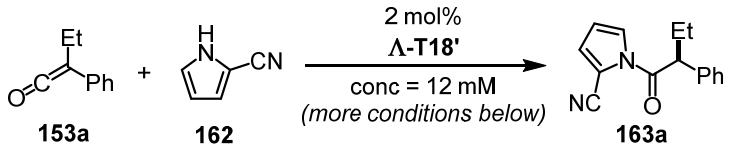

153a **162** **163a**

entry	*t* (°C)	solvent	time (h)	conv[a] (%)	crude ee[b] (%)	yield (%)	isolated ee[b] (%)
1	25	THF	18	full	69	n.d.	n.d.
2	25	Et_2O	18	full	84	93	86
3	25	CH_2Cl_2	18	≤ 10	59	n.d.	n.d.
4	25	MeCN	6.5	≤ 50	30	n.d.	n.d.
5	25	1,4-dioxane	17	full	81	83	81
6	25	EtOAc	24	full	80	n.d.	n.d.
7	25	*m*-xylene	15	full	87	99	86
8	25	C_6H_5Cl	15	full	82	n.d.	n.d.
9	25	CPME	14	full	86	86	86
10	25	DME	20	full	76	n.d.	n.d.
11	25	*o*-xylene	19	full	86	88	86
12	25	MTBE	14	full	86	93	87
13	25	toluene	5.5	full	86	92	86

[a]Estimated from TLC analysis. [b]Enantioselectivities determined by chiral HPLC analysis.

Based on the solvent screening from Table 17, toluene and MTBE were chosen as solvents of choice (entries 12 and 13) although other solvents had given comparable yields and enantio-selectivities (e.g., Et_2O, *m*-xylene, CPME, and *o*-xylene). For this decision, additional factors were taken into consideration, such as 1.) permanent availability, e.g., perfectly anhydrous, pure toluene was permanently available from a solvent still, and 2.) ease of use, e.g., for the reaction **153 + 162 → 163** the required ketenes (**153**) are slowly added as diluted solutions via a microliter syringe – Et_2O with its high vapor pressure, its low boiling point, and its low viscosity would have been less suitable for practical reasons.

Next, two additional ketenes, *o*-tolyl ethyl ketene (**153b**) and phenyl isopropyl ketene (**153c**), were prepared and screened with toluene and MTBE as solvents. These reactions were performed at both rt and 0 °C. The results of this screening are summarized in Table 18.

Table 18. Reaction conditions screening with ketenes **153a**, **153b**, and **153c**.

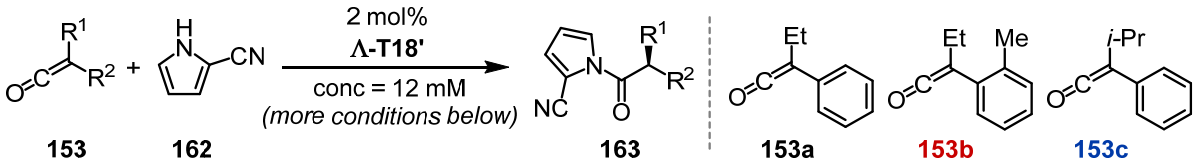

entry	ketene	*t* (°C)	solvent	time (h)	conv[a] (%)	yield (%)	isolated ee[b] (%)	product
1[c]	**153a**	rt	MTBE	14	full	93	87	**163a**
2[c]	**153a**	rt	toluene	5.5	full	92	86	**163a**
3	**153b**	rt	MTBE	18	full	98	83	**163b**
4	**153b**	rt	toluene	20	full	98	80	**163b**
5	**153c**	rt	MTBE	18	full	99	90	**163c**
6	**153c**	rt	toluene	19	full	99	91	**163c**
7	**153a**	0	MTBE	48	full	96	89	**163a**
8	**153b**	0	MTBE	48	full	99	84	**163b**
9	**153c**	0	toluene	48	full	99	93	**163c**

[a]Indicated by TLC analysis. [b]Enantioselectivities determined by chiral HPLC analysis. [c]Results copied from Table 17 for comparison and clarity.

The results from Table 18 were interpreted as follows:

Entries 1–6 indicated that MTBE was a slightly better solvent for unbranched ketenes such as **153a** and **153b** and that toluene was a slightly better one for branched ketenes such as **153c**. Admittedly, the differences are small and in consideration of the few results this could be a random result or limited to those three substrates. However, due to the lack of time for further investigations it was decided to generally use MTBE as solvent for unbranched ketenes and toluene as solvent for branched ketenes.

Moreover, it was investigated whether the enantioselectivities could be improved by a reduction of the temperature to 0 °C (entries 7–9). And indeed, desired *N*-acyl pyrroles **163a–c** were provided at 0 °C within 48 h with improved enantioselectivities of 84–93% ee and still isolated in virtually quantitative yields of 96–99%.

Next, five additional ketenes **153d–h** were synthesized. All eight prepared ketene substrates **153a–h** including already mentioned **153a–c** are depicted in Figure 20.

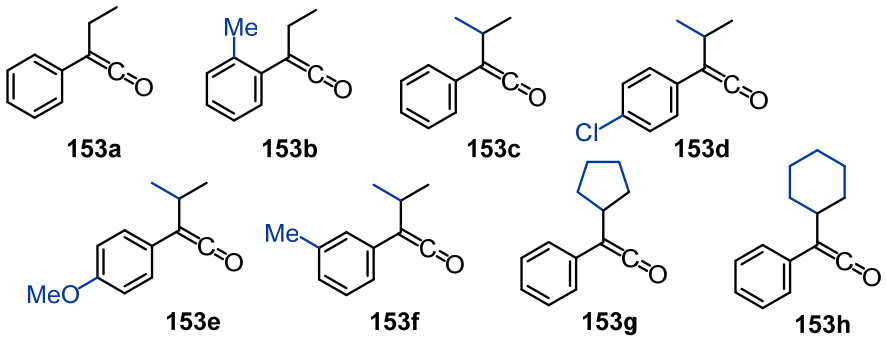

Figure 20. Aryl alkyl ketenes **153a–h** were prepared and used as substrates in the reaction **153** + **162** → **163** with **Λ-T18'** as catalyst (see Table 19). Modifications with respect to phenyl ethyl ketene (**153a**) are highlighted in blue.

Substrates **153a–h** were then screened as substrates with the optimized conditions from Table 18, entries 7–8. The results of these experiments are summarized in Table 19.

Table 19. Scope: asymmetric addition of 2-cyanopyrrole to aryl alkyl ketenes (**153** + **162** → **143**).[a]

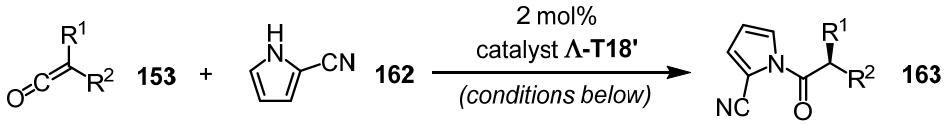

entry	R^1	R^2	yield (%)[b]	ee (%)[b]	product
1[c]	Et	Ph	96	89	**163a** (*S*)
2[c]	Et	*o*-Tol	99	84	**163b** (*S*)
3	*i*-Pr	Ph	99	93	**163c** (*S*)
4	*i*-Pr	*p*-Cl-Ph	99	90	**163d** (*S*)
5	*i*-Pr	*p*-OMe-Ph	99	91	**163e** (*S*)
6	*i*-Pr	*m*-Tol	99	95	**163f** (*S*)
7[d]	*i*-Pr	*m*-Tol	98	95	**163f** (*S*)
8	Cyclopentyl	Ph	99	93	**163g** (*S*)
9[d]	Cyclopentyl	Ph	99	93	**163g** (*S*)
10	Cyclohexyl	Ph	99	93	**163h** (*S*)

[a]Standard reaction conditions: ketene (**153**; 1.0 eq; 100−130 µmol) and 2-cyanopyrrole (**162**; 2.0 eq) with catalyst **Λ-T18'** (2 mol%) in toluene (conc = 12 mM) at 0 °C for 48 h. [b]Isolated yields; enantioselectivities determined from isolated products by chiral HPLC analysis. [c]Solvent: MTBE used instead of toluene. [d]Scaled-up reactions, entry 7: 194 mg (1.12 mmol) of ketene **153f**; entry 9: 209 mg (1.12 mmol) of ketene **153g**.

With phenyl ethyl ketene (**153a**) as substrate, *N*-acyl pyrrole **163a** was provided in 89% ee (Table 19, entry 1). Addition of a methyl group in the *ortho*-position of the ketene's phenyl ring (ketene **153b**) caused the ee to drop to 84% for product **163b** (entry 2). However, replacement of phenyl ethyl ketene (**153a**) by phenyl isopropyl ketene (**153c**) improved the ee of product **163c** to 93% (entry 3). Introduction of a chloro-substituent with ketene **153d** and a methoxy-substituent with ketene **153e** in the *para*-position of phenyl isopropyl ketene's phenyl ring provided corresponding products **163d** (entry 4) and **163e** (entry 5) with slightly diminished, but still high selectivity (90% ee for **163d** and 91% ee for **163e**). The highest selectivity was found for *m*-tolyl isopropyl ketene (**153f**) which yielded product **163f** in 95% ee (entry 6). Finally, phenyl isopropyl ketene's isopropyl group was replaced by a cyclopentyl group (**153g**; entry 8) and a cyclohexyl group (**153h**; entry 10). In both cases, corresponding products **163g** and **163h** were obtained in 93% ee.

Exemplarily, two reactions with ketenes **153f** and **153g** were scaled up by a factor of about ten (~1 mmol scale). Also in case of the scaled-up experiments, products **163f** and **163g** were obtained in excellent yields (98% and 99%) and with identical selectivities as in case of the corresponding standard scale experiments (entries 7 and 9, compare with entries 6 and 8).

Notably, all products from Table 19 (**163a–h**) could be obtained in virtually quantitative yields (96–99%). Absolute configurations of chiral *N*-acyl pyrroles **163d–h** were assigned as

S-configured by comparison of optical rotation values with literature values.[26c] Experimental details for the reactions **153** + **162** → **163** as well as stereochemistry assignment details for *N*-acyl pyrroles **163a–h** are provided in the experimental section.

It is worth noting that Fu and co-workers have demonstrated that *α*-chiral *N*-acyl pyrroles (**163**) are useful compounds from a synthetic point of view, as they can be easily converted into *α*-chiral acids, esters, amides, aldehydes, and alcohols.[26c] Taking this and the large number of nucleophilic catalysts reported to date into account, it was surprising to find that no other publication dealing with this transformation had been published when the presented experiments were performed.[93]

2.3.8 Mechanistic Experiments I: Steglich Rearrangement and Black Rearrangement

Now, attention was turned to the mechanisms of the established stereogenic intramolecular *O* → *C* acyl migration reactions with **Λ-T18'** as catalyst, that is to say the Steglich rearrangement of *O*-acylated azlactones from chapter 2.3.2 (**13** → **14**), the Black rearrangement of *O*-acylated benzofuranones from chapter 2.3.3 (**142** → **143**), and the Steglich-type rearrangements of *O*-acylated oxindoles from chapter 2.3.5 (**147** → **148**, **149** → **150**, **151** → **152**).

The objectives here were to experimentally proof the anticipated mechanisms and to attempt to rationally understand the catalyst's manner of enantioinduction. The latter was considered as important as the development of catalyst **Λ-T18'** had rather been the outcome of a systematic screening strategy than of a rational design strategy (see chapters 2.2, 2.3.1–2.3.7). It was envisioned – in case the catalyst's manner of enantioinduction could be put on a rational basis – that this might significantly simplify future improvements of catalyst **Λ-T18'** or even offer the possibility to custom tailor **Λ-T18'** or **Λ-T18'**-derived catalysts to specific substrates or vice versa – if applicable, also with the support of computational methods.

The proposed mechanism for the Black rearrangements **142** → **143** with **Λ-T18'** as catalyst is depicted in Scheme 36 using the example of substrate **142i**.[22b,86]

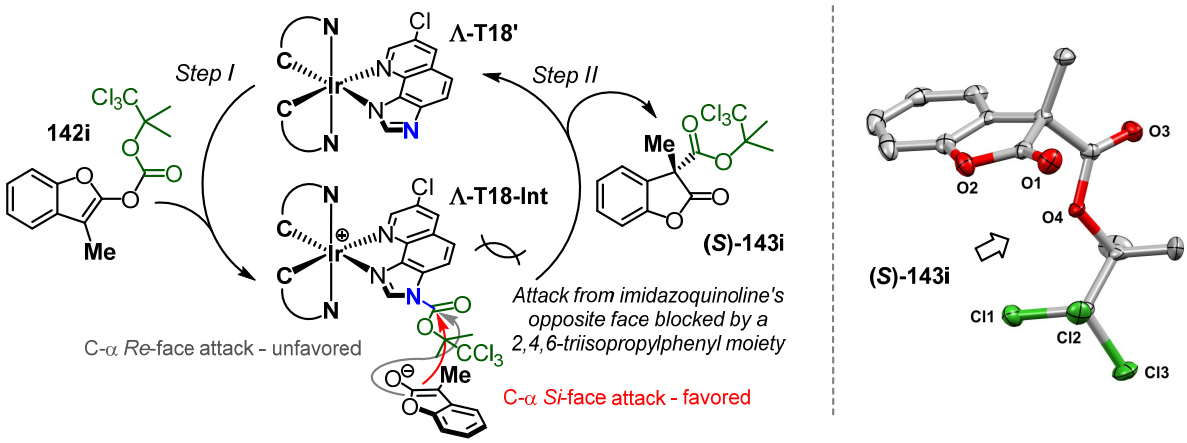

Scheme 36. *Left:* Proposed mechanism for Black rearrangements of *O*-acylated benzofuranones (**142** → **143**) with catalyst **Λ-T18'** using the example of substrate **142i**.[22b,86] The Steglich rearrangements of *O*-acylated azlactones (**13** → **14**) from chapter 2.3.2 (see Scheme 39) and the Steglich-type rearrangements of *O*-acylated oxindoles (**147** → **148**, **149** → **150**, **151** → **152**) from chapter 2.3.5 are supposed to follow an analogous mechanism. *Right:* Structure of **(*S*)-143i** from the crystal structure of a crystal which was grown from **143i** (batch with 93% ee; see chapter 2.3.3, Table 13, entry 13 and Figure 19 for details).[85] [Scheme on the left side reproduced and adapted with permission from ref. 84. Copyright © 2017, American Chemical Society]

At first, the imidazoquinoline ligand's nucleophilic nitrogen atom reacts with the carbonate group of substrate **142i**, which results in the formation of *N*-acylated intermediate **Λ-T18-Int**, which is a salt that consists of a +1 charged iridium(III) complex cation and its associated benzofuranone enolate counteranion (Scheme 36, Step I). In order to support the formation of

anticipated **Λ-T18-Int** experimentally, its analog ***rac*-T18-TfO** was prepared as shown in Scheme 37.

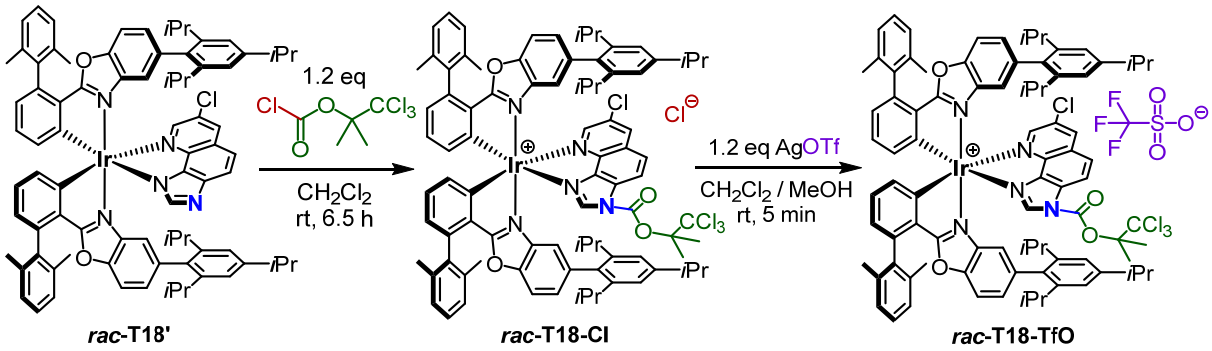

Scheme 37. Preparation of ***rac*-T18-Cl** and ***rac*-T18-TfO** from ***rac*-T18'** and 2,2,2-trichloro-1,1-dimethylethyl chloroformate and silver triflate. While all attempts failed to crystallize chloride salt ***rac*-T18-Cl**, triflate salt ***rac*-T18-TfO** could be readily crystallized and studied via XRD analysis (see Figure 21). Further experimental details are provided in the experimental section.

In this context, it is worth mentioning that ***rac*-T18'** was, in an additional experiment, quantitatively converted into **Λ-T18-Cl** within less than 10 min at rt when ***rac*-T18'** was mixed in an NMR tube with 3 eq of 2,2,2-trichloro-1,1-dimethylethyl chloroformate in CD_2Cl_2 (conc = 25 mM; further details are provided in the experimental section).

In **T18-TfO**, the reactive enolate counteranion of intermediate **T18-Int** is replaced by an inert triflate counteranion and accordingly **T18-TfO** serves as a catalysis intermediate analog for **T18-Int**. A crystal structure for ***rac*-T18-TfO** could be obtained, which allowed to deduce the three-dimensional structure of **Λ-T18-TfO**, which is depicted in Figure 21.

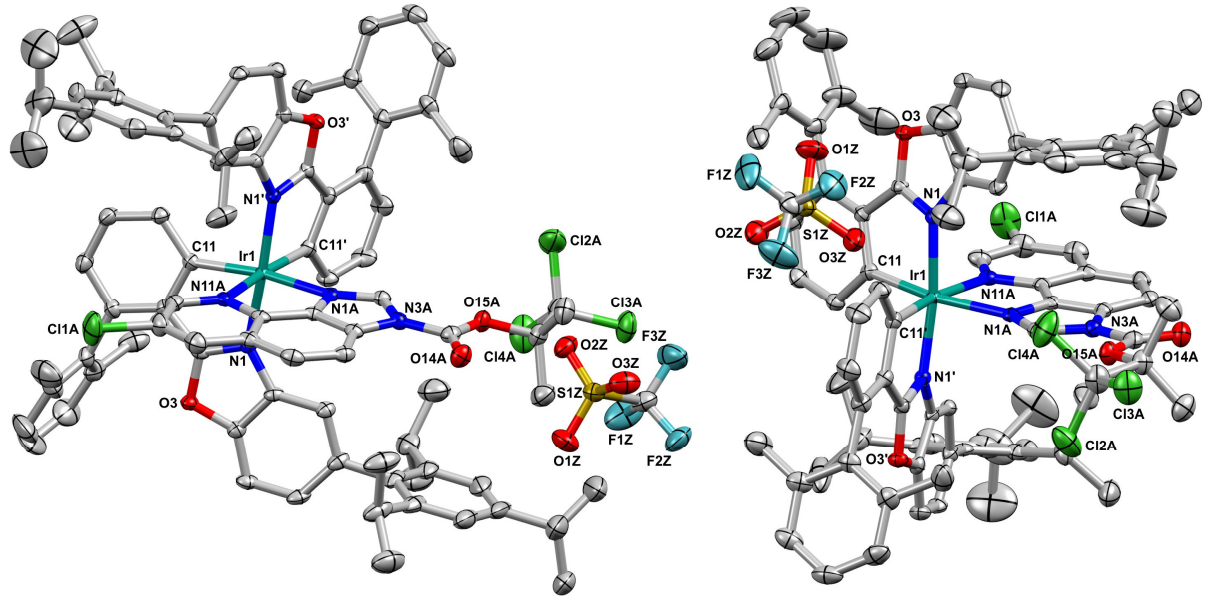

Figure 21. Three-dimensional structure of catalysis intermediate analog **Λ-T18-TfO** from two different perspectives, deduced from a crystal structure of ***rac*-T18-TfO**. Positional disorder and co-crystallized solvent molecules are omitted for clarity; 60% probability of thermal ellipsoids.[85] Detailed crystallographic data of ***rac*-T18-TfO** is provided in the experimental section.

Returning to Scheme 36, product **143i** is finally formed via nucleophilic attack of the reactive, nucleophilic benzofuranone enolate onto the *N*-acylated complex cation, which goes along with regeneration of catalyst **Λ-T18'** (Scheme 36, Step II). The stereochemical outcome of the reaction depends on with which of its prochiral faces the enolate approaches and reacts with the catalyst-bound acyl group. In this context, it is important to note that the enolate is only able to approach the acyl group from one of both imidazoquinoline faces as the opposite face is completely shielded by a bulky 2,4,6-triisopropylphenyl group (see Figure 21 and 23). In the case of Λ-configured catalyst **Λ-T18'**, the approach and reaction of the benzofuranone enolate with its *Si*-face oriented toward the catalyst-bound acyl group is obviously favored, leading to predominant formation of the *S*-enantiomer in case of product **143i** (Scheme 36).

One could expect that intermediates of type **Λ-T18-Int** interchange their electrostatically associated enolate counterions, which would lead to partial formation of scrambled products. Indeed, when a crossover experiment was performed with substrates **142g** and **142i**, scrambled products **143b** and **143e** were formed in addition to non-scrambled products **143g** and **143i** (Scheme 38; more details are provided in the experimental section).

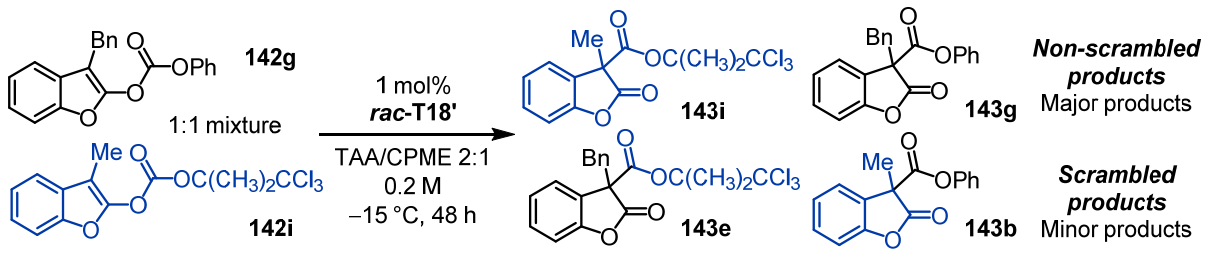

Scheme 38. Crossover experiment with *O*-acylated benzofuranones **142g** and **142i** with ***rac*-T18'** as catalyst. Non-scrambled and scrambled products were formed in a ratio of **143i**:**143g**:**143e**:**143b** of about 4.5:4.5:1:1 according to ^{1}H NMR analysis of the crude product mixture.

Additional evidence for the mechanism proposed in Scheme 36 is provided by the fact that protonated precatalyst **T18** is, in contrast to catalyst **T18'**, not catalytically active in absence of a Brønsted base (see chapter 2.3.2 for details) and that the *N*-methylated form of catalyst **T18'**, **T18-Me**, is not catalytically active at all – neither in the absence nor in the presence of a Brønsted base (details about the preparation of **T18-Me** and details about the experiments with **T18-Me** are provided in the experimental section).

The Steglich rearrangement of *O*-acylated azlactones from chapter 2.3.2 and the Steglich-type rearrangements of *O*-acylated oxindoles from chapter 2.3.5 are supposed to follow an analogous mechanism. The mechanism for the Steglich rearrangements from chapter 2.3.2 is depicted in Scheme 39 using the example of substrate **13e**.[22a,23h]

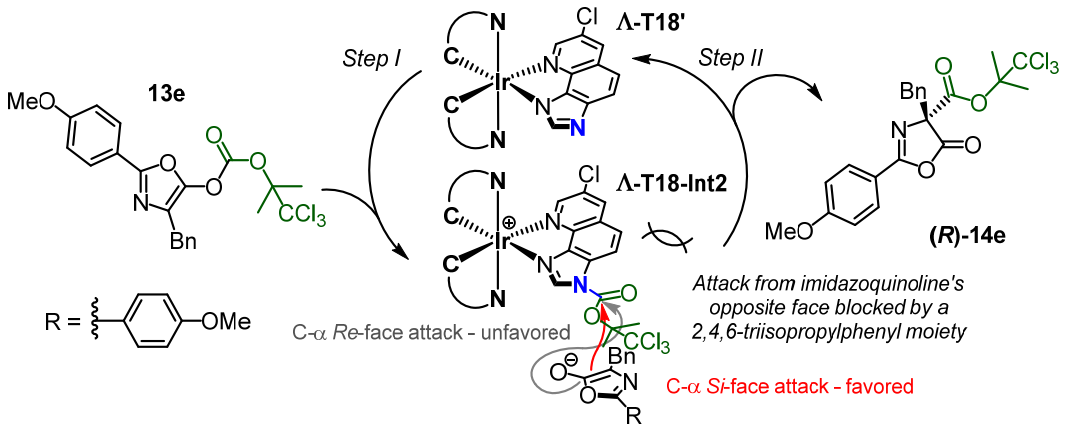

Scheme 39. Proposed mechanism for the Steglich rearrangement of *O*-acylated azlactones (**13** → **14**) catalyzed by **Λ-T18'** using the example of substrate **13e**.[22a,23h] Note the similarity to the catalysis cycle from Scheme 36.

As shown in Scheme 39, the mechanism is basically identical with the mechanism from Scheme 36, apart from the fact that the formed enolate counteranion of catalysis intermediate **Λ-T18-Int2** is not a benzofuranone enolate but an azlactone enolate. Eventually, approach and reaction of the azlactone enolate with its *Si*-face oriented toward the catalyst-bound acyl group lead to predominant formation of the *R*-enantiomer in case of product **14e** (Scheme 39, Step II). As the migrating acyl group of *O*-acylated azlactone **13e** is identical with the one of *O*-acylated benzofuranone **142i**, the complex cation of catalysis intermediate **Λ-T18-Int2** from Scheme 39 is identical with the complex cation of catalysis intermediate **Λ-T18-Int** from Scheme 36. As a result, **Λ-T18-TfO** (Scheme 37 and Figure 21) serves as a catalysis intermediate analog for both depicted catalytic cycles.

With the combined aid of...

- ...the unambiguous assignment of the primarily employed enantiomer of catalyst **T18'** as Λ-enantiomer (=**Λ-T18'**) by circular dichroism spectra comparisons (details in the experimental section),...
- ...the crystal structure obtained for racemic catalysis intermediate analog ***rac*-T18-TfO** and the three-dimensional structure of **Λ-T18-TfO** deduced from it (see Scheme 37 and Figure 21) and the crystal structure obtained for racemic catalyst ***rac*-T18'** and the three-dimensional structure of **Λ-T18'** deduced from it (see chapter 2.3.2, Figure 16),...
- ...and the unambiguous assignment of *C*-acylated benzofuranone product **143i** (93% ee) from Table 13, entry 13 – synthesized with catalyst **Λ-T18'** – as predominantly *S*-configured by both XRD analysis and comparison of optical rotation data of products **143b–i** with literature data (details are provided in the experimental section),...

...the time had now come to shed light on the catalyst's manner of enantioinduction. In that regard, it was decided to mainly focus on Black rearrangements of *O*-acylated benzofuranones (**142** → **143**).

Referring to the chiral complex cations of **Λ-T18-Int** (see Scheme 36), **Λ-T18-Int2** (see Scheme 39), and **Λ-T18-TfO** (see Scheme 37 and Figure 21), which are identical for all three species as explained above, the following has to be considered when trying to unveil the catalyst's manner of enantioinduction: The *N*-bound acyl group of the complex cation gives, in theory, rise to two coplanar conformers A and B, both allowing favorable conjugation with the neighboring π-system (Figure 22). However, only conformer A is found in the crystal structure obtained for ***rac*-T18-TfO** (see Figure 21).

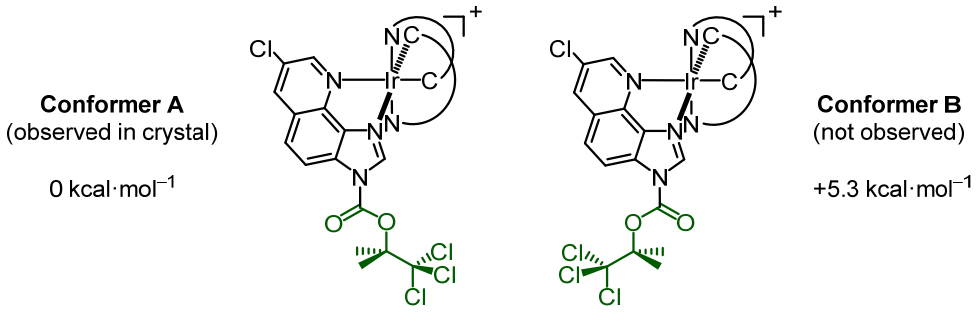

Figure 22. Schematic representations of both possible π-conjugated conformers of the cation of **Λ-T18-Int**, **Λ-T18-Int2**, and **Λ-T18-TfO** and their calculated relative energies (details are given in the text below).

To exclude a misleading crystal packing effect and to ascertain the energy difference between both conformers A and B, it was intended to confirm this XRD-based finding by a quantum chemical calculation. With the aid of Vladimir A. Larionov, postdoctoral researcher at that time in the Meggers laboratory in Marburg, Michael G. Medvedev (M. G. M.), a theoretical chemist from Moscow affiliated with the 'A. N. Nesmeyanov Institute of Organoelement Compounds RAS'[94] and with the 'N. D. Zelinsky Institute of Organic Chemistry RAS',[95] could be won for this task and the subsequent quantum chemical calculations as an external cooperation partner.

M. G. M. performed a quantum chemical modeling of both conformations of the complex cation of **Λ-T18-TfO** in the absence of crystal effects at the PBE0[96]-D3[97]/IMCP-SR1[98,99]//PBE0-D3/SBKJC[100] SMD[101] (butanol) level of theory for which M. G. M. relied on the XRD-derived three-dimensional structure of **Λ-T18-TfO** from Figure 21 (full computational details are provided in the experimental section). The PBE0 functional was chosen as it is known to be accurate for organic chemistry calculations[96b] and has recently been shown to be well-grounded in theory[96c] and the IMCP-SR1 basis set was chosen as it incorporates scalar-relativistic effects, which are important for heavy elements, such as iridium in case of

the studied system and,[99] moreover, retains the correct nodal structures of atoms.[98a] Solvent effects were accounted for by M. G. M. by means of the SMD universal solvation model.[101] M. G. M.'s calculations revealed that conformer A is indeed 5.3 kcal·mol^{-1} lower in energy than conformer B, which proves that conformer B's contribution to the overall reaction is most probably negligible for further mechanistic considerations (Figure 22).[102]

Having ruled out excessive conformational freedom of the *N*-bound acyl group with this calculation, it was now possible to shed light on the prochiral recognition mode of the *N*-acylated catalysis intermediate and hence on the underlying manner of enantioinduction of catalyst **Λ-T18'**.

At first, a Connolly surface or molecular surface with a probe radius of r = 1.4 Å was added to the XRD-derived complex cation structure of intermediate analog **Λ-T18-TfO** (see Figure 21) in order examine its active site accessibility with regard to the benzofuranone enolate's approach and stereogenic attack (Figure 23; Connolly surface modeling conceived and performed by T. C.).[103,104]

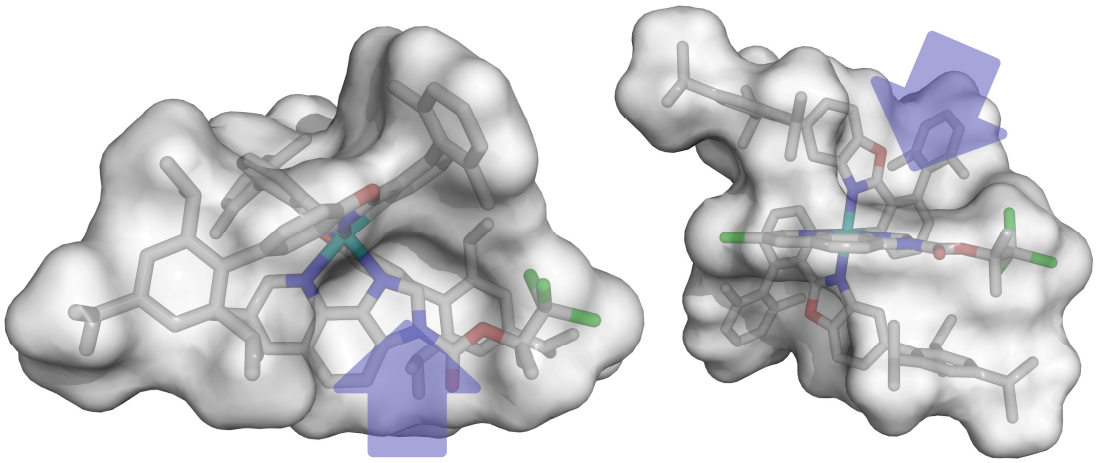

Figure 23. *Left*: Molecular surface (probe radius r = 1.4 Å) of the complex cation of **Λ-T18-TfO** derived from the crystal structure obtained for ***rac*-T18-TfO** (see Figure 21)[103–105] with view on the sterically accessible face of the *N*-acylated imidazoquinoline ligand. *Right*: Same structure as left, tilted by 90° resulting in a view on the edge of the *N*-acylated imidazoquinoline ligand. The blue arrows in both representations point into the chiral molecular cavity (details provided in the text). [Reproduced with permission from ref. 84. Copyright © 2017, American Chemical Society]

This approach was considered appropriate for the following reasons: After the formation of the *N*-acylated catalysis intermediate, the enolate has to closely approach the electrophilic carbonyl moiety of the acyl group to react with it. In this regard, it is apparent from Figures 21 and 23 that there are basically no functionalities in the *N*-acylated catalysis intermediate which could interact with the approaching enolate via pronounced non-covalent interactions, such as hydrogen-bonding interactions or dipole-dipole interactions.[106] For this reason, it was anticipated that the enolate's spatial approach would be mainly governed by steric repulsions, weak Van der Waals interactions, and the separation of charge between

complex cation and enolate anion. Moreover, the catalyst's structural rigidity and the clearly proved conformational preference of its *N*-attached acyl group (see Figure 22 and the associated discussion) renders a preliminary active site accessibility inspection via a molecular surface survey feasible.

As depicted in Figure 23, the target carbonyl moiety of the acyl group is nestled down in a chiral molecular pocket or molecular cavity, which a prochiral enolate has to enter in order to react with the acyl group. The "bottom" of this cavity consists of a part of the *N*-acylated imidazoquinoline ligand including the target electrophilic carbonyl moiety. And the "walls" of this cavity are shaped of, from left to right, a 2,4,6-triisopropylphenyl moiety, the cyclometalated benzoxazole ligand the latter is bound to, a 2,6-dimethylphenyl moiety being also part of this benzoxazole ligand, and finally the tail of the *N*-bound acyl group, which in case of the cation of **Λ-T18-TfO** is the CMe_2CCl_3 fragment. Figure 23 clearly shows that the second face of the imidazoquinoline ligand is, in contrast, effectively shielded by another 2,4,6-triisopropylphenyl moiety. Keeping these considerations at the back of one's mind, the catalyst screenings from chapter 2.3.2 and the eventual selection of precatalyst **Λ-T18** / catalyst **Λ-T18'** become more intelligible as Figure 23 clearly visualizes that appropriate choice of the substituents in the catalyst is essential for both high enantioselectivity and activity.

To confirm these mechanistic considerations and to establish the mechanism in greater detail, cooperation partner M. G. M. was asked to perform a quantum chemical modeling of a Black rearrangement's stereogenic step with substrate **142i** and catalyst **Λ-T18'**. However, the computational complexity of this system made it necessary to switch over to less complex catalyst model **Λ-T18'-QM**, which is depicted in Figure 24, and also to less complex benzofuranone substrate **142h**, in which **142i**'s CMe_2CCl_3 group is replaced by a methyl group (see chapter 2.3.2, Figure 17). Importantly, in catalyst model **Λ-T18'-QM** the shape of the active center and of the mentioned molecular cavity of **Λ-T18'** remains entirely untouched (details in the experimental section).

Simplified model of catalyst **Λ-T18'**:

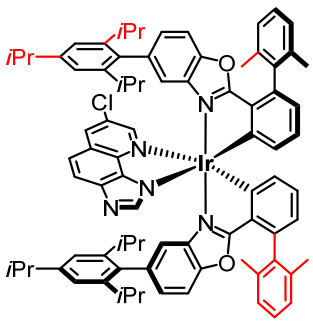

Λ-T18'-QM

Figure 24. Simplified model of catalyst **Λ-T18'** named **Λ-T18'-QM**. Removed fragments are shown in red. Importantly, the shape of the catalyst's active center and molecular cavity remains entirely untouched in **Λ-T18'-QM**. More details are provided in the experimental section.

Using an approach which has recently been developed and applied by M. G. M. and colleagues to locate all 728 transitions states (TSs) feasible for an SpnF-catalyzed formal Diels–Alder cycloaddition,[107] four TSs were located at the PBE0[96]-D3[97]/IMCP-SR1[98,99]//PBE0-D3/SBKJC[100] SMD[101] (butanol) level of theory (details in the experimental section). As parameters for *tert*-amyl alcohol (TAA) were unavailable for the SMD solvation model,[101] the alcohol's influence was taken into consideration with the according parameters for *n*-butanol as already before in case of the conformational analysis of the *N*-acylated complex cation. This was considered appropriate as alcohols had been found − at least in terms of enantioselectivity − to generally exert a positive and similar influence on Black rearrangements (**142 → 143**) with **Λ/Δ-T18'** as catalyst (see chapter 2.3.3, Table 12).

Based on the computed transition states and their relative energies (see Table 20 and Figure 25), the stereochemical outcome of the reaction **142h → 143h** was then calculated by M. G. M. and with this also the modeling itself reaffirmed: In order to account for the interplay between the located transition states, the Curtin–Hammett principle was invoked by M. G. M., which, in its modern sense, states that the rate (and so the efficacy) of a particular reaction path is determined by the relative energies of the corresponding TSs, assuming that the rates of substrate conformer interconversions are much higher than the rates of the chemical reaction.[108] For any two different transition states with energies E_1 and E_2, their contributions to the reaction C_1 and C_2 are connected by Eq. 2, in which R is the gas constant and T the temperature (in Kelvin).[108]

$$\frac{C_1}{C_2} = exp\left(\frac{E_2 - E_1}{RT}\right) \qquad \text{(Eq. 2)}$$

Eq. 2 was used by M. G. M. to calculate the contribution ratios between each TS and the lowest TS at the reaction temperature of −30 °C (T = 243.15 K). The individual percentaged contributions were then calculated by considering the cumulative contribution to be 100%. The calculated contributions of all four TSs are summarized in Table 20 together with their types and their computed relative energies.

Table 20. Types, relative energies, and calculated contributions of each of the four transition states.

transition state (TS)[a]	type / attacking face	relative energy (kcal·mol^{-1})[b]	contribution (C; in %)[c]
TS-*Re*-A	*Re*	+1.808	1.6
TS-*Re*-B	*Re*	+0.480	24.3
TS-*Si*-A	*Si*	0.000	65.6
TS-*Si*-B	*Si*	+0.981	8.6

[a]The corresponding transition states are depicted in Figure 25. [b]Calculated at the PBE0-D3/IMCP-SR1 SMD(butanol) level of theory. [c]Calculated invoking the Curtin–Hammett principle (Eq. 2).

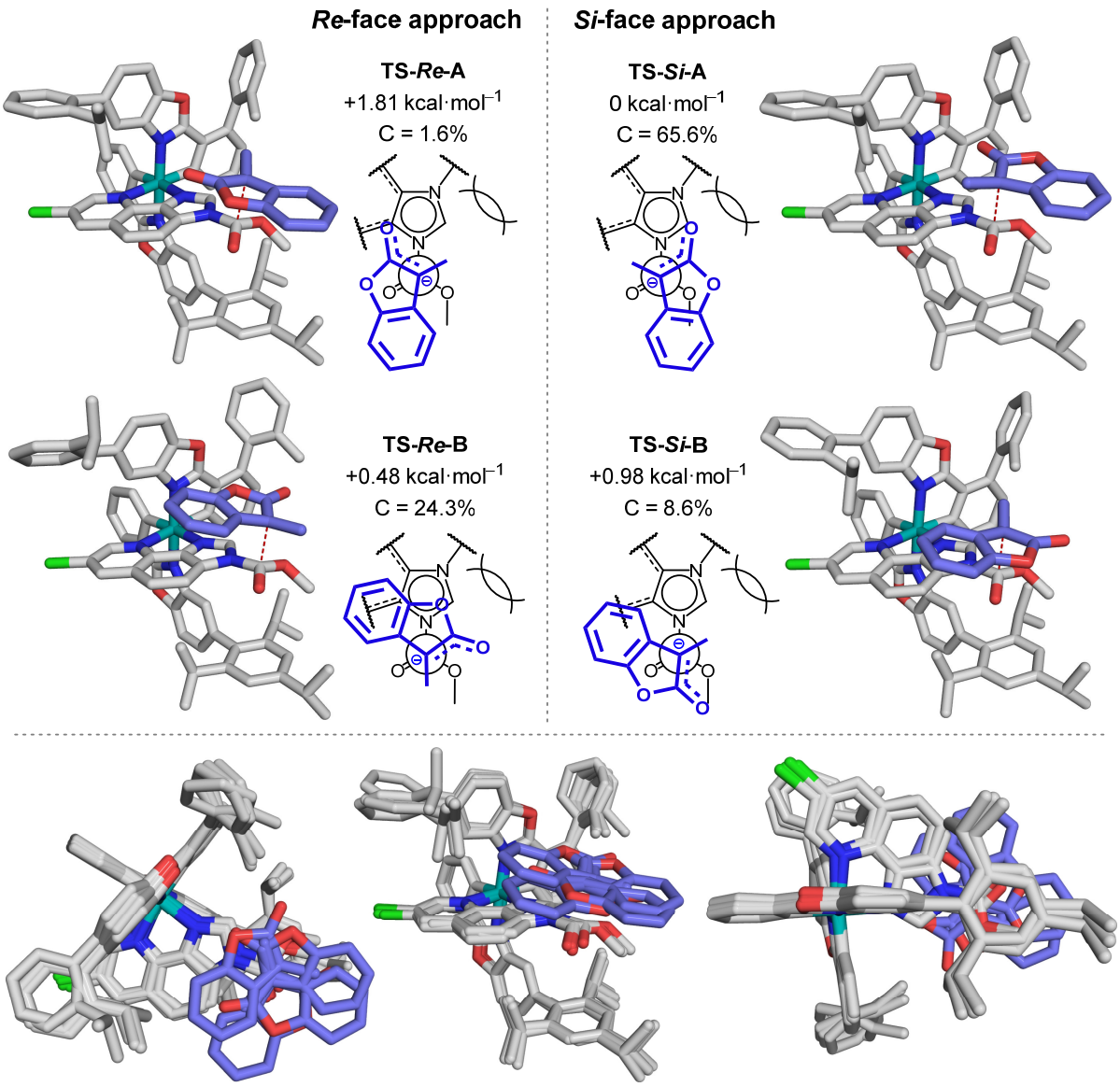

Figure 25. Quantum chemical modeling of the stereogenic step of the Black rearrangement **142h** → **143h** with **Λ-T18'-QM** as catalyst model.[105] *Top*: Three-dimensional representations of the four calculated transition states with their Newman projections (views along the forming C-C bonds) and with their relative energies and their Curtin–Hammett-based contributions (C). *Bottom*: Superpositions of the four calculated TSs from three different perspectives. The carbon atoms of the approaching enolate are highlighted in blue and the forming C-C bonds are indicated with red dashes.

With the contributions of each TS to the overall reaction, the stereochemical outcome of the Black rearrangement **142h** → **143h** with catalyst model **Λ-T18'-QM** was calculated to be 48.4% ee (*R*), which, in consideration of the applied approximations, is in a very good agreement with the observed 70% ee (*R*). One might raise the question whether the energy differences between the four calculated TSs (see Table 20, Figure 25) are not somewhat too low for reliable conclusions. As far as that is concerned, it has to be considered that the studied transition states only differ in weak interactions, which allows to compute their relative energies with a high accuracy in the range of ~0.1 kcal·mol^{-1}[109] Moreover, the particular calculations for the studied system benefit from an error cancellation, which rises

from the fact that the studied transition states are very similar, so systematic errors in them largely cancel out.[107,110] The later is in part a consequence of the rigid framework of the catalyst which results in a constrained, well-defined active site.

Three-dimensional representations of the four calculated TSs and their Newman projections with views along the forming C-C bonds are shown in Figure 25 together with their calculated relative energies and their Curtin–Hammett-based contributions. The energetically most favored transition state TS-*Si*-A with 65.6% calculated contribution is shown in Figure 26 with individual molecular surfaces added to the *N*-acylated catalysis intermediate (grey surface) and the approaching enolate (blue surface; probe radius $r = 1.4$ Å for both surfaces; Connolly surface modeling conceived and performed by T. C. with M. G. M.'s calculated 3D-model for TS-*Si*-A).[103–105] Figure 26 serves to illustrate the spatial situation of that reactive approach in general and for transition state TS-*Si*-A in particular.

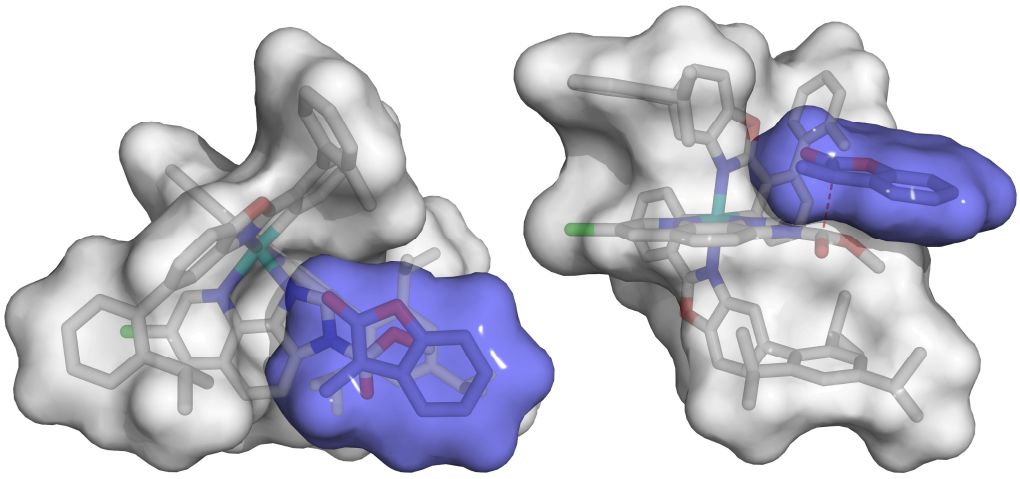

Figure 26. Quantum chemical modeling of the stereogenic step of the Black rearrangement **142h → 143h** with **Λ-T18'-QM** as catalyst model. Main contributing transition state TS-*Si*-A with molecular surfaces added to both the *N*-acylated complex cation (grey surface) and the approaching enolate (blue surface; both surfaces are Connolly surfaces with a probe radius of $r = 1.4$ Å; angles of view are identical with Figure 23).[103–105] The forming C-C bond is indicated with red dashes. [Reproduced with permission from ref. 84. Copyright © 2017, American Chemical Society]

In summary, the quantum chemical modeling...

- ...was able to put the catalyst's manner of enantioinduction on a rational basis and helped to understand the results of the catalyst screening from chapter 2.3.2,...
- ...confirmed the underlying idea of a chiral rigid molecular cavity or molecular pocket, which must be entered by an enolate in order to react with the acyl group's carbonyl moiety to form the chiral rearrangement product (see Figures 22–26),...
- ...confirmed that the approach of the enolate is mainly governed by nondirectional steric repulsions and Van der Waals interactions (see Figure 25),...

- ...correctly predicted the stereochemical outcome of the transformation **142h** → **143h** with 48.4% ee (*R*-configuration; computed) vs. 70% ee (*R*-configuration; experimental).

The results also clearly indicate that the unique rigid framework of **Λ-T18'** with its constrained and well-defined active site represents a well-suited scaffold for the rational design of related catalysts: It should readily allow it to custom tailor **Λ-T18'**-derived catalysts to specific substrates, or to identify suitable substrates for **Λ-T18'** via *in silico* screenings. Such *in silico* screenings could range from simple molecular surface based active site accessibility considerations (see Figure 23) to compute-intensive but much more informative DFT-based screenings with the here presented methods (see Figure 25 and 26). What kind of approach is selected of course depends on what computing resources are available and which efforts are projected and feasible.[111] However, in consideration of the protracted and time-consuming experimental search for "the best" nucleophilic stereogenic-only-at-metal catalyst described in chapters 2.2, 2.3.1, and 2.3.2, *in silico* screenings could have the potential to accelerate and facilitate catalyst enhancement and development in the future and could contribute to decreased research expenses.

The usefulness of the here presented calculations and considerations shall be shortly demonstrated: Inspection of Figures 23, 25 and 26 illustrates that a small migrating acyl group results in a wider molecular cavity, which understandably may result in diminished selectivity, e.g., in case of benzofuranone substrate **142h** (see chapter 2.3.3, Table 13). A closer look at the four TSs depicted in Figure 25 and at the most favorable transition state TS-*Si*-A depicted in Figure 26 also renders the poor result for benzofuranone substrate **142a** (see chapter 2.3.3, Table 13) consequential as the occurring all-planar, rigid phenyl-substituted enolate is hardly able to enter the resulting, comparatively small molecular cavity, which manifests in a sluggish reaction and a poor selectivity. Similarly, the extremely sluggish reaction observed with gliocladin C precursor **147** from chapter 2.3.5, Table 15 is just consequential: Also here the formed rigid and bulky enolate is hardly able to enter the resulting molecular cavity − in case the preceding nucleophilic attack is not already precluded by excessive steric congestion.

2.3.9 Mechanistic Experiments II: Addition of 2-Cyanopyrrole to Aryl Alkyl Ketenes

Now, attention was turned to the mechanism of the asymmetric addition of 2-cyanopyrrole (**162**) to aryl alkyl ketenes (**153**) providing *α*-chiral *N*-acyl pyrroles (**163**) from chapters 2.3.6 and 2.3.7. For the asymmetric addition of 2-cyanopyrrole (**162**) to aryl alkyl ketenes (**153**) two pathways are reasonable which are depicted in Scheme 40 using the example of ketene substrate **153c**.[26c,34]

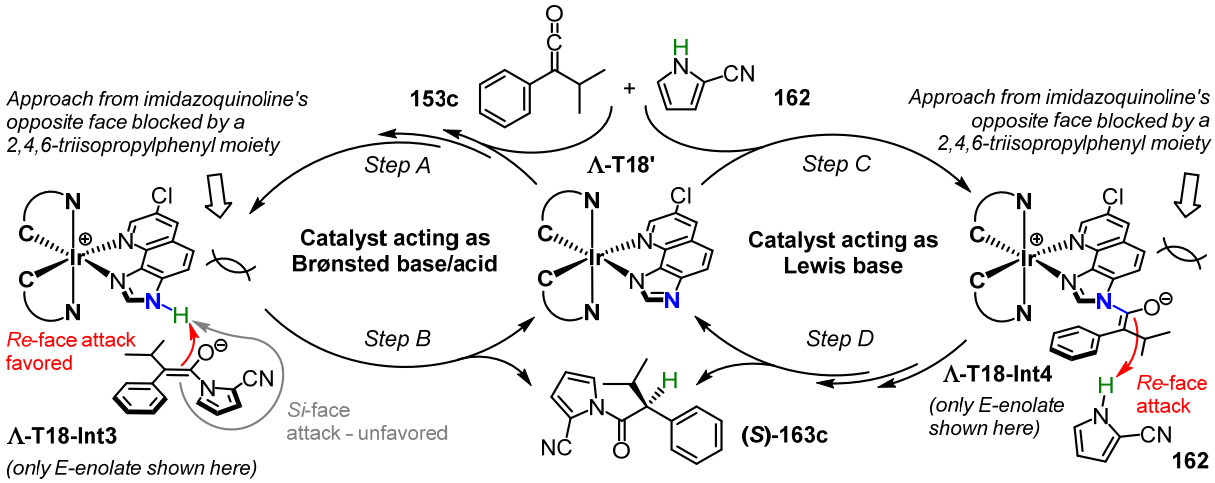

Scheme 40. Reasonable pathways for the reaction of aryl alkyl ketenes (**153**) with 2-cyanopyrrole (**162**) catalyzed by **Λ-T18'** using the example of ketene substrate **153c**.[26c,34] [Reproduced and adapted with permission from ref. 84. Copyright © 2017, American Chemical Society]

The first reasonable pathway starts with proton transfer from 2-cyanopyrrole (**162**) to catalyst **Λ-T18'** followed by addition of the generated pyrrolate to ketene **153c**, which eventually results in formation of **Λ-T18-Int3**, a salt consisting of an *N*-protonated +1 charged iridium(III) complex cation and its associated ketene enolate counteranion (Scheme 40, Step A). On the assumption that this pathway is operational, the observed stereochemical outcome originates from the circumstance that chiral Brønsted acid **Λ-T18-Int3** preferentially protonates the prochiral ketene enolate from the *Re*-face, which leads to predominant formation of the *S*-enantiomer of product **163c** (Scheme 40, Step B). In Scheme 40, the *E*-enolate is arbitrarily drawn. However, in case this pathway is operational, the ketene enolate might be existent as an *E*/*Z* mixture.[34a] As discussed for the acyl migration reactions, the ketene enolate can only approach the protonated imidazoquinoline ligand from one face as the other one is sterically obstructed (see chapter 2.3.8, Figure 23).

The second reasonable pathway starts with addition of catalyst **Λ-T18'** to ketene **153c**, which results in formation of zwitterionic iridium(III) complex **Λ-T18-Int4**, which might again exist as an *E*/*Z* mixture (Scheme 40, Step C; *E*-form arbitrarily drawn).[34a] In case this pathway is operational, preferred proton transfer to the *Re*-face of the catalyst-bound ketene enolate from

2-cyanopyrrole (**162**) eventually leads to predominant formation of the *S*-enantiomer of product **163c** (Scheme 40, Step D). Again, 2-cyanopyrrole (**162**) can only approach the imidazoquinoline ligand from one face as the other one is sterically obstructed.

In an attempt to clarify which of both cycles from Scheme 40 is in operation, the following observations were made: When ***rac*-T18'** was mixed in dry CD_2Cl_2 with excess *p*-chlorophenyl isopropyl ketene (**153d**) at room temperature, only ^{1}H NMR signals belonging to **153d** and ***rac*-T18'** were found but no indication for the formation of a zwitterionic species like **Λ-T18-Int4**. This result is in agreement with observations made by Fu and co-workers for their DMAP-derived catalyst **(–)-7b** (see Scheme 3 in chapter 1.2) and speaks, at first, against the right cycle from Scheme 40.[26c] However, ion pair formation was also not observed when ***rac*-T18'** was mixed with excess 2-cyanopyrrole (**162**) under identical conditions, only a weak hydrogen-bonding interaction between the *N*-bound proton of **162** and the nitrogen atom of ***rac*-T18'** could be observed (details of both experiments are provided in the experimental section). This is in contrast to observations made by Fu and co-workers for catalyst **(–)-7b**, who report about ion pair formation for this experiment.[26c] Based on their NMR observations together with additional experimental data, primarily kinetic data, Fu and co-workers carefully assumed that the Brønsted base/acid mechanism should be in operation in case of catalyst **(–)-7b**.[26c]

In contrast, a recent thorough computational study from Cheong and co-workers arrived at the conclusion that the nucleophilic pathway should be in operation in case of **(–)-7b**.[34] For the reaction between phenyl methyl ketene and 2-cyanopyrrole (**162**) catalyzed by **(–)-7b**, Cheong and co-workers revealed that...

- ...the decisive rate determining step (RDS) of the nucleophilic pathway is favored by 8.3 kcal·mol^{-1} over the RDS of the Brønsted base/acid pathway[34]...
- ...the NMR-observed ion pair formed between 2-cyanopyrrole (**162**) and catalyst **(–)-7b** is merely the unproductive resting state of the catalyst[34]...
- ...the NMR-based non-observation of a zwitterionic intermediate formed between a ketene and **(–)-7b** is consequential as that step is endergonic[34]...
- ...the experimental primary kinetic isotope effect (KIE) of $k_H / k_D \sim 5$ found by Fu and co-workers coincides with the computed KIE for the nucleophilic pathway (computed: $k_H / k_D = 5$) but *not* with the computed KIE for the Brønsted base/acid pathway (computed: $k_H / k_D = 1$; k_H is here the rate constant for the reaction with common 2-cyanopyrrole (**162**) and k_D the rate constant for the reaction with *N*-deuterated 2-cyanopyrrole (**162-D**).[34]

Being aware of the different structures and properties of Fu's catalyst **(–)-7b** and catalyst **Λ-T18'**, it is at the moment assumed, in consideration of the recent calculations from Cheong and co-workers for catalyst **(–)-7b**, that for catalyst **Λ-T18'** the nucleophilic catalysis pathway is in operation as well (Scheme 40, right cycle). At least, it can concluded for sure that the lone-pair of the imidazoquinoline's nitrogen atom is indispensable for this reaction either way as mixing of *N*-methylated catalyst (**Λ-T18-Me**) with ketene **153c** and 2-cyanopyrrole (**162**) resulted in no formation of addition product **163c** (experimental details and the preparation procedure for **Λ-T18-Me** are provided in the experimental section).

To clarify which of both pathways from Scheme 40 is in operation or at least predominantly in operation, a clever combination of *in vitro* and *in silico* experiments as presented by Cheong and co-workers seems to be the most viable approach.[34] Accordingly, the following tasks should be performed:

- Both pathways from Scheme 40 should be studied with catalyst **Λ-** or **Δ-T18'** or with a suitable simplified model (for example **Δ-T18'-QM**; see Figure 24) by explicit quantum chemical calculations with the aim to obtain the reaction coordinate diagrams for both pathways with the energies of their individual transition states and intermediates. This would reveal the RDSs of both pathways and their crucial difference in energy.[34]
- Next, it should be verified whether the above mentioned experimental results for ***rac*-T18'** with *p*-chlorophenyl isopropyl ketene (**153d**) and 2-cyanopyrrole (**162**) are in accordance with the reaction pathway featuring the energetically favored RDS.[34]
- Then, the rate constants (k) for the reaction between an aryl alkyl ketene (**153**) and 2-cyanopyrrole (**162**; rate constant: k_H) and the reaction between the same aryl alkyl ketene (**153**) and *N*-deuterated 2-cyanopyrrole (**162-D**; rate constant k_D) should be experimentally determined with ***rac*-T18'** as catalyst, which provides the experimental primary KIE (k_H / k_D). Next, the KIEs should be computed for both pathways.[34] If the computed KIEs are not identical or very similar for both pathways, the computed KIE should resemble the experimental KIE of the operational pathway.[34]
- Finally, the stereochemical outcome could be computed for both the favored and the unfavored pathway. If they are not identical or very similar, the computed stereochemical outcome of the favored pathway should resemble the experimental stereochemical outcome.[34]

2.4 Summary and Outlook

In summary, complex **Λ/Δ-T18'** has been developed and demonstrated to be a versatile, highly active, for several transformations highly enantioselective, air- and moisture-stable chiral nucleophilic catalyst featuring a bidentate deprotonated imidazoquinoline ligand as its catalytic site and an octahedral Ir(III) stereocenter as its exclusive element of chirality (Figure 27).

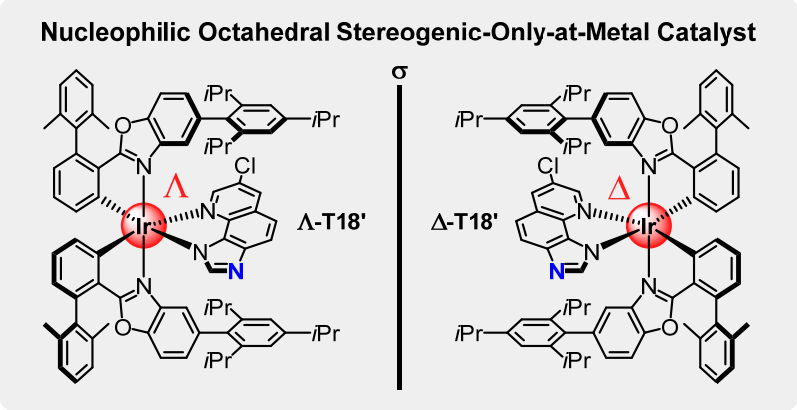

Figure 27. Structural formulas of nucleophilic stereogenic-only-at-metal catalyst **Λ-T18'** (left) and its enantiomer **Δ-T18'** (right). The catalytically active nucleophilic nitrogen atom is highlighted in blue and the octahedral Ir(III) stereocenter is highlighted in red.

Starting from preliminary research results from two former PhD students from the Meggers laboratory, namely Zhijie Lin (see chapter 2.2.1)[75a] and Xiaodong Shen (see chapter 2.2.2),[76] 28 different Ir(III) complexes **Λ-T1**−**Λ-T28** (see chapters 2.3.1 and 2.3.2, Figures 12−14,) were synthesized and evaluated and complex **Λ/Δ-T18** eventually selected as the most promising nucleophilic catalyst candidate based on the results from Steglich rearrangement reaction **13a** → **14a**, which accordingly served as a probe reaction (see chapter 2.3.2, Tables 5−7).

In has been revealed that initially formed and isolated complex **Λ/Δ-T18** is catalytically inactive and that instead its deprotonated form **Λ/Δ-T18'**, formed by mild Brønsted base treatment from **Λ/Δ-T18**, is the actual catalytically active species (see chapter 2.3.2, Table 4 and Scheme 31; additional experiments are provided in the experimental section). Moreover, it has been demonstrated that **Λ-T18'** and **Δ-T18'** are both available with >99% ee with the employed synthetic route (see chapter 2.3.2, Scheme 32) and their absolute configurations have been unambiguously assigned via CD spectroscopy (see chapter 2.3.2, Figure 15; additional experimental data is provided in the experimental section).

The versatility of newly designed nucleophilic stereogenic-only-at-metal catalyst **Λ/Δ-T18'** could be successfully demonstrated for three asymmetric transformations (Scheme 41):

- For the Steglich rearrangement of *O*-acylated azlactones (**13**) to *C*-acylated azlactones (**14**) going along with the formation of a quaternary stereocenter (9 examples; up to 99% yield and up to 96% ee; see chapter 2.3.2 for details),...
- ...for the related Black rearrangement of *O*-acylated benzofuranones (**142**) to *C*-acylated benzofuranones (**143**) going along with the formation of an all-carbon quaternary stereocenter (9 examples; up to 99% yield and up to 94% ee; see chapter 2.3.3 for details),...
- ...and finally for the addition of 2-cyanopyrrole (**162**) to aryl alkyl ketenes (**153**) yielding *α*-chiral *N*-acyl pyrroles (**163**; 8 examples, up to 99% yield and up to 95% ee; see chapters 2.3.6 and 2.3.7 for details), a reaction for which catalyst **Λ/Δ-T18'** is, after Fu's planar-chiral catalyst **(–)-7b**, the only other reported chiral catalyst so far.[26c,93]

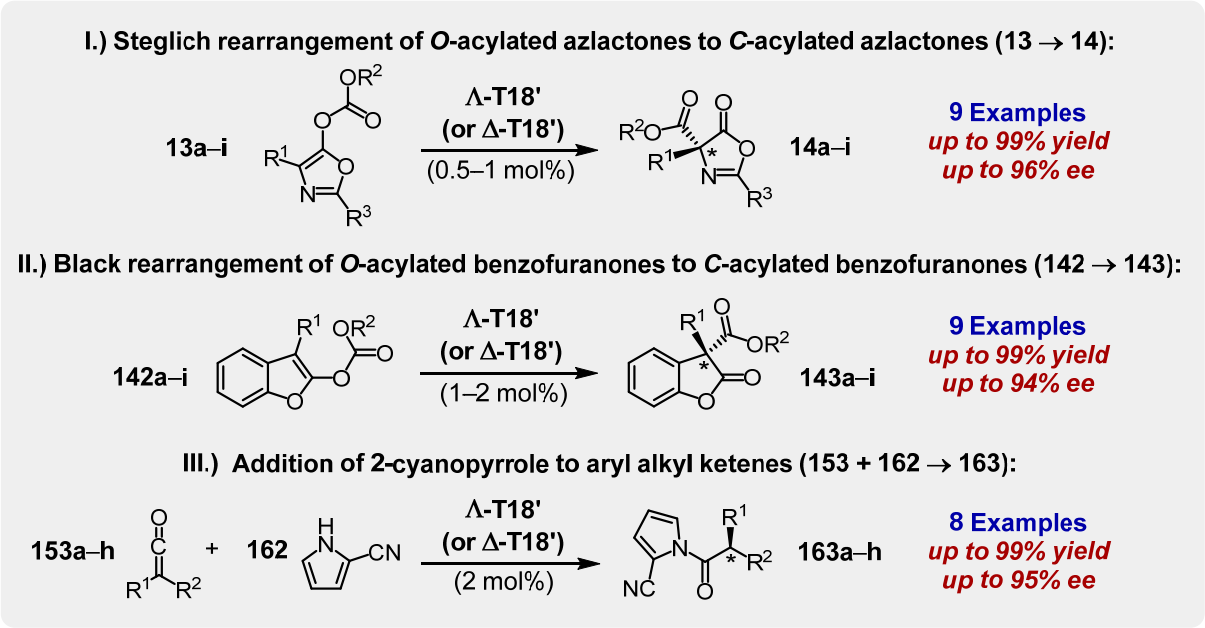

Scheme 41. Successfully established reactions with catalyst **Λ-T18'**. Enantiomeric catalyst **Δ-T18'** can also be employed which leads to products with opposite configurations.

Notably, it was possible to perform these transformations with just 0.5–2 mol% of catalyst **Λ/Δ-T18'**, partially at temperatures as low as −30 °C, which underlines the catalyst's high activity (Scheme 41).

In case of one Black rearrangement, it has been demonstrated that the catalyst can be easily recovered in high yield after reaction completion without any deterioration of its enantiopurity and reused again (reisolation of **Λ-T18'**: 94% reisolated yield and a reisolated ee of >99%; see chapter 2.3.3, Table 13 and the associated text).

With crystal structures of active catalyst ***rac*-T18'** (chapter 2.3.2, Figure 16) and *N*-acylated catalysis intermediate analog ***rac*-T18-TfO** (chapter 2.3.8, Figure 21), analysis of the degree of conformational freedom in the complex cation of catalysis intermediate analog **Λ-T18-TfO** (chapter 2.3.8, Figure 22; DFT-based conformational analysis performed by

cooperation partner M. G. M.), and via analysis of the active site accessibility of the latter (chapter 2.3.8, Figure 23), it has been shed light on the catalyst's manner of prochiral recognition and enantioinduction. And in case of the Black rearrangements (**142** → **143**), the herefrom deduced mechanistic conclusions have been explicitely confirmed and further refined with a quantum chemical modeling of a Black rearrangement's stereogenic step (**142h** → **143h**), which also correctly predicted the stereochemical outcome of the studied reaction (chapter 2.3.8, Figures 24–26; quantum chemical modeling of the stereogenic step and prediction of the stereochemical outcome performed by cooperation partner M. G. M.).

In case of the reaction between 2-cyanopyrrole (**162**) and aryl alkyl ketenes (**153**) to give *α*-chiral *N*-acyl pyrroles (**163**) it remains somewhat elusive for now whether the reaction follows a Brønsted base/acid pathway or a nucleophilic pathway (Scheme 40). An additional study should be performed here according to the proposed procedure described in the last paragraph of chapter 2.3.9 in order to clarify which of both pathways is in operation. Under consideration of the aforementioned computational study from Cheong and co-workers, it is at the moment assumed that a nucleophilic catalysis pathway is in operation.[34]

The key results of this research project have been published in *ACS Catalysis* as a research article (*ACS Catal.* **2017**, *7*, 5152–5162),[84] which has recently been highlighted in *Synfacts* (*Synfacts* **2017**, *13*, 0945).[112] Some of the complex syntheses of **Λ-T1**−**Λ-T28** which were performed according to Scheme 30, Route II have been included in a publication in *Chemistry – A European Journal* (*Chem. – Eur. J.* **2017**, *23*, 12363–12371), which deals with the aforementioned post-complexation modification of bis-cyclometalated Ir(III) complexes via Suzuki-Miyaura cross-couplings (see chapter 2.3.1, Scheme 30 and the associated text).

Future experimental studies with **Λ/Δ-T18'** or derivatives thereof should aim at identifying other suitable asymmetric transformations beyond those depicted in Scheme 41. In this regard, reinvestigation of the intermolecular *C*-acylation of silyl ketenes acetals (**144** + **145** → **146**) from chapter 2.3.4 could be promising as product **146da** had been obtained there with encouraging 66% ee (see Table 14). That result could be taken as a starting point for an extensive substrate and conditions screening. And also the Steglich-type rearrangements of *O*-acylated oxindoles (**149** → **150**) from chapter 2.3.5 could be interesting in that regard as product **150b** had been obtained there in 96% yield with encouraging 59% ee (see Table 15).

Moreover, it would be interesting to shed more light on the iridium center's electronic influence on the attached imidazoquinoline ligand and to elucidate its influence on the activity of catalyst **T18'** as a whole.

In this regard, it would be also highly interesting to reveal whether catalyst **Λ/Δ-T18'** or a similar catalyst of that type could be combined with photochemistry. A suggestion for such an application is shown in Scheme 42 with catalyst **Λ-T18'**:

In the envisioned merger of nucleophilic catalysis with photochemistry from Scheme 42, an acylation agent R(C=O)X or an alkylating agent RX first reacts with catalyst **Λ-T18'**. This results in the formation of acylated **Λ-T18-A1** or alkylated **Λ-T18-B1**. Importantly, R should be able to stabilize a radical which forms upon homolysis of the R-N bond (**Λ-T18-B1**) or of the R(CO)-N bond (**Λ-T18-A1**), for instance by resonance. The next steps are only shown for **Λ-T18-B1** but they are analog for *N*-acylated **Λ-T18-A1**.

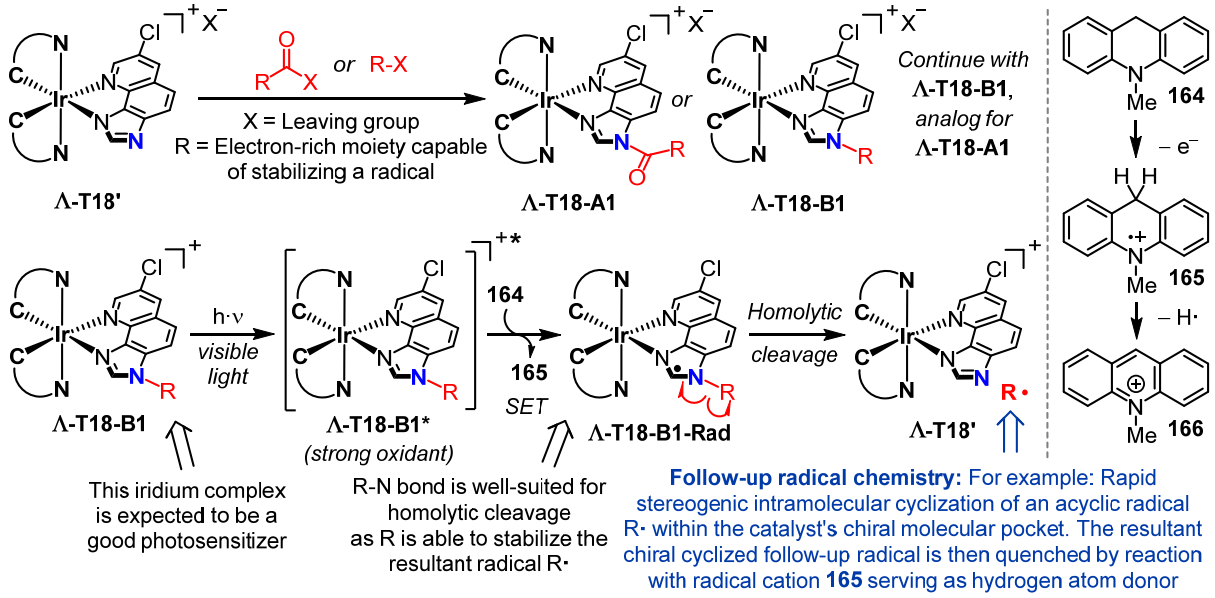

Scheme 42. Envisioned merger of nucleophilic catalysis with photochemistry with catalyst **Λ-T18'**. Detailed explanations are provided in the text.

Λ-T18-B1 is expected to be a good photosensitizer and **Λ-T18-B1** is expected to become a strong oxidant upon photoexcitation, which allows an easy single-electron transfer (SET) reduction of excited **Λ-T18-B1*** by a suitable reductant, e.g., *N*-methyl dihydroacridine (**164**).[73] This results in the formation of radical species **Λ-T18-B1-Rad** and the *N*-methyl dihydroacridine radical cation (**165**). Radical species **Λ-T18-B1-Rad** may now undergo homolysis of its R-N bond, which results in the formation of (resonance stabilized) radical R· and regeneration of catalyst **Λ-T18'**. In case R· is an acyclic, flexible species capable of undergoing a stereogenic intramolecular radical cyclization reaction, catalyst **Λ-T18'** might be able to control the stereochemical outcome of that cyclization: The chiral environment of **Λ-T18-B1** and **Λ-T18-B1-Rad** forces the chain of residue R into a certain conformation (see chapter 2.3.8, Figures 23–26 for an illustration). In case the catalyst is able to force the chain in or at least close to a reactive conformation leading to one of both enantiomers, the catalyst

should be able to control the stereochemical outcome of the reaction as rapid intramolecular radical cyclization after homolysis of **Λ-T18-B1*** would then "conserve" the catalyst-dictated conformation of initially formed radical R·. The resultant chiral cyclized follow-up radical is eventually quenched by the *N*-methyl dihydroacridine radical cation (**165**), which becomes oxidized to the *N*-methyl acridinium cation (**166**). Anyway, Scheme 42 only represents a suggestion for a merger of nucleophilic catalysis with photochemistry and other applications might be conceived.

Catalyst **Λ-T18'** represents, in contrast to all other presented kinetically-inert stereogenic-at-metal catalysts from the Meggers group (see chapter 1.4, Figure 8), a monofunctional catalyst in which the imidazoquinoline ligand acts as the single catalytically active site. Accordingly, it could be attempted to develop a bi- or multifunctional nucleophilic catalyst starting from **Λ-T18'**. In this regard, Suga's recently reported bifunctional BINOL-derived nucleophilic catalyst **39** could serve as a source of inspiration (Scheme 43).[23g]

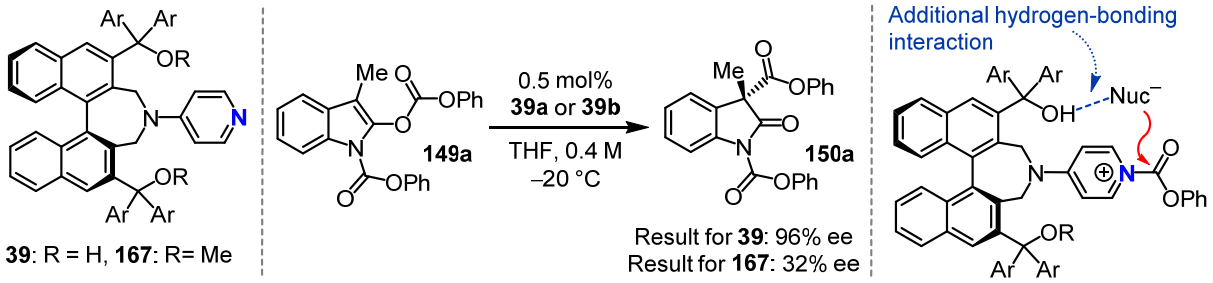

Scheme 43. In Suga's BINOL-derived nucleophilic catalyst **39**, the hydrogen-bonding interaction between the approaching enolate and the acylated catalyst is crucial for an efficient enantioinduction in case of the rearrangement of *N*,*O*-diacylated oxindoles (**149** → **150**).[23g] In case the hydroxy groups of **39** are methylated (**167**), the enantiomeric excess of products **150** drops significantly.[23g] A similar interaction could be employed to render a catalyst based on **Λ-T18'** bi- or multifunctional.

In case of Suga's catalyst **39**, its hydroxy groups proved to be crucial for an efficient enantioinduction for the rearrangement of *N*,*O*-diacylated oxindoles (**149** → **150**), which has also been confirmed by quantum chemical calculations (Scheme 43).[23g] The reason for that is that the enolate (Nuc^-) synergistically interacts with the catalyst's hydroxy groups via hydrogen-bonding, which significantly contributes to the prochiral recognition (Scheme 43).[23g]

A similar interaction could be implemented in a 2nd generation of catalyst **Λ-T18'** to render the catalyst bi- or multifunctional and to improve its enantioselectivity. A good basis for such considerations are the calculated transition states for the Black rearrangement **142h** → **143h** with simplified model catalyst **Λ-T18'-QM** from chapter 2.3.8, Figures 25 and 26: As can be seen from the three-dimensional representation of the most favored transition state TS-*Si*-A, the negatively charged part of the approaching enolate comes in close proximity to one of the methyl groups of one of the 2,6-dimethylphenyl groups of catalyst **Λ-T18'** (Figure 28).

Accordingly, an appropriately oriented hydrogen-bond donor or a positively charged moiety could be installed in lieu of the respective methyl group in order to synergistically interact with the approaching enolate and to co-direct its approach (Figure 28).

However, it has to be considered that this modification could also positively affect transition state TS-*Re*-B (see chapter 2.3.8, Figure 25), which is the main contributing transition state leading to the undesired enantiomer. Accordingly, it might be challenging to improve **Λ-T18'** with such a secondary interaction, at least in case of Black rearrangements (**142** → **143**).

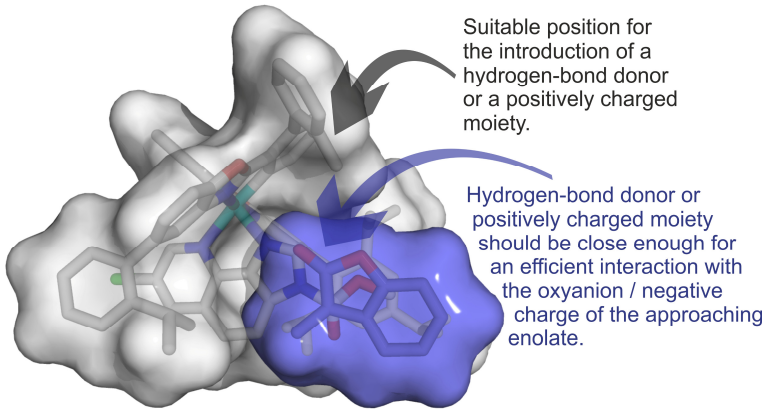

Figure 28. Energetically most favored transition state TS-*Si*-A of the Black rearrangement **142h** → **143h** for model catalyst **Λ-T18'-QM** from chapter 2.3.8, Figure 26.[103-105] As can be seen in this three-dimensional representation, one of both methyl groups of one of the 2,6-dimethylphenyl substituent of **Λ-T18'** seems to be a good position to install a hydrogen-bond donor or a positively charged moiety, which could then interact with the approaching enolate's oxyanion / negative charge and accordingly render the catalyst bifunctional.

Close inspection of the four calculated transition states from chapter 2.3.8, Figure 25 reveals that there could be another, much easier way to "improve" the enantioselectivity of the Black rearrangements (**142** → **143**) with catalyst **Λ-T18'**: Aforementioned transition state TS-*Re*-B, which is according to Figure 25 the main contributing transition state leading to the undesired enantiomer, seems to be the only transition state which would significantly suffer from the introduction of a bulky substituent R^3 at the 6-position of the *O*-acylated benzofuranone substrates (**142**; Figure 29), e.g., from the introduction of a *tert*-butyl group.

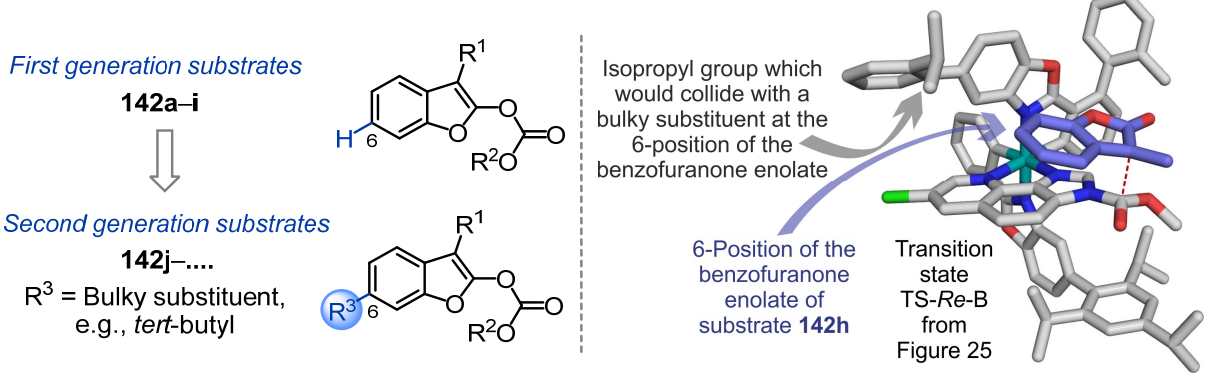

Figure 29. *O*-Acylated benzofuranones (**142**) with a bulky substituent R^3 at their 6-position could be intrinsically favored substrates for catalyst **Λ/Δ-T18'** according to the representations of the computed transition states from chapter 2.3.8, Figure 25. The representation on the right side shows transition state TS-*Re*-B from Figure 25 and pinpoints the steric interaction which could emerge from the introduction of a bulky substituent.

The reason for that is that bulky groups R^3 should collide with one of the isopropyl groups of one of the triisopropylphenyl substituents of **Λ-T18'** (see Figures 25 and 29) in case of that particular transition state. Accordingly, such substrates could be potentially predestined for catalyst **Λ-T18'**.

And finally, there remains another challenge which could be addressed: As presented in chapter 1.4, catalysts **Λ-89** and **Λ-(*R*,*R*)-90** were developed as improved C_2-symmetric versions of catalysts **Λ-81** and **Λ-85**. A similar strategy could be utilized to improve catalyst **Λ-T18'** in terms of activity and maybe also in terms of enantioselectivity (Figure 30).

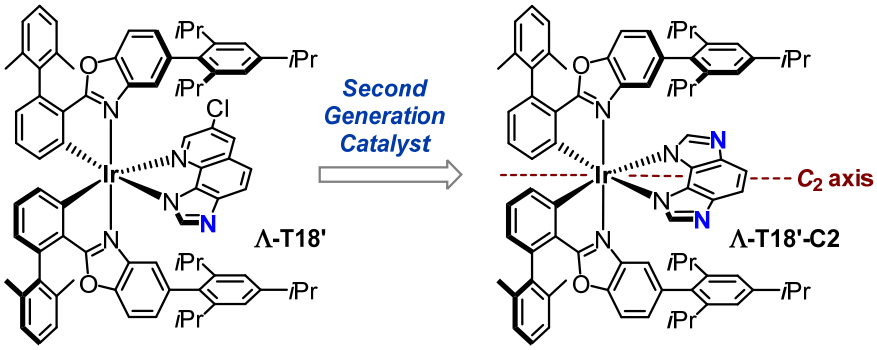

Figure 30. Suggested catalyst enhancement: Replacement of the imidazoquinoline ligand of **Λ-T18'** by a bis-imidazoquinoline ligand would result in C_2-symmetric catalyst **Λ-T18'-C2**, which might exhibit a higher catalytic activity than **Λ-T18'** due to the presence of two indistinguishable catalytic sites and which might also provide enhanced enantioselectivities.

3. Bifunctional Stereogenic-Only-at-Metal Enamine/Hydrogen-Bonding Catalyst

3.1 Aim of the Project

Before the attention was turned to the nucleophilic stereogenic-only-at-metal catalyst project from chapter 2., it was intended to develop a bifunctional stereogenic-only-at-metal catalyst based on Ir(III) complex **Λ-T29** as parent structure (Scheme 44), which was envisioned to catalyze Michael additions of enolizable aldehydes and / or ketones to nitroalkenes and / or nitroacrylates by means of cooperative enamine/hydrogen-bonding catalysis.

Scheme 44 shows an example for a Michael addition which was envisioned to be catalyzed by complex **Λ-T29**, namely the addition of 2-phenylacetaldehyde (**167a**) to isopropyl (*Z*)-3-nitro-2-phenylacrylate (**168a**) yielding Michael addition product **169aa**.

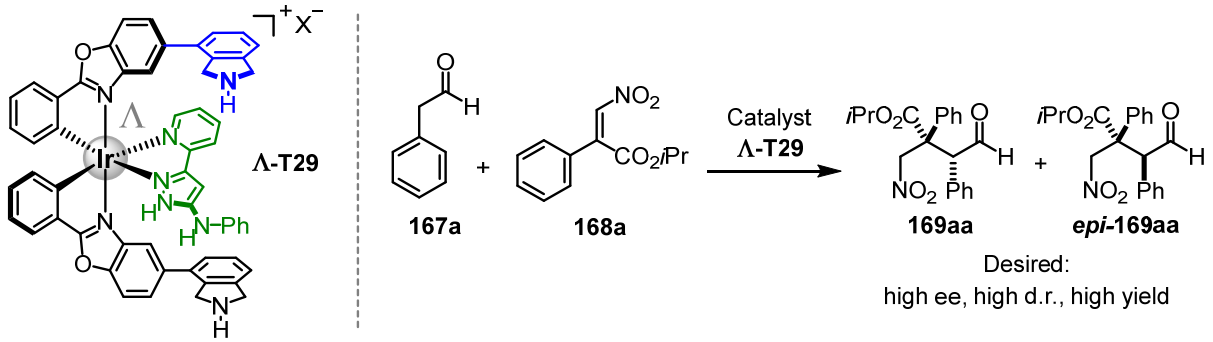

Scheme 44. *Left:* Complex **Λ-T29** as parent structure of the envisioned bifunctional stereogenic-only-at-metal enamine/hydrogen-bonding catalyst. *Right:* Envisioned Michael addition of 2-phenylacetaldehyde (**167a**) to isopropyl (*Z*)-3-nitro-2-phenylacrylate (**168a**) yielding Michael addition product **169aa** with **Λ-T29** as catalyst.

Complex **Λ-T29** represents a kinetically-inert, bis-cyclometalated, phenylbenzoxazole-based Ir(III) complex, which features an octahedral Ir(III) stereocenter as its exclusive element of chirality (highlighted in grey). As in case of the nucleophilic catalysts presented in chapter 2., the iridium center is not directly involved in the (envisioned) catalytic cycle (see Scheme 45) but plays a crucial role in spatially arranging both organocatalytic entities required for cooperative bifunctional catalysis, which are...

- ...an *N*-phenyl-3-(pyridin-2-yl)-1*H*-pyrazol-5-amine ligand (highlighted in green), which is supposed to activate nitroalkenes and / or nitroacrylates by double hydrogen-bonding, just as the amidopyrazole ligands in catalysts **Λ-81**, **Λ-85**, **Λ-89**, and **Λ-(*R*,*R*)-90** (see chapter 1.4, Schemes 15−18)...
- ...and an isoindoline moiety (highlighted in blue) attached to the cyclometalated phenylbenzoxazole ligands, which is supposed to activate enolizable aldehydes or ketones by the formation of an enamine intermediate, just as the cyclic secondary amine in catalyst **Λ-99** (see chapter 1.4, Schemes 20).

Accordingly, catalyst **Λ-T29** was intended − figuratively speaking − to be a merger of double-hydrogen bonding catalysts **Λ-81**, **Λ-85**, **Λ-89**, or **Λ-(*R*,*R*)-90** and single-hydrogen-bonding/enamine catalyst **Λ-99**.

The envisioned catalytic cycle for **Λ-T29** is depicted in Scheme 45 using aldehyde **167a** and nitroacrylate **168a** as substrate examples.

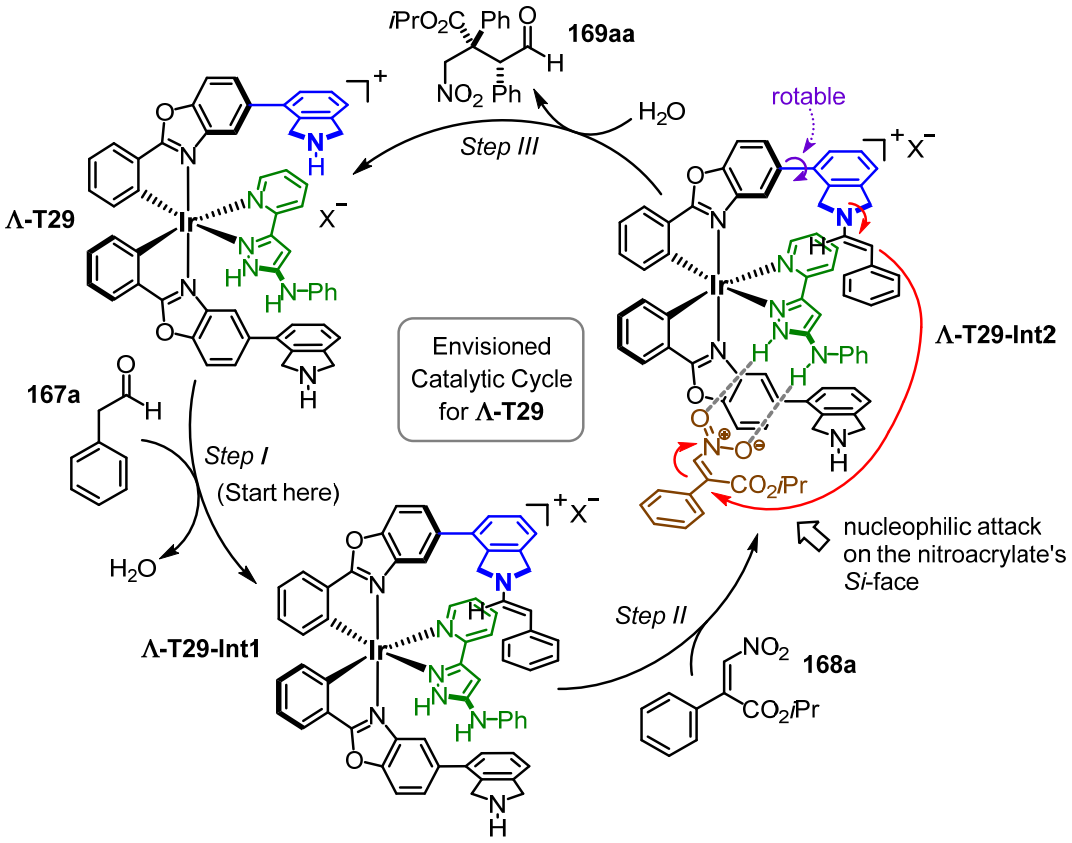

Scheme 45. Envisioned catalytic cycle for the Michael addition of 2-phenylacetaldehyde (**167a**) to isopropyl (*Z*)-3-nitro-2-phenylacrylate (**168a**) with **Λ-T29** as catalyst. This scheme is not able to give a precise picture of the spatial situation, please refer to Figure 31 to get an impression of the spatial situation in **Λ-T29** and intermediates **Λ-T29-Int1** and **Λ-T29-Int2**.

At first, **Λ-T29** was expected to react with enolizable aldehyde **167a** in a condensation reaction to form intermediate enamine **Λ-T29-Int1** (Scheme 45, Step I). Next, nitroacrylate **168a** was expected to bind to **Λ-T29-Int1** in a non-covalent fashion with the aminopyrazole moiety acting as double hydrogen-bond donor, resulting in the formation of ternary complex **Λ-T29-Int2** (Step II; Steps I and II may also take place in reverse order). The intermediate enamine, in theory now well-aligned with the nitroacrylate (see Figure 31 for an illustration), was then expected to "intramolecularly" attack the nitroacrylate in a conjugate fashion to give Michael addition product **169aa** and catalyst **Λ-T29** after hydrolysis (Step III).

Importantly, the double hydrogen-bonded nitroacrylate in Scheme 45 faces the intermediate enamine with its *Si*-face. In theory, it could also face it with its *Re*-face. However, modeling

suggested that the latter would result in steric clashes with the catalyst's phenylbenzoxazole framework. This circumstance was anticipated to ensure a good prochiral recognition.

Figure 31 shows another envisioned catalyst, complex **Λ-T30**, which differs from **Λ-T29** by the fact that the phenyl rings of its phenylbenzoxazole ligands feature additional 2,6-dimethylphenyl substituents. In addition to the structure of **Λ-T30**'s corresponding ternary intermediate **Λ-T30-Int2**, a three-dimensional representation of **Λ-T30-Int2** is shown in Figure 31, which serves to illustrate the spatial situation in the catalyst and in the intermediates in general.

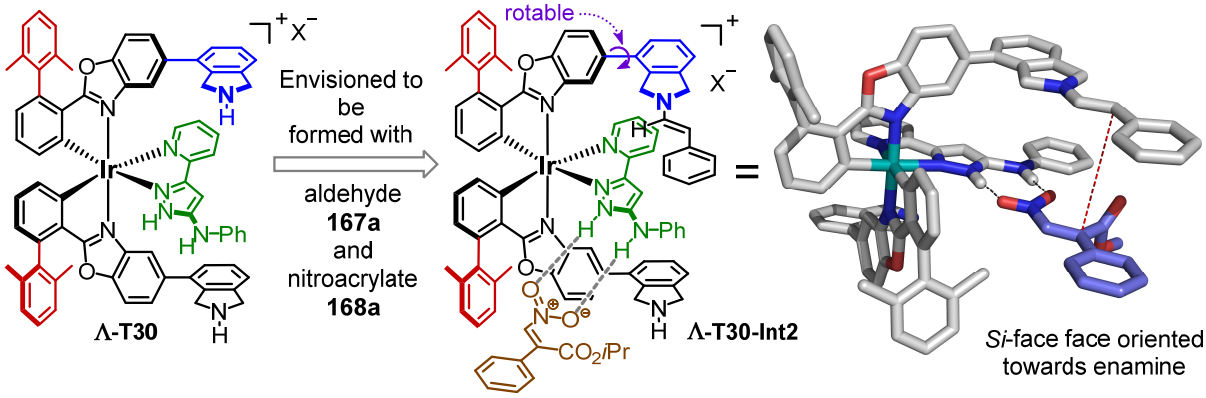

Figure 31. *Left*: Envisioned catalyst **Λ-T30** featuring additional 2,6-dimethylphenyl substitutents (red). *Center*: **Λ-T30**'s corresponding ternary intermediate **Λ-T30-Int2** formed from **Λ-T30**, **167a**, and **168a**. *Right:* Three-dimensional representation of **Λ-T30-Int2**. The two gray dashes represent the hydrogen bonds between the nitroacrylate's nitro group and the aminopyrazole moiety and the red dashes connect the nucleophilic C-atom of the enamine moiety with the electrophilic C-atom of the underlying nitroacrylate to illustrate their proximity.[105]

As depicted in Figure 31, the nucleophilic C-atom of intermediate enamine **Λ-T30-Int2** should be perfectly aligned with the electrophilic C-atom of the nitroacrylate for a reaction (red dashes). It is also apparent that the opposite binding mode of the nitroacrylate, that is to say with its *Re*-face facing the enamine, should be unfavorable due to steric interactions with the catalyst's phenylbenzoxazole framework and also with one of the 2,6-dimethylphenyl substituents. Accordingly, the introduction of the 2,6-dimethylphenyl substituents in case of advanced catalyst **Λ-T30** was envisioned to result in an improved version of parent catalyst **Λ-T29**.

Figure 31 also hints at the possibility that such a catalyst might not only be able to control the enantioselectivity but also the diastereoselectivity. Under the assumption that *Si*-face orientation with regard to the nitroacrylate, as depicted in Figure 31, is energetically favorable, only the enamine conformer which is drawn in Figure 31 is perfectly aligned with the underlying nitroacrylate. This is crucial as the conformer of the enamine − i.e., with its *Re*- or with its *Si*-face towards the nitroacrylate − determines the emerging configuration at the *α*-position of resulting aldehyde **169aa**.

It is worth mentioning that aldehyde **167a** could also form an enamine with the remaining isoindoline moiety which is present in **Λ-T29** and **Λ-T30**. However, as that isoindoline moiety is lacking an appropriately oriented double hydrogen-bonding motif, it was anticipated that this enamine would just constitute an unproductive resting state of both catalysts and would, if at all, only insignificantly contribute to the reaction.

In order to synthesize complexes of type **Λ-T29**, a significant problem had to be overcome at first: A method had to be devised to assemble optically pure complexes of type **Λ-T29** featuring free secondary amines / isoindolines (Figure 32).

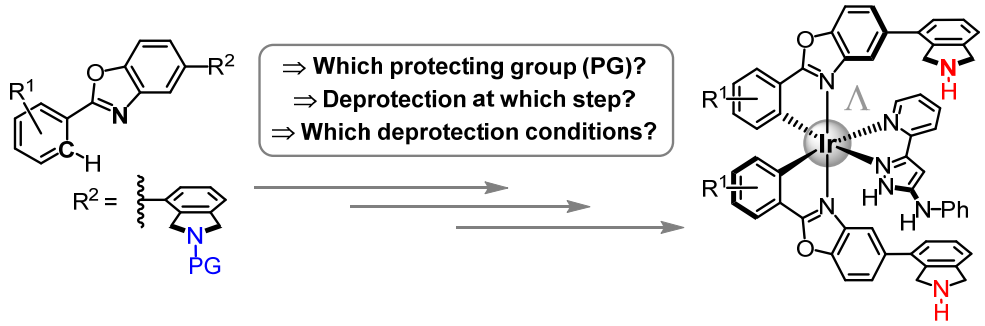

Figure 32. Synthetic problem: How to assemble optically pure complexes of type **Λ-T29** featuring free secondary amines / isoindolines?

This was considered challenging as the standard synthesis of bis-cyclometalated Ir(III) complexes proceeds via Ir(III) dimers of type $[Ir^{III}(C\hat{}N)_2(\mu\text{-}Cl)]_2$ (C^N: cyclometaled ligand).[77] And they are commonly prepared by means of heating of the respective ligand to be cyclometalated in the presence of $IrCl_3 \cdot 3H_2O$ in an alcoholic mixture (often 2-ethoxyethanol / water) at > 100 °C (Nonoyama's method)[77] – which are conditions that free amines in ligands to be cyclometalated do not tolerate.[113] Moreover, organic and organometallic compounds with aliphatic amines are usually highly basic, which implicates that they considerably tail on conventional silica gel columns, often even when large amounts of a base modifier are present in the eluent. For this reason, it was planned to protect the isoindoline moieties of the phenylbenzoxazole ligands to be cyclometalated with a suitable protecting group being able to withstand the cyclometalation conditions, and to cleave this protecting group as late as possible in the course of the synthesis.

3.2 Results and Discussion

3.2.1 Preparation and Characterization of the Envisioned Iridium(III) Complexes

The conceived protection-deprotection strategy from Figure 32 could indeed be implemented by relying on carboxybenzyl (Cbz) as protecting group and by cleaving the Cbz groups in the final step of **Λ-T29**'s synthesis with a modified version of Birkofer's decarbobenzoxylation procedure.[114] Scheme 46 shows the synthesis scheme for complex **Λ-T29** with the applied conditions and the obtained yields.

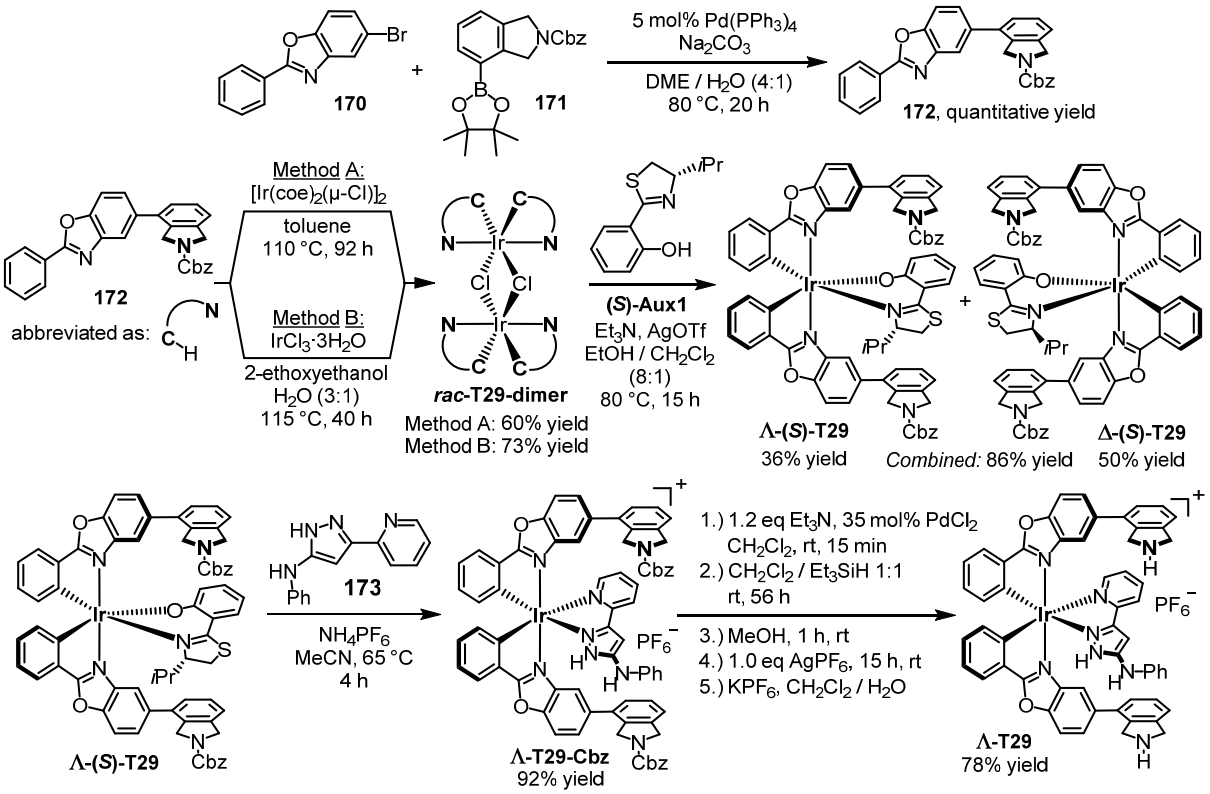

Scheme 46. Synthesis of complex **Λ-T29** starting from brominated phenylbenzoxazole **170** and *N*-Cbz-protected isoindoline boronic acid **171**. Details are provided in the experimental section.

First, brominated phenylbenzoxazole **170** and *N*-Cbz-protected isoindoline boronic acid **171** were subjected to Suzuki-Miyaura cross-coupling to give *N*-Cbz-protected isoindoline-functionalized phenylbenzoxazole **172**. Initially, it was expected that the Cbz group in **172** would not withstand the comparatively harsh cyclometalation conditions with $IrCl_3 \cdot 3H_2O$ in 2-ethoxyethanol and water at > 100 °C to give ***rac*-T29-dimer** ($[Ir^{III}(C\hat{}N)_2(\mu\text{-}Cl)]_2$; C^N represents cyclometalated **172**) according to Nonoyama's procedure.[77] Accordingly, a milder method was evaluated at first, namely the reaction between **172** and iridium(I) precursor $[Ir^{I}(coe)_2(\mu\text{-}Cl)]_2$ (coe = cyclooctene) in dry toluene at 110 °C, which had not been reported at that time for 2-phenylbenzoxazoles as cyclometalating ligands (C^N) but for structurally related 2-phenylpyridines.[115,116] And indeed, ***rac*-T29-dimer** could be obtained in 60% yield

with this method under non-optimized conditions (Scheme 46, Method A). It was found to be imperative to perform this reaction with strictly degassed toluene due to the sensitivity of Ir(I) precursor $[Ir^{I}(coe)_2(\mu\text{-}Cl)]_2$ to oxidation. However, Nonoyama's procedure was additionally tested.[77] Unexpectedly, compound ***rac*-T29-dimer** was formed smoothly with Nonoyama's procedure and could be isolated in 73% yield (Method B).

The next steps were performed with modifications of procedures which were established in the Meggers laboratory: First, ***rac*-T29-dimer** was cleaved with auxiliary ligand **(*S*)-Aux1** to give diastereomeric iridium(III) complexes **Λ-(*S*)-T29** and **Δ-(*S*)-T29**, which were separated and purified via standard silica flash chromatography.[79] Next, auxiliary ligand **(*S*)-Aux1** was cleaved off and replaced by pyridylpyrazole ligand **173** to give complex **Λ-T29-Cbz**.[38a] Cleavage of both Cbz groups of **Λ-T29-Cbz** was planned as the final step en route to **Λ-T29**. It was originally planned to realize this step by means of Pd(0)-catalyzed hydrogenolytic cleavage with palladium on charcoal (Pd/C) as catalyst. This is commonly considered as the method of choice for *N*-Cbz cleavage as it is economic, easy to perform, tolerates a broad range of functional groups, and usually proceeds in the absence of side reactions.[117] However, when attempts were made to cleave off the Cbz groups from **Λ-T29-Cbz** by means of that, no conversion could be found apart from some decomposition in a few cases (Table 21).

Table 21. Hydrogenolytic Cbz-cleavage experiments with compounds **Λ-T29-Cbz**, **Λ-(*S*)-T29**, **Λ-T29-acac**, **172**, and **Λ-(*S*)-V1**.

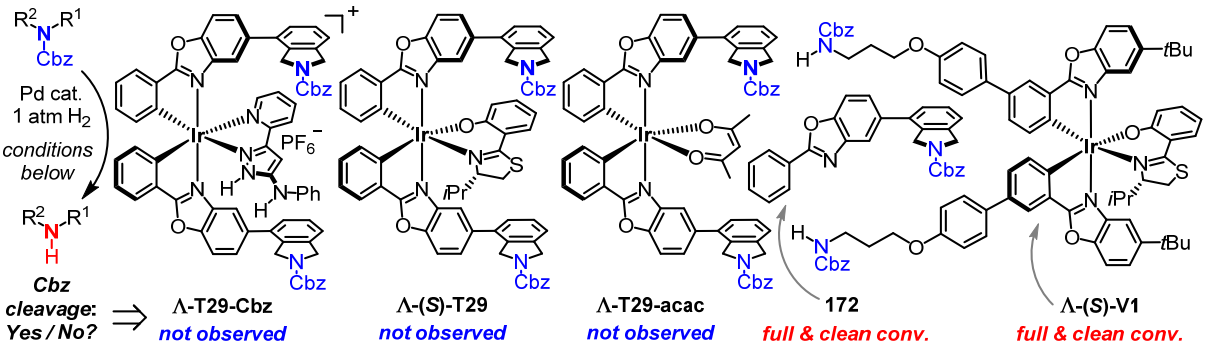

entry	substrate	Pd source (wt%)	Pd loading (mol%)	solvent	conc (mM)	*t* (°C)	time (h)	conv
1	**Λ-T29-Cbz**	Pd/C (10)	21	EtOH	14	rt	3	no conv
2	**Λ-T29-Cbz**	Pd/C (10)	23	THF / MeOH 4:1	13	rt	13	no conv[a]
3	**Λ-T29-Cbz**	Pd/C (10)	28	EtOAc / MeOH 4:1	14	rt	13	no conv
4	**Λ-T29-Cbz**	$Pd(OH)_2$/C (20)	22	THF / MeOH 1:1	10	rt	19	no conv
5	**Λ-T29-Cbz**	Pd/C (10)	42	THF / MeOH 1:1	10	40	19	no conv[a]
6	**Λ-T29-Cbz**	Pd/C (10)	22	THF / EtOH 1:4	12	75	19	no conv[a]
7	**Λ-(*S*)-T29**	Pd/C (10)	20	THF / EtOH 1:4	13	rt	19	no conv
8	**Λ-T29-acac**	Pd/C (10)	32	THF / EtOH 1:4	12	rt	19	no conv
9	**172**	Pd/C (10)	21	THF / EtOH 1:4	12	rt	19	full and clean[b]
10	**Λ-(*S*)-V1**[70]	Pd/C (10)	30	EtOAc / MeOH 1:4	6	rt	24	full and clean[c]

[a]Unclean reaction, decomposition products observed by TLC. [b]Desired amine isolated in 73% yield (non-optimized conditions). [c]Desired bisamine isolated in 93% yield (optimized conditions).[70]

The outcome did also not change when higher palladium loadings and elevated temperatures were applied (Table 21, entries 5–6). It was initially assumed that the salt character of **Λ-T29-Cbz** would impede its interaction with the palladium's surface and hence preclude Cbz cleavage. However, when attempts were made to cleave the Cbz groups of neutral complexes **Λ-(*S*)-T29** and **Λ-T29-acac**, no conversion was found either (entries 7–8). In contrast, purely organic ligand **172** could be deprotected without any problems (entry 9). Surprisingly and in contrast to **Λ-T29-Cbz**, **Λ-(*S*)-T29**, and **Λ-T29-acac**, it was possible to cleave off both *N*-Cbz groups from complex **Λ-(*S*)-V1** without any problems (entry 10). Complex **Λ-(*S*)-V1** has recently been utilized in the Meggers laboratory as a precursor for the covalent immobilization of a Lewis acidic stereogenic-only-at-metal catalyst.[70]

Finally, when a strongly modified version of Birkofer's decarbobenzoxylation procedure was applied,[114] which relies on *in situ* reduction of a Pd(II) species to Pd(0) with an amine as reductant and triethylsilane as transfer hydrogenation reagent,[114] both Cbz groups of **Λ-T29-Cbz** could be cleaved off smoothly and desired catalyst **Λ-T29** could be isolated in a respectable yield of 78% (see Scheme 46, final step).

In order to verify **Λ-T29**'s enantiopurity, a small sample of isolated **Λ-T29** was reprotected with CbzCl to **Λ-T29-Cbz** (chiral HPLC conditions had been already established at that time for **T29-Cbz**). Chiral HPLC analysis revealed >99% ee for reprotected **Λ-T29-Cbz**, which indirectly proved that desired **Λ-T29** had indeed >99% ee (Figure 33).

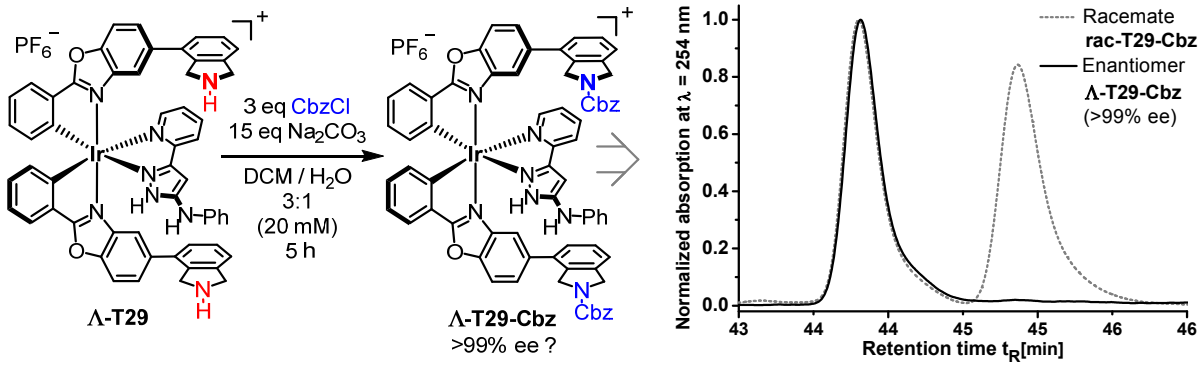

Figure 33. *Left*: Reprotection of **Λ-T29**. *Right*: Superposition of absorption-normalized excerpts of the chiral HPLC traces of ***rac*-T29-Cbz** and **Λ-T29-Cbz**. Chiral HPLC conditions: Chiralpak IB column (5 µm, 25 cm x 4.6 mm); eluent: MeCN / 0.1% TFA (aq); 40:60 → 80:20 (gradient; 40 min) → 80:20 (isocratic; 10 min), λ = 254 nm, flow = 0.75 mL/min, *t* (column) = 35 °C.

The same synthetic strategy was next utilized to synthesize 2,6-dimethylphenyl substituted complex **Λ-T30** (Scheme 47). In contrast to **Λ-T29** (see Scheme 46), *tert*-butyl-substituted salicyloxazoline auxiliary ligand **(*S*)-Aux2** was used instead of isopropyl-substituted salicylthiazoline auxiliary ligand **(*S*)-Aux1** as the diastereomers formed with **(*S*)-Aux1** had proven to be virtually inseparable via flash chromatography.

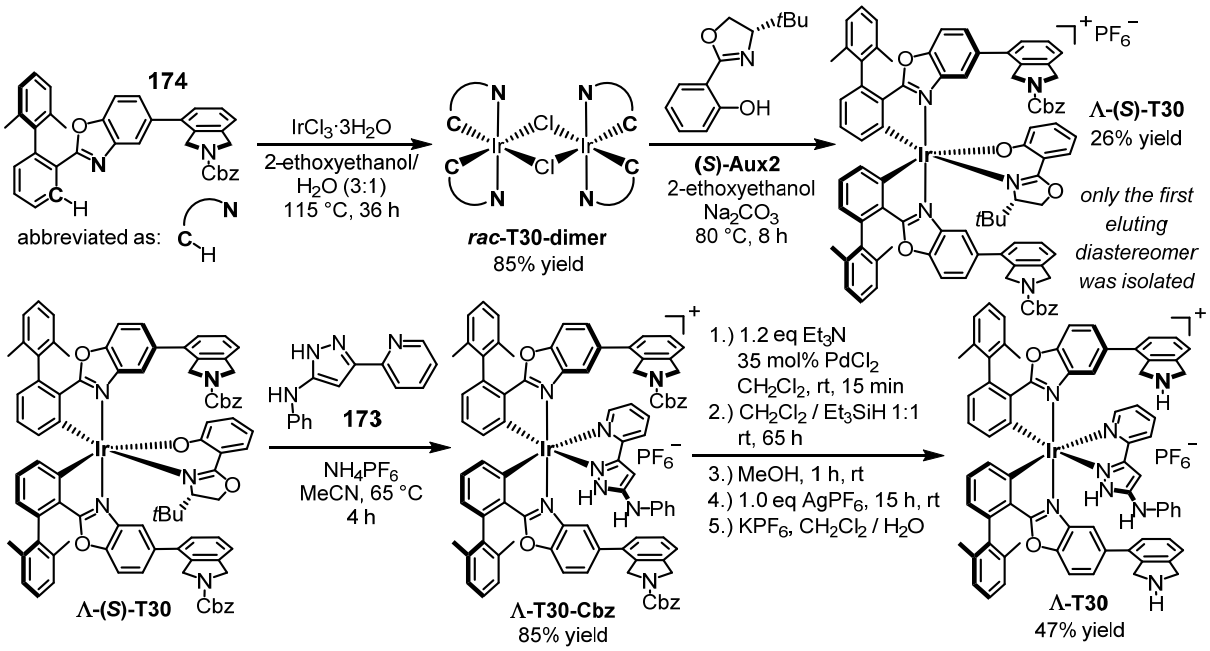

Scheme 47. Synthesis of complex **Λ-T30** starting from *N*-Cbz-protected isoindoline-functionalized phenylbenzoxazole ligand **174**.

As the synthesis routes from Schemes 46 and 47 had proven to be reliable, it was now speculated whether it would be possible to replace the catalytically essential pyridylpyrazole ligand of **Λ-T29** by the according C_2-symmetric bispyrazole ligand (Figure 34).

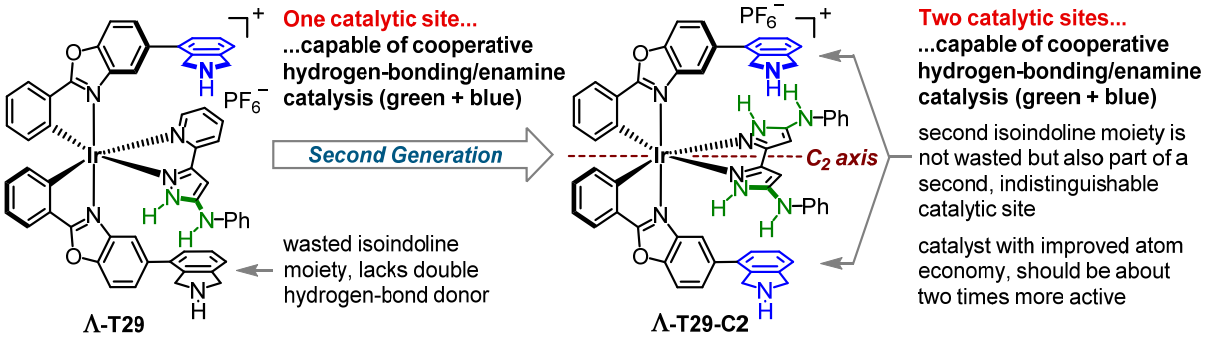

Figure 34. Envisioned catalyst enhancement: Replacement of the dissymmetric pyridylpyrazole ligand of **Λ-T29** by a symmetric bispyrazole ligand should result in the enhanced C_2-symmetric catalyst **Λ-T29-C2**.

As explained in chapter 3.1, catalyst **Λ-T29** features one bifunctional cooperative catalytic site, which consists of one of both isoindoline moieties of **Λ-T29** (Figure 34, *left*, highlighted in blue) and the aminopyrazole moiety (Figure 34, *left*, highlighted in green). While examining the catalyst's structure, it was recognized that catalysts of type **Λ-T29** suffered from a "design flaw" as they comprise a second, basically wasted isoindoline moiety lacking an appropriately positioned double hydrogen-bond donor required for cooperative catalysis. Accordingly, it was envisioned to synthesize C_2-symmetric bispyrazole-based complex

Λ-T29-C2, which would comprise two indistinguishable catalytic sites capable of cooperative enamine/hydrogen-bonding catalysis (Figure 34, *right*).

At that time, no literature reports dealing with metalorganic transition metal complexes with bispyrazoles as bidentate ligands were available. Accordingly, to investigate whether bispyrazole ligands would coordinate to the Ir(III) center of bis-cyclometalated complexes in the anticipated manner and to study their stability and general properties, bispyrazole ligand **180** was prepared following a straightforward synthetic route from H.-D. Stachel (Scheme 48).[118] It is worth noting that this synthesis route does not require any time-consuming chromatography to provide **180** analytically pure (details are provided in the experimental section).

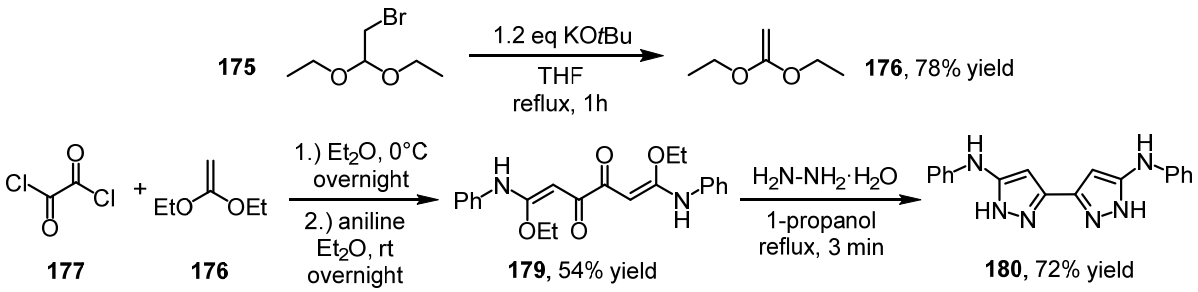

Scheme 48. Bispyrazole **180** was prepared according to a synthetic route reported by H.-D. Stachel.[118]

Next, it was attempted to synthesize racemic bispyrazole probe complex ***rac*-T31-C2** from Ir(III) dimer ***rac*-T31-dimer** (Scheme 49). And indeed, when ***rac*-T31-dimer** was stirred with bispyrazole **180** in CH_2Cl_2 / MeOH 4:1 in the presence of silver hexafluorophosphate at rt for 3 h, desired bispyrazole complex ***rac*-T31-C2** was formed and could be isolated in 92% yield.

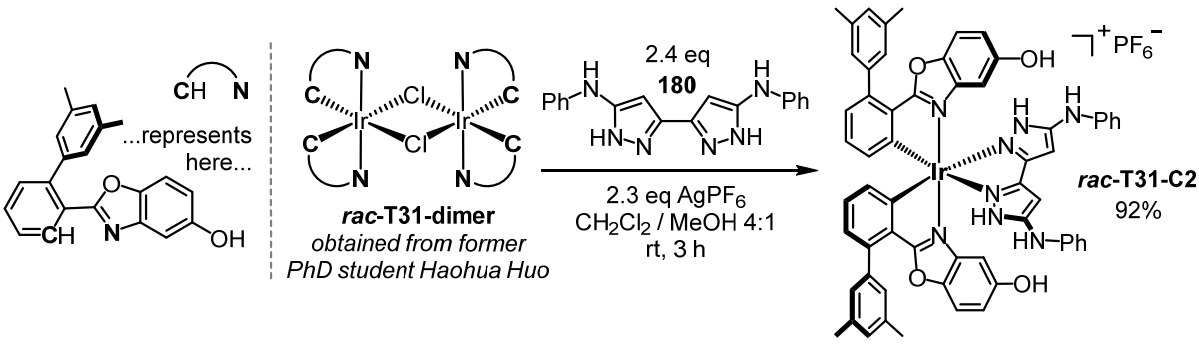

Scheme 49. Synthesis of racemic bispyrazole complex ***rac*-T31-C2**.

Importantly, bispyrazole probe complex ***rac*-T31-C2** proved to be stable towards silica gel flash chromatography and NMR experiments confirmed the anticipated formation of a C_2-symmetric complex (Figure 35). In order to study the stability of complex ***rac*-T31-C2** in solution, this NMR-tube was left standing at rt for 4.5 d (non-degassed, non-dry DMSO-d_6 as solvent). No sign of any decomposition of ***rac*-T31-C2** could be observed (Figure 35).

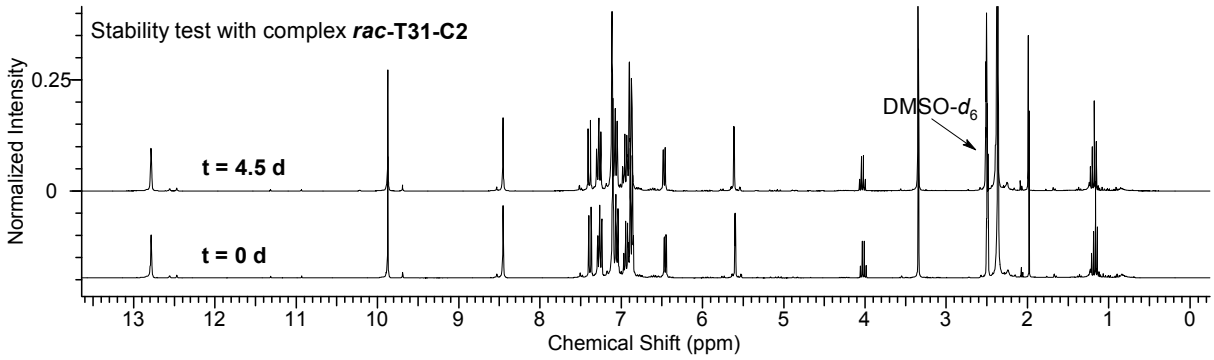

Figure 35. Complex ***rac*-T31-C2** was kept in non-degassed and non-dry DMSO-d_6 at rt for 4.5 d. No change in the ^{1}H NMR signal pattern and accordingly no sign of a any decomposition was found.

From these experiments with bispyrazole ligand **180** and bispyrazole probe complex ***rac*-T31-C2** it was concluded...

- ...that bispyrazole ligands of type **180** indeed coordinate the Ir(III) center and, moreover, in the anticipated fashion, which results in C_2-symmetric complexes such as ***rac*-T31-C2**,...
- ...that the resulting complexes should be sufficiently stable in solution and towards silica gel chromatography to serve as feasible scaffolds for the design of kinetically-inert stereogenic-at-metal catalysts,...
- ...and that the remarkably simple and straightforward synthetic route to amine-functionalized bispyrazoles from H.-D. Stachel (Scheme 48), which had rarely been used by other researchers at that time,[118] should pave the way to the rapid synthesis of a library of bispyrazole ligands to be evaluated, which would facilitate the design of bispyrazole-based stereogenic-at-metal catalysts.

Having with complexes **Λ-T29** and **Λ-T30** two of the envisioned enamine/hydrogen-bonding catalysts in hand, their catalytic properties were investigated next (chapter 3.2.2).

3.2.2 Catalytic Properties of the Prepared Complexes

With complexes **Λ-T29**, ***rac*-T29** (synthesis in the experimental section), and **Λ-T30** in hand, it was next attempted to use them as catalysts for the asymmetric Michael addition of enolizable aldehydes and / or ketones to nitroacrylates and / or nitroolefins.

The initial results for the experiments with aldehydes / ketones **167a–f** and nitroacrylates **168a–b** with **Λ-T29** as intended catalyst are summarized in Table 22. Similar reaction conditions were applied which had proven suitable in case of the reduction of nitroalkenes with a Hantzsch ester with catalyst **Λ-81** (see chapter 1.4, Scheme 15)[38a] and in case of the Friedel–Crafts alkylation of indoles with nitroacrylates with catalyst **Λ-85** (see chapter 1.4, Scheme 16).[38b] In case of all experiments from Table 22, 4 mol% of **Λ-T29** were employed together with 6 mol% of $NaBArF_{24}$ to enhance the solubility of complex **Λ-T29** in the non-polar solvents via *in situ* anion exchange.[49] Prior to this, it had been verified that $NaBArF_{24}$ neither promoted any unwanted side-reactions nor catalyzed any background reaction.

Table 22. Attempted conjugate additions of enolizable aldehydes / ketones **167a–f** to nitroacrylates **168a–b** with complex **Λ-T29** as intended catalyst.

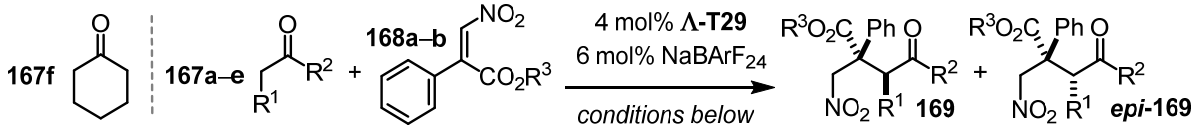

entry	R^1, R^2 (**167**)[a]	eq of **167**	R^3 (**168**)	solvent	conc (M)	*t* (°C)	time (h)	result
1	hexyl, H (**167b**)	1.5	*i*Pr (**168a**)	toluene	0.7	rt	20 h / 4 d	n.c. / n.c.[b]
2	Ph, H (**167a**)	1.5	*i*Pr (**168a**)	toluene	0.7	rt	15 h / 2 w	n.c. / n.c.[c]
3	Ph, H (**167a**)	1.5	Me (**168b**)	toluene	0.7	rt	17 h / 2 w	n.c. / n.c.[c]
4	Ph, H (**167a**)	1.5	Me (**168b**)	CH_2Cl_2	0.7	rt	17 h / 2 w	n.c. / n.c.[c]
5	Ph, H (**167a**)	6.0	*i*Pr (**168a**)	toluene	0.7	45	26 h / 4 d	n.c. / n.c.[c]
6	H, H (**167c**)	2.0	*i*Pr (**168a**)	toluene	0.7	rt	–	cat. decomp.[d]
7	Me, H (**167d**)	3.0	*i*Pr (**168a**)	toluene	0.7	rt	19 h / 2 w	n.c. / n.c.
8	OMe, Me (**167e**)	1.5	*i*Pr (**168a**)	toluene	0.7	rt	19 h / 2 w	n.c. / n.c.
9	cyclohexanone (**167f**)	1.5	*i*Pr (**168a**)	toluene	0.7	rt	19 h / 2 w	n.c. / n.c.

[a]All employed aldehydes were distilled before use. [b]N.c. = no conversion. [c]Considerable self-aldolization of the aldehyde observed (confirmed by NMR). [d]Catalyst decomposition within minutes (confirmed by TLC).

As shown in Table 22, catalyst **Λ-T29** was not able to catalyze any of the screened reactions between nitroacrylates **168a–b** and enolizable aldehydes / ketones **168a–f**. In case of phenylacetaldehyde (**167a**), considerable amounts of self-aldolization products were observed after prolonged reaction times, which were not formed when **Λ-T29** was absent (entries 2–5). This indicated that at least one of both isoindoline moieties of **Λ-T29** was accessible to phenylacetaldehyde (**167a**) but apparently **Λ-T29** only catalyzed its self-aldolization instead of the desired conjugate addition to nitroacrylates **168a–b**.

Next, the intended reaction between aldehyde **167a** and nitroacrylate **168a** was repeated with the reaction conditions from Table 22, entry 2 but complex **Λ-T29** was replaced by 8 mol% isoindoline hydrochloride salt **181** and 8 mol% Et_3N (Scheme 50). Et_3N was added to deprotonate hydrochloride salt **181** *in situ*. 8 mol% of **181** were used to account for the two isoindoline moieties that are present in complex **Λ-T29**.

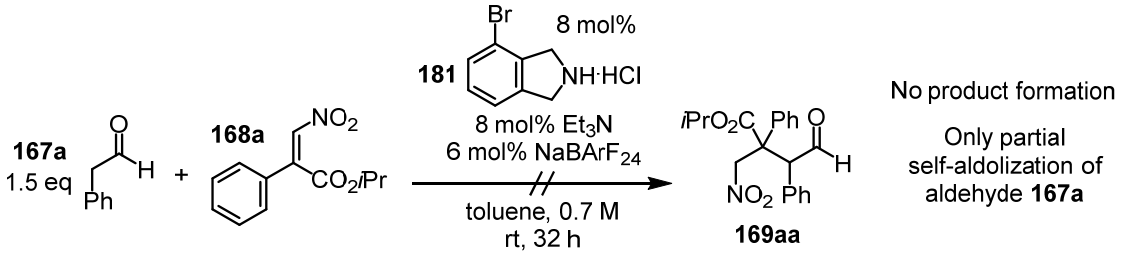

Scheme 50. Attempted synthesis of **169aa** from **167a** and **168a** with **181** and Et_3N. Aldehyde **167a** was freshly distilled before use.

The experiment from Scheme 50 virtually gave the same result as the experiment from Table 22, entry 2: only partial self-aldolization of **167a** could be observed. This indicated that **Λ-T29** did not act as intended, i.e., not as a cooperative catalyst, at least not in case of substrates **167a** and **168a**, and this supported that at least one of both isoindoline moieties of **Λ-T29** catalyzed the self-aldolization of **167a**.

Subsequently, a similar experiment was performed with octanal (**167b**) and *trans*-*β*-nitrostyrene (**182**) as substrates (Scheme 51).

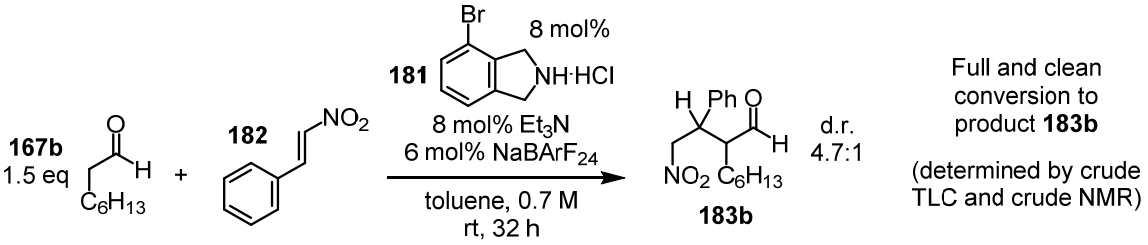

Scheme 51. Synthesis of **183b** from **167b** and **182** with **181** and Et_3N. Aldehyde **167b** was freshly distilled before use.

In contrast, this experiment provided desired **183b** smoothly within 32 h with a d.r. of 4.7:1. Now, it was investigated whether catalysts of type **Λ-T29** would give similar results with *trans*-*β*-nitrostyrene (**182**) and, moreover, whether these complexes would be able to provide products **183** with reasonable levels of enantioselectivity and diastereoselectivity (Table 23).

Table 23. Experiments with enolizable aldehydes / ketones (**167a–f**) and *trans*-*β*-nitrostyrene (**182**) with complexes ***rac*-T29**, **Λ-T29**, and **Λ-T30**.

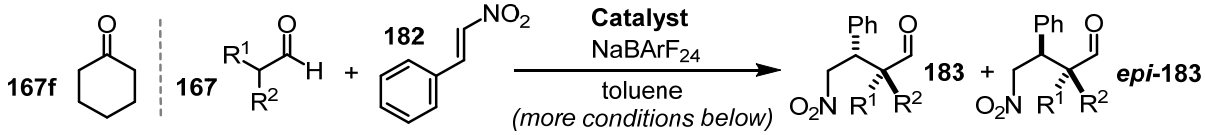

entry	R^1, R^2 (**167**)[a]	eq of **167**	catalyst	cat. loading (mol%)	$NaBArF_{24}$ (mol%)	conc (M)	*t* (°C)	time	result
1	hexyl, H (**167b**)	1.5	***rac*-T29**	4	6	0.7	rt	30 h	full conv (**183b**) 69% isolated yield d.r. 2.5:1[b]
2	hexyl, H (**167b**)	1.5	***rac*-T29**	1	1.5	0.7	rt	14 d	incomplete (**183b**) 25% isolated yield d.r. 3:1[b]
3	Me, Me (**167g**)	1.5	***rac*-T29**	2	3	0.7	rt	14 d	incomplete (**183g**) 10% isolated yield
4	Ph, Me (**167h**)	1.5	***rac*-T29**	2	3	0.7	rt	14 d	incomplete (**183h**) 12% isolated yield d.r. not determined
5	Et, Et (**167i**)	1.5	***rac*-T29**	4	6	0.7	rt	14 d	no trace of conv
6	Bu, Me (**167j**)	1.5	***rac*-T29**	2	3	0.7	rt	14 d	no trace of conv
7	*t*-Bu, H (**167k**)	5.0	***rac*-T29**	2	3	0.7	rt	14 d	no trace of conv
8	cyclohexanone (**167f**)	5.0	***rac*-T29**	2	3	0.7	rt	14 d	incomplete (**183f**) 46% isolated yield d.r. 3:1[b]
9	hexyl, H (**167b**)	1.5	**Λ-T29**	4	6	0.7	rt	28 h	full conv (**183b**) d.r. 2.9:1[c] major: 17% ee[d] minor: 14% ee[d]
10	hexyl, H (**167b**)	1.5	**Λ-T30**	4	6	0.7	rt	28 h	full conv (**183b**) d.r. 1.8:1[c] major: 19% ee[d] minor: 33% ee[d]

[a]All employed aldehydes were distilled before use. [b]D.r. determined from isolated product by ^{1}H NMR analysis. [c]D.r determined from crude product mixture by ^{1}H NMR analysis. [d]Enanioselectivity determined from crude product mixture by chiral HPLC analysis (HPLC traces for entries 9 and 10 are shown in Figure 36)

And indeed, with 4 mol% of complex ***rac*-T29** and substrates **167b** and **182**, product **183b** was smoothly provided within 30 h and subsequently isolated in reasonable 69% yield with an isolated d.r. of 2.5:1 (Table 23, entry 1). However, when the loading of complex ***rac*-T29** was reduced to 1 mol%, the reaction became exceptionally sluggish (entry 2). For sterically demanding *α*-branched aldehydes, either a sluggish reaction was observed (entries 3–4) or no conversion at all (entries 5–7). Also with cyclohexanone (**167f**) as substrate a sluggish reaction was observed (entry 8). It was concluded from these results that, if at all, only non-*α*-branched aldehydes, such as octanal (**167b**), were applicable under the used conditions at catalyst loadings of approx. 4 mol%.

Eventually, enantiopure catalysts **Λ-T29** and **Λ-T30** were employed as catalysts for the reaction between octanal (**167b**) and *trans*-*β*-nitrostyrene (**182**; entries 9–10). As expected, both reactions proceeded smoothly to completion within 28 h. NMR analysis of the crude

product mixtures of both experiments revealed d.r. values for **183b** of 2.9:1 (**Λ-T29**; entry 9) and 1.8:1 (**Λ-T30**; entry 10). For **Λ-T29**, chiral HPLC analysis of the crude product mixture revealed 17% ee for the major diastereomer of **183b** and 14% ee for the minor one (entry 9). For **Λ-T30**, chiral HPLC analysis revealed 19% ee for the major diastereomer of **183b** and 33% ee for the minor one (entry 10). Both chiral HPLC traces are shown in Figure 36.

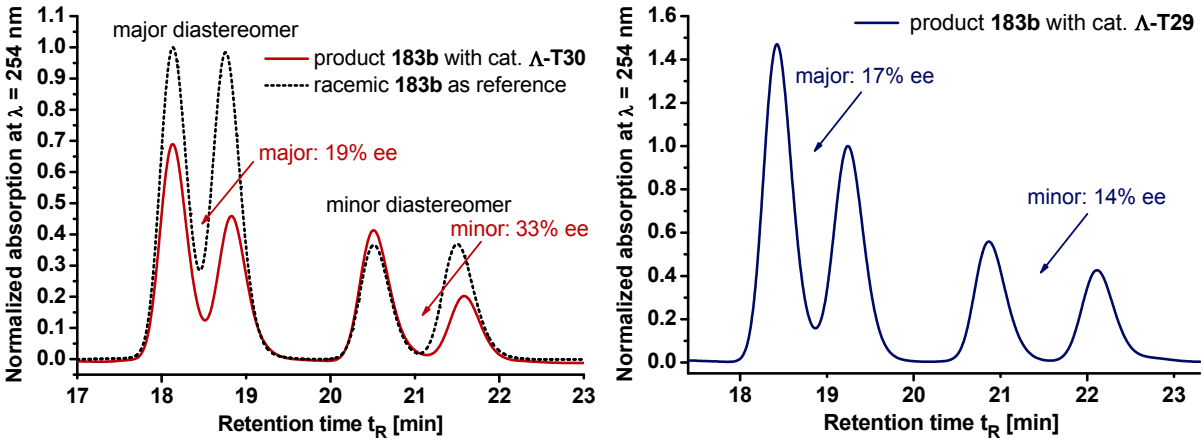

Figure 36. Excerpts from the chiral HPLC traces of racemic **183b** and enantioenriched products **183b** obtained with catalysts **Λ-T29** (Table 23, entry 9) and **Λ-T30** (Table 23, entry 10). All traces are normalized relative to the HPLC trace of racemic **183b**. Chiral HPLC conditions: Chiralpak AD-H column (5 µm, 25 cm x 4.6 mm); *n*-hexane / *i*-PrOH 95:5, λ = 220 nm, flow = 0.5 mL/min, *t* (column) = 14 °C.

In addition to the overall less promising catalysis results with catalysts of type **Λ-T29**, another not yet mentioned issue eventually led to the termination of the enamine/hydrogen-bonding catalyst project:

During experimentation with catalysts of type **Λ-T29**, problems with the stability of such isoindoline-functionalized Ir(III) complexes became apparent: While all their *N*-Cbz-protected precursors were found to be stable in solution for weeks, quick decomposition of the deprotected complexes within a couple of hours could be observed. This was initially noticed as brightly orange complex solutions gradually turned dark. The decompositions of the respective complexes were later on confirmed by TLC and NMR analysis. Moreover, such darkened complex batches displayed a reduced catalytic activity compared to freshly prepared complex batches.

Although this decomposition was not studied in detail, it appears to be the result of an oxidation of the deprotected isoindoline moieties. This (presumable) oxidation might be simple autoxidation or in part actively phototriggered by the respective Ir(III) complexes themselves.[73]

3.3 Summary and Outlook

In summary, the stereogenic-only-at-metal enamine/hydrogen-bonding catalyst project was eventually terminated for the following reasons:

- Because of the ascertained narrow reaction scope (see Tables 22 and 23).
- Because of the strong indication that complexes of type **Λ-T29** do not, as anticipated, act as cooperative bifunctional catalysts (see Tables 22 and 23 as well as Schemes 50 and 51).
- Because of the low stereoselectivities found for product **183b** which was synthesized with catalysts **Λ-T29** and **Λ-T30** (see Table 23, entries 10–11 and Figure 36).
- And finally, because of the ascertained low stability of complexes of type **Λ-T29** in solution, which appears to be the result of a high susceptibility to oxidation.

Especially the second and the fourth point here indicate a serious "design flaw", which should be addressed first of all in case a resumption of this project is considered.

Although the designed catalysts did not meet the expected properties, several important tasks could be accomplished:

- A synthetic access could be established to complexes of type **Λ-T29**, which relies on the one hand on 1.) previously developed synthetic methods from the Meggers laboratory[79] and on the other hand on 2.) a protection-deprotection strategy with carboxybenzyl (Cbz) as *N*-protecting group and a modified version of Birkofer's decarbobenzoxylation procedure for late-stage Cbz cleavage (see Schemes 46 and 47).[114]

  It is worth mentioning in this context that the *N*-Cbz-protected isoindoline moieties of complexes of type **Λ-T29** could be nowadays, most likely, much more conveniently introduced by means of a post-complexation cross-coupling protocol, which has recently been developed in the Meggers laboratory[78] and which has been utilized to synthesize some of complexes **Λ-T1**–**Λ-T28** from chapter 2. (see chapter 2.3.1, Scheme 30, Route II).
- With the synthesis of bispyrazole **180** (Scheme 48) and its use as a bidentate ligand in proof-of-principle complex ***rac*-T31-C2** (Scheme 49 and Figure 35), the way was paved to the development of kinetically-inert C_2-symmetric bispyrazole-based Ir(III) catalysts (see Figure 38 below).[63,64]

Some of the knowledge and know-how which could be attained in the course of this project later on significantly contributed to other, successfully accomplished projects:

- Accumulated knowledge in terms of *N*-Cbz-protections and -deprotections in bis-cyclometalated Ir(III) complexes later on significantly accelerated the synthetic implementation of polymer-supported Lewis acidic stereogenic-only-at-metal catalyst **Λ-V1** (Figure 37).[70]

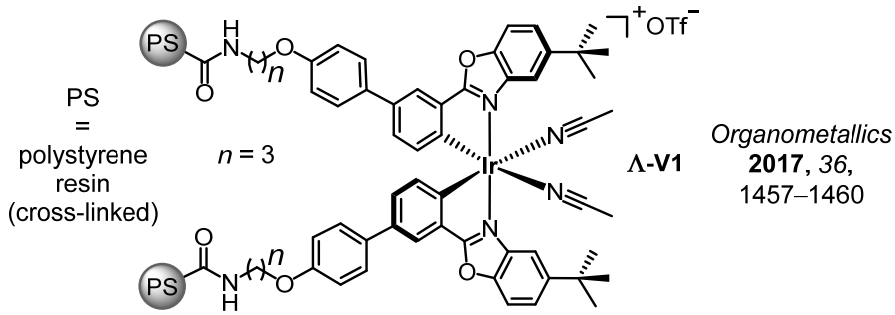

Figure 37. Polymer-supported Lewis acidic stereogenic-only-at-metal catalyst **Λ-V1**.[70]

- Due to the termination of the enamine/hydrogen-bonding catalyst project, the development of C_2-symmetric versions of such catalysts (see Figure 34) was also discontinued. However, the performed preliminary experiments, i.e., experimental verification of H.-D. Stachel's route to amine-functionalized bispyrazoles (see Scheme 48),[118] synthesis of proof-of-principle bispyrazole complex ***rac*-T31-C2** (see Scheme 49), and confirmation of ***rac*-T31-C2**'s C_2-symmetry and its ascertained stability (see Figure 35), paved the way for the development of C_2-symmetric catalysts **Λ-89** (see chapter 1.4, Scheme 17)[63] and **Λ-(*R*,*R*)-90** (see Scheme 18).[64]

  For an illustration, **Λ-89** and **Λ-(*R*,*R*)-90** are shown in Figure 38 together with their first generation counterparts **Λ-81** and **Λ-85**.

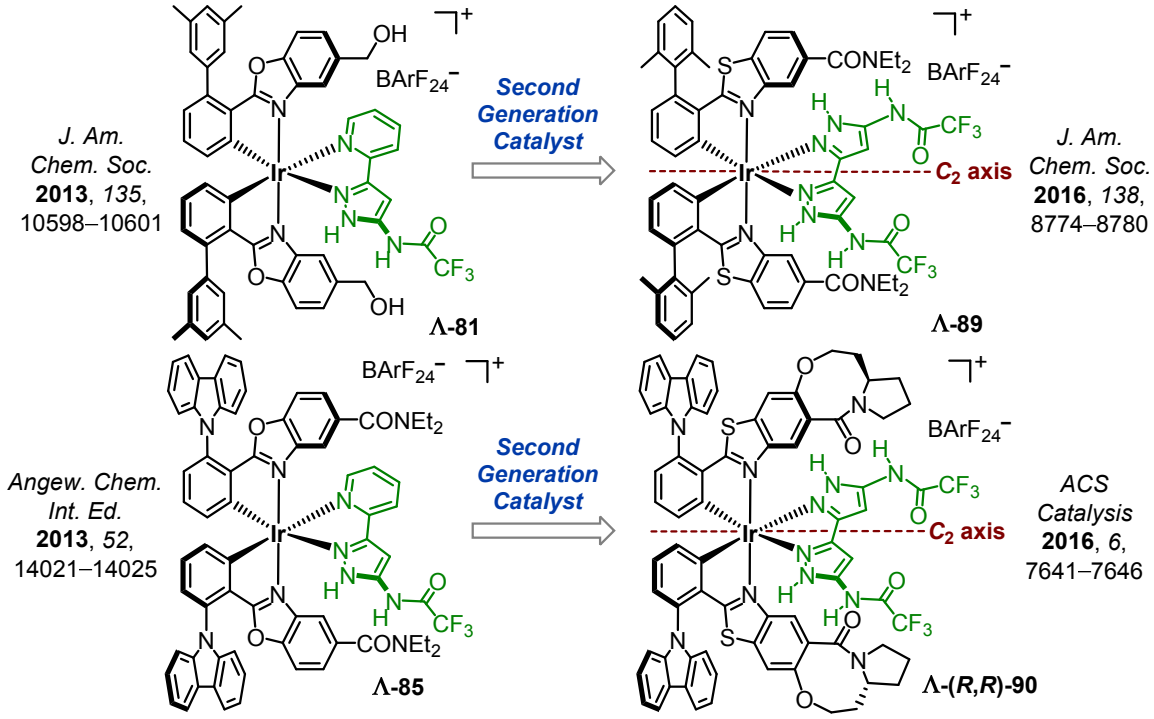

Figure 38. First generation catalysts **Λ-81**[38a] and **Λ-85**[38b] and their second generation counterparts **Λ-89**[63] and **Λ-(*R*,*R*)-90**.[64]

4. Experimental Section

4.1 General Experimental Remarks

Water and / or oxygen sensitive reactions were carried out under a positive pressure of nitrogen gas in flame-dried glassware using standard Schlenk techniques. Solvents were freshly distilled under nitrogen atmosphere from calcium hydride (DMF, CH_3CN, CH_2Cl_2), sodium / benzophenone (THF), or sodium (Et_2O, toluene). All other dry solvents were either freshly prepared from HPLC or reagent grade solvents by storage over appropriate freshly dehydrated molecular sieves or purchased as dry solvents from commercial suppliers (*Acros*, *Alfa Aesar*, *Sigma Aldrich*, *TCI*) in septum sealed bottles containing molecular sieves. When dry solvents were not required, solvents were either used in HPLC or reagent grade quality. Triethylamine used for chromatographic purifications was distilled prior to use. 2-Cyano-pyrrole used for the asymmetric synthesis of *N*-acyl pyrroles was purchased from *Alfa Aesar* (product number L15330; 99%) and used without further purification. Whenever the term 'room temperature' (rt) is used, it means that the reaction or operation was performed at an ambient temperature of 25 °C without active thermostatization. Reactions were monitored by thin layer chromatography (TLC) with silica gel coated fluorescent aluminum sheets (*type 60 F_{254}* from *Merck KGaA*). TLC spots were detected by irradiation with UV light by fluorescence quenching (excitation at $\lambda = 254$ nm) or by fluorescence of fluorescent spots (excitation at $\lambda = 366$ nm). In case TLC spots were not or less UV active, TLC sheets were stained with CAM stain (cerium ammonium molybdate stain; Hanessian's stain). Flash chromatography (f. c.) was performed with standard silica gel *type 60 M* (0.04–0.063 mm, 230–400 mesh) from *Macherey-Nagel* and chromatographic purifications were performed under standard atmosphere. NMR spectra were recorded on a *Bruker AV 250 MHz*, a *Bruker AV II 300 MHz*, a *Bruker AV III 500 MHz*, a *Bruker AV III HD 500 MHz* and a *Bruker AV II 600 MHz* spectrometer. All ^{13}C NMR spectra were acquired using ^{1}H decoupling during acquisition. ^{1}H spectra were calibrated using the residual solvent signals and ^{13}C spectra using the deuterated solvent signals as internal standards. Chemical shifts are given in ppm, multiplicities are given as s (singlet), d (doublet), t (triplet), q (quartet), sept (septet), m (multiplet). In case of multiplets (m), the ppm ranges are reported. NMR spectra were recorded at 300 K if not stated otherwise. Infrared spectra were recorded from 4000–400 cm^{-1} on a *Bruker Alpha ATR FT-IR* instrument. Mass spectra were either recorded on a *Finnigan LTQ-FT* (*Thermo Fisher Scientific*) mass spectrometer (APCI and ESI method) or on an *AccuTOF-GCv* (*JEOL*) mass spectrometer (CI, EI, and FD method). For all reported *m/z* values, it was ensured that the observed isotopic pattern was in accordance with the expected isotopic pattern. Chiral HPLC analysis was performed using an *Agilent 1200 Series*, an *Agilent 1260 Infinity*, and a

Shimadzu LC-2030C HPLC system, each equipped with a variable wavelength detector. Optical activity of isolated chiral products was determined using a *P8000-T* polarimeter (*A. Krüss Optronic GmbH*) and a 50.0 mm polarimeter cell, optical activity is given as specific rotation $[\alpha]_D^{23}$ (*c*, solvent) at the sodium D line (λ = 589 nm) at 23 °C in the indicated solvent and the concentration *c* is given in the unit g/100 mL. Correct polarimeter operation and measurement were ensured by reproduction of the specific rotation of commercial L-valine.[119] CD spectra were recorded on a *JASCO J-810 spectropolarimeter* using a thermostatted CD cell (25.0 °C) with a path length of d = 1.0 mm. Catalysis reactions carried out at ≤ 0 °C were conducted using a coverable immersion bath (filled with *i*-PrOH as immersion liquid) equipped with a magnetic stirrer which was kept at the indicated temperature with a *TC50E-F* cryostat (*Huber Kaeltemaschinenbau AG*). The experimental setup ensured that the cooling bath temperature did not oscillate more than ±2 °C around the set temperature throughout the reaction. The cooling bath was permanently monitored with a second external thermometer to preclude incorrect temperature readings. All catalysis experiments with less than 100 mg of substrate and / or product were performed using a *Mettler Toledo XP204* high precision analytical balance and the purified product solutions in each case filtered through a CH_2Cl_2-rinsed disposable pipette equipped with a small cotton plug in order to remove possible traces of dust and silica gel to provide accurate yields. All other reactions were performed using an *Ohaus Pioneer P114C* analytical balance.

4.2 Cyclometalating Ligands of the Ir(III) Complexes from Chapter 2.

4.2.1 Benzoxazole Ligand 186

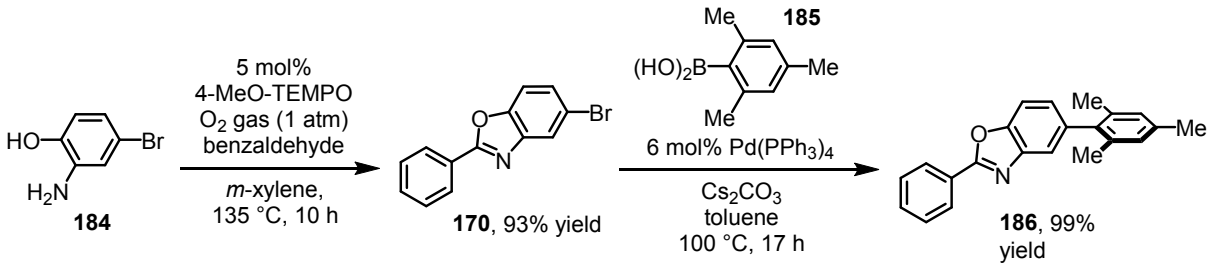

Scheme 52. Synthesis of benzoxazole ligand **186**.

Bromobenzoxazole 170. Compound **170** was prepared following a method reported by Han et al.[120] A flask (250 mL) was charged with aminophenol **184**[121] (4.00 g, 21.3 mmol, 1.00 eq), benzaldehyde (2.28 mL, 22.4 mmol, 1.05 eq), and *m*-xylene (63 mL). The flask was equipped with a reflux condenser and the mixture stirred at 135 °C for 40 min. After cooling to rt, 4-MeO-TEMPO (200 mg, 1.07 mmol, 5.0 mol%) was added and the mixture put under an atmosphere of oxygen gas using a balloon. Then, the mixture was stirred at 135 °C for 10 h under an atmosphere of oxygen gas. After cooling to rt, TLC (hexanes/EtOAc 15:1) indicated full conversion and all volatiles were removed *in vacuo*. The dark residue was dissolved in CH_2Cl_2, adsorbed on silica gel, and purified by flash chromatography (hexanes/EtOAc 50:1 → 40:1). After drying in vacuo, desired bromobenzoxazole **170** was obtained as a colorless solid (5.40 g, 19.7 mmol, 93%). ^{1}H NMR (300 MHz, $CDCl_3$): δ = 8.29–8.17 (m, 2H), 7.90 (t, J = 1.2 Hz, 1H), 7.59–7.48 (m, 3H), 7.47–7.43 (m, 2H) ppm; ^{13}C NMR (75 MHz, $CDCl_3$): δ = 164.3, 149.9, 143.9, 132.1, 129.1 (2C), 128.2, 127.9 (2C), 126.8, 123.2, 117.5, 111.9 ppm.

Benzoxazole Ligand 186. A flask (25 mL) was charged with bromobenzoxazole **170** (452 mg, 1.65 mmol, 1.00 eq), 2,4,6-trimethylphenylboronic acid (**185**, 406 mg, 2.48 mmol, 1.50 eq), and Cs_2CO_3 (1.08 g, 3.31 mmol, 2.01 eq). Dry toluene (5 mL) was added and the mixture purged with nitrogen gas for 5 min. Then, $Pd(PPh_3)_4$ (114 mg, 99 µmol, 6.0 mol%) was added, the flask equipped with a reflux condenser, and the mixture stirred at 100 °C for 17 h under nitrogen atmosphere. After cooling to rt, TLC (hexanes/Et_2O 40:3) indicated full conversion and the mixture was filtered through a glass filter (porosity G3) and the filter cake rinsed with CH_2Cl_2. All volatiles were removed from the filtrate *in vacuo*, the residue dissolved in CH_2Cl_2, adsorbed on silica gel, and purified by flash chromatography (hexanes/Et_2O 40:3). After drying *in vacuo*, desired benzoxazole ligand **186** was obtained as a colorless oil which crystallized on standing (514 mg, 1.64 mmol, 99%). ^{1}H NMR (300 MHz, $CDCl_3$): δ = 8.35–8.25 (m, 2H), 7.64 (dd, J = 8.3 Hz, J = 0.6 Hz, 1H), 7.60–7.49 (m, 4H), 7.14 (dd, J = 8.3 Hz, J = 1.5 Hz, 1H), 6.99 (s, 2H), 2.37 (s, 3H), 2.04 (s, 6H) ppm; ^{13}C NMR (75 MHz, $CDCl_3$):

δ = 163.5, 149.8, 142.5, 138.6, 137.9, 136.8, 136.3 (2C), 131.6, 129.0 (2C), 128.3 (2C), 127.7 (2C), 127.3, 126.7, 120.7, 110.5, 21.1, 20.9 (2C) ppm; IR (film): $\tilde{\nu}$ = 1555, 1465, 1449, 1259, 1202, 1053, 1024, 850, 813, 776, 706, 688 cm^{-1}; HRMS (ESI): *m/z* calcd for $C_{22}H_{19}N_1O_1H_1$: 314.1539 $[M+H]^+$; found: 314.1536.

4.2.2 Benzoxazole Ligand 189

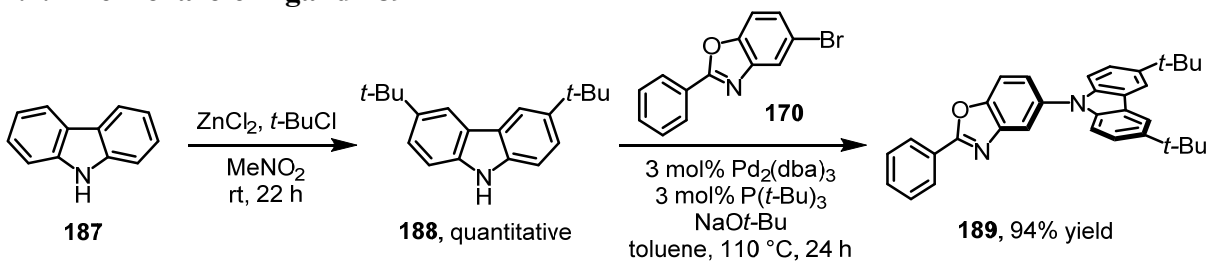

Scheme 53. Synthesis of benzoxazole ligand **189**.

3,6-Di-*tert*-butylcarbazole (188). Compound **188** was prepared following a protocol reported by Hou et al.[122] A flask (250 mL) was charged with $ZnCl_2$ (5.50 g, 40.4 mmol, 3.06 eq) and the flask with the $ZnCl_2$ rigorously flame-dried *in vacuo* (heat gun, ~450 °C). After cooling to rt, a flame-dried stir bar and carbazole (**187**; 2.20 g, 13.2 mmol, 1.00 eq) were added and the flask evacuated and refilled with nitrogen gas (3x). Dry nitromethane (66 mL) and *tert*-butyl chloride (4.40 mL, 40.4 mmol, 3.06 eq) were added and the mixture stirred at rt for 22 h under nitrogen atmosphere. The mixture was then quenched by the addition of water (100 mL), the organic layer separated, and the aqueous layer extracted with CH_2Cl_2 (4x). The organic layer was washed with water (2x) and brine (1x) and dried over Na_2SO_4. All volatiles were removed *in vacuo*, the crude residue dissolved in CH_2Cl_2, adsorbed on silica gel (45 °C), and purified by short-column chromatography (hexanes/EtOAc 10:1 → 5:1). After solvent removal and drying *in vacuo*, desired 3,6-di-*tert*-butylcarbazole (**188**) was obtained as pale-beige, crystalline solid (3.73 g, 13.3 mmol, quantitative). ^{1}H NMR (300 MHz, $CDCl_3$): δ = 8.12 (dd, J = 1.9 Hz, J = 0.6 Hz, 2H), 7.49 (dd, J = 8.6 Hz, J = 2.0 Hz, 2H), 7.32 (d, J = 8.5 Hz, 2H), 1.49 (s, 18H) ppm (N*H* signal not found); HRMS (ESI): *m/z* calcd for $C_{20}H_{25}N_1H_1$: 280.2060 $[M+H]^+$; found: 280.2059.

Benzoxazole Ligand 189. Benzoxazole ligand **189** was prepared following a protocol reported by Qiu et al.[123] A flame-dried flask (250 mL) was charged with benzoxazole **170** (1.53 g, 5.58 mmol, 1.00 eq), 3,6-di-*tert*-butylcarbazole (**188**; 1.71 g, 6.12 mmol, 1.10 eq), and NaO*t*-Bu (803 mg, 8.36 mmol, 1.50 eq). The flask was then evacuated for 40 min and refilled with nitrogen gas. Dry toluene (120 mL), $Pd_2(dba)_3$ (154 mg, 168 µmol, 3.0 mol%), and P(*t*-Bu)$_3$ (38 µL, 157 µmol, 2.8 mol%) were added via syringe and the mixture stirred at 110 °C for 24 h under nitrogen atmosphere. After cooling to rt, the mixture was quenched by

the addition of MeOH and the resulting mixture passed through a short silica plug, which was subsequently rinsed with EtOAc. All volatiles were removed *in vacuo*, the residue dissolved in CH_2Cl_2, adsorbed on silica gel, and purified by flash chromatography (hexanes/EtOAc 50:1 → 40:1). After solvent removal and drying *in vacuo*, desired benzoxazole ligand **189** was obtained as a white solid foam (2.47 g, 5.23 mmol, 94%). ^{1}H NMR (300 MHz, $CDCl_3$): δ = 8.38–8.29 (m, 2H), 8.20 (d, J = 1.3 Hz, 2H), 7.99 (d, J = 1.5 Hz, 1H), 7.77 (dd, J = 8.6 Hz, J = 0.5 Hz, 1H), 7.62–7.52 (m, 4H), 7.49 (dd, J = 8.6 Hz, J = 2.0 Hz, 2H), 7.37 (d, J = 8.7 Hz, 2H), 1.50 (s, 18H) ppm; ^{13}C NMR (75 MHz, $CDCl_3$): δ = 164.6, 149.7, 143.4, 143.1 (2C), 139.8 (2C), 135.2, 132.1, 129.2 (2C), 128.0 (2C), 127.0, 124.5, 123.8 (2C), 123.5 (2C), 118.8, 116.4 (2C), 111.6, 109.2 (2C), 34.9 (2C), 32.2 (6C) ppm; IR (film): $\tilde{\nu}$ = 2955, 1553, 1482, 1292, 1258, 1234, 808, 701, 662, 612 cm^{-1}; HRMS (ESI): *m/z* calcd for $C_{33}H_{33}N_2O_1$: 473.2587 $[M+H]^+$; found: 473.2584.

4.2.3 Benzoxazole Ligand 195

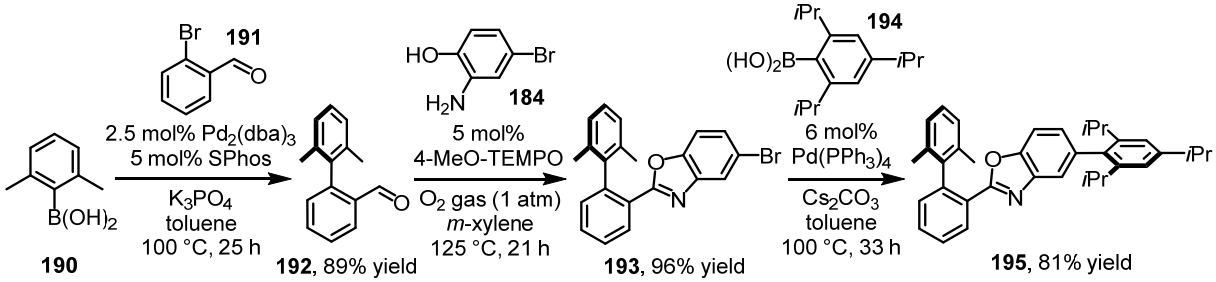

Scheme 54. Synthesis of benzoxazole ligand **195**.

Aldehyde 192. Compound **192** was prepared following a method reported by Buchwald et al.[124] A flame-dried flask (100 mL) was charged with 2,6-dimethylphenylboronic acid (**190**; 4.78 g, 30.3 mmol, 1.47 eq), K_3PO_4 (12.7 g, 59.8 mmol, 2.90 eq), and SPhos (411 mg, 1.00 mmol, 4.9 mol%) and the flask evacuated and refilled with nitrogen gas (3x). Dry toluene (40 mL), Pd_2dba_3 (460 mg, 500 µmol, 2.4 mol%), and 2-bromobenzaldehyde (**191**; 2.40 mL, 20.6 mmol, 1.00 eq) were added, the flask equipped with a reflux condenser, and the mixture stirred at 100 °C for 25 h under an atmosphere of nitrogen gas. After cooling to rt, TLC (hexanes/EtOAc 10:1) indicated full conversion and the mixture was diluted with CH_2Cl_2 and filtered through a plug of silica gel, which was rinsed with a CH_2Cl_2/MeOH mixture. All volatiles were removed from the filtrate *in vacuo*, the residue dissolved in CH_2Cl_2, adsorbed on silica gel, and purified by flash chromatography (hexanes/EtOAc 50:1). After drying *in vacuo*, desired aldehyde **192** was obtained as a crystalline colorless solid (3.85 g, 18.3 mmol, 89%). ^{1}H NMR (300 MHz, $CDCl_3$): δ = 9.66 (d, J = 0.9 Hz, 1H), 8.05 (dd, J = 7.8 Hz, J = 1.0 Hz, 1H), 7.68 (ddd, J = 7.6 Hz, J = 7.6 Hz, J = 1.5 Hz, 1H), 7.51 (dddd, J = 7.6 Hz, J = 7.6 Hz, J = 0.9 Hz, J = 0.9 Hz, 1H), 7.26–7.19 (m, 2H), 7.18–7.10 (m, 2H),

1.98 (s, 6H) ppm; ^{13}C NMR (75 MHz, $CDCl_3$): δ = 192.3, 145.2, 137.3, 136.4, 134.5, 133.8, 130.6, 128.1, 127.9, 127.6 (2C), 127.4, 21.0 (2C) ppm; one overlapping C signal could not be located; IR (film): $\tilde{\nu}$ = 1691, 1654, 1595, 1461, 1447, 1394, 1257, 1240, 1194, 829, 767, 749, 687, 639, 566, 431 cm^{-1}; HRMS (ESI): *m/z* calcd for $C_{15}H_{14}O_1Na_1$: 233.0937 [*M*+Na]$^+$; found: 233.0937.

Bromobenzoxazole 193. Compound **193** was prepared following a method reported by Han et al.[120] A flask (100 mL) was charged with aldehyde **192** (2.50 g, 11.9 mmol, 1.00 eq), aminophenol **184**[121] (2.23 g, 11.9 mmol, 1.00 eq), and *m*-xylene (37 mL). The flask was equipped with a reflux condenser and the mixture stirred at 125 °C for 45 min. After cooling to rt, 4-MeO-TEMPO (115 mg, 617 µmol, 5.2 mol%) was added and the mixture put under an atmosphere of oxygen gas using a balloon. Then, the mixture was stirred at 125 °C for 21 h under an atmosphere of oxygen gas. After cooling to rt, TLC (hexanes/EtOAc 10:1) indicated full conversion and all volatiles were removed *in vacuo*. The dark residue was dissolved in CH_2Cl_2, adsorbed on silica gel, and purified by flash chromatography (hexanes/EtOAc 50:1). After drying *in vacuo*, desired bromobenzoxazole **193** was obtained as a pale-yellow crystalline solid (4.32 g, 11.4 mmol, 96%). ^{1}H NMR (300 MHz, $CDCl_3$): δ = 8.31 (dd, *J* = 7.7 Hz, *J* = 1.3 Hz, 1H), 7.79 (d, *J* = 1.9 Hz, 1H), 7.62 (ddd, *J* = 7.5 Hz, *J* = 7.5 Hz, *J* = 1.5 Hz, 1H), 7.53 (ddd, *J* = 7.6 Hz, *J* = 7.6 Hz, *J* = 1.4 Hz, 1H), 7.33 (dd, *J* = 8.6 Hz, *J* = 2.0 Hz, 1H), 7.30–7.24 (m, 1H), 7.18 (dd, *J* = 8.4 Hz, *J* = 6.7 Hz, 1H), 7.12–7.03 (m, 3H), 1.95 (s, 6H) ppm; ^{13}C NMR (75 MHz, $CDCl_3$): δ = 164.7, 149.9, 143.4, 141.6, 140.6, 135.9, 131.9, 131.1, 130.6, 127.9, 127.7, 127.4, 127.2 (2C), 126.1, 123.1, 117.1, 111.7, 20.7 (2C) ppm; one overlapping C signal could not be located; IR (film): $\tilde{\nu}$ = 1570, 1534, 1455, 1440, 1420, 1329, 1303, 1258, 1194, 1072, 1040, 1033, 910, 857, 821, 802, 767, 749, 707, 681, 589, 400 cm^{-1}; HRMS (ESI): *m/z* calcd for $C_{21}H_{16}{}^{79}Br_1N_1O_1Na_1$: 400.0307 [*M*+Na]$^+$; found: 400.0302.

Benzoxazole Ligand 195. A flask (50 mL) was charged with bromobenzoxazole **193** (2.31 g, 6.11 mmol, 1.00 eq), 2,4,6-triisopropylphenylboronic acid (**194**; 2.11 g, 8.50 mmol, 1.39 eq), and Cs_2CO_3 (3.96 g, 12.2 mmol, 1.99 eq). Dry toluene (27 mL) was added and the mixture purged with nitrogen gas for 10 min. Then, $Pd(PPh_3)_4$ (422 mg, 365 µmol, 6.0 mol%) was added, the flask equipped with a reflux condenser, and the mixture stirred at 100 °C for 33 h under nitrogen atmosphere. After cooling to rt, TLC (hexanes/EtOAc 10:1) indicated full conversion and the mixture was passed through a glass filter (type G3) and the filter cake rinsed with CH_2Cl_2. All volatiles were removed from the filtrate *in vacuo*, the residue dissolved in CH_2Cl_2, adsorbed on silica gel, and purified by flash chromatography (hexanes/EtOAc 50:1). After drying *in vacuo*, desired benzoxazole ligand **195** was obtained as an off-white solid

(2.47 g, 4.92 mmol, 81%). ^{1}H NMR (300 MHz, $CDCl_3$): δ = 8.47 (dd, J = 7.6 Hz, J = 1.4 Hz, 1H), 7.61 (ddd, J = 7.5 Hz, J = 7.5 Hz, J = 1.6 Hz, 1H), 7.54 (ddd, J = 7.6 Hz, J = 7.6 Hz, J = 1.6 Hz, 1H), 7.52–7.48 (m, 1H), 7.32–7.08 (m, 5H), 7.05 (s, 2H), 7.02 (dd, J = 8.3 Hz, J = 1.7 Hz, 1H), 2.94 (sept, J = 6.9 Hz, 1H), 2.56 (sept, J = 6.9 Hz, 2H), 2.00 (s, 6H), 1.31 (d, J = 7.0 Hz, 6H), 1.07 (d, J = 7.0 Hz, 6H), 1.04 (d, J = 7.0 Hz, 6H) ppm; ^{13}C NMR (75 MHz, $CDCl_3$): δ = 164.2, 149.9, 148.2, 146.9 (2C), 141.5, 141.3, 141.1, 137.4, 136.6, 136.0, 131.6, 131.2, 130.7, 127.7, 127.3, 127.1 (2C), 126.9, 126.5, 120.9, 120.7 (2C), 109.9, 34.4, 30.4 (2C), 24.4 (2C), 24.3 (2C), 24.2 (2C), 20.9 (2C) ppm, one overlapping signal could not be located; IR (film): $\tilde{\nu}$ = 2959, 2868, 1458, 1322, 1258, 1200, 1029, 911, 880, 816, 768, 734 cm^{-1}; HRMS (ESI): *m/z* calcd for $C_{36}H_{39}N_1O_1H_1$: 502.3104 [M+H]$^+$; found: 502.3110.

4.2.4 Benzoxazole Ligand 196

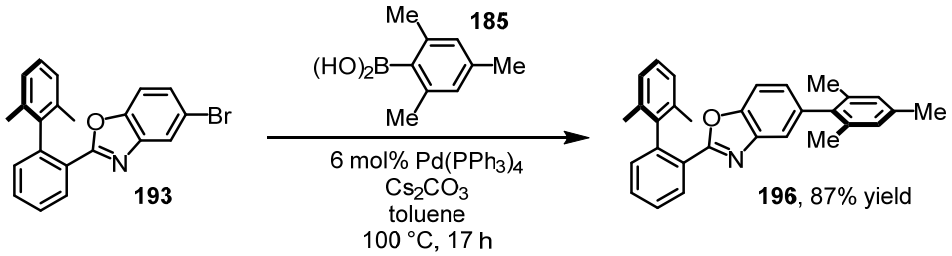

Scheme 55. Synthesis of benzoxazole ligand **196**.

Benzoxazole Ligand 196. A flask (25 mL) was charged with bromobenzoxazole **193** (1.15 g, 3.04 mmol, 1.00 eq), 2,4,6-trimethylphenylboronic acid (**185**; 748 mg, 4.56 mmol, 1.50 eq), and Cs_2CO_3 (1.99 g, 6.11 mmol, 2.01 eq). Dry toluene (10 mL) was added and the mixture purged with nitrogen gas for 10 min. Then, $Pd(PPh_3)_4$ (211 mg, 182 µmol, 6.0 mol%) was added, the flask equipped with a reflux condenser, and the mixture stirred at 100 °C for 17 h under nitrogen atmosphere. After cooling to rt, TLC (hexanes/Et_2O 40:3) indicated full conversion and the mixture was passed through a glass filter (type G3) and the filter cake subsequently rinsed with CH_2Cl_2. All volatiles were removed from the filtrate *in vacuo*, the residue dissolved in CH_2Cl_2, adsorbed on silica gel, and purified by flash chromatography (hexanes/Et_2O 40:3). After drying *in vacuo*, desired benzoxazole ligand **196** was obtained as an off-white solid (1.11 g, 2.65 mmol, 87%). ^{1}H NMR (300 MHz, $CDCl_3$): δ = 8.35 (dd, J = 7.7 Hz, J = 1.3 Hz, 1H), 7.53 (ddd, J = 7.4 Hz, J = 7.4 Hz, J = 1.6 Hz, 1H), 7.45 (ddd, J = 7.6 Hz, J = 7.6 Hz, J = 1.5 Hz, 1H), 7.40–7.35 (m, 1H), 7.24–6.96 (m, 5H), 6.90 (dd, J = 8.3 Hz, J = 1.5 Hz, 1H), 6.86 (s, 2H), 2.25 (s, 3H), 1.91 (s, 6H), 1.89 (s, 6H) ppm; ^{13}C NMR (75 MHz, $CDCl_3$): δ = 164.0, 149.8, 141.7, 141.4, 140.9, 138.7, 137.7, 136.9, 136.3, 136.0, 131.7, 131.2, 130.7, 128.3 (2C), 127.7, 127.3, 127.2 (2C), 126.5, 126.4, 120.6, 110.4, 21.2, 21.0 (2C), 20.8 (2C) ppm (two overlapping C signals could not be located); IR (film):

$\tilde{\nu}$ = 1461, 1257, 1197, 1027, 817, 766, 709, 430 cm^{-1}; HRMS (ESI): *m/z* calcd for $C_{30}H_{27}N_1O_1H_1$: 418.2165 $[M+H]^+$; found: 418.2170.

4.2.5 Benzothiazole Ligand 199

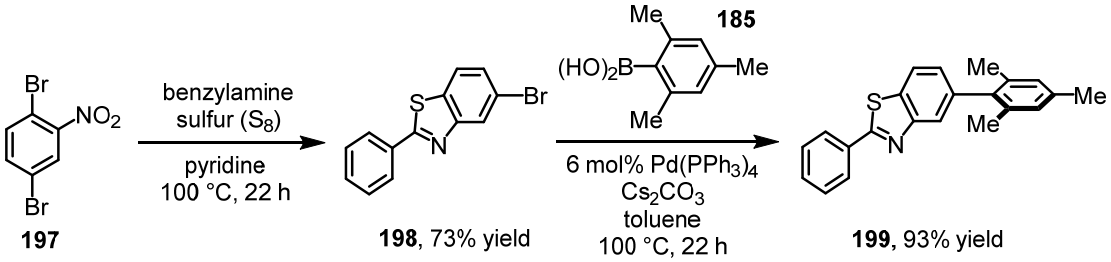

Scheme 56. Synthesis of benzothiazole ligand **199**.

Bromobenzothiazole 198. Compound **198** was prepared following a method reported by Al-Mourabit et al.[125] A flame-dried flask was charged with pyridine (2.0 mL), 2,5-dibromonitrobenzene (**197**; 2.81 g, 10.0 mmol, 1.00 eq), benzylamine (2.75 mL, 25.2 mmol, 2.52 eq), and elemental sulfur (481 mg, 15.0 mmol, 1.50 eq). The mixture was stirred at 100 °C under nitrogen atmosphere for 22 h. After cooling to rt, the resulting suspension was taken up in CH_2Cl_2/MeOH, adsorbed on silica gel (45 °C), and purified by flash chromatography (hexanes/EtOAc 100:1 → 75:1). After solvent removal and drying *in vacuo*, desired bromobenzothiazole **198** was obtained as a colorless crystalline solid (2.11 g, 7.27 mmol, 73%). ^{1}H NMR (300 MHz, $CDCl_3$): δ = 8.22 (d, J = 1.7 Hz, 1H), 8.11–8.02 (m, 2H), 7.74 (d, J = 8.5 Hz, 1H), 7.55–7.43 (m, 4H) ppm; HRMS (ESI): *m/z* calcd for $C_{13}H_9{}^{79}Br_1N_1S_1$: 289.9637 $[M+H]^+$; found: 289.9637.

Benzothiazole Ligand 199. A flask (25 mL) was charged with bromobenzothiazole **198** (1.00 g, 3.45 mmol, 1.00 eq), boronic acid **185** (854 mg, 5.21 mmol, 1.51 eq), cesium carbonate (2.26 g, 6.94 mmol, 2.01 eq), and toluene (11 mL). The mixture was purged with nitrogen gas for 5 min. $Pd(PPh_3)_4$ (240 mg, 208 µmol, 6.0 mol%) was then added and the mixture stirred at 100 °C for 22 h under nitrogen atmosphere. After cooling to rt, the mixture was diluted with CH_2Cl_2 and passed through a glass filter (porosity G4), which was subsequently rinsed with CH_2Cl_2. All volatiles were removed from the filtrate *in vacuo*, the crude product dissolved in CH_2Cl_2, adsorbed on silica gel, and purified by flash chromatography (Hex/EtOAc 30:1 → 20:1). After solvent removal and drying *in vacuo*, desired benzothiazole ligand **199** was obtained as pale-yellow solid foam (1.05 g, 3.20 mmol, 93%). ^{1}H NMR (300 MHz, $CDCl_3$): δ = 8.18–8.08 (m, 2H), 7.95 (dd, J = 8.1 Hz, J = 0.6 Hz, 1H), 7.90 (dd, J = 1.5 Hz, J = 0.6 Hz, 1H), 7.56–7.46 (m, 3H), 7.19 (dd, J = 8.1 Hz, J = 1.5 Hz, 1H), 7.03–6.95 (m, 2H), 2.36 (s, 3H), 2.05 (s, 6H) ppm; ^{13}C NMR (75 MHz, $CDCl_3$): δ = 168.8, 154.4, 139.9, 138.4, 137.0, 136.2, 133.7, 133.4, 131.3, 129.2 (2C), 128.4 (2C), 127.8 (2C), 127.2,

123.9, 121.7, 21.2, 21.0 (2C) ppm (one overlapping C signal could not be located); IR (film): $\tilde{\nu}$ = 1479, 1445, 1243, 962, 887, 848, 814, 760, 690 cm^{-1}; HRMS (ESI): *m/z* calcd for $C_{22}H_{20}N_1S_1$: 330.1322 [*M*+H]$^+$; found: 330.1314.

4.2.6 Benzoxazole Ligand 202

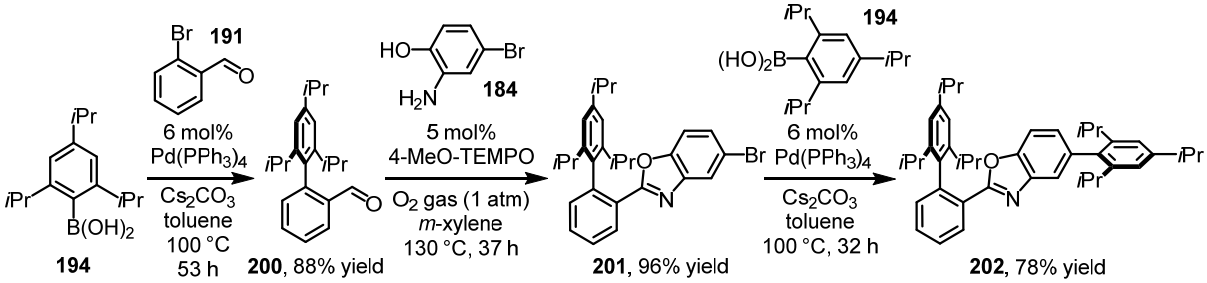

Scheme 57. Synthesis of benzoxazole ligand **202**.

Aldehyde 200. A flame-dried flask (100 mL) was charged with boronic acid **194** (3.04 g, 12.3 mmol, 1.30 eq) and cesium carbonate (6.15 g, 18.9 mmol, 2.00 eq). Toluene (35 mL) was added and the mixture purged with nitrogen gas for 5 min. $Pd(PPh_3)_4$ (690 mg, 597 µmol, 6.3 mol%) and 2-bromobenzaldehyde (**191**; 1.10 mL, 9.42 mmol, 1.00 eq) were then added and the mixture stirred at 100 °C for 53 h under nitrogen atmosphere. After cooling to rt, the salts were filtered off by passing the mixture through a glass filter (porosity G3), which was subsequently rinsed with CH_2Cl_2. All volatiles were removed from the filtrate *in vacuo*, the residue taken up in CH_2Cl_2, adsorbed on silica gel, and purified by flash chromatography (hexanes/EtOAc 40:1 → 20:1). After solvent removal and drying *in vacuo*, desired aldehyde **200** was obtained as a colorless crystalline solid (2.57 g, 8.33 mmol, 88%). ^{1}H NMR (300 MHz, $CDCl_3$): δ = 9.71 (d, *J* = 0.8 Hz, 1H), 8.04 (ddd, *J* = 7.8 Hz, *J* = 1.5 Hz, *J* = 0.5 Hz, 1H), 7.63 (td, *J* = 7.5 Hz, *J* = 1.6 Hz, 1H), 7.55–7.45 (m, 1H), 7.26 (ddd, *J* = 7.6 Hz, *J* = 1.3 Hz, *J* = 0.4 Hz, 1H), 7.11–7.06 (m, 2H), 2.96 (sept, *J* = 6.9 Hz, 1H), 2.44 (sept, *J* = 6.9 Hz, 2H), 1.32 (d, *J* = 7.0 Hz, 6H), 1.07 (d, *J* = 6.8 Hz, 6H), 1.03 (d, *J* = 6.8 Hz, 6H) ppm; HRMS (ESI): *m/z* calcd for $C_{22}H_{28}O_1Na_1$: 331.2032 [*M*+Na]$^+$; found: 331.2037.

Bromobenzoxazole 201. Compound **201** was prepared following a method reported by Han et al.[120] A flask (50 mL) was charged with aldehyde **200** (1.60 g, 5.19 mmol, 1.00 eq), aminophenol **184**[121] (982 mg, 5.22 mmol, 1.01 eq), and *m*-xylene (18 mL). The flask was equipped with a reflux condenser and the mixture stirred at 130 °C for 50 min. After cooling to rt, 4-MeO-TEMPO (48.4 mg, 262 µmol, 5.1 mol%) was added and the mixture put under an atmosphere of oxygen gas using a balloon. Then, the mixture was stirred at 130 °C for 37 h under an atmosphere of oxygen gas. After cooling to rt, TLC (hexanes/EtOAc 10:1) indicated full conversion and all volatiles were removed *in vacuo*. The dark residue was dissolved in

CH_2Cl_2, adsorbed on silica gel, and purified by flash chromatography (hexanes/EtOAc 30:1 → 15:1). After drying *in vacuo*, desired bromobenzoxazole **201** was obtained as a pale-yellow crystalline solid (2.38 g, 5.00 mmol, 96%). ^{1}H NMR (300 MHz, $CDCl_3$): δ = 8.38–8.27 (m, 1H), 7.79 (d, J = 1.7 Hz, 1H), 7.63–7.47 (m, 2H), 7.37–7.27 (m, 2H), 7.06–6.99 (m, 2H), 6.95 (d, J = 8.5 Hz, 1H), 2.96 (sept, J = 6.9 Hz, 1H), 2.49 (sept, J = 6.8 Hz, 2H), 1.32 (d, J = 6.8 Hz, 6H), 1.05 (d, J = 6.8 Hz, 6H), 0.87 (d, J = 7.0 Hz, 6H) ppm; HRMS (ESI): *m/z* calcd for $C_{28}H_{30}{}^{79}Br_1N_1O_1Na_1$: 498.1403 $[M+Na]^+$; found: 498.1421.

Benzoxazole Ligand 202. A flame-dried flask (25 mL) was charged with bromobenzoxazole **201** (1.26 g, 2.64 mmol, 1.00 eq), boronic acid **194** (860 mg, 3.47 mmol, 1.31 eq), and cesium carbonate (1.72 g, 5.28 mmol, 2.00 eq). The flask was evacuated for 15 min and then carefully refilled with nitrogen gas. Toluene (12 mL) and $Pd(PPh_3)_4$ (186 mg, 161 µmol, 6.1 mol%) were added and the mixture stirred at 100 °C for 32 h under nitrogen atmosphere. After cooling to rt, the salts were filtered off by passing the mixture through a glass filter (porosity G3), which was subsequently rinsed with CH_2Cl_2. All volatiles were removed from the filtrate *in vacuo*, the remaining residue taken up in CH_2Cl_2, adsorbed on silica gel, and purified by flash chromatography (hexanes/EtOAc 70:1). After solvent removal, desired benzoxazole ligand **202** was obtained as a colorless solid (1.23 g, 2.05 mmol, 78%). ^{1}H NMR (300 MHz, $CDCl_3$): δ = 8.50–8.38 (m, 1H), 7.60–7.52 (m, 2H), 7.52–7.48 (m, 1H), 7.39–7.31 (m, 1H), 7.12–7.03 (m, 5H), 7.01 (dd, J = 8.2 Hz, J = 1.6 Hz, 1H), 3.08–2.87 (m, 2H), 2.66–2.44 (m, 4H), 1.35 (d, J = 7.0 Hz, 6H), 1.32 (d, J = 6.8 Hz, 6H), 1.14–1.01 (m, 18H), 0.94 (d, J = 6.8 Hz, 6H) ppm; ^{13}C NMR (75 MHz, $CDCl_3$): δ = 164.4, 149.7, 148.4, 148.2, 147.0 (2C), 146.4 (2C), 141.4, 141.2, 137.3, 136.7, 135.8, 132.1, 130.9, 130.2, 127.5 (2C), 126.9, 121.0, 120.7 (2C), 120.5 (2C), 109.5, 34.6, 34.4, 30.8 (2C), 30.4 (2C), 24.8 (2C), 24.4 (4C), 24.2 (4C), 23.5 (2C) ppm; IR (film): $\tilde{\nu}$ = 2960, 2928, 2869, 1458, 911, 879, 815, 769, 732 cm^{-1}; HRMS (ESI): *m/z* calcd for $C_{43}H_{53}N_1O_1H_1$: 600.4200 $[M+H]^+$; found: 600.4213.

4.2.7 Benzoxazole Ligand 206

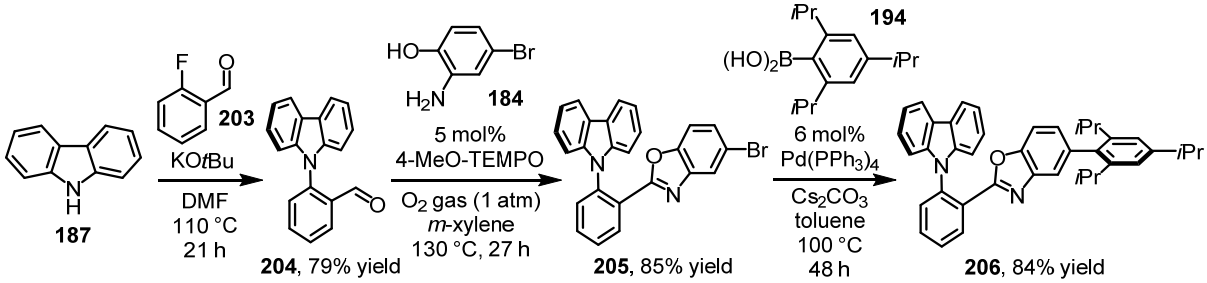

Scheme 58. Synthesis of benzoxazole ligand **206**.

Aldehyde 204. A flame-dried three-neck flask equipped with a reflux condenser was charged with carbazole (**187**; 2.50 g, 15.0 mmol, 1.00 eq) and KO*t*Bu (2.51 g, 22.4 mmol, 1.50 eq).

Dry DMF (60 mL) was added and the mixture stirred at 110 °C while 2-fluorobenzaldehyde (**203**; 2.40 mL, 22.8 mmol, 1.52 eq) was added dropwise over 30 min via syringe and the mixture then stirred at 110 °C for 21 h under nitrogen atmosphere. After cooling to rt, the mixture was diluted with CH_2Cl_2 and water, the organic layer separated, and the aqueous layer extracted with CH_2Cl_2 (5x). The combined organic layers were dried over Na_2SO_4, all volatiles removed *in vacuo*, the residue dissolved in CH_2Cl_2, adsorbed on silica gel, and purified by flash chromatography (hexanes/EtOAc 30:1). After solvent removal and drying *in vacuo*, desired aldehyde **204** was obtained as a pale-yellow crystalline solid (3.23 g, 11.9 mmol, 79%). ^{1}H NMR (300 MHz, $CDCl_3$): δ = 9.61 (d, J = 0.9 Hz, 1H), 8.23 (dd, J = 7.8 Hz, J = 1.8 Hz, 1H), 8.21–8.15 (m, 2H), 7.85 (ddd, J = 7.7 Hz, J = 7.5 Hz, J = 1.7 Hz, 1H), 7.68 (tt, J = 7.6 Hz, J = 1.0 Hz, 1H), 7.55 (dd, J = 7.9 Hz, J = 0.8 Hz, 1H), 7.48–7.39 (m, 2H), 7.38–7.30 (m, 2H), 7.22–7.15 (m, 2H) ppm; HRMS (ESI): *m/z* calcd for $C_{19}H_{13}N_1O_1Na_1$: 294.0889 $[M+Na]^+$; found: 294.0902.

Bromobenzoxazole 205. Bromobenzoxazole **205** was prepared following a method reported by Han et al.[120] A flask (100 mL) was charged with aldehyde **204** (1.71 g, 6.30 mmol, 1.00 eq), aminophenol **184**[121] (1.18 g, 6.28 mmol, 1.00 eq), and *m*-xylene (21 mL). The flask was equipped with a reflux condenser and the mixture stirred at 130 °C for 50 min. After cooling to rt, 4-MeO-TEMPO (59.2 mg, 318 µmol, 5.1 mol%) was added and the mixture put under an atmosphere of oxygen gas using a balloon. Then, the mixture was stirred at 130 °C for 27 h under an atmosphere of oxygen gas. After cooling to rt, TLC (hexanes/EtOAc 10:1) indicated full conversion and all volatiles were removed *in vacuo*. The dark residue was dissolved in CH_2Cl_2, adsorbed on silica gel, and purified by flash chromatography (hexanes/EtOAc 30:1 → 15:1). After drying *in vacuo*, desired bromobenzoxazole **205** was obtained as a colorless solid foam (2.35 g, 5.35 mmol, 85%). ^{1}H NMR (300 MHz, $CDCl_3$): δ = 8.38 (dd, J = 7.7 Hz, J = 1.7 Hz, 1H), 8.10–8.01 (m, 2H), 7.68 (td, J = 7.6 Hz, J = 1.7 Hz, 1H), 7.61 (dd, J = 7.6 Hz, J = 1.5 Hz, 1H), 7.59–7.53 (m, 2H), 7.24–7.09 (m, 4H), 7.07 (dd, J = 8.7 Hz, J = 1.9 Hz, 1H), 7.03–6.95 (m, 2H), 6.63 (d, J = 8.5 Hz, 1H) ppm; HRMS (ESI): *m/z* calcd for $C_{25}H_{15}{}^{79}Br_1N_2O_1Na_1$: 461.0260 $[M+Na]^+$; found: 461.0284.

Benzoxazole Ligand 206. A flame-dried flask (25 mL) was charged with bromobenzoxazole **205** (1.10 g, 2.50 mmol, 1.00 eq), boronic acid **194** (890 mg, 3.59 mmol, 1.43 eq), and cesium carbonate (1.63 g, 5.00 mmol, 2.00 eq). The flask was evacuated for 5 min and then carefully refilled with nitrogen gas. Toluene (12 mL) and $Pd(PPh_3)_4$ (180 mg, 156 µmol, 6.2 mol%) were added and the mixture stirred at 100 °C for 48 h under nitrogen atmosphere. After cooling to rt, the salts were filtered off by passing the mixture through a glass filter (porosity G3), which was subsequently rinsed with CH_2Cl_2. All volatiles were removed from the filtrate

in vacuo, the remaining residue taken up in CH_2Cl_2, adsorbed on silica gel, and purified by flash chromatography (hexanes/EtOAc 30:1 → 20:1). After solvent removal, desired benzoxazole ligand **206** was obtained as a colorless solid foam (1.18 g, 2.10 mmol, 84%). ^{1}H NMR (300 MHz, $CDCl_3$): δ = 8.49 (dd, J = 7.7 Hz, J = 1.7 Hz, 1H), 8.13–8.02 (m, 2H), 7.69 (td, J = 7.5 Hz, J = 1.8 Hz, 1H), 7.62 (td, J = 7.5 Hz, J = 1.6 Hz, 1H), 7.56 (dd, J = 7.6 Hz, J = 1.7 Hz, 1H), 7.28 (d, J = 1.1 Hz, 1H), 7.25–7.10 (m, 4H), 7.06-6.99 (m, 2H), 6.93 (s, 2H), 6.79 (dd, J = 8.3 Hz, J = 1.5 Hz, 1H), 6.72 (d, J = 8.3 Hz, 1H), 2.83 (sept, J = 6.9 Hz, 1H), 2.34 (sept, J = 6.8 Hz, 2H), 1.20 (d, J = 6.8 Hz, 6H), 0.93 (d, J = 7.0 Hz, 6H), 0.90 (d, J = 7.0 Hz, 6H) ppm; ^{13}C NMR (75 MHz, $CDCl_3$): δ = 161.5, 149.6, 148.2, 146.8 (2C), 142.2, 141.2, 137.4, 136.6, 136.5, 132.8, 131.9, 131.1, 129.1, 127.2, 126.8, 126.0 (2C), 123.8, 120.9, 120.7 (2C), 120.3 (2C), 119.9 (2C), 109.8, 109.7 (2C), 34.4, 30.3 (2C), 24.3 (2C), 24.2 (4C) ppm (two overlapping C signals could not be located); IR (film): $\tilde{\nu}$ = 2960, 2928, 1602, 1455, 1318, 1232, 911, 816, 745, 727 cm^{-1}; HRMS (ESI): *m/z* calcd for $C_{40}H_{39}N_2O_1$: 563.3057 $[M+H]^+$; found: 563.3075.

4.2.8 Benzoxazole Ligand 210

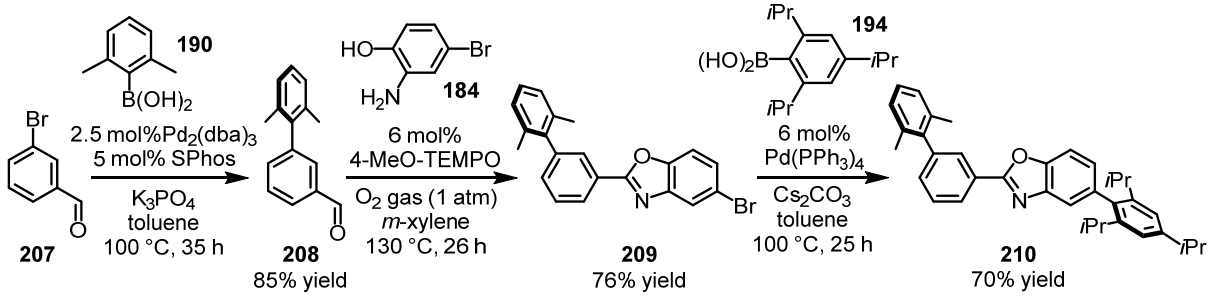

Scheme 59. Synthesis of benzoxazole ligand **210**.

Aldehyde 208. Compound **208** was prepared following a method reported by Buchwald et al.[124] A flame-dried flask was charged with 2,6-dimethylphenylboronic acid (**190**; 2.82 g, 18.8 mmol, 1.57 eq), K_3PO_4 (7.74 g, 36.4 mmol, 3.03 eq), and SPhos (243 mg, 0.59 mmol, 4.9 mol%). The flask was evacuated for 30 min and then carefully refilled with nitrogen gas. Dry toluene (24 mL), 3-bromobenzaldehyde (**207**; 1.40 mL, 12.0 mmol, 1.00 eq), and $Pd_2(dba)_3$ (270 mg, 0.30 mmol, 2.5 mol%) were added and the mixture stirred at 100 °C for 35 h under nitrogen atmosphere. After cooling to rt, the mixture was diluted with CH_2Cl_2, passed through a plug of celite, and all volatiles removed from the filtrate *in vacuo*. The residue was dissolved in CH_2Cl_2, adsorbed on silica gel, and purified by flash chromatography (hexanes/EtOAc 50:1). After solvent removal and drying *in vacuo*, desired aldehyde **208** was obtained as a colorless oil (2.14 g, 10.2 mmol, 85%). ^{1}H NMR (300 MHz, $CDCl_3$): δ = 10.06 (s, 1H), 7.88 (dt, J = 7.6 Hz, J = 1.5 Hz, 1H), 7.69 (td, J = 1.7 Hz, J = 0.4 Hz, 1H), 7.61 (t,

J = 7.6 Hz, 1H), 7.44 (dt, *J* = 7.6 Hz, *J* = 1.5 Hz, 1H), 7.24–7.16 (m, 1H), 7.16–7.09 (m, 2H), 2.02 (s, 6H) ppm; HRMS (ESI): *m/z* calcd for $C_{15}H_{15}O_1$: 211.1117 $[M+H]^+$; found: 211.1124.

Bromobenzoxazole 209. Bromobenzoxazole **209** was prepared following a method reported by Han et al.[120] A flask was charged with aldehyde **208** (1.20 g, 5.70 mmol, 1.05 eq), aminophenol **184**[121] (1.02 g, 5.42 mmol, 1.00 eq), and *m*-xylene (20 mL). The flask was equipped with a reflux condenser and the mixture stirred at 130 °C for 1 h. After cooling to rt, 4-MeO-TEMPO (57.5 mg, 0.31 mmol, 5.7 mol%) was added and the mixture put under an atmosphere of oxygen gas using a balloon. Then, the mixture was stirred at 130 °C for 26 h under an atmosphere of oxygen gas. After cooling to rt, all volatiles were removed *in vacuo*, the dark residue dissolved in CH_2Cl_2, adsorbed on silica gel, and purified by flash chromatography (hexanes/EtOAc 40:1). After drying *in vacuo*, desired bromobenzoxazole **209** was obtained as a colorless solid (1.65 g, 4.36 mmol, 76%). ^{1}H NMR (300 MHz, $CDCl_3$): δ = 8.23 (dt, *J* = 7.9 Hz, *J* = 1.4 Hz, 1H), 8.06 (t, *J* = 1.5 Hz, 1H), 7.90 (dd, *J* = 1.6 Hz, *J* = 0.7 Hz, 1H), 7.61 (t, *J* = 7.7 Hz, 1H), 7.50–7.41 (m, 2H), 7.37 (dt, *J* = 7.6 Hz, *J* = 1.4 Hz, 1H), 7.24–7.17 (m, 1H), 7.17–7.10 (m, 2H), 2.07 (s, 6H) ppm; HRMS (ESI): *m/z* calcd for $C_{21}H_{17}{}^{79}Br_1N_1O_1$: 378.0488 $[M+H]^+$; found: 378.0499.

Benzoxazole Ligand 210. A flame-dried flask was charged with bromobenzoxazole **209** (1.01 g, 2.67 mmol, 1.00 eq), boronic acid **194** (860 mg, 3.47 mmol, 1.30 eq), and cesium carbonate (1.76 g, 5.41 mmol, 2.03 eq). The flask was evacuated for 15 min and then carefully refilled with nitrogen gas. Toluene (13 mL) and $Pd(PPh_3)_4$ (186 mg, 0.16 mmol, 6.0 mol%) were added and the mixture stirred at 100 °C for 25 h under nitrogen atmosphere. After cooling to rt, the mixture was diluted with CH_2Cl_2 and passed through a plug of celite. The crude product was adsorbed on silica gel and purified by flash chromatography (hexanes/EtOAc 10:1). After solvent removal and drying *in vacuo*, desired benzoxazole ligand **210** was obtained as a colorless foam (936 mg, 1.87 mmol, 70%). ^{1}H NMR (300 MHz, $CDCl_3$): δ = 8.29 (ddd, *J* = 7.8 Hz, *J* = 1.7 Hz, *J* = 1.2 Hz, 1H), 8.12 (t, *J* = 1.4 Hz, 1H), 7.67–7.55 (m, 3H), 7.37 (dt, *J* = 7.7 Hz, *J* = 1.3 Hz, 1H), 7.25–7.11 (m, 4H), 7.09 (s, 2H), 2.97 (sept, *J* = 6.9 Hz, 1H), 2.63 (sept, *J* = 6.9 Hz, 2H), 2.09 (s, 6H), 1.33 (d, *J* = 6.8 Hz, 6H), 1.09 (d, *J* = 6.8 Hz, 12H) ppm; ^{13}C NMR (75 MHz, $CDCl_3$): δ = 163.7, 149.8, 148.3, 146.9 (2C), 142.3, 142.1, 140.9, 137.8, 136.6, 136.1 (2C), 132.6, 129.4, 128.5, 127.6, 127.6, 127.6 (2C), 127.3, 126.2, 121.1, 120.8 (2C), 110.3, 34.5, 30.5 (2C), 24.4 (2C), 24.3 (2C), 24.2 (2C), 21.0 (2C) ppm; IR (film): $\tilde{\nu}$ = 2959, 1551, 1461, 1262, 1200, 1058, 878, 840, 806, 769, 738, 730, 702 cm^{-1}; HRMS (ESI): *m/z* calcd for $C_{36}H_{40}N_1O_1$: 502.3104 $[M+H]^+$; found: 502.3119.

4.2.9 Benzoxazole Ligand 217

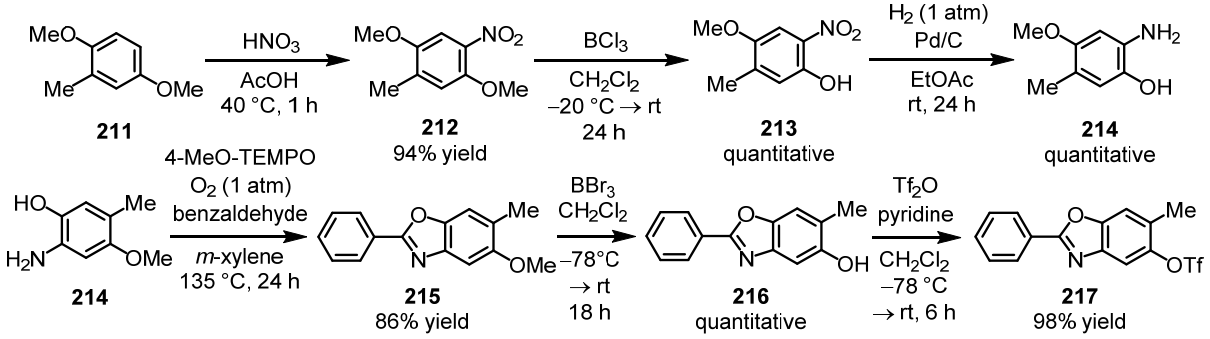

Scheme 60. Synthesis of benzoxazole ligand **217**.

Compound 212. Compound **212** was synthesized following a protocol from Neeb et al.[126] A round-bottom flask (250 mL) was charged with 2,5-dimethoxytoluene (**211**; 8.70 mL, 60.0 mmol, 1.00 eq) and acetic acid (30 mL). The resulting mixture was warmed to 40 °C and 65% HNO_3 (4.80 mL, 67.8 mmol, 1.13 eq) in acetic acid (15 mL) was added dropwise over 15 min. After stirring at 40 °C for 1 h, the mixture was allowed to cool to rt and the formed yellow precipitate was filtered off, thoroughly washed with water, and dried *in vacuo*. Desired compound **212** was obtained as a bright yellow powder without the need for further purification (11.1 g, 56.4 mmol, 94%). ^{1}H NMR (300 MHz, $CDCl_3$): δ = 7.39 (s, 1H), 6.89 (s, 1H), 3.92 (s, 3H), 3.83 (s, 3H), 2.27 (s, 3H) ppm; HRMS (ESI): *m/z* calcd for $C_9H_{12}N_1O_4$: 198.0761 $[M+H]^+$, found: 198.0760.

Compound 213. Compound **213** was synthesized following a protocol from Neeb et al.[126] A flame-dried nitrogen-flask (250 mL) was charged with compound **212** (6.00 g, 30.4 mmol, 1.00 eq) and dry CH_2Cl_2 (30 mL). The solution was cooled to −20 °C and BCl_3 (1M in CH_2Cl_2; 31.0 mL, 31.0 mmol, 1.02 eq) was added dropwise over 10 min. Then, the mixture was allowed to warm to rt and stirred for 24 h under nitrogen atmosphere. The mixture was carefully quenched with aqueous sat. Na_2CO_3 and diluted with CH_2Cl_2 and H_2O. The organic layer was separated and the aqueous layer was extracted with CH_2Cl_2 (3x). The combined organic layers were dried over Na_2SO_4 and the solvent removed *in vacuo*. Desired product **213** was obtained in form of yellow-orange crystals without the need for further purification (5.56 g, 30.4 mmol, quantitative). ^{1}H NMR (300 MHz, $CDCl_3$): δ = 10.45 (s, 1H), 7.38 (s, 1H), 6.93 (s, 1H), 3.84 (s, 3H), 2.26 (s, 3H) ppm; ^{13}C NMR (75 MHz, $CDCl_3$): δ = 151.4, 150.3, 140.8, 131.2, 121.1, 103.5, 56.1, 17.1 ppm.

Compound 214. Compound **214** was synthesized following a protocol from Neeb et al.[126] A nitrogen-flask (500 mL) was charged with compound **213** (5.54 g, 30.2 mmol, 1.00 eq) and EtOAc (150 mL). The resulting solution was purged with nitrogen gas for 10 min. Then, Pd/C (10 wt%; 0.45 g, 0.42 mmol, 1.4 mol%) was added under nitrogen atmosphere. The nitrogen

atmosphere was replaced by a hydrogen atmosphere via H_2-balloon and the mixture vigorously stirred for 24 h under hydrogen atmosphere. The resulting mixture was filtered through a plug of celite, which was subsequently thoroughly rinsed with EtOAc. All volatiles were removed from the filtrate and the obtained residue was dried *in vacuo*. Desired product **214** was obtained in form of an off-white crystalline solid without the need for further purification (4.63 g, 30.2 mmol, quantitative). ^{1}H NMR (300 MHz, DMSO-d_6): δ = 8.28 (s, 1H), 6.41 (s, 1H), 6.26 (s, 1H), 4.32 (s, 2H), 3.61 (s, 3H), 1.94 (s, 3H) ppm; HRMS (ESI): *m/z* calcd for $C_8H_{12}N_1O_2$: 154.0863 $[M+H]^+$, found: 154.0863.

Compound 215. Compound **215** was prepared following a method reported by Han et al.[120] A nitrogen-flask (250 mL) was charged with compound **214** (1.30 g, 8.49 mmol, 1.00 eq), *m*-xylene (28 mL), and benzaldehyde (0.91 mL, 8.95 mmol, 1.05 eq). This mixture was heated to 135 °C for 30 min. After cooling to rt, 4-MeO-TEMPO (86 mg, 0.46 mmol, 5.4 mol%) was added and the flask's atmosphere replaced by an oxygen atmosphere (O_2-balloon) and the mixture stirred at 135 °C for 24 h under oxygen atmosphere. After cooling to rt, all volatiles were removed *in vacuo*, the residue dissolved in CH_2Cl_2 and adsorbed on silica gel, and the crude product purified by flash chromatography (hexanes/EtOAc 20:1 → 15:1). After drying *in vacuo*, desired product **215** was obtained as an off-white crystalline solid (1.75 g, 7.31 mmol, 86%). ^{1}H NMR (300 MHz, $CDCl_3$): δ = 8.28–8.13 (m, 2H), 7.54–7.46 (m, 3H), 7.33 (s, 1H), 7.19 (s, 1H), 3.89 (s, 3H), 2.34 (s, 3H) ppm; HRMS (ESI): *m/z* calcd for $C_{15}H_{14}N_1O_2$: 240.1019 $[M+H]^+$, found: 240.1018.

Compound 216. A nitrogen-flask (250 mL) was charged with compound **215** (1.74 g, 7.27 mmol, 1.00 eq) and dried *in vacuo* for 1 h. Then, dry CH_2Cl_2 (52 mL) was added under nitrogen atmosphere. The resulting solution was cooled to −78 °C and BBr_3 (2.50 mL, 25.9 mmol, 3.57 eq) was added dropwise over 15 min. The mixture was then allowed to warm to rt and stirred for 18 h. Then, the mixture was cooled to 0 °C and carefully quenched with aqueous sat. Na_2CO_3 and the resulting mixture diluted with EtOAc and H_2O. The organic layer was separated and the aqueous layer extracted with EtOAc (3x). The combined organic layers were washed with brine and dried over Na_2SO_4. All volatiles were removed and the residue dried *in vacuo*. Desired product **216** was obtained as an off-white crystalline solid without the need for further purification (1.66 g, 7.37 mmol, quantitative). ^{1}H NMR (500 MHz, DMSO-d_6): δ = 9.51 (s, 1H), 8.16–8.10 (m, 2H), 7.62–7.53 (m, 3H), 7.47 (s, 1H), 7.12 (s, 1H), 2.25 (s, 3H) ppm; HRMS (ESI): *m/z* calcd for $C_{14}H_{12}N_1O_2$: 226.0863 $[M+H]^+$, found: 226.0861.

Benzoxazole Ligand 217. A nitrogen-flask (250 mL) was charged with compound **216** (1.64 g, 7.28 mmol, 1.00 eq) and dried *in vacuo* for 1 h. Then, dry CH_2Cl_2 (96 mL) and dry

pyridine (5.50 mL, 68.0 mmol, 9.34 eq) were added under nitrogen atmosphere. The mixture was cooled to −78 °C and Tf_2O (1.80 mL, 10.7 mmol, 1.47 eq) was added dropwise over 5 min. The mixture was stirred at −78 °C for 30 min and then allowed to warm to 0 °C and stirred for 1 h. Next, the mixture was allowed to warm to rt and stirred for another 5 h. The reaction was quenched by the addition of H_2O and the quenched mixture was stirred for 10 min at rt. The organic layer was separated, the aqueous layer extracted with CH_2Cl_2 (4x), the combined organic layers dried over Na_2SO_4, and the solvent removed *in vacuo*. The residue was dissolved in CH_2Cl_2, adsorbed on silica gel, and purified by short-column chromatography (hexanes/EtOAc 6:1). After drying *in vacuo*, desired benzoxazole ligand **217** was obtained as an off-white crystalline solid (2.55 g, 7.14 mmol, 98%). ^{1}H NMR (300 MHz, acetone-d_6): δ = 8.27–8.18 (m, 2H), 7.78 (s, 1H), 7.74 (s, 1H), 7.69–7.56 (m, 3H), 2.53 (s, 3H) ppm; ^{13}C NMR (75 MHz, acetone-d_6): δ = 165.6, 150.8, 146.2, 142.1, 133.1, 130.1 (2C), 129.5, 128.5 (2C), 127.4, 119.6 (q, $J_{C\text{-}F}$ = 319 Hz), 114.0, 113.5, 17.1 ppm; ^{19}F NMR (282 MHz, acetone-d_6): δ = –74.9 (s, 3F, CF_3) ppm; IR (film): $\tilde{\nu}$ = 1550, 1460, 1414, 1246, 1206, 1133, 1054, 883, 834, 777, 697, 598, 502, 438 cm^{-1}; HRMS (ESI): *m/z* calcd for $C_{15}H_{11}F_3N_1O_4S_1$: 358.0355 $[M+H]^+$, found: 358.0354.

4.2.10 Benzoxazole Ligand 222

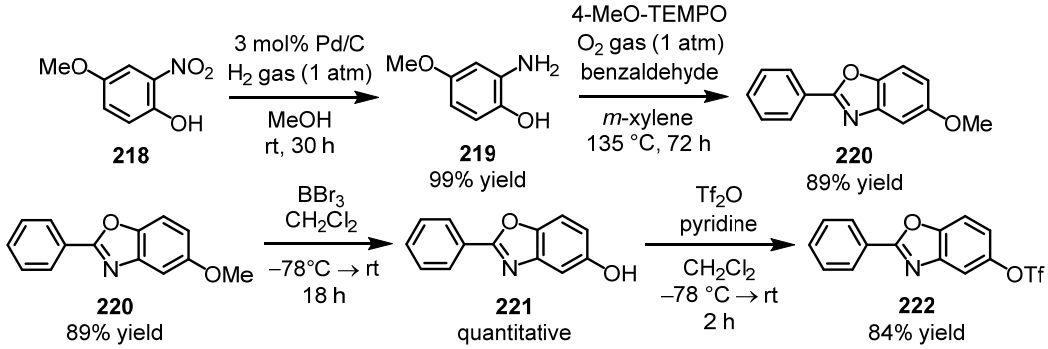

Scheme 61. Synthesis of benzoxazole ligand **222**.

Compound 219. A nitrogen-flask (1 L) was charged with 4-methoxy-2-nitrophenol (**218**; 12.1 g, 71.8 mmol, 1.00 eq), MeOH (300 mL), and Pd/C (10 wt%; 2.43 g, 2.30 mmol, 3.2 mol%). The resultant mixture was purged with nitrogen gas for 10 min. Then, the flask's nitrogen atmosphere was replaced by a hydrogen atmosphere with an H_2-ballon and the mixture vigorously stirred at rt under hydrogen atmosphere for 30 h. The mixture was purged with nitrogen gas for 15 min and then passed through a plug of celite, which was subsequently rinsed with EtOAc/MeOH 1:1. All volatiles were removed from the filtrate *in vacuo*, which gave desired product **219** as an off-white, almost colorless crystalline solid without the need for further purification (9.91 g, 71.2 mmol, 99%). ^{1}H NMR (300 MHz, DMSO-d_6): δ = 8.42 (s,

1H), 6.52 (d, *J* = 8.5 Hz, 1H), 6.20 (d, *J* = 3.0 Hz, 1H), 5.95 (dd, *J* = 8.5 Hz, *J* = 2.8 Hz, 1H), 4.52 (s, 2H), 3.58 (s, 3H) ppm; HRMS (ESI): *m/z* calcd for $C_7H_{10}N_1O_2$ $[M+H]^+$: 140.0706, found: 140.0706.

Compound 220. A flask (250 mL) was charged with compound **219** (3.50 g, 25.1 mmol, 1.00 eq), *m*-xylene (80 mL), and benzaldehyde (2.70 mL, 26.4 mmol, 1.05 eq). The resulting mixture was heated to 135 °C for 1 h. After cooling to rt, 4-MeO-TEMPO (252 mg, 1.36 mmol, 5.4 mol%) was added, the atmosphere in the flask replaced with an oxygen atmosphere (O_2-balloon), and the mixture stirred at 135 °C for 72 h under oxygen atmosphere. After cooling to rt, all volatiles were removed *in vacuo*, the residue dissolved in CH_2Cl_2 and adsorbed on silica gel, and the crude product purified by flash chromatography (hexanes/EtOAc 1:1). After drying *in vacuo*, desired product **220** was obtained as a pale-beige solid (5.01 g, 22.2 mmol, 89%). ^{1}H NMR (300 MHz, CDCl3): δ = 8.29–8.18 (m, 2H), 7.57–7.49 (m, 3H), 7.47 (d, *J* = 8.9 Hz, 1H), 7.27 (d, *J* = 2.6 Hz, 1H), 6.96 (dd, *J* = 8.9 Hz, *J* = 2.6 Hz, 1H), 3.88 (s, 3H) ppm; HRMS (ESI): *m/z* calcd for $C_{14}H_{12}N_1O_2$ $[M+H]^+$: 226.0868, found: 226.0874.

Compound 221. A nitrogen-flask (100 mL) was charged with compound **220** (3.00 g, 13.3 mmol, 1.00 eq) and dry CH_2Cl_2 (45 mL). The resulting solution was cooled to −78 °C and BBr_3 (4.60 mL, 11.9 mmol, 3.60 eq) was added dropwise over 10 min. Then, the mixture was allowed to warm to rt and stirred for 24 h. Subsequently, the mixture was cooled to 0 °C and carefully quenched with aqueous sat. Na_2CO_3 and the resulting mixture diluted with EtOAc and H_2O. The organic layer was separated, the aqueous layer extracted with EtOAc (3x), and the combined organic layers washed with brine and dried over Na_2SO_4. All volatiles were removed *in vacuo*, the residue dissolved in CH_2Cl_2 and adsorbed on silica gel, and the crude product purified by flash chromatography (hexanes/EtOAc 15:1). After solvent removal and drying *in vacuo*, desired product **221** was obtained as a beige solid (2.79 g, 13.2 mmol, quantitative). ^{1}H NMR (500 MHz, DMSO-d_6): δ = 9.51 (s, 1H), 8.16–8.10 (m, 2H), 7.62–7.53 (m, 3H), 7.47 (s, 1H), 7.12 (s, 1H), 2.25 (s, 3H) ppm; HRMS (ESI): *m/z* calcd for $C_{14}H_{12}N_1O_2$: 226.0863 $[M+H]^+$, found: 226.0861.

Benzoxazole Ligand 222. A nitrogen-flask (500 mL) was charged with compound **221** (3.00 g, 14.2 mmol, 1.00 eq), dry CH_2Cl_2 (175 mL), and dry pyridine (10.7 mL, 133 mmol, 9.34 eq). The mixture was cooled to −78 °C and Tf_2O (3.51 mL, 5.89 mmol, 1.47 eq) was added dropwise over 10 min. The mixture was stirred at −78 °C for 30 min and then allowed to warm to rt and stirred for 1.5 h. The reaction was quenched by the addition of H_2O, the organic layer was separated, and the aqueous layer extracted with CH_2Cl_2 (4x). The combined organic layers were dried over Na_2SO_4 and the solvent removed *in vacuo*. The crude product was dissolved in CH_2Cl_2, adsorbed on silica gel, and purified by short-column chromato-

graphy (hexanes/EtOAc 3:1). After solvent removal and drying *in vacuo*, desired benzoxazole ligand **222** was obtained as an off-white solid (4.10 g, 11.9 mmol, 84%). ^{1}H NMR (300 MHz, CD_2Cl_2): δ = 8.30–8.20 (m, 2H), 7.71 (d, J = 2.5 Hz, 1H), 7.67 (d, J = 8.9 Hz, 1H), 7.64–7.51 (m, 3H), 7.31 (dd, J = 8.9 Hz, J = 2.6 Hz, 1H) ppm; ^{13}C NMR (75 MHz, CD_2Cl_2): δ = 166.0, 150.4, 146.8, 143.8, 132.7, 129.5 (2C), 128.3 (2C), 126.9, 119.2 (q, $J_{C\text{-}F}$ = 322 Hz, CF_3), 118.8, 113.7, 112.0 ppm; ^{19}F NMR (282 MHz, CD_2Cl_2): δ = –73.2 ppm; IR (film): $\tilde{\nu}$ = 1550, 1423, 1228, 1197, 1133, 1096, 1055, 1020, 947, 876, 816, 788, 701, 599, 499 cm^{-1}; HRMS (ESI): *m/z* calcd for $C_{36}H_{40}N_1O_1$: 502.3104 $[M+H]^+$; found: 502.3119.

4.3 Cyclometalating Ligands of the Ir(III) Complexes from Chapter 3.

4.3.1 Benzoxazole Ligand 172

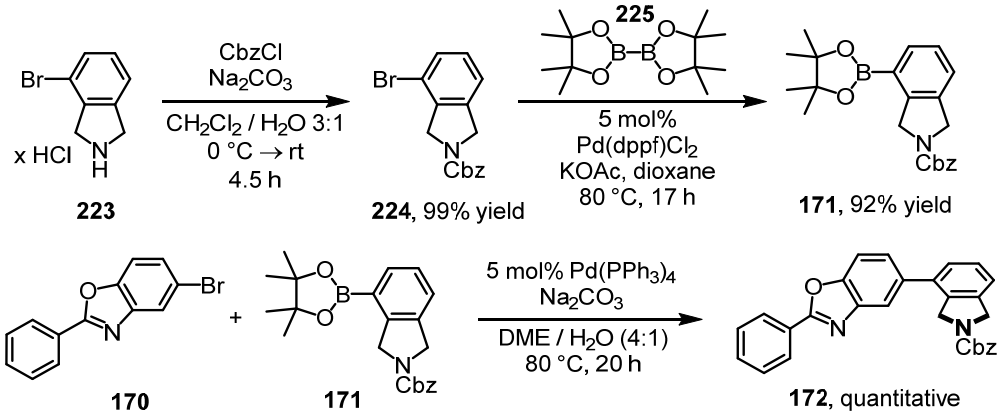

Scheme 62. Synthesis of *N*-Cbz-protected benzoxazole ligand **172**.

Compound 224. A flask (25 mL) was charged with 4-bromoisoindoline hydrochloride (**223**; 301 mg, 1.28 mmol, 1.00 eq), CH_2Cl_2 (13 mL), and water (4.3 mL). The mixture was cooled to 0 °C and Na_2CO_3 (814 mg, 7.68 mmol, 6.00 eq) and CbzCl (230 µL, 1.61 mmol, 1.26 eq) were added under stirring. The mixture was allowed to warm to rt and intensely stirred for 4.5 h. Then, the mixture was quenched by the addition of aqueous sat. NH_4Cl, the organic layer separated, and the aqueous layer extracted with CH_2Cl_2 (2x). The combined organic layers were dried over Na_2SO_4, all volatiles removed *in vacuo*, the residue dissolved in CH_2Cl_2 and adsorbed on silica gel, and the crude product purified by flash chromatography (hexanes/EtOAc 9:1 → 5:1). After solvent removal and drying *in vacuo*, desired compound **224** was obtained as a white solid (422 mg, 1.27 mmol, 99%). ^{1}H NMR (300 MHz, $CDCl_3$): δ = 7.52–7.28 (m, 6H), 7.25–7.10 (m, 2H), 5.31–5.18 (m, 2H), 4.93–4.79 (m, 2H), 4.79–4.66 (m, 2H) ppm; HRMS (ESI): *m/z* calcd for $C_{16}H_{14}{}^{79}Br_1N_1O_2Na_1$ $[M+Na]^+$: 354.0100, found: 354.0096.

Boronic acid 171. A flask (100 mL) was charged with compound **224** (3.12 g, 9.39 mmol, 1.00 eq), bis(pinacolato)diboron (**225**; 3.02 g, 11.9 mmol, 1.27 eq), KOAc (1.85 g, 18.9 mmol,

2.01 eq), and dioxane (48 mL). This mixture was purged with nitrogen gas for 15 min. Then, Pd(dppf)Cl_2 (345 mg, 472 µmol, 5.0 mol%) was added and the mixture stirred at 80 °C for 17 h under nitrogen atmosphere. After cooling to rt, the mixture was diluted with CH_2Cl_2 and the salts filtered off with a glass filter (porosity G3). All volatiles were removed from the filtrate *in vacuo*, the residue dissolved in CH_2Cl_2 and adsorbed on silica gel, and the crude product purified by flash chromatography (hexanes/EtOAc 10:1 → 6:1). After solvent removal and drying *in vacuo*, desired boronic acid **171** was obtained as a colorless crystalline solid (3.26 g, 8.60 mmol, 92%). ^{1}H NMR (300 MHz, $CDCl_3$): δ = 7.80–7.65 (m, 1H), 7.53–7.18 (m, 7H), 5.33–5.13 (m, 2H), 5.03–4.84 (m, 2H), 4.81–4.66 (m, 2H), 1.39–1.23 (m, 12H) ppm; HRMS (ESI): *m/z* calcd for $C_{22}H_{27}B_1N_1O_4$ $[M+H]^+$: 380.2032, found: 380.2027.

***N*-Cbz-Protected Benzoxazole Ligand 172.** A flask was charged with bromobenzoxazole **170** (1.61 g, 5.86 mmol, 1.00 eq), boronic acid **171** (2.55 g, 6.72 mmol, 1.15 eq), 1,2-dimethoxyethane (60 mL), and water (15 mL). Na_2CO_3 (1.36 g, 12.8 mmol, 2.19 eq) was carefully added to this mixture under stirring. The resulting mixture was then purged with nitrogen gas for 15 min followed by the addition of $Pd(PPh_3)_4$ (340 mg, 294 µmol, 5.0 mol%). The mixture was then stirred at 80 °C for 20 h under nitrogen atmosphere. After cooling to rt, the mixture was diluted with EtOAc and water, the organic layer was separated, and the aqueous layer extracted with EtOAc (2x). The combined organic layers were washed with brine, dried over Na_2SO_4, and all volatiles removed *in vacuo*. The residue was dissolved in CH_2Cl_2, adsorbed on silica gel, and purified by flash chromatography (hexanes/EtOAc 6:1 → 3:1). After solvent removal and drying *in vacuo*, desired compound **172** was obtained as a pale-yellow solid (2.66 g, 5.95 mmol, quantitative). ^{1}H NMR (300 MHz, $CDCl_3$): δ = 8.38–8.21 (m, 2H), 7.80 (dd, J = 5.3 Hz, J = 1.3 Hz, 1H), 7.64 (dd, J = 8.3 Hz, J = 1.7 Hz, 1H), 7.60–7.51 (m, 3H), 7.48–7.22 (m, 9H), 5.20 (d, J = 8.1 Hz, 2H), 4.93–4.74 (m, 4H) ppm; ^{13}C NMR: complex spectrum due to hindered rotation of the Cbz group (signals split up and broadened); IR (film): $\tilde{\nu}$ = 1700, 1461, 1449, 1409, 1362, 1347, 1099, 776, 755, 705, 689 cm^{-1}; HRMS (ESI): *m/z* calcd for $C_{29}H_{23}N_2O_3$: 447.1703 $[M+H]^+$; found: 447.1695.

4.3.2 Benzoxazole Ligand 174

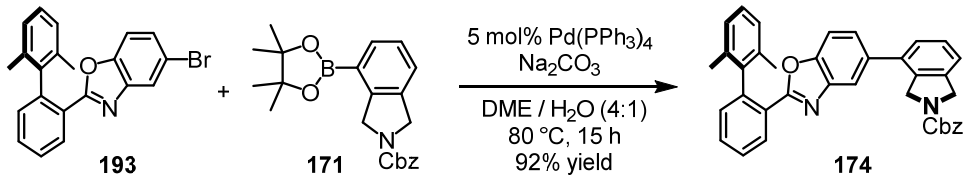

Scheme 63. Synthesis of *N*-Cbz-protected benzoxazole ligand **174**.

Benzoxazole Ligand 174. A flask was charged with bromobenzoxazole **193** (2.00 g, 5.28 mmol, 1.00 eq), boronic acid **171** (2.30 g, 6.06 mmol, 1.15 eq), 1,2-dimethoxyethane (55 mL), and water (13 mL). Na_2CO_3 (1.12 g, 10.6 mmol, 2.00 eq) was added to this mixture under stirring. The resulting mixture was purged with nitrogen gas for 15 min followed by the addition of $Pd(PPh_3)_4$ (310 mg, 268 μmol, 5.1 mol%). The mixture was stirred at 80 °C for 15 h under nitrogen atmosphere. After cooling to rt, the mixture was diluted with EtOAc and water, the organic layer was separated, and the aqueous layer extracted with EtOAc (2x). The combined organic layers were washed with brine, dried over Na_2SO_4, and all volatiles removed *in vacuo*. The residue was dissolved in CH_2Cl_2, adsorbed on silica gel, and purified by flash chromatography (hexanes/EtOAc 10:1 → 5:1). After solvent removal and drying *in vacuo*, desired *N*-Cbz-protected benzoxazole ligand **174** was obtained as a pale-yellow solid (2.68 g, 4.87 mmol, 92%). ^{1}H NMR (300 MHz, $CDCl_3$): δ = 8.46–8.34 (m, 1H), 7.69 (s, 1H), 7.63 (td, J = 7.5 Hz, J = 1.5 Hz, 1H), 7.56 (td, J = 7.6 Hz, J = 1.3 Hz, 1H), 7.46–7.22 (m, 11H), 7.19 (d, J = 7.7 Hz, 1H), 7.15–7.06 (m, 2H), 5.20 (d, J = 7.2 Hz, 2H), 4.83 (d, J = 7.0 Hz, 2H), 4.78 (d, J = 10.4 Hz, 2H), 1.99 (s, 3H), 1.99 (s, 3H) ppm; ^{13}C NMR: complex spectrum due to hindered rotation of the Cbz group (signals split up and broadened); IR (film): $\tilde{\nu}$ = 1697, 1459, 1446, 1415, 1362, 1347, 1201, 1184, 1089, 1029, 916, 819, 791, 757, 744, 713, 697, 654 cm^{-1}; HRMS (ESI): *m/z* calcd for $C_{37}H_{31}N_2O_3$: 551.2329 $[M+H]^+$; found: 551.2308.

4.4 Chiral Auxiliary Ligands (*S*)-Aux1 and (*S*)-Aux2

4.4.1 Salicylthiazoline Auxiliary Ligand (*S*)-Aux1

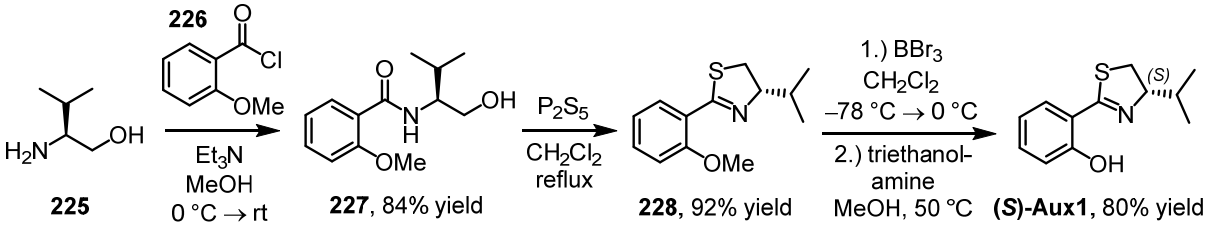

Scheme 64. Synthesis of salicylthiazoline auxiliary ligand **(*S*)-Aux1**.

Compound 227. Compound **227** was synthesized following a protocol reported by Aitken et al.[127] A flask (500 mL) was charged with methanol (245 mL), Et_3N (6.97 mL, 50.0 mmol, 1.10 eq), and L-valinol[128] (**225**; 4.69 g, 45.5 mmol, 1.00 eq). The mixture was cooled to 0 °C and 2-methoxybenzoyl chloride (**226**; 7.45 mL, 50.0 mmol, 1.10 eq) was added dropwise via syringe and the mixture allowed to warm to rt. After stirring at rt for 2 h, full conversion was indicated by TLC analysis (hexanes/EtOAc 1:1). All volatiles were removed *in vacuo* and the residue taken up in 250 mL EtOAc/H_2O (1:1). The organic layer was separated and the aqueous layer extracted with EtOAc (3x). The combined organic layers were washed with brine, dried over Na_2SO_4, the solvent removed *in vacuo*, the remaining oil dissolved in CH_2Cl_2 and adsorbed on silica gel, and the crude product purified by short-column chromatography (hexanes/EtOAc 2:1 → 1:2). After solvent removal and drying *in vacuo*, desired compound **227** was obtained as a colorless oil which slowly crystallized on standing (9.10 g, 38.3 mmol, 84%). ^{1}H NMR (300 MHz, $CDCl_3$): δ = 8.19 (dd, J = 7.7 Hz, J = 1.9 Hz, 1H), 8.14 (s, 1H), 7.46 (ddd, J = 8.3 Hz, J = 7.3 Hz, J = 1.8 Hz, 1H), 7.08 (td, J = 7.6 Hz, J = 0.9 Hz, 1H), 6.99 (d, J = 8.3 Hz, 1H), 4.05–3.93 (m, 1H), 3.98 (s, 3H), 3.80 (dd, J = 11.1 Hz, J = 3.5 Hz, 1H), 3.73 (dd, J = 11.0 Hz, J = 6.8 Hz, 1H), 3.33 (s, 1H), 2.11–1.94 (m, 1H), 1.03 (d, J = 7.1 Hz, 3H), 1.00 (d, J = 7.1 Hz, 3H) ppm; HRMS (ESI): *m/z* calcd for $C_{13}H_{19}N_1O_3H_1$: 238.1438 $[M+H]^+$; found: 238.1443.

Compound 228. Compound **228** was synthesized following a protocol reported by Aitken et al.[127] A flame-dried flask (250 mL) was charged with compound **227** (4.61 g, 19.4 mmol, 1.00 eq), dry CH_2Cl_2 (115 mL), and phosphorus pentasulfide (6.80 g, 30.6 mmol, 1.57 eq). The flask was equipped with a reflux condenser and the resulting suspension stirred at reflux for 46 h under nitrogen atmosphere after which clean and full conversion was indicated by TLC analysis. The yellow precipitate was filtered off with a glass filter (porosity G3) and the resultant filter cake thoroughly rinsed with CH_2Cl_2. The filtrate was washed with aqueous 2 M NaOH (2x 40 mL), water, and brine and the resulting organic layer dried over Na_2SO_4. All volatiles were removed *in vacuo*, the remaining oil dissolved in CH_2Cl_2, adsorbed on

silica gel, and purified by flash chromatography (hexanes/EtOAc 10:1). After solvent removal and drying *in vacuo*, desired product **228** was obtained as a pale-yellow colorless oil (4.23 g, 18.0 mmol, 92%). ^{1}H NMR (300 MHz, $CDCl_3$): δ = 7.86 (dd, J = 7.7 Hz, J = 1.7 Hz, 1H), 7.38 (ddd, J = 8.3 Hz, J = 7.4 Hz, J = 1.7 Hz, 1H), 6.99 (dd, J = 7.6 Hz, J = 1.1 Hz, 1H), 6.94 (dd, J = 8.1 Hz, J = 0.7 Hz, 1H), 4.41–4.28 (m, 1H), 3.89 (s, 3H), 3.32 (dd, J = 10.8 Hz, J = 8.9 Hz, 1H), 3.05 (dd, J = 10.8 Hz, J = 9.8 Hz, 1H), 2.21–2.02 (m, 1H), 1.11 (d, J = 6.8 Hz, 3H), 1.02 (d, J = 6.8 Hz, 3H) ppm; HRMS (ESI): *m/z* calcd for $C_{13}H_{17}N_1O_1S_1H_1$: 236.1104 $[M+H]^+$; found: 236.1105.

Auxiliary Ligand (*S*)-Aux1. A flame-dried flask (10 mL) was charged with compound **228** (200 mg, 850 µmol, 1.00 eq) and dry CH_2Cl_2 (5 mL). The resulting solution was cooled to −78 °C and BBr_3 (100 µL, 1.05 mmol, 1.24 eq) was added dropwise under stirring at –78 °C. The mixture was then allowed to warm to rt and after 3 h stirring at rt full conversion was indicated by TLC analysis. The mixture was quenched via dropwise addition of triethanolamine (2 mL, 15.1 mmol, 17.8 eq) whereupon a yellow precipitate formed. The resulting yellow suspension was taken up in water (50 mL) and EtOAc (50 mL), the organic layer was separated, and the aqueous layer extracted with EtOAc. The combined organic layers were dried over $MgSO_4$ and all volatiles were removed *in vacuo*. The resulting yellow oil was dissolved in MeOH (3 mL) and triethanolamine (3 mL) and the resulting mixture was stirred at 50 °C for 3 h. After cooling to rt, the mixture was taken up in water (50 mL) and EtOAc (50 mL), the organic layer was separated, and the aqueous layer extracted with EtOAc. The combined organic layers were dried over $MgSO_4$, the solvent removed *in vacuo*, and the resulting oil purified by flash chromatography (hexanes/EtOAc 20:1). After solvent removal and drying *in vacuo*, desired thiazoline auxiliary ligand **(*S*)-Aux1** was obtained as a viscous yellow oil (151 mg, 682 µmol, 80%). ^{1}H NMR (300 MHz, $CDCl_3$): δ = 12.85 (s, 1H), 7.44−7.31 (m, 2H), 7.05 (dd, J = 8.3 Hz, J = 0.8 Hz, 1H), 6.88 (dd, J = 7.6 Hz, J = 1.1 Hz, 1H), 4.54–4.40 (m, 1H), 3.41 (dd, J = 11.0 Hz, J = 8.7 Hz, 1H), 3.11 (dd, J = 10.9 Hz, J = 9.5 Hz, 1H), 2.14–1.96 (m, 1H), 1.11 (d, J = 6.6 Hz, 3H), 1.05 (d, J = 6.8 Hz, 3H) ppm; ^{13}C NMR (75 MHz, $CDCl_3$): δ = 171.5, 159.5, 133.3, 130.7, 119.0, 117.3, 116.3, 82.2, 34.1, 33.3, 19.7, 19.4 ppm; IR (film): $\tilde{\nu}$ = 1594, 1569, 1489, 1456, 1254, 1218, 1154, 1025, 991, 959, 946, 814, 748, 689 cm^{-1}; HRMS (ESI): *m/z* calcd for $C_{12}H_{15}N_1O_1S_1H$: 222.0947 $[M+H]^+$; found: 222.0945.

4.4.2 Salicyloxazoline Auxiliary Ligand (*S*)-Aux2

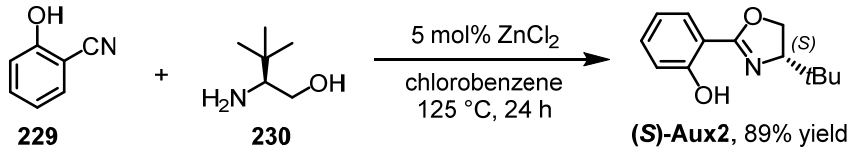

Scheme 65. Synthesis of salicyloxazoline auxiliary ligand **(*S*)-Aux2**.

Auxiliary Ligand (*S*)-Aux2. Auxiliary ligand **(*S*)-Aux2** was synthesized following a procedure from Iwata et al.[80b] A flame-dried flask (25 mL) was charged with zinc chloride (54.0 mg, 396 µmol, 5 mol%) and rigorously flame-dried *in vacuo* (heat gun; approx. 5 min at 450 °C). After cooling to rt, a flame-dried stir bar, 2-hydroxybenzonitrile (**229**; 944 mg, 7.92 mmol, 1.00 eq), L-*tert*-leucinol (**230**; 1.20 g, 11.6 mmol, 1.47 eq), and dry chlorobenzene (8.0 mL) were added and the mixture stirred at 125 °C (reflux) for 24 h under nitrogen atmosphere. After cooling to rt, the solvent was removed *in vacuo*, the residue taken up in CH_2Cl_2 and water, the organic layer separated, and the aqueous layer extracted with CH_2Cl_2 (3x). The combined organic layers were dried over Na_2SO_4, adsorbed on silica gel (40 °C), and purified by flash chromatography (hexanes/EtOAc 20:1). After solvent removal and drying *in vacuo*, desired **(*S*)-Aux2** was obtained as a colorless liquid which crystallized on standing at 4 °C (1.55 g, 7.08 mmol, 89%). $[\alpha]_D^{23}$ = −20 (*c* 1.0, $CHCl_3$); ^{1}H NMR (300 MHz, $CDCl_3$): δ = 12.40 (s, 1H), 7.64 (dd, *J* = 7.7 Hz, *J* = 1.7 Hz, 1H), 7.37 (ddd, *J* = 8.4 Hz, *J* = 7.3 Hz, *J* = 1.7 Hz, 1H), 7.02 (dd, *J* = 8.4 Hz, *J* = 0.8 Hz, 1H), 6.92–6.82 (m, 1H), 4.35 (dd, *J* = 10.0 Hz, *J* = 8.5 Hz, 1H), 4.22 (dd, *J* = 8.5 Hz, *J* = 7.7 Hz, 1H), 4.11 (dd, *J* = 10.0 Hz, *J* = 7.7 Hz, 1H), 0.95 (s, 9H) ppm; ^{13}C NMR (75 MHz, $CDCl_3$): δ = 165.2, 160.2, 133.4, 128.1, 118.6, 116.8, 110.7, 75.0. 68.2, 33.9, 25.9 (3C) ppm; IR (film): $\tilde{\nu}$ = 2958, 1641, 1619, 1491, 1361, 1310, 1259, 1232, 1155, 1129, 1075, 1058, 959, 752, 668 cm^{-1}; HRMS (ESI): *m/z* calcd for $C_{13}H_{17}N_1O_2H$: 220.1332 $[M+H]^+$; found: 220.1330.

4.5 Achiral Non-Cyclometalating Ligands from Chapter 2.

4.5.1 Imidazoquinoline Ligand 233

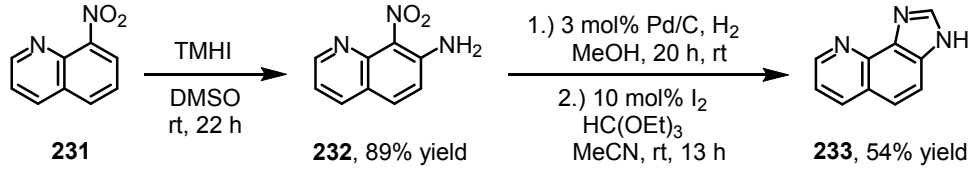

Scheme 66. Synthesis of imidazoquinoline ligand **233**.

8-Nitroquinolin-7-amine (232). Compound **232** was prepared according to a modified procedure reported by Grzegożek.[129] A flame-dried flask (100 mL) was charged with 8-nitro-

quinoline (**231**; 1.75 g, 10.0 mmol, 1.00 eq), 1,1,1-trimethylhydrazinium iodide[130] (3.06 g, 15.1 mmol, 1.51 eq), and dry DMSO (60 mL). The mixture was cooled with a water bath and KO*t*Bu (3.38 g, 30.1 mmol, 3.01 eq) was added to the mixture at once. After 10 min, the mixture was allowed to stir at rt for 22 h under an atmosphere of nitrogen gas. TLC analysis (hexanes/EtOAc 1:1) indicated full conversion and the mixture was quenched with aqueous NH_4Cl and diluted with water and CH_2Cl_2. The organic layer was separated, the aqueous layer extracted with CH_2Cl_2 (10x), the combined organic layers washed with water (2x) and brine, dried over Na_2SO_4, and the crude product adsorbed on silica gel and purified by flash chromatography ($CHCl_3$/EtOAc 1:1[131]). After solvent removal and drying *in vacuo*, desired product **232** was obtained as an orange crystalline solid (1.68 g, 8.88 mmol, 89%). ^{1}H NMR (300 MHz, DMSO-d_6): δ = 8.72 (dd, J = 4.4 Hz, J = 1.8 Hz, 1H), 8.17 (dd, J = 8.1 Hz, J = 1.7 Hz, 1H), 7.81 (d, J = 9.1 Hz, 1H), 7.29 (dd, J = 8.1 Hz, J = 4.3 Hz, 1H), 7.19 (d, J = 9.1 Hz, 1H), 6.85 (s, 2H) ppm.

Imidazoquinoline Ligand 233. A flask (100 mL) was charged with 8-nitroquinolin-7-amine **232** (700 mg, 3.70 mmol, 1.00 eq) and MeOH (24 mL). The mixture was purged with nitrogen gas for 5 min. Then, Pd/C (10 wt%; 113 mg, 106 µmol, 3 mol%) was added and the mixture put under an atmosphere of hydrogen gas using a balloon. The mixture was vigorously stirred for 20 h at rt under an atmosphere of hydrogen gas. Then, the mixture was purged with nitrogen gas for 5 min and filtered through a plug of celite, which was thoroughly rinsed with CH_2Cl_2/MeOH 1:1. The filtrate was concentrated *in vacuo* and the remaining brown solid transferred into a new flask (25 mL). The subsequent construction of the imidazole ring was achieved with a modified procedure reported by Zhang et al.[132] Iodine (95 mg, 0.37 mmol, 10 mol%), dry MeCN (5 mL), and triethyl orthoformate (0.81 mL, 4.92 mmol, 1.33 eq) were added, the flask sealed with a septum, and the mixture stirred at rt for 13 h. Then, all volatiles were removed *in vacuo*, the residue taken up in CH_2Cl_2/MeOH, adsorbed on silica gel, and purified by flash chromatography (EtOAc/MeOH 10:1). After solvent removal and drying *in vacuo*, desired imidazoquinoline ligand **233** was obtained as a brown solid (341 mg, 2.02 mmol, 54%). ^{1}H NMR (300 MHz, CD_3OD): δ = 8.86 (dd, J = 4.3 Hz, J = 1.5 Hz, 1H), 8.37 (dd, J = 8.3 Hz, J = 1.5 Hz, 1H), 8.31 (s, 1H) ppm; ^{13}C NMR (75 MHz, DMSO-d_6): δ = 140.8, 132.3, 131.2, 130.6, 128.8, 122.7, 117.3, 114.5, 111.8, 109.5 ppm; IR (film): $\tilde{\nu}$ = 3038, 2811, 1530, 1361, 1243, 940, 819, 796, 765, 700, 627 cm^{-1}; HRMS (ESI): *m/z* calcd for $C_{10}H_7N_3H_1$: 170.0713 $[M+H]^+$; found: 170.0712.

4.5.2 Imidazoquinoline Ligand 236

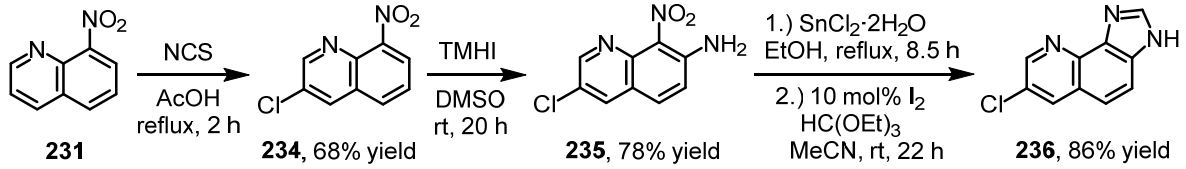

Scheme 67. Synthesis of imidazoquinoline ligand **236**.

3-Chloro-8-nitroquinoline (234). Compound **234** was prepared following a modified procedure reported by Gershon et al.[133] A two-neck flask (100 mL) equipped with a reflux condenser was charged with acetic acid (40 mL) and 8-nitroquinoline (**231**; 2.52 g, 14.5 mmol, 1.00 eq). The mixture was heated to 105 °C and NCS (3.39 g, 24.5 mmol, 1.75 eq) was added portionwise over a period of 1 h. When the addition was complete, the mixture was stirred at 120 °C (reflux) for 2 h. After cooling to rt, TLC (hexanes/EtOAc 6:1) indicated full conversion and the mixture was poured into water (300 mL) and the mixture stirred vigorously for 5 min. The formed yellow precipitate was filtered off (glass filter; porosity G4), the precipitate dissolved in CH_2Cl_2, and the resulting organic layer dried over Na_2SO_4. The crude product was dissolved in CH_2Cl_2, adsorbed on silica gel, and purified by flash chromatography (hexanes/EtOAc 10:1 → 8:1). After drying *in vacuo*, desired product **234** was obtained as a yellow crystalline solid (2.05 g, 9.83 mmol, 68%). ^{1}H NMR (300 MHz, $CDCl_3$): δ = 8.94 (d, J = 2.3 Hz, 1H), 8.24 (d, J = 2.3 Hz, 1H), 8.10–7.90 (m, 2H), 7.66 (dd, J = 7.7 Hz, J = 7.7 Hz, 1H) ppm; ^{13}C NMR (75 MHz, $CDCl_3$): δ = 152.0, 148.4, 137.6, 134.1, 131.2, 130.7, 129.3, 126.8, 124.0 ppm; IR (film): $\tilde{\nu}$ = 3064, 1528, 1490, 1356, 1189, 1092, 910, 763, 653 cm^{-1}; HRMS (ESI): *m/z* calcd for $C_9H_5Cl_1N_2O_2Na$: 230.9932 [M+Na]$^+$; found: 230.9933.

3-Chloro-8-nitroquinolin-7-amine (235). Compound **235** was prepared according to a modified procedure reported by Grzegożek.[129] A flame-dried flask (250 mL) was charged with 3-chloro-8-nitroquinoline (**234**; 1.50 g, 7.19 mmol, 1.00 eq), 1,1,1-trimethylhydrazinium iodide[130] (2.25 g, 11.1 mmol, 1.55 eq), and dry DMSO (40 mL). The mixture was cooled with a water bath and KO*t*Bu (2.46 g, 21.9 mmol, 3.05 eq) was added to the mixture at once. After 10 min, the mixture was allowed to stir at rt for 20 h under an atmosphere of nitrogen gas. TLC (hexanes/EtOAc 1:1) indicated full conversion and the mixture was quenched with aqueous sat. NH_4Cl and diluted with water (500 mL) and CH_2Cl_2 (250 mL). The organic layer was separated and the aqueous layer extracted with CH_2Cl_2 (6x). The combined organic layers were washed with water (2x) and brine, dried over Na_2SO_4, adsorbed on silica gel, and purified by flash chromatography ($CHCl_3$/EtOAc 6:1 → 3:1[131]). After drying *in vacuo*,

desired product **235** was obtained as an orange crystalline solid (1.25 g, 5.59 mmol, 78%). ^{1}H NMR (300 MHz, DMSO-d_6): δ = 8.71 (d, J = 2.5 Hz, 1H), 8.36 (d, J = 2.5 Hz, 1H), 7.80 (d, J = 9.3 Hz, 1H), 7.25 (d, J = 9.1 Hz, 1H), 7.01 (s, 2H) ppm; ^{13}C NMR (75 MHz, DMSO-d_6): δ = 149.5, 143.6, 140.5, 134.2, 130.9, 127.7, 124.5, 121.5, 120.3 ppm; IR (film): $\tilde{\nu}$ = 3416, 3302, 3176, 1639, 1548, 1503, 1471, 1272, 1107, 900, 576, 526 cm^{-1}; HRMS (ESI): *m/z* calcd for $C_9H_6Cl_1N_3O_2H$: 224.0221 [M+H]$^+$; found: 224.0223.

Imidazoquinoline Ligand 236. A flask (25 mL) was charged with compound **235** (461 mg, 2.06 mmol, 1.00 eq), $SnCl_2 \cdot 2H_2O$ (1.48 g, 6.56 mmol, 3.18 eq), and EtOH (14 mL) and the mixture was stirred at reflux for 8.5 h. After cooling to rt, the mixture was diluted with water and EtOAc and the pH of the aqueous layer was set to pH ≥ 12 with aqueous 2 M NaOH. The organic layer was separated and the aqueous layer extracted with EtOAc (3x). The combined organic layers were dried over Na_2SO_4 and the solvent removed *in vacuo*, which yielded a brown crystalline solid which was dried *in vacuo* and transferred into a new flask (25 mL). The subsequent construction of the imidazole ring was achieved with a modified procedure reported by Zhang et al.[132] Iodine (52 mg, 205 µmol, 10 mol%), dry MeCN (6.3 mL), and triethyl orthoformate (650 µL, 3.91 mmol, 1.90 eq) were added, the flask sealed with a septum and the mixture stirred at rt for 22 h. All volatiles were removed *in vacuo*, the dark residue taken up in CH_2Cl_2/MeOH, adsorbed on silica gel, and purified by flash chromatography (EtOAc/MeOH 30:1). After solvent removal and drying *in vacuo*, desired imidazoquinoline ligand **236** was obtained as a brown solid (357 mg, 1.76 mmol, 86%). ^{1}H NMR (300 MHz, DMSO-d_6): δ = 13.62 (s, 1H), 8.91 (d, J = 2.5 Hz, 1H), 8.64 (d, J = 2.5 Hz, 1H), 8.39 (s, 1H), 7.94 (d, J = 8.7 Hz, 1H), 7.71 (d, J = 8.9 Hz, 1H) ppm; ^{13}C NMR (75 MHz, DMSO-d_6): δ = 147.4, 141.5, 140.6, 136.7, 134.8, 130.8, 125.9, 125.1, 121.1, 120.1 ppm; IR (film): $\tilde{\nu}$ = 2576, 1718, 1479, 1359, 1308, 1270, 1180, 1103, 948, 919, 885, 854, 796, 755, 697, 628, 514 cm^{-1}; HRMS (ESI): *m/z* calcd for $C_{10}H_6N_3Cl_1Na$: 226.0142 [M+Na]$^+$; found: 226.0149.

4.5.3 Imidazoquinoline Ligand 238

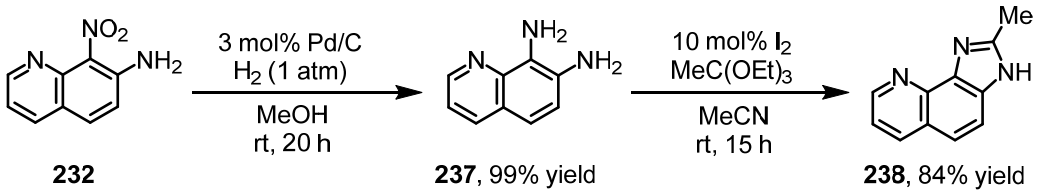

Scheme 68. Synthesis of imidazoquinoline ligand **238**.

Quinoline-7,8-diamine (237). A flask (100 mL) was charged with 8-nitroquinolin-7-amine (**232**; 700 mg, 3.70 mmol, 1.00 eq), Pd/C (10 wt%; 112 mg, 105 µmol, 3 mol%), and MeOH

(24 mL). The resulting mixture was purged with nitrogen gas for 10 min. Then, the mixture was placed under an atmosphere of hydrogen gas (H_2-ballon) and vigorously stirred for 20 h. The resulting mixture was purged with nitrogen gas for 10 min, diluted with CH_2Cl_2/MeOH, and passed through a short plug of celite, which was subsequently rinsed with CH_2Cl_2/MeOH. All volatiles were removed from the filtrate and the residue dried *in vacuo*. Desired quinoline-7,8-diamine (**237**) was obtained as a dark-brown solid without the need for further purification (588 mg, 3.69 mmol, quantitative). ^{1}H NMR (300 MHz, CD_3OD): δ = 8.62 (dd, J = 4.3 Hz, J = 1.5 Hz, 1H), 8.02 (dd, J = 8.3 Hz, J = 1.5 Hz, 1H), 7.21–7.13 (m, 2H), 7.11 (d, J = 8.7 Hz, 1H) ppm (the signals belonging to the NH_2 groups could not be found due to rapid exchange); HRMS (ESI): *m/z* calcd for $C_9H_9N_3H$: 160.0869 [M+H]$^+$; found: 160.0873.

Imidazoquinoline Ligand 238. Compound **238** was synthesized following a method reported by Zhang et al.[132] A flask was charged with quinoline-7,8-diamine (**237**; 170 mg, 1.07 mmol, 1.00 eq), iodine (27.4 mg, 108 µmol, 10 mol%), triethyl orthoacetate (270 µL, 1.47 mmol, 1.38 eq), and dry MeCN (1.7 mL). The mixture was stirred at rt for 15 h under an atmosphere of nitrogen gas. The resulting dark slurry was then diluted with CH_2Cl_2/MeOH 1:1, adsorbed on silica gel, and purified by flash chromatography (EtOAc/MeOH 20:1 → 15:1). After solvent removal and drying *in vacuo*, desired imidazoquinoline ligand **238** was obtained as a light-brown nacre-like crystalline solid (165 mg, 901 µmol, 84%). ^{1}H NMR (300 MHz, CD_3OD): δ = 8.81 (dd, J = 4.4 Hz, J = 1.6 Hz, 1H), 8.30 (dd, J = 8.2 Hz, J = 1.6 Hz, 1H), 7.60 (d, J = 8.7 Hz, 1H), 7.50 (d, J = 8.7 Hz, 1H), 7.42 (dd, J = 8.2 Hz, J = 4.4 Hz), 2.66 (s, 3H) ppm; ^{13}C NMR (75 MHz, CD_3OD): δ = 152.4, 150.3, 141.9, 139.5, 138.2, 132.3, 126.5, 123.4, 121.0, 118.9, 14.5 ppm; IR (film): $\tilde{\nu}$ = 1608, 1541, 1508, 1428, 1396, 1362, 1328, 1304, 1255, 1019, 825, 799, 767, 707, 650, 532, 500, 412 cm^{-1}; HRMS (ESI): *m/z* calcd for $C_{11}H_9N_3H_1$: 184.0869 [M+H]$^+$; found: 184.0873.

4.5.4 Imidazoquinoline Ligand 241

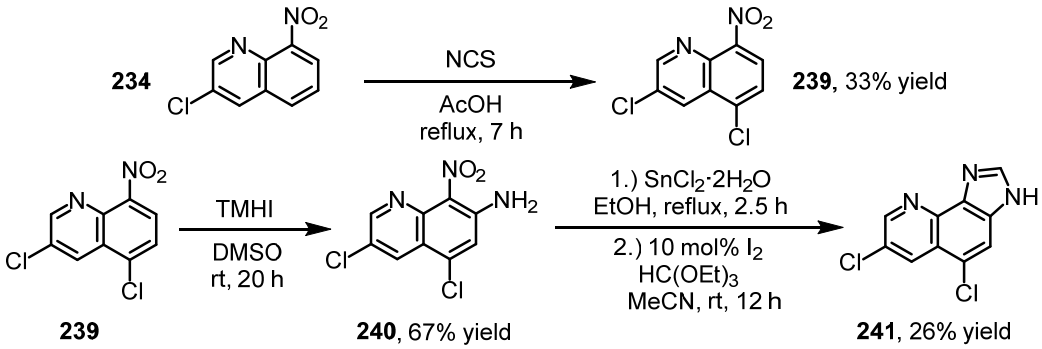

Scheme 69. Synthesis of imidazoquinoline ligand **241**.

3,5-Dichloro-8-nitroquinoline (239). A flask (50 mL) was charged with 3-chloro-8-nitroquinoline (**234**; 283 mg, 1.36 mmol, 1.00 eq) and glacial acetic acid (5 mL). The mixture was

heated to 110 °C, NCS (210 mg, 1.57 mmol, 1.16 eq) was added at once, and the mixture stirred at 110 °C for 15 min. As TLC indicated incomplete conversion, additional NCS (113 mg, 0.85 mmol, 0.62 eq) was added and the mixture stirred at 110 °C for 6.5 h. As TLC now indicated full conversion, the mixture was allowed to cool to rt, all volatiles were removed *in vacuo*, and acetic acid traces removed as an azeotrope with toluene (4x). The crude residue was dissolved in CH_2Cl_2, adsorbed on silica gel, and purified by flash chromatography (hexanes/EtOAc 50:1 → 40:1). After solvent removal and drying *in vacuo*, desired dichlorinated compound **239** was obtained as a colorless crystalline solid (108 mg, 444 µmol, 33%). ^{1}H NMR (300 MHz, $CDCl_3$): $\delta = 9.00$ (d, $J = 2.3$ Hz, 1H), 8.63 (d, $J = 2.3$ Hz, 1H), 7.99 (d, $J = 8.1$ Hz, 1H), 7.75 (d, $J = 8.1$ Hz, 1H) ppm; HRMS (ESI): *m/z* calcd for $C_9H_4Cl_2N_2O_2H$: 242.9723 $[M+H]^+$; found: 242.9723.

Compound 240. Compound **240** was prepared according to a modified procedure reported by Grzegożek.[129] A flask (10 mL) was charged with compound **239** (107 mg, 440 µmol, 1.00 eq) and dried *in vacuo* for 1 h. Then, 1,1,1-trimethylhydrazinium iodide[130] (130 mg, 643 µmol, 1.46 eq), dry DMSO (3.2 mL), and KO*t*Bu (143 mg, 1.27 mmol, 2.89 eq) were added and the mixture stirred at rt for 20 h under nitrogen atmosphere. Then, the mixture was diluted with CH_2Cl_2 and quenched by the addition of aqueous NH_4Cl. The organic layer was separated and the aqueous layer extracted with CH_2Cl_2 (10x). The combined organic layers were washed with brine and dried over Na_2SO_4. All volatiles were removed *in vacuo*, the residue dissolved in CH_2Cl_2/MeOH, adsorbed on silica gel, and purified by flash chromatography ($CHCl_3$/EtOAc 3:1[131]). After solvent removal and drying *in vacuo*, desired compound **240** was obtained as an orange-brown solid (76.4 mg, 296 µmol, 67%). ^{1}H NMR (300 MHz, DMSO-d_6): $\delta = 8.82$ (d, $J = 2.5$ Hz, 1H), 8.37 (dd, $J = 2.3$ Hz, 1H), 7.46 (s, 1H), 7.15 (s, 2H) ppm.

Imidazoquinoline Ligand 241. A flask (10 mL) was charged with compound **240** (76.0 mg, 294 µmol, 1.00 eq), $SnCl_2 \cdot 2H_2O$ (204 mg, 904 µmol, 3.07 eq), and EtOH (1.6 mL) and the mixture was stirred at reflux for 2.5 h. After cooling to rt, the mixture was diluted with water and EtOAc and the pH of the aqueous layer was set to pH ≥ 12 with aqueous 2 M NaOH. The organic layer was separated and the aqueous layer extracted with EtOAc (3x). The combined organic layers were dried over Na_2SO_4 and the solvent removed *in vacuo*, which yielded a yellow-brown solid which was dried *in vacuo* and transferred into a new flask (10 mL). The subsequent construction of the imidazole ring was achieved with a modified procedure reported by Zhang et al.[132] Iodine (8.1 mg, 31.9 µmol, 11 mol%), dry MeCN (0.8 mL), and triethyl orthoformate (75 µL, 454 µmol, 1.55 eq) were added, the flask sealed with a septum and the mixture stirred at rt for 12 h. Then, the dark slurry was diluted with CH_2Cl_2/MeOH and

the crude product adsorbed on silica gel and purified by flash chromatography (EtOAc/MeOH 100:1). After solvent removal and drying *in vacuo*, desired dichlorinated imidazoquinoline ligand **241** was obtained as an orange-grey solid (18.4 mg, 77.3 µmol, 26%). ^{1}H NMR (300 MHz, DMSO-d_6): δ = 13.81 (s, 1H), 9.03 (d, J = 2.3 Hz, 1H), 8.66 (d, J = 2.3 Hz, 1H), 8.43 (s, 1H), 8.18 (s, 1H) ppm; IR (film): $\tilde{\nu}$ = 3344, 1610, 1540, 1495, 1451, 1423, 1340, 1283, 1259, 1208, 1022, 959, 809, 781 cm^{-1}; HRMS (ESI): *m/z* calcd for $C_{10}H_5Cl_2N_3H$: 237.9933 $[M+H]^+$; found: 237.9935.

4.5.5 Imidazoquinoline Ligand 245

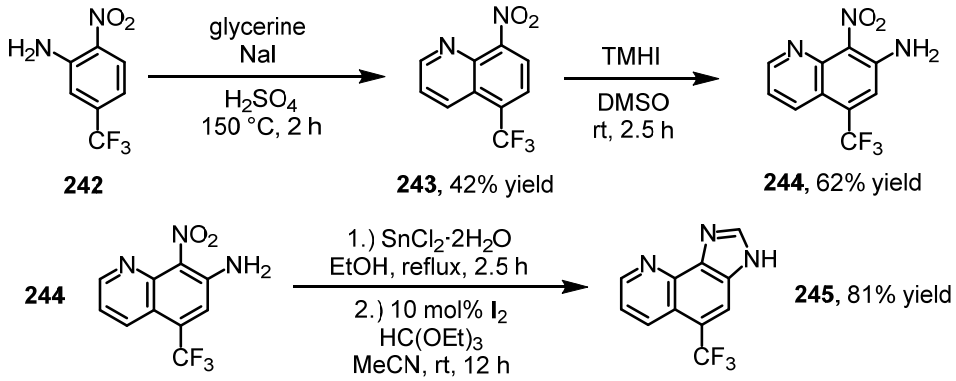

Scheme 70. Synthesis of imidazoquinoline ligand **245**.

8-Nitro-5-(trifluoromethyl)quinoline (243). A flask (10 mL) was charged with glycerin (1.58 g, 21.5 mmol, 4.24 eq) and the glycerin heated to 160 °C for 1 h 15 min. The resulting mixture was allowed to cool to 110 °C and 2-nitro-5-(trifluoromethyl)aniline (**242**; 1.05 g, 5.07 mmol, 1.00 eq) and NaI (25.1 mg, 167 µmol, 3.3 mol%) were added and the mixture heated to 150 °C. Concentrated H_2SO_4 (1.11 mL, 20.8 mmol, 4.11 eq) was carefully added dropwise at 150 °C under stirring and the mixture was stirred for 1 h at 150 °C. After cooling to rt, the resulting dark slurry was diluted with large amounts of water and CH_2Cl_2, the organic layer separated, the aqueous layer extracted with CH_2Cl_2 (5x), and the combined organic layers dried over Na_2SO_4. All volatiles were removed *in vacuo*, the residue dissolved in CH_2Cl_2, adsorbed on silica gel, and purified by flash chromatography (hexanes/EtOAc 6:1). After solvent removal and drying *in vacuo*, desired quinoline **243** was obtained as an orange crystalline solid (511 mg, 2.11 mmol, 42%). ^{1}H NMR (300 MHz, $CDCl_3$): δ = 9.13 (dd, J = 4.3 Hz, J = 1.5 Hz, 1H), 8.58 (dquin, J = 8.8 Hz, J = 1.8 Hz, 1H), 8.10–7.93 (m, 2H), 7.71 (dd, J = 8.9 Hz, J = 4.2 Hz, 1H) ppm; HRMS (ESI): *m/z* calcd for $C_{10}H_5F_3N_2O_2H$: 243.0376 $[M+H]^+$; found: 243.0375.

Compound 244. Compound **244** was prepared according to a modified procedure reported by Grzegożek.[129] A flame-dried flask (10 mL) was charged with quinoline **243** (292 mg,

1.21 mmol, 1.00 eq), 1,1,1-trimethylhydrazinium iodide[130] (293 mg, 1.45 mmol, 1.20 eq), dry DMSO (7.5 mL), and KO*t*Bu (406 mg, 3.62 mmol, 2.99 eq) and the mixture stirred at rt for 2.5 h under nitrogen atmosphere. The mixture was diluted with CH_2Cl_2 and quenched by the addition of aqueous NH_4Cl, the organic layer separated, and the aqueous layer extracted with CH_2Cl_2 (8x). The combined organic layers were washed with brine, dried over Na_2SO_4, all volatiles removed *in vacuo*, the residue dissolved in CH_2Cl_2/MeOH and adsorbed on silica gel, and the crude product purified by flash chromatography ($CHCl_3$/EtOAc 10:1[131]). After solvent removal and drying *in vacuo*, desired compound **244** was obtained as an orange-brown crystalline solid (192 mg, 747 µmol, 62%). ^{1}H NMR (300 MHz, DMSO-d_6): δ = 8.84 (dd, J = 4.3 Hz, J = 1.3 Hz, 1H), 8.25 (dt, J = 8.5 Hz, J = 1.8 Hz, 1H), 7.77 (s, 1H), 7.45 (dd, J = 8.5 Hz, J = 4.3 Hz, 1H), 7.02 (s, 2H) ppm; HRMS (ESI): *m/z* calcd for $C_{10}H_6F_3N_3O_2H$: 258.0485 $[M+H]^+$; found: 258.0485.

Imidazoquinoline Ligand 245. A flask (25 mL) was charged with compound **244** (295 mg, 1.15 mmol, 1.00 eq), $SnCl_2 \cdot 2H_2O$ (776 mg, 3.44 mmol, 3.00 eq), and EtOH (6.0 mL) and the mixture was stirred at reflux for 2.5 h. After cooling to rt, the mixture was diluted with water and EtOAc and the pH of the aqueous layer was set to pH ≥ 12 with aqueous 2 M NaOH. The organic layer was separated and the aqueous layer extracted with EtOAc (4x). The combined organic layers were dried over Na_2SO_4 and the solvent removed *in vacuo*, which yielded a yellow-brown solid which was dried *in vacuo* and transferred into a new flask (10 mL). The subsequent construction of the imidazole ring was achieved with a modified procedure reported by Zhang et al.[132] Iodine (29 mg, 114 µmol, 10 mol%), dry MeCN (2.5 mL), and triethyl orthoformate (290 µL, 1.74 µmol, 1.52 eq) were added, the flask sealed with a septum and the mixture stirred at rt for 12 h. Then, the dark slurry was diluted with CH_2Cl_2/MeOH and the crude product adsorbed on silica gel and purified by flash chromatography (EtOAc/MeOH 60:1). After solvent removal and drying *in vacuo*, desired trifluoromethylated ligand **245** was obtained as a brown crystalline solid (221 mg, 933 µmol, 81%). ^{1}H NMR (300 MHz, DMSO-d_6): δ = 14.07 (s, 1H), 9.07 (dd, J = 4.2 Hz, J = 1.4 Hz, 1H), 8.64–8.54 (m, 2H), 8.53 (s, 1H), 8.40 (s, 1H), 7.74 (dd, J = 8.7 Hz, J = 4.3 Hz, 1H) ppm; IR (film): $\tilde{\nu}$ = 1342, 1279, 1222, 1139, 1103, 944, 879, 786, 698, 630 cm^{-1}; HRMS (ESI): *m/z* calcd for $C_{11}H_6F_3N_3Na$: 260.0406 $[M+Na]^+$; found: 260.0407.

4.5.6 Imidazoquinoline Ligand 251

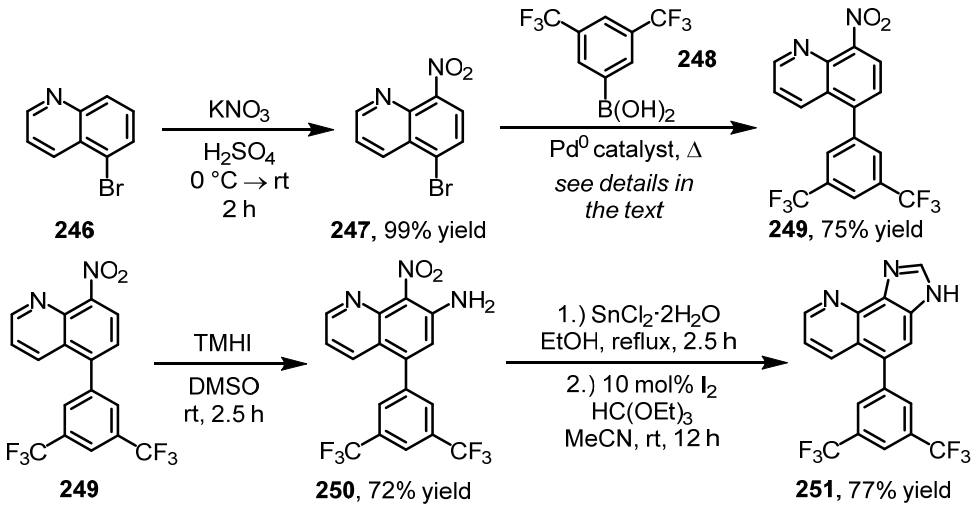

Scheme 71. Synthesis of imidazoquinoline ligand **251**.

5-Bromo-8-nitroquinoline (247). A flask (25 mL) was charged with 5-bromoquinoline (**246**; 2.50 g, 12.0 mmol, 1.00 eq) and concentrated H_2SO_4 (10 mL) was added at 0 °C. Then, KNO_3 (1.98 g, 19.6 mmol, 1.63 eq) was added portionwise over 15 min. The resulting mixture was then allowed to warm to rt and stirred for 2 h. Then, the resulting mixture was poured into ice-water, CH_2Cl_2 was added, the organic layer separated, and the aqueous layer extracted with CH_2Cl_2 (6x). The combined organic layers were washed with brine, dried over Na_2SO_4, and the solvent removed *in vacuo*. After drying *in vacuo*, desired compound **247** was obtained as a colorless solid without the need for further purification (3.01 g, 11.9 mmol, 99%). ^{1}H NMR (300 MHz, $CDCl_3$): $\delta = 9.09$ (dd, $J = 4.2$ Hz, $J = 1.6$ Hz, 1H), 8.63 (dd, $J = 8.7$ Hz, $J = 1.7$ Hz, 1H), 7.98–7.85 (m, 2H), 7.67 (dd, $J = 8.6$ Hz, $J = 4.2$ Hz, 1H) ppm; HRMS (ESI): *m/z* calcd for $C_9H_5Br_1N_2O_2Na$: 274.9427 $[M+Na]^+$; found: 274.9429.

Compound 249. A flame-dried flask (10 mL) was charged with compound **247** (300 mg, 1.19 mmol, 1.00 eq), 3,5-bis(trifluoromethyl)phenylboronic acid (**248**; 465 mg, 1.80 mmol, 1.52 eq), and Na_2CO_3 (369 mg, 3.48 mmol, 2.94 eq). 1,2-Dimethoxyethane (4.2 mL) and water (0.42 mL) were added and the mixture purged with nitrogen gas for 10 min. The mixture was stirred at 90 °C under nitrogen atmosphere for 40 h. TLC (hexanes/EtOAc 3:1) indicated that the reaction was incomplete. The mixture was diluted with water and EtOAc, the organic layer separated, the aqueous layer extracted with EtOAc (3x), the combined organic layers dried over Na_2SO_4, and the solvent removed *in vacuo*. As crude ^{1}H NMR indicated a ratio **249**/**247** of about 2:1 and as product **249** and substrate **247** proved to be hardly resolvable by standard flash chromatography, the obtained crude product was put in a new flask (10 mL) and boronic acid **248** (163 mg, 634 µmol, 0.53 eq), Cs_2CO_3 (260 mg, 798 µmol, 0.67 eq), and toluene (2.2 mL) were added and the resulting mixture degassed (4x;

freeze-pump-thaw technique). $Pd(PPh_3)_4$ (29 mg, 25.1 µmol, 2.1 mol%) was added and the resulting mixture stirred at 100 °C for 31 h under nitrogen atmosphere. As TLC indicated full conversion, the mixture was allowed to cool to rt, diluted with CH_2Cl_2 and the salts removed by filtration through a glass filter (porosity G4). All volatiles were removed from the filtrate *in vacuo*, the residue dissolved in CH_2Cl_2, and the crude product purified by flash chromatography (hexanes/EtOAc 10:1). After solvent removal and drying *in vacuo*, desired compound **249** was obtained as an off-white solid (345 mg, 893 µmol, 75%). ^{1}H NMR (300 MHz, $CDCl_3$): $\delta = 9.12$ (dd, $J = 4.2$ Hz, $J = 1.5$ Hz, 1H), 8.11 (dd, $J = 8.6$ Hz, $J = 1.6$ Hz, 1H), 8.10 (d, $J = 7.6$ Hz, 1H), 8.06 (s, 1H), 7.93 (s, 2H), 7.63 (d, $J = 7.7$ Hz, 1H), 7.61 (dd, $J = 8.7$ Hz, $J = 4.2$ Hz, 1H) ppm; HRMS (ESI): *m/z* calcd for $C_{17}H_8F_6N_2O_2H$: 387.0563 $[M+H]^+$; found: 387.0562.

Compound 250. Compound **250** was prepared according to a modified procedure reported by Grzegożek.[129] A flame-dried flask (25 mL) was charged with compound **249** (340 mg, 880 µmol, 1.00 eq). Then, 1,1,1-trimethylhydrazinium iodide[130] (217 mg, 1.07 mmol, 1.22 eq), dry DMSO (5.5 mL), and KO*t*Bu (302 mg, 2.69 mmol, 3.06 eq) were added and the mixture stirred at rt for 2.5 h under nitrogen atmosphere. The mixture was diluted with CH_2Cl_2 and quenched by the addition of aqueous NH_4Cl. The organic layer was separated, the aqueous layer extracted with CH_2Cl_2 (8x), and the combined organic layers washed with brine and dried over Na_2SO_4. All volatiles were removed *in vacuo*, the residue dissolved in CH_2Cl_2/MeOH, adsorbed on silica gel, and purified by flash chromatography ($CHCl_3$/EtOAc 10:1[131]). After solvent removal and drying *in vacuo*, desired compound **250** was obtained as a yellow-green crystalline solid (255 mg, 636 µmol, 72%). ^{1}H NMR (300 MHz, DMSO-d_6): $\delta = 8.77$ (dd, $J = 4.3$ Hz, $J = 1.7$ Hz, 1H), 8.39–8.15 (m, 3H), 7.83 (dd, $J = 8.3$ Hz, $J = 1.7$ Hz, 1H), 7.31 (dd, $J = 8.5$ Hz, $J = 4.3$ Hz, 1H), 7.24 (s, 1H), 6.88 (s, 2H) ppm; HRMS (ESI): *m/z* calcd for $C_{17}H_9F_6N_3O_2H$: 402.0672 $[M+H]^+$; found: 402.0672.

Imidazoquinoline Ligand 251. A flask (25 mL) was charged with compound **250** (252 mg, 628 µmol, 1.00 eq), $SnCl_2 \cdot 2H_2O$ (430 mg, 1.91 mmol, 3.03 eq), and EtOH (4.0 mL) and the mixture was stirred at reflux for 2.5 h. After cooling to rt, the mixture was diluted with water and EtOAc and the pH of the aqueous layer was set to pH ≥ 12 with aqueous 2 M NaOH. The organic layer was separated and the aqueous layer extracted with EtOAc (4x). The combined organic layers were dried over Na_2SO_4 and the solvent removed *in vacuo*, which yielded an ocher-green solid which was dried *in vacuo* and transferred into a new flask (10 mL). The subsequent construction of the imidazole ring was achieved with a modified procedure reported by Zhang et al.[132] Iodine (18 mg, 70.9 µmol, 11 mol%), dry MeCN (1.5 mL), and triethyl orthoformate (160 µL, 962 µmol, 1.53 eq) were added, the flask sealed with a septum,

and the mixture stirred at rt for 12 h. Then, the dark slurry was diluted with CH_2Cl_2/MeOH and the crude product adsorbed on silica gel and purified by flash chromatography (EtOAc/MeOH 60:1). After solvent removal and drying *in vacuo*, desired imidazoquinoline ligand **251** was obtained as a pale-ocher solid (186 mg, 487 µmol, 77%). ^{1}H NMR (300 MHz, DMSO-d_6): δ = 13.80 (s, 1H), 8.98 (dd, J = 4.3 Hz, J = 1.5 Hz, 1H), 8.43 (s, 1H), 8.22 (s, 3H), 8.13 (dd, J = 8.5 Hz, J = 1.5 Hz, 1H), 7.98 (s, 1H), 7.56 (dd, J = 8.6 Hz, J = 4.2 Hz, 1H) ppm; IR (film): $\tilde{\nu}$ = 1382, 1351, 1287, 1165, 1116, 924, 894, 846, 788, 716, 683, 629 cm^{-1}; HRMS (ESI): *m/z* calcd for $C_{18}H_9F_6N_3H$: 382.0773 $[M+H]^+$; found: 382.0773.

4.5.7 Imidazoquinoline Ligand 252

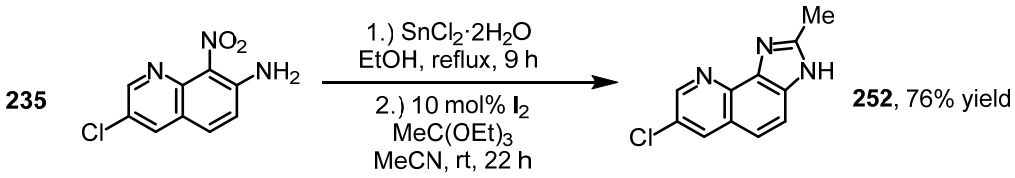

Scheme 72. Synthesis of imidazoquinoline ligand **252**.

Imidazoquinoline Ligand 252. A flask was charged with 3-chloro-8-nitroquinolin-7-amine (**235**; 1.00 g, 4.47 mmol, 1.00 eq), $SnCl_2 \cdot 2H_2O$ (3.07 g, 13.6 mmol, 3.04 eq), and EtOH (23 mL) and the mixture was stirred at reflux for 9 h. After cooling to rt, the mixture was diluted with water and EtOAc and the pH of the aqueous layer was set to pH ≥ 12 with aqueous 2 M NaOH. The organic layer was separated and the aqueous layer extracted with EtOAc (3x). The combined organic layers were dried over Na_2SO_4 and the solvent removed *in vacuo*, which yielded the according intermediate diamine as a brown-yellow solid (866 mg, 4.47 mmol, quantitative). 80.3 mg (415 µmol, set as 1.00 eq) of this intermediate product were then transferred into a new flask (10 mL). The subsequent construction of the imidazole ring was achieved with a modified procedure reported by Zhang et al.[132] Iodine (10.4 mg, 41.0 µmol, 10 mol%), dry MeCN (0.67 mL), and triethyl orthoacetate (105 µL, 573 µmol, 1.38 eq) were added, the flask sealed with a septum, and the mixture stirred at rt for 22 h. The dark slurry was diluted with CH_2Cl_2/MeOH and the crude product adsorbed on silica gel and purified by flash chromatography (EtOAc/MeOH 30:1 → 20:1). After solvent removal and drying *in vacuo*, desired imidazoquinoline ligand **252** was obtained as a brown-ocher solid (68.8 mg, 316 µmol, 76%). ^{1}H NMR (300 MHz, DMSO-d_6): δ = 13.43 (s, 1H), 8.87 (d, J = 2.5 Hz, 1H), 8.61 (d, J = 1.9 Hz, 1H), 7.83 (d, J = 8.7 Hz, 1H), 7.65 (d, J = 8.7 Hz, 1H), 2.57 (s, 3H) ppm; IR (film): $\tilde{\nu}$ = 2229, 1508, 1389, 1359, 1312, 1277, 1097, 1007, 911, 886, 795, 701, 669, 625, 521, 475 cm^{-1}; HRMS (ESI): *m/z* calcd for $C_{11}H_8Cl_1N_3H$: 218.0480 $[M+H]^+$; found: 218.0488.

4.5.8 Imidazoquinoline Ligand 255

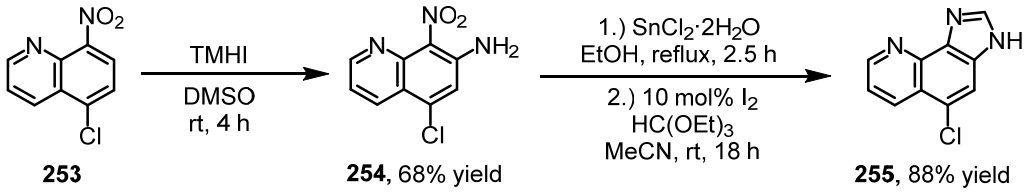

253 **254**, 68% yield **255**, 88% yield

Scheme 73. Synthesis of imidazoquinoline ligand **255**.

5-Chloro-8-nitroquinolin-7-amine (254). Compound **254** was prepared according to a modified procedure reported by Grzegożek.[129] A flame-dried flask (25 mL) was charged with 5-chloro-8-nitroquinoline **254**[134] (339 mg, 1.63 mmol, 1.00 eq). Then, 1,1,1-trimethylhydrazinium iodide[130] (497 mg, 2.46 mmol, 1.51 eq), dry DMSO (11 mL), and KO*t*Bu (548 mg, 4.88 mmol, 2.99 eq) were added and the mixture stirred at rt for 4 h under nitrogen atmosphere. The mixture was diluted with CH_2Cl_2, quenched by the addition of aqueous NH_4Cl, the organic layer separated, the aqueous layer extracted with CH_2Cl_2 (10x), and the combined organic layers were washed with brine and dried over Na_2SO_4. All volatiles were removed *in vacuo*, the residue dissolved in CH_2Cl_2/MeOH, adsorbed on silica gel, and purified by flash chromatography ($CHCl_3$/EtOAc 5:1 → 2:1[131]). After solvent removal and drying *in vacuo*, desired 5-chloro-8-nitroquinolin-7-amine (**254**) was obtained as a yellow-orange crystalline solid (248 mg, 1.11 mmol, 68%). ^{1}H NMR (300 MHz, DMSO-d_6): δ = 8.81 (dd, J = 4.3 Hz, J = 1.7 Hz, 1H), 8.36 (dd, J = 8.4 Hz, J = 1.6 Hz, 1H), 7.43 (dd, J = 8.3 Hz, J = 4.3 Hz, 1H), 7.41 (s, 1H), 6.98 (s, 2H) ppm; HRMS (ESI): *m/z* calcd for $C_9H_6N_3O_2Cl_1H$: 224.0221 $[M+H]^+$; found: 224.0226.

Imidazoquinoline Ligand 255. A flask (25 mL) was charged with compound **254** (240 mg, 1.07 mmol, 1.00 eq), $SnCl_2 \cdot 2H_2O$ (736 mg, 3.26 mmol, 3.04 eq), and EtOH (5.5 mL) and the mixture was stirred at reflux for 2.5 h. After cooling to rt, the mixture was diluted with water and EtOAc and the pH of the aqueous layer was set to pH ≥ 12 with aqueous 2 M NaOH. The organic layer was separated and the aqueous layer extracted with EtOAc (3x). The combined organic layers were dried over Na_2SO_4 and the solvent removed *in vacuo*, which yielded the according intermediate diamine as a pale-brown solid (217 mg, 1.12 mmol, quantitative). 100 mg of the intermediate diamine (516 µmol, set as 1.00 eq) were then transferred into a new flask. The subsequent construction of the imidazole ring was achieved with a modified procedure reported by Zhang et al.[132] Iodine (13.0 mg, 51.2 µmol, 9.9 mol%), dry MeCN (1.0 mL), and triethyl orthoformate (130 µL, 789 µmol, 1.53 eq) were added, the flask sealed with a septum and the mixture stirred at rt for 18 h. Then, the dark slurry was diluted with CH_2Cl_2/MeOH and the crude product adsorbed on silica gel and purified by flash

chromatography (EtOAc/MeOH 10:1). After solvent removal and drying *in vacuo*, desired imidazoquinoline ligand **255** was obtained as brown-grey solid (92.5 mg, 454 µmol, 88%). ^{1}H NMR (300 MHz, DMSO-d_6): δ = 13.81 (s, 1H), 9.02 (dd, J = 4.2 Hz, J = 1.4 Hz, 1H), 8.66 (dd, J = 8.6 Hz, J = 1.4 Hz, 1H), 8.40 (s, 1H), 8.11 (s, 1H), 7.70 (dd, J = 8.5 Hz, J = 4.3 Hz, 1H) ppm; IR (film): $\tilde{\nu}$ = 1617, 1519, 1349, 1287, 1149, 928, 859, 776, 718, 626, 578, 437 cm^{-1}; HRMS (ESI): *m/z* calcd for $C_{10}H_6Cl_1N_3Na$: 226.0142 [M+Na]$^+$; found: 226.0150.

4.5.9 Imidazoquinoline Ligand 260

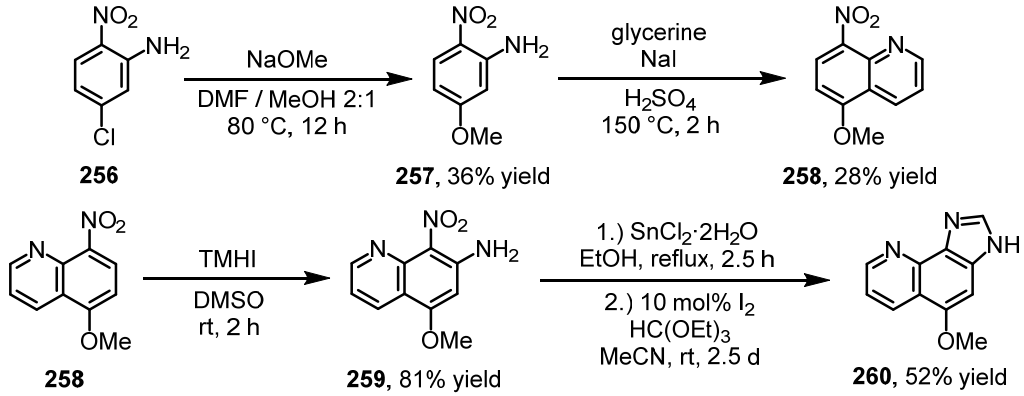

Scheme 74. Synthesis of imidazoquinoline ligand **260**.

5-Methoxy-2-nitroaniline (257). A flame-dried flask (100 mL) was charged with 5-chloro-2-nitroaniline (**256**; 5.00 g, 29.0 mmol, 1.00 eq) and dry DMF (25 mL). A solution of NaOMe (4.50 g, 83.3 mmol, 2.17 eq) in dry MeOH (11 mL) was added and the resulting mixture stirred at 80 °C for 12 h under nitrogen atmosphere. Then, the mixture was allowed to cool to rt and diluted with water and EtOAc. The organic layer was separated, the aqueous layer extracted with CH_2Cl_2 (2x), and the combined organic layers washed with brine (2x) and dried over Na_2SO_4. The solvent was removed *in vacuo*, the crude product dissolved in CH_2Cl_2, adsorbed on silica gel, and purified by flash chromatography (hexanes/EtOAc 3:1 → 3:2). Desired 5-methoxy-2-nitroaniline (**257**) was obtained as a crystalline solid (1.77 g, 10.5 mmol, 36%). ^{1}H NMR (300 MHz, $CDCl_3$): δ = 8.06 (d, J = 9.6 Hz, 1H), 6.27 (dd, J = 9.5 Hz, J = 2.5 Hz, 1H), 6.22 (s, 2H), 6.15 (d, J = 2.5 Hz, 1H), 3.82 (s, 3H) ppm; HRMS (ESI): *m/z* calcd for $C_7H_8N_2O_3Na$: 191.0438 [M+Na]$^+$; found: 191.0428.

5-Methoxy-8-nitroquinoline (258). A flask was charged with glycerin (2.05 mL, 27.8 mmol, 2.69 eq) and the glycerin stirred at 160 °C for 1 h. Then, the mixture was allowed to cool to rt and compound **257** (1.65 g, 9.80 mmol, 1.00 eq) and NaI (31.0 mg, 0.21 mmol, 2.0 mol%) were added and the mixture heated to 150 °C. Concentrated H_2SO_4 (1.29 mL, 24.2 mmol, 2.34 eq) was added dropwise and the resulting mixture stirred at 150 °C for 1 h. After cooling to rt, the mixture was diluted with water and CH_2Cl_2, the organic layer separated, and the

aqueous layer extracted with CH_2Cl_2 (5x). The combined organic layers were dried over Na_2SO_4 and all volatiles were removed *in vacuo*. The resulting residue was dissolved in CH_2Cl_2, adsorbed on silica gel, and purified by flash chromatography (hexanes/EtOAc 2:1). After solvent removal and drying *in vacuo*, desired 5-methoxy-8-nitroquinoline (**258**) was obtained as a yellow-orange crystalline solid (560 mg, 2.74 mmol, 28%). ^{1}H NMR (300 MHz, $CDCl_3$): δ = 9.08 (dd, J = 4.2 Hz, J = 1.8 Hz, 1H), 8.62 (dd, J = 8.5 Hz, J = 1.7 Hz, 1H), 8.18 (d, J = 8.5 Hz, 1H), 7.51 (dd, J = 8.6 Hz, J = 4.2 Hz, 1H), 6.84 (d, J = 8.7 Hz, 1H), 4.09 (s, 3H) ppm; HRMS (ESI): *m/z* calcd for $C_{10}H_8N_2O_3Na$: 227.0427 $[M+Na]^+$; found: 227.0429.

Compound 259. Compound **259** was prepared according to a modified procedure reported by Grzegożek.[129] A flame-dried flask (25 mL) was charged with 5-methoxy-8-nitroquinoline (**258**; 0.55 g, 2.69 mmol, 1.00 eq). Then, 1,1,1-trimethylhydrazinium iodide[130] (0.66 g, 3.28 mmol, 1.22 eq), dry DMSO (5.5 mL), and KO*t*Bu (0.92 g, 8.23 mmol, 3.06 eq) were added and the mixture stirred at rt for 2 h under nitrogen atmosphere. The mixture was diluted with CH_2Cl_2, quenched by the addition of aqueous NH_4Cl, the organic layer separated, the aqueous layer extracted with CH_2Cl_2 (8x), and the combined organic layers dried over Na_2SO_4. All volatiles were removed *in vacuo*, the residue dissolved in CH_2Cl_2/MeOH, adsorbed on silica gel, and purified by flash chromatography ($CHCl_3$/EtOAc 1:1[131]). After solvent removal and drying *in vacuo*, desired compound **259** was obtained as a yellow-orange crystalline solid (0.48 g, 2.19 mmol, 81%). ^{1}H NMR (300 MHz, DMSO-d_6): δ = 8.73 (dd, J = 4.4 Hz, J = 1.8 Hz, 1H), 8.26 (dd, J = 8.2 Hz, J = 1.8 Hz, 1H), 7.27 (dd, J = 8.3 Hz, J = 4.3 Hz, 1H), 7.22 (s, 2H), 6.60 (s, 1H), 3.96 (s, 3H) ppm; HRMS (ESI): *m/z* calcd for $C_{10}H_9N_3O_3H$: 220.0717 $[M+H]^+$; found: 220.0717.

Imidazoquinoline Ligand 260. A flask (25 mL) was charged with compound **259** (420 mg, 1.92 mmol, 1.00 eq), $SnCl_2 \cdot 2H_2O$ (1.31 g, 5.82 mmol, 3.03 eq), and EtOH (6 mL) and the mixture was stirred at reflux for 2.5 h. After cooling to rt, the mixture was diluted with water and EtOAc and the pH of the aqueous layer was set to pH ≥ 12 with aqueous 2 M NaOH. The organic layer was separated and the aqueous layer extracted with EtOAc (4x). The combined organic layers were washed with brine, dried over Na_2SO_4, and the solvent removed *in vacuo*, which yielded the according intermediate diamine as a pale-brown solid (0.39 g, 2.06 mmol, quantitative). All of the obtained diamine was then transferred into a new flask. The subsequent construction of the imidazole ring was achieved with a modified procedure reported by Zhang et al.[132] Iodine (53.0 mg, 0.21 mmol, 11 mol%), dry MeCN (1.50 mL), and triethyl orthoformate (0.49 mL, 2.94 mmol, 1.53 eq) were added, the flask sealed with a septum, and the mixture stirred at rt for 2.5 d. Then, the dark slurry was diluted with CH_2Cl_2/MeOH, the crude product adsorbed on silica gel, and purified by flash chromatography (EtOAc/MeOH

20:1 → 10:1). After solvent removal and drying *in vacuo*, desired imidazoquinoline ligand **260** was obtained as an olive-green solid (0.20 g, 1.00 mmol, 52%). ^{1}H NMR (300 MHz, methanol-d_4): δ = 8.88 (dd, J = 4.3 Hz, J = 1.5 Hz, 1H), 8.70 (dd, J = 8.4 Hz, J = 1.4 Hz, 1H), 8.19 (s, 1H), 7.50 (dd, J = 8.4 Hz, J = 4.4 Hz, 1H), 7.23 (s, 1H), 4.07 (s, 3H) ppm (N*H* signal not observed due to rapid H-D exchange).

4.5.10 *N*-Methylated Imidazoquinoline Ligand 262

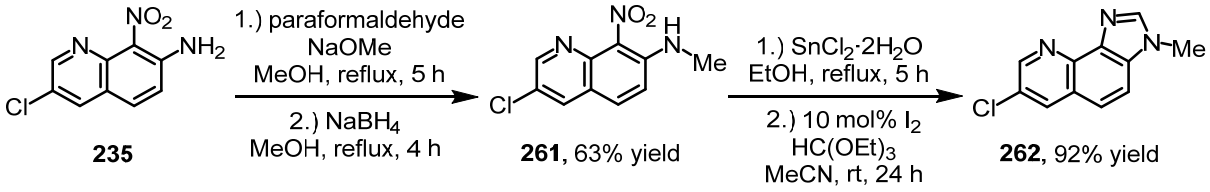

Scheme 75. Synthesis of imidazoquinoline ligand **262**.

3-Chloro-*N*-methyl-8-nitroquinolin-7-amine (261). Compound **261** was synthesized based on a modified protocol from Skrydstrup et al.[135] A flame-dried flask (100 mL) was charged with compound **235** (500 mg, 2.24 mmol, 1.00 eq), NaOMe (906 mg, 16.8 mmol, 7.50 eq), paraformaldehyde (504 mg, 16.8 mmol, 7.51 eq), and dry MeOH (60 mL). The flask was equipped with a reflux condenser and the mixture stirred at 70 °C (reflux) for 5 h under nitrogen atmosphere. Then, the mixture was cooled to 0 °C, $NaBH_4$ (633 mg, 16.7 mmol, 7.48 eq) carefully added, and the mixture stirred at reflux for another 4 h under nitrogen atmosphere. After cooling to rt, the mixture was diluted with water and EtOAc, the organic layer separated, and the aqueous layer extracted with EtOAc (4x). The combined organic layers were dried over Na_2SO_4, the solvent removed *in vacuo*, the crude residue dissolved in CH_2Cl_2/MeOH, adsorbed on silica gel, and purified by flash chromatography (toluene/acetone 15:1). After drying *in vacuo*, desired product **261** was obtained as a brown crystalline solid (335 mg, 1.41 mmol, 63%). ^{1}H NMR (300 MHz, DMSO-d_6): δ = 8.71 (d, J = 2.5 Hz, 1H), 8.37 (d, J = 2.5 Hz, 1H), 7.89 (d, J = 9.4 Hz, 1H), 7.34 (d, J = 9.4 Hz, 1H), 7.15–7.00 (m, 1H), 2.93 (d, J = 4.7 Hz, 3H) ppm; HRMS (ESI): *m/z* calcd for $C_{10}H_8Cl_1N_3O_2Na$: 260.0197 $[M+Na]^+$; found: 260.0201.

***N*-Methylated Imidazoquinoline Ligand 262.** A flask (25 mL) was charged with compound **261** (392 mg, 1.65 mmol, 1.00 eq), $SnCl_2 \cdot 2H_2O$ (1.21 g, 5.36 mmol, 3.25 eq), and EtOH (11 mL) and the mixture was stirred at reflux for 5 h. After cooling to rt, the mixture was diluted with water and EtOAc and the pH of the aqueous layer was set to pH ≥ 12 with 2 M NaOH (aq). The organic layer was separated and the aqueous layer extracted with EtOAc (4x). The combined organic layers were dried over Na_2SO_4 and the solvent removed *in vacuo*, which yielded a brown solid which was dried *in vacuo* and transferred into a new flask

(25 mL). The subsequent construction of the imidazole ring was achieved with a modified procedure reported by Zhang et al.[132] Iodine (43 mg, 0.17 mmol, 10 mol%), dry MeCN (5.1 mL), and triethyl orthoformate (520 µL, 3.13 mmol, 1.90 eq) were added, the flask sealed with a septum, and the mixture stirred at rt for 24 h. All volatiles were removed *in vacuo*, the residue taken up in CH_2Cl_2/MeOH, adsorbed on silica gel, and purified by flash chromatography (EtOAc/MeOH 10:1 → 5:1). After drying *in vacuo*, desired *N*-methylated imidazoquinoline ligand **262** was obtained as a beige solid (331 mg, 1.52 mmol, 92%). ^{1}H NMR (300 MHz, DMSO-d_6): δ = 8.89 (s, 1H), 8.61 (d, J = 2.5 Hz, 1H), 8.37 (s, 1H), 7.95 (d, J = 8.7 Hz, 1H), 7.79 (d, J = 8.7 Hz, 1H), 3.99 (s, 3H) ppm; ^{13}C NMR (75 MHz, DMSO-d_6): δ = 147.9, 143.6, 139.7, 138.1, 134.8, 134.2, 125.7, 124.9, 121.9, 113.5, 31.1 ppm; IR (film): $\tilde{\nu}$ = 1516, 1365, 1342, 1104, 896, 793, 698, 634 cm^{-1}; HRMS (ESI): *m/z* calcd for $C_{11}H_8Cl_1N_3Na$: 240.0299 [*M*+Na]$^+$; found: 240.0305.

4.5.11 2-(1*H*-Pyrazol-3-yl)pyridine Ligand (265)

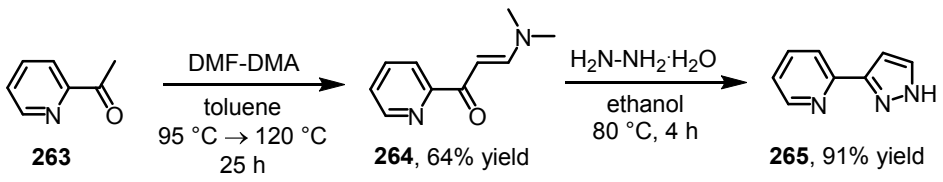

Scheme 76. Synthesis of 2-(1*H*-pyrazol-3-yl)pyridine ligand (**265**).

Compound 264. Compound **264** was synthesized according to a protocol from Milani et al.[136] A flame-dried flask (25 mL) was charged with 2-acetylpyridine (**263**; 1.16 mL, 10.3 mmol, 1.00 eq), *N*,*N*-dimethylformamide dimethyl acetal (3.14 mL, 23.7 mmol, 2.29 eq), and toluene (6.5 mL). The mixture was stirred at 95 °C for 24 h and evolving MeOH was continuously distilled off. Finally, the temperature was raised to 120 °C for 1 h to remove residual MeOH and to push the reaction to completion. Subsequently, the mixture was allowed to cool to rt, all volatiles removed, and the remaining residue dried *in vacuo*, which yielded desired compound **264** as a yellow-brown crystalline solid without the need for further purification (1.16 g, 6.57 mmol, 64%). ^{1}H NMR (300 MHz, $CDCl_3$): δ = 8.67−8.47 (m, 1H), 8.13 (dd, J = 7.9 Hz, J = 0.9 Hz, 1H), 7.89 (d, J = 12.5 Hz, 1H), 7.79 (td, J = 7.7 Hz, J = 1.8 Hz, 1H), 7.35 (ddd, J = 7.6 Hz, J = 4.8 Hz, J = 1.2 Hz, 1H), 6.45 (d, J = 12.7 Hz, 1H), 3.15 (s, 3H), 2.98 (s, 3H) ppm; HRMS (ESI): *m/z* calcd for $C_{10}H_{12}N_2O_1H$: 177.1022 [*M*+H]$^+$; found: 177.1022.

2-(1*H*-Pyrazol-3-yl)pyridine (265). Compound **265** was synthesized according to a protocol from Thiel et al.[137] A flask (10 mL) was charged with compound **264** (151 mg, 857 µmol, 1.00 eq) and EtOH (1.5 mL). Then, hydrazine hydrate (80 wt%; 320 µL, 5.26 mmol, 6.14 eq)

was added and the resulting mixture stirred at 80 °C for 4 h. After cooling to rt, all volatiles were removed *in vacuo* and the resulting yellow crystalline solid was recrystallized from EtOAc (ca. 0.3–0.5 mL). The recrystallized precipitate was washed with hexanes and after drying *in vacuo*, desired 2-(1*H*-pyrazol-3-yl)pyridine (**265**) was obtained as a colorless crystalline solid (114 mg, 782 µmol, 91%). ^{1}H NMR (300 MHz, $CDCl_3$): δ = 12.14 (s, 1H), 8.70 (dt, J = 4.9 Hz, J = 1.3 Hz, 1H), 7.83–7.70 (m, 2H), 7.67 (d, J = 2.1 Hz, 1H), 7.28–7.19 (m, 1H), 6.83 (d, J = 2.1 Hz, 1H) ppm; ^{13}C NMR (75 MHz, $CDCl_3$): δ = 149.5, 149.3, 145.0, 137.4, 137.2, 122.9, 120.5, 103.7 ppm; IR (film): $\tilde{\nu}$ = 1590, 1501, 1416, 759, 704, 615, 403 cm^{-1}; HRMS (ESI): *m/z* calcd for $C_8H_7N_3H$: 146.0713 $[M+H]^+$; found: 146.0712.

4.6 Achiral Non-Cyclometalating Ligands from Chapter 3.

4.6.1 *N*-Phenyl-3-(pyridin-2-yl)-1*H*-pyrazol-5-amine Ligand (173)

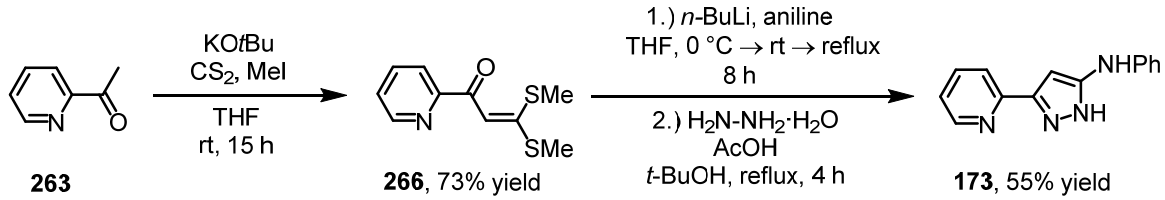

Scheme 77. Synthesis of *N*-phenyl-3-(pyridin-2-yl)-1*H*-pyrazol-5-amine (**173**).

Compound 266. Compound **266** was synthesized according to a modified procedure from Junjappa et al.[138] A flame-dried flask (250 mL) was charged with KO*t*Bu (9.70 g, 86.4 mmol, 2.11 eq) and dry THF (200 mL). The flask was cooled with a water bath and 2-acetylpyridine (**263**; 4.60 mL, 41.0 mmol, 1.00 eq) was added dropwise over 10 min under stirring. The resulting mixture was stirred at rt for 15 min whereupon a pale-yellow suspension was formed. Then, carbon disulfide (2.62 mL, 43.7 mmol, 1.07 eq) was added dropwise over 30 min at rt. Next, methyl iodide (5.40 mL, 86.7 mmol, 2.12 eq) was added dropwise over 40 min and the mixture was stirred at rt for 15 h under nitrogen atmosphere. The resulting mixture was poured into ice-water (0.5 L) and the resulting suspension vigorously stirred for 1.5 h. The resulting yellow precipitate was filtered off with a glass filter (porosity G3), thoroughly washed with water, and dried *in vacuo*. Desired compound **266** was obtained as a yellow powder without the need for further purification (6.76 g, 30.0 mmol, 73%). ^{1}H NMR (300 MHz, $CDCl_3$): δ = 8.64 (d, J = 4.0 Hz, 1H), 8.17 (d, J = 7.9 Hz, 1H), 7.84 (td, J = 7.7 Hz, J = 1.7 Hz, 1H), 7.64 (s, 1H), 7.40 (ddd, J = 7.5 Hz, J = 4.8 Hz, J = 1.1 Hz, 1H), 2.64 (s, 3H), 2.55 (s, 3H) ppm; HRMS (ESI): *m/z* calcd for $C_{10}H_{12}N_1O_1S_2$: 226.0355 $[M+H]^+$; found: 226.0355.

***N*-Phenyl-3-(pyridin-2-yl)-1*H*-pyrazol-5-amine (173).** Compound **173** was synthesized according to a modified procedure from Junjappa et al.[138] A flame-dried flask (250 mL) was charged with aniline (1.78 mL, 19.5 mmol, 1.10 eq) and dry THF (75 mL). The mixture was cooled to 0 °C and *n*-BuLi (2.5 M in hexanes; 7.80 mL, 19.5 mmol, 1.10 eq) was added dropwise over 10 min. The resulting mixture was stirred for 30 min at 0 °C and then allowed to warm to rt and stirred for 45 min. Then, compound **266** (4.00 g, 17.8 mmol, 1.00 eq) in dry THF (35 mL) was added dropwise over 15 min at 0 °C. The resulting mixture was allowed to warm to rt and stirred for 2.5 h and then stirred at 65 °C (reflux) for 8 h. After cooling to rt, the mixture was diluted with water and EtOAc and the organic layer separated and the aqueous layer extracted with EtOAc (3x). The combined organic layers were washed with brine, dried over Na_2SO_4, the solvent removed *in vacuo*, the residue dissolved in CH_2Cl_2 and adsorbed on silica gel, and the intermediate crude product purified by flash chromatography (hexanes/EtOAc 3:1). After solvent removal and drying *in vacuo*, a yellow crystalline solid (4.37 g; intermediate dithioketene acetal) was obtained, which was transferred into a new flask (100 mL). *t*-BuOH (80 mL), hydrazine hydrate (80 wt%; 1.50 mL, 24.7 mmol, 1.53 eq), and acetic acid (1.10 mL, 19.2 mmol, 1.19 eq) were added and the mixture stirred at reflux for 4 h. After cooling to rt, the resulting mixture was diluted with water and EtOAc, the organic layer separated, and the aqueous layer extracted with EtOAc (5x). The combined organic layers were washed with brine, dried over Na_2SO_4, and the solvent removed *in vacuo*. The resulting residue was dissolved in CH_2Cl_2, adsorbed on silica gel, and purified by flash chromatography (hexanes/EtOAc 2:1 → 1:2). After solvent removal and drying *in vacuo*, *N*-phenyl-3-(pyridin-2-yl)-1*H*-pyrazol-5-amine (**173**) was obtained as a colorless crystalline solid (2.32 g, 9.81 mmol, 55%). ^{1}H NMR (300 MHz, DMSO-d_6): δ = 12.69 (s, 1H), 8.60 (d, J = 4.7 Hz, 1H), 8.48 (s, 1H), 7.95–7.75 (m, 2H), 7.43–7.27 (m, 3H), 7.27–7.12 (m, 2H), 6.71 (t, J = 7.3 Hz, 1H), 6.44 (d, J = 2.1 Hz, 1H) ppm; ^{13}C NMR (75 MHz, DMSO-d_6): δ = 152.2, 149.3, 148.1, 143.8, 141.5, 135.2, 128.7 (2C), 122.8, 119.8, 117.9, 114.8 (2C), 92.2 ppm; IR (film): $\tilde{\nu}$ = 3259, 1597, 1549, 1494, 1458, 1433, 1421, 997, 757, 740, 704, 687, 622, 489, 462, 401 cm^{-1}; HRMS (ESI): *m/z* calcd for $C_{14}H_{12}N_4H$: 237.1135 $[M+H]^+$; found: 237.1129.

4.6.2 Bispyrazole Ligand 180

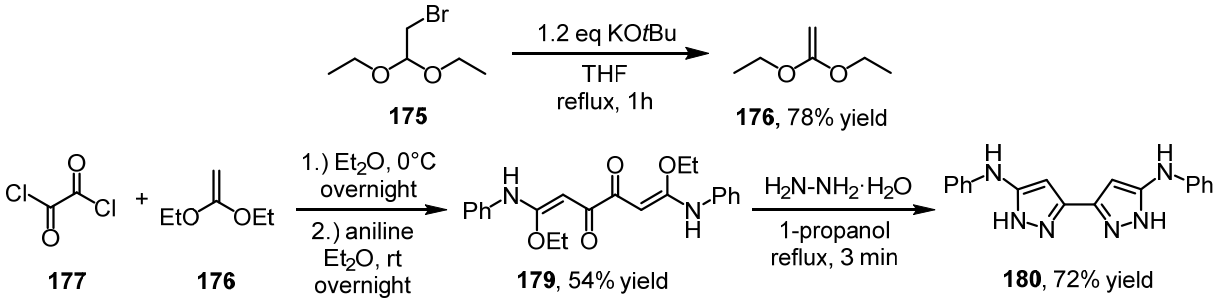

Scheme 78. Synthesis of bispyrazole ligand **180**.

1,1-Diethoxyethene (176). Compound **176** was prepared following a literature protocol from DeHaven-Hudkins et al.[139] A flame-dried flask (250 mL) was charged with dry THF (75 mL) and KO*t*Bu (22.3 g, 199 mmol, 1.19 eq). The flask was cooled to 0 °C and bromo-acetaldehyde diethyl acetal (**175**; 25.1 mL, 167 mmol, 1.00 eq) was added dropwise over 30 min. The mixture was subsequently stirred at 70 °C (reflux) for 1 h under nitrogen atmosphere. After cooling to rt, THF was carefully removed *in vacuo* and the residue transferred with dry CH_2Cl_2 into a new flame-dried flask (100 mL). The solvent was carefully removed *in vacuo* and the product purified by short-path distillation (70−75 °C, 180−190 mbar). Desired 1,1-diethoxyethene (**176**; 15.0 g, 129 mmol, 78%) was obtained as a clear colorless liquid and stored in a well-sealed Schlenk tube (note that **176** is moisture-sensitive). ^{1}H NMR (300 MHz, $CDCl_3$): δ = 3.79 (q, J = 7.0 Hz, 4H), 3.05 (s, 2H), 1.29 (t, J = 7.1 Hz, 6H) ppm; ^{13}C NMR (75 MHz, CD_2Cl_2): δ = 165.1, 63.7 (2C), 55.7, 14.5 (2C) ppm; IR (film): $\tilde{\nu}$ = 2982, 1642, 1372, 1274, 1046, 972, 875, 709 cm^{-1}; HRMS (ESI): *m/z* calcd for $C_6H_{12}O_2H$: 117.0910 $[M+H]^+$; found: 117.0910.

Compound 179. Compound **179** was prepared following a protocol from H.-D. Stachel.[118a,b] A flame-dried flask (100 mL) was charged with dry Et_2O (46 mL) and 1,1-diethoxyethene (**176**; 4.70 g, 40.4 mmol, 6.05 eq). The resulting solution was cooled to 0 °C and oxalyl chloride (**177**; 570 µL, 6.69 mmol, 1.00 eq) was added dropwise, which resulted in the formation of a yellow precipitate. This mixture was stirred at 0 °C overnight under nitrogen atmosphere. The next day, the clear yellow supernatant was carefully removed with a syringe and the yellow precipitate repeatedly washed with dry, ice-cold Et_2O (4x 15 mL) under nitrogen atmosphere. The resulting supernatant was each time carefully removed with a syringe (the yellow precipitate, which is the according moisture-sensitive intermediate oxalylketene acetal,[118a,b] is virtually insoluble in Et_2O). Then, dry Et_2O (20 mL) and aniline (1.59 mL, 17.5 mmol, 2.61 eq) were added to the remaining precipitate and the mixture stirred at rt overnight under nitrogen atmosphere. The next day, the resulting yellow precipitate was

filtered off with a glass filter (porosity G4) and washed with ice-cold Et_2O. After drying *in vacuo*, desired compound **179** was obtained as a bright yellow powder (1.37 g, 3.61 mmol, 54%) without the need for further purification. ^{1}H NMR (300 MHz, CD_2Cl_2): δ = 13.01 (s, 2H), 7.46−7.27 (m, 8H), 7.20−7.05 (m, 2H), 6.01 (s, 2H), 4.32 (q, J = 7.0 Hz, 4H), 1.47 (t, J = 7.0 Hz, 6H) ppm; ^{13}C NMR (75 MHz, CD_2Cl_2): δ = 185.1 (2C), 167.9 (2C), 138.1 (2C), 129.6 (4C), 124.8 (2C), 122.2 (4C), 74.7 (2C), 66.3 (2C), 14.7 (2C) ppm; IR (film): $\tilde{\nu}$ = 1622, 1574, 1554, 1510, 1493, 1463, 1440, 1393, 1369, 1311, 1275, 1203, 1152, 1046, 779, 749, 689, 652, 463 cm^{-1}; HRMS (ESI): *m/z* calcd for $C_{22}H_{24}N_2O_4H$: 381.1809 [M+H]$^+$; found: 381.1800.

Bispyrazole Ligand 180. Bispyrazole ligand **180** was prepared following a protocol from H.-D. Stachel.[118c] A flask (25 mL) was charged with compound **179** (500 mg, 1.31 mmol, 1.00 eq) and 1-propanol (12 mL). The mixture was heated to 100 °C (reflux) and hydrazine hydrate (80% wt%; 480 µL, 7.90 mmol, 6.01 eq) was added at once under stirring when substrate **179** was completely dissolved. The mixture was stirred at 100 °C for 3 min whereupon the yellow color of the mixture disappeared. The resulting mixture was allowed to cool to rt whereupon a colorless crystalline precipitate formed. To accelerate and to push the precipitation to completion, the mixture was kept at −20 °C for 1 h. Then, the colorless precipitate was filtered off with a glass filter (porosity G4) and washed with hexanes (insoluble) and Et_2O (slightly soluble). After drying *in vacuo*, desired bispyrazole ligand **180** (300 mg, 949 µmol, 72%) was obtained as a colorless crystalline powder without the need for further purification. ^{1}H NMR (300 MHz, DMSO-d_6): δ = 12.45 (s, 2H), 8.51 (s, 2H), 7.35 (d, J = 7.8 Hz, 4H), 7.19 (t, J = 7.6 Hz, 4H), 6.72 (t, J = 6.6 Hz, 2H). 6.26 (s, 2H) ppm; ^{13}C NMR (75 MHz, DMSO-d_6): δ = 152.0 (2C), 143.8 (2C), 132.7 (2C), 128.7 (4C), 118.0 (2C), 114.8 (4C), 90.8 (2C) ppm; IR (film): $\tilde{\nu}$ = 3421, 1593, 1532, 1497, 1484, 1454, 1236, 1008, 793, 748, 692, 502 cm^{-1}; HRMS (ESI): *m/z* calcd for $C_{18}H_{16}N_6H$: 317.1509 [M+H]$^+$; found: 317.1504.

4.7 Synthesis of Iridium(III) Complexes Λ/Δ-T1–Λ/Δ-T28 from Chapter 2.

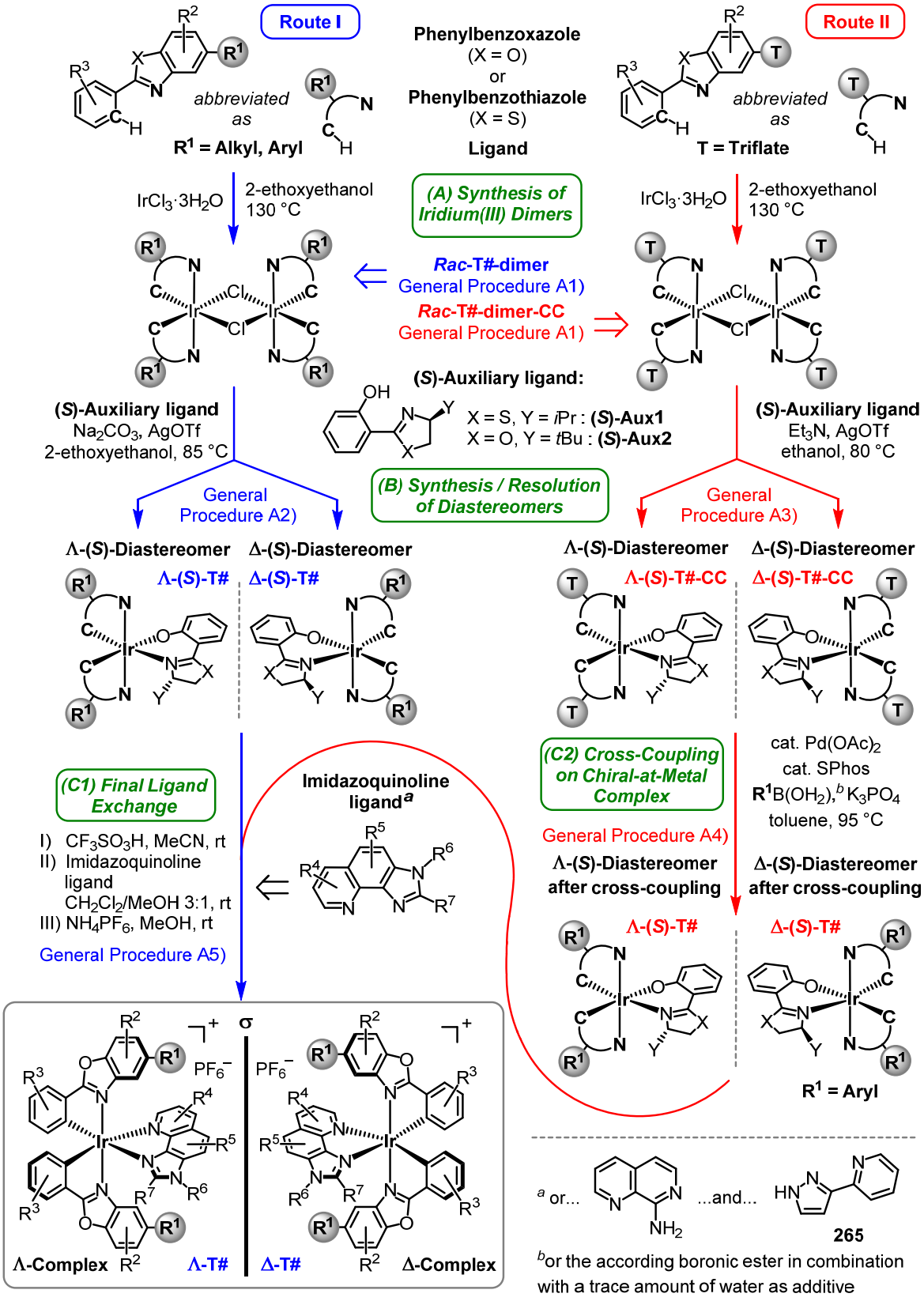

Scheme 79. General synthesis routes for iridium(III) complexes **Λ/Δ-T1–Λ/Δ-T28**.

Scheme 79 reproduces and specifies Scheme 30 from chapter 2.3.1 and serves to illustrate the notation system which is used below for complexes **Λ/Δ-T1–Λ/Δ-T28** and their precursors.

In case of Route I (Scheme 79; highlighted in blue), the precursing auxiliary complex of a final complex **Λ/Δ-T#** (# is a placeholder for a complex number) is denoted as **Λ/Δ-(*S*)-T#** (for example for **Λ-T1**: **Λ-(*S*)-T1**). And the precursing iridium(III) dimer of an auxiliary complex **Λ/Δ-(*S*)-T#** is denoted as ***rac*-T#-dimer** (for example for **Λ-(*S*)-T1**: ***rac*-T1-dimer**).

In case of Route II (Scheme 79; highlighted in red), the OTf-functionalized dimers are denoted as ***rac*-T#-dimer-CC** and the according OTf-functionalized auxiliary complexes, which are employed in the post-complexation cross-coupling step, are denoted as **Λ/Δ-(*S*)-T#-CC**.

Remark: In case a complex **Λ/Δ-T#** is synthesized from a precursor of another complex **Λ/Δ-T#** whose synthesis has already been presented, the precursor keeps the original number (#) of the complex with which it has been presented first (no double numbering!).

4.7.1 General Procedures A1)–A5)

General Procedure A1).

Synthesis of Iridium(III) Dimers (*rac*-T#-dimer and *rac*-T#-dimer-CC).

Iridium(III) dimers (***rac*-T#-dimer** and ***rac*-T#-dimer-CC**) were synthesized according to a modified version of Nonoyama's procedure.[77] A flask was charged with $IrCl_3 \cdot 3H_2O$ (1.00 eq), the indicated amount of the respective phenylbenzoxazole or phenylbenzothiazole ligand (2.0–2.4 eq), and 2-ethoxyethanol (conc = 30 mM) and the mixture purged with nitrogen gas for 15 min. Then, the flask was equipped with a reflux condenser and the mixture stirred at 130 °C for the indicated time under exclusion of light under nitrogen atmosphere. After cooling to rt, aqueous 1 M HCl (3–4 times the volume of the reaction mixture) was added under stirring whereupon a yellow precipitate formed. This precipitate was filtered off with a glass filter (porosity G3) and thoroughly washed with 1 M HCl and finally with a small amount of MeOH. The precipitate was dissolved in CH_2Cl_2, passed as solution through the filter, and the resulting clear organic layer dried over Na_2SO_4. After solvent removal and drying *in vacuo*, the desired iridium(III) dimer (***rac*-T#-dimer** or ***rac*-T#-dimer-CC**) was obtained.

General Procedure A2).

Synthesis / Resolution of Λ-(*S*)- and Δ-(*S*)-Diastereomers (*rac*-T#-dimer → Λ/Δ-(*S*)-T#).

A flask was charged with the respective iridium(III) dimer (***rac*-T#-dimer**; 1.00 eq), auxiliary ligand **(*S*)-Aux1** or **(*S*)-Aux2** (2.50 eq), Na_2CO_3 (15.0 eq), AgOTf (2.25 eq), and 2-ethoxyethanol (conc = 10 mM) and the mixture was purged with nitrogen gas for 5–10 min. Then, the mixture was stirred at 85 °C for 8 h under exclusion of light under nitrogen atmosphere.

After cooling to rt, the mixture was diluted with CH_2Cl_2 and passed through a short plug of silica gel with CH_2Cl_2 as eluent to remove the salts. All volatiles were removed *in vacuo* (40 °C) and the crude diastereomer mixture purified and resolved by standard flash chromatography with the indicated eluent. After drying *in vacuo*, diastereomers **Λ-(*S*)-T#** and **Δ-(*S*)-T#** were obtained (in most cases, only **Λ-(*S*)-T#** was isolated and purified).

General Procedure A3).

Synthesis and Resolution of OTf-Functionalized Λ-(*S*)- and Δ-(*S*)-Diastereomers (*rac*-T#-dimer-CC → Λ/Δ-(*S*)-T#-CC).[78]

A flask was charged with the respective OTf-functionalized iridium(III) dimer (***rac*-T#-dimer-CC**; 1.00 eq), auxiliary ligand **(*S*)-Aux1** or **(*S*)-Aux2** (2.50 eq), Et_3N (10 eq), AgOTf (2.25 eq), and ethanol (conc = 15 mM) and the mixture purged with nitrogen gas for 5−10 min. Then, the mixture was stirred at 80 °C for the indicated time under exclusion of light under nitrogen atmosphere. After cooling to rt, the mixture was diluted with CH_2Cl_2 and passed through a short plug of silica gel with CH_2Cl_2 as eluent to remove the salts. All volatiles were removed from the filtrate *in vacuo* (40 °C) and the crude Λ/Δ-diastereomer mixture purified and resolved by standard flash chromatography with the indicated eluent. After drying *in vacuo*, diastereomers **Λ-(*S*)-T#-CC** and **Δ-(*S*)-T#-CC** were obtained (in most cases, only **Λ-(*S*)-T#-CC** was isolated and purified).

Remark: General procedure A3) is a modified version of general procedure A2) since OTf-functionalized complexes are <u>not</u> compatible with the conditions from general procedure A2) (the triflate groups are cleaved off under those conditions).

General Procedure A4).

Post-Complexation Cross-Coupling with OTf-Functionalized Λ-(*S*)- and Δ-(*S*)-Diastereomers (Λ/Δ-(*S*)-T#-CC → Λ/Δ-(*S*)-T#).[78]

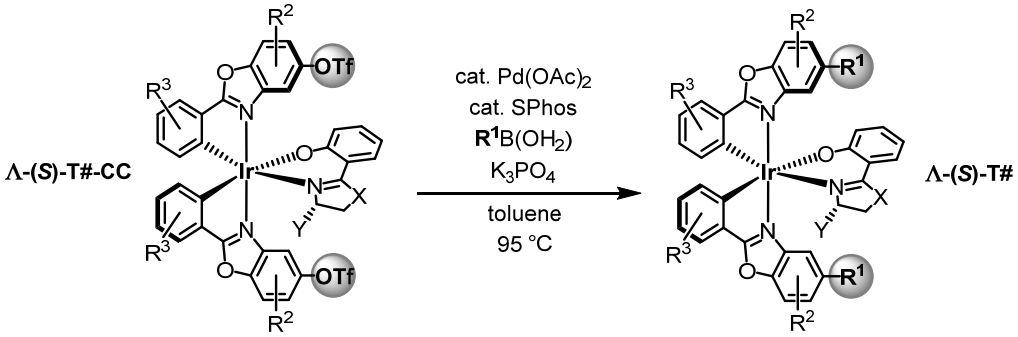

Scheme 80: Post-complexation Suzuki-Miyaura cross-couplings with OTf-functionalized diastereomers.[78]

A Schlenk tube (10 mL; threaded PTFE plug) was charged with finely ground K_3PO_4 (4.00 eq) and a PTFE stir bar and the Schlenk tube flame-dried *in vacuo* for 5 min (heat gun;

approx. 300 °C). Then, the respective OTf-functionalized diastereomer **Λ-** or **Δ-(*S*)-T#-CC** (1.00 eq), SPhos (20 mol%), $Pd(OAc)_2$ (12 mol%), and the respective boronic acid or boronic ester (4.00 eq) were added. The Schlenk tube was evacuated for 5 min and then carefully refilled with nitrogen gas. Dry and degassed toluene (conc = 50–60 mM) was added, the Schlenk tube sealed, and the mixture stirred at 95 °C under nitrogen atmosphere and under exclusion of light for the indicated time. Subsequently, all volatiles were removed *in vacuo* and the desired crude product purified by flash chromatography with the indicated eluent. After drying *in vacuo*, the desired cross-coupled diastereomer **Λ-** or **Δ-(*S*)-T#** was obtained.

General Procedure A5).

Synthesis of Λ- and Δ-Complexes / Precatalysts (Λ/Δ-(*S*)-T# → Λ/Δ-T#).

A flask was charged with the respective diastereomer **Λ-** or **Δ-(*S*)-T#** (1.00 eq) and MeCN (conc = 10 mM). Triflic acid (5.00 eq) was added and the resulting mixture stirred for 15 min at rt. Then, all volatiles were removed *in vacuo* (40 °C) and the resulting bisacetonitrile intermediate (**Λ-** or **Δ-T#-(MeCN)$_2$**, both depicted in Figure 39) purified by short-column chromatography. Eluent was in all cases hexanes/EtOAc/MeCN 4:2:1 → 4:4:2.[140]

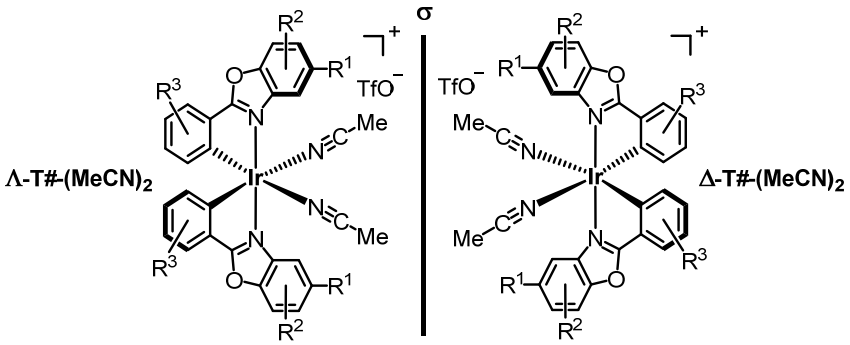

Figure 39. Intermediate bisacetonitrile complexes **Λ-** and **Δ-T#-(MeCN)$_2$**.[140]

Then, a new flask was charged with the purified bisacetonitrile intermediate (**Λ-** or **Δ-T#-(MeCN)$_2$**), the respective imidazoquinoline ligand (3.00 eq), and a 3:1 mixture of CH_2Cl_2/MeOH (conc = 10 mM). The resulting mixture was stirred overnight (≥ 15 h) at rt.[81] All volatiles were then removed *in vacuo* (40 °C), NH_4PF_6 (100 eq) and MeOH (conc = 5 mM) added, and the resulting mixture vigorously stirred for 2 h at rt.[82] Again, all volatiles were removed *in vacuo* (40 °C) and the crude product purified by flash chromatography with the indicated eluent. After drying *in vacuo*, the desired Λ- or Δ-configured complex / precatalyst (**Λ-** or **Δ-T#**) was obtained.

4.7.2 Synthetic Procedures and Characterizations

4.7.2.1 Precatalyst Λ-T1

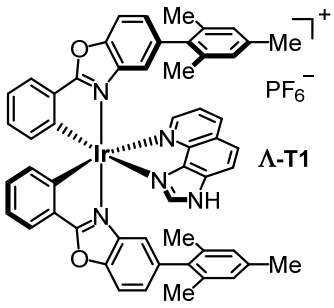

Precatalyst **Λ-T1** was prepared according to general procedures A1), A2), and A5) from benzoxazole ligand **186**, $IrCl_3 \cdot 3H_2O$, auxiliary ligand **(*S*)-Aux1**, and imidazoquinoline ligand **233**.

***Rac*-T1-dimer.** General procedure A1) was followed using benzoxazole ligand **186** (512 mg, 1.63 mmol, 2.40 eq) and $IrCl_3 \cdot 3H_2O$ (239 mg, 678 µmol, 1.00 eq); reaction time: 20 h; Ir(III) dimer ***rac*-T1-dimer** was obtained as an orange crystalline solid (458 mg, 269 µmol, 79%). ^{1}H NMR (300 MHz, CD_2Cl_2): δ = 8.22 (d, J = 1.3 Hz, 4H), 7.45 (d, J = 8.3 Hz, 4H), 7.32 (dd, J = 7.6 Hz, J = 1.1 Hz, 4H), 7.11 (dd, J = 8.5 Hz, J = 1.7 Hz, 4H), 7.02 (s, 4H), 6.83–6.69 (m, 8H), 6.54 (td, J = 7.6 Hz, J = 1.5 Hz, 4H), 6.00 (d, J = 7.6 Hz, 4H), 2.30 (s, 12H), 2.21 (s, 12H), 1.79 (s, 12H) ppm; HRMS (ESI): *m/z* calcd for $C_{88}H_{72}Cl_2Ir_2N_4O_4Na$: 1727.4073 $[M+Na]^+$; found: 1727.4080.

Λ-(*S*)-T1. General procedure A2) was followed using ***rac*-T1-dimer** (502 mg, 294 µmol) and auxiliary ligand **(*S*)-Aux1**; the crude diastereomer mixture was adsorbed on silica gel (40 °C) and purified and resolved by f. c. with hexanes/EtOAc 15:1; only the Λ-(*S*)-diastereomer was isolated and characterized; diastereomer **Λ-(*S*)-T1** was obtained as an orange solid (208 mg, 201 µmol, 34%). ^{1}H NMR (500 MHz, CD_2Cl_2): δ = 7.75 (dd, J = 7.6 Hz, J = 0.8 Hz, 1H), 7.74–7.65 (m, 4H), 7.30 (dd, J = 8.1 Hz, J = 1.8 Hz, 1H), 7.25 (d, J = 1.3 Hz, 1H), 7.20 (ddd, J = 8.5 Hz, J = 7.2 Hz, J = 1.6 Hz, 2H), 7.00–6.86 (m, 7H), 6.81–6.76 (m, 2H), 6.66 (d, J = 7.5 Hz, 1H), 6.52 (d, J = 7.5 Hz, 1H), 6.48 (dd, J = 8.5 Hz, J = 1.0 Hz, 1H), 6.20 (ddd, J = 8.1 Hz, J = 6.8 Hz, J = 1.2 Hz, 1H), 4.60 (ddd, J = 7.9 Hz, J = 3.4 Hz, J = 3.2 Hz, 1H), 2.79–2.69 (m, 2H), 2.34 (s, 3H), 2.28 (s, 3H), 2.06 (s, 3H), 2.03 (s, 3H), 1.95 (s, 3H), 1.61 (s, 3H), 0.80–0.69 (m, 1H), 0.20 (t, J = 7.3 Hz, 6H) ppm; HRMS (ESI): *m/z* calcd for $C_{56}H_{50}IrN_3O_3SNa$: 1060.3097 $[M+Na]^+$; found: 1060.3089.

Precatalyst Λ-T1. General procedure A5) was followed using **Λ-(*S*)-T1** (20.2 mg, 19.5 µmol) and imidazoquinoline ligand **233**; eluent for f. c.: CH_2Cl_2/MeOH 40:1; precatalyst **Λ-T1** was obtained as a greenish yellow solid (19.4 mg, 17.2 µmol, 88%). ^{1}H NMR (500 MHz, CD_2Cl_2): δ = 11.10 (s, 1H), 8.34 (dd, J = 8.2 Hz, J = 0.9 Hz, 1H), 8.09 (dd, J = 5.0 Hz, J = 1.1 Hz, 1H), 8.00–7.94 (m, 2H), 7.90 (dd, J = 7.6 Hz, J = 0.8 Hz, 1H), 7.88–7.83 (m, 2H), 7.65 (d, J = 8.5 Hz, 1H), 7.63 (d, J = 8.9 Hz, 1H), 7.41 (dd, J = 8.2 Hz, J = 5.0 Hz, 1H), 7.19 (td, J = 7.5 Hz, J = 0.9 Hz, 1H), 7.17–7.10 (m, 2H), 7.10–7.00 (m, 3H), 6.91 (s, 1H), 6.89–6.80 (m, 4H), 6.74 (s, 1H), 6.04 (d, J = 1.1 Hz, 1H), 5.17 (d, J = 1.1 Hz, 1H), 2.27 (s, 3H), 2.26 (s, 3H), 1.98 (s, 3H), 1.88 (s, 3H), 1.23 (s, 3H), 1.11 (s, 3H) ppm;

^{13}C NMR (125 MHz, CD_2Cl_2): δ = 178.4, 178.3, 151.8, 149.7, 149.6, 146.2, 144.0, 143.4, 142.7, 141.5, 140.2, 139.9, 138.8, 138.4, 138.1, 137.8, 137.5, 137.4, 137.3, 136.0, 135.8, 135.7, 135.5, 134.5, 134.2, 133.4, 133.1, 133.0, 130.5, 130.4, 129.1, 129.0, 128.6, 128.6, 128.4, 128.0, 127.1, 126.9, 125.9, 125.7, 123.6 (2C), 123.1, 117.2, 116.7, 115.8, 112.5, 112.2, 21.3, 21.2, 21.1, 21.0, 20.4, 20.3 ppm; IR (film): $\tilde{\nu}$ = 1443, 1380, 836, 734, 705, 552 cm^{-1}; HRMS (ESI): *m/z* calcd for $C_{54}H_{43}IrN_5O_2$: 986.3044 [*M*–PF_6]$^+$; found: 986.3034.

4.7.2.2 Complex Λ-T2

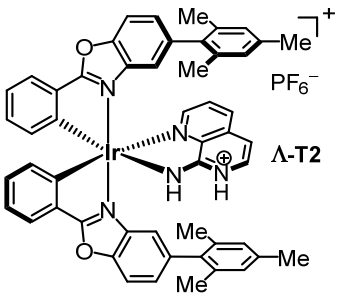

A flask was charged with diastereomer **Λ-(*S*)-T1** (see 4.7.2.1; 24.9 mg, 24.0 µmol, 1.00 eq), 1,7-naphthyridin-8-amine (3.0 mg, 20.7 µmol, 0.86 eq → 1,7-naphthyridin-8-amine elutes with complex **Λ-T2**), NH_4PF_6 (39.0 mg, 239 µmol, 9.97 eq), and MeCN (2.0 mL). The mixture was stirred at 65 °C for 12 h under nitrogen atmosphere and under exclusion of light. TLC indicated full conversion with respect to 1,7-naphthyridin-8-amine. All volatiles were removed *in vacuo* (40 °C) and the crude product purified by flash chromatography (CH_2Cl_2/MeOH 100:1). After solvent removal and drying *in vacuo*, desired complex **Λ-T2** was obtained as a yellow-orange solid (13.0 mg, 11.7 µmol, 57%). ^{1}H NMR (500 MHz, CD_2Cl_2): δ = 7.88 (dd, *J* = 5.0 Hz, *J* = 1.3 Hz, 1H), 7.85 (dd, *J* = 7.7 Hz, *J* = 0.8 Hz, 1H), 7.81 (dd, *J* = 7.7 Hz, *J* = 1.0 Hz, 1H), 7.77 (s, 1H), 7.72 (d, *J* = 8.6 Hz, 1H), 7.69 (d, *J* = 8.6 Hz, 1H), 7.66 (dd, *J* = 8.2 Hz, *J* = 1.3 Hz, 1H), 7.40 (d, *J* = 1.1 Hz, 1H), 7.34 (dd, *J* = 8.2 Hz, *J* = 5.2 Hz, 1H), 7.21 (dd, *J* = 8.5 Hz, *J* = 1.6 Hz, 1H), 7.16–7.10 (m, 2H), 7.09 (d, *J* = 7.1 Hz, 1H), 7.05 (td, *J* = 7.5 Hz, *J* =1.1 Hz, 1H), 7.00 (td, *J* = 7.5 Hz, *J* =1.4 Hz, 1H), 6.92 (td, *J* = 7.5 Hz, *J* =1.5 Hz, 1H), 6.90 (s, 1H), 6.88–6.83 (m, 2H), 6.81 (s, 1H), 6.79 (d, *J* = 7.3 Hz, 1H), 6.67 (d, *J* = 7.5 Hz, 1H), 6.16 (d, *J* = 7.1 Hz, 1H), 2.27 (s, 3H), 2.24 (s, 3H), 2.00 (s, 3H), 1.89 (s, 3H), 1.71 (s, 3H), 1.54 (s, 3H) ppm (two N*H* signals could not be found due to rapid exchange); ^{13}C NMR (125 MHz, CD_2Cl_2): δ = 178.6, 178.3, 161.1, 152.7, 151.6, 149.9, 149.7, 146.7, 144.7, 140.5, 139.8, 138.4, 138.4, 137.7, 137.7, 137.6, 137.4, 136.4, 136.4, 136.1, 135.9, 135.9, 135.6, 134.3, 134.1, 133.1, 132.7, 132.3, 130.6, 130.0, 129.2, 129.0, 128.8, 128.6 (2C), 128.3, 127.7, 126.9, 126.7, 123.1, 122.9, 117.8, 115.7, 112.6, 112.0, 102.9, 21.3, 21.2, 21.1, 21.1, 20.8, 20.7 ppm; IR (film): $\tilde{\nu}$ = 1638, 1588, 1514, 1433, 1383, 1284, 1226, 1154, 1026, 815, 736, 631, 512 cm^{-1}; HRMS (ESI): *m/z* calcd for $C_{52}H_{43}Ir_1N_5O_2$: 962.3044 [*M*–PF_6]$^+$; found: 962.3032.

4.7.2.3 Complex *rac*-T3

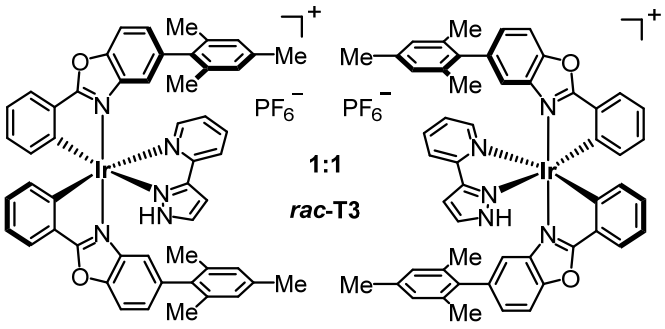

An amber glass vial was charged with iridium(III) dimer ***rac*-T1-dimer** (see 4.7.2.1; 35.1 mg, 20.6 µmol, 1.00 eq), 2-(1*H*-pyrazol-3-yl)pyridine ligand (**265**, 7.5 mg, 51.7 µmol, 2.51 eq), $AgPF_6$ (22.5 mg, 89.0 µmol, 4.32 eq), and CH_2Cl_2/MeOH 2:1 (6 mL) and the mixture was stirred at rt for 20 h under exclusion of light. All volatiles were removed *in vacuo* (40 °C) and the crude product purified by flash chromatography (CH_2Cl_2/MeOH 35:1). After solvent removal and drying *in vacuo*, desired racemic complex ***rac*-T3** was obtained as a green crystalline solid (35.8 mg, 32.3 µmol, 78%). ^{1}H NMR (300 MHz, CD_2Cl_2): δ = 8.07 (d, J = 5.5 Hz, 1H), 7.97 (d, J = 7.9 Hz, 1H), 7.90–7.82 (m, 3H), 7.75–7.66 (m, 3H), 7.25–7.11 (m, 5H), 7.06 (td, J = 7.6 Hz, J = 1.5 Hz, 1H), 7.03 (td, 7.6 Hz, J = 1.4 Hz, 1H), 6.98 (d, J = 2.9 Hz, 1H), 6.93–6.83 (m, 4H), 6.73 (t, J = 7.4 Hz, 2H), 5.61 (d, J = 1.4 Hz, 1H), 5.55 (d, J = 1.5 Hz, 1H), 2.28 (s, 3H), 2.28 (s, 3H), 1.96 (s, 3H), 1.91 (s, 3H), 1.69 (s, 3H), 1.66 (s, 3H) ppm (N*H* signal could not be found due to rapid exchange); IR (film): $\tilde{\nu}$ = 1591, 1517, 1448, 1381, 1256, 1039, 836, 772, 735, 553 cm^{-1}; HRMS (ESI): *m/z* calcd for $C_{52}H_{43}Ir_1N_5O_2$: 962.3044 [M–PF_6]$^+$; found: 962.3028.

4.7.2.4 Precatalyst Λ-T4

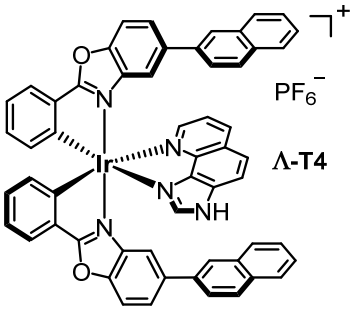

General procedure A5) was followed using **Λ-(*S*)-T4** (13.0 mg, 12.3 µmol; obtained from PhD student T. Mietke; contained **(*S*)-Aux1** as coordinating auxiliary ligand) and imidazoquinoline ligand **233**; eluent for f. c.: CH_2Cl_2/MeOH 50:1; precatalyst **Λ-T4** was obtained as a greenish yellow solid (11.5 mg, 10.0 µmol, 82%). ^{1}H NMR (500 MHz, CD_2Cl_2): δ = 8.56 (dd, J = 8.4 Hz, J = 1.3 Hz, 1H), 8.30 (dd, J = 5.0 Hz, J = 1.2 Hz, 1H), 8.23 (s, 1H), 8.12 (d, J = 8.9 Hz, 1H), 7.99 (s, 1H), 7.98 (s, 1H), 7.92–7.84 (m, 5H), 7.82 (d, J = 8.9 Hz, 1H), 7.80 (dd, J = 8.0 Hz, J = 0.6 Hz, 1H), 7.77 (dd, J = 8.6 Hz, J = 1.7 Hz, 1H), 7.74 (dd, J = 3.4 Hz, J = 0.6 Hz, 1H), 7.72 (dd, J = 3.3 Hz, J = 0.6 Hz, 1H), 7.68–7.65 (m, 2H), 7.61 (dd, J = 8.4 Hz, J = 5.0 Hz, 1H), 7.58–7.46 (m, 4H), 7.34 (d, J = 1.6 Hz, 1H), 7.24 (dd, J = 8.6 Hz, J = 1.9 Hz, 1H), 7.19 (td, J = 7.5 Hz, J = 1.1 Hz, 1H), 7.15 (td, J = 7.5 Hz, J = 1.0 Hz, 1H), 7.11–7.06 (m, 2H), 7.04 (td, J = 7.5 Hz, J = 1.5 Hz, 1H), 6.89–6.85 (m, 2H), 6.50 (dd, J = 1.7 Hz, J = 0.6 Hz, 1H), 5.76 (dd, J = 1.8 Hz, J = 0.5 Hz, 1H) ppm, N*H* signal could not be found due to rapid exchange; ^{13}C NMR (125 MHz, CD_2Cl_2): δ = 178.8, 178.7, 152.2, 150.4,

150.3, 146.2, 144.3, 143.6, 143.2 (2C), 142.0, 140.4, 140.2, 139.2, 139.1, 138.9, 137.3, 136.8, 134.5, 134.2, 134.1, 134.0, 133.7, 133.4, 133.3, 133.3, 130.3, 130.3, 129.9, 129.1, 128.8, 128.4, 128.3, 128.2, 127.4, 127.3, 127.2, 127.1, 127.0, 127.0, 126.3, 126.2 (2C), 126.0, 125.7, 125.6, 125.5, 124.9, 123.7 (2C), 123.3, 117.6, 113.9, 113.5, 113.0, 112.8 ppm; IR (film): $\tilde{\nu}$ = 1589, 1446, 1379, 1260, 1037, 835, 804, 735, 703, 552, 474 cm^{-1}; HRMS (ESI): *m/z* calcd for $C_{56}H_{35}Ir_1N_5O_2$: 1002.2419 $[M–PF_6]^+$; found: 1002.2404.

4.7.2.5 Precatalyst Λ-T5

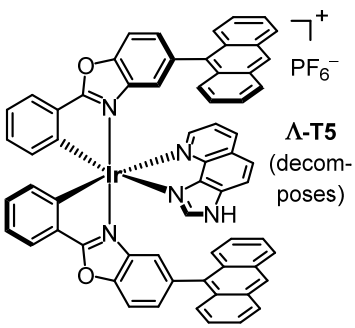

It was attempted to synthesize precatalyst **Λ-T5** from the according diastereomer (**Λ-(*S*)-T5**; obtained from PhD student T. Mietke; contained **(*S*)-Aux1** as auxiliary ligand) and imidazoquinoline ligand **233** according to general procedure A5). However, the resulting product complex, supposably **Λ-T5**, decomposed in solution and hence the scheduled experiments with **Λ-T5** were cancelled.

4.7.2.6 Precatalyst Λ-T6

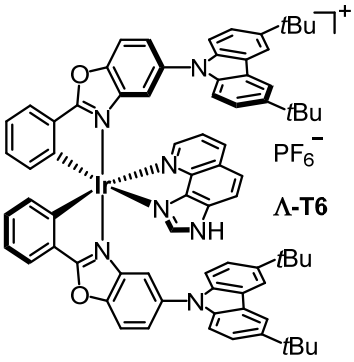

Precatalyst **Λ-T6** was prepared according to general procedures A1), A2), and A5) from benzoxazole ligand **189**, $IrCl_3 \cdot 3H_2O$, auxiliary ligand **(*S*)-Aux1**, and imidazoquinoline ligand **233**.

***Rac*-T6-dimer.** General procedure A1) was followed using benzoxazole ligand **189** (970 mg, 2.05 mmol, 2.05 eq) and $IrCl_3 \cdot 3H_2O$ (353 mg, 1.00 mmol, 1.00 eq); reaction time: 24 h. ***Rac*-T6-dimer**, which was prepared according to general procedure A1), was additionally purified via flash chromatography: Crude ***rac*-T6-dimer** was dissolved in CH_2Cl_2, adsorbed on silica gel (36 °C), and purified by f. c. (hexanes/EtOAc 20:1). After solvent removal and drying *in vacuo*, dimer ***rac*-T6-dimer** was obtained as an orange solid (644 mg, 275 µmol, 55%). ^{1}H NMR (500 MHz, CD_2Cl_2): δ = 8.60 (d, J = 2.0 Hz, 4H), 8.20 (d, J = 1.8 Hz, 8H), 7.56 (dd, J = 8.8 Hz, J = 2.2 Hz, 4H), 7.42 (dd, J = 8.7 Hz, J = 1.6 Hz, 8H), 7.35–7.29 (m, 12H), 6.78–6.73 (m, 4H), 6.63–6.59 (m, 8H), 6.14–6.10 (m, 4H), 1.49 (s, 72H) ppm; HRMS (ESI): *m/z* calcd for $C_{132}H_{124}Cl_2Ir_2N_8O_4Na$: 2364.8295 $[M+Na]^+$; found: 2364.8276.

Λ-(*S*)-T6. General procedure A2) was followed using ***rac*-T6-dimer** (339 mg, 145 µmol) and auxiliary ligand **(*S*)-Aux1**; the crude diastereomer mixture was purified and resolved by f. c. with CH_2Cl_2/hexanes 2:1; only the Λ-(*S*)-diastereomer was isolated and characterized; diastereomer **Λ-(*S*)-T6** was obtained as an orange-red solid (98.6 mg, 72.7 µmol, 25%). ^{1}H NMR

(500 MHz, CD_2Cl_2): δ = 8.19 (d, J = 10.1 Hz, 2H), 8.13 (d, J = 2.1 Hz, 1H), 8.11 (d, J = 1.6 Hz, 2H), 7.88 (d, J = 8.7 Hz, 1H), 7.85 (dd, J = 8.2 Hz, J = 0.9 Hz, 1H), 7.79 (dd, J = 7.6 Hz, J = 0.9 Hz, 1H), 7.74 (dd, J = 7.6 Hz, J = 0.9 Hz, 1H), 7.69 (dd, J = 8.8 Hz, J = 2.2 Hz, 1H), 7.65–7.60 (m, 2H), 7.52 (d, J = 8.0 Hz, 1H), 7.48 (d, J = 8.7 Hz, 1H), 7.40 (d, J = 8.9 Hz, 1H), 7.38–7.30 (m, 3H), 7.26 (d, J = 8.2 Hz, 2H), 7.21 (d, J = 8.5 Hz, 1H), 7.03 (td, J = 7.5 Hz, J = 1.3 Hz, 1H), 7.01–6.93 (m, 2H), 6.88 (td, J = 7.5 Hz, J = 1.5 Hz, 1H), 6.77 (d, J = 7.6 Hz, 1H), 6.66 (ddd, J = 8.6 Hz, J = 6.8 Hz, J = 1.8 Hz, 1H), 6.54 (d, J = 7.3 Hz, 1H), 6.36 (dd, J = 8.6 Hz, J = 1.0 Hz, 1H), 6.19 (ddd, J = 8.1 Hz, J = 6.8 Hz, J = 1.1 Hz, 1H), 4.70–4.62 (m, 1H), 2.52–2.44 (m, 2H), 1.53–1.43 (m, 36H), 0.87–0.77 (m, 1H), 0.20 (d, J = 7.1 Hz, 3H), 0.15 (d, J = 7.1 Hz, 3H) ppm; HRMS (ESI): *m/z* calcd for $C_{78}H_{77}Ir_1N_5O_3S_1$: 1356.5377 $[M+H]^+$; found: 1356.5388.

Precatalyst Λ-T6. General procedure A5) was followed using **Λ-(*S*)-T6** (30.3 mg, 22.3 µmol) and imidazoquinoline ligand **233**; eluent for f. c.: CH_2Cl_2/MeOH 100:1; precatalyst **Λ-T6** was obtained as a yellow crystalline solid (18.1 mg, 12.5 µmol, 56%). ^{1}H NMR (600 MHz, CD_2Cl_2): δ = 11.08 (s, 1H), 8.17 (d, J = 1.9 Hz, 2H), 8.15 (d, J = 8.8 Hz, 1H), 8.12 (d, J = 1.7 Hz, 2H), 8.11–8.06 (m, 3H), 7.96–7.88 (m, 3H), 7.83 (d, J = 5.2 Hz, 1H), 7.81 (d, J = 5.2 Hz, 1H), 7.58 (dd, J = 8.7 Hz, J = 2.0 Hz, 1H), 7.53 (dd, J = 8.7 Hz, J = 2.0 Hz, 1H), 7.50–7.25 (m, 4H), 7.22 (dd, J = 7.6 Hz, J = 1.0 Hz, 1H), 7.18 (td, J = 7.5 Hz, J = 0.8 Hz, 1H), 7.16 (dd, J = 8.3 Hz, J = 4.8 Hz, 1H), 7.12 (td, J = 7.6 Hz, J = 1.4 Hz, 1H), 7.09 (td, J = 7.5 Hz, J = 1.4 Hz, 1H), 6.92 (d, J = 7.6 Hz, 1H), 6.87 (d, J = 7.6 Hz, 1H), 6.45 (d, J = 1.9 Hz, 1H), 5.70 (d, J = 2.1 Hz, 1H), 1.58–1.45 (m, 36H) ppm (the signals of four protons could not be located due to severe signal broadening → probably due to hindered rotation of the carbazole moieties); ^{13}C NMR (150 MHz, CD_2Cl_2): δ = 179.5, 179.4, 152.0, 149.1, 148.8, 146.4, 144.4, 144.1, 143.9, 143.6, 143.0, 141.6, 139.4, 139.2, 139.2, 139.1, 139.0, 137.3, 137.0, 134.5, 134.1, 134.0, 133.6, 133.2, 130.0, 129.9, 127.4, 127.3, 125.9, 125.9, 124.6, 124.3, 124.2, 124.2, 12.9, 123.9, 123.8, 123.2, 117.4, 117.3, 116.9, 113.9, 113.7, 113.1, 112.7, 109.1, 108.5, 35.3, 35.2, 32.4, 32.3 ppm (severe signal broadening → probably due to hindered rotation of the carbazole moieties); IR (film): $\tilde{\nu}$ = 2955, 1592, 1483, 1444, 1369, 1295, 1260, 1232, 838, 735, 705, 612, 554 cm^{-1}; HRMS (ESI): *m/z* calcd for $C_{76}H_{69}Ir_1N_7O_2$: 1304.5144 $[M–PF_6]^+$; found: 1304.5126.

4.7.2.7 Precatalyst Λ-T7

I.) Synthesis of Boronic Ester 269[141]

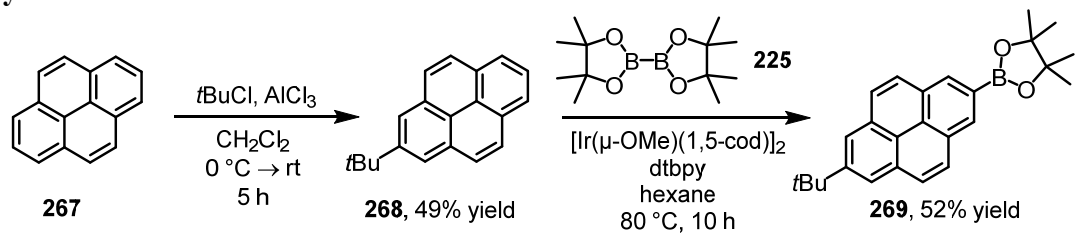

Scheme 81. Synthesis of pinacol boronic ester **269** starting from pyrene (**267**).[141]

2-(*tert*-Butyl)pyrene (268). Compound **268** was prepared according to a modified literature protocol from Marder et al.[141] A flame-dried flask (100 mL) was charged with pyrene (**267**; 5.00 g, 24.7 mmol, 1.00 eq), dry CH_2Cl_2 (50 mL), and *tert*-butyl chloride (3.04 mL, 27.2 mmol, 1.10 eq). The mixture was cooled to 0 °C and $AlCl_3$ (3.29 g, 24.7 mmol, 1.00 eq) was added portionwise giving a red suspension. Then, the mixture was allowed to warm to rt and stirred for 5 h. The mixture was quenched by the careful addition of water at 0 °C, diluted with CH_2Cl_2, and stirred vigorously for 10 min. The organic layer was separated and the aqueous layer extracted with CH_2Cl_2 (3x). The combined organic layers were washed with brine, dried over Na_2SO_4, and the solvent removed *in vacuo*. The resulting brown crude product was recrystallized from methanol to give 2-(*tert*-butyl)pyrene (**268**; 3.01 g, 11.7 mmol, 49%) as a beige solid. ^{1}H NMR (300 MHz, $CDCl_3$): δ = 8.26–8.11 (m, 4H), 8.10–7.91 (m, 5H), 1.59 (s, 9H) ppm; ^{13}C NMR (75 MHz, $CDCl_3$): δ = 149.2, 131.2 (2C), 131.2, 127.7 (2C), 127.6, 127.4 (2C), 125.6 (2C), 124.9 (2C), 122.4 (2C), 122.2, 35.4, 32.1 (3C) ppm; HRMS (ESI): *m/z* calcd for $C_{20}H_{18}$ $[M+H]^+$: 259.1492; found 259.1487.

Boronic ester 269. Compound **269** was prepared according to a modified literature protocol from Marder et. al.[141] A flame-dried Schlenk tube (10 mL; threaded PTFE plug) equipped with a stir bar was charged with $[Ir(\mu\text{-}OMe)(1,5\text{-}cod)]_2$ (33.7 mg, 50.8 µmol, 1.3 mol%), 4,4'-di-*tert*-butyl-2,2'-bipyridine (dtbpy; 27.3 mg, 102 µmol, 2.6 mol%), and bis(pinacolato)-diboron (**225**; 50.0 mg, 197 µmol, 5.0 mol%). Dry *n*-hexane (2 mL) was added and the resulting suspension heated to 50 °C under nitrogen atmosphere until the yellow suspension had turned into a red solution. The resulting red solution was transferred with a syringe into another flame-dried Schlenk tube (10 mL; threaded PTFE plug) which contained a solution of 2-(*tert*-butyl)pyrene (**268**; 1.01 g, 3.91 mmol, 1.00 eq) and bis(pinacolato)diboron (**225**; 1.27 g, 5.00 mmol, 1.28 eq) in dry *n*-hexane (10 mL). The resulting mixture was then stirred in the sealed Schlenk tube at 80 °C for 16 h under nitrogen atmosphere. Then, the resulting reaction mixture was filtered through a plug of silica gel which was thoroughly rinsed with excess CH_2Cl_2 (0.5 L). The solvent was removed *in vacuo* to give a yellow solid residue

which was purified via recrystallization from hexanes. The obtained recrystallized precipitate was washed with cold hexanes and after drying *in vacuo*, desired boronic ester **269** was obtained as a beige solid (0.79 g, 2.06 mmol, 53%). ^{1}H NMR (300 MHz, $CDCl_3$): δ = 8.61 (s, 2H), 8.21 (s, 2H), 8.09 (d, J = 9.0 Hz, 2H), 8.04 (d, J = 9.0 Hz, 2H), 1.59 (s, 9H), 1.47 (s, 12H) ppm; ^{13}C NMR (75 MHz, $CDCl_3$): δ = 149.7, 131.7 (2C), 131.3 (2C), 130.4 (2C), 127.8 (2C), 127.6 (2C), 126.5, 123.0, 122.3 (2C), 84.3 (2C), 35.4, 32.1 (3C), 25.2 (4C) ppm (one C signal could not be observed (*C*-B)); IR (film): $\tilde{\nu}$ = 2966, 1460, 1358, 1323, 1294, 1231, 1135, 964, 900, 886, 846, 807, 714 cm^{-1}; HRMS (ESI): *m/z* calcd for $C_{26}H_{29}B_1O_2Na$ $[M+Na]^+$: 407.2157, found: 407.2161.

II.) Synthesis of Precatalyst Λ-T7

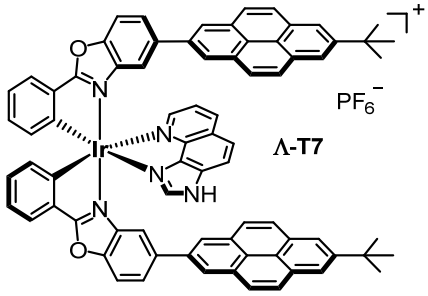

Precatalyst **Λ-T7** was prepared according to general procedures A1), A3), A4), and A5) from benzoxazole ligand **222**, $IrCl_3 \cdot 3H_2O$, auxiliary ligand **(*S*)-Aux1**, boronic ester **269**, and imidazoquinoline ligand **233**.

***Rac*-T7-dimer-CC.** General procedure A1) was followed using benzoxazole ligand **222** (2.50 g, 7.30 mmol, 2.10 eq) and $IrCl_3 \cdot 3H_2O$ (1.34 g, 3.48 mmol, 1.00 eq); reaction time: 24 h; in contrast to general procedure A1), ***rac*-T7-dimer-CC** was not purified by precipitation but via flash chromatography. Accordingly, all volatiles were removed *in vacuo* after reaction completion and the crude dimer purified by f. c. (CH_2Cl_2/hexanes 1:1). ***Rac*-T7-dimer-CC** was obtained as an orange solid (2.51 g, 1.37 mmol, 79%). ^{1}H NMR (300 MHz, CD_2Cl_2): δ = 8.20 (d, J = 2.5 Hz, 4H), 7.70 (dd, J = 7.6 Hz, J = 1.1 Hz, 4H), 7.56 (d, J = 9.1 Hz, 4H), 7.16 (dd, J = 9.1 Hz, J = 2.6 Hz, 4H), 6.95 (td, J = 7.5 Hz, J = 0.7 Hz, 4H), 6.74 (td, J = 7.6 Hz, J = 1.4 Hz, 4H), 6.12 (d, J = 7.7 Hz, 4H) ppm.

Λ-(*S*)-T7-CC. General procedure A3) was followed using ***rac*-T7-dimer-CC** (500 mg, 274 µmol); reaction time: 8 h; the crude diastereomer mixture was purified and resolved by f. c. with CH_2Cl_2/hexanes 6:1 → 8:1 → 10:1; only the Λ-(*S*)-diastereomer was isolated and characterized; diastereomer **Λ-(*S*)-T7-CC** was obtained as a red-orange solid (220 mg, 201 µmol, 37%). ^{1}H NMR (300 MHz, CD_2Cl_2): δ = 7.88 (d, J = 2.6 Hz, 1H), 7.80 (d, J = 9.0 Hz, 1H), 7.76 (ddd, J = 7.8 Hz, J = 1.5 Hz, J = 0.6 Hz, 1H), 7.74 (d, J = 8.9 Hz, 1H), 7.69 (ddd, J = 7.6 Hz, J = 1.5 Hz, J = 0.5 Hz, 1H), 7.46 (dd, J = 8.1 Hz, J = 1.7 Hz, 1H), 7.43–7.34 (m, 3H), 7.16 (ddd, J = 8.6 Hz, J = 6.8 Hz, J = 1.8 Hz, 1H), 7.00 (dd, J = 7.4 Hz, J = 1.1 Hz, 1H), 6.95 (dd, J = 7.3 Hz, J = 1.0 Hz, 1H), 6.89 (td, J = 7.5 Hz, J = 1.7 Hz, 1H), 6.83 (td, J = 7.5 Hz, J = 1.4 Hz, 1H), 6.68 (dd, J = 8.7 Hz, J = 1.1 Hz, 1H), 6.62 (d, J = 7.5 Hz,

1H), 6.37–6.27 (m, 2H), 4.64 (dt, J = 10.2 Hz, J = 2.1 Hz, 1H), 3.37 (dd, J = 11.9 Hz, J = 9.8 Hz, 1H), 3.01 (dd, J = 11.9 Hz, J = 1.9 Hz, 1H), 0.75–0.59 (m, 1H), 0.25 (d, J = 7.2 Hz, 3H), 0.22 (d, J = 7.2 Hz, 3H) ppm.

Λ-(*S*)-T7. General procedure A4) was followed using **Λ-(*S*)-T7-CC** (50.0 mg, 45.6 µmol); instead of toluene, a 10:1 mixture of toluene and H_2O was used as solvent; employed boronic ester: **269**; reaction time: 16 h; the crude product was purified by f. c. with CH_2Cl_2/hexanes 6:1 → CH_2Cl_2; **Λ-(*S*)-T7** was obtained as an orange solid (46.9 mg, 35.7 µmol, 78%). ^{1}H NMR (300 MHz, CD_2Cl_2): δ = 8.52 (d, J = 1.5 Hz, 1H), 8.45 (s, 2H), 8.32 (s, 2H), 8.26 (d, J = 12 Hz, 4H), 8.12 (s, 4H), 8.10–7.98 (m, 5H), 7.94–7.83 (m, 3H), 7.81–7.72 (m, 3H), 7.67 (d, J = 8.4 Hz, 1H), 7.38 (ddd, J = 8.6 Hz, J = 6.8 Hz, J = 1.8 Hz, 1H), 7.09 (dd, J = 8.6 Hz, J = 1.0 Hz, 1H), 7.04 (td, J = 7.5 Hz, J = 1.1 Hz, 1H), 6.99–6.88 (m, 2H), 6.82–6.72 (m, 2H), 6.59 (ddd, J = 8.1 Hz, J = 6.8 Hz, J = 1.2 Hz, 1H), 6.53 (d, J = 7.2 Hz, 1H), 4.98–4.86 (m, 1H), 3.16 (dd, J = 11.6 Hz, J = 9.9 Hz, 1H), 2.85 (dd, J = 11.7 Hz, J = 1.1 Hz, 1H), 1.61 (s, 9H), 1.61 (s, 9H), 1.06–0.83 (m, 1H), 0.29 (d, J = 7.0 Hz, 3H), 0.09 (d, J = 7.0 Hz, 3H) ppm; ^{13}C NMR (75 MHz, CD_2Cl_2): δ = 179.3, 179.0, 168.2, 167.4, 151.1, 150.7, 150.5, 150.4, 150.1, 150.0, 140.8, 140.6, 140.1, 139.9, 138.3, 137.7, 135.4, 134.5, 134.4, 132.5, 132.5, 132.2 (3C), 132.0 (2C), 131.8, 131.7 (2C), 131.6 (2C), 131.2, 128.7 (2C), 128.6 (2C), 128.0 (2C), 127.7 (2C), 126.8, 126.5, 126.0, 125.6, 125.0, 124.5, 124.4, 124.2 (2C), 124.1 (2C), 123.3, 123.2 (3C), 123.1 (2C), 122.6, 121.5, 118.9, 117.4, 115.4, 114.1, 112.6, 112.2, 86.5, 35.8 (2C), 32.3 (6C), 32.2, 28.0, 19.1, 14.6 ppm; IR (film): $\tilde{\nu}$ = 2956, 1594, 1557, 1517, 1439, 1377, 1195, 1010, 877, 811, 737, 709 cm^{-1}; HRMS (ESI): *m/z* calcd for $C_{78}H_{62}Ir_1N_3O_3S_1Na$: 1336.4041 $[M+Na]^+$, found: 1336.4074.

Precatalyst Λ-T7. General procedure A5) was followed using **Λ-(*S*)-T7** (27.2 mg, 25.5 µmol) and imidazoquinoline ligand **233**; eluent for f. c.: CH_2Cl_2/MeOH 100:1; precatalyst **Λ-T7** was obtained as a greenish yellow solid (17.3 mg, 14.9 µmol, 59%). ^{1}H NMR (600 MHz, CD_2Cl_2): δ = 11.74 (s, 1H), 8.58 (dd, J = 8.5 Hz, J = 0.9 Hz, 1H), 8.35–8.31 (m, 2H), 8.29 (s, 2H), 8.24 (s, 2H), 8.22 (d, J = 9.0 Hz, 1H), 8.16–8.08 (m, 6H), 8.05 (d, J = 9.0 Hz, 1H), 8.01 (d, J = 9.0 Hz, 2H), 7.93 (dd, J = 7.7 Hz, J = 0.9 Hz, 1H), 7.92–7.87 (m, 4H), 7.80–7.73 (m, 3H), 7.66 (s, 2H), 7.60 (dd, J = 8.5 Hz, J = 5.1 Hz, 1H), 7.21 (td, J = 7.5 Hz, J = 0.8 Hz, 1H), 7.16 (td, J = 7.5 Hz, J = 0.8 Hz, 1H), 7.10 (td, J = 7.5 Hz, J = 1.5 Hz, 1H), 7.06 (td, J = 7.5 Hz, J = 1.3 Hz, 1H), 6.95 (d, J = 7.5 Hz, 1H), 6.91 (d, J = 7.5 Hz, 1H), 6.76 (d, J = 1.5 Hz, 1H), 5.83 (d, J = 1.5 Hz, 1H), 1.60 (s, 9H), 1.55 (s, 9H) ppm; ^{13}C NMR (150 MHz, CD_2Cl_2): δ = 178.8, 178.7, 152.3, 150.5, 150.4, 150.3, 150.2, 146.2, 144.4, 143.6, 143.3, 142.1, 140.8, 140.7, 139.3, 139.1, 138.9, 137.3, 136.6, 134.6, 134.2, 133.7, 133.5, 133.3, 132.2 (2C), 131.9 (2C), 131.6 (2C), 131.5 (2C), 130.3, 130.3,

129.2 (2C), 129.1 (2C), 127.8 (2C), 127.4 (2C), 127.2, 127.1, 126.2, 126.2, 126.2, 126.1, 124.4, 124.4, 123.7, 123.7, 123.5 (2C), 123.4 (3C), 123.3 (2C), 123.0 (3C), 122.9, 117.6, 114.3, 114.1, 113.1, 112.9, 35.8, 35.7, 32.2 (3C), 32.2 (3C) ppm; IR (film): $\tilde{\nu}$ = 2960, 1595, 1443, 1382, 1261, 1090, 1035, 843, 738, 711, 557 cm^{-1}; HRMS (ESI): *m/z* calcd for $C_{76}H_{55}Ir_1N_5O_2$: 1262.3987 $[M–PF_6]^+$; found: 1262.3997.

4.7.2.8 Precatalyst Λ-T8

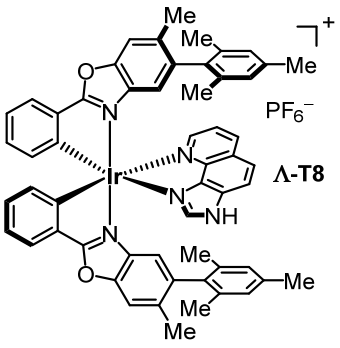

Precatalyst **Λ-T8** was prepared according to general procedures A1), A3), A4), and A5) from benzoxazole ligand **217**, $IrCl_3 \cdot 3H_2O$, auxiliary ligand **(*S*)-Aux1**, 2,4,6-trimethylphenylboronic acid, and imidazoquinoline ligand **233**.

***Rac*-T8-dimer-CC.** General procedure A1) was followed using benzoxazole ligand **217** (510 mg, 1.43 mmol, 2.04 eq) and $IrCl_3 \cdot 3H_2O$ (246 mg, 698 µmol, 1.00 eq); reaction time: 24 h; in contrast to general procedure A1), ***rac*-T8-dimer-CC** was not purified by precipitation but via flash chromatography. Accordingly, all volatiles were removed *in vacuo* after reaction completion and the crude product purified by f. c. (CH_2Cl_2/hexanes 1:1). Ir(III) dimer ***rac*-T8-dimer-CC** was obtained as an orange solid (584 mg, 310 µmol, 89%). ^{1}H NMR (500 MHz, CD_2Cl_2): δ = 8.10 (s, 4H), 7.65 (dd, J = 7.6 Hz, J = 0.9 Hz, 4H), 7.45 (s, 4H), 6.93 (ddd, J = 7.4 Hz, J = 7.6 Hz, J = 0.7 Hz, 4H), 6.72 (ddd, J = 7.9 Hz, J = 7.3 Hz, J = 1.4 Hz, 4H), 6.12 (d, J = 7.8 Hz, 4H), 2.47 (s, 12H) ppm; ^{19}F NMR (471 MHz, CD_2Cl_2): δ = −73.9 (s, 3F, 4x C*F*$_3$) ppm; HRMS (ESI): *m/z* calcd for $C_{60}H_{36}Cl_2F_{12}Ir_2N_4O_{16}S_4Na$: 1902.9324 $[M+Na]^+$, found: 1902.9318.

Λ-(*S*)-T8-CC. General procedure A3) was followed using ***rac*-T8-dimer-CC** (585 mg, 311 µmol); reaction time: 8 h; the crude diastereomer mixture was purified and resolved by f. c. with CH_2Cl_2/hexanes 3:1; only the Λ-(*S*)-diastereomer was isolated and characterized; diastereomer **Λ-(*S*)-T8-CC** was obtained as a red-orange solid (282 mg, 250 µmol, 40%). ^{1}H NMR (500 MHz, CD_2Cl_2): δ = 7.89 (s, 1H), 7.73 (dd, J = 7.8 Hz, J = 1.0 Hz, 1H), 7.68 (s, 1H), 7.65–7.59 (m, 1H), 7.53 (d, J = 5.9 Hz, 1H), 7.49–7.43 (m, 1H), 7.40 (s, 1H), 7.16–7.07 (m, 1H), 6.95 (ddd, J = 7.5 Hz, J = 7.5 Hz, J = 1.0 Hz, 2H), 6.87 (ddd, J = 7.5 Hz, J = 7.5 Hz, J = 1.4 Hz, 1H), 6.84–6.79 (m, 1H), 6.71–6.66 (m, 1H), 6.65 (d, J = 7.7 Hz, 1H), 6.34 (d, J = 7.7 Hz, 1H), 6.32–6.26 (m, 1H), 4.63–4.55 (m, 1H), 3.42 (dd, J = 11.7 Hz, J = 10.1 Hz, 1H), 2.98 (d, J = 11.7 Hz, 1H), 2.55 (s, 3H), 2.48 (s, 3H), 0.77–0.62 (m, 1H), 0.27 (d, J = 7.0 Hz, 3H), 0.24 (d, J = 7.0 Hz, 3H) ppm; ^{13}C NMR (125 MHz, CD_2Cl_2): δ = 180.5, 180.0, 169.7, 167.9, 151.6, 150.5, 150.0, 149.6, 147.1, 145.7, 138.0, 137.9, 135.4, 134.1,

133.9, 133.1, 132.5, 132.0, 130.6, 130.4, 129.9, 129.3, 127.2, 126.9, 124.5, 122.6, 121.6, 119.2 (q, $J_{C\text{-}F}$ = 320 Hz), 119.0 (q, $J_{C\text{-}F}$ = 321 Hz), 118.5, 114.8, 114.4, 114.1, 111.7, 110.3, 85.0, 32.4, 27.3, 19.2, 17.9, 17.3, 14.3 ppm; ^{19}F NMR (471 MHz, CD_2Cl_2): δ = −73.9 (s, 3F, CF_3), −74.2 (s, 3F, CF_3) ppm; IR (film): $\tilde{\nu}$ = 1594, 1557, 1518, 1463, 1414, 1205, 1130, 1063, 1012, 961, 882, 851, 735, 607, 508, 446 cm^{-1}; HRMS (ESI): *m/z* calcd for $C_{42}H_{32}F_6Ir_1N_3O_9S_3Na$: 1148.0724 [*M*+Na]$^+$, found: 1148.0725.

Λ-(*S*)-T8. General procedure A4) was followed using **Λ-(*S*)-T8-CC** (30.2 mg, 26.8 µmol); boronic acid: 2,4,6-trimethylphenylboronic acid; reaction time: 11 h; the crude product was purified by f. c. with CH_2Cl_2/hexanes 3:1 → CH_2Cl_2; **Λ-(*S*)-Ir8** was obtained as a bright orange solid (26.8 mg, 25.2 µmol, 94%). ^{1}H NMR (300 MHz, CD_2Cl_2): δ = 7.71 (dd, *J* = 7.6 Hz, *J* = 0.8 Hz, 1H), 7.64 (dd, *J* = 7.6 Hz, *J* = 1.0 Hz, 1H), 7.61 (s, 1H), 7.58 (s, 1H), 7.48 (s, 1H), 7.24 (dd, *J* = 8.1 Hz, *J* = 1.7 Hz, 1H), 7.11 (s, 1H), 7.02–6.83 (m, 7H), 6.81 (s, 1H), 6.75 (dd, *J* = 7.5 Hz, *J* = 1.5 Hz, 1H), 6.61 (d, *J* = 7.2 Hz, 1H), 6.55–6.47 (m, 1H), 6.41 (dd, *J* = 8.7 Hz, *J* = 1.1 Hz, 1H), 6.14 (ddd, *J* = 8.1 Hz, *J* = 6.8 Hz, *J* = 1.1 Hz, 1H), 4.53 (ddd, *J* = 9.6 Hz, *J* = 2.3 Hz, *J* = 2.3 Hz, 1H), 2.71 (dd, *J* = 11.7 Hz, *J* = 2.1 Hz, 1H), 2.62 (dd, *J* = 11.5 Hz, *J* = 9.4 Hz, 1H), 2.34 (s, 3H), 2.29 (s, 3H), 2.10 (s, 3H), 2.08 (s, 3H), 1.94 (s, 3H), 1.93 (s, 3H), 1.87 (s, 3H), 1.54 (s, 3H), 0.83–0.62 (m, 1H), 0.20 (d, *J* = 7.0 Hz, 1H), 0.18 (d, *J* = 7.0 Hz, 1H) ppm. ^{13}C NMR (75 MHz, CD_2Cl_2): δ = 178.0, 177.8, 169.0, 168.3, 151.1, 150.4, 150.2, 149.9, 139.9, 139.8, 137.6, 137.6, 137.5, 137.5, 137.3, 137.1, 136.7, 136.2, 136.1, 135.7, 135.0, 134.9, 134.7, 133.6, 133.5, 132.6, 132.0, 131.9, 131.6, 131.4, 128.8, 128.6, 128.5, 128.5, 126.4, 126.0, 124.1, 122.2, 121.1, 119.1, 118.7, 116.7, 113.3, 113.1, 112.5, 85.1, 32.2, 27.7, 21.5, 21.4, 20.8, 20.6, 20.3, 20.3, 19.2, 14.5 ppm; IR (film): $\tilde{\nu}$ = 2957, 2917, 1596, 1557, 1518, 1441, 1378, 1280, 1194, 1153, 1036, 1011, 849, 736, 445 cm^{-1}; HRMS (ESI): *m/z* calcd for $C_{58}H_{54}Ir_1N_3O_3S_1Na$: 1088.3410 [*M*+Na]$^+$, found: 1088.3456.

Precatalyst Λ-T8. General procedure A5) was followed using **Λ-(*S*)-T8** (35.4 mg, 33.2 µmol) and imidazoquinoline ligand **233**; eluent for f. c.: CH_2Cl_2/MeOH 100:1 → 50:1; precatalyst **Λ-T8** was obtained as a greenish yellow solid (23.2 mg, 20.0 µmol, 60%). ^{1}H NMR (300 MHz, CD_2Cl_2): δ = 11.15 (s, 1H), 8.24 (dd, *J* = 8.3 Hz, *J* = 1.1 Hz, 1H), 8.03 (dd, *J* = 5.1 Hz, *J* = 1.1 Hz, 1H), 7.93 (d, *J* = 8.9 Hz, 1H), 7.90 (s, 1H), 7.86 (dd, *J* = 7.7 Hz, *J* = 0.9 Hz, 1H), 7.84–7.78 (m, 2H), 7.54 (s, 1H), 7.50 (s, 1H), 7.32 (dd, *J* = 8.3 Hz, *J* = 4.9 Hz, 1H), 7.22–7.08 (m, 2H), 7.05 (td, *J* = 7.5 Hz, *J* = 1.5 Hz, 1H), 7.01 (td, *J* = 7.6 Hz, *J* = 1.8 Hz, 1H), 6.91 (s, 1H), 6.89–6.79 (m, 4H), 6.76 (s, 1H), 5.92 (s, 1H), 4.86 (s, 1H), 2.28 (s, 6H), 1.97 (s, 3H), 1.91 (s, 3H), 1.86 (s, 3H), 1.74 (s, 3H), 1.17 (s, 3H), 1.04 (s, 3H) ppm; ^{13}C NMR (75 MHz, CD_2Cl_2): δ = 177.6, 177.6, 151.8, 150.2, 150.2, 146.0, 144.1, 143.2, 142.6, 141.6, 140.3, 139.8, 138.7, 137.8, 137.4, 136.8, 136.7, 136.7, 136.2, 136.0, 135.8,

135.6 (2C), 135.6, 135.3, 134.6, 134.2, 133.2, 133.0, 132.8, 130.7, 130.7, 128.9, 128.9, 128.5 (2C), 126.8, 126.7, 125.8, 125.6, 123.5 (2C), 122.9, 117.1, 116.0, 115.0, 113.6, 113.3, 21.3, 21.3, 20.4 (2C), 20.3, 20.3, 20.0 (2C) ppm; IR (film): $\tilde{\nu}$ = 1450, 1380, 834, 775, 736, 704, 553 cm^{-1}; HRMS (ESI): *m/z* calcd for $C_{56}H_{47}Ir_1N_5O_2$: 1014.3358 $[M–PF_6]^+$; found: 1014.3364.

4.7.2.9 Precatalyst Λ-T9

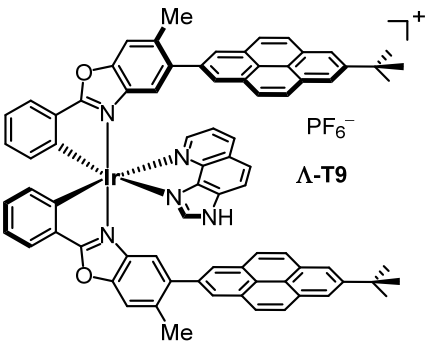

Precatalyst **Λ-T9** was prepared according to general procedures A4) and A5) from OTf-functionalized diastereomer **Λ-(*S*)-T8-CC** (see 4.7.2.8), boronic ester **269** (see 4.7.2.7), and imidazoquinoline ligand **233**.

Λ-(*S*)-T9. General procedure A4) was followed using **Λ-(*S*)-T8-CC** (70.1 mg, 62.3 µmol); instead of toluene, a 10:1 mixture of toluene and H_2O was used as solvent; employed boronic ester: **269**; reaction time: 14 h; the crude product was purified by f. c. with CH_2Cl_2/hexanes 3:1 → 6:1; diastereomer **Λ-(*S*)-T9** was obtained as an orange solid (71.5 mg, 53.3 µmol, 86%). ^{1}H NMR (600 MHz, CD_2Cl_2): δ = 8.32 (s, 2H), 8.31 (s, 2H), 8.29 (s, 2H), 8.16 (d, *J* = 9.0 Hz, 2H), 8.15–8.11 (m, 4H), 8.08 (d, *J* = 9.0 Hz, 2H), 8.05 (s, 2H), 7.99 (s, 1H), 7.77 (ddd, *J* = 7.6 Hz, *J* = 7.6 Hz, *J* = 1.0 Hz, 1H), 7.73 (ddd, *J* = 7.7 Hz, *J* = 1.4 Hz, *J* = 0.5 Hz, 1H), 7.70 (s, 1H), 7.61 (dd, *J* = 8.2 Hz, *J* = 1.7 Hz, 1H), 7.61 (s, 1H), 7.57 (s, 1H), 7.02 (ddd, *J* = 7.5 Hz, *J* = 7.5 Hz, *J* = 1.1 Hz, 1H), 6.98–6.91 (m, 2H), 6.84–6.77 (m, 3H), 6.57 (dd, *J* = 8.2 Hz, *J* = 1.1 Hz, 1H), 6.51 (d, *J* = 7.5 Hz, 1H), 6.31 (ddd, *J* = 8.0 Hz, *J* = 6.7 Hz, *J* = 1.2 Hz, 1H), 4.81 (ddd, *J* = 9.9 Hz, *J* = 2.3 Hz, *J* = 2.3 Hz, 1H), 2.69 (dd, *J* = 11.4 Hz, *J* = 9.9 Hz, 1H), 2.63–2.54 (m, 1H), 2.57 (s, 3H), 2.49 (s, 3H), 1.64 (s, 9H), 1.63 (s, 9H), 0.99–0.89 (m, 1H), 0.26 (d, *J* = 7.0 Hz, 3H), 0.09 (d, *J* = 7.0 Hz, 3H) ppm; ^{13}C NMR (150 MHz, CD_2Cl_2): δ = 178.3, 178.1, 168.4, 167.4, 151.0, 150.5, 150.3, 150.2, 150.0, 149.8, 141.4, 141.2, 138.9, 138.7, 137.4, 137.2, 135.4, 134.5, 134.5, 134.0, 133.6, 132.4, 132.1, 131.9, 131.7, 131.6 (3C), 131.6 (2C), 131.4 (2C), 131.3, 131.3 (2C), 128.6 (2C), 128.3 (2C), 128.0 (2C), 127.8 (2C), 126.5 (2C), 126.5, 126.7 (2C), 126.1, 124.4, 124.2, 124.0, 123.2, 123.1 (2C), 123.0 (2C), 122.3, 121.2, 120.1, 118.7, 117.7, 113.6, 113.4, 113.0, 86.0, 35.8, 35.8, 32.3 (9C), 32.1, 27.6, 22.1, 21.7, 19.0, 14.5 ppm; IR (film): $\tilde{\nu}$ = 3041, 2956, 2867, 1595, 1556, 1517, 1441, 1378, 1254, 1226, 1192, 1150, 1126, 1033, 1009, 874, 848, 801, 715, 444 cm^{-1}; HRMS (ESI): *m/z* calcd for $C_{80}H_{66}Ir_1N_3O_3S_1Na$: 1364.4353 $[M+Na]^+$, found: 1364.4386.

Precatalyst Λ-T9. General procedure A5) was followed using **Λ-(*S*)-T9** (71.0 mg, 52.9 µmol) and imidazoquinoline ligand **233**; eluent for f. c.: CH_2Cl_2/MeOH 100:1; precatalyst **Λ-T9** was obtained as a greenish yellow solid (35.2 mg, 24.5 µmol, 46%). ^{1}H NMR

(500 MHz, CD_2Cl_2): δ = 11.21 (s, 1H), 8.31 (s, 2H), 8.29 (s, 2H), 8.17–8.08 (m, 7H), 8.03 (s, 1H), 8.02 (s, 1H), 8.01–7.95 (m, 4H), 7.88 (dd, J = 7.6 Hz, J = 0.9 Hz, 1H), 7.84 (dd, J = 7.6 Hz, J = 0.9 Hz, 1H), 7.71 (s, 2H), 7.60 (s, 1H), 7.55 (s, 1H), 7.47 (s, 2H), 7.19 (td, J = 7.6 Hz, J = 1.0 Hz, 1H), 7.16–7.11 (s, 2H), 7.08 (td, J = 7.6 Hz, J = 1.6 Hz, 1H), 7.06 (td, J = 7.6 Hz, J = 1.5 Hz, 1H), 6.94 (d, J = 7.3 Hz, 1H), 6.88 (d, J = 7.5 Hz, 1H), 6.37 (s, 1H), 5.23 (s, 1H), 2.39 (s, 3H), 2.35 (s, 3H), 1.62 (9H), 1.59 (9H) ppm; ^{13}C NMR (150 MHz, CD_2Cl_2): δ = 177.9, 177.9, 152.1, 150.3, 150.2, 150.2, 150.1, 146.0, 144.3, 143.4, 142.9, 141.9, 141.7, 141.3, 138.7, 138.2, 138.0, 136.7, 136.0, 135.6, 135.1, 134.6, 134.1, 133.3, 133.1, 132.9, 131.6 (2C), 131.5 (2C), 131.5 (2C), 131.2 (2C), 130.5, 130.5, 129.0 (2C), 128.8 (2C), 127.5 (2C), 127.4 (2C), 126.9, 126.8, 126.0, 125.8, 125.6 (2C), 125.5 (2C), 124.1, 124.0, 123.6, 123.5, 123.3 (2C), 123.3 (2C), 123.1, 123.0, 123.0, 117.3, 117.0, 116.4, 113.7, 113.7, 35.8, 35.8, 32.2 (3C), 32.2 (3C), 21.9, 21.6 ppm; IR (film): $\tilde{\nu}$ = 2958, 1596, 1447, 1383, 1038, 840, 728, 557 cm^{-1}; HRMS (ESI): *m/z* calcd for $C_{78}H_{59}Ir_1N_5O_2$: 1290.4300 [*M*–PF_6]$^+$; found: 1290.4313.

4.7.2.10 Precatalyst Λ-T10

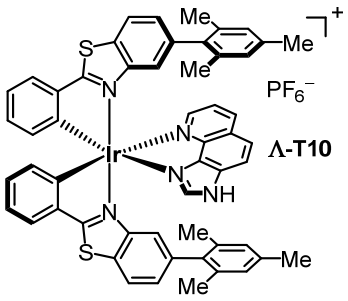

Precatalyst **Λ-T10** was prepared according to general procedures A1), A2), and A5) from benzothiazole ligand **199**, $IrCl_3 \cdot 3H_2O$, auxiliary ligand **(*S*)-Aux1**, and imidazoquinoline ligand **233**.

***Rac*-T10-dimer.** General procedure A1) was followed using benzothiazole ligand **199** (1.04 g, 3.16 mmol, 2.05 eq) and $IrCl_3 \cdot 3H_2O$ (542 mg, 1.54 mmol, 1.00 eq); reaction time: 11.5 h; Ir(III) dimer ***rac*-T10-dimer** was obtained as a deeply red solid (1.40 g, 0.79 mmol, quantitative). ^{1}H NMR (300 MHz, CD_2Cl_2): δ = 9.00–8.87 (m, 4H), 8.01 (d, J = 8.1 Hz, 4H), 7.65 (d, J = 7.9 Hz, 4H), 7.32 (dd, J = 8.2 Hz, J = 1.2 Hz, 4H), 7.00–6.84 (m, 12H), 6.67 (td, J = 7.5 Hz, J = 1.2 Hz, 4H), 6.37 (d, J = 7.7 Hz, 4H), 2.30 (s, 12H), 2.11 (s, 12H), 1.99 (s, 12H) ppm; HRMS (ESI): *m/z* calcd for $C_{88}H_{72}Cl_1Ir_2N_4S_4$: 1733.3572 [*M*–Cl]$^+$; found: 1733.3632.

Λ-(*S*)-T10. General procedure A2) was followed using ***rac*-T10-dimer** (501 mg, 283 µmol) and auxiliary ligand **(*S*)-Aux1**; the crude diastereomer mixture was dissolved in CH_2Cl_2, adsorbed on silica gel (40 °C), and purified and resolved by f. c. with hexanes/EtOAc 20:1 → 10:1; only the Λ-(*S*)-diastereomer was isolated and characterized; diastereomer **Λ-(*S*)-T10** was obtained as a red solid (156 mg, 146 µmol, 26%). ^{1}H NMR (500 MHz, CD_2Cl_2): δ = 8.60 (d, J = 1.1 Hz, 1H), 7.93 (d, J = 8.3 Hz, 1H), 7.91 (d, J = 8.1 Hz, 1H), 7.74 (d, J = 7.5, 1H), 7.65 (dd, J = 7.6 Hz, J = 0.8 Hz, 1H), 7.56 (d, J = 1.1 Hz, 1H), 7.23 (d, J = 1.5 Hz, 1H), 7.22

(d, J = 1.3 Hz, 1H), 7.18 (dd, J = 8.2 Hz, J = 1.7 Hz, 1H), 6.98 (s, 1H), 6.95–6.87 (m, 3H), 6.84 (s, 1H), 6.83–6.79 (m, 1H), 6.75 (td, J = 7.5 Hz, J = 1.5 Hz, 1H), 6.71–6.64 (m, 3H), 6.31 (d, J = 7.5, 1H), 6.26 (dd, J = 8.6 Hz, J = 0.9 Hz, 1H), 6.15–6.10 (m, 1H), 4.34 (d, J = 10.5 Hz, 1H), 2.51 (dd, J = 11.7 Hz, J = 1.5 Hz, 1H), 2.32 (s, 3H), 2.25 (s, 3H), 2.19 (dd, J = 11.6 Hz, J = 9.7 Hz, 1H), 2.05 (s, 3H), 1.99 (s, 6H), 1.51 (s, 3H), 0.69–0.57 (m, 1H), 0.24 (d, J = 7.2 Hz, 3H), 0.10 (d, J = 7.2 Hz, 3H) ppm; HRMS (ESI): *m/z* calcd for $C_{56}H_{50}Ir_1N_3O_1S_3Na$: 1092.2637 $[M+Na]^+$; found: 1092.2642.

Precatalyst Λ-T10. General procedure A5) was followed using **Λ-(*S*)-T10** (25.0 mg, 23.4 µmol) and imidazoquinoline ligand **233**; eluent for f. c.: CH_2Cl_2/MeOH 35:1; precatalyst **Λ-T10** was obtained as a yellow-orange crystalline solid (14.3 mg, 12.3 µmol, 53%). ^{1}H NMR (500 MHz, CD_2Cl_2): δ = 11.21 (s, 1H), 8.04 (dd, J = 8.3 Hz, J = 1.0 Hz, 1H), 7.94–7.78 (m, 7H), 7.77 (d, J = 9.0 Hz, 1H), 7.20–7.05 (m, 4H), 7.00 (dd, J = 8.3 Hz, J = 1.5 Hz, 1H), 6.93 (td, J = 7.6 Hz, J = 1.4 Hz, 1H), 6.91–6.86 (m, 2H), 6.83 (s, 1H), 6.81 (s, 1H), 6.73 (s, 1H), 6.70 (d, J = 7.7 Hz, 1H), 6.66 (d, J = 7.7 Hz, 1H), 6.55 (d, J = 0.9 Hz, 1H), 5.43 (d, J = 0.9 Hz, 1H), 2.30 (s, 3H), 2.28 (s, 3H), 1.90 (s, 3H), 1.74 (s, 3H), 0.94 (s, 3H), 0.92 (s, 3H) ppm; ^{13}C NMR (125 MHz, CD_2Cl_2): δ = 182.1, 181.6, 150.6, 150.5, 150.1, 147.2, 144.4, 143.8, 141.9, 141.9, 141.6, 141.5, 141.5, 141.1, 138.6, 138.1, 137.5, 137.4, 137.2, 135.6, 135.5, 135.5, 135.1, 134.7, 134.4, 133.1, 132.2, 131.9, 130.2, 130.0, 128.9, 128.7, 128.3, 128.2, 128.1, 127.4, 126.9, 126.8, 126.0, 125.7, 123.7, 123.6, 123.6, 123.4, 123.0, 124.5, 119.4, 116.9, 21.3, 21.1, 21.0, 20.8, 20.3, 20.0 ppm; IR (film): $\tilde{\nu}$ = 1442, 1410, 841, 764, 733, 557 cm^{-1}; HRMS (ESI): *m/z* calcd for $C_{54}H_{43}Ir_1N_5S_2$: 1018.2584 $[M–PF_6]^+$; found: 1018.2594.

4.7.2.11 Precatalyst Λ-T11

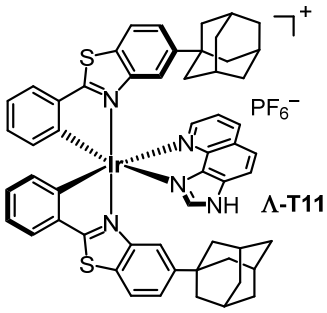

Precatalyst **Λ-T11** was prepared according to general procedures A2) and A5) from iridium(III) dimer ***rac*-T11-dimer** (received from former PhD student Haohua Huo), auxiliary ligand **(*S*)-Aux1**, and imidazoquinoline ligand **233**.

Λ-(*S*)-T11. General procedure A2) was followed using ***rac*-T11-dimer** (122 mg, 66.5 µmol) and auxiliary ligand **(*S*)-Aux1**; the crude diastereomer mixture was dissolved in CH_2Cl_2, adsorbed on silica gel (40 °C), and purified and resolved by f. c. with hexanes/EtOAc 20:1; only the Λ-(*S*)-diastereomer was isolated and characterized; diastereomer **Λ-(*S*)-T11** was obtained as a red solid (36.0 mg, 32.7 µmol, 25%). ^{1}H NMR (300 MHz, CD_2Cl_2): δ = 8.93 (d, J = 1.7 Hz, 1H), 7.86 (d, J = 8.5 Hz, 1H), 7.80–7.68 (m, 3H), 7.61 (dd, J = 7.6 Hz, J = 0.9 Hz, 1H), 7.49 (dt, J = 8.7 Hz, J = 1.8 Hz, 2H), 7.29 (dd, J = 8.1 Hz, J = 1.7 Hz, 1H), 6.98 (ddd, J = 8.6 Hz,

J = 6.8 Hz, *J* = 1.8 Hz, 1H), 6.93–6.84 (m, 2H), 6.82–6.76 (m, 1H), 6.72 (td, *J* = 7.5 Hz, *J* = 1.3 Hz, 1H), 6.69–6.59 (m, 2H), 6.17–6.07 (m, 2H), 4.47 (dt, *J* = 9.9 Hz, *J* = 2.0 Hz, 1H), 3.43 (dd, *J* = 11.4 Hz, *J* = 9.7 Hz, 1H), 2.98 (dd, *J* = 11.5 Hz, *J* = 1.7 Hz, 1H), 2.25–1.48 (m, 30H), 0.74–0.56 (m, 1H), 0.32 (d, *J* = 7.0 Hz, 3H), 0.03 (d, *J* = 6.8 Hz, 3H) ppm; HRMS (ESI): *m/z* calcd for $C_{58}H_{58}IrN_3OS_3Na$: 1124.3263 $[M+Na]^+$; found: 1124.3304.

Precatalyst Λ-T11. General procedure A5) was followed using **Λ-(*S*)-T11** (35.8 mg, 32.5 µmol) and imidazoquinoline ligand **233**; eluent for f. c.: CH_2Cl_2/MeOH 100:1 → 50:1; precatalyst **Λ-T11** was obtained as a greenish yellow crystalline solid (28.6 mg, 23.9 µmol, 74%). ^{1}H NMR (500 MHz, CD_2Cl_2): δ = 11.50 (s, 1H), 8.47 (dd, *J* = 8.3 Hz, *J* = 1.2 Hz, 1H), 8.19 (dd, *J* = 5.0 Hz, *J* = 1.3 Hz, 1H), 8.11 (d, *J* = 0.7 Hz, 1H), 8.03 (d, *J* = 9.0 Hz, 1H), 7.92 (d, *J* = 9.0 Hz, 1H), 7.85 (dd, *J* = 7.7 Hz, *J* = 0.9 Hz, 1H), 7.81 (dd, *J* = 7.7 Hz, *J* = 0.9 Hz, 1H), 7.78–7.72 (m, 2H), 7.61 (dd, *J* = 8.3 Hz, *J* = 5.0 Hz, 1H), 7.33 (dd, *J* = 8.5 Hz, *J* = 1.7 Hz, 1H), 7.30 (dd, *J* = 8.5 Hz, *J* = 1.7 Hz, 1H), 7.11 (td, *J* = 7.5 Hz, *J* = 1.0 Hz, 1H), 7.06 (td, *J* = 7.5 Hz, *J* = 1.0 Hz, 1H), 6.89 (td, *J* = 7.5 Hz, *J* = 1.5 Hz, 1H), 6.85 (td, *J* = 7.5 Hz, *J* = 1.3 Hz, 1H), 6.58 (d, *J* = 7.3 Hz, 1H), 6.54 (d, *J* = 1.7 Hz, 1H), 6.51 (d, *J* = 7.5 Hz, 1H), 6.25 (d, *J* = 1.7 Hz, 1H), 2.03–1.06 (m, 30H) ppm; ^{13}C NMR (125 MHz, CD_2Cl_2): δ = 181.8, 181.5, 152.7, 152.3, 150.6, 150.5, 150.4, 146.8, 143.9, 143.8, 142.1, 141.7, 141.6, 141.5, 138.6, 134.4, 134.3, 133.3, 132.1, 131.8, 128.9, 128.7, 126.6, 126.4, 126.3, 125.8, 124.1, 123.9, 123.8, 123.5, 123.4, 123.1, 122.9, 117.0, 115.3, 115.0, 43.4 (3C), 43.2 (3C), 36.9 (3C), 36.8 (3C), 36.5, 36.3, 29.1 (3C), 29.1 (3C) ppm; IR (film): $\tilde{\nu}$ = 2900, 1441, 839, 766, 732, 668, 554, 454 cm^{-1}; HRMS (ESI): *m/z* calcd for $C_{56}H_{51}IrN_5S_2$: 1050.3211 $[M–PF_6]^+$; found: 1050.3208.

4.7.2.12 Precatalyst Λ-T12

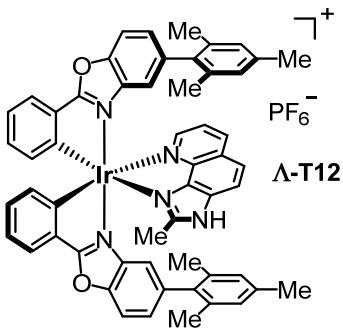

Precatalyst **Λ-T12** was prepared according to general procedure A5) from diastereomer **Λ-(*S*)-T1** (see 4.7.2.1; 25.0 mg, 24.1 µmol) and imidazoquinoline ligand **238**; eluent for f. c.: CH_2Cl_2/MeOH 100:1 → 50:1; precatalyst **Λ-T12** was obtained as a yellow crystalline solid (15.4 mg, 13.4 µmol, 56%). ^{1}H NMR (300 MHz, CD_2Cl_2): δ = 10.75 (s, 1H), 8.28 (dd, *J* = 8.4 Hz, *J* = 1.0 Hz, 1H), 8.06 (dd, *J* = 5.1 Hz, *J* = 1.1 Hz, 1H), 7.94–7.81 (m, 3H), 7.75 (d, *J* = 8.9 Hz, 1H), 7.68 (d, *J* = 8.5 Hz, 1H), 7.64 (d, *J* = 8.5 Hz, 1H), 7.35 (dd, *J* = 8.4 Hz, *J* = 5.0 Hz, 1H), 7.24–7.11 (m, 3H), 7.11–7.00 (m, 3H), 6.92 (s, 1H), 6.90–6.80 (m, 4H), 6.75 (s, 1H), 6.05 (d, *J* = 1.1 Hz, 1H), 5.12 (d, *J* = 1.1 Hz, 1H), 2.28 (s, 3H), 2.27 (s, 3H), 2.02 (s, 3H), 1.98 (s, 3H), 1.88 (s, 3H), 1.31 (s, 3H), 1.12 (s, 3H) ppm; ^{13}C NMR

(75 MHz, CD_2Cl_2): δ = 178.5, 178.3, 155.2, 151.6, 149.7, 149.7, 146.4, 144.6, 143.6, 141.8, 140.6, 140.0, 138.8, 138.6, 138.1, 137.9, 137.5, 137.5, 137.3, 135.8, 135.8, 135.7, 135.6, 134.5, 134.1, 133.7, 133.5, 133.1, 130.6, 130.5, 129.1 (2C), 128.7 (2C), 128.5, 128.1, 127.1, 127.1, 125.6, 124.6, 123.7, 123.6, 122.6, 116.7, 116.5, 115.9, 112.6, 112.4, 21.3, 21.3, 21.0, 21.0, 20.5, 20.4, 13.3 ppm; IR (film): $\tilde{\nu}$ = 1611, 1592, 1518, 1466, 1449, 1428, 1380, 1041, 843, 735, 705, 557 cm^{-1}; HRMS (ESI): *m/z* calcd for $C_{55}H_{45}Ir_1N_5O_2$: 1000.3201 $[M–PF_6]^+$; found: 1000.3239.

4.7.2.13 Precatalyst Λ-T13

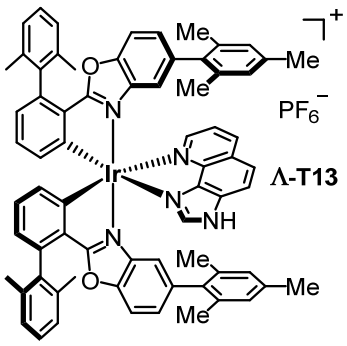

Precatalyst **Λ-T13** was prepared according to general procedures A1), A2), and A5) from benzoxazole ligand **196**, $IrCl_3 \cdot 3H_2O$, auxiliary ligand **(*S*)-Aux1**, and imidazoquinoline ligand **233**.

***Rac*-T13-dimer.** General procedure A1) was followed using benzoxazole ligand **196** (1.08 g, 2.59 mmol, 2.00 eq) and $IrCl_3 \cdot 3H_2O$ (457 mg, 1.30 mmol, 1.00 eq); reaction time: 45 h; Ir(III) dimer ***rac*-T13-dimer** was obtained as an orange solid (1.37 g, 646 µmol, 99%) which was employed in the next step without characterization.

Λ-(*S*)-T13. General procedure A2) was followed using ***rac*-T13-dimer** (500 mg, 236 µmol) and auxiliary ligand **(*S*)-Aux1**; the crude diastereomer mixture was adsorbed on silica gel (40 °C) and purified and resolved by f. c. with hexanes/EtOAc 30:1; only the Λ-(*S*)-diastereomer was isolated and characterized; diastereomer **Λ-(*S*)-T13** was obtained as an orange solid (86.3 mg, 69.3 µmol, 15%). ^{1}H NMR (500 MHz, CD_2Cl_2): δ = 7.57 (dd, *J* = 1.7 Hz, *J* = 0.6 Hz, 1H), 7.32–7.21 (m, 7H), 7.19–7.12 (m, 3H), 7.07 (ddd, *J* = 8.5 Hz, *J* = 1.6 Hz, *J* = 0.8 Hz, 2H), 6.97–6.86 (m, 5H), 6.80–6.75 (m, 2H), 6.64 (dd, *J* = 7.4 Hz, *J* = 1.0 Hz, 1H), 6.59 (dd, *J* = 7.3 Hz, *J* = 1.1 Hz, 1H), 6.56 (dd, *J* = 7.6 Hz, *J* = 1.0 Hz, 1H), 6.49 (dd, *J* = 8.6 Hz, *J* = 1.1 Hz, 1H), 6.44 (dd, *J* = 7.7 Hz, *J* = 0.9 Hz, 1H), 6.18 (ddd, *J* = 8.1 Hz, *J* = 6.8 Hz, *J* = 1.2 Hz, 1H), 4.90 (dt, *J* = 10.0 Hz, *J* = 2.5 Hz, 1H), 2.84 (dd, *J* = 11.6 Hz, *J* = 2.1 Hz, 1H), 2.77 (dd, *J* = 11.6 Hz, *J* = 9.8 Hz, 1H), 2.33 (s, 3H), 2.27 (s, 3H), 2.12 (s, 3H), 2.07 (s, 3H), 2.02 (s, 3H), 2.00 (s, 3H), 1.88 (s, 3H), 1.83 (s, 3H), 1.78 (s, 3H), 1.57 (s, 3H), 0.98–0.87 (m, 1H), 0.35 (d, *J* = 7.0 Hz, 3H), 0.15 (d, *J* = 7.0 Hz, 3H) ppm; HRMS (ESI): *m/z* calcd for $C_{72}H_{66}IrN_3O_3SNa$: 1268.4351 $[M+Na]^+$; found: 1268.4355.

Precatalyst Λ-T13. General procedure A5) was followed using **Λ-(*S*)-T13** (22.8 mg, 18.3 µmol) and imidazoquinoline ligand **233**; eluent for f. c.: CH_2Cl_2/MeOH 35:1; precatalyst **Λ-T13** was obtained as a greenish yellow solid (18.1 mg, 13.5 µmol, 74%). ^{1}H NMR (500 MHz, CD_2Cl_2): δ = 11.46 (s, 1H), 8.35 (dd, *J* = 8.4 Hz, *J* = 1.1 Hz, 1H), 8.19 (dd,

J = 5.0 Hz, *J* = 1.2 Hz, 1H), 8.02–7.97 (m, 2H), 7.86 (d, *J* = 8.8 Hz, 1H), 7.43 (dd, *J* = 8.3 Hz, *J* = 5.0 Hz, 1H), 7.33–7.15 (m, 8H), 7.10 (t, *J* = 7.6 Hz, 1H), 7.06 (t, *J* = 7.6 Hz, 1H), 6.99 (dd, *J* = 8.4 Hz, *J* = 1.7 Hz, 1H), 6.93 (dd, *J* = 7.5 Hz, *J* = 1.1 Hz, 1H), 6.91 (dd, *J* = 8.5 Hz, *J* = 1.6 Hz, 1H), 6.90–6.86 (m, 2H), 6.84–6.79 (m, 4H), 6.72 (s, 1H), 6.00 (d, *J* = 1.1 Hz, 1H), 5.20 (d, *J* = 1.1 Hz, 1H), 2.26 (s, 3H), 2.25 (s, 3H), 2.09 (s, 3H), 2.07 (s, 3H), 2.06 (s, 3H), 2.04 (s, 3H), 1.94 (s, 3H), 1.84 (s, 3H), 1.14 (s, 3H), 1.03 (s, 3H) ppm; ^{13}C NMR (125 MHz, CD_2Cl_2): δ = 178.3, 178.2, 151.2, 149.5, 149.4, 148.3, 145.5, 144.0, 142.4 (2C), 142.2, 141.5, 140.1, 139.7, 139.7, 139.7, 138.9, 138.0, 137.8, 137.7, 137.4 (2C), 137.3, 136.7, 136.6, 136.4, 136.1, 135.9, 135.7, 135.6, 135.4, 133.2, 133.2, 133.1, 132.8, 132.8, 129.1, 128.9, 128.6, 128.6, 128.5, 128.5, 128.3, 128.1, 128.1, 127.9, 127.9, 127.8, 127.7, 127.6, 125.9, 125.7, 125.3, 125.2, 123.0, 117.3, 116.5, 115.6, 112.4, 112.0, 21.3, 21.2, 21.2, 21.1, 21.1, 21.1 (2C), 21.0, 20.3, 20.2 ppm; IR (film): $\tilde{\nu}$ = 1569, 1464, 1439, 1412, 841, 771, 708, 556 cm^{-1}; HRMS (ESI): *m/z* calcd for $C_{70}H_{59}IrN_5O_2$: 1194.4299 [*M*–PF_6]$^+$; found: 1194.4314.

4.7.2.14 Precatalyst Λ-T14

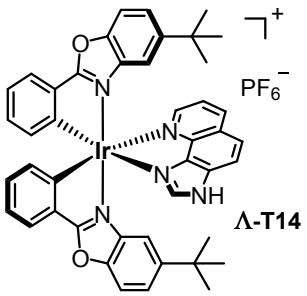

General procedure A5) was followed using diastereomer **Λ-(*S*)-T14**[69] (obtained from former PhD student Haohua Huo; 36.1 mg, 39.5 µmol, 1.00 eq; contained **(*S*)-Aux1** as coordinating auxiliary ligand) and imidazoquinoline ligand **233**; eluent for f. c.: CH_2Cl_2/MeOH 100:1; precatalyst **Λ-T14** was obtained as a greenish yellow crystalline solid (30.1 mg, 29.9 µmol, 76%). ^{1}H NMR (500 MHz, CD_2Cl_2): δ = 11.46 (s, 1H), 8.54 (dd, *J* = 8.2 Hz, *J* = 1.1 Hz, 1H), 8.27 (dd, *J* = 5.1 Hz, *J* = 1.2 Hz, 1H), 8.18 (d, *J* = 1.0 Hz, 1H), 8.07 (d, *J* = 9.0 Hz, 1H), 7.96 (d, *J* = 9.0 Hz, 1H), 7.82 (ddd, *J* = 7.6 Hz, *J* = 7.0 Hz, *J* = 1.0 Hz, 2H), 7.63 (dd, *J* = 8.4 Hz, *J* = 5.0 Hz, 1H), 7.54 (d, *J* = 5.3 Hz, 1H), 7.52 (d, *J* = 5.3 Hz, 1H), 7.38 (dd, *J* = 8.8 Hz, *J* = 1.9 Hz, 1H), 7.34 (dd, *J* = 8.8 Hz, *J* = 1.9 Hz, 1H), 7.16 (td, *J* = 7.5 Hz, *J* = 1.0 Hz, 1H), 7.11 (td, *J* = 7.5 Hz, *J* = 1.0 Hz, 1H), 7.04 (td, *J* = 7.5 Hz, *J* = 1.4 Hz, 1H), 6.99 (td, *J* = 7.5 Hz, *J* = 1.3 Hz, 1H), 6.79 (d, *J* = 7.6 Hz, 1H), 6.76 (d, *J* = 7.6 Hz, 1H), 6.05 (d, *J* = 1.7 Hz, 1H), 5.59 (d, *J* = 1.7 Hz, 1H), 1.04 (s, 9H), 0.87 (s, 9H) ppm; ^{13}C NMR (125 MHz, CD_2Cl_2): δ = 178.1, 178.0, 151.9, 151.1, 150.5, 148.8, 148.7, 145.9, 144.2, 143.3, 142.9, 141.9, 139.1, 138.1, 138.1, 134.3, 134.0, 133.3, 133.1, 132.9, 130.6, 130.5, 126.8, 126.6, 126.1, 125.9, 124.3, 124.0, 123.4 (2C), 123.4, 117.1, 111.9 (2C), 111.7, 111.5, 35.3, 35.2, 31.6 (3C), 31.5 (3C) ppm; IR (film): $\tilde{\nu}$ = 1594, 1444, 1384, 842, 737, 558 cm^{-1}; HRMS (ESI): *m/z* calcd for $C_{44}H_{39}IrN_5O_2$: 862.2730 [*M*–PF_6]$^+$; found: 862.2734.

4.7.2.15 Precatalyst Λ-T15

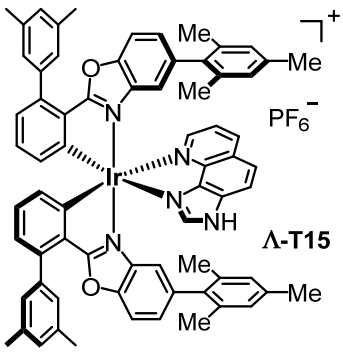

Precatalst **Λ-T15** was prepared according to general procedures A4) and A5) from diastereomer **Λ-(*S*)-T15-CC** (obtained from PhD student Thomas Mietke; contained **(*S*)-Aux1** as coordinating auxiliary ligand), 2,4,6-trimethylphenylboronic acid, and imidazoquinoline ligand **233**.

Λ-(*S*)-T15. General procedure A4) was followed using **Λ-(*S*)-T15-CC** (80.8 mg, 61.9 µmol) and 2,4,6-trimethylphenylboronic acid; reaction time: 8 h; the crude diastereomer mixture was purified by f. c. (CH_2Cl_2/hexanes 1:1 → 2:1); **Λ-(*S*)-T15** was obtained as an orange solid (56.4 mg, 45.3 µmol, 73%). ^{1}H NMR (300 MHz, CD_2Cl_2): δ = 7.76–7.72 (m, 1H), 7.43 (d, J = 8.5 Hz, 1H), 7.39 (d, J = 8.3 Hz, 1H), 7.31 (dd, J = 8.1 Hz, J = 1.7 Hz, 1H), 7.24 (d, J = 0.9 Hz, 1H), 7.19–7.05 (m, 8H), 7.04–6.85 (m, 6H), 6.85–6.73 (m, 3H), 6.63 (dd, J = 7.3 Hz, J = 1.4 Hz, 1H), 6.59 (dd, J = 7.5 Hz, J = 1.4 Hz, 1H), 6.56 (dd, J = 8.7 Hz, J = 1.1 Hz, 1H), 6.22 (ddd, J = 8.1 Hz, J = 6.8 Hz, J = 1.3 Hz, 1H), 4.71–4.60 (m, 1H), 2.83–2.60 (m, 2H), 2.45 (s, 6H), 2.39 (s, 6H), 2.33 (s, 3H), 2.28 (s, 3H), 2.03 (s, 3H), 2.00 (s, 3H), 1.95 (s, 3H), 1.54 (s, 3H), 0.85–0.69 (m, 1H), 0.31 (d, J = 7.0 Hz, 3H), 0.17 (d, J = 7.0 Hz, 3H) ppm; ^{13}C NMR (125 MHz, CD_2Cl_2): δ = 178.8, 178.4, 169.2, 167.8, 153.5, 152.6, 149.4, 149.3, 144.0, 143.5, 140.9, 140.7, 140.1, 139.8, 138.9, 138.8, 138.4, 138.2, 137.9 (2C), 137.7 (2C), 137.4, 137.1, 136.8, 136.5, 136.1, 135.9, 134.1, 133.8, 133.7, 131.5, 131.5, 131.2, 130.9, 129.7, 129.6, 129.3, 129.0, 128.7, 128.6, 128.6, 128.5, 128.4, 127.8, 127.5, 126.8, 125.2, 124.3, 124.0, 119.8, 118.5, 116.9, 113.5, 112.1, 111.2, 85.0, 39.4, 32.3, 27.8, 21.8, 21.7, 21.4, 21.3 (2C), 21.3, 21.1, 20.6, 19.4, 14.5, 14.4, 11.4 ppm; IR (film): $\tilde{\nu}$ = 2956, 2921, 1603, 1561, 1523, 1464, 1438, 1402, 1355, 1265, 1011, 850, 816, 791, 743, 710 cm^{-1}; HRMS (ESI): *m/z* calcd for $C_{72}H_{66}Ir_1N_3O_3S_1Na$: 1268.4351 [*M*+Na]$^+$, found: 1268.4344.

Precatalyst Λ-T15. General procedure A5) was followed using **Λ-(*S*)-T15** (42.8 mg, 34.4 µmol) and imidazoquinoline ligand **233**; eluent for f. c.: CH_2Cl_2/MeOH 50:1; precatalyst **Λ-T15** was obtained as a greenish yellow solid (40.9 mg, 30.5 µmol, 89%). ^{1}H NMR (500 MHz, CD_2Cl_2): δ = 11.30 (s, 1H), 8.35 (dd, J = 8.3 Hz, J = 0.9 Hz, 1H), 8.19 (dd, J = 5.0 Hz, J = 1.0 Hz, 1H), 8.07 (s, 1H), 8.00 (d, J = 8.9 Hz, 1H), 7.87 (d, J = 9.0 Hz, 1H), 7.46 (dd, J = 8.3 Hz, J = 5.0 Hz, 1H), 7.34 (d, J = 9.0 Hz, 1H), 7.32 (d, J = 8.7 Hz, 1H), 7.19–7.12 (m, 6H), 7.10–7.00 (m, 5H), 6.95 (dd, J = 8.4 Hz, J = 1.5 Hz, 1H), 6.90 (s, 1H), 6.86 (dd, J = 4.9 Hz, J = 3.8 Hz, 1H), 6.84–6.80 (m, 3H), 6.73 (s, 1H), 6.04 (d, J = 1.1 Hz, 1H), 5.14 (d, J = 1.1 Hz, 1H), 2.42 (s, 6H), 2.42 (s, 6H), 2.27 (s, 3H), 2.26 (s, 3H), 1.96 (s, 3H), 1.84 (s, 3H), 1.17 (s, 3H), 1.06 (s, 3H) ppm; ^{13}C NMR (125 MHz, CD_2Cl_2): δ = 178.3, 178.2, 151.6,

149.3, 149.2, 148.4, 145.6, 144.4, 144.2, 143.9, 142.6, 141.5, 140.1, 140.1, 140.0, 139.7, 138.8, 138.1 (2C), 138.0 (2C), 137.8, 137.7, 137.4, 137.4, 137.3, 135.9, 135.7, 135.7, 135.3, 133.3, 133.1, 133.0, 132.6, 132.2, 130.0, 129.9, 129.0, 129.0, 128.6, 128.5, 128.3, 127.8 (3C), 127.8 (3C), 127.7, 127.7, 126.4, 126.3, 125.9, 125.7, 123.2, 117.2, 116.6, 115.6, 112.3, 112.0, 21.7 (2C), 21.7 (2C), 21.3, 21.2, 21.1, 21.0, 20.3, 20.3 ppm; IR (film): $\tilde{\nu}$ = 1567, 1466, 1436, 1407, 1266, 844, 710, 557 cm^{-1}; HRMS (ESI): *m/z* calcd for $C_{70}H_{59}Ir_1N_5O_2$: 1194.4299 $[M-PF_6]^+$; found: 1194.4302.

4.7.2.16 Precatalyst Λ-T16

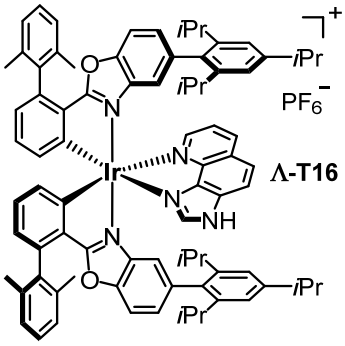

General procedure A5) was followed using diastereomer **Λ-(*S*)-T18** (see 4.7.2.18; 15.3 mg, 10.8 µmol) and imidazoquinoline ligand **233**; eluent for f. c.: CH_2Cl_2/MeOH 100:1; precatalyst **Λ-T16** was obtained as a greenish yellow crystalline solid (13.8 mg, 9.15 µmol, 85%). ^{1}H NMR (500 MHz, CD_2Cl_2): δ = 11.31 (s, 1H), 8.26 (dd, *J* = 8.4 Hz, *J* = 0.9 Hz, 1H), 8.06 (dd, *J* = 4.9 Hz, *J* = 1.0 Hz, 1H), 7.92 (s, 1H), 7.89 (d, *J* = 8.9 Hz, 1H), 7.74 (d, *J* = 8.9 Hz, 1H), 7.35 (dd, *J* = 8.4 Hz, *J* = 5.1 Hz, 1H), 7.33–7.26 (m, 2H), 7.26–7.16 (m, 6H), 7.10 (t, *J* = 7.6 Hz, 1H), 7.05 (t, *J* = 7.5 Hz, 1H), 7.03–6.99 (m, 2H), 6.96–6.91 (m, 3H), 6.91–6.86 (m, 2H), 6.84–6.76 (m, 3H), 6.13 (d, *J* = 1.0 Hz, 1H), 5.30 (d, *J* = 1.0 Hz, 1H), 2.95–2.81 (m, 2H), 2.35 (sept, *J* = 6.8 Hz, 1H), 2.25 (sept, *J* = 6.9 Hz, 1H), 2.10–2.01 (m, 12H), 1.80–1.66 (m, 2H), 1.29–1.21 (m, 12H), 1.09 (d, *J* = 6.8 Hz, 3H), 1.03 (d, *J* = 6.8 Hz, 3H), 1.01 (d, *J* = 6.8 Hz, 3H), 0.92 (d, *J* = 7.0 Hz, 3H), 0.76 (d, *J* = 7.0 Hz, 3H), 0.74 (d, *J* = 7.0 Hz, 3H), 0.15 (d, *J* = 6.8 Hz, 3H), 0.06 (d, *J* = 6.8 Hz, 3H) ppm; ^{13}C NMR (125 MHz, CD_2Cl_2): δ = 178.3, 178.2, 150.9, 149.6, 149.5 (2C), 149.1, 148.5, 146.9, 146.8, 146.6, 146.3, 145.4, 143.9, 142.4, 142.2, 142.0, 141.3, 140.2, 139.8, 139.7, 139.6, 138.9, 137.8, 137.5, 136.7, 136.5, 136.4, 136.0, 135.7, 135.5, 133.2 133.2, 133.2, 132.8, 132.8, 128.6, 128.3, 128.2, 128.1, 128.0, 127.9, 127.8, 127.7 (2C), 126.0, 125.8, 125.4, 125.3, 122.8, 121.2, 121.1, 120.8, 120.7, 117.3, 116.7, 115.9, 112.1, 111.7, 34.9, 34.8, 30.9, 30.8, 30.5, 30.3, 25.1, 24.9, 24.4 (2C), 24.3 (2C), 24.3, 24.0, 23.9, 23.7, 23.4, 23.3, 21.2, 21.1, 21.1 (2C) ppm (one overlapping signal could not be located); IR (film): $\tilde{\nu}$ = 2960, 1570, 1460, 1414, 845 cm^{-1}; HRMS (ESI): *m/z* calcd for $C_{82}H_{83}IrN_5O_2$: 1362.6179 $[M–PF_6]^+$; found: 1362.6134.

4.7.2.17 Precatalyst Λ-T17

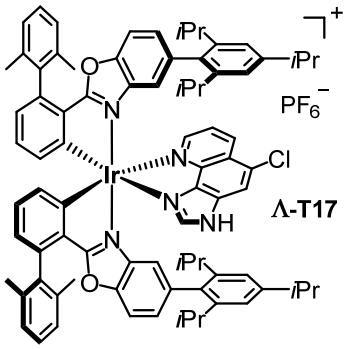

General procedure A5) was followed using diastereomer **Λ-(*S*)-T18** (see 4.7.2.18; 15.1 mg, 10.7 µmol) and imidazoquinoline ligand **255**; eluent for f. c.: CH_2Cl_2/MeOH 100:1; precatalyst **Λ-T17** was obtained as a yellow-green crystalline solid (8.7 mg, 5.6 µmol, 53%). ^{1}H NMR (500 MHz, CD_2Cl_2): δ = 11.03 (s, 1H), 8.52 (dd, J = 8.5 Hz, J = 1.0 Hz, 1H), 8.10 (dd, J = 5.0 Hz, J = 1.0 Hz, 1H), 8.02 (s, 1H), 7.90 (s, 1H), 7.43 (dd, J = 8.6 Hz, J = 5.0 Hz, 1H), 7.32–7.26 (m, 2H), 7.25–7.16 (m, 6H), 7.10 (t, J = 7.6 Hz, 1H), 7.05 (t, J = 7.6 Hz, 1H), 7.04–6.99 (m, 2H), 6.97–6.91 (m, 3H), 6.90 (d, J = 1.5 Hz, 1H), 6.88 (dd, J = 7.5 Hz, J = 1.0 Hz, 1H), 6.84 (d, J = 1.6 Hz, 1H), 6.81 (dd, J = 7.7 Hz, J = 0.9 Hz, 1H), 6.77 (dd, J = 7.6 Hz, J = 0.9 Hz, 1H), 6.09 (d, J = 1.1 Hz, 1H), 5.27 (d, J = 1.0 Hz, 1H), 2.93–2.82 (m, 2H), 2.34 (sept, J = 6.9 Hz, 1H), 2.24 (sept, J = 6.9 Hz, 1H), 2.07 (s, 3H), 2.05 (s, 6H), 2.96 (s, 3H), 1.80–1.70 (m, 2H), 1.25 (d, J = 7.0 Hz, 6H), 1.25 (d, J = 6.9 Hz, 6H), 1.08 (d, J = 6.9 Hz, 3H), 1.04 (d, J = 6.9 Hz, 3H), 1.00 (d, J = 6.9 Hz, 3H), 0.91 (d, J = 6.9 Hz, 3H), 0.78 (d, J = 6.9 Hz, 3H), 0.76 (d, J = 6.9 Hz, 3H), 0.19 (d, J = 6.9 Hz, 3H), 0.07 (d, J = 6.9 Hz, 3H) ppm; ^{13}C NMR (125 MHz, CD_2Cl_2): δ = 178.3, 178.2, 151.5, 149.5, 149.4 (2C), 149.2, 148.4, 146.9, 146.8, 146.6, 146.3, 145.1, 143.8, 143.1, 142.5, 142.2, 140.6, 140.2, 139.8, 139.6, 139.6, 137.7, 137.5, 136.7, 136.6 (2C), 136.5, 136.4, 135.9, 135.6, 135.5, 133.3, 133.1, 132.8 (2C), 129.6, 128.5, 128.4, 128.3, 128.2, 128.1, 128.0, 127.9, 127.8, 127.7 (2C), 125.4, 125.4, 124.3, 123.2, 121.2, 121.1, 120.8 (2C), 117.4, 116.6, 115.8, 112.1, 111.8, 34.8 (2C), 30.9, 30.8, 30.5, 30.4, 25.1, 24.9, 24.4, 24.3 (2C), 24.3, 24.1, 23.9, 23.9, 23.7, 23.3, 23.2, 21.2, 21.1, 21.1, 21.1 ppm; IR (film): $\tilde{\nu}$ = 2959, 2926, 1572, 1464, 1444, 1413, 1261, 845, 772, 558 cm^{-1}; HRMS (ESI): *m/z* calcd for $C_{82}H_{82}Cl_1Ir_1N_5O_2$: 1396.5784 $[M–PF_6]^+$; found: 1396.6061.

4.7.2.18 Precatalysts *rac*-, Λ-, and Δ-T18, Catalysts *rac*-, Λ-, and Δ-T18', and Bisacetonitrile Intermediates Λ- and Δ-T18-(MeCN)$_2$

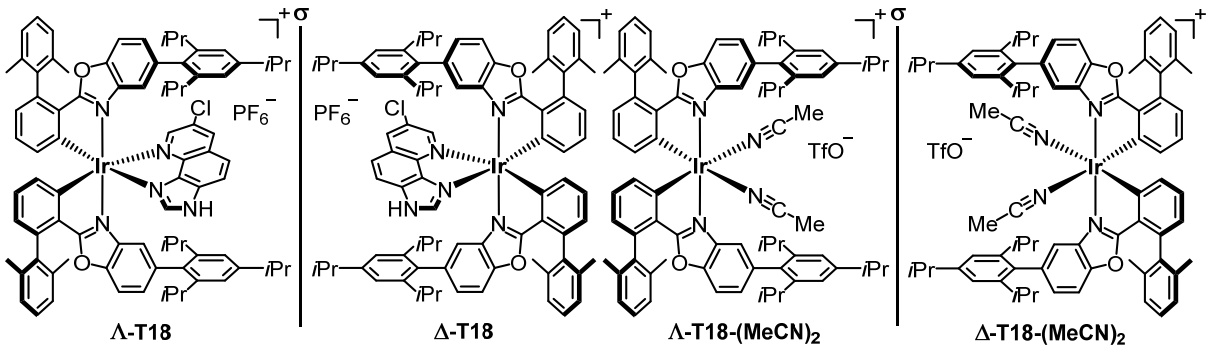

Precatalysts **Λ-** and **Δ-T18** as well as bisacetonitrile intermediates **Λ-** and **Δ-T18-(MeCN)$_2$** were prepared according to general procedures A1), A2), and A5) from benzoxazole ligand **195**, $IrCl_3 \cdot 3H_2O$, auxiliary ligand **(*S*)-Aux2**, and imidazoquinoline ligand **236** (ligand **236** is not required for the synthesis of **Λ/Δ-T18-(MeCN)$_2$**).

***Rac*-T18-dimer.** General procedure A1) was followed using $IrCl_3 \cdot 3H_2O$ (531 mg, 1.51 mmol, 1.00 eq) and benzoxazole ligand **195** (1.50 g, 2.99 mmol, 1.99 eq); reaction time: 35 h; Ir(III) dimer ***rac*-T18-dimer** was obtained as a red-orange solid (1.85 g, 753 µmol, quantitative). ^{1}H NMR and ^{13}C NMR: NMR characterization unfeasible due to complex spectra; IR (film): $\tilde{\nu}$ = 2959, 2927, 2029, 1569, 1458, 1413, 1413, 1358, 1101, 817, 770, 710 cm^{-1}; HRMS (ESI): *m/z* calcd for $C_{144}H_{152}Cl_1Ir_2N_4O_4$: 2422.0772 [*M*–Cl]$^+$; found: 2422.0791; XRD: X-ray quality crystals of ***rac*-T18-dimer** were obtained by slow diffusion of MeOH into a concentrated acetone solution of ***rac*-T18-dimer** at rt (vapor diffusion technique). Crystal structure and crystallographic data are provided in the crystallographic section.

Diastereomers Λ-(*S*)-T18 and Δ-(*S*)-T18. General procedure A2) was followed using iridium(III) dimer ***rac*-T18-dimer** (203 mg, 82.6 µmol, 1.00 eq) and auxiliary ligand **(*S*)-Aux2**; the obtained crude diastereomer mixture was purified and resolved by f. c. with hexanes/ CH_2Cl_2 2:1 → 1:1 → 1:2. After solvent removal and drying *in vacuo*, both diastereomers **Λ-(*S*)-T18** (first eluting) and **Δ-(*S*)-T18** (second eluting) were obtained as orange solids (**Λ-(*S*)-T18**: 52.7 mg, 37.3 µmol, 23%; **Δ-(*S*)-T18**: 96.5 mg, 68.3 µmol, 41%; combined yield: 64%).

Analytical data for **Λ-(*S*)-T18**: ^{1}H NMR (500 MHz, CD_2Cl_2): δ = 7.90 (d, J = 1.4 Hz, 1H), 7.39 (d, J = 1.1 Hz, 1H), 7.36 (dd, J = 8.2 Hz, J = 1.9 Hz, 1H), 7.33 (d, J = 8.4 Hz, 1H), 7.28 (d, J = 7.5 Hz, 1H), 7.25–7.18 (m, 4H), 7.17–7.08 (m, 6H), 7.05 (d, J = 1.7 Hz, 1H), 6.95 (d, J = 1.7 Hz, 1H), 6.91–6.84 (m, 2H), 6.76 (d, J = 2.9 Hz, 1H), 6.75 (s, 1H), 6.64 (dd, J = 7.4 Hz, J = 0.9 Hz, 1H), 6.61 (dd, J = 5.7 Hz, J = 2.8 Hz, 1H), 6.35 (dd, J = 8.6 Hz,

J = 1.0 Hz, 1H), 6.27 (dd, *J* = 7.8 Hz, *J* = 1.0 Hz, 1H), 6.05 (ddd, *J* = 8.1 Hz, *J* = 6.9 Hz, *J* = 1.1 Hz, 1H), 4.21 (dd, *J* = 9.7 Hz, *J* = 2.7 Hz, 1H), 3.91 (t, *J* = 9.1 Hz, 1H), 3.73 (dd, *J* = 8.5 Hz, *J* = 2.7 Hz, 1H), 2.98 (sept, *J* = 6.9 Hz, 1H), 2.90 (sept, *J* = 6.9 Hz, 1H), 2.68 (sept, *J* = 6.9 Hz, 1H), 2.65 (sept, *J* = 6.9 Hz, 1H), 2.55 (sept, *J* = 6.9 Hz, 1H), 2.48 (sept, *J* = 6.9 Hz, 1H), 2.12 (s, 3H), 2.01 (s, 3H), 1.91 (s, 3H), 1.88 (s, 3H), 1.33 (d, *J* = 7.0 Hz, 3H), 1.33 (d, *J* = 6.9 Hz, 3H), 1.27 (d, *J* = 6.9 Hz, 3H), 1.27 (d, *J* = 6.9 Hz, 3H), 1.23 (d, *J* = 6.8 Hz, 3H), 1.16–1.09 (m, 9H), 1.04 (d, *J* = 6.8 Hz, 3H), 1.02 (d, *J* = 6.9 Hz, 3H), 0.96 (d, *J* = 6.9 Hz, 3H), 0.68 (d, *J* = 6.8 Hz, 3H), 0.31 (s, 9H) ppm; ^{13}C NMR (125 MHz, CD_2Cl_2): δ = 179.2 (C_q), 178.3 (C_q), 173.1 (C_q), 167.4 (C_q), 152.9 (C_q), 151.7 (C_q), 149.8 (C_q), 149.3 (C_q), 149.2 (C_q), 148.7 (C_q), 147.3 (3C; C_q), 147.0 (C_q), 141.7 (C_q), 141.2 (C_q), 140.6 (C_q), 140.5 (C_q), 139.2 (C_q), 139.1 (C_q), 138.9 (C_q), 138.8 (C_q), 137.4 (C_q), 136.9 (C_q), 136.7 (C_q), 136.5 (C_q), 136.4 (C_q), 136.2 (C_q), 134.6 (CH_{arom}), 133.8 (CH_{arom}), 131.5 (CH_{arom}), 130.8 (CH_{arom}), 130.7 (CH_{arom}), 130.6 (CH_{arom}), 130.5 (C_q), 129.5 (C_q), 127.8 (CH_{arom}), 127.6 (2C; CH_{arom}), 127.6 (CH_{arom}), 127.6 (CH_{arom}), 127.4 (2C; CH_{arom}), 127.0 (CH_{arom}), 124.2 (CH_{arom}), 123.8 (CH_{arom}), 122.6 (CH_{arom}), 121.2 (CH_{arom}), 121.1 (3C; CH_{arom}), 120.2 (CH_{arom}), 116.7 (CH_{arom}), 112.5 (CH_{arom}), 112.1 (C_q), 111.5 (CH_{arom}), 110.8 (CH_{arom}), 76.3 (*C*H(Me)$_3$), 68.4 (S(*C*H$_2$)), 35.4 (*C*(Me)$_3$), 35.0 (*C*H(Me)$_2$), 34.9 (*C*H(Me)$_2$), 31.0 (*C*H(Me)$_2$), 30.9 (*C*H(Me)$_2$), 30.9 (*C*H(Me)$_2$), 30.6 (*C*H(Me)$_2$), 25.9 (3C; C(*C*H$_3$)$_3$), 25.2 (CH$_3$), 24.8 (CH$_3$), 24.8 (CH$_3$), 24.6 (CH$_3$), 24.5 (2C; CH$_3$), 24.4 (2C; CH$_3$), 24.4 (CH$_3$), 24.3 (CH$_3$), 24.2 (CH$_3$), 23.8 (CH$_3$), 21.2 (CH$_3$), 21.2 (CH$_3$), 21.0 (CH$_3$), 20.9 (CH$_3$) ppm; IR (film): $\tilde{\nu}$ = 2960, 2927, 1607, 1573, 1465, 1409, 1357, 771 cm^{-1}; HRMS (ESI): *m/z* calcd for $C_{85}H_{92}IrN_3O_4Na$: 1434.6618 [*M*+Na]$^+$; found: 1434.6668; CD (MeOH, 0.20 mM): λ, nm (Δε, M^{-1}·cm^{-1}) 472 (−7), 446 (−8), 368 (+44), 344 (+34), 333 (+43), 309 (−43), 299 (−47), 249 (+11), 220 (−40), 212 (+6).

Analytical data for **Δ-(*S*)-T18**: ^{1}H NMR (500 MHz, CD_2Cl_2): δ = 7.49 (d, *J* = 1.1 Hz, 1H), 7.44 (d, *J* = 1.1 Hz, 1H), 7.34–7.26 (m, 3H), 7.25–7.18 (m, 6H), 7.09 (dd, *J* = 8.5 Hz, *J* = 1.7 Hz, 1H), 7.05 (dd, *J* = 8.4 Hz, *J* = 1.5 Hz, 1H), 7.01 (d, *J* = 1.6 Hz, 1H), 6.99 (d, *J* = 1.5 Hz, 1H), 6.97 (d, *J* = 1.6 Hz, 1H), 6.92 (d, *J* = 1.6 Hz, 1H), 6.90–6.83 (m, 2H), 6.74 (t, *J* = 7.6 Hz, 1H), 6.69 (dd, *J* = 7.4 Hz, *J* = 1.0 Hz, 1H), 6.64–6.59 (m, 2H), 6.56 (dd, *J* = 7.7 Hz, *J* = 1.0 Hz, 1H), 6.40 (dd, *J* = 8.5 Hz, *J* = 0.7 Hz, 1H), 6.15 (ddd, *J* = 7.8 Hz, *J* = 7.0 Hz, *J* = 0.9 Hz, 1H), 4.26 (dd, *J* = 8.9 Hz, *J* = 1.8 Hz, 1H), 3.09 (t, *J* = 8.7 Hz, 1H), 2.96–2.82 (m, 3H), 2.52 (sept, *J* = 6.8 Hz, 1H), 2.42 (sept, *J* = 6.8 Hz, 1H), 2.37 (sept, *J* = 6.9 Hz, 1H), 2.19 (s, 3H), 2.17 (sept, *J* = 6.9 Hz, 1H), 2.14 (s, 3H), 1.98 (s, 3H), 1.98 (s, 3H), 1.28–1.23 (m, 12H), 1.10–1.05 (m, 6H), 1.03 (d, *J* = 6.9 Hz, 3H), 0.99 (d, *J* = 6.8 Hz, 3H), 0.88–0.83 (m, 9H), 0.82 (d, *J* = 6.8 Hz, 3H), 0.52 (s, 9H) ppm; ^{13}C NMR (125 MHz,

CD_2Cl_2): δ = 180.0 (C_q), 179.3 (C_q), 171.5 (C_q), 167.4 (C_q), 155.2 (C_q), 151.2 (C_q), 149.6 (C_q), 149.2 (C_q), 148.8 (C_q), 148.8 (C_q), 147.2 (C_q), 147.2 (C_q), 147.0 (C_q), 146.8 (C_q), 141.8 (C_q), 141.3 (C_q), 140.7 (C_q), 140.7 (C_q), 139.6 (C_q), 138.9 (C_q), 138.7 (C_q), 138.4 (C_q), 137.0 (C_q), 136.9 (C_q), 136.8 (C_q), 136.6 (C_q), 136.4 (C_q), 136.1 (C_q), 135.8 (CH_{arom}), 133.2 (CH_{arom}), 131.9 (CH_{arom}), 131.5 (CH_{arom}), 131.1 (CH_{arom}), 129.6 (CH_{arom}), 128.9 (C_q), 128.2 (CH_{arom}), 128.0 (C_q), 127.8 (CH_{arom}), 127.8 (CH_{arom}), 127.4 (CH_{arom}), 127.6 (2C; CH_{arom}), 127.5 (CH_{arom}), 127.5 (CH_{arom}), 123.5 (CH_{arom}), 123.3 (CH_{arom}), 122.3 (CH_{arom}), 121.2 (CH_{arom}), 120.9 (CH_{arom}), 120.7 (CH_{arom}), 120.6 (CH_{arom}), 118.4 (CH_{arom}), 118.4 (CH_{arom}), 113.5 (C_q), 112.8 (CH_{arom}), 110.9 (CH_{arom}), 110.8 (CH_{arom}), 73.0 (*C*H(Me)$_3$), 70.9 (S(*C*H$_2$)), 35.2 (*C*(Me)$_3$), 34.9 (*C*H(Me)$_2$), 34.8 (*C*H(Me)$_2$), 30.9 (*C*H(Me)$_2$), 30.7 (*C*H(Me)$_2$), 30.5 (*C*H(Me)$_2$), 30.5 (*C*H(Me)$_2$), 26.6 (3C; C(*C*H$_3$)$_3$), 25.6 (CH_3), 25.2 (CH_3), 24.9 (CH_3), 24.7 (CH_3), 24.5 (CH_3), 24.4 (CH_3), 24.4 (CH_3), 24.4 (CH_3), 24.3 (CH_3), 24.2 (CH_3), 23.9 (CH_3), 23.7 (CH_3), 21.6 (CH_3), 21.5 (CH_3), 21.1 (CH_3), 20.9 (CH_3) ppm; IR (film): $\tilde{\nu}$ = 2960, 2928, 1610, 1572, 1465, 1409, 1356, 771 cm^{-1}; HRMS (ESI): *m/z* calcd for $C_{85}H_{92}IrN_3O_4Na$: 1434.6618 [*M*+Na]$^+$; found: 1434.6674; CD (MeOH, 0.20 mM): λ, nm (Δε, $M^{-1}\cdot cm^{-1}$) 465 (+15), 455 (+15), 368 (−17), 345 (−12), 332 (−16), 286 (+33), 251 (−26), 222 (+20), 215 (+1).

Precatalyst Λ-T18 and Bisacetonitrile intermediate Λ-T18-(MeCN)$_2$.

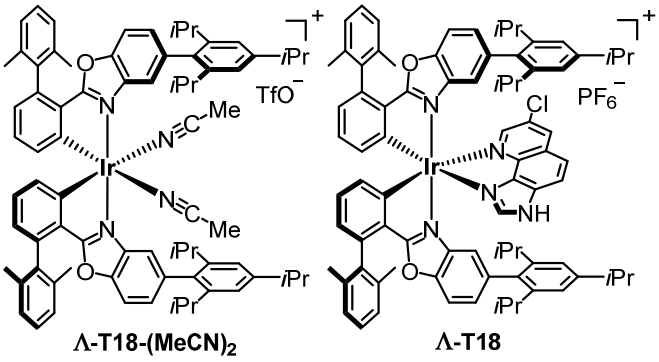

General procedure A5) was followed using **Λ-(*S*)-T18** (83.2 mg, 58.9 µmol, 1.00 eq) and imidazoquinoline ligand **236**; intermediate bisacetonitrile complex **Λ-T18-(MeCN)$_2$** was isolated and fully characterized; eluent for final f. c.: CH_2Cl_2/MeOH 100:1; precatalyst **Λ-T18** was obtained as a greenish yellow crystalline solid (78.8 mg, 51.1 µmol, 87%).

Precatalyst Δ-T18 and Bisacetonitrile intermediate Δ-T18-(MeCN)$_2$.

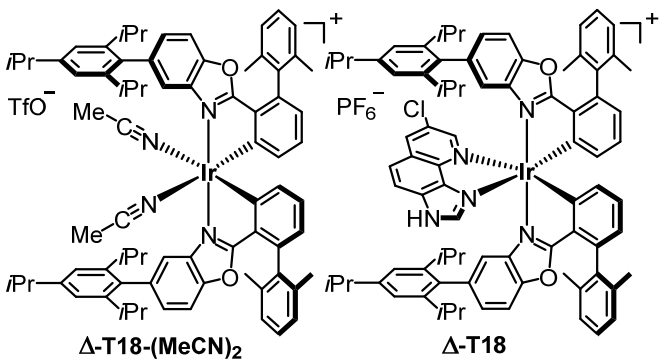

General procedure A5) was followed using **Δ-(*S*)-T18** (90.5 mg, 64.1 µmol, 1.00 eq) and imidazoquinoline ligand **236**; intermediate bisacetonitrile complex **Δ-T18-(MeCN)$_2$** was isolated and fully characterized; eluent for final f. c.: CH_2Cl_2/MeOH 100:1; precatalyst **Δ-T18** was obtained as a greenish yellow crystalline solid (81.8 mg, 53.0 µmol, 83%).

I.) Analytical data for precatalyst **Λ/Δ-T18**: ^{1}H NMR (500 MHz, CD_2Cl_2): δ = 11.38 (s, 1H), 8.23 (d, J = 1.9 Hz, 1H), 7.97 (s, 1H), 7.94 (d, J = 7.7 Hz, 1H), 7.93 (s, 1H), 7.68 (d, J = 8.9 Hz, 1H), 7.33–7.27 (m, 2H), 7.27–7.16 (m, 6H), 7.13 (t, J = 7.6 Hz, 1H), 7.08–7.01 (m, 3H), 6.99 (dd, J = 8.4 Hz, J = 1.6 Hz, 1H), 6.98–6.94 (m, 2H), 6.92–6.88 (m, 2H), 6.86 (dd, J = 7.6 Hz, J = 1.0 Hz, 1H), 6.84 (d, J = 1.6 Hz, 1H), 6.71 (dd, J = 7.6 Hz, J = 0.9 Hz, 1H), 6.23 (d, J = 1.2 Hz, 1H), 5.20 (d, J = 1.1 Hz, 1H), 2.95–2.83 (m, 2H), 2.36 (sept, J = 6.9 Hz, 1H), 2.24 (sept, J = 6.9 Hz, 1H), 2.09 (s, 3H), 2.08 (s, 3H), 2.06 (s, 3H), 2.04 (s, 3H), 1.81–1.70 (m, 2H), 1.28–1.23 (m, 12H), 1.10 (d, J = 6.9 Hz, 3H), 1.03 (t, J = 7.0 Hz, 6H), 0.94 (d, J = 6.8 Hz, 3H), 0.81 (d, J = 6.8 Hz, 3H), 0.74 (d, J = 6.9 Hz, 3H), 0.16 (d, J = 6.8 Hz, 3H), 0.05 (d, J = 6.8 Hz, 3H) ppm; ^{13}C NMR (125 MHz, CD_2Cl_2): δ = 178.2 (C_q), 178.1 (C_q), 150.2 (CH_{arom}), 149.6 (C_q), 149.5 (C_q), 149.5 (C_q), 149.3 (C_q), 147.6 (C_q), 146.9 (C_q), 146.8 (C_q), 146.5 (C_q), 146.2 (C_q), 144.3 (C_q), 142.6 (C_q), 142.3 (C_q), 141.9 (C_q), 141.1 (C_q), 140.3 (C_q), 140.0 (C_q), 139.6 (C_q), 139.5 (C_q), 137.7 (C_q), 137.4 (CH_{arom}), 137.3 (C_q), 136.6 (C_q), 136.5 (C_q), 136.4 (C_q), 136.0 (C_q), 135.5 (C_q), 135.5 (C_q), 133.4 (C_q), 133.4 (CH_{arom}), 133.3 (CH_{arom}), 132.9 (CH_{arom}), 132.7 (CH_{arom}), 130.3 (C_q), 128.6 (C_q), 128.4 (C_q), 128.3 (CH_{arom}), 128.2 (2C, CH_{arom}), 128.0 (CH_{arom}), 127.9 (CH_{arom}), 127.8 (CH_{arom}), 127.7 (CH_{arom}), 127.6 (CH_{arom}), 125.9 (C_q), 125.7 (CH_{arom}), 125.5 (CH_{arom}), 124.9 (CH_{arom}), 121.2 (CH_{arom}), 121.1 (CH_{arom}), 120.8 (CH_{arom}), 120.7 (CH_{arom}), 118.7 (CH_{arom}), 116.6 (CH_{arom}), 115.9 (CH_{arom}), 112.2 (CH_{arom}), 111.8 (CH_{arom}), 34.9 ($CH(Me)_2$), 34.9 ($CH(Me)_2$), 30.9 ($CH(Me)_2$), 30.8 ($CH(Me)_2$), 30.5 ($CH(Me)_2$), 30.3 ($CH(Me)_2$), 25.0 (CH_3), 24.9 (CH_3), 24.5 (CH_3), 24.5 (CH_3), 24.3 (2C; CH_3), 24.3 (CH_3), 24.0 (CH_3), 23.9 (CH_3), 23.7 (CH_3), 23.3 (2C; CH_3), 21.3 (CH_3), 21.1 (CH_3), 21.1 (CH_3), 21.1 (CH_3) ppm; ^{19}F NMR (282 MHz, CD_2Cl_2): δ = −72.3 (d, $J_{F\text{-}P}$ = 711 Hz, PF_6) ppm; ^{31}P NMR (101 MHz, CD_2Cl_2): −143.6 (sept, $J_{F\text{-}P}$ = 711 Hz, PF_6); IR (film): $\tilde{\nu}$ = 2960, 2928, 1569, 1461, 1415, 845, 773, 558 cm^{-1}.

HPLC analysis of precatalyst **Λ/Δ-T18**: See HPLC analysis of catalyst **Λ/Δ-T18'**, please note the remark there.

Circular dichroism data for precatalyst **Λ-T18**:

CD (MeCN, 0.20 mM): λ, nm (Δε, M^{-1}·cm^{-1}) 418 (−13), 360 (+25), 339 (+32), 317 (+39), 286 (+7), 273 (+14), 257 (−82), 240 (−21), 233 (−23), 228 (−21), 223 (−24), 211 (+5).

Circular dichroism data for precatalyst **Δ-T18**:

CD (MeCN, 0.20 mM): λ, nm (Δε, M^{-1}·cm^{-1}) 417 (+13), 360 (−26), 338 (−33), 315 (−41), 284 (−8), 272 (−15), 257 (+83), 240 (+21), 234 (+26), 227 (+21), 220 (+24), 212 (−9).

II.) Analytical data for bisacetonitrile intermediate **Λ/Δ-T18-(MeCN)$_2$**: ^{1}H NMR (300 MHz, CD_3CN): δ = 7.56 (d, J = 0.9 Hz, 2H), 7.41 (d, J = 8.4 Hz, 2H), 7.36–7.19 (m, 8H), 7.17–7.09 (m, 4H), 6.93 (t, J = 7.6 Hz, 2H), 6.72 (dd, J = 7.5 Hz, J = 0.8 Hz, 2H), 6.44 (dd, J = 7.6 Hz, J = 0.8 Hz, 2H), 2.94 (sept, J = 6.9 Hz, 2H), 2.72–2.49 (m, 4H), 1.99 (s, 6H), 1.86 (s, 6H), 1.26 (d, J = 6.8 Hz, 12H), 1.15–1.04 (m, 18H), 1.01 (d, J = 6.8 Hz, 6H) ppm (due to a rapid $CH_3CN \rightarrow CD_3CN$ exchange, a signal belonging to CH_3CN is missing (6H, 2x C*H*$_3$CN)); ^{13}C NMR (75 MHz, CD_3CN): δ = 178.3 (2C), 150.3 (2C), 149.8 (2C), 147.7 (2C), 147.6 (2C), 145.1 (2C), 142.2 (2C), 140.5 (2C), 140.1 (2C), 138.6 (2C), 136.9 (2C), 136.8 (2x 2C), 133.0 (2C), 132.1 (2C), 129.1 (2C), 128.9 (2C), 128.8 (2C), 128.3 (2x 2C), 125.8 (2C), 122.2 (d, $J_{C\text{-}F}$ = 321 Hz, 1C; *C*F$_3$SO$_3$), 121.8 (2C), 121.8 (2C), 118.3 (2C), 112.2 (2C), 35.1 (2C), 31.4 (4C), 24.8 (2C), 24.7 (2C), 24.4 (2x 2C), 24.2 (2C), 24.1 (2C), 20.8 (2C), 20.8 (2C) ppm (due to a rapid $CH_3CN \rightarrow CD_3CN$ exchange, the signals belonging to CH_3CN are missing (4C, 2x *C*H$_3$*C*N)); ^{19}F NMR (282 MHz, CD_3CN): −78.5 (s, 3F, C*F*$_3$SO$_3$) ppm; IR (film): $\tilde{\nu}$ = 2960, 1570, 1457, 1416, 1263, 1169, 1032, 773, 639 cm^{-1}; HRMS (ESI): *m/z* calcd for $C_{76}H_{82}IrN_4O_2$: 1275.6069 [M–CF_3SO_3]$^+$; found: 1275.6074.

Circular dichroism data for intermediate **Λ-T18-(MeCN)$_2$**:

CD (MeCN, 0.20 mM): λ, nm (Δε, M^{-1}·cm^{-1}) 405 (−15), 354 (+30), 335 (+25), 322 (+2), 316 (+7), 262 (−22), 245 (+5), 237 (±0), 231 (+2), 218 (−33).

Circular dichroism data for intermediate **Δ-T18-(MeCN)$_2$**:

CD (MeCN, 0.20 mM): λ, nm (Δε, M^{-1}·cm^{-1}) 405 (+16), 354 (−33), 335 (−26), 322 (−2), 316 (−7), 262 (+24), 246 (−5), 237 (+2), 231 (−2), 217 (+31).

Active Catalysts Λ-T18' and Δ-T18'

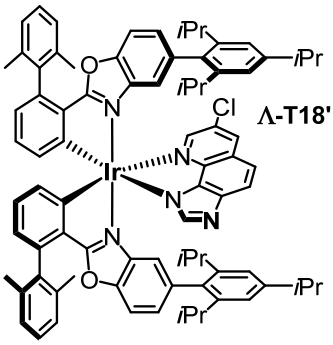

Catalyst Λ-T18'. Precatalyst **Λ-T18** (78.8 mg, 51.1 μmol) was dissolved in CH_2Cl_2 (2 mL) and passed through a disposable glass pipette charged with a slurry of CH_2Cl_2-swelled piperidinomethylated polystyrene beads (200–400 mesh, f = 3−4 mmol/g; pipette packing dimensions in diameter x length: 0.5 cm x 8.0 cm).[83] The polystyrene beads were rinsed with CH_2Cl_2 until the eluent became virtually colorless. After solvent removal and drying *in vacuo*, catalyst **Λ-T18'** was obtained analytically pure as a greenish yellow crystalline solid (70.8 mg, 50.7 μmol, 99%).

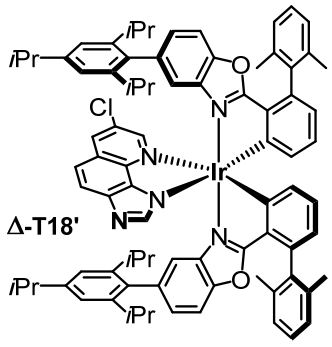

Catalyst Δ-T18'. Following the procedure described above for catalyst **Λ-T18'**, precatalyst **Δ-T18** (81.8 mg, 53.0 μmol) was converted to active catalyst **Δ-T18'**. Catalyst **Δ-T18'** was obtained as a greenish yellow crystalline solid (73.4 mg, 52.6 μmol, 99%). Alternatively, catalyst **Λ-** and **Δ-T18'** can be obtained analytically pure by washing a CH_2Cl_2 solution of **Λ/Δ-T18** with aqueous 0.3 M NaOH followed by repetitive washing of the organic layer with water (5x) and drying of the organic layer over Na_2SO_4.

Analytical data for active catalyst **Λ/Δ-T18'**:

^{1}H NMR (500 MHz, CD_2Cl_2): δ = 7.99 (d, J = 2.0 Hz, 1H), 7.76 (d, J = 8.7 Hz, 1H), 7.74 (d, J = 2.0 Hz, 1H), 7.60 (s, 1H), 7.31–7.20 (m, 4H), 7.20–7.06 (m, 6H), 7.04–6.99 (m, 2H), 6.97 (d, J = 1.5 Hz, 1H), 6.93 (dd, J = 8.4 Hz, J = 1.7 Hz, 1H), 6.91–6.86 (m, 5H), 6.86–6.81 (m, 2H), 6.06 (d, J = 1.2 Hz, 1H), 5.54 (d, J = 1.1 Hz, 1H), 2.92 (sept, J = 6.8 Hz, 1H), 2.88 (sept, J = 6.8 Hz, 1H), 2.40–2.27 (m, 2H), 2.13 (s, 3H), 2.12 (s, 3H), 2.07 (s, 3H), 2.06 (s, 3H), 1.76 (sept, J = 6.9 Hz, 1H), 1.71 (sept, J = 6.9 Hz, 1H), 1.29 (d, J = 6.8 Hz, 3H), 1.29 (d, J = 7.0 Hz, 3H), 1.28–1.24 (m, 6H), 1.07 (d, J = 6.7 Hz, 3H), 1.06 (d, J = 6.8 Hz, 3H), 1.02 (d, J = 6.9 Hz, 3H), 0.99 (d, J = 6.7 Hz, 3H), 0.79 (d, J = 6.9 Hz, 3H), 0.75 (d, J = 6.9 Hz, 3H), 0.18 (d, J = 6.9 Hz, 3H), 0.07 (d, J = 6.7 Hz, 3H) ppm. ^{13}C NMR (125 MHz, CD_2Cl_2): δ = 178.6 (C_q), 178.3 (C_q), 153.2 (C_q), 150.8 (CH_{arom}), 149.5 (C_q), 149.4 (C_q), 149.0 (C_q), 148.9 (C_q), 148.2 (C_q), 147.1 (C_q), 147.0 (C_q), 146.7 (CH_{arom}), 146.7 (C_q), 146.6 (C_q), 146.6 (C_q), 144.0 (C_q), 142.3 (C_q), 141.9 (C_q), 141.5 (C_q), 140.2 (C_q), 140.2 (C_q), 139.6 (C_q), 139.4 (C_q), 138.0 (C_q), 138.0 (C_q), 136.8 (C_q), 136.6 (C_q), 136.4 (C_q), 136.3 (C_q), 136.2 (CH_{arom}), 136.2 (C_q), 135.9 (C_q), 133.5 (CH_{arom}), 133.3 (CH_{arom}), 132.8 (CH_{arom}), 132.0 (CH_{arom}), 129.2 (C_q), 128.5 (C_q), 128.0 (CH_{arom}), 127.9 (CH_{arom}), 127.7 (2C; CH_{arom}), 127.7 (CH_{arom}), 127.5 (CH_{arom}), 127.4 (CH_{arom}), 126.8 (CH_{arom}), 125.6 (C_q), 124.4 (CH_{arom}), 124.4 (CH_{arom}), 124.0 (CH_{arom}), 124.0 (C_q), 121.0 (CH_{arom}), 120.8 (CH_{arom}), 120.7 (CH_{arom}), 120.5 (CH_{arom}), 117.7 (CH_{arom}), 117.6 (CH_{arom}), 116.8 (CH_{arom}), 111.5 (CH_{arom}), 111.1 (CH_{arom}), 34.9 (CH(Me)$_2$), 34.8 (CH(Me)$_2$), 30.9 (CH(Me)$_2$), 30.8 (CH(Me)$_2$), 30.5 (CH(Me)$_2$), 30.3 (CH(Me)$_2$), 25.1 (CH_3), 25.0 (CH_3), 24.5 (CH_3), 24.4 (CH_3), 24.3 (CH_3) 24.3 (CH_3), 24.2 (CH_3), 24.1 (CH_3), 23.8 (CH_3), 23.7 (CH_3), 23.4 (CH_3), 23.3 (CH_3), 21.2 (2C; CH_3), 21.2 (CH_3), 21.0 (CH_3) ppm; ^{19}F NMR (282 MHz, CD_2Cl_2): Only noise, no signals (absence of the PF_6^- counteranion in neutral **Λ/Δ-T18'**); ^{31}P NMR (101 MHz, CD_2Cl_2): Only noise, no signals (absence of the PF_6^- counteranion in neutral **Λ/Δ-T18'**). IR (film): $\tilde{\nu}$ = 2960, 2927, 1569, 1508, 1460, 1412, 1360, 1279, 1258, 1184, 802, 772 cm^{-1}.

Chiral HPLC: Chiralpak IC column (5 µm, 250 mm x 4.6 mm); eluent A: *n*-hexane with 2.0 vol% ethanol and 0.3 vol% diethylamine as modifiers; eluent B: isopropanol; linear gradient: 95:5 A/B → 88:12 A/B over 20 min; λ = 254 nm, flow = 0.5 mL/min, *t* (column) = 10 °C; t_{R1} (**Λ-T18'**) = 14.6 min, t_{R2} (**Δ-T18'**) = 16.6 min. Determined enantiomeric excess: >99% ee for both **Λ-** and **Δ-T18'**.

Remark: Chiral HPLC conditions for precatalyst **Λ/Δ-T18** and catalyst **Λ/Δ-T18'** are identical under the aforementioned conditions as a small amount of injected **Λ/Δ-T18** is instantly deprotonated to **Λ/Δ-T18'** by the basic eluent modifier diethylamine.

Analytical data for precatalyst **Λ-T18** and catalyst **Λ-T18'**:

HRMS (ESI): *m/z* calcd for $C_{82}H_{82}Cl_1Ir_1N_5O_2$: 1396.5781 $[M–PF_6]^+$ (**Λ-T18**) $[M+H]^+$ (**Λ-T18'**); found (for both): 1396.5796.

Analytical data for precatalyst **Δ-T18** and catalyst **Δ-T18'**:

HRMS (ESI): *m/z* calcd for $C_{82}H_{82}Cl_1Ir_1N_5O_2$: 1396.5781 $[M–PF_6]^+$ (**Δ-T18**) $[M+H]^+$ (**Δ-T18'**); found (for both): 1396.5809.

Racemic Precatalyst *rac*-T18 and Racemic Catalyst *rac*-T18'

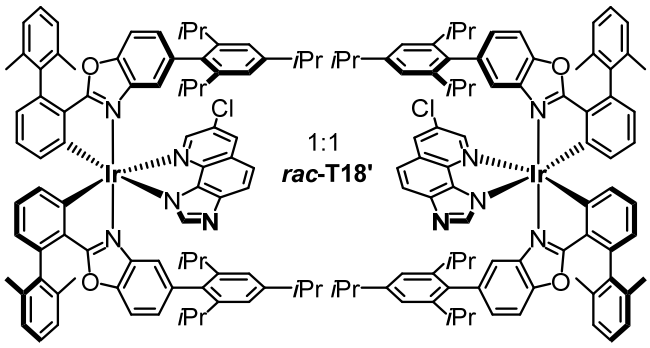

A flask (25 mL) was charged with iridium(III) dimer ***rac*-T18-dimer** (450 mg, 183 µmol, 1.00 eq), imidazoquinoline **236** (87.0 mg, 427 µmol, 2.33 eq), $AgPF_6$ (111 mg, 439 µmol, 2.40 eq), and a 5:1 mixture of CH_2Cl_2/MeOH (18 mL) and the mixture stirred for 24 h under exclusion of light. Then, the mixture was diluted with CH_2Cl_2 and passed through a short plug of silica gel with CH_2Cl_2 as eluent to remove the salts. All volatiles were removed *in vacuo* (40 °C) and the crude product purified by flash chromatography (CH_2Cl_2/MeOH 100:1). After solvent removal and drying *in vacuo*, desired racemic precatalyst ***rac*-T18** was obtained as a greenish yellow crystalline solid (380 mg, 246 µmol, 67%). Active catalyst ***rac*-T18'** was obtained from precatalyst ***rac*-T18** as described above for enantiopure **Λ-** and **Δ-T18'**.

XRD: X-ray quality crystals of ***rac*-T18'** were grown at rt by slow evaporation of CH_2Cl_2 from a CH_2Cl_2/MeCN solution of ***rac*-T18'**. Crystal structure and crystallographic data are provided in the crystallographic section.

4.7.2.19 Precatalyst Λ-T19

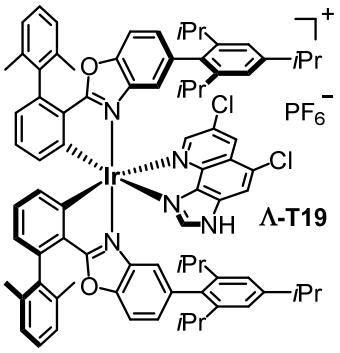

Precatalyst **Λ-T19** was prepared according to general procedure A5) from diastereomer **Λ-(*S*)-T18** (see 4.7.2.18; 12.3 mg, 8.7 µmol) and imidazoquinoline ligand **241**; eluent for f. c.: CH_2Cl_2/MeOH 100:1; precatalyst **Λ-T19** was obtained as a yellow-green solid (8.1 mg, 5.1 µmol, 59%). ^{1}H NMR (500 MHz, CD_2Cl_2): δ = 8.50 (d, J = 1.8 Hz, 1H), 8.05 (s, 1H), 7.98 (d, J = 2.0 Hz, 1H), 7.96 (s, 1H), 7.33–7.17 (m, 8H), 7.13 (t, J = 7.6 Hz, 1H), 7.09–6.99 (m, 4H), 6.99–6.96 (m, 2H), 6.91 (d, J = 1.7 Hz, 1H), 6.90 (dd, J = 7.5 Hz, J = 0.9 Hz, 1H), 6.86 (d, J = 1.7 Hz, 1H), 6.85 (dd, J = 7.7 Hz, J = 0.9 Hz, 1H), 6.71 (dd, J = 7.7 Hz, J = 0.9 Hz, 1H), 6.18 (d, J = 1.1 Hz, 1H), 5.20 (d, J = 1.1 Hz, 1H), 2.95–2.85 (m, 2H), 2.36 (sept, J = 6.9 Hz, 1H), 2.25 (sept, J = 6.9 Hz, 1H), 2.09 (s, 3H), 2.08 (s, 3H), 2.05 (s, 3H), 2.04 (s, 3H), 1.87-1.73 (m, 2H), 1.26 (d, J = 7.0 Hz, 6H), 1.25 (d, J = 7.0 Hz, 6H), 1.10 (d, J = 6.8 Hz, 3H), 1.05 (d, J = 7.0 Hz, 3H), 1.02 (d, J = 6.8 Hz, 3H), 0.94 (d, J = 6.8 Hz, 3H), 0.84 (d, J = 6.8 Hz, 3H), 0.77 (d, J = 6.8 Hz, 3H), 0.20 (d, J = 7.0 Hz, 3H), 0.07 (d, J = 6.8 Hz, 3H) ppm (N*H* signal could not be found due to rapid exchange); ^{13}C NMR (125 MHz, CD_2Cl_2): δ = 178.2, 178.1, 151.0, 149.6, 149.5, 149.5, 149.4, 147.5, 146.9, 146.8, 146.5, 146.3, 144.1, 143.7, 142.7, 142.4, 141.8, 140.5, 140.4, 140.1, 139.5, 139.5, 137.6, 137.3, 136.6, 136.5, 136.4, 136.0, 135.5 (2C), 135.4, 133.5, 133.2, 132.9, 132.7, 131.1, 128.6, 128.4, 128.3, 128.3, 128.3, 128.0, 127.9, 127.8, 127.8, 127.6, 125.8, 125.6, 124.4, 121.3, 121.2, 120.9, 120.8, 118.5, 116.6, 115.9 (2C), 112.3, 111.9, 35.0, 34.9, 30.9, 30.9, 30.6, 30.4, 25.1, 24.9, 24.5, 24.3 (2C), 24.3, 24.2, 24.0, 23.9, 23.7, 23.3, 23.2, 21.3, 21.1, 21.1 (2C) ppm (one ^{13}C signal could not be located); IR (film): $\tilde{\nu}$ = 2960, 2927, 1569, 1460, 1415, 1365, 845, 773, 558 cm^{-1}; HRMS (ESI): *m/z* calcd for $C_{82}H_{81}Cl_2Ir_1N_5O_2$: 1430.5385 $[M–PF_6]^+$; found: 1430.5375.

4.7.2.20 Precatalyst Λ-T20

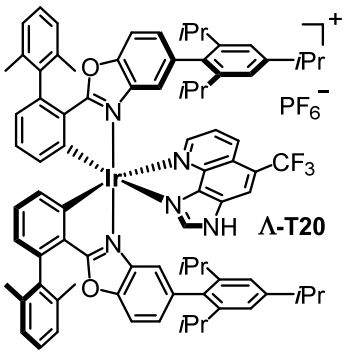

Precatalyst **Λ-T20** was prepared according to general procedure A5) from diastereomer **Λ-(*S*)-T18** (see 4.7.2.18; 13.5 mg, 9.6 µmol) and imidazoquinoline ligand **245**; eluent for f. c.: CH_2Cl_2/MeOH 100:1; precatalyst **Λ-T20** was obtained as a yellow-green solid (8.8 mg, 5.6 µmol, 58%). ^{1}H NMR (500 MHz, CD_2Cl_2): δ = 8.48 (d, J = 8.5 Hz, 1H), 8.32 (s, 1H), 8.18 (dd, J = 4.9 Hz, J = 0.8 Hz, 1H), 8.02 (s, 1H), 7.46 (dd, J = 8.7 Hz, J = 5.0 Hz, 1H), 7.32–7.27 (m, 2H), 7.25–7.16 (m, 6H), 7.11 (t, J = 7.6 Hz, 1H), 7.06 (t,

J = 7.6 Hz, 1H), 7.02 (d, J = 1.6 Hz, 1H), 7.00 (dd, J = 8.4 Hz, J = 1.6 Hz, 1H), 6.98 (dd, J = 8.4 Hz, J = 1.6 Hz, 1H), 6.95–6.93 (m, 2H), 6.91–6.87 (m, 2H), 6.82 (d, J = 1.6 Hz, 1H), 6.80 (dd, J = 1.8 Hz, J = 1.0 Hz, 1H), 6.78 (dd, J = 1.8 Hz, J = 1.1 Hz, 1H), 5.91 (d, J = 1.1 Hz, 1H), 5.39 (d, J = 0.9 Hz, 1H), 2.95–2.82 (m, 2H), 2.38–2.25 (m, 2H), 2.07 (s, 3H), 2.06 (s, 3H), 2.04 (s, 3H), 2.03 (s, 3H), 1.80–1.67 (m, 2H), 1.25 (d, J = 6.9 Hz, 6H), 1.24 (dd, J = 6.9 Hz, J = 0.9 Hz, 6H), 1.08 (d, J = 6.9 Hz, 3H), 1.05 (d, J = 6.9 Hz, 3H), 1.00 (d, J = 6.8 Hz, 3H), 0.94 (d, J = 6.8 Hz, 3H), 0.78 (d, J = 6.9 Hz, 3H), 0.75 (d, J = 6.9 Hz, 3H), 0.11 (d, J = 6.9 Hz, 3H), 0.08 (d, J = 6.8 Hz, 3H) ppm (N*H* signal could not be found due to rapid exchange); ^{13}C NMR (125 MHz, CD_2Cl_2): δ = 178.3, 178.3, 151.5, 149.6, 149.5, 149.4, 149.2, 148.6, 146.9, 146.7, 146.6, 146.2, 145.6, 145.1, 144.0, 143.9, 142.5, 142.3, 140.2, 139.9, 139.6, 139.6, 137.6, 137.6, 136.7, 136.5, 136.4, 136.3, 135.9, 135.5, 135.5, 133.3, 133.0, 132.8, 132.7, 128.5, 128.4, 128.3, 128.2, 128.1, 128.0, 127.9, 127.8, 127.7, 127.7, 125.4, 125.3, 123.5, 122.2, 121.2, 121.0, 120.8 (2C), 117.9, 116.4, 115.9, 112.1, 111.8, 34.8 (2C), 30.9, 30.8, 30.5, 30.3, 25.1, 24.9, 24.4, 24.3, 24.3, 24.2, 24.2, 24.0, 23.8, 23.8, 23.3, 23.0, 21.2, 21.1, 21.1 (2C) ppm (three ^{13}C signals could not be located; complicated spectrum due to C-F coupling); IR (film): $\tilde{\nu}$ = 2960, 1569, 1413, 1351, 1181, 1126, 842, 773, 710, 556 cm^{-1}; HRMS (ESI): *m/z* calcd for $C_{83}H_{82}F_3Ir_1N_5O_2$: 1430.6053 $[M–PF_6]^+$; found: 1430.6033.

4.7.2.21 Precatalyst Λ-T21

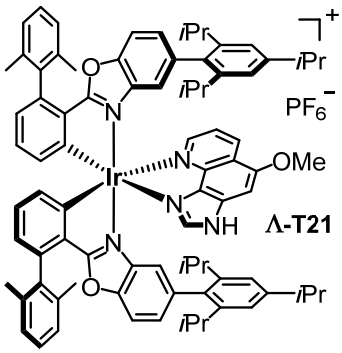

Precatalyst **Λ-T21** was prepared according to general procedure A5) from diastereomer **Λ-(*S*)-T18** (see 4.7.2.18; 9.0 mg, 6.4 µmol) and imidazoquinoline ligand **260**; eluent for f. c.: CH_2Cl_2/MeOH 100:1; precatalyst **Λ-T21** was obtained as a yellow-green crystalline solid (8.0 mg, 5.2 µmol, 82%). ^{1}H NMR (500 MHz, CD_2Cl_2): δ = 10.86 (s, 1H), 8.46 (dd, J = 8.4 Hz, J = 1.3 Hz, 1H), 8.01 (dd, J = 5.0 Hz, J = 1.2 Hz, 1H), 7.71 (s, 1H), 7.31–7.22 (m, 4H), 7.22–7.15 (m, 6H), 7.08 (t, J = 7.6 Hz, 1H), 7.03 (t, J = 7.6 Hz, 1H), 7.03–6.99 (m, 2H), 6.95–6.91 (m, 3H), 6.90 (d, J = 1.7 Hz, 1H), 6.87 (dd, J = 7.4 Hz, J = 1.0 Hz, 1H), 6.82 (d, J = 1.7 Hz, 1H), 6.80 (dd, J = 7.7 Hz, J = 0.9 Hz, 1H), 6.77 (dd, J = 7.6 Hz, J = 1.0 Hz, 1H), 6.18 (d, J = 1.1 Hz, 1H), 5.25 (d, J = 1.1 Hz, 1H), 3.98 (s, 3H), 2.95–2.81 (m, 2H), 2.35 (sept, J = 6.9 Hz, 1H), 2.23 (sept, J = 6.9 Hz, 1H), 2.06 (s, 3H), 2.05 (s, 3H), 2.04 (s, 6H), 1.84–1.70 (m, 2H), 1.26 (d, J = 6.8 Hz, 6H), 1.24 (d, J = 7.0 Hz, 6H), 1.08 (d, J = 7.0 Hz, 3H), 1.03 (d, J = 7.0 Hz, 3H), 0.99 (d, J = 7.0 Hz, 3H), 0.90 (d, J = 7.0 Hz, 3H), 0.78 (d, J = 7.1 Hz, 3H), 0.76 (d, J = 7.0 Hz, 3H), 0.21 (d, J = 6.8 Hz, 3H), 0.11 (d,

J = 7.0 Hz, 3H) ppm; HRMS (ESI): *m/z* calcd for $C_{83}H_{85}Ir_1N_5O_3$: 1392.6285 $[M–PF_6]^+$; found: 1392.6283.

4.7.2.22 Precatalyst Λ-T22

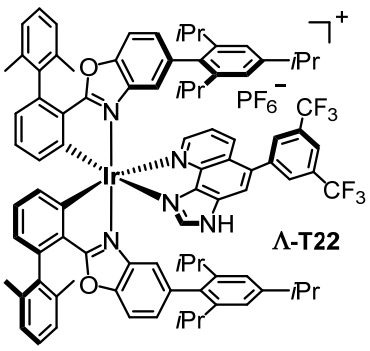

Precatalyst **Λ-T22** was prepared according to general procedure A5) from diastereomer **Λ-(*S*)-T18** (see 4.7.2.18; 13.5 mg, 9.6 µmol) and imidazoquinoline ligand **251**; eluent for f. c.: CH_2Cl_2/MeOH 100:1; precatalyst **Λ-T22** was obtained as a yellow-green solid (10.9 mg, 6.3 µmol, 66%). ^{1}H NMR (500 MHz, CD_2Cl_2): δ = 11.35 (s, 1H), 8.17 (dd, *J* = 5.0 Hz, *J* = 1.1 Hz, 1H), 8.08–8.04 (m, 2H), 8.01 (s, 1H), 7.95 (s, 1H), 7.79 (s, 2H), 7.39 (dd, *J* = 8.6 Hz, *J* = 5.0 Hz, 1H), 7.32–7.28 (m, 2H), 7.27–7.15 (m, 6H), 7.12 (t, *J* = 7.6 Hz, 1H), 7.08 (t, *J* = 7.5 Hz, 1H), 7.05–7.02 (m, 2H), 6.98 (dd, *J* = 8.4 Hz, *J* = 1.6 Hz, 1H), 6.95 (dd, *J* = 7.5 Hz, *J* = 1.0 Hz, 1H), 6.94–6.89 (m, 3H), 6.82 (dd, *J* = 1.7 Hz, *J* = 1.1 Hz, 1H), 6.80 (dd, *J* = 1.7 Hz, *J* = 1.1 Hz, 1H), 6.79 (d, *J* = 1.6 Hz, 1H), 6.02 (d, *J* = 1.1 Hz, 1H), 5.49 (d, *J* = 1.0 Hz, 1H), 2.89 (sept, *J* = 7.0 Hz, 1H), 2.83 (sept, *J* = 7.0 Hz, 1H), 2.34 (sept, *J* = 6.9 Hz, 1H), 2.29 (sept, *J* = 6.9 Hz, 1H), 2.09 (s, 3H), 2.07 (s, 3H), 2.06 (s, 3H), 2.05 (s, 3H), 1.90–1.76 (m, 2H), 1.25 (d, *J* = 7.0 Hz, 6H), 1.20 (d, *J* = 7.0 Hz, 3H), 1.19 (d, *J* = 6.9 Hz, 3H), 1.09 (d, *J* = 6.9 Hz, 3H), 1.05 (d, *J* = 7.1 Hz, 3H), 1.03 (d, *J* = 7.0 Hz, 3H), 0.93 (d, *J* = 6.9 Hz, 3H), 0.81 (d, *J* = 6.8 Hz, 3H), 0.79 (d, *J* = 7.0 Hz, 3H), 0.21 (d, *J* = 6.9 Hz, 3H), 0.02 (d, *J* = 6.9 Hz, 3H) ppm; ^{13}C NMR (125 MHz, CD_2Cl_2): δ = 178.4, 178.3, 151.4, 149.6, 149.6, 149.5, 149.2, 148.4, 146.9, 146.8, 146.5, 146.0, 144.9, 144.0, 143.2, 142.5, 142.3, 141.5, 140.3, 139.9, 139.9, 139.6, 139.6, 137.7 (2C), 136.8, 136.7, 136.5, 136.4, 135.9, 135.8, 135.6, 135.4, 133.4, 133.0 (2C), 132.9, 132.8, 132.7, 132.5, 130.7, 128.5, 128.3, 128.2, 128.1, 128.0, 127.9, 127.8, 127.8, 127.7, 125.5, 124.5, 123.4, 123.1, 121.3, 121.1, 120.8, 120.8, 118.3, 116.5, 115.8, 112.3, 111.9, 34.9, 34.7, 31.0, 30.8, 30.6, 30.3, 25.2, 25.0, 24.7, 24.3, 24.3 (3C), 24.2, 23.9, 23.7, 23.3, 23.1, 21.2, 21.1, 21.1 (2C) ppm (five ^{13}C signals could not be located; complicated spectrum due to C-F couplings); IR (film): $\tilde{\nu}$ = 2961, 1570, 1459, 1416, 1373, 1279, 1181, 1140, 845, 774 cm^{-1}; HRMS (ESI): *m/z* calcd for $C_{90}H_{85}F_6Ir_1N_5O_2$: 1574.6241 $[M–PF_6]^+$; found: 1574.6199.

4.7.2.23 Precatalyst Λ-T23

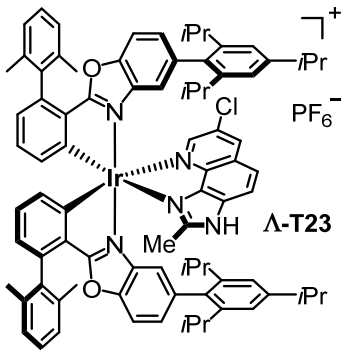

Precatalyst **Λ-T23** was prepared according to general procedure A5) from diastereomer **Λ-(*S*)-T18** (see 4.7.2.18; 20.5 mg, 14.5 µmol) and imidazoquinoline ligand **252**; eluent for f. c.: CH_2Cl_2/MeOH 100:1; precatalyst **Λ-T23** was obtained as a yellow-green solid (11.9 mg, 7.7 µmol, 53%). ^{1}H NMR (500 MHz, CD_2Cl_2): δ = 10.90 (s, 1H), 8.18 (d, J = 1.9 Hz, 1H), 7.90 (d, J = 1.9 Hz, 1H), 7.82 (d, J = 8.8 Hz, 1H), 7.58 (d, J = 9.0 Hz, 1H), 7.33–7.28 (m, 2H), 7.27–7.21 (m, 5H), 7.20–7.17 (d, J = 6.9 Hz, 1H), 7.13 (t, J = 7.6 Hz, 1H), 7.07 (t, J = 7.6 Hz, 1H), 7.04 (dd, J = 8.3 Hz, J = 1.6 Hz, 1H), 7.03–7.00 (m, 2H), 6.97–6.94 (m, 2H), 6.92 (d, J = 1.6 Hz, 1H), 6.90 (dd, J = 7.5 Hz, J = 1.0 Hz, 1H), 6.87 (dd, J = 7.7 Hz, J = 1.0 Hz, 1H), 6.84 (d, J = 1.6 Hz, 1H), 6.64 (dd, J = 7.7 Hz, J = 1.0 Hz, 1H), 6.15 (d, J = 1.1 Hz, 1H), 5.13 (d, J = 1.1 Hz, 1H), 2.96–2.84 (m, 2H), 2.39 (sept, J = 6.8 Hz, 1H), 2.22 (sept, J = 6.9 Hz, 1H), 2.15 (s, 3H), 2.09 (s, 3H), 2.07 (s, 6H), 1.99 (s, 3H), 1.78 (sept, J = 6.9 Hz, 1H), 1.72 (sept, J = 6.9 Hz, 1H), 1.27 (d, J = 7.2 Hz, 6H), 1.26 (d, J = 7.0 Hz, 6H), 1.10 (d, J = 6.9 Hz, 3H), 1.04 (d, J = 6.9 Hz, 3H), 1.01 (d, J = 6.8 Hz, 3H), 0.92 (d, J = 6.9 Hz, 3H), 0.82 (d, J = 6.9 Hz, 3H), 0.76 (d, J = 7.0 Hz, 3H), 0.12 (d, J = 6.9 Hz, 3H), 0.04 (d, J = 6.9 Hz, 3H) ppm; ^{13}C NMR (125 MHz, CD_2Cl_2): δ = 178.2, 178.1, 155.6, 150.1, 149.6, 149.6, 149.5, 149.3, 147.8, 146.8, 146.6, 146.5, 146.2, 145.5, 142.6, 142.5, 141.4, 141.3, 140.5, 140.1, 139.5, 139.5, 137.6, 137.4, 137.2, 136.6 (2C), 136.1, 136.0, 135.5, 135.3, 134.1, 133.4, 133.2, 133.0, 132.1, 129.6, 128.5, 128.3, 128.3, 128.2, 128.1, 127.9 (2C), 127.8, 127.8, 127.6, 125.7, 125.4 (2C), 123.8, 121.1, 121.1, 120.8, 120.6, 118.1, 116.4, 116.1, 112.1, 112.0, 34.9, 34.8, 30.9, 30.9, 30.5, 30.4, 25.0, 24.9, 24.5, 24.4, 24.3 (2C), 24.2, 24.1, 23.7, 23.7, 23.3, 23.2, 21.3, 21.2, 21.1, 21.0, 13.9 ppm; IR (film): $\tilde{\nu}$ = 2960, 1568, 1457, 1413, 841, 773, 737, 707, 557 cm^{-1}; HRMS (ESI): *m/z* calcd for $C_{83}H_{84}Cl_1Ir_1N_5O_2$: 1410.5937 $[M-PF_6]^+$; found: 1410.5925.

4.7.2.24 Precatalyst *rac*-T24

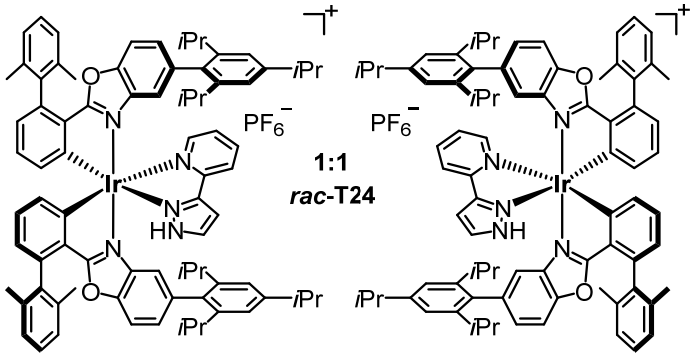

An amber glass vial was charged with iridium(III) dimer **Λ-(*S*)-T18** (see 4.7.2.18; 20.6 mg, 8.38 µmol, 1.00 eq), 2-(1*H*-pyrazol-3-yl)pyridine ligand (**265**; 3.3 mg, 23 µmol, 2.7 eq), $AgPF_6$ (5.5 mg, 22 µmol, 2.6 eq), and CH_2Cl_2/ MeOH 10:1 (0.88 mL) and the mixture stirred at rt for 20 h under exclusion of light. All volatiles were removed *in vacuo*

(40 °C) and the crude product purified by flash chromatography (CH_2Cl_2/MeOH 100:1). After solvent removal and drying *in vacuo*, desired complex ***rac*-T24** was obtained as a green-yellow solid (16.6 mg, 11.2 µmol, 67%). ^{1}H NMR (300 MHz, CD_2Cl_2): δ = 8.13 (d, J = 5.5 Hz, 1H), 7.83–7.67 (m, 3H), 7.33–6.84 (m, 20H), 6.70 (d, J = 7.6 Hz, 1H), 6.56 (d, J = 7.7 Hz, 1H), 5.61 (d, J = 0.9 Hz, 1H), 5.37 (d, J = 1.1 Hz, 1H), 2.98–2.79 (m, 2H), 2.44–2.20 (m, 2H), 2.11 (s, 3H), 2.05 (s, 3H), 2.11–1.88 (m, 2H), 1.90 (s, 3H), 1.84 (s, 3H), 1.26 (d, J = 7.1, 12H), 1.06 (d, J = 6.9 Hz, 3H), 1.04 (d, J = 6.6 Hz, 3H), 0.92 (d, J = 7.0 Hz, 3H), 0.90 (d, J = 7.0 Hz, 3H), 0.86 (d, J = 6.8 Hz, 6H), 0.73 (d, J = 7.0 Hz, 3H), 0.68 (d, J = 6.8 Hz, 3H) ppm (N*H* signal could not be found due to rapid exchange); IR (film): $\tilde{\nu}$ = 2960, 1569, 1457, 1414, 841, 773, 557 cm^{-1}; HRMS (ESI): *m/z* calcd for $C_{80}H_{83}Ir_1N_5O_2$: 1338.6178 [M−PF_6]$^+$; found: 1338.6194.

4.7.2.25 Precatalyst Λ-T25

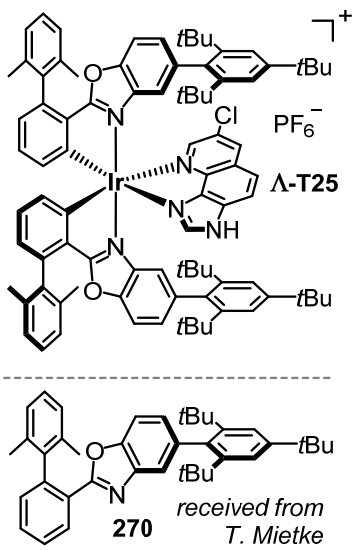

Precatalyst **Λ-T25** was prepared according to general procedures A1), A2), and A5) from benzoxazole ligand **270** (see left; received from PhD student Thomas Mietke), $IrCl_3 \cdot 3H_2O$, auxiliary ligand **(*S*)-Aux2**, and imidazoquinoline ligand **236**.

***Rac*-T25-dimer.** General procedure A1) was followed using benzoxazole ligand **270** (168 mg, 309 µmol, 1.89 eq) and $IrCl_3 \cdot 3H_2O$ (57.6 mg, 163 µmol, 1.00 eq); reaction time: 24 h; Ir(III) dimer ***rac*-T25-dimer** was obtained as an orange solid (205 mg, 78.1 µmol, quantitative). ***Rac*-T25-dimer** was pushed forward into the next step without characterization.

Λ-(*S*)-T25. General procedure A2) was followed using ***rac*-T25-dimer** (199 mg, 75.8 µmol) and auxiliary ligand **(*S*)-Aux2**; the crude diastereomer mixture was purified and resolved by preparative TLC with CH_2Cl_2/hexanes 2:1 as eluent; only the Λ-(*S*)-diastereomer was isolated; diastereomer **Λ-(*S*)-T25** was obtained as an orange-red solid (30.9 mg, 20.7 µmol, 27%). ^{1}H NMR (500 MHz, CD_2Cl_2): δ = 8.03–8.00 (m, 1H), 7.55 (d, J = 2.1 Hz, 1H), 7.53 (d, J = 2.0 Hz, 1H), 7.49 (d, J = 1.4 Hz, 1H), 7.48 (d, J = 2.0 Hz, 1H), 7.41–7.35 (m, 2H), 7.32 (dd, J = 8.4 Hz, J = 1.7 Hz, 1H), 7.29–7.09 (m, 9H), 6.84–6.78 (m, 2H), 6.76 (t, J = 7.5 Hz, 1H), 6.68 (dd, J = 7.6 Hz, J = 1.1 Hz, 1H), 6.62–6.56 (m, 2H), 6.28 (dd, J = 8.6 Hz, J = 1.0 Hz, 1H), 6.09–6.02 (m, 2H), 4.18 (dd, J = 9.5 Hz, J = 2.5 Hz, 1H), 3.91 (t, J = 8.9 Hz, 1H), 3.82 (dd, J = 8.3 Hz, J = 2.5 Hz, 1H), 2.12 (s, 3H), 2.02 (s, 3H), 1.82 (s, 3H), 1.77 (s, 3H), 1.39 (s, 9H), 1.34 (s, 9H), 1.12 (s, 9H), 1.04 (s, 9H), 0.99 (s, 9H),

0.82 (s, 9H), 0.31 (s, 9H) ppm; HRMS (ESI): *m/z* calcd for $C_{91}H_{104}Ir_1N_3O_4H$: 1496.7739 $[M+H]^+$; found: 1496.7730.

Precatalyst Λ-T25. General procedure A5) was followed using **Λ-(*S*)-T25** (20.2 mg, 13.5 µmol) and imidazoquinoline ligand **236**; eluent for f. c.: CH_2Cl_2/MeOH 100:1; precatalyst **Λ-T25** was obtained as a yellow-green crystalline solid (17.5 mg, 10.8 µmol, 80%). ^{1}H NMR (500 MHz, CD_2Cl_2): δ = 11.28 (s, 1H), 8.19 (d, J = 2.0 Hz, 1H), 7.98 (s, 1H), 7.96 (dd, J = 8.9 Hz, J = 1.0 Hz, 1H), 7.93 (d, J = 2.0 Hz, 1H), 7.96 (d, J = 9.0 Hz, 1H), 7.47 (d, J = 2.0 Hz, 1H), 7.40 (d, J = 2.0 Hz, 1H), 7.34 (d, J = 2.0 Hz, 1H), 7.32–7.16 (m, 9H), 7.13–7.06 (m, 3H), 7.03 (t, J = 7.7 Hz, 1H), 6.95 (dd, J = 7.5 Hz, J = 0.9 Hz, 1H), 6.88 (dd, J = 7.5 Hz, J = 1.1 Hz, 1H), 6.77 (dd, J = 7.7 Hz, J = 0.9 Hz, 1H), 6.61 (dd, J = 7.7 Hz, J = 0.9 Hz, 1H), 6.38 (d, J = 1.2 Hz, 1H), 5.26 (d, J = 1.2 Hz, 1H), 2.11 (s, 3H), 2.07 (s, 3H), 2.06 (s, 3H), 2.04 (s, 3H), 1.33 (s, 9H), 1.32 (s, 9H), 1.03 (s, 9H), 0.96 (s, 9H), 0.34 (s, 9H), 0.31 (s, 9H) ppm; HRMS (ESI): *m/z* calcd for $C_{88}H_{94}Cl_1Ir_1N_5O_2$: 1480.6721 $[M–PF_6]^+$; found: 1480.6775.

4.7.2.26 Precatalyst Λ-T26

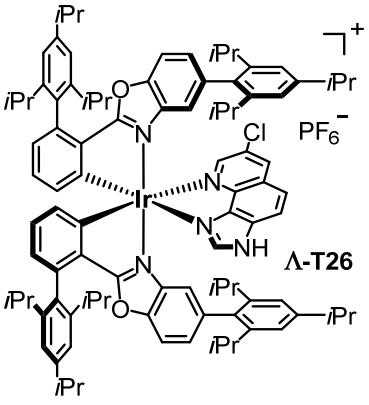

Precatalyst **Λ-T26** was prepared according to general procedures A1), A2), and A5) from benzoxazole ligand **202**, $IrCl_3 \cdot 3H_2O$, auxiliary ligand **(*S*)-Aux2**, and imidazoquinoline ligand **236**.

***Rac*-T26-dimer.** General procedure A1) was followed using benzoxazole ligand **202** (451 mg, 752 µmol, 1.76 eq) and $IrCl_3 \cdot 3H_2O$ (151 mg, 428 µmol, 1.00 eq); reaction time: 22 h; Ir(III) dimer ***rac*-T26-dimer** was obtained as an orange solid (504 mg, 176 µmol, 94%). ***Rac*-T26-dimer** was pushed forward into the next step without characterization.

Λ-(*S*)-T26: General procedure A2) was followed using ***rac*-T26-dimer** (212 mg, 74.4 µmol) and auxiliary ligand **(*S*)-Aux2**; the crude diastereomer mixture was purified and resolved by f. c. with CH_2Cl_2/hexanes 2:1; only the Λ-(*S*)-diastereomer was isolated; diastereomer **Λ-(*S*)-T26** was obtained as an orange-red solid (39.5 mg, 25.6 µmol, 17%). IR (film): $\tilde{\nu}$ = 2960, 2929, 2870, 1607, 1572, 1462, 1359 cm^{-1}; HRMS (ESI): *m/z* calcd for $C_{99}H_{120}Ir_1N_3O_4Na$: 1630.8812 $[M+Na]^+$; found: 1630.9024. **Λ-(*S*)-T26** was pushed forward into the next step without further characterization.

Precatalyst Λ-T26. General procedure A5) was followed using **Λ-(*S*)-T26** (14.2 mg, 8.83 µmol) and imidazoquinoline ligand **236**; eluent for f. c.: CH_2Cl_2/MeOH 200:1;

precatalyst **Λ-T26** was obtained as a yellow-green solid (7.6 mg, 4.4 µmol, 50%). ^{1}H NMR (500 MHz, CD_2Cl_2): δ = 11.32 (s, 1H), 8.24 (d, J = 1.8 Hz, 1H), 7.99–7.93 (m, 3H), 7.68 (d, J = 9.0 Hz, 1H), 7.22 (d, J = 1.7 Hz, 1H), 7.19 (d, J = 1.7 Hz, 1H), 7.18–7.15 (m, 2H), 7.14 (d, J = 3.9 Hz, 1H), 7.12 (d, J = 4.0 Hz, 1H), 7.06 (t, J = 7.5 Hz, 1H), 7.04–6.97 (m, 5H), 6.96 (d, J = 1.7 Hz, 1H), 6.94 (dd, J = 7.6 Hz, J = 0.8 Hz, 1H), 6.91 (d, J = 1.7 Hz, 1H), 6.85 (d, J = 1.5 Hz, 1H), 6.71 (dd, J = 7.5 Hz, J = 0.9 Hz, 1H), 6.58 (dd, J = 7.5 Hz, J = 0.9 Hz, 1H), 6.22 (d, J = 1.1 Hz, 1H), 5.12 (d, J = 1.3 Hz, 1H), 3.09–2.99 (m, 2H), 2.94–2.83 (m, 2H), 2.70 (sept, J = 6.8 Hz, 1H), 2.63 (sept, J = 6.8 Hz, 1H), 2.62–2.50 (m, 2H), 2.37 (sept, J = 6.8 Hz, 1H), 2.23 (sept, J = 6.9 Hz, 1H), 1.86–1.74 (m, 2H), 1.42–1.34 (m, 12H), 1.26 (d, J = 7.0 Hz, 12H), 1.22 (d, J = 6.8 Hz, 3H), 1.18 (d, J = 6.8 Hz, 3H), 1.11 (d, J = 6.8 Hz, 3H), 1.09 (d, J = 6.6 Hz, 3H), 1.07 (d, J = 7.0 Hz, 3H), 1.04 (d, J = 7.0 Hz, 3H), 1.03–1.00 (m, 9H), 0.94 (d, J = 6.8 Hz, 3H), 0.92 (d, J = 7.0 Hz, 3H), 0.88 (d, J = 6.8 Hz, 3H), 0.82 (d, J = 7.0 Hz, 3H), 0.75 (d, J = 7.0 Hz, 3H), 0.18 (d, J = 6.8 Hz, 3H), 0.12 (d, J = 6.8 Hz, 3H) ppm; ^{13}C NMR (125 MHz, CD_2Cl_2): δ = 178.4, 178.4, 150.2, 149.7, 149.6, 149.5, 149.3, 149.3, 149.2, 147.1 (2C), 147.0 (2C), 146.9, 146.6, 146.6, 146.4, 144.0, 142.5, 142.4 (2C), 142.3, 142.1, 141.2, 140.3, 140.1, 137.6, 137.5, 137.2, 135.5, 135.4, 134.5 (2C), 133.5, 132.8, 132.8, 132.3, 132.3, 130.1, 129.9, 129.7, 128.3, 127.6, 126.7, 126.5, 125.9, 125.0, 121.4, 121.3, 121.3, 121.2, 121.1, 121.1, 120.9, 120.7, 118.7, 116.7, 115.8, 111.8, 111.5, 35.1, 35.1, 35.0, 34.9, 31.7, 31.5, 31.3, 31.3, 30.9, 30.8, 30.4, 30.3, 25.1, 25.0, 24.9 (2C), 24.8, 24.7 (3C), 24.6 (2C), 24.6, 24.5, 24.3, 24.3, 24.3 24.2, 24.1 (4C), 24.0, 23.8, 23.5 (2C) ppm; IR (film): $\tilde{\nu}$ = 2960, 2928, 1568, 1461, 1421, 846 cm^{-1}; HRMS (ESI): *m/z* calcd for $C_{96}H_{110}Cl_1Ir_1N_5O_2$: 1592.7975 $[M–PF_6]^+$; found: 1592.8004.

4.7.2.27 Precatalyst Λ-T27

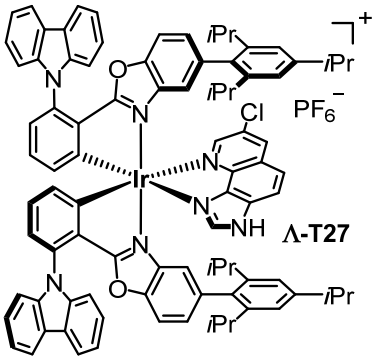

Precatalyst **Λ-T27** was prepared according to general procedures A1), A2), and A5) from benzoxazole ligand **206**, $IrCl_3 \cdot 3H_2O$, auxiliary ligand **(*S*)-Aux2**, and imidazoquinoline ligand **236**.

***Rac*-T27-dimer.** General procedure A1) was followed using benzoxazole ligand **206** (501 mg, 890 µmol, 1.99 eq) and $IrCl_3 \cdot 3H_2O$ (158 mg, 448 µmol, 1.00 eq); reaction time: 35 h; Ir(III) dimer ***rac*-T27-dimer** was obtained as an orange solid (483 mg, 179 µmol, 80%). ***Rac*-T27-dimer** was pushed forward into the next step without characterization.

Λ-(*S*)-T27. General procedure A2) was followed using ***rac*-T27-dimer** (199 mg, 73.6 µmol) and auxiliary ligand **(*S*)-Aux2**; the crude diastereomer mixture was purified and resolved by

f. c. with CH_2Cl_2/hexanes 3:2 → 1:1; only the Λ-(*S*)-diastereomer was isolated; **Λ-(*S*)-T27** was obtained as an orange-red solid (93.9 mg, 61.2 µmol, 42%). **Λ-(*S*)-T27** was pushed forward into the next step without characterization.

Precatalyst Λ-T27. General procedure A5) was followed using **Λ-(*S*)-T27** (14.1 mg, 9.2 µmol) and imidazoquinoline ligand **236**; eluent for f. c.: CH_2Cl_2/MeOH 200:1; precatalyst **Λ-T27** was obtained as a yellow-green solid (5.1 mg, 3.1 µmol, 33%). ^{1}H NMR (500 MHz, CD_2Cl_2): δ = 11.41 (s, 1H), 8.33–8.23 (m, 5H), 8.21 (s, 1H), 8.13 (d, *J* = 1.9 Hz, 1H), 7.94 (d, *J* = 9.0 Hz, 1H), 7.70 (d, *J* = 9.0 Hz, 1H), 7.48–7.28 (m, 12H), 7.26 (d, *J* = 8.2 Hz, 1H), 7.23 (d, *J* = 8.1 Hz, 1H), 7.22–7.16 (m, 2H), 7.07–7.04 (m, 1H), 7.01 (d, *J* = 1.5 Hz, 1H), 6.97–6.89 (m, 6H), 6.87 (d, *J* = 1.5 Hz, 1H), 6.82 (d, *J* = 1.5 Hz, 1H), 6.09 (d, *J* = 0.9 Hz, 1H), 5.20 (s, 1H), 2.95–2.83 (m, 2H), 2.29 (sept, *J* = 6.9 Hz, 1H), 2.19 (sept, *J* = 6.8 Hz, 1H), 1.72–1.57 (m, 2H), 1.25 (d, *J* = 6.8 Hz, 12H), 1.05 (d, *J* = 6.9 Hz, 3H), 1.04–0.99 (m, 6H), 0.95 (d, *J* = 6.8 Hz, 3H), 0.76 (d, *J* = 6.8 Hz, 3H), 0.70 (d, *J* = 6.8 Hz, 3H), 0.84 (d, *J* = 6.8 Hz, 3H), 0.06 (d, *J* = 6.8 Hz, 3H) ppm; ^{13}C NMR (125 MHz, CD_2Cl_2): δ = 176.3, 176.2, 150.4, 149.6, 149.4, 149.4, 149.2, 148.8, 146.8, 146.7, 146.5, 146.1, 145.2, 143.2, 142.7, 142.6, 142.5, 142.5, 141.8, 141.1, 140.8, 140.4, 137.8, 137.2 (2C), 137.0, 136.9, 135.3, 135.1, 134.7, 134.7, 134.2, 134.1, 133.4, 130.4, 129.2, 128.8, 128.8, 128.2, 127.1, 126.8, 126.6, 126.5, 126.0, 125.5, 125.2, 125.1, 124.4, 124.3, 124.2, 124.2, 121.3, 121.2, 121.1, 121.0, 121.0, 120.9, 120.8, 120.8, 120.7, 120.7, 120.6, 120.5, 118.8, 116.5, 115.9, 112.2, 111.8, 110.4, 110.3, 110.2, 109.7, 34.9, 34.8, 30.9, 30.8, 30.4, 30.3, 25.1, 25.0, 24.5, 24.4, 24.3, 24.3, 24.3, 24.1, 23.8, 23.6, 23.2, 23.2 ppm; IR (film): $\tilde{\nu}$ = 2960, 2928, 1574, 1456, 1425, 1228, 845, 748 cm^{-1}; HRMS (ESI): *m/z* calcd for $C_{90}H_{80}Cl_1Ir_1N_7O_2$: 1518.5687 $[M–PF_6]^+$; found: 1518.5708.

4.7.2.28 Precatalyst Λ-T28

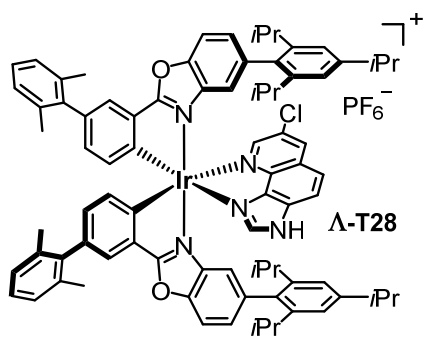

Precatalyst **Λ-T28** was prepared according to general procedures A1), A2), and A5) from benzoxazole ligand **210**, $IrCl_3 \cdot 3H_2O$, auxiliary ligand **(*S*)-Aux2**, and imidazoquinoline ligand **236**.

***Rac*-T28-dimer.** General procedure A1) was followed using benzoxazole ligand **210** (399 mg, 796 µmol, 1.80 eq) and $IrCl_3 \cdot 3H_2O$ (156 mg, 443 µmol, 1.00 eq); reaction time: 23 h; Ir(III) dimer ***rac*-T28-dimer** was obtained as an orange solid (437 mg, 178 µmol, 89%). ***Rac*-T28-dimer** was pushed forward into the next step without characterization.

Λ-(*S*)-T28. General procedure A2) was followed using ***rac*-T28-dimer** (202 mg, 82.0 µmol) and auxiliary ligand **(*S*)-Aux2**; the crude diastereomer mixture was purified and resolved by

f. c. with CH_2Cl_2/hexanes 1:1; only the Λ-(*S*)-diastereomer was isolated; **Λ-(*S*)-T28** was obtained as an orange-red solid (20.6 mg, 14.6 µmol, 18%) and pushed into the next step without characterization.

Precatalyst Λ-T28. General procedure A5) was followed using **Λ-(*S*)-T28** (20.6 mg, 14.6 µmol) and imidazoquinoline ligand **236**; eluent for f. c.: CH_2Cl_2/MeOH 200:1; precatalyst **Λ-T28** was obtained as a yellow-green solid (16.0 mg, 10.6 µmol, 73%). ^{1}H NMR (500 MHz, CD_2Cl_2): δ = 11.32 (s, 1H), 8.24 (d, *J* = 1.9 Hz, 1H), 7.98 (d, *J* = 9.0 Hz, 1H), 7.95 (s, 1H), 7.78 (d, *J* = 1.9 Hz, 1H), 7.76 (d, *J* = 2.2 Hz, 1H), 7.72 (d, *J* = 2.2 Hz, 1H), 7.70 (d, *J* = 9.0 Hz, 1H), 7.66–7.61 (m, 2H), 7.23–7.10 (m, 9H), 7.04 (d, *J* = 1.5 Hz, 1H), 7.01 (d, *J* = 7.7 Hz, 1H), 6.98–6.92 (m, 3H), 6.90 (dd, *J* = 7.9 Hz, *J* = 1.9 Hz, 1H), 6.87 (d, *J* = 1.5 Hz, 1H), 6.43 (d, *J* = 1.0 Hz, 1H), 5.26 (d, *J* = 1.0 Hz, 1H), 2.98–2.83 (m, 2H), 2.44 (sept, *J* = 6.9 Hz, 1H), 2.31 (sept, *J* = 6.8 Hz, 1H), 2.14 (s, 6H), 2.10 (s, 3H), 2.10 (s, 3H), 1.91–1.77 (m, 2H), 1.27 (d, *J* = 7.1 Hz, 12H), 1.11 (d, *J* = 6.9 Hz, 3H), 1.04 (d, *J* = 6.9 Hz, 3H), 1.02 (d, *J* = 6.9 Hz, 3H), 0.97 (d, *J* = 6.9 Hz, 3H), 0.85 (d, *J* = 6.9 Hz, 3H), 0.80 (d, *J* = 6.9 Hz, 3H), 0.19 (d, *J* = 6.9 Hz, 3H), 0.07 (d, *J* = 6.7 Hz, 3H) ppm; IR (film): $\tilde{\nu}$ = 2960, 2927, 1604, 1531, 1456, 1371, 1258, 1184, 1090, 1042, 943, 842, 771, 739, 557 cm^{-1}; HRMS (ESI): *m/z* calcd for $C_{82}H_{82}Cl_1Ir_1N_5O_2$: 1396.5781 $[M–PF_6]^+$; found: 1396.5778.

4.7.2.29 *N*-Methylated Catalyst Λ-T18-Me

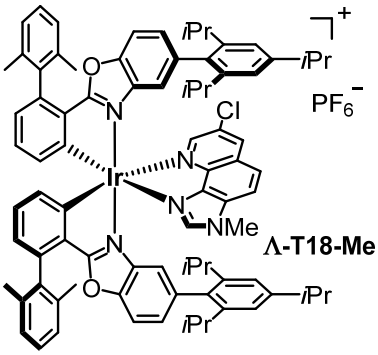

General procedure A5) was followed using diastereomer **Λ-(*S*)-T18** (see 4.7.2.18; 85.3 mg, 60.4 µmol) and *N*-methylated imidazoquinoline ligand **262**; eluent for f. c.: CH_2Cl_2/MeOH 100:1 → 50:1; *N*-methylated complex **Λ-T18-Me** was obtained as a greenish-yellow crystalline solid (63.0 mg, 40.5 µmol, 67%). ^{1}H NMR (300 MHz, CD_2Cl_2): δ = 8.30 (d, *J* = 1.9 Hz, 1H), 7.99 (d, *J* = 1.9 Hz, 1H), 7.85–7.72 (m, 3H), 7.36–7.17 (m, 8H), 7.14 (t, *J* = 7.6 Hz, 1H), 7.11–6.95 (m, 6H), 6.95–6.88 (m, 2H), 6.87–6.78 (m, 2H), 6.71 (d, *J* = 7.6 Hz, 1H), 6.00 (d, *J* = 0.9 Hz, 1H), 5.28 (d, *J* = 0.9 Hz, 1H), 3.81 (s, 3H), 3.00–2.79 (m, 2H), 2.38 (sept, *J* = 6.8 Hz, 1H), 2.25 (sept, *J* = 6.8 Hz, 1H), 2.12–1.98 (m, 12H), 1.88–1.67 (m, 2H), 1.35–1.20 (m, 12H), 1.11 (d, *J* = 7.0 Hz, 3H), 1.09–0.99 (m, 6H), 0.95 (d, *J* = 7.0 Hz, 3H), 0.85–0.73 (m, 6H), 0.15 (d, *J* = 6.8 Hz, 3H), 0.05 (d, *J* = 6.8 Hz, 3H) ppm; ^{13}C NMR (75 MHz, CD_2Cl_2): δ = 178.3, 178.2, 150.7, 149.7, 149.6 (2C), 149.5, 147.2, 147.0, 146.9, 146.5, 146.3, 144.2, 144.1, 142.8, 142.5, 142.1, 141.7, 140.2, 140.1, 139.6, 139.4, 137.7, 137.6, 137.5, 136.6 (2C), 136.2, 136.0, 135.7, 135.4, 134.8, 133.6, 133.2, 133.0, 132.5, 130.8, 128.5, 128.4 (2C), 128.4, 128.1, 128.0, 127.9 (3C), 127.8, 126.1, 125.9,

125.6 (2C), 121.3, 121.0, 121.0, 120.8, 116.5, 116.2, 116.1, 112.1, 112.1, 35.0 (2C), 33.6, 31.0, 30.9, 30.5, 30.5, 25.1 (2C), 24.5, 24.4 (2C), 24.4 (2C), 24.3, 23.9, 23.7, 23.4, 23.3, 21.3, 21.1, 21.1, 21.1 ppm; ^{19}F NMR (282 MHz, CD_2Cl_2): $\delta = -73.4$ (d, $J_{F\text{-}P} = 710$ Hz, PF_6) ppm; ^{31}P NMR (101 MHz, CD_2Cl_2): −144.0 (sept, $J_{F\text{-}P} = 710$ Hz, PF_6) ppm; IR (film): $\tilde{\nu} = 2959$, 1568, 1458, 1414, 837, 772, 734, 705, 556 cm^{-1}; HRMS (ESI): *m/z* calcd for $C_{83}H_{84}Cl_1Ir_1N_5O_2$: 1410.5938 $[M–PF_6]^+$; found: 1410.5936.

4.8 Synthesis of Iridium(III) Complexes Λ-T29, Λ-T30, *rac*-T31-C2 from Chapter 3.

4.8.1 Complex Λ-T29

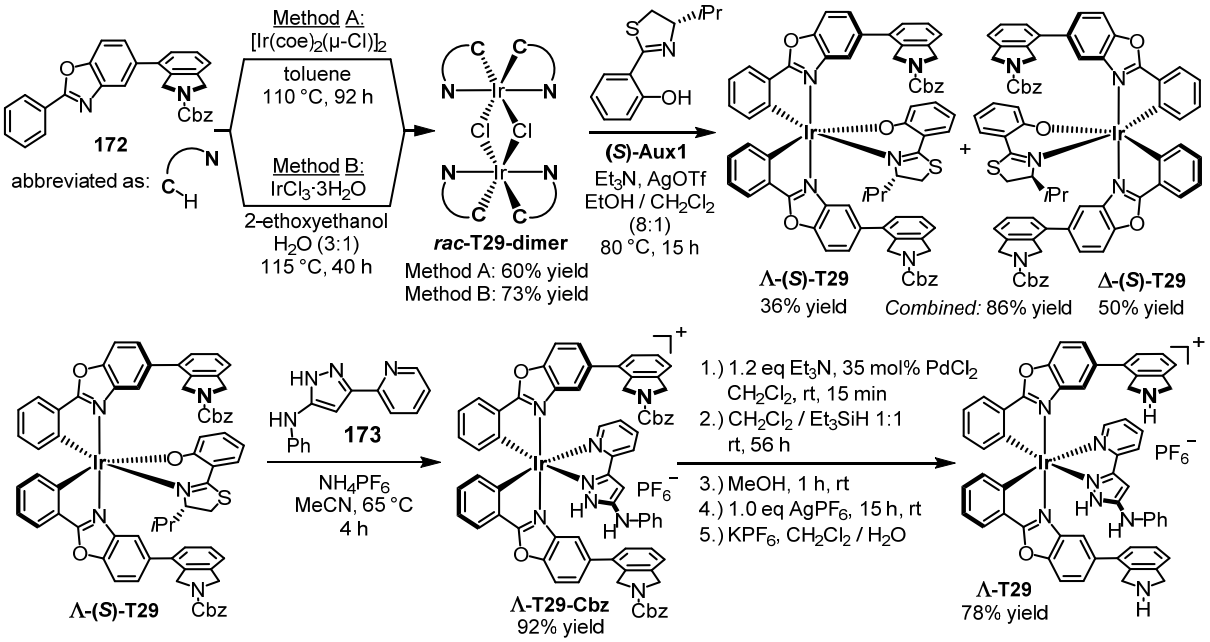

Scheme 82. Synthesis of complex **Λ-T29** from phenylbenzoxazole **172**, $IrCl_3 \cdot 3H_2O$, and aminopyrazole **173**.

***Rac*-T29-dimer.** *Method A.*[116] *Although Ir(I) complex [Ir(coe)$_2$(μ-Cl)]$_2$ is insensitive as a solvent-free powder, it becomes quickly oxidized in solution, in particular at elevated temperatures. Consequently, rigorous exclusion of oxygen was found to be imperative for this protocol.* A flame-dried flask (10 mL) was charged with benzoxazole ligand **172** (311 mg, 697 μmol, 4.17 eq) and $[Ir(coe)_2(\mu\text{-}Cl)]_2$ (150 mg, 167 μmol, 1.00 eq). Then, the flask was evacuated and carefully refilled with nitrogen gas (3x). Dry and degassed toluene (6.5 mL; from a solvent still, additionally degassed (3x) via freeze-pump-thaw technique) was added and the mixture stirred at 110 °C for 92 h under nitrogen atmosphere and under exclusion of light, which gave a clear, deeply orange solution. After cooling to rt, all volatiles were removed *in vacuo* and the crude product purified via flash chromatography (CH_2Cl_2/MeOH 400:1 → 250:1 → 150:1). After solvent removal and drying *in vacuo*, desired ***rac*-T29-dimer** was obtained as a deeply orange solid (223 mg, 100 μmol, 60%).

Method B.[77] A flask (50 mL) was charged with $IrCl_3 \cdot 3H_2O$ (193 mg, 547 µmol, 1.00 eq), benzoxazole ligand **172** (500 mg, 1.12 mmol, 2.05 eq), and a 3:1 mixture of 2-ethoxyethanol and H_2O (24 mL). The resulting mixture was purged with nitrogen gas for 10 min. Then, the mixture was stirred at 115 °C for 40 h under exclusion of light. After cooling to rt, H_2O (25 mL) was added which caused the formation of a yellow precipitate. The precipitate was filtered off and thoroughly washed with excess water and a small amount of Et_2O (20 mL). The precipitate was then dissolved in CH_2Cl_2, the resulting organic layer dried over Na_2SO_4, and the organic layer passed through a plug of celite which was subsequently rinsed with CH_2Cl_2. After solvent removal and drying *in vacuo*, desired ***rac*-T29-dimer** was obtained as a brown-orange solid without the need for further purification (449 mg, 201 µmol, 73%).

^{1}H NMR (500 MHz, $CDCl_3$): δ = 8.60–8.38 (m, 4H), 7.61–6.99 (m, 44H), 6.90–6.52 (m, 8H), 6.30–6.10 (m, 4H), 5.39–4.51 (m, 24H) ppm; ^{13}C NMR (125 MHz, $CDCl_3$): δ = 178.0–177.8 (4x C_q), 155.1–154.8 (4x C_q), 149.4–149.1 (4x C_q), 144.9–144.1 (4x C_q), 140.5–140.0 (4x C_q), 138.1–137.5 (4x C_q), 137.4–136.9 (8x C_q), 136.2–135.9 (4x C_q), 134.9–134.3 (4x C_q), 133.2–132.5 (4x CH), 132.5–131.7 (4x CH), 129.3–128.9 (4x C_q), 128.9–127.7 (28x CH), 125.8–125.4 (4x CH), 124.5–123.7 (4x CH), 122.3–121.4 (8x CH), 118.5–117.6 (4x CH), 111.1–110.5 (4x CH), 67.5–66.7 (4x CH_2), 53.1–52.6 (4x CH_2), 52.4–51.9 (4x CH_2) ppm (^{1}H and ^{13}C signals are split up into complex signals due to hindered rotation of the four Cbz groups); IR (film): $\tilde{\nu}$ = 1699, 1589, 1446, 1408, 1386, 1362, 1346, 1282, 1099, 1072, 1037, 779, 769, 726, 696, 454 cm^{-1}; HRMS (ESI): *m/z* calcd for $C_{116}H_{84}Cl_2Ir_2N_8O_{12}$: 2259.4736 [*M*+Na]$^+$; found: 2259.4724.

Λ-(*S*)-T29 and Δ-(*S*)-T29. A flask (10 mL) was charged with ***rac*-T29-dimer** (100 mg, 44.9 µmol, 1.00 eq), auxiliary ligand **(*S*)-Aux1** (24.8 mg, 112 µmol, 2.50 eq), AgOTf (27.5 mg, 107 µmol, 2.38 eq), and an 8:1 mixture of ethanol and CH_2Cl_2 (8.2 mL). The mixture was purged with nitrogen gas for 5 min. Then, Et_3N (62.5 µL, 448 µmol, 10.0 eq) was added and the mixture stirred at 80 °C for 15 h under exclusion of light and under nitrogen atmosphere. After cooling to rt, the solvent was removed *in vacuo* and the crude diastereomer mixture purified and resolved via flash chromatography (CH_2Cl_2/MeOH 300:1 → 200:1). Both diastereomers were isolated as deeply orange solids (**Λ-(*S*)-T29**: 42.4 mg, 32.5 µmol, 36%; **Δ-(*S*)-T29**: 58.4 mg, 44.8 µmol, 50%).

Analytic data for **Λ-(*S*)-T29**:

^{1}H NMR (500 MHz, CD_2Cl_2): δ = 7.90–7.85 (m, 1H), 7.79–7.64 (m, 4H), 7.58–7.17 (m, 19H), 7.16–7.05 (m, 1H), 7.05–6.90 (m, 3H), 6.90–6.82 (m, 1H), 6.81–6.73 (m, 1H), 6.71–6.65 (m, 1H), 6.61–6.49 (m, 1H), 6.44–6.34 (m, 1H), 6.32–6.16 (m, 1H), 5.31–4.45 (m, 12H), 4.44–4.21 (m, 1H), 3.00–2.91 (m, 1H), 2.88–2.77 (m, 1H), 0.90–0.74 (m, 1H), 0.26–0.12 (m,

6H) ppm (^{1}H signals are split up into complex signals due to hindered rotation of the two Cbz groups); HRMS (ESI): *m/z* calcd for $C_{70}H_{56}Ir_1N_5O_7S_1H$: 1304.3607 $[M+H]^+$; found: 1304.3591.

Analytic data for **Δ-(*S*)-T29**:

^{1}H NMR (400 MHz, $CDCl_3$): δ = 8.00–7.89 (m, 1H), 7.82–6.63 (m, 30H), 6.53–6.36 (m, 2H), 6.31–6.11 (m, 1H), 5.33–5.09 (m, 4H), 4.94–4.47 (m, 8H), 3.65–3.53 (m, 1H), 2.91–2.63 (m, 2H), 2.04–1.89 (m, 1H), 0.70–0.54 (m, 3H), 0.07–0.04 (m, 3H) ppm (^{1}H signals are split up into complex signals due to hindered rotation of the two Cbz groups); HRMS (ESI): *m/z* calcd for $C_{70}H_{56}Ir_1N_5O_7S_1H$: 1304.3607 $[M+H]^+$; found: 1304.3590.

Λ-T29-Cbz. A flask (10 mL) was charged with **Λ-(*S*)-T29** (34.8 mg, 26.7 µmol, 1.00 eq), aminopyrazole ligand **173** (14.6 mg, 61.8 µmol, 2.31 eq), NH_4PF_6 (21.9 mg, 134 µmol, 5.03 eq), and MeCN (2.7 mL). The mixture was purged with nitrogen gas for 5 min and then stirred at 65 °C for 4 h. After cooling to rt, all volatiles were removed *in vacuo* and the crude product purified by flash chromatography (CH_2Cl_2/MeOH 300:1 → 100:1). After solvent removal and drying *in vacuo*, **Λ-T29-Cbz** was obtained as a yellow solid (35.9 mg, 24.5 µmol, 92%). ^{1}H NMR (300 MHz, CD_2Cl_2): δ = 12.22–11.70 (m, 1H), 10.75–10.40 (m, 1H), 8.18–6.60 (m, 38H), 6.45–6.20 (m, 1H), 6.05–5.78 (m, 1H), 5.28–4.99 (m, 4H), 4.88–4.14 (m, 8H) ppm (^{1}H signals are split up into complex signals due to hindered rotation of the two Cbz groups); HRMS (ESI): *m/z* calcd for $C_{72}H_{54}Ir_1N_8O_6$: 1319.3797 $[M–PF_6]^+$; found: 1319.3798.

Complex Λ-T29. A flask (10 mL) was charged with **Λ-T29-Cbz** (39.7 mg, 27.1 µmol, 1.00 eq) and $PdCl_2$ (1.7 mg, 9.6 µmol, 35 mol%). The flask was evacuated and carefully refilled with nitrogen gas (3x). Then, CH_2Cl_2 (1.3 mL) and Et_3N (4.6 µL, 33 µmol, 1.2 eq) were added and the mixture vigorously stirred at rt for 15 min under nitrogen atmosphere. Then, Et_3SiH (1.30 mL, 8.14 mmol, 300 eq) was added at once and the mixture vigorously stirred at rt for 56 h under nitrogen atmosphere after which TLC (CH_2Cl_2/MeOH 10:1 + trace of Et_3N) indicated full conversion. MeOH (6 mL) was added and the mixture stirred at rt until the gas evolution ceased (1 h). Then, a solution of $AgPF_6$ (6.9 mg, 27.3 µmol, 1.01 eq) in MeOH (2 mL) was added and the mixture stirred for 15 min at rt under exclusion of light. The resulting mixture was passed through a glass filter (porosity G4), all volatiles removed *in vacuo*, and the crude product purified by flash chromatography (CH_2Cl_2/MeOH/Et_3N 500:20:10 → 500:30:10 → 500:40:10). After solvent removal, the product was taken up in CH_2Cl_2 and the organic layer washed with water (2x), aqueous KPF_6 (1x), and again with water (2x). After solvent removal and drying *in vacuo*, **Λ-T29** was obtained as a yellow-ocher solid (25.4 mg, 21.2 µmol, 78%). Chiral HPLC analysis: >99% ee according to the applied indirect procedure, which is explained in detail in chapter 3.2.1. ^{1}H NMR (600 MHz,

DMSO-d_6): δ = 12.38–12.25 (m, 1H), 8.43 (s, 1H), 8.00–7.76 (m, 6H), 7.72 (d, J = 7.1 Hz, 1H), 7.49 (d, J = 8.6 Hz, 2H), 7.30–7.22 (m, 2H), 7.17–6.85 (m, 11H), 6.83 (dd, J = 6.0 Hz, J = 1.8 Hz, 1H), 6.71 (d, J = 7.4 Hz, 1H), 6.63–6.51 (m, 3H), 6.43 (d, J = 1.0 Hz, 1H), 6.00 (d, J = 1.0 Hz, 1H), 4.80–3.20 (br m, 3H), 4.33 (d, J = 14.0 Hz, 1H), 4.15 (s, 2H), 4.06–3.92 (m, 4H), 3.84 (d, J = 13.8 Hz, 1H) ppm; ^{13}C NMR (125 MHz, DMSO-d_6): δ = 177.9 (C_q), 177.6 (C_q), 156.8 (C_q), 155.6 (C_q), 152.4 (C_q), 151.9 (C_q), 150.6 (CH), 149.7 (C_q), 148.9 (C_q), 148.9 (C_q), 144.4 (C_q), 142.3 (C_q), 141.2 (C_q), 138.9 (CH), 138.7 (C_q), 138.3 (C_q), 138.2 (C_q), 138.1 (C_q), 137.9 (C_q), 137.3 (C_q), 134.8 (C_q), 134.6 (C_q), 133.5 (CH), 132.8 (2x CH), 131.9 (CH), 129.6 (C_q), 128.7 (2x CH), 128.5 (C_q), 127.6 (CH), 127.5 (CH), 126.9 (CH), 126.7 (CH), 126.2 (CH), 125.7 (CH), 125.6 (CH), 125.5 (CH), 122.0 (CH), 121.9 (2x CH), 121.6 (CH), 121.2 (CH), 119.3 (CH), 116.8 (CH), 115.5 (CH), 113.7 (2x CH), 113.5 (CH), 112.5 (CH), 112.1 (CH), 90.2 (CH), 52.1 (CH_2), 51.7 (2x CH_2), 51.6 (CH_2) ppm; IR (film): $\tilde{\nu}$ = 1561, 1504, 1446, 1405, 1177, 770, 746, 709 cm^{-1}; HRMS (ESI): *m/z* calcd for $C_{56}H_{42}Ir_1N_8O_2$: 1051.3060 [M–PF_6]$^+$, found: 1051.3047.

4.8.2 Complex Λ-T30

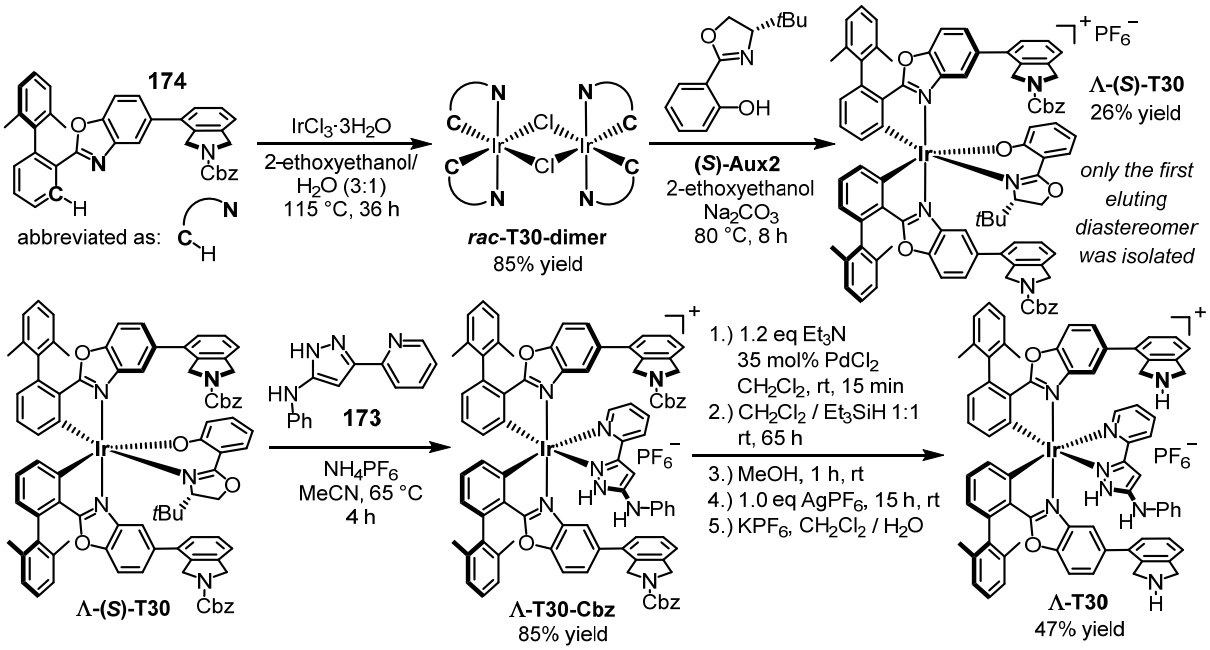

Scheme 83. Synthesis of complex **Λ-T30** from phenylbenzoxazole **174**, $IrCl_3 \cdot 3H_2O$, and aminopyrazole **173**.

***Rac*-T30-dimer.** A flask (50 mL) was charged with $IrCl_3 \cdot 3H_2O$ (304 mg, 862 µmol, 1.00 eq), benzoxazole ligand **174** (1.00 g, 1.82 mmol, 2.11 eq), and a 3:1 mixture of 2-ethoxyethanol and H_2O (40 mL). The resulting mixture was purged with nitrogen gas for 15 min. Then, the mixture was stirred at 115 °C for 36 h under exclusion of light and under nitrogen atmosphere. After cooling to rt, H_2O (50 mL) was added, which caused the formation of a yellow precipitate. The precipitate was filtered off and thoroughly washed with excess water and a small

amount of Et_2O (20 mL). The precipitate was then dissolved in CH_2Cl_2, the resulting organic layer dried over Na_2SO_4, and the organic layer passed through a plug of celite which was subsequently rinsed with CH_2Cl_2. After solvent removal and drying *in vacuo*, desired ***rac*-T30-dimer** was obtained as an orange solid without the need for further purification (977 mg, 368 µmol, 85%).

^{1}H NMR (300 MHz, CD_2Cl_2): δ = 8.15–7.96 (m, 4H), 7.60–6.74 (m, 52H), 6.74–6.53 (m, 4H), 6.50–6.32 (m, 4H), 6.19–5.98 (m, 4H), 5.33–4.71 (m, 20H), 4.34–4.11 (m, 4H), 1.80–1.61 (m, 12H), 1.39–1.19 (m, 12H) ppm (^{1}H signals are split up into complex signals due to hindered rotation of the four Cbz groups); HRMS (ESI): *m/z* calcd for $C_{74}H_{58}Ir_1N_4O_6$: 1291.3987 $[½M-Cl]^+$; found: 1291.3999.

Λ-(*S*)-T30. A flask (25 mL) was charged with ***rac*-T30-dimer** (300 mg, 113 µmol, 1.00 eq), auxiliary ligand **(*S*)-Aux2** (62.0 mg, 283 µmol, 2.50 eq), Na_2CO_3 (182 mg, 1.72 mmol, 15.2 eq), and 2-ethoxyethanol (11.5 mL). The mixture was purged with nitrogen gas for 15 min and then stirred at 80 °C for 8 h under exclusion of light and under nitrogen atmosphere. After cooling to rt, all volatiles were removed *in vacuo* and the remaining residue purified by flash chromatography (CH_2Cl_2/MeOH/Et_3N 500:1:1 → 500:3:1). Only the Λ-(*S*)-diastereomer was isolated; diastereomer **Λ-(*S*)-T30** was obtained as a red-orange solid (88.9 mg, 58.9 µmol, 26%). ^{1}H NMR: Complex ^{1}H signals due to hindered rotation of the two Cbz groups, interpretation unfeasible; HRMS (ESI): *m/z* calcd for $C_{87}H_{75}Ir_1N_5O_8$: 1510.5249 $[M+H]^+$, found: 1510.5225.

Λ-T30-Cbz. A flask (10 mL) was charged with **Λ-(*S*)-T30** (88.9 mg, 58.9 µmol, 1.00 eq), aminopyrazole ligand **173** (32.7 mg, 138 µmol, 2.35 eq), NH_4PF_6 (48.2 mg, 296 µmol, 5.02 eq), and MeCN (6.0 mL). The mixture was purged with nitrogen gas for 5 min and then stirred at 65 °C for 4 h. After cooling to rt, all volatiles were removed *in vacuo* and the crude product purified by flash chromatography (CH_2Cl_2 300:1 → 150:1). After solvent removal and drying *in vacuo*, desired **Λ-T30-Cbz** was obtained as a green-yellow solid (83.8 mg, 50.1 µmol, 85%). ^{1}H NMR (300 MHz, CD_2Cl_2): δ = 13.19–12.94 (m, 1H), 10.93–10.73 (m, 1H), 8.34–6.38 (m, 42H), 6.35–6.15 (m, 1H), 5.89–5.69 (m, 1H), 5.28–5.02 (m, 4H), 4.89–3.86 (m, 8H), 2.41–1.80 (m, 12H) ppm (^{1}H signals are split up into complex signals due to hindered rotation of the two Cbz groups); IR (film): $\tilde{\nu}$ = 1702, 1576, 1463, 1445, 1408, 1349, 1283, 1179, 1100, 838, 769, 747, 696, 556 cm^{-1}; HRMS (ESI): *m/z* calcd for $C_{88}H_{70}Ir_1N_8O_6$: 1527.5051 $[M–PF_6]^+$, found: 1527.5040.

Complex Λ-T30. A flask (25 mL) was charged with **Λ-T30-Cbz** (107 mg, 64.0 µmol, 1.00 eq) and $PdCl_2$ (35 mg, 19.7 µmol, 31 mol%). The flask was evacuated and then carefully refilled with nitrogen gas (3x). Then, CH_2Cl_2 (3.0 mL) and Et_3N (10.7 µL, 76.8 µmol,

1.20 eq) were added and the mixture vigorously stirred at rt for 15 min under nitrogen atmosphere. Et_3SiH (3.1 mL, 19.4 mmol, 303 eq) was added at once and the mixture vigorously stirred at rt for 65 h under nitrogen atmosphere after which TLC (CH_2Cl_2/MeOH 10:1 + a trace of Et_3N) indicated full conversion. The flask was cooled to 0 °C and MeOH (15 mL) was added and the mixture stirred at rt until the gas evolution ceased (1 h). Then, a solution of $AgPF_6$ (16 mg, 63 µmol, 1.0 eq) in MeOH (2 mL) was added and the mixture stirred at rt for 15 min under exclusion of light. The resulting mixture was passed through a glass filter (porosity G4), all volatiles removed *in vacuo* (40 °C), and the crude product purified by flash chromatography (CH_2Cl_2/MeOH/Et_3N 500:15:10 → 500:20:10). After solvent removal, the residue was taken up in CH_2Cl_2 and the organic layer washed with water (2x), aqueous KPF_6 (1x), and again with water (2x). After solvent removal and drying *in vacuo*, **Λ-T30** was obtained as a yellow-ocher solid (42.2 mg, 30.0 µmol, 47%). ^{1}H NMR (500 MHz, DMSO-d_6): δ = 12.41–12.20 (m, 1H), 8.40 (s, 1H), 8.00–7.85 (m, 2H), 7.81 (t, J = 7.4 Hz, 1H), 7.44–7.30 (m, 4H), 7.29–7.09 (m, 10H), 7.08–6.97 (m, 6H), 6.97–6.87 (m, 2H), 6.76 (d, J = 6.9 Hz, 1H), 6.73 (d, J = 7.3 Hz, 1H), 6.65 (d, J = 7.3 Hz, 1H), 6.62 (d, J = 7.6 Hz, 1H), 6.57 (t, J = 6.7 Hz, 1H), 6.55–6.48 (m, 2H), 6.42 (s, 1H), 5.99 (s, 1H), 4.17–3.70 (m, 8H), 3.38 (br s, 2H), 2.08 (s, 3H), 1.96 (s, 3H), 1.88 (s, 3H), 1.84 (s, 3H) ppm; ^{13}C NMR (100 MHz, DMSO-d_6): δ = 177.8 (C_q), 177.7 (C_q), 157.5 (C_q), 156.8 (C_q), 153.7 (C_q), 152.9 (C_q), 150.2 (CH), 149.5 (C_q), 148.5 (C_q), 148.5 (C_q), 144.4 (C_q), 143.2 (C_q), 142.6 (C_q), 140.9 (C_q), 140.4 (C_q), 139.6 (C_q), 139.4 (C_q), 139.3 (2x C_q), 139.0 (CH), 138.5 (C_q), 138.4 (C_q), 137.7 (C_q), 136.8 (C_q), 135.4 (2x C_q), 135.3 (C_q), 135.0 (C_q), 134.5 (C_q), 134.5 (C_q), 132.4 (CH), 131.7 (CH), 131.5 (CH), 131.1 (CH), 128.5 (2x CH), 127.7 (C_q), 127.4 (CH), 127.3 (2x CH), 127.2 (CH), 127.1 (3x CH), 127.0 (CH), 126.6 (CH), 126.5 (C_q), 126.4 (CH), 125.6 (CH), 125.4 (CH), 123.2 (CH), 122.3 (CH), 121.9 (CH), 121.8 (CH), 121.4 (CH), 119.5 (CH), 116.7 (CH), 115.6 (CH), 113.9 (2x CH), 113.5 (CH), 111.9 (CH), 111.3 (CH), 90.1 (CH), 52.4 (CH_2), 52.3 (CH_2), 52.2 (CH_2), 52.0 (CH_2), 20.7 (CH_3), 20.3 (CH_3), 20.3 (CH_3), 20.2 (CH_3) ppm; IR (film): $\tilde{\nu}$ = 1599, 1561, 1504, 1459, 1446, 1405, 1260, 1177, 822, 770, 747, 709 cm^{-1}; HRMS (ESI): *m/z* calcd for $C_{72}H_{58}Ir_1N_8O_2$: 1259.4313 [M–PF_6]$^+$, found: 1259.4137.

4.8.3 Bispyrazole Complex *rac*-T31-C2

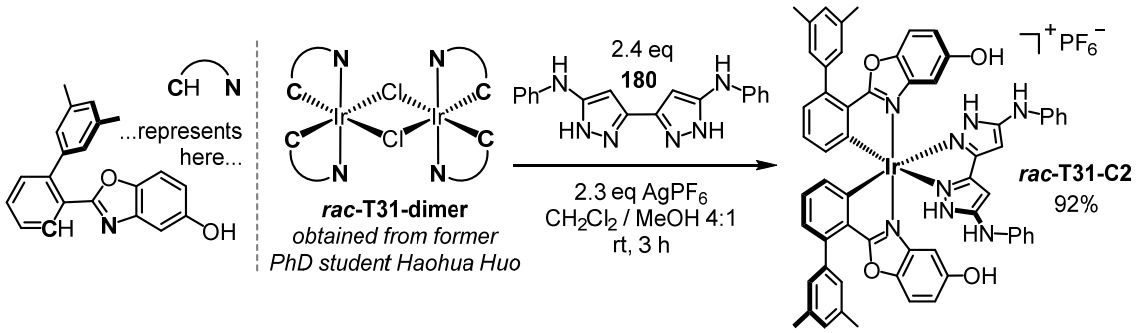

Scheme 84. Synthesis of complex ***rac*-T31-C2** from Ir(III) dimer ***rac*-T31-dimer** and bispyrazole ligand **180**.

An amber glas vial with a stir bar was charged with ***rac*-T31-dimer** (obtained from former PhD student Haohua Huo; 34.1 mg, 15.2 µmol, 1.00 eq), bispyrazole ligand **180** (12.5 mg, 39.5 µmol, 2.60 eq), $AgPF_6$ (10.0 mg, 39.6 µmol, 2.60 eq), and a 4:1 mixture of CH_2Cl_2 and MeOH (1.0 mL) and the resulting mixture stirred at rt for 3 h. As TLC (CH_2Cl_2/MeOH 35:1) indicated full, all volatiles were removed *in vacuo* and the crude product purified by flash chromatography (CH_2Cl_2/MeOH 300:1 → 200:1). After solvent removal and drying *in vacuo*, desired bispyrazole complex ***rac*-T31-C2** was obtained as a yellow solid (48.5 mg, 31.4 µmol, 92%). ^{1}H NMR (500 MHz, DMSO-d_6): δ = 12.79 (s, 2H), 9.86 (s, 2H), 8.44 (s, 2H), 7.39 (d, J = 9.2 Hz, 2H), 7.30–7.24 (m, 4H), 7.15–7.08 (m, 6H), 7.07 (s, 2H), 7.05 (s, 2H), 6.95 (t, J = 7.7 Hz, 2H), 6.92–6.84 (m, 8H), 6.47 (dd, J = 7.6 Hz, J = 0.8 Hz, 2H), 5.61 (d, J = 2.4 Hz, 2H), 2.37 (s, 12H) ppm; ^{13}C NMR (125 MHz, DMSO-d_6): δ = 177.2 (2x C_q), 156.1 (2x C_q), 148.2 (2x C_q), 148.0 (2x C_q), 146.7 (2x C_q), 142.7 (2x C_q), 142.2 (2x C_q), 142.1 (2x C_q), 139.5 (2x C_q), 137.3 (2x C_q), 136.7 (4x C_q), 131.8 (2x CH), 131.2 (2x CH), 129.4 (4x CH), 129.1 (2x CH), 127.1 (4x CH), 126.9 (2x C_q), 124.8 (2x CH), 120.5 (2x CH), 115.6 (4x CH), 114.0 (2x CH), 112.2 (2x CH), 100.3 (2x CH), 90.8 (2x CH), 21.0 (4x CH_3) ppm; IR (film): $\tilde{\nu}$ = 1571, 1478, 1439, 1410, 1163, 830, 794, 740, 689, 557 cm^{-1}; HRMS (ESI): *m/z* calcd for $C_{60}H_{48}Ir_1N_8O_4$: 1137.3427 [M–PF_6]$^+$, found: 1137.3465.

4.9 Synthesis of Catalysis Substrates

4.9.1 *O*-Acylated Azlactones (13a–i)

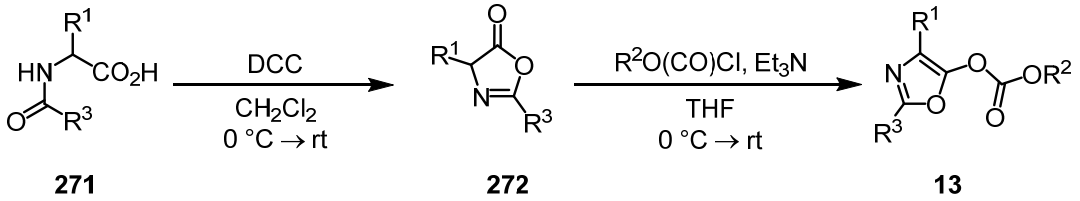

271 **272** **13**

Scheme 85. Synthesis of *O*-acylated azlactones (**13**) from *N*-acylated acids (**271**).

Literature reported *O*-acylated azlactones **13a–c**,[22a] **13d**,[142] and **13e**[143] were synthesized according to the reported procedures. **13f–i** were synthesized analogously: First, the respective *N*-acylated acids (**271**) were synthesized either by a Schotten–Baumann reaction of the respective *α*-amino acid and the appropriate acid chloride or by *N*-acylation of the respective *α*-amino acid ester hydrochloride and subsequent ester saponification.[22a] The *N*-acylated acids (**271**) were then subjected to DCC-promoted cyclization to the according azlactones (**272**), which were finally acylated with the appropriate chloroformates to give *O*-acylated azlactones (**13**; Scheme 85).

4.9.1.1 General Procedures B1)–B3)

General Procedure B1). Synthesis of *N*-acylated acids (**271**).[22a]

A flask was charged with the indicated *α*-amino acid ester hydrochloride (1.00 eq) and dry CH_2Cl_2 (conc = 0.3 M). The mixture was cooled to 0 °C and the indicated amounts of acid chloride and Et_3N were added. The mixture was kept at 0 °C for 10 min and then allowed to warm to rt and stirred for the indicated time. Then, the mixture was diluted with CH_2Cl_2 and washed with 1 M HCl (2x), aqueous $NaHCO_3$, and brine and dried over Na_2SO_4. All volatiles were removed *in vacuo* and the remaining residue was suspended in a 2:1 mixture of MeOH and aqueous 2 M NaOH (conc = 0.35 M; recommended: dissolve residue first in MeOH, then add aqueous NaOH). The resulting suspension was vigorously stirred until a clear solution was obtained (1 h). MeOH was then selectively removed *in vacuo* and the remaining aqueous layer was diluted with water and washed with CH_2Cl_2 (2x). The resulting organic layer was disposed and the remaining aqueous layer acidified to pH ≤ 2 with 1 M HCl, which caused the formation of a white precipitate. CH_2Cl_2 was added causing precipitate dissolution. The resulting organic layer was separated, the aqueous layer extracted with CH_2Cl_2 (3x), and the combined organic layers dried over Na_2SO_4. After solvent removal and drying *in vacuo*, the desired *N*-acylated acid (**271**) was obtained without the need for further purification.

General Procedure B2). DCC-promoted cyclization of *N*-acylated acids to azlactones (**271** → **272**).[22a]

A flame-dried flask was charged with the indicated *N*-acylated acid (**271**; 1.00 eq) and dry CH_2Cl_2 (conc = 0.15 M). The mixture was cooled to 0 °C, DCC added (1.01 eq), and the resulting mixture allowed to warm to rt and stirred for the indicated time under nitrogen atmosphere. The resulting white precipitate was filtered off with a glass filter (porosity G3), which was subsequently rinsed with CH_2Cl_2. The filtrate was concentrated *in vacuo* and the resulting crude product purified by short-column chromatography with the indicated eluent. After drying *in vacuo*, the desired azlactone (**272**) was obtained.

General Procedure B3). Acylation of azlactones to *O*-acylated azlactones (**272** → **13**).[22a]

A flame-dried flask was charged with the indicated azlactone (**272**; 1.00 eq) and dry THF (conc = 0.1 M). The mixture was cooled to 0 °C, the indicated amounts of Et_3N and chloroformate were added, and the mixture was allowed to warm to rt and stirred for the indicated time. Then, the mixture was diluted with MTBE and 1 M HCl. The aqueous layer was extracted with MTBE (1x) and the combined organic layers were washed with 1 M HCl and brine and dried over Na_2SO_4. After solvent removal, the remaining residue was dissolved in CH_2Cl_2, adsorbed on silica gel (40 °C), and purified by flash chromatography with the indicated eluent. After drying *in vacuo*, the desired *O*-acylated azlactone (**13**) was obtained.

4.9.1.2 Synthetic Procedures and Characterizations

Benzyl (4-benzyl-2-(4-methoxyphenyl)oxazol-5-yl) carbonate (13a)[22a]

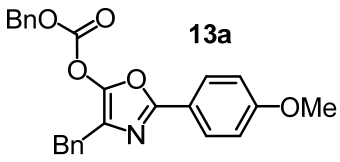

13a was synthesized according to procedures reported by Fu et al.[22a] in a three-step synthesis starting with 1.) Schotten–Baumann reaction between phenylalanine (1.00 eq) and *p*-anisoyl chloride followed by 2.) DCC-promoted cyclization and finally 3.) *O*-acylation with benzyl chloroformate. **13a** was obtained as a pale-yellow oil which slowly crystallized on standing to an almost colorless solid (2.43 g, 5.84 mmol, 77% over three steps). ^{1}H NMR (300 MHz, $CDCl_3$): δ = 7.89 (d, J = 8.9 Hz, 2H), 7.48–7.15 (m, 10H), 6.92 (d, J = 9.1 Hz, 2H), 5.21 (s, 2H), 3.92–3.77 (m, 5H) ppm; ^{13}C NMR (75 MHz, $CDCl_3$): δ = 161.5, 155.4, 151.6, 146.1, 137.7, 134.0, 129.2, 129.0 (2C), 128.9 (2C), 128.8 (2C), 128.6 (2C), 127.9 (2C), 126.6, 123.1, 120.0, 114.3 (2C), 71.8, 55.5, 31.6 ppm; IR (film): $\tilde{\nu}$ = 1765, 1496, 1255, 1215, 1161, 1109, 1029, 953, 831, 739, 693, 513 cm^{-1}; HRMS (EI): *m/z* calcd for $C_{25}H_{21}N_1O_5$: 415.1420 $[M]^+$; found: 415.1413.

Benzyl (4-isobutyl-2-(4-methoxyphenyl)oxazol-5-yl) carbonate (13b)[22a]

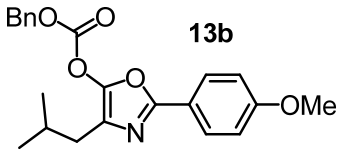

13b was synthesized according to procedures reported by Fu et al.[22a] in a three-step synthesis starting with 1.) *N*-acylation of leucine methyl ester hydrochloride (1.00 eq) with *p*-anisoyl chloride and subsequent saponification with aqueous 2 M NaOH in MeOH followed by 2.) DCC-promoted cyclization and finally 3.) *O*-acylation with benzyl chloroformate. **13b** was obtained as a colorless oil (709 mg, 1.86 mmol, 77% over three steps). ^{1}H NMR (300 MHz, $CDCl_3$): δ = 7.98–7.81 (m, 2H), 7.53–7.32 (m, 5H), 7.02–6.85 (m, 2H), 5.32 (s, 2H), 3.85 (s, 3H), 2.32 (d, J = 7.0 Hz, 2H), 2.13–1.92 (m, 1H), 0.93 (d, J = 6.6 Hz, 6H) ppm; ^{13}C NMR (75 MHz, $CDCl_3$): δ = 161.6, 155.2, 151.9, 146.2, 134.2, 129.3, 129.0 (2C), 128.8 (2C), 127.9 (2C), 123.5, 120.1, 114.3 (2C), 71.8, 55.5, 33.9, 27.7, 22.5 (2C) ppm; IR (film): $\tilde{\nu}$ = 1785, 1450, 1254, 1218, 1174 cm^{-1}; HRMS (ESI): *m/z* calcd for $C_{22}H_{23}N_1O_5Na$: 404.1468 [*M*+Na]$^+$; found: 404.1476.

Benzyl (2-(4-methoxyphenyl)-4-methyloxazol-5-yl) carbonate (13c)[22a]

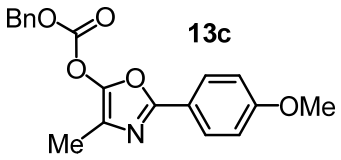

13c was synthesized according to procedures reported by Fu et al.[22a] in a three-step synthesis starting with 1.) *N*-acylation of alanine methyl ester hydrochloride (1.00 eq) with *p*-anisoyl chloride and subsequent saponification with aqueous 2 M NaOH in MeOH followed by 2.) DCC-promoted cyclization and finally 3.) *O*-acylation with benzyl chloroformate. **13c** was obtained as a colorless crystalline solid (548 mg, 1.61 mmol, 48% over three steps). ^{1}H NMR (300 MHz, $CDCl_3$): δ = 7.89 (d, J = 8.9 Hz, 2H), 7.56–7.32 (m, 5H), 6.94 (d, J = 8.9 Hz, 2H), 5.33 (s, 2H), 3.85 (s, 3H), 2.12 (s, 3H) ppm; ^{13}C NMR (75 MHz, $CDCl_3$): δ = 161.6, 155.1, 151.8, 145.8, 134.1, 129.3, 129.0 (2C), 128.8 (2C), 127.8 (2C), 120.1, 120.0, 114.4 (2C), 71.9, 55.5, 10.3 ppm; IR (film): $\tilde{\nu}$ = 1782, 1498, 1251, 1204, 1175, 1028, 837, 742 cm^{-1}; HRMS (ESI): *m/z* calcd for $C_{19}H_{17}N_1O_5Na$: 362.0999 [*M*+Na]$^+$; found: 362.0998.

4-Benzyl-2-(4-methoxyphenyl)oxazol-5-yl methyl carbonate (13d)[22a,142]

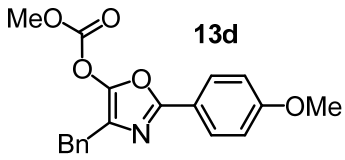

13d was synthesized according to procedures reported by Fu[22a] and Smith[142] in a three-step synthesis starting with 1.) Schotten–Baumann reaction between phenylalanine (1.00 eq) and *p*-anisoyl chloride[22a] followed by 2.) DCC-promoted cyclization[22a] and finally 3.) *O*-acylation with methyl chloroformate.[142] **13d** was obtained as a pale yellow oil which slowly crystallized on standing to an almost colorless solid (579 mg, 1.70 mmol, 68% over three steps). ^{1}H NMR (300 MHz, $CDCl_3$): δ = 7.89 (d, J = 8.7 Hz, 2H),

7.41–7.12 (m, 5H), 6.93 (d, J = 8.7 Hz, 2H), 3.92–3.85 (m, 5H), 3.85 (s, 3H) ppm; ^{13}C NMR (75 MHz, $CDCl_3$): δ = 161.7, 155.4, 152.2, 146.1, 137.7, 129.1 (2C), 128.6 (2C), 128.0 (2C), 126.6, 123.0, 119.9, 114.3 (2C), 56.6, 55.5, 31.6 ppm; IR (film): $\tilde{\nu}$ = 1786, 1612, 1498, 1222, 1169, 1028, 924, 705 cm^{-1}; HRMS (ESI): *m/z* calcd for $C_{19}H_{17}N_1O_5H$: 340.1179 $[M+H]^+$; found: 340.1180.

4-Benzyl-2-(4-methoxyphenyl)oxazol-5-yl 3,3,3-trichloro-2,2-dimethylpropanoate (13e)[22a,142]

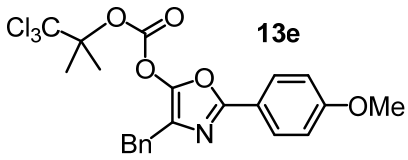

13e was synthesized according to procedures reported by Fu[22a] and Smith[142] in a three-step synthesis starting with 1.) Schotten–Baumann reaction between phenylalanine (1.00 eq) and *p*-anisoyl chloride[22a] followed by 2.) DCC-promoted cyclization[22a] and finally 3.) *O*-acylation with 2,2,2-trichloro-1,1-dimethylethyl chloroformate.[142] **13e** was obtained as a colorless crystalline solid (1.20 g, 2.49 mmol, 79% over three steps). ^{1}H NMR (300 MHz, $CDCl_3$): δ = 7.94–7.86 (m, 2H), 7.36–7.15 (m, 5H), 6.98–6.88 (m, 2H), 3.89 (s, 2H), 3.85 (s, 3H), 1.92 (s, 6H) ppm; ^{13}C NMR (75 MHz, $CDCl_3$): δ = 161.6, 155.4, 148.3, 145.7, 137.6, 129.0 (2C), 128.6 (2C), 127.9 (2C), 126.7, 123.2, 120.0, 114.3 (2C), 104.6, 92.3, 55.5, 31.8, 21.1 (2C) ppm; IR (film): $\tilde{\nu}$ = 1787, 1613, 1498, 1230, 1208, 1145, 1025, 802, 738, 708 cm^{-1}; HRMS (ESI): *m/z* calcd for $C_{22}H_{20}Cl_3N_1O_5H$: 484.0480 $[M+H]^+$; found: 484.0480.

Benzyl (4-benzyl-2-(4-(*tert*-butyl)phenyl)oxazol-5-yl) carbonate (13f)

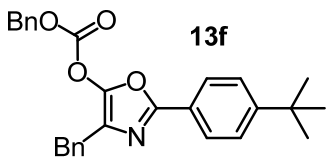

***N*-acylated Acid 271f.** General procedure B1) was followed: Phenylalanine methyl ester hydrochloride (1.89 g, 8.76 mmol, 1.00 eq), 4-*tert*-butylbenzoyl chloride (1.71 mL, 8.76 mmol, 1.00 eq), Et_3N (2.54 mL, 18.3 mmol, 2.09 eq); reaction time: 24 h; **271f** was obtained as a white solid (2.33 g, 7.17 mmol, 82%). ^{1}H NMR (300 MHz, $CDCl_3$): δ = 10.92 (s, 1H), 7.56 (d, J = 8.3 Hz, 2H), 7.35 (d, J = 8.3 Hz, 2H), 7.28–7.04 (m, 5H), 6.64–6.29 (m, 1H), 5.10–4.92 (m, 1H), 3.29 (dd, J = 13.9 Hz, J = 5.6 Hz, 1H), 3.18 (dd, J = 14.0 Hz, J = 5.9 Hz, 1H), 1.24 (s, 9H) ppm.

Azlactone 272f. General procedure B2) was followed: *N*-Acylated acid **271f** (2.33 g, 7.17 mmol); reaction time: 24 h; eluent: CH_2Cl_2/MeOH 200:1; **272f** was obtained as a pale yellow solid (1.57 g, 5.11 mmol, 71%). ^{1}H NMR (300 MHz, $CDCl_3$): δ = 7.75 (d, J = 8.6 Hz, 2H), 7.36 (d, J = 8.6 Hz, 2H), 7.25–7.03 (m, 5H), 4.57 (dd, J = 6.5 Hz, J = 5.0 Hz, 1H), 3.26 (dd, J = 14.0 Hz, J = 4.9 Hz, 1H), 3.08 (dd, J = 14.0 Hz, J = 6.6 Hz, 1H), 1.24 (s, 9H) ppm.

***O*-Acylated Azlactone 13f.** General procedure B3) was followed: Azlactone **272f** (1.43 g, 4.65 mmol), benzyl chloroformate (0.73 mL, 5.12 mmol, 1.10 eq), Et_3N (0.74 mL, 5.35 mmol, 1.15 eq); reaction time: 20 h; eluent: hexanes/MTBE 15:1; **13f** was obtained as a pale yellow oil which crystallized on standing (1.56 g, 3.53 mmol, 76%). ^{1}H NMR (300 MHz, $CDCl_3$): δ = 7.78 (d, J = 8.6 Hz, 2H), 7.34 (d, J = 8.7 Hz, 2H), 7.31–7.05 (m, 10H), 5.11 (s, 2H), 3.77 (s, 2H), 1.24 (s, 9H) ppm; ^{13}C NMR (75 MHz, $CDCl_3$): δ = 155.4, 153.8, 151.5, 146.3, 137.7, 134.0, 129.2, 129.0 (2C), 128.9 (2C), 128.7 (2C), 128.5 (2C), 126.6, 126.0 (2C), 125.7 (2C), 124.5, 123.3, 71.7, 35.0, 31.6, 31.3 (3C) ppm; IR (film): $\tilde{\nu}$ = 1783, 1203, 1116, 901, 839, 740, 699, 552 cm^{-1}; HRMS (ESI): *m/z* calcd for $C_{28}H_{27}N_1O_4Na$: 464.1832 [M+Na]$^+$; found: 464.1834.

Benzyl (4-benzyl-2-(naphthalen-1-yl)oxazol-5-yl) carbonate (13g)

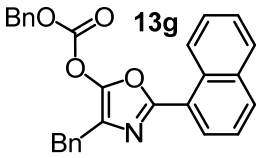

***N*-acylated Acid 271g.** General procedure B1) was followed: Phenylalanine methyl ester hydrochloride (2.00 g, 9.25 mmol, 1.00 eq), 1-naphthoyl chloride (1.40 mL, 9.29 mmol, 1.00 eq), Et_3N (2.70 mL, 19.4 mmol, 2.09 eq); reaction time: 23 h; **271g** was obtained as a colorless crystalline solid (2.93 g, 9.17 mmol, 99%). ^{1}H NMR (300 MHz, DMSO-d_6): δ = 12.84 (s, 1H), 8.85 (d, J = 8.3 Hz, 1H), 8.03–7.82 (m, 3H), 7.61–7.18 (m, 9H), 4.78 (ddd, J = 11.0 Hz, J = 8.3 Hz, J = 4.3 Hz, 1H), 3.25 (dd, J = 13.8 Hz, J = 4.3 Hz, 1H), 3.01 (dd, J = 13.8 Hz, J = 11.0 Hz, 1H) ppm.

Azlactone 272g. General procedure B2) was followed: *N*-Acylated acid **271g** (2.91 g, 9.11 mmol); reaction time: 22 h; eluent: CH_2Cl_2/MeOH 200:1; **272g** was obtained as a white crystalline solid (2.65 g, 8.79 mmol, 97%). ^{1}H NMR (300 MHz, $CDCl_3$): δ = 8.94 (d, J = 8.5 Hz, 1H), 7.98–7.85 (m, 2H), 7.85–7.75 (m, 1H), 7.59–7.43 (m, 2H), 7.39 (t, J = 7.7 Hz, 1H), 7.31–7.06 (m, 5H), 4.76 (dd, J = 6.2 Hz, J = 5.1 Hz, 1H), 3.39 (dd, J = 13.9 Hz, J = 5.1 Hz, 1H), 3.22 (dd, J = 13.9 Hz, J = 6.3 Hz, 1H) ppm.

***O*-Acylated Azlactone 13g.** General procedure B3) was followed: Intermediate **272g** (603 mg, 2.00 mmol), benzyl chloroformate (315 µL, 2.21 mmol, 1.10 eq), Et_3N (310 µL, 2.22 mmol, 1.11 eq); reaction time: 14 h; eluent: hexanes/MTBE 9:2 → 3:1; **13g** was obtained as a colorless crystalline solid (764 mg, 1.75 mmol, 88%). ^{1}H NMR (300 MHz, $CDCl_3$): δ = 9.08 (d, J = 8.7 Hz, 1H), 8.02 (d, J = 7.4 Hz, 1H), 7.85 (d, J = 8.3 Hz, 1H), 7.80 (d, J = 7.9 Hz, 1H), 7.60-7.03 (m, 13H), 5.16 (s, 2H), 3.88 (s, 2H) ppm; ^{13}C NMR (75 MHz, $CDCl_3$): δ = 155.3, 151.5, 146.6, 137.8, 134.1, 134.0, 131.4, 130.3, 129.3, 129.1 (2C), 129.0 (2C), 128.8 (2C), 128.7, 128.6 (2C), 127.9, 127.7, 126.7, 126.4, 126.3, 125.0, 123.6, 123.4, 71.9, 31.8 ppm; IR

(film): $\tilde{\nu}$ = 1783, 1663, 1204, 1137, 773, 736, 702 cm^{-1}; HRMS (ESI): *m/z* calcd for $C_{28}H_{21}N_1O_4Na$: 458.1363 [*M*+Na]$^+$; found: 458.1363.

Benzyl (4-benzyl-2-(naphthalen-2-yl)oxazol-5-yl) carbonate (13h)

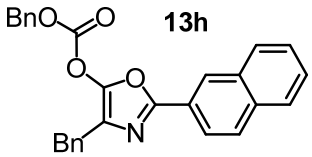

13h

***N*-acylated Acid 271h.** General procedure B1) was followed: Phenylalanine methyl ester hydrochloride (3.00 g, 13.9 mmol, 1.00 eq), 2-naphthoyl chloride (2.09 mL, 13.9 mmol, 1.00 eq), Et_3N (4.05 mL, 29.1 mmol, 2.09 eq); reaction time: 24 h; **271h** was obtained as a colorless crystalline solid (3.80 g, 11.9 mmol, 86%). ^{1}H NMR (300 MHz, DMSO-d_6): δ = 12.78 (s, 1H), 8.86 (d, *J* = 8.3 Hz, 1H), 8.41 (s, 1H), 8.06–7.92 (m, 3H), 7.87 (dd, *J* = 8.5 Hz, *J* = 1.6 Hz, 1H), 7.66–7.54 (m, 2H), 7.38–7.22 (m, 4H), 7.22–7.13 (m, 1H), 4.77–4.60 (m, 1H), 3.23 (dd, *J* = 13.8 Hz, *J* = 4.7 Hz, 1H), 3.12 (dd, *J* = 13.7 Hz, *J* = 10.4 Hz, 1H) ppm.

Azlactone 272h: General procedure B2) was followed: *N*-acylated acid **271h** (3.44 g, 10.8 mmol); reaction time: 24 h; eluent: CH_2Cl_2/MeOH 200:1; **272h** was obtained as colorless crystalline solid (2.90 g, 9.62 mmol, 89%). ^{1}H NMR (300 MHz, $CDCl_3$): δ = 8.25 (s, 1H), 7.90 (dd, *J* = 8.7 Hz, *J* = 1.7 Hz, 1H), 7.83–7.67 (m, 3H), 7.53–7.35 (m, 2H), 7.28–6.99 (m, 5H), 4.62 (dd, *J* = 6.6 Hz, *J* = 4.9 Hz, 1H), 3.29 (dd, *J* = 14.0 Hz, *J* = 5.0 Hz, 1H), 3.11 (dd, *J* = 14.0 Hz, *J* = 6.7 Hz, 1H) ppm.

***O*-Acylated Azlactone 13h:** General procedure B3) was followed: Azlactone **272h** (2.82 g, 9.36 mmol, 1.00 eq), benzyl chloroformate (1.47 mL, 10.3 mmol, 1.10 eq), Et_3N (1.50 mL, 10.8 mmol, 1.15 eq); reaction time: 24 h; eluent: hexanes/MTBE 6:1; **13h** was obtained as a pale yellow oil which crystallized on standing (3.47 g, 7.97 mmol, 85%). ^{1}H NMR (300 MHz, $CDCl_3$): δ = 8.54 (s, 1H), 8.16 (dd, *J* = 8.7 Hz, *J* = 1.7 Hz, 1H), 8.03–7.84 (m, 3H), 7.64–7.54 (m, 2H), 7.54–7.27 (m, 10H), 5.33 (s, 2H), 4.05 (s, 2H) ppm; ^{13}C NMR (75 MHz, $CDCl_3$): δ = 155.3, 151.5, 146.5, 137.6, 134.1, 133.9, 133.0, 129.1, 129.0 (2C), 128.8 (2C), 128.7 (2C), 128.7, 128.6, 128.5 (2C), 127.9, 127.2, 126.7, 126.6, 126.0, 124.4, 123.7, 122.9, 71.7, 31.6 ppm; IR (film): $\tilde{\nu}$ = 1782, 1658, 1202, 1127, 1066, 955, 898, 820, 741, 698, 471 cm^{-1}; HRMS (ESI): *m/z* calcd for $C_{28}H_{21}N_1O_4Na$: 458.1363 [*M*+Na]$^+$; found: 458.1368.

Benzyl (4-benzyl-2-(*tert*-butyl)oxazol-5-yl) carbonate (13i)

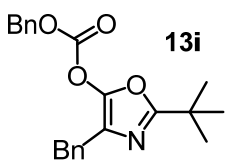

13i

***N*-acylated Acid 271i:** General procedure B1) was followed: Phenylalanine methyl ester hydrochloride (3.00 g, 13.9 mmol, 1.00 eq), pivaloyl chloride (1.71 mL, 13.9 mmol, 1.00 eq), Et_3N (4.10 mL, 29.4 mmol, 2.11 eq); reaction time: 21 h; **271i** was obtained as a white crystalline solid (3.34 g, 13.4 mmol, 96%). ^{1}H NMR (300 MHz, $CDCl_3$): δ = 10.55 (s, 1H), 7.38–7.21 (m,

3H), 7.21–7.10 (m, 2H), 6.14 (d, J = 7.4 Hz, 1H), 4.96–4.78 (m, 1H), 3.27 (dd, J = 14.0 Hz, J = 5.6 Hz, 1H), 3.15 (dd, J = 14.0 Hz, J = 6.0 Hz, 1H), 1.13 (s, 9H) ppm.

Azlactone 272i: General procedure B2) was followed: *N*-acylated acid **271i** (3.32 g, 13.3 mmol); reaction time: 18 h; eluent: CH_2Cl_2/MeOH 100:1; **272i** was obtained as a colorless oil (2.86 g, 12.4 mmol, 93%). ^{1}H NMR (300 MHz, $CDCl_3$): δ = 7.34–7.07 (m, 5H), 4.47 (t, J = 5.0 Hz, 1H), 3.28 (dd, J = 13.7 Hz, J = 5.2 Hz, 1H), 3.18 (dd, J = 13.7 Hz, J = 4.8 Hz, 1H), 1.06 (s, 9H) ppm.

***O*-Acylated Azlactone 13i:** General procedure B3) was followed: Azlactone **272i** (1.60 g, 6.92 mmol), benzyl chloroformate (3.06 mmol, 21.4 mmol, 3.10 eq), Et_3N (3.06 mL, 21.9 mmol, 3.17 eq); reaction time: 40 h; eluent: hexanes/MTBE 10:1; **1i** was obtained as a colorless oil which crystallized on standing (1.72 g, 4.71 mmol, 68%). ^{1}H NMR (300 MHz, $CDCl_3$): δ = 7.36–7.23 (m, 5H), 7.19–7.04 (m, 5H), 5.07 (s, 2H), 3.70 (s, 2H), 1.26 (s, 9H) ppm; ^{13}C NMR (75 MHz, $CDCl_3$): δ = 164.6, 151.5, 145.9, 137.8, 134.1, 129.2, 129.0 (2C), 128.9 (2C), 128.7 (2C), 128.5 (2C), 126.5, 121.1, 71.6, 33.9, 31.7, 28.5 (3C) ppm; IR (film): $\tilde{\nu}$ = 1782, 1208, 1144, 1104, 738, 702 cm^{-1}; HRMS (ESI): *m/z* calcd for $C_{22}H_{23}N_1O_4Na$: 388.1519 $[M+Na]^+$; found: 388.1523.

4.9.2 *O*-Acylated Benzofuranones (142a–i)

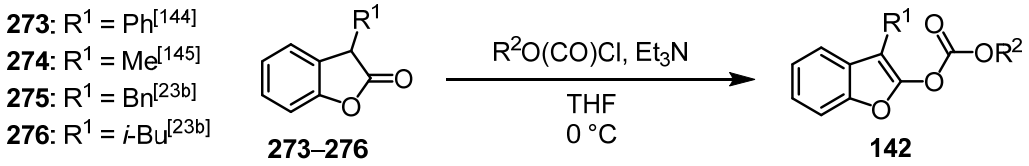

Scheme 86. Synthesis of *O*-acylated benzofuranones (**142**) from benzofuran-2(3*H*)-ones (**273–276**).

O-Acylated benzofuranones (**142**) were synthesized from the corresponding 3-substituted benzofuran-2(3*H*)-ones (**273–276**) and the latter were synthesized according to literature procedures (Scheme 86).[23b,144,145]

4.9.2.1 General Procedure C1). Synthesis of *O*-acylated benzofuranones (**142**).[23b]

A flame-dried flask was charged with the appropriate benzofuran-2(3*H*)-one (**273–276**; 1.00 eq) and dry THF (conc = 0.3 M). The mixture was cooled to 0 °C and the indicated amounts of Et_3N and chloroformate were added. The mixture was stirred at 0 °C for the indicated time and then diluted with Et_2O and quenched with 0.1 M HCl. The organic layer was separated and the aqueous layer extracted with Et_2O (3x). The combined organic layers were washed with brine and dried over Na_2SO_4. All volatiles were removed *in vacuo*, the obtained residue dissolved in CH_2Cl_2, adsorbed on silica gel (40 °C), and purified by flash chromatography, which yielded the desired *O*-acylated benzofuranone (**142**).

4.9.2.2 Synthetic Procedures and Characterizations

3-Phenylbenzofuran-2(3*H*)-one (273)

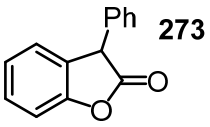

Compound **273** was synthesized according to a protocol from Lee et al.[144] A flask (250 mL) was charged with mandelic acid (15.2 g, 100 mmol, 1.00 eq) and phenol (13.3 g, 141 mmol, 1.41 eq). The flask was cooled to 0 °C and H_2SO_4 (70 wt%; 40 mL) was added and the resulting mixture stirred at 0 °C for 30 min. Subsequently, the mixture was stirred at 115 °C for 45 min. After cooling to rt, the resulting mixture was poured into ice-water and the mixture extracted with CH_2Cl_2 (3x). The combined organic layers were washed water (1x), aqueous $NaHCO_3$ (1x), and brine (1x) and dried over Na_2SO_4. After solvent removal and drying *in vacuo*, a pale-yellow crystalline solid was obtained, which was recrystallized from ethanol (15 mL). The recrystallized precipitate was filtered off and washed with ice-cold EtOH and hexanes. After drying *in vacuo*, 3-phenylbenzofuran-2(3*H*)-one (**273**) was obtained as a colorless crystalline solid (5.60 g, 26.6 mmol, 27%). ^{1}H NMR (300 MHz, $CDCl_3$): δ = 7.35–7.20 (m, 4H), 7.19–7.04 (m, 5H), 4.80 (s, 1H) ppm; HRMS (ESI): *m/z* calcd for $C_{14}H_{10}O_2Na$: 233.0573 $[M+Na]^+$; found: 233.0577.

3-Methylbenzofuran-2(3*H*)-one (274)

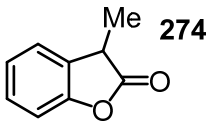

Compound **274** was synthesized according to a protocol from Piccolo et al.[145] A flame-dried flask (250 mL) was charged phenol (2.43 g, 25.8 mmol, 1.00 eq) and the flask cooled to 0 °C. $TiCl_4$ (2.85 mL, 26.0 mmol, 1.01 eq) was added and the mixture stirred at 0 °C for 30 min. Then, ethyl pyruvate (2.88 mL, 25.9 mmol, 1.00 eq) was added and the mixture stirred at 10 °C for 10 min. Next, Zn powder (2.58 g, 39.5 mmol, 1.53 eq) and glacial acetic acid (20 mL; *caution: gas evolution!*) were added at 0 °C. The mixture was allowed to warm to rt and CH_2Cl_2 was selectively removed from the mixture under reduced pressure. The remaining mixture was stirred at 90 °C (reflux) for 3 h. After cooling to rt, Et_2O (100 mL) and aqueous 10% HCl (100 mL) were added and the mixture violently stirred at rt for 3 h. The organic layer was separated, the aqueous layer extracted with Et_2O (3x), and the combined organic layers washed with water and dried over Na_2SO_4. All volatiles were removed *in vacuo* and traces of acetic acid were removed as an azeotrope with toluene (3x). The resulting residue was dissolved in CH_2Cl_2, adsorbed on silica gel, and purified by flash chromatography (hexanes/EtOAc 30:1). After solvent removal and drying *in vacuo*, 3-methylbenzofuran-2(3*H*)-one (**274**) was obtained as a clear colorless oil (1.76 g, 11.9 mmol, 46%). ^{1}H NMR (300 MHz, $CDCl_3$): δ = 7.35–7.21 (m, 2H), 7.19–7.05 (m, 2H), 3.72 (q, *J* = 7.6 Hz, 1H), 1.57

(d, J = 7.7 Hz, 3H) ppm; HRMS (ESI): *m/z* calcd for $C_9H_8O_2Na$: 171.0417 $[M+Na]^+$; found: 171.0420.

3-Benzylbenzofuran-2(3*H*)-one (275)

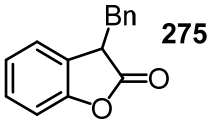

Compound **275** was synthesized according to a protocol from Smith et al.[23b] A flame-dried flask was charged with NaH (60 wt% in mineral oil; 1.25 g, 31.3 mmol, 1.15 eq) and dry DMF (6 mL). 2-Methoxyphenylacetonitrile (4.00 g, 27.2 mmol, 1.00 eq) was added and the mixture stirred at rt for 1 h. The resulting mixture was cooled to 0 °C and benzyl bromide (3.40 mL, 28.6 mmol, 1.05 eq) was added and the mixture allowed to warm to rt and stirred for 15 h. The mixture was then quenched by the addition of aqueous sat. NH_4Cl and Et_2O and the organic layer was separated. The aqueous layer was extracted with Et_2O (3x) and the combined organic layers were washed with sat. NaCl and dried over Na_2SO_4. After solvent removal and drying *in vacuo*, a yellow oil was obtained as intermediate product (6.80 g). Half of this intermediate product (i.e., 3.40 g) were transferred into a new flask (250 mL), aqueous 48% HBr (75 mL) was added, and the resulting mixture stirred at reflux for 4 d. After cooling to rt, the mixture was neutralized with aqueous 3 M NaOH while ice was continuously added for cooling. The resulting mixture was extracted with Et_2O (4x) and the combined organic layers were washed with brine and dried over Na_2SO_4. All volatiles were removed *in vacuo*, the residue dissolved in CH_2Cl_2, adsorbed on silica gel, and purified by flash chromatography (hexanes/Et_2O 40:1 → 30:1). After solvent removal and drying *in vacuo*, desired 3-benzylbenzofuran-2(3*H*)-one (**275**) was obtained as a yellow oil which crystallized on standing (1.26 g, 5.62 mmol, 41%). ^{1}H NMR (300 MHz, $CDCl_3$): δ = 7.34–7.21 (m, 4H), 7.21–7.13 (m, 2H), 7.08–6.98 (m, 2H), 6.85–6.77 (m, 1H), 4.02 (dd, J = 9.0 Hz, J = 4.8 Hz, 1H), 3.51 (dd, J = 13.8 Hz, J = 4.9 Hz, 1H), 3.05 (dd, J = 13.8 Hz, J = 8.9 Hz, 1H) ppm; HRMS (ESI): *m/z* calcd for $C_{15}H_{12}O_2Na$: 247.0730 $[M+Na]^+$; found: 247.0729.

3-Isobutylbenzofuran-2(3*H*)-one (276)

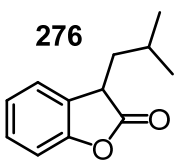

Compound **276** was synthesized according to a procedure from Smith et al.[23b] A flame-dried flask was charged with NaH (60 wt% in mineral oil; 0.62 g, 15.5 mmol, 1.14 eq) and dry DMF (3.5 mL). 2-Methoxyphenylacetonitrile (2.00 g, 13.6 mmol, 1.00 eq) was added and the mixture stirred at rt for 1 h. The resulting mixture was cooled to 0 °C and isobutyl iodide (1.60 mL, 13.9 mmol, 1.02 eq) was added. As the mixture became barely stirrable, additional dry DMF (4 mL) was added. The mixture was then allowed to warm to rt and stirred for 15 h. Then, the mixture was quenched by the addition of aqueous sat. NH_4Cl and Et_2O and the organic layer was separated.

The aqueous layer was extracted with Et_2O (3x) and the combined organic layers were washed with brine and dried over Na_2SO_4. After solvent removal and drying *in vacuo*, aqueous 48% HBr (70 mL) was added and the mixture stirred at reflux for 48 h. After cooling to rt, the mixture was neutralized with aqueous 3 M NaOH while ice was continuously added for cooling. The resulting mixture was extracted with Et_2O (3x) and the combined organic layers were washed with brine and dried over Na_2SO_4. All volatiles were removed *in vacuo*, the residue dissolved in CH_2Cl_2, adsorbed on silica gel, and purified by flash chromatography (hexanes/Et_2O 40:1 → 30:1). After solvent removal and drying *in vacuo*, 3-isobutylbenzofuran-2(3*H*)-one (**276**) was obtained as a pale-yellow oil (1.30 g, 6.92 mmol, 51%). ^{1}H NMR (300 MHz, $CDCl_3$): δ = 7.34–7.21 (m, 2H), 7.18–7.06 (m, 2H), 3.72 (t, J = 7.1 Hz, 1H), 2.02 (sept, J = 6.8 Hz, 1H), 1.96–1.84 (m, 1H), 1.82–1.68 (m, 1H), 1.00 (d, J = 6.6 Hz, 3H), 0.97 (d, J = 6.6 Hz, 3H) ppm; ^{13}C NMR (75 MHz, $CDCl_3$): δ = 177.6, 153.8, 128.8, 128.1, 124.5, 124.1, 110.9, 41.7, 40.6, 25.3, 22.7, 22.3 ppm.

Phenyl (3-phenylbenzofuran-2-yl) carbonate (142a)[86b]

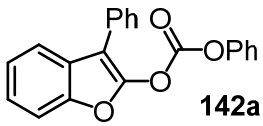

142a

General procedure C1) was followed: Benzofuranone **273** (567 mg, 2.70 mmol), phenyl chloroformate (340 µL, 2.71 mmol, 1.00 eq), Et_3N (570 µL, 4.09 mmol, 1.52 eq); reaction time: 1 h; eluent: hexanes/Et_2O 30:1; **142a** was obtained as a colorless oil (704 mg, 2.13 mmol, 79%). ^{1}H NMR (300 MHz, $CDCl_3$): δ = 7.73–7.52 (m, 3H), 7.49–7.00 (m, 11H) ppm; ^{13}C NMR (75 MHz, $CDCl_3$): δ = 151.0, 150.0, 150.0, 148.9, 130.1, 129.8 (2C), 129.2 (2C), 128.4 (2C), 127.9, 127.7, 126.9, 124.8, 123.8, 120.7 (2C), 120.5, 111.6, 105.1 ppm; IR (film): $\tilde{\nu}$ = 1795, 1453, 1223, 1163, 1015, 744, 693 cm^{-1}; HRMS (ESI): *m/z* calcd for $C_{21}H_{14}O_4Na$: 353.0784 [M+Na]$^+$; found: 353.0786.

3-Methylbenzofuran-2-yl phenyl carbonate (142b)[23b]

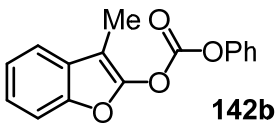

142b

General procedure C1) was followed: Benzofuranone **274** (449 mg, 3.03 mmol), phenyl chloroformate (570 µL, 4.54 mmol, 1.50 eq), Et_3N (640 µL, 4.59 mmol, 1.52 eq); reaction time: 1.5 h; eluent: hexanes/Et_2O 10:1; **142b** was obtained as a colorless crystalline solid (791 mg, 2.95 mmol, 97%). ^{1}H NMR (300 MHz, $CDCl_3$): δ = 7.44–7.30 (m, 4H), 7.27–7.16 (m, 5H), 2.12 (s, 3H) ppm; ^{13}C NMR (75 MHz, $CDCl_3$): δ = 151.0, 150.3, 149.8, 149.3, 129.9 (2C), 129.6, 126.9, 124.3, 123.1, 120.8 (2C), 119.6, 111.2, 98.8, 6.7 ppm; IR (film): $\tilde{\nu}$ = 1793, 1452, 1215, 1165, 1109, 1001, 742 cm^{-1}; HRMS (ESI): *m/z* calcd for $C_{16}H_{12}O_4Na$: 291.0628 [M+Na]$^+$; found: 291.0632.

Benzyl (3-methylbenzofuran-2-yl) carbonate (142c)[86b]

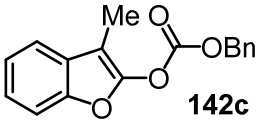

142c

General procedure C1) was followed: Benzofuranone **274** (320 mg, 2.16 mmol), benzyl chloroformate (440 mL, 3.09 mmol, 1.43 eq), Et_3N (440 µL, 3.16 mmol, 1.46 eq); reaction time: 1 h; eluent: hexanes/Et_2O 20:1; **142c** was obtained as a colorless crystalline solid (554 mg, 1.96 mmol, 91%). ^{1}H NMR (300 MHz, $CDCl_3$): δ = 7.41–7.24 (m, 7H), 7.22–7.11 (m, 2H), 5.24 (s, 2H), 2.03 (s, 3H) ppm; ^{13}C NMR (75 MHz, $CDCl_3$): δ = 151.9, 149.7, 149.6, 134.3, 129.6, 129.2, 128.9 (2C), 128.7 (2C), 124.2, 123.0, 119.5, 111.1, 98.6, 71.6, 6.7 ppm; IR (film): $\tilde{\nu}$ = 1779, 1452, 1220, 1177, 1132, 740, 698 cm^{-1}; HRMS (ESI): *m/z* calcd for $C_{17}H_{14}O_4Na$: 305.0784 [*M*+Na]$^+$; found: 305.0788.

Isopropyl (3-methylbenzofuran-2-yl) carbonate (142d)

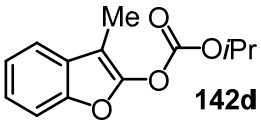

142d

General procedure C1) was followed: Benzofuranone **274** (237 mg, 1.60 mmol), isopropyl chloroformate (2.0 M in toluene, 1.20 mL, 2.40 mmol, 1.50 eq), Et_3N (335 µL, 2.40 mmol, 1.50 eq); reaction time: 2 h; eluent: hexanes/Et_2O 10:1; **142d** was obtained as a colorless crystalline solid (355 mg, 1.52 mmol, 95%). ^{1}H NMR (300 MHz, $CDCl_3$): δ = 7.41–7.34 (m, 1H), 7.33–7.26 (m, 1H), 7.23–7.11 (m, 2H), 4.95 (sept, *J* = 6.3 Hz, 1H), 2.05 (s, 3H), 1.33 (d, *J* = 6.4 Hz, 6H) ppm; ^{13}C NMR (75 MHz, $CDCl_3$): δ = 151.3, 149.8, 149.7, 129.7, 124.0, 123.0, 119.4, 111.1, 98.4, 74.9, 21.7 (2C), 6.7 ppm; IR (film): $\tilde{\nu}$ = 1776, 1455, 1230, 1191, 1176, 1132, 1095, 908, 741 cm^{-1}; HRMS (APCI): *m/z* calcd for $C_{13}H_{14}O_4H$: 235.0965 [*M*+H]$^+$; found: 235.0964.

3-Benzylbenzofuran-2-yl (1,1,1-trichloro-2-methylpropan-2-yl) carbonate (142e)[22b]

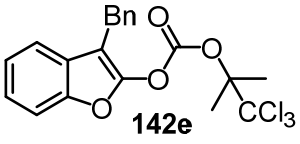

142e

General procedure C1) was followed: Benzofuranone **275** (180 mg, 803 µmol), 2,2,2-trichloro-1,1-dimethylethyl chloroformate (262 mg, 1.09 mmol, 1.36 eq), Et_3N (160 µL, 1.15 mmol, 1.43 eq); reaction time: 2.5 h; eluent: hexanes/Et_2O 20:1; **142e** was obtained as a colorless crystalline solid (325 mg, 761 µmol, 95%). ^{1}H NMR (300 MHz, $CDCl_3$): δ = 7.32 (d, *J* = 8.1 Hz, 1H), 7.25–7.02 (m, 8H), 3.88 (s, 2H), 1.89 (s, 6H) ppm; ^{13}C NMR (75 MHz, $CDCl_3$): δ = 149.9, 149.7, 148.8, 138.4, 128.7, 128.7 (2C), 128.7 (2C), 128.6, 126.6, 124.3, 123.2, 120.1, 111.2, 104.8, 102.1, 92.2, 28.7, 21.2 (2C) ppm; IR (film): $\tilde{\nu}$ = 1785, 1454, 1237, 1203, 1138, 1101, 800, 743, 702 cm^{-1}; HRMS (ESI): *m/z* calcd for $C_{20}H_{17}Cl_3O_4Na$: 449.0085 [*M*+Na]$^+$; found: 449.0082.

3-Isobutylbenzofuran-2-yl phenyl carbonate (142f)[23b]

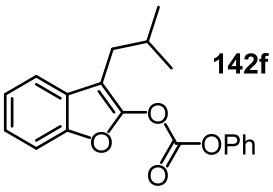

General procedure C1) was followed: Benzofuranone **276** (260 mg, 1.38 mmol), phenyl chloroformate (260 µL, 2.07 mmol, 1.50 eq), Et_3N (290 µL, 2.08 mmol, 1.51 eq); reaction time: 1.5 h; eluent: hexanes/ Et_2O 20:1; **142f** was obtained as a colorless oil (391 mg, 1.26 mmol, 91%). ^1H NMR (300 MHz, $CDCl_3$): δ = 7.46–7.40 (m, 1H), 7.40–7.29 (m, 3H), 7.26–7.12 (m, 5H), 2.45 (d, J = 7.2 Hz, 2H), 1.99 (sept, J = 6.8 Hz, 1H), 0.91 (d, J = 6.6 Hz, 6H) ppm; ^{13}C NMR (75 MHz, $CDCl_3$): δ = 151.0, 150.4, 149.9, 149.7, 129.9 (2C), 129.2, 126.9, 124.2, 123.1, 120.8 (2C), 120.1, 111.3, 102.5, 31.6, 28.4, 22.8 (2C) ppm; IR (film): $\tilde{\nu}$ = 1794, 1456, 1208, 1164, 1007, 742, 686 cm^{-1}; HRMS (ESI): *m/z* calcd for $C_{19}H_{18}O_4Na$: 333.1097 $[M+Na]^+$; found: 333.1098.

3-Benzylbenzofuran-2-yl phenyl carbonate (142g)[23b]

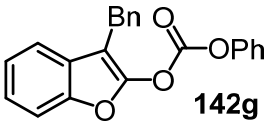

General procedure C1) was followed: Benzofuranone **275** (250 mg, 1.11 mmol), phenyl chloroformate (220 µL, 1.75 mmol, 1.57 eq), Et_3N (240 µL, 1.72 mmol, 1.55 eq); reaction time: 3 h; eluent: hexanes/Et_2O 40:1 → 30:1; **142g** was obtained as a colorless crystalline solid (315 mg, 914 µmol, 82%). ^1H NMR (300 MHz, $CDCl_3$): δ = 7.36–7.02 (m, 14H), 3.90 (s, 2H) ppm; ^{13}C NMR (75 MHz, $CDCl_3$): δ = 150.9, 150.2, 149.9, 149.7, 138.3, 129.8 (2C), 128.7 (2C), 128.7 (2C), 128.6, 126.8, 126.6, 124.4, 123.2, 120.7 (2C), 120.2, 111.3, 102.2, 28.7 ppm; IR (film): $\tilde{\nu}$ = 1792, 1453, 1189, 1158, 1099, 1010, 740, 694, 499 cm^{-1}; HRMS (ESI): *m/z* calcd for $C_{22}H_{16}O_4Na$: 367.0941 $[M+Na]^+$; found: 367.0942.

Methyl (3-methylbenzofuran-2-yl) carbonate (142h)

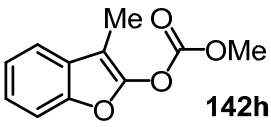

General procedure C1) was followed: Benzofuranone **274** (280 mg, 1.89 mmol), methyl chloroformate (220 µL, 2.85 mmol, 1.51 eq), Et_3N (400 µL, 2.87 mmol, 1.52 eq); reaction time: 2 h; eluent: hexanes/Et_2O 20:1; **142h** was obtained as a colorless oil (360 mg, 1.75 mmol, 92%; *product is volatile in vacuo*). ^1H NMR (300 MHz, $CDCl_3$): δ = 7.42–7.35 (m, 1H), 7.33–7.27 (m, 1H), 7.24–7.12 (m, 2H), 3.89 (s, 3H), 2.05 (s, 3H) ppm; ^{13}C NMR (75 MHz, $CDCl_3$): δ = 152.5, 149.7, 149.6, 129.6, 124.2, 123.0, 119.5, 111.1, 98.5, 56.4, 6.6 ppm; IR (film): $\tilde{\nu}$ = 1783, 1665, 1446, 1233, 1178, 1130, 925, 743, 438 cm^{-1}; HRMS (ESI): *m/z* calcd for $C_{11}H_{10}O_4Na$: 229.0471 $[M+Na]^+$; found: 229.0471.

3-Methylbenzofuran-2-yl (1,1,1-trichloro-2-methylpropan-2-yl) carbonate (142i)

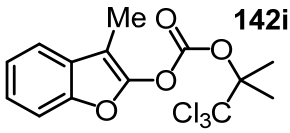

General procedure C1) was followed: Benzofuranone **274** (337 mg, 2.27 mmol), 2,2,2-trichloro-1,1-dimethylethyl chloroformate (729 mg, 3.04 mmol, 1.34 eq), Et_3N (440 µL, 3.16 mmol, 1.39 eq); reaction time: 1.5 h; eluent: hexanes/Et_2O 20:1; **142i** was obtained as a colorless crystalline solid (769 mg, 2.19 mmol, 96%). ^{1}H NMR (300 MHz, $CDCl_3$): δ = 7.42–7.35 (m, 1H), 7.34–7.27 (m, 1H), 7.23–7.13 (m, 2H), 2.07 (s, 3H), 1.95 (s, 6H) ppm; ^{13}C NMR (75 MHz, $CDCl_3$): δ = 149.8, 149.3, 148.9, 129.6, 124.2, 123.1, 119.5, 111.1, 104.8, 98.7, 92.2, 21.3, 6.7 ppm; IR (film): $\tilde{\nu}$ = 1785, 1454, 1237, 1188, 1140, 1109, 801, 744 cm^{-1}; HRMS (FD): *m/z* calcd for $C_{14}H_{13}Cl_3O_4$: 349.9879 $[M]^+$; found: 349.9880.

4.9.3 Aryl Alkyl Ketenes (153a–h)

Aryl alkyl ketenes (**153**) were synthesized in a two-step procedure (Scheme 87). In case the required *α*-alkyl-*α*-arylacetic acids (**277**) were not available, they were synthesized beforehand from a commercial precursor. The *α*-alkyl-*α*-arylacetic acids acids (**277**) were converted to the according acid chlorides (**278**) via thionyl chloride treatment and the resulting acid chlorides (**278**) were finally converted to the desired ketenes (**153**) via base-induced *β*-elimination.

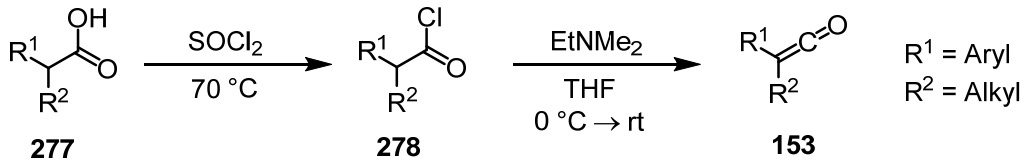

Scheme 87. Synthesis of aryl alkyl ketenes (**153**) from *α*-alkyl-*α*-arylacetic acids (**277**).

$EtNMe_2$ was employed as base for the final *β*-elimination step due to its high volatility, which ensured its easy removal from the ketenes during their distillative purification.[26a]

4.9.3.1 General Procedures D1)–D3)

General Procedure D1). Synthesis of *α*-alkyl-*α*-arylacetic acids (**277**) from *α*-arylacetic acids:[146]

A flame-dried flask was charged with the indicated commercial *α*-arylacetic acid (1.00 eq) and dry THF (conc = 0.35 M). The mixture was cooled to −78 °C and *n*-BuLi (2.5 M in hexanes, 4.00 eq) was added over 10 min and the mixture stirred for 2 h at −78 °C. The indicated alkyl bromide (4.00 eq) was added and the mixture allowed to warm to rt and stirred for the indicated time. Then, the mixture was quenched with 0.1 M HCl, diluted with CH_2Cl_2, the organic layer separated, and the aqueous layer extracted with CH_2Cl_2 (3x). The combined organic layers were washed with aqueous 10% $Na_2S_2O_3$ and dried over Na_2SO_4. After drying

in vacuo, the desired *α*-alkyl-*α*-arylacetic acid (**277**) was obtained without the need for further purification.

General Procedure D2). Synthesis of acid chlorides from *α*-alkyl-*α*-arylacetic acids (**277** → **278**).

A flame-dried flask was charged with the respective *α*-alkyl-*α*-arylacetic acid (**277**; 1.00 eq) and thionyl chloride (2.50 eq) and the flask equipped with a reflux condenser. Then, the mixture was stirred at 70 °C (reflux) for the indicated time under nitrogen atmosphere. After cooling to rt, excess thionyl chloride was carefully removed *in vacuo* and the remaining crude acid chloride (**278**) purified via short-path distillation at the indicated pressure and temperature.

General Procedure D3). Synthesis of aryl alkyl ketenes from acid chlorides (**153** → **278**).[26a] A flame-dried flask was charged with the respective acid chloride (**278**; 1.00 eq) and dry THF (conc = 0.50 M). The mixture was cooled to 0 °C and $EtNMe_2$ (4.00 eq) was added under stirring. Then, the mixture was allowed to warm to rt and stirred for the indicated time under nitrogen atmosphere. The formed white precipitate ($EtNMe_2 \cdot HCl$) was filtered off using a flame-dried Schlenk frit (porosity G4) equipped with a flame-dried receiving flask. The filtered off precipitate was thoroughly rinsed under nitrogen atmosphere with dry THF. Then, solvent and excess $EtNMe_2$ were carefully removed from the filtrate *in vacuo* and remaining crude ketene (**153**) distilled via short-path distillation at the indicated pressure and temperature.

Remark: All operations were performed under strict exclusion of moisture and air and all isolated ketenes were immediately stored after their distillation in well-sealed, flame-dried Schlenk mini-tubes (5 mL; threaded PTFE plug) at −20 °C under exclusion of light and under nitrogen atmosphere and used for catalysis experiments within two weeks after preparation.

4.9.3.2 Synthetic Procedures and Characterizations

Phenyl ethyl ketene (153a)[147]

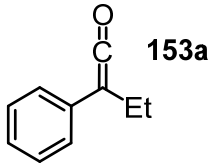

2-Phenylbutanoyl chloride (278a). General procedure D2) was followed: Commercial 2-phenylbutanoic acid (**277a**; 10.5 g, 63.6 mmol); reaction time: 18 h; distillation: 110–150 °C (15 mbar); **278a** was obtained as a colorless oil (11.6 g, 63.5 mmol, quant.). ^{1}H NMR (300 MHz, C_6D_6): δ = 7.10–6.92 (m, 5H), 3.49 (t, J = 7.5 Hz, 1H), 1.96–1.77 (m, 1H), 1.61–1.42 (m, 1H), 0.57 (t, J = 7.5 Hz, 3H) ppm; ^{13}C NMR (75 MHz, C_6D_6): δ = 175.0, 136.6, 129.6 (2C), 129.0 (2C), 128.6, 65.6, 27.0, 11.8 ppm.

Phenyl ethyl ketene (153a). General procedure D3) was followed: 2-Phenylbutanoyl chloride (**278a**, 2.70 g, 14.8 mmol); reaction time: 15 h; distillation: 40–50 °C (1.0 mbar); **153a** was obtained as a yellow oil (1.84 g, 12.6 mmol, 85%). ^{1}H NMR (300 MHz, C_6D_6): δ = 7.14–6.80 (m, 5H), 1.97 (q, J = 7.4 Hz, 2H), 0.86 (t, J = 7.4 Hz, 3H) ppm; ^{13}C NMR (75 MHz, C_6D_6): δ = 206.2, 133.4, 129.6 (2C), 124.8, 124.8 (2C), 42.4, 17.4, 13.1 ppm.

o-Tolyl ethyl ketene (153b)[26c]

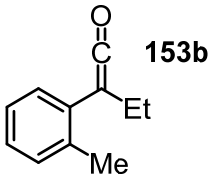

2-(*o*-Tolyl)butanoyl chloride (278b). General procedure D2) was followed: 2-(*o*-Tolyl)butanoic acid[146] (**277b**; 6.06 g, 34.0 mmol); reaction time: 8 h; distillation: 100–125 °C (5 mbar); **278b** was obtained as a pale yellow oil (6.51 g, 33.1 mmol, 97%). ^{1}H NMR (300 MHz, C_6D_6): δ = 7.09–6.88 (m, 4H), 3.86 (t, J = 7.4 Hz, 1H), 2.09 (s, 3H), 1.99–1.80 (m, 1H), 1.64-1.44 (m, 1H), 0.59 (t, J = 7.4 Hz, 3H) ppm; ^{13}C NMR (75 MHz, C_6D_6): δ = 174.9, 137.3, 135.3, 131.6, 128.5, 127.7, 127.5, 61.2, 27.0. 20.0, 11.8 ppm.

***o*-Tolyl ethyl ketene (153b).** General procedure D3) was followed: 2-(*o*-Tolyl)butanoyl chloride (**278b**; 2.94 g, 14.9 mmol); reaction time: 15 h; distillation: 40–50 °C (1.0 mbar); **153b** was obtained as a yellow oil (1.92 g, 12.0 mmol, 80%). ^{1}H NMR (300 MHz, C_6D_6): δ = 7.12–6.84 (m, 4H), 2.15 (s, 3H), 2.08 (q, J = 7.4 Hz, 2H), 0.88 (t, J = 7.4 Hz, 3H) ppm; ^{13}C NMR (75 MHz, C_6D_6): δ = 201.2, 136.2, 131.4, 131.3, 127.4, 127.1, 126.4, 38.3, 21.1, 20.5, 13.4 ppm.

Phenyl isopropyl ketene (153c)[148]

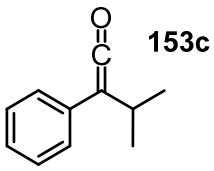

3-Methyl-2-phenylbutanoyl chloride (278c). General procedure D2) was followed: 3-Methyl-2-phenylbutanoic acid[149] (**277c**; 8.96 g, 50.3 mmol); reaction time: 8 h; distillation: 85–110 °C (5 mbar); **278c** was obtained as a pale yellow oil (9.69 g, 49.3 mmol, 98%). ^{1}H NMR (300 MHz, C_6D_6): δ = 7.11–6.95 (m, 5H), 3.42 (d, J = 10.0 Hz, 1H), 2.30–2.10 (m, 1H), 0.90 (d, J = 6.4 Hz, 3H), 0.46 (d, J = 6.6 Hz, 3H) ppm; ^{13}C NMR (75 MHz, C_6D_6): δ = 174.8, 135.7, 129.5 (2C), 129.5 (2C), 128.7, 72.2, 32.5, 21.4, 20.0 ppm.

Phenyl isopropyl ketene (153c). General procedure D3) was followed: 3-Methyl-2-phenyl-butanoyl chloride (**278c**; 3.03 g, 15.4 mmol); reaction time: 15 h; distillation: 40–50 °C (1.0 mbar); **153c** was obtained as a yellow oil (1.97 g, 12.3 mmol, 80%). ^{1}H NMR (300 MHz, C_6D_6): δ = 7.14–6.83 (m, 5H), 2.44 (sept, J = 6.6 Hz, 1H), 0.95 (d, J = 6.6 Hz, 6H) ppm; ^{13}C NMR (75 MHz, C_6D_6): δ = 205.2, 133.0, 129.7 (2C), 125.6 (2C), 125.0, 48.5, 24.5, 22.3 (2C) ppm.

***p*-Chlorophenyl isopropyl ketene (153d)[148]**

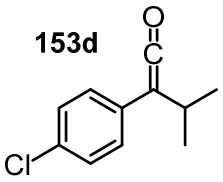

2-(4-Chlorophenyl)-3-methylbutanoyl chloride (278d). General procedure D2) was followed: Commercial 2-(4-chlorophenyl)-3-methylbutanoic acid (**277d**; 7.05 g, 33.2 mmol); reaction time: 20 h; distillation: 120–130 °C (5 mbar); **278d** was obtained as a pale yellow oil (7.28 g, 31.5 mmol, 95%). ^{1}H NMR (300 MHz, C_6D_6): δ = 7.05–6.91 (m, 2H), 6.80–6.65 (m, 2H), 3.26 (d, J = 10.0 Hz, 1H), 2.16–1.95 (m, 1H), 0.84 (d, J = 6.6 Hz, 3H), 0.37 (d, J = 6.8 Hz, 3H) ppm; ^{13}C NMR (75 MHz, C_6D_6): δ = 174.5, 134.9, 134.1, 130.7 (2C), 129.7 (2C), 71.2, 32.3, 21.3, 19.8 ppm.

***p*-Chlorophenyl isopropyl ketene (153d).** General procedure D3) was followed: 2-(4-Chlorophenyl)-3-methylbutanoyl chloride (**278d**; 2.34 g, 10.1 mmol); reaction time: 15 h; distillation: 60–65 °C (0.5 mbar); **153d** was obtained as a yellow oil (1.73 g, 8.88 mmol, 88%). ^{1}H NMR (300 MHz, C_6D_6): δ = 7.09–6.98 (m, 2H), 6.63–6.51 (m, 2H), 2.27 (sept, J = 6.7 Hz, 1H), 0.88 (d, J = 6.6 Hz, 6H) ppm; ^{13}C NMR (75 MHz, C_6D_6): δ = 204.2, 131.6, 130.4, 129.8 (2C), 126.7 (2C), 48.1, 24.4, 22.2 (2C) ppm.

***p*-Methoxyphenyl isopropyl ketene (153e)[26i]**

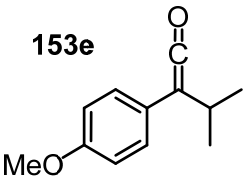

2-(4-Methoxyphenyl)-3-methylbutanoic acid (277e). General procedure D1) was followed: Commercial 4-methoxyphenylacetic acid (4.99 g, 30.0 mmol); alkyl bromide: 2-bromopropane; reaction time: 22 h; **277e** was obtained as a colorless crystalline solid (6.05 g, 29.1 mmol, 97%); ^{1}H NMR (300 MHz, DMSO-d_6): δ = 12.18 (s, 1H), 7.22 (d, J = 8.7 Hz, 2H), 6.88 (d, J = 8.7 Hz, 2H), 3.73 (s, 3H), 3.03 (d, J = 10.4 Hz, 1H), 2.25–2.05 (m, 1H), 0.98 (d, J = 6.4 Hz, 3H), 0.63 (d, J = 6.6 Hz, 3H) ppm; ^{13}C NMR (75 MHz, DMSO-d_6): δ = 174.9, 158.2, 130.7, 129.2 (2C), 113.7 (2C), 58.4, 55.0, 31.0, 21.2, 19.8 ppm; IR (film): $\tilde{\nu}$ = 2961, 1701, 1510, 1297, 1255, 1179, 1029, 830 cm^{-1}; HRMS (ESI): *m/z* calcd for $C_{12}H_{16}O_3Na$: 231.0992 $[M+Na]^+$; found: 231.0994.

2-(4-Methoxyphenyl)-3-methylbutanoyl chloride (278e). General procedure D2) was followed: 2-(4-Methoxyphenyl)-3-methylbutanoic acid (**277e**; 6.20 g, 29.8 mmol); reaction time: 2.5 h; distillation: 100–130 °C (5 mbar); **278e** was obtained as a yellow oil (6.16 g, 27.2 mmol, 91%). ^{1}H NMR (300 MHz, C_6D_6): δ = 6.99 (d, J = 8.7 Hz, 2H), 6.68 (d, J = 8.7 Hz, 2H), 3.41 (d, J = 10.2 Hz, 1H), 3.36–3.21 (m, 3H), 2.33–2.12 (m, 1H), 0.94 (d, J = 6.6 Hz, 3H), 0.52 (d, J = 6.6 Hz, 3H) ppm; ^{13}C NMR (75 MHz, C_6D_6): δ = 175.0, 160.4, 130.6 (2C), 127.5, 115.1 (2C), 71.4, 55.2, 32.4, 21.5, 20.0 ppm.

***p*-Methoxyphenyl isopropyl ketene (153e).** General procedure D3) was followed: 2-(4-Methoxyphenyl)-3-methylbutanoyl chloride (**278e**, 2.12 g, 9.35 mmol); reaction time: 45 h; distillation: 70 °C (0.7 mbar); **153e** was obtained as a yellow oil (1.30 g, 6.81 mmol, 73%). ^{1}H NMR (300 MHz, C_6D_6): δ = 6.94–6.83 (m, 2H), 6.80–6.68 (m, 2H), 3.32 (s, 3H), 2.46 (sept, J = 6.7 Hz, 1H), 0.99 (d, J = 6.6 Hz, 6H) ppm; ^{13}C NMR (75 MHz, C_6D_6): δ = 206.7, 158.2, 127.5 (2C), 124.2, 115.5 (2C), 55.2, 47.1, 25.2, 22.4 (2C) ppm.

***m*-Tolyl isopropyl ketene (153f)**

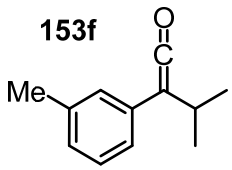

3-Methyl-2-(*m*-tolyl)butanoic acid (277f). General procedure D1) was followed: Commercial *m*-tolylacetic acid (3.81 g, 25.4 mmol); alkyl bromide: 2-bromopropane; reaction time: 26 h; **277f** was obtained as a colorless crystalline solid (4.87 g, 25.3 mmol, quant.); ^{1}H NMR (300 MHz, $CDCl_3$): δ = 10.74 (s, 1H), 7.27–7.03 (m, 4H), 3.11 (d, J = 10.6 Hz, 1H), 2.43–2.23 (m, 1H), 2.35 (s, 3H), 1.09 (d, J = 6.6 Hz, 3H), 0.72 (d, J = 6.6 Hz, 3H) ppm; ^{13}C NMR (75 MHz, $CDCl_3$): δ = 180.4, 138.3, 137.8, 129.5, 128.6, 128.4, 125.8, 60.1, 31.6, 21.6, 21.6, 20.3 ppm. IR (film): $\tilde{\nu}$ = 3022, 1700, 1290, 1210, 780, 718 cm^{-1}; HRMS (ESI): *m/z* calcd for $C_{12}H_{16}O_2Na$: 215.1043 $[M+Na]^+$; found: 215.1045.

3-Methyl-2-(*m*-tolyl)butanoyl chloride (278f). General procedure D2) was followed: 3-Methyl-2-(*m*-tolyl)butanoic acid (**277f**; 4.84 g, 25.2 mmol); reaction time: 4 h; distillation: 70 °C (0.4 mbar); **278f** was obtained as a colorless oil (5.13 g, 24.3 mmol, 97%). ^{1}H NMR (300 MHz, C_6D_6): δ = 7.01 (t, J = 7.7 Hz, 1H), 6.69–6.79 (m, 3H), 3.43 (d, J = 10.2 Hz, 1H), 2.34–2.12 (m, 1H), 2.02 (s, 3H), 0.93 (d, J = 6.4 Hz, 3H), 0.49 (d, J = 6.6 Hz, 3H) ppm; ^{13}C NMR (75 MHz, C_6D_6): δ = 174.9, 139.2, 135.7, 130.1, 129.6, 129.5, 126.6, 72.3, 32.6, 21.6, 21.5, 20.1 ppm.

***m*-Tolyl isopropyl ketene (153f).** General procedure D3) was followed: 3-Methyl-2-(*m*-tolyl)butanoyl chloride (**278f**; 2.11 g, 10.0 mmol); reaction time: 43 h; distillation: 45−55 °C (0.4 mbar); **153f** was obtained as a yellow oil (1.34 g, 7.71 mmol, 77%). ^{1}H NMR (300 MHz, C_6D_6): δ = 7.07 (d, J = 7.6 Hz, 1H), 6.88–6.69 (m, 3H), 2.50 (sept, J = 6.8 Hz, 1H), 2.08 (s, 3H), 0.99 (d, J = 6.8 Hz, 6H) ppm; ^{13}C NMR (75 MHz, C_6D_6): δ = 205.5, 139.1, 132.9, 129.6, 126.5, 126.0, 122.9, 48.4, 24.5, 22.4 (2C), 21.8 ppm.

Phenyl cyclopentyl ketene (153g)[148]

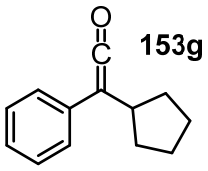

2-Cyclopentyl-2-phenylacetyl chloride (278g). General procedure D2) was followed: Commercial 2-cyclopentyl-2-phenylacetic acid (**277g**; 5.75 g, 28.2 mmol); reaction time: 5 h; distillation: 85 °C (0.3 mbar); **278g** was obtained as a pale yellow oil (6.02 g, 27.0 mmol, 96%). ^{1}H NMR (300 MHz, C_6D_6): δ = 7.13–6.89 (m, 5H), 3.52 (d, J = 10.8 Hz, 1H), 2.52–2.25 (m, 1H), 1.99–1.75 (m, 1H), 1.52–0.94 (m, 6H), 0.80–0.56 (m, 1H) ppm; ^{13}C NMR (75 MHz, C_6D_6): δ = 174.8, 136.6, 129.6 (2C), 129.2 (2C), 128.7, 70.4, 44.0, 31.9, 31.0, 25.8, 25.3 ppm.

Phenyl cyclopentyl ketene (153g). General procedure D3) was followed: 2-Cyclopentyl-2-phenylacetyl chloride (**278g**; 2.18 g, 9.79 mmol); reaction time: 38 h; distillation: 70–75 °C (0.5 mbar); **153g** was obtained as a yellow oil (1.19 g, 6.36 mmol, 65%). ^{1}H NMR (300 MHz, C_6D_6): δ = 7.17–7.04 (m, 2H), 7.01–6.85 (m, 2H), 2.56 (quint, J = 7.4 Hz, 1H), 1.87–1.67 (m, 2H), 1.58–1.30 (m, 4H), 1.30–1.11 (m, 2H) ppm; ^{13}C NMR (75 MHz, C_6D_6): δ = 205.6, 133.8, 129.6 (2C), 125.4 (2C), 124.9, 46.5, 35.0, 33.1 (2C), 25.2 (2C) ppm.

Phenyl cyclohexyl ketene (153h)[148]

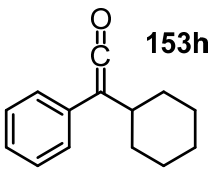

2-Cyclohexyl-2-phenylacetyl chloride (278h). General procedure D2) was followed: Commercial 2-cyclohexyl-2-phenylacetic acid (**277h**, 4.98 g, 22.8 mmol); reaction time: 4 h; distillation: 110–120 °C (0.5 mbar); **278h** was obtained as a pale yellow oil (5.28 g, 22.3 mmol, 98%). ^{1}H NMR (300 MHz, C_6D_6): δ = 7.15–6.87 (m, 5H), 3.54 (d, J = 10.2 Hz, 1H), 2.11–1.79 (m, 2H), 1.63–0.72 (m, 9H), 0.58–0.35 (m, 1H) ppm; ^{13}C NMR (75 MHz, C_6D_6): δ = 174.8, 135.3, 129.6 (4C), 128.7, 71.4, 41.7, 32.2, 30.4, 26.7, 26.4, 26.3 ppm.

Phenyl cyclohexyl ketene (153h). General procedure D3) was followed: 2-Cyclohexyl-2-phenylacetyl chloride (**278h**; 2.00 g, 8.45 mmol); reaction time: 44 h; distillation: 80–90 °C (0.4 mbar); **153h** was obtained as a yellow oil (1.26 g, 6.29 mmol, 75%). ^{1}H NMR (300 MHz, C_6D_6): δ = 7.18–6.84 (m, 5H), 2.30–2.09 (m, 1H), 1.93–1.74 (m, 2H), 1.64–0.82 (m, 8H) ppm; ^{13}C NMR (75 MHz, C_6D_6): δ = 205.4, 132.9, 129.7 (2C), 125.7 (2C), 125.0, 47.3, 33.8, 33.2 (2C), 26.9 (2C), 26.7 ppm.

4.9.4 *O*-Acylated Oxindoles (147a–b, 149a–b, 151)

Gliocladin C Precursors 147a and 147b[90,150]

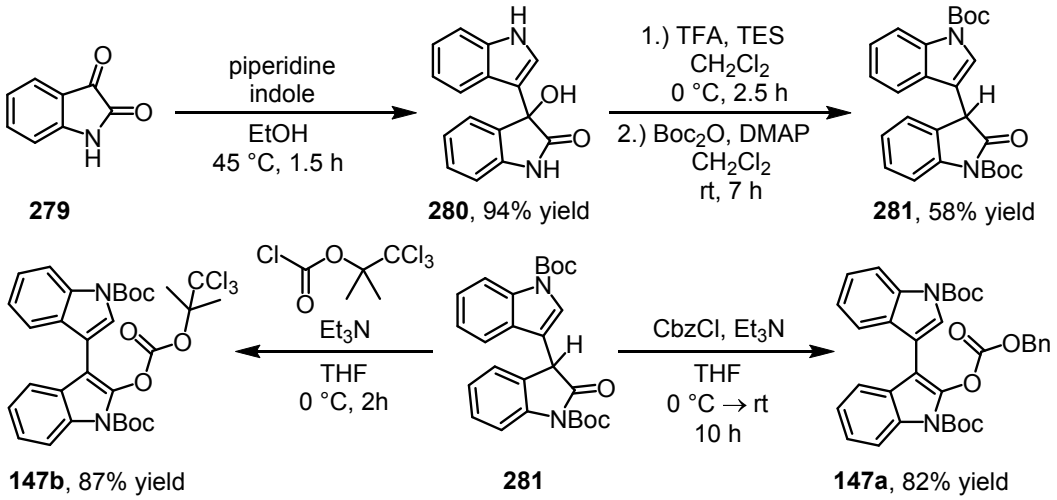

Scheme 88. Synthesis of gliocladin C precursors **147a** and **147a**.

Compound 280. Compound **280** was synthesized according to a modified protocol from Bergman et al.[150] A flask (250 mL) was charged with isatin (**279**; 2.21 g, 15.0 mmol, 1.00 eq), indole (1.76 g, 15.0 mmol, 1.00 eq), ethanol (45 mL), and piperidine (148 µL, 1.50 mmol, 10 mol%). The resulting mixture was stirred at 45 °C for 1.5 h. After cooling to rt, all volatiles were removed *in vacuo*, the crude product dissolved in MeOH, adsorbed on silica gel, and purified by short-column flash chromatography (hexanes/EtOAc 1:1 → EtOAc). After drying *in vacuo*, compound **280** was obtained as a beige crystalline solid (3.71 g, 14.0 mmol, 94%). ^{1}H NMR (300 MHz, DMSO-d_6): δ = 10.98 (d, J = 1.3 Hz, 1H), 10.34 (s, 1H), 7.44–7.31 (m, 2H), 7.31–7.20 (m, 2H), 7.09 (d, J = 2.6 Hz, 1H), 7.04 (td, J = 7.6 Hz, J = 1.1 Hz, 1H), 7.00–6.83 (m, 3H), 6.36 (s, 1H) ppm; HRMS (ESI): *m/z* calcd for $C_{16}H_{12}N_2O_2Na$: 287.0791 $[M+Na]^+$; found: 287.0793.

Compound 281. Compound **281** was synthesized according to a protocol from Overman et al.[90] A flask (250 mL) was charged with compound **280** (3.65 g, 13.8 mmol, 1.00 eq), evacuated for 2 h, and carefully refilled with nitrogen gas. Dry CH_2Cl_2 (55 mL) and triethylsilane (6.60 mL, 41.4 mmol, 3.00 eq) were added and the resulting mixture cooled to 0 °C. Trifluoroacetic acid (5.20 mL, 68.0 mmol, 4.92 eq) was added dropwise over 5 min and the resulting mixture stirred at 0 °C for 2.5 h. The mixture was then quenched at 0 °C by the addition of aqueous 5% sodium citrate (330 mL). This mixture was diluted with EtOAc and the organic layer separated. The aqueous layer was extracted with EtOAc (3x), the combined organic layers washed with water and brine, and the solvent removed *in vacuo*. Solvent traces were removed from the residue as an azeotrope with *m*-xylene (2x 50 mL). The obtained solid was then triturated with hexanes (70 mL) and the hexane layer removed by filtration through a

glass filter (porosity G3). The precipitate was collected, dried *in vacuo*, and transferred into a new flask (250 mL). CH_2Cl_2 (90 mL) was added and the resulting suspension cooled with a water bath. Then, Boc_2O (8.38 g, 38.4 mmol, 2.78 eq) and DMAP (268 mg, 2.19 mmol, 16 mol%) were added (*caution*: *gas evolution!*). The resulting mixture was stirred at rt for 7 h under nitrogen atmosphere whereupon the suspension turned into a solution. Then, MeOH (45 mL) was added and the mixture stirred at rt for 16 h. Subsequently, the resulting mixture was diluted with EtOAc and aqueous sat. NH_4Cl. The organic layer was separated and the aqueous layer extracted with EtOAc (3x). The combined organic layers were dried over Na_2SO_4 and the solvent removed *in vacuo*. The crude product was dissolved in CH_2Cl_2, adsorbed on silica gel, and purified by flash chromatography (hexanes/EtOAc 20:1 → 10:1). After drying *in vacuo*, compound **281** was obtained as a pale-yellow solid foam (3.60 g, 8.02 mmol, 58%). ^{1}H NMR (300 MHz, $CDCl_3$): δ = 8.14 (d, J = 8.3 Hz, 1H), 7.97 (d, J = 8.1 Hz, 1H), 7.49 (s, 1H), 7.43–7.35 (m, 1H), 7.34–7.11 (m, 5H), 1.66 (s, 9H), 1.64 (s, 9H) ppm; HRMS (ESI): *m/z* calcd for $C_{26}H_{28}N_2O_5Na$: 471.1890 [M+Na]$^+$; found: 471.1891.

Gliocladin C Precursor 147a. Compound **147a** was synthesized according to a modified protocol from Overman et al.[90] A flame-dried flask (10 mL) was charged with compound **281** (400 mg, 892 µmol, 1.00 eq), dry THF (3.6 mL), and Et_3N (300 µL, 2.16 mmol, 2.42 eq). This mixture was cooled to 0 °C and CbzCl (280 µL, 1.96 mmol, 2.20 eq) was added. The resulting mixture was allowed to warm to rt and stirred for 10 h at rt and then quenched by the addition of aqueous sat. NH_4Cl. The mixture was diluted with water and EtOAc, the organic layer separated, the aqueous layer extracted with EtOAc (2x), and the combined organic layers washed with water (2x) and dried over Na_2SO_4. The solvent was removed *in vacuo*, the residue dissolved in CH_2Cl_2 and adsorbed on silica gel (40 °C), and the crude product purified by flash chromatography (hexanes/Et_2O 10:1 → 5:1). After drying *in vacuo*, gliocladin C precursor **147a** was obtained as a colorless solid foam (426 mg, 731 µmol, 82%). ^{1}H NMR (300 MHz, $CDCl_3$): δ = 8.23 (d, J = 8.3 Hz, 1H), 8.18 (d, J = 8.3 Hz, 1H), 7.76 (s, 1H), 7.56 (t, J = 7.7 Hz, 2H), 7.42–7.33 (m, 2H), 7.33–7.13 (m, 7H), 5.22 (s, 2H), 1.70 (s, 9H), 1.63 (s, 9H) ppm; ^{13}C NMR (75 MHz, $CDCl_3$): δ = 152.5, 149.8, 149.0, 138.2, 135.7, 134.4, 132.6, 129.8, 128.8, 128.7 (2C), 128.4 (2C), 127.0, 125.1, 124.9, 124.8, 123.4, 122.9, 121.1, 120.2, 115.7, 115.4, 110.7, 102.9, 84.9, 84.0, 71.2, 28.4 (3C), 28.3 (3C) ppm; IR (film): $\tilde{\nu}$ = 1778, 1734, 1453, 1363, 1315, 1249, 1213, 1149, 1115, 1068, 738 cm^{-1}; HRMS (ESI): *m/z* calcd for $C_{34}H_{34}N_2O_7Na$: 605.2258 [M+Na]$^+$; found: 605.2259.

Gliocladin C precursor 147b. Compound **147b** was synthesized according to a modified protocol from Overman et al.[90] A flame-dried flask (25 mL) was charged with compound **281** (800 mg, 1.78 mmol, 1.00 eq), dry THF (7.2 mL), and Et_3N (300 µL, 2.16 mmol, 1.21 eq).

This mixture was cooled to 0 °C and 2,2,2-trichloro-1,1-dimethylethyl chloroformate (471 mg, 1.96 mmol, 1.10 eq) was added. The resulting mixture was stirred at 0 °C for 2 h and then quenched by the addition of aqueous sat. NH_4Cl and diluted with water and EtOAc. The organic layer was separated, the aqueous layer extracted with EtOAc (2x), and the combined organic layers washed with water (1x) and brine (1x) and dried over Na_2SO_4. The solvent was removed *in vacuo*, the residue dissolved in CH_2Cl_2 and adsorbed on silica gel (40 °C), and the crude product purified by flash chromatography (hexanes/Et_2O 20:1 → 10:1). After solvent removal and drying *in vacuo*, gliocladin C precursor **147b** was obtained as a colorless solid foam (1.01 g, 1.55 mmol, 87%). ^{1}H NMR (300 MHz, $CDCl_3$): δ = 8.23 (d, J = 8.1 Hz, 1H), 8.12 (d, J = 8.5 Hz, 1H), 7.76 (s, 1H), 7.56 (t, J = 7.4 Hz, 2H), 7.42–7.32 (m, 2H), 7.30–7.17 (m, 2H), 1.87 (s, 6H), 1.71 (s, 9H), 1.69 (s, 9H) ppm; ^{13}C NMR (75 MHz, $CDCl_3$): δ = 149.7, 149.1, 148.9, 138.2, 135.7, 132.4, 129.7, 126.8, 124.9, 124.8, 124.8, 123.4, 122.9, 121.1, 120.3, 115.6, 115.4, 110.7, 105.0, 102.7, 91.8, 85.0, 84.1, 28.4 (3C), 28.4 (3C), 21.1 (2C) ppm; IR (film): $\tilde{\nu}$ = 1783, 1736, 1453, 1365, 1315, 1248, 1211, 1154, 1115, 1069, 802, 742 cm^{-1}; HRMS (ESI): *m/z* calcd for $C_{31}H_{33}Cl_3N_2O_7Na$: 673.1246 [*M*+Na]$^+$; found: 673.1250.

N,O-Diacylated Oxindoles (149a–b)

N,O-Diacylated Oxindole 149a

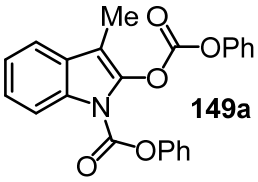

Compound **149a** was synthesized according to a procedure from Suga et al.[23f] A flame-dried flask (25 mL) was charged with commercial 3-methyl-2-oxindole (386 mg, 2.62 mmol, 1.00 eq) and dry THF (10 mL). Et_3N (1.55 mL, 11.1 mmol, 4.24 eq) and phenyl chloroformate (1.32 mL, 10.5 mmol, 4.02 eq) were added and the mixture stirred at rt for 1 h. The mixture was then diluted with CH_2Cl_2 and quenched with 1 M HCl. The organic layer was separated and the aqueous layer extracted with CH_2Cl_2 (3x). The combined organic layers were dried over Na_2SO_4, the solvent removed *in vacuo*, the crude product dissolved in CH_2Cl_2, adsorbed on silica gel (42 °C), and purified by short-column chromatography (hexanes/Et_2O 10:1). After drying *in vacuo*, desired *N,O*-diacylated oxindole **149** was obtained as a colorless oil which crystallized on standing (1.02 g, 2.63 mmol, quant.). ^{1}H NMR (300 MHz, $CDCl_3$): δ = 8.14–8.02 (m, 1H), 7.50–7.10 (m, 11H), 7.09–6.98 (m, 2H), 2.19 (s, 3H) ppm; ^{13}C NMR (75 MHz, $CDCl_3$): δ = 151.3, 151.1, 150.2, 148.7, 137.4, 132.4, 129.9 (2C), 129.7 (2C), 128.3, 126.8, 126.7, 125.3, 123.9, 121.7 (2C), 120.9 (2C), 119.2, 115.7, 106.5, 7.2 ppm; IR (film): $\tilde{\nu}$ = 1789, 1747, 1455, 1355, 1328, 1187, 1070, 999, 741, 687 cm^{-1}; HRMS (ESI): *m/z* calcd for $C_{23}H_{17}N_1O_5Na$: 410.0999 [*M*+Na]$^+$; found: 410.1007.

N,O-Diacylated Oxindole 149b

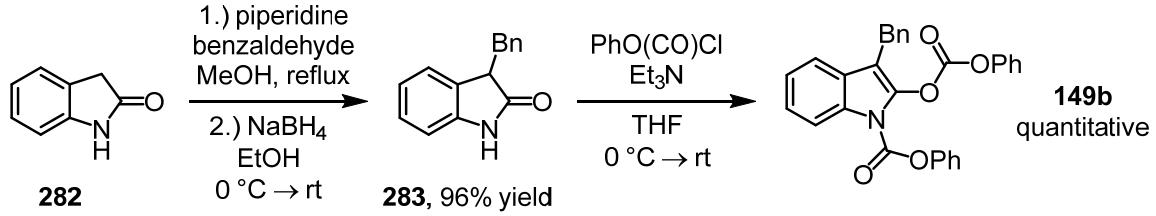

Scheme 89. Synthesis of *N,O*-diacylated oxindole **149b**.

2-Benzylindolin-2-one (283). Compound **283** was synthesized according to a protocol from Melchiorre et al.[151] A flame-dried flask was charged with commercial indolin-2-one (**282**; 500 mg, 3.76 mmol, 1.00 eq), dry MeOH (4.0 mL), piperidine (740 µL, 7.49 mmol, 2.00 eq), and benzaldehyde (420 µL, 4.13 mmol, 1.10 eq). The resulting mixture was stirred at reflux for 3.5 h. After cooling to rt, all volatiles were removed and the resulting yellow-orange solid dried *in vacuo*. Then, dry MeOH (12 mL) was added, the resulting suspension cooled to 0 °C, and $NaBH_4$ (500 mg, 13.2 mmol, 3.52 eq) carefully added (*gas evolution!*). After the gas evolution had ceased, the mixture was allowed to warm to rt and stirred for 1 h under nitrogen atmosphere. Then, the mixture was quenched by the addition of aqueous NH_4Cl and diluted with water and EtOAc. The organic layer was separated, the aqueous layer extracted with EtOAc (3x), and the combined organic layers dried over Na_2SO_4. All volatiles were removed *in vacuo*, the crude product dissolved in CH_2Cl_2, adsorbed on silica gel, and purified by short-column flash chromatography (hexanes/EtOAc 3:1). After drying *in vacuo*, desired 2-benzylindolin-2-one (**283**) was obtained as a pale-yellow crystalline solid (803 mg, 3.59 mmol, 96%). ^{1}H NMR (300 MHz, $CDCl_3$): δ = 9.08 (s, 1H), 7.23–7.01 (m, 6H), 6.86–6.72 (m, 2H), 6.65 (d, J = 7.4 Hz, 1H), 3.67 (dd, J = 9.3 Hz, J = 4.5 Hz, 1H), 3.41 (dd, J = 13.8 Hz, J = 4.5 Hz, 1H), 2.85 (dd, J = 13.6 Hz, J = 9.3 Hz, 1H) ppm; HRMS (ESI): *m/z* calcd for $C_{15}H_{13}N_1O_1H$: 224.1070 $[M+H]^+$; found: 224.1072.

***N,O*-Diacylated oxindole 149b.** Compound **149b** was synthesized according to a protocol from Suga et al.[23f] A flame-dried flask (10 mL) was charged with 2-benzylindolin-2-one (**283**; 350 mg, 1.57 mmol, 1.00 eq) and dry THF (5 mL). Et_3N was added (550 µL, 3.95 mmol, 2.52 eq) and the mixture cooled to 0 °C. Then, phenyl chloroformate (490 µL, 3.91 mmol, 2.50 eq) was added and the mixture allowed to warm to rt and stirred for 2 h. The mixture was diluted with CH_2Cl_2 and quenched with 1 M HCl. The organic layer was separated and the aqueous layer extracted with CH_2Cl_2 (2x). The combined organic layers were dried over Na_2SO_4, the solvent removed *in vacuo*, the crude product dissolved in CH_2Cl_2, adsorbed on silica gel (40 °C), and purified by short-column chromatography (hexanes/Et_2O 10:1). After drying *in vacuo*, *N,O*-diacylated oxindole **149b** was obtained as a colorless crystalline solid

(730 mg, 1.58 mmol, quant.). ^{1}H NMR (300 MHz, $CDCl_3$): δ = 8.19 (d, J = 8.1 Hz, 1H), 7.53–7.11 (m, 16H), 7.09–7.01 (m, 2H), 4.12 (s, 2H) ppm; ^{13}C NMR (75 MHz, $CDCl_3$): δ = 151.2, 151.1, 150.2, 148.7, 138.6, 138.0, 132.6, 129.9 (2C), 129.7 (2C), 129.3, 128.8 (3C), 127.5, 126.8, 126.7, 126.6, 125.3, 124.0, 121.7 (2C), 120.9 (2C), 119.8, 115.8, 109.5, 29.0 ppm; IR (film): $\tilde{\nu}$ = 2923, 1790, 1748, 1718, 1456, 1360, 1329, 1229, 1186, 1112, 1015, 745, 692 cm^{-1}; HRMS (ESI): *m/z* calcd for $C_{29}H_{21}NO_5Na$: 486.1312 [*M*+Na]$^+$; found: 486.1313.

O-Acylated, *N*-Methylated Indole 151

Compound **151** was synthesized according to a procedure from Trost et al. (Scheme 90).[152]

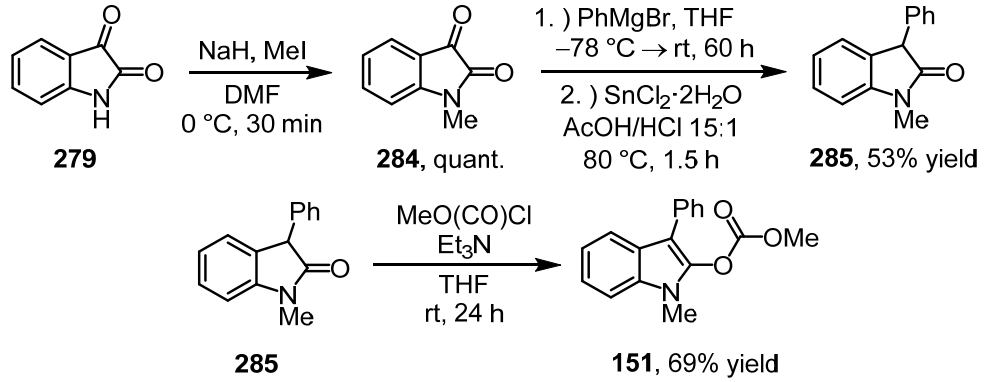

Scheme 90. Synthesis of *O*-acylated, *N*-methylated indole **151**.[152]

Compound 284. A flame-dried flask was charged with isatin (**279**; 4.00 g, 27.2 mmol, 1.00 eq) and dry DMF (80 mL) and the mixture cooled to 0 °C. Sodium hydride (60 wt% in mineral oil; 1.30 g, 32.6 mmol, 1.20 eq) was gradually added to the mixture under stirring. 5 min after addition completion, methyl iodide (2.54 mL, 40.8 mmol, 1.50 eq) was added and the mixture stirred at 0 °C for 30 min. The resulting mixture was quenched by the addition of aqueous sat. NH_4Cl and diluted with water and EtOAc. The organic layer was separated and the aqueous layer extracted with EtOAc (4x). The combined organic layers were washed with water (3x) and brine and dried over $MgSO_4$. After solvent removal and drying *in vacuo*, compound **284** was obtained as a red solid without the need for further purification (4.64 g, 28.8 mmol, quant.). ^{1}H NMR (300 MHz, $CDCl_3$): δ = 7.64–7.52 (m, 2H), 7.11 (td, J = 7.6 Hz, J = 0.8 Hz, 1H), 6.88 (d, J = 7.9 Hz, 1H), 3.23 (s, 3H) ppm; HRMS (ESI): *m/z* calcd for $C_9H_7N_1O_2Na$: 184.0369 [*M*+Na]$^+$; found: 184.0372.

Compound 285. A flame-dried flask was charged with compound **284** (0.50 g, 3.10 mmol, 1.00 eq) and dry THF (80 mL) and the resulting mixture cooled to –78 °C. Then, a solution of PhMgBr (3 M in Et_2O; 1.19 mL, 3.57 mmol, 1.15 eq) was added dropwise. The mixture was stirred at –78 °C for 1 h and then allowed to warm to rt and stirred for 60 h. The resulting

mixture was quenched with aqueous sat. NH_4Cl, diluted with water and CH_2Cl_2, the organic layer separated, and the aqueous layer extracted with CH_2Cl_2 (3x). The combined organic layers were washed with brine and dried over $MgSO_4$. The solvent was removed *in vacuo*, which yielded a yellow oil which was transferred into a new flask (250 mL). A 15:1 mixture of glacial acetic acid and concentrated HCl (90 mL) as well as $SnCl_2 \cdot 2H_2O$ (1.68 g, 7.44 mmol, 2.00 eq) were added and the mixture stirred at 80 °C (reflux) for 1.5 h. After cooling to rt, the mixture was diluted with Et_2O and water and the organic layer separated. The aqueous layer was extracted with Et_2O (3x) and the combined organic layers washed with aqueous 1 M NaOH and dried over $MgSO_4$. The solvent was removed *in vacuo*, the crude product dissolved in CH_2Cl_2, adsorbed on silica gel, and purified by flash chromatography (hexanes/Et_2O 7:3). Desired product **285** was obtained as a pale yellow crystalline solid (0.37 g, 1.65 mmol, 53%). ^{1}H NMR (300 MHz, $CDCl_3$): δ = 7.46–7.24 (m, 4H), 7.24–7.13 (m, 3H), 7.11–7.02 (m, 1H), 6.90 (d, J = 7.7 Hz, 1H), 4.61 (s, 1H), 3.26 (s, 3H) ppm.

***O*-Acylated, *N*-methylated indole 151.** A flame-dried flask was charged with sodium hydride (60 wt% in mineral oil; 38.0 mg, 950 µmol, 1.15 eq) and dry THF (5.0 mL). Compound **285** (185 mg, 830 µmol, 1.00 eq) was added and the resulting mixture stirred at rt for 30 min. Methyl chloroformate (74.0 µL, 950 µmol, 1.15 eq) was added and the mixture stirred for 24 h at rt. The mixture was diluted with water and Et_2O and the organic layer separated. The aqueous layer was extracted with Et_2O (3x) and the combined organic layers washed with brine and dried over Na_2SO_4. The solvent was removed *in vacuo*, the crude product dissolved in CH_2Cl_2, adsorbed on silica gel, and purified by flash chromatography (hexanes/Et_2O 8:2). After solvent removal and drying *in vacuo*, desired *O*-acylated, *N*-methylated indole **151** was obtained as a colorless solid (160 mg, 570 µmol, 69%). ^{1}H NMR (300 MHz, $CDCl_3$): δ = 7.82 (d, J = 7.9 Hz, 1H), 7.65–7.55 (m, 2H), 7.51–7.40 (m, 2H), 7.37–7.24 (m, 3H), 7.24–7.15 (m, 1H), 3.89 (s, 3H), 3.68 (s, 3H) ppm; ^{13}C NMR (75 MHz, $CDCl_3$): δ = 153.1, 139.0, 133.1, 132.8, 128.9 (2C), 128.5 (2C), 126.3, 124.9, 122.3, 120.7, 119.8, 109.4, 56.4, 28.5 ppm (one signal could not be located due to low S/N ratio); IR (film): $\tilde{\nu}$ = 1773, 1574, 1474, 1433, 1405, 1369, 1235, 1139, 1081, 924, 770, 739, 698, 640, 496, 442 cm^{-1}; HRMS (ESI): *m/z* calcd for $C_{17}H_{15}N_1O_3Na$: 304.0944 $[M+Na]^+$; found: 304.0944.

4.9.5 Silyl Ketene Acetals (145a–d)

Silyl Ketene Acetal 145a

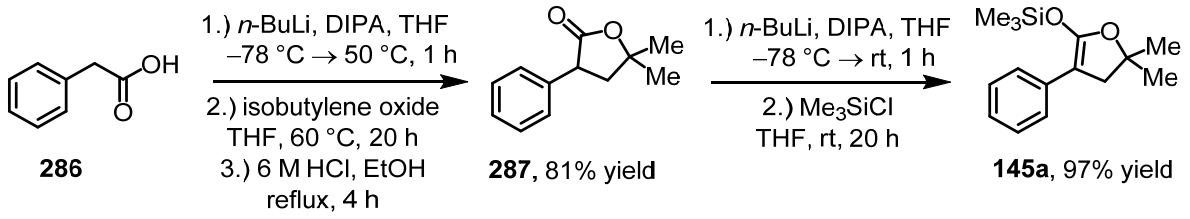

Scheme 91. Synthesis of silyl ketene acetal **145a**.

Compound 287. Compound **287** was synthesized according to a protocol from Fu et al.[89] A flask (250 mL) was charged with dry THF (40 mL) and diisopropylamine (6.55 mL, 46.7 mmol, 3.12 eq). This mixture was cooled to –78 °C and *n*-BuLi (2.5 M in hexanes; 18.1 mL, 45.2 mmol, 3.02 eq) was added. The resulting mixture was stirred at –78 °C for 15 min and then allowed to stir at 0 °C for 10 min. Phenylacetic acid (**286**; 2.04 g, 15.0 mmol, 1.00 eq) in dry THF (15 mL) was added and the mixture stirred at 50 °C for 1 h under nitrogen atmosphere. Then, the mixture was allowed to cool to rt and isobutylene oxide (1.35 mL, 15.2 mmol, 1.01 eq) was added and the resulting mixture stirred at 60 °C for 20 h under nitrogen atmosphere. After cooling to rt, water (35 mL) was added and the mixture vigorously stirred at 70 °C (reflux) for 2 h. After cooling to rt, the mixture was diluted with Et_2O and water, the aqueous layer separated, washed with Et_2O (3x), and the organic layers disposed. Traces of Et_2O were selectively removed from the aqueous layer *in vacuo*. Then, aqueous 6 M HCl (25 mL) and EtOH (50 mL) were added to the aqueous layer and the resulting mixture stirred at 80 °C (reflux) for 4 h. After cooling to rt, the mixture was extracted with $CHCl_3$ (4x) and the resulting organic layer washed with aqueous $NaHCO_3$ and brine and dried over Na_2SO_4. After solvent removal and drying *in vacuo*, compound **287** was obtained as a colorless crystalline solid without the need for further purification (2.32 g, 12.2 mmol, 81%). ^{1}H NMR (300 MHz, $CDCl_3$): δ = 7.40–7.07 (m, 5H), 3.95 (dd, J = 11.7 Hz, J = 9.3 Hz, 1H), 2.49 (dd, J = 12.8 Hz, J = 9.3 Hz, 1H), 2.15 (t, J = 12.3 Hz, 1H), 1.46 (s, 3H), 1.41 (s, 3H) ppm; HRMS (ESI): *m/z* calcd for $C_{12}H_{14}O_2Na$ $[M+Na]^+$: 214.0886, found: 214.0887.

Silyl Ketene Acetal 145a. Compound **145a** was synthesized according to a protocol from Fu et al.[89] A flame-dried flask (50 mL) was charged with dry THF (10 mL) and diisopropylamine (1.64 mL, 11.7 mmol, 1.06 eq). This mixture was cooled to –78 °C and *n*-BuLi (2.5 M in hexanes; 4.68 mL, 11.7 mmol, 1.06 eq) was added and the mixture stirred at –78 °C for 1 h. Then, compound **287** (2.10 g, 11.0 mmol, 1.00 eq) was added in dry THF (13 mL) and the resulting mixture stirred at –78 °C for 1 h. Me_3SiCl (1.50 mL, 11.8 mmol, 1.07 eq) was added at –78 °C, the mixture allowed to warm to rt, and the mixture stirred at rt for 20 h under

nitrogen atmosphere. Then, the solvent was carefully removed *in vacuo* (*moisture exclusion!*) and the remaining residue taken up in dry pentane. The resulting mixture was passed under nitrogen atmosphere through a flame-dried Schlenk frit (porosity G4) charged with a plug of flame-dried florisil (60–100 mesh) and which was equipped with a flame-dried receiving flask. The solvent was removed from the resulting clear filtrate *in vacuo* (*exclusion of moisture!*), which yielded silyl ketene acetal **145a** after drying *in vacuo* as a pale yellow oil (2.79 g, 10.6 mmol, 97%; *moisture-sensitive*). ^{1}H NMR (300 MHz, C_6D_6): δ = 7.80–7.65 (m, 2H), 7.54–7.38 (m, 2H), 7.21–7.09 (m, 1H), 2.68 (s, 2H), 1.30 (s, 6H), 0.35 (s, 9H) ppm; ^{13}C NMR (75 MHz, C_6D_6): δ = 153.5, 137.3, 128.8 (2C), 124.7 (2C), 123.7, 82.9, 81.5, 43.9, 28.9 (2C), 0.9 (3C) ppm.

Silyl Ketene Acetal 145b

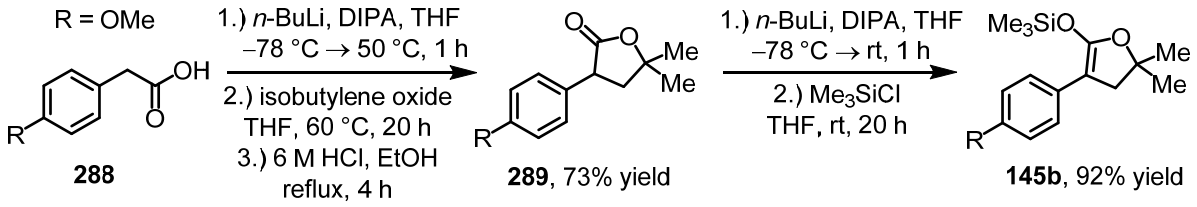

Scheme 92. Synthesis of silyl ketene acetal **145b**.

Compound 289. Compound **289** was synthesized according to a protocol from Fu et al.[89] A flask (250 mL) was charged with dry THF (40 mL) and diisopropylamine (8.13 mL, 58.0 mmol, 3.86 eq). This mixture was cooled to –78 °C and *n*-BuLi (2.5 M in hexanes; 22.0 mL, 55.0 mmol, 3.66 eq) was added. The resulting mixture was stirred at –78 °C for 15 min and then allowed to stir at 0 °C for 10 min. (4-Methoxyphenyl)acetic acid (**288**; 2.50 g, 15.0 mmol, 1.00 eq) in dry THF (15 mL) was then added and the mixture stirred at 50 °C for 1 h under nitrogen atmosphere. The mixture was allowed to cool to rt and isobutylene oxide (1.35 mL, 15.2 mmol, 1.01 eq) was added and the resulting mixture stirred at 60 °C for 20 h under nitrogen atmosphere. After cooling to rt, water (35 mL) was added and the resulting mixture vigorously stirred at 70 °C (reflux) for 2 h. After cooling to rt, the mixture was diluted with Et_2O and water, the aqueous layer separated, washed with Et_2O (3x), and the organic layers disposed. Traces of Et_2O were selectively removed from the aqueous layer *in vacuo*. Then, aqueous 6 M HCl (25 mL) and EtOH (50 mL) were added to the aqueous layer and the resulting mixture stirred 80 °C (reflux) for 4 h. After cooling to rt, the mixture was extracted with $CHCl_3$ (4x) and the resulting organic layer washed with aqueous $NaHCO_3$ and brine and dried over Na_2SO_4. After solvent removal and drying *in vacuo*, desired compound **289** was obtained as a pale yellow crystalline solid without the need for

further purification (2.42 g, 11.0 mmol, 73%). ^{1}H NMR (300 MHz, $CDCl_3$): δ = 7.20 (d, J = 8.7 Hz, 2H), 6.89 (d, J = 8.1 Hz, 2H), 3.98 (dd, J = 11.8 Hz, J = 9.2 Hz, 1H), 3.79 (s, 3H), 2.54 (dd, J = 12.7 Hz, J = 9.2 Hz, 1H), 2.19 (t, J = 12.3 Hz, 1H), 1.53 (s, 3H), 1.48 (s, 3H) ppm; HRMS (ESI): *m/z* calcd for $C_{13}H_{16}O_3Na$ $[M+Na]^+$: 243.0992, found: 243.0993.

Silyl Ketene Acetal 145b. Compound **145b** was synthesized according to a protocol from Fu et al.[89] A flame-dried flask (50 mL) was charged with dry THF (10 mL) and diisopropylamine (1.48 mL, 10.6 mmol, 1.06 eq). This mixture was cooled to –78 °C and *n*-BuLi (2.5 M in hexanes; 4.20 mL, 10.5 mmol, 1.05 eq) was added and the mixture stirred at –78 °C for 1 h. Then, compound **289** (2.20 g, 9.99 mmol, 1.00 eq) was added in dry THF (11 mL) and the mixture stirred at –78 °C for 1 h. Me_3SiCl (1.35 mL, 10.6 mmol, 1.06 eq) was added at −78 °C, the mixture allowed to warm to rt, and the mixture stirred at rt for 20 h under nitrogen atmosphere. Then, the solvent was removed *in vacuo* (*moisture exclusion!*) and the remaining residue taken up in dry pentane. The resulting mixture was passed under nitrogen atmosphere through a flame-dried Schlenk frit (porosity G4) charged with a plug of flame-dried florisil (60–100 mesh) and which was equipped with a flame-dried receiving flask. The solvent was removed from the clear filtrate *in vacuo* (*exclusion of moisture!*), which yielded desired silyl ketene acetal **145b** after drying *in vacuo* as an off-white crystalline solid (2.68 g, 9.15 mmol, 92%; *moisture-sensitive*). ^{1}H NMR (300 MHz, C_6D_6): δ = 7.62−7.48 (m, 2H), 7.05−6.91 (m, 2H), 3.41 (s, 3H), 1.22 (s, 2H), 0.26 (s, 9H) ppm; ^{13}C NMR (75 MHz, C_6D_6): δ = 157.0, 152.2, 130.1, 125.8 (2C), 114.6 (2C), 82.4, 81.1, 55.2, 44.3, 29.0 (2C), 0.9 (3C) ppm.

Silyl Ketene Acetal 145c

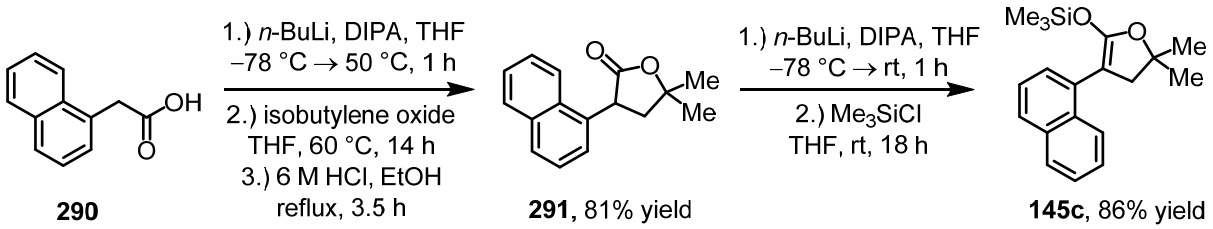

Scheme 93. Synthesis of silyl ketene acetal **145c**.

Compound 291. Compound **291** was synthesized according to a protocol from Fu et al.[89] A flask (250 mL) was charged with dry THF (60 mL) and diisopropylamine (7.01 mL, 50.0 mmol, 3.11 eq). This mixture was cooled to –78 °C and *n*-BuLi (2.5 M in hexanes; 19.3 mL, 48.3 mmol, 3.00 eq) was added. The resulting mixture was stirred at –78 °C for 30 min and then allowed to stir at 0 °C for 10 min. 1-Naphthaleneacetic acid (**290**; 3.00 g, 16.1 mmol, 1.00 eq) in dry THF (12 mL) was added and the mixture stirred at 50 °C for 1 h under nitrogen atmosphere. The mixture was allowed to cool to rt and isobutylene oxide

(1.45 mL, 16.3 mmol, 1.01 eq) was added and the resulting mixture stirred at 60 °C for 14 h under nitrogen atmosphere. After cooling to rt, water (36 mL) was added and the resulting mixture vigorously stirred at 70 °C (reflux) for 2 h. After cooling to rt, the mixture was diluted with Et_2O and water, the aqueous layer separated, washed with Et_2O (3x), and the organic layers disposed. Traces of Et_2O were selectively removed from the aqueous layer *in vacuo*. Then, aqueous 6 M HCl (35 mL) and EtOH (60 mL) were added to the aqueous layer and the mixture stirred at 80 °C (reflux) for 3.5 h. After cooling to rt, the resulting mixture was extracted with $CHCl_3$ (3x) and the organic layer washed with aqueous $NaHCO_3$ and brine and dried over Na_2SO_4. After solvent removal and drying *in vacuo*, desired compound **291** was obtained as a pale yellow crystalline solid without the need for further purification (3.13 g, 13.0 mmol, 81%). ^{1}H NMR (300 MHz, $CDCl_3$): δ = 7.98−7.72 (m, 3H), 7.62−7.38 (m, 4H), 4.71 (dd, J = 10.5 Hz, J = 9.7 Hz, 1H), 2.73 (dd, J = 12.9 Hz, J = 9.5 Hz, 1H), 2.29 (dd, J = 12.9 Hz, J = 10.7 Hz, 1H), 1.58 (s, 3H), 1.56 (s, 3H) ppm; HRMS (ESI): *m/z* calcd for $C_{16}H_{16}O_2Na$ $[M+Na]^+$: 263.1043, found: 263.1041.

Silyl Ketene Acetal 145c. Compound **145c** was synthesized according to a protocol from Fu et al.[89] A flame-dried flask (50 mL) was charged with dry THF (10 mL) and diisopropylamine (1.15 mL, 8.20 mmol, 1.10 eq). This mixture was cooled to –78 °C and *n*-BuLi (2.5 M in hexanes; 3.19 mL, 7.98 mmol, 1.06 eq) was added and the mixture stirred at –78 °C for 1 h. Then, compound **291** (1.80 g, 7.49 mmol, 1.00 eq) was added in dry THF (10 mL) and the mixture stirred at –78 °C for 1 h. Me_3SiCl (1.01 mL, 7.96 mmol, 1.06 eq) was added at −78 °C, the mixture allowed to warm to rt, and the mixture stirred at rt for 18 h under nitrogen atmosphere. Then, the solvent was removed *in vacuo* (*moisture exclusion!*) and the remaining residue taken up in dry pentane. The resulting mixture was passed under nitrogen atmosphere through a flame-dried Schlenk frit (porosity G4) charged with a plug of flame-dried florisil (60–100 mesh) and which was equipped with a flame-dried receiving flask. The solvent was removed from the clear filtrate *in vacuo* (*exclusion of moisture!*), which yielded silyl ketene acetal **145c** after drying *in vacuo* as a pale yellow crystalline solid (2.02 g, 6.48 mmol, 86%; *moisture-sensitive*). ^{1}H NMR (300 MHz, C_6D_6): δ = 8.35 (d, J = 8.5 Hz, 1H), 7.72 (d, J = 7.9 Hz, 1H), 7.58 (d, J = 7.9 Hz, 1H), 7.50−7.25 (m, 4H), 2.83 (s, 2H), 1.34 (s, 3H), 0.06 (s, 9H) ppm; ^{13}C NMR (75 MHz, C_6D_6): δ = 152.9, 135.2, 135.0, 132.8, 129.1, 127.9, 126.7, 126.3, 126.1, 126.0, 125.4, 81.9, 81.6, 47.4, 28.8 (2C), 0.6 (3C) ppm.

Silyl Ketene Acetal 145d

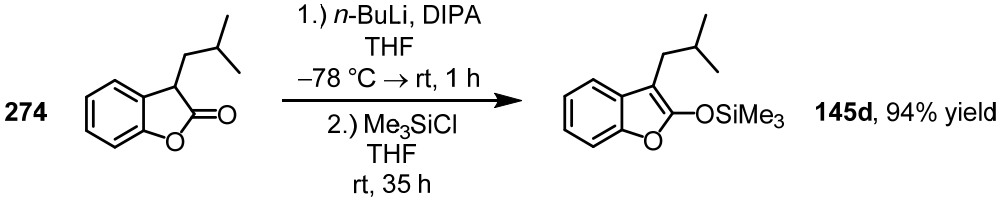

Scheme 94. Synthesis of silyl ketene acetal **145d**.

Silyl Ketene Acetal 145d. Compound **145d** was synthesized according to a modified protocol from Fu et al.[89] A flame-dried flask (50 mL) was charged with dry THF (7.2 mL) and diisopropylamine (850 µL, 6.06 mmol, 1.12 eq). This mixture was cooled to –78 °C and *n*-BuLi (2.5 M in hexanes; 2.35 mL, 5.88 mmol, 1.09 eq) was added and the mixture stirred at –78 °C for 1 h. Then, benzofuranone **274** (1.03 g, 5.41 mmol, 1.00 eq) was added in dry THF (7.2 mL) and the mixture stirred at –78 °C for 1 h. Me_3SiCl (740 µL, 5.83 mmol, 1.08 eq) was added at –78 °C, the mixture allowed to warm to rt, and the mixture stirred at rt for 35 h under nitrogen atmosphere. The solvent was removed *in vacuo* (*exclusion of moisture!*) and the remaining residue taken up in dry pentane. The resulting mixture was passed under nitrogen atmosphere through a flame-dried Schlenk frit (porosity G4) charged with a plug of flame-dried florisil (60–100 mesh) and which was equipped with a flame-dried receiving flask. The solvent was removed from the clear filtrate *in vacuo* (*exclusion of moisture!*), which yielded silyl ketene acetal **145d** after drying *in vacuo* as a colorless oil (1.34 g, 5.11 mmol, 94%; *moisture-sensitive*). ^{1}H NMR (300 MHz, C_6D_6): δ = 7.36–7.28 (m, 1H), 7.25 (d, J = 8.1 Hz, 1H), 7.18–7.08 (m, 1H), 7.02 (t, J = 7.7 Hz, 1H), 2.45 (d, J = 7.2 Hz, 2H), 2.03 (sept, J = 6.8 Hz, 1H), 0.96 (d, J = 6.6 Hz, 6H), 0.23 (s, 9H) ppm; ^{13}C NMR (75 MHz, C_6D_6): δ = 156.6, 149.2, 132.0, 123.2, 122.1, 118.9, 110.6, 92.6, 32.2, 29.2, 23.1 (2C), 0.5 (3C) ppm.

4.9.6 Nitroacrylates (168a–b)

Nitroacrylate 168a

Nitroacrylate **168a** was synthesized according to a protocol from List et al.[153]

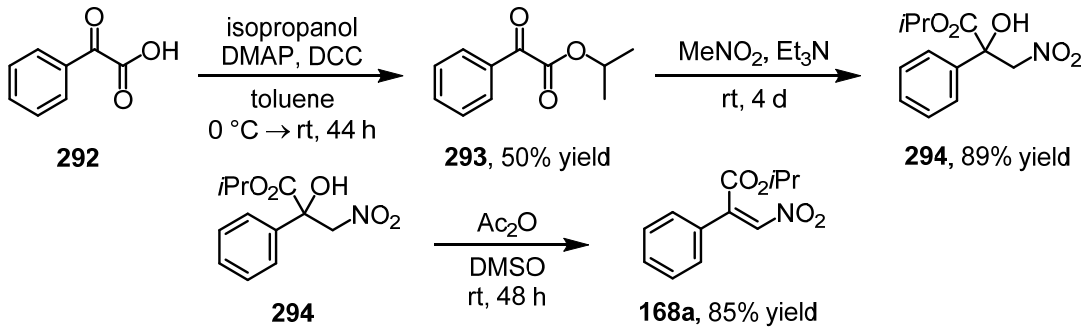

Scheme 95. Synthesis of nitroacrylate **168a**.[153]

Isopropyl 2-oxo-2-phenylacetate (293). A flame-dried flask (100 mL) was charged with dry toluene (48 mL) and phenylglyoxalic acid (**292**; 3.00 g, 20.0 mmol, 1.00 eq). The mixture was cooled to 0 °C and DCC (4.12 g, 20.0 mmol, 1.00 eq) and isopropanol (3.20 mL, 41.8 mmol, 2.09 eq) were added. The mixture was then allowed to warm to rt and stirred at rt for 44 h under nitrogen atmosphere. Subsequently, the resulting mixture was passed through a plug of celite which was subsequently rinsed with toluene. All volatiles were removed from the filtrate *in vacuo*, the crude product dissolved in CH_2Cl_2, adsorbed on silica gel, and purified by flash chromatography (hexanes/EtOAc 20:1). After solvent removal and drying *in vacuo*, product **293** was obtained as a quite volatile, pale-yellow oil (1.92 g, 10.0 mmol, 50%). ^{1}H NMR (300 MHz, $CDCl_3$): δ = 8.05–7.93 (m, 2H), 7.70–7.61 (m, 1H), 7.56–7.46 (m, 2H), 5.32 (sept, J = 6.3 Hz, 1H), 1.41 (d, J = 6.2 Hz, 6H) ppm; HRMS (ESI): *m/z* calcd for $C_{11}H_{12}O_3Na$: 215.0690 $[M+Na]^+$; found: 215.0675.

Compound 294. A flask (100 mL) was charged with compound **293** (1.91 g, 9.94 mmol, 1.00 eq), nitromethane (40 mL), and Et_3N (300 µL, 2.15 mmol, 0.22 eq) and the mixture was stirred at rt in a septum-sealed flask. TLC (hexanes/EtOAc 10:1) indicated incomplete conversion after 2 d and after 4 d almost complete conversion (small trace of **293** still visible on TLC). The reaction was stopped after 4 d and the solvent removed *in vacuo*. The crude product was dissolved in CH_2Cl_2, adsorbed on silica gel, and purified by flash chromatography (hexanes/EtOAc 15:1 → 10:1). After solvent removal and drying *in vacuo*, compound **294** was obtained as a colorless crystalline solid (2.23 g, 8.81 mmol, 89%). ^{1}H NMR (300 MHz, $CDCl_3$): δ = 7.73–7.54 (m, 2H), 7.51–7.32 (m, 3H), 5.35–5.09 (m, 2H), 4.67 (d, J = 14.0 Hz, 1H), 4.23 (s, 1H), 1.35 (d, J = 6.2 Hz, 3H), 1.29 (d, J = 6.4 Hz, 3H) ppm; HRMS (ESI): *m/z* calcd for $C_{12}H_{15}N_1O_5Na$: 276.0842 $[M+Na]^+$; found: 276.0840.

Nitroacrylate 168a. A flame-dried flask (25 mL) was charged with compound **294** (1.41 g, 5.55 mmol, 1.00 eq), dry DMSO (17.5 mL), and acetic anhydride (1.60 mL, 16.9 mmol, 3.05 eq). The mixture was stirred at rt for 48 h under nitrogen atmosphere. Then, the mixture was diluted with water and CH_2Cl_2, the organic layer separated, and the aqueous layer extracted with CH_2Cl_2 (4x). The combined organic layers were washed with aqueous $NaHCO_3$ and dried over Na_2SO_4. The solvent was removed *in vacuo*, the crude product dissolved in CH_2Cl_2, adsorbed on silica gel (42 °C), and purified by flash chromatography (hexanes/EtOAc 30:1 → 25:1). After solvent removal and drying *in vacuo*, desired nitroacrylate **168a** was obtained as a pale yellow crystalline solid (1.11 g, 4.72 mmol, 85%). ^{1}H NMR (300 MHz, $CDCl_3$): δ = 7.59–7.41 (m, 5H), 7.34 (s, 1H), 5.38 (sept, J = 6.3 Hz, 1H), 1.39 (d, J = 6.4 Hz, 6H) ppm; ^{13}C NMR (75 MHz, $CDCl_3$): δ = 164.4, 143.6, 134.4, 132.2, 129.9, 129.7 (2C), 127.6 (2C), 71.0, 21.7 (2C) ppm; IR (film): $\tilde{\nu}$ = 1725, 1622, 1514, 1447,

1360, 1340, 1247, 1207, 1180, 1096, 1018, 907, 850, 825, 767, 748, 687, 678, 669, 586 cm^{-1}; HRMS (ESI): *m/z* calcd for $C_{12}H_{13}N_1O_4Na$: 258.0737 $[M+Na]^+$; found: 258.0734.

Nitroacrylate 168b

Nitroacrylate **168b** was synthesized according to a protocol from List et al.[153]

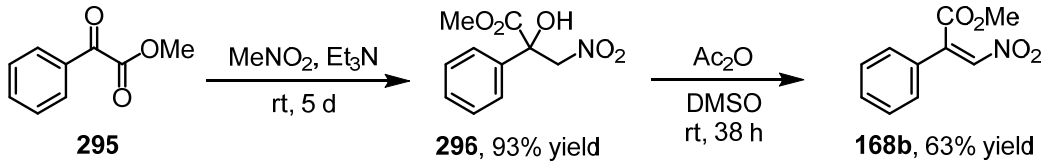

Scheme 96. Synthesis of nitroacrylate **168b**.[153]

Compound 296. A flask (50 mL) was charged with commercial methyl benzoylformate (**295**; 1.45 mL, 10.2 mmol, 1.00 eq), nitromethane (40 mL), and Et_3N (300 µL, 2.15 mmol, 0.22 eq) and the mixture stirred at rt in a septum-sealed flask. TLC (hexanes/EtOAc 10:1) indicated incomplete conversion after 2 d and complete conversion after 5 d. The solvent was removed *in vacuo*, the crude product dissolved in CH_2Cl_2, adsorbed on silica gel, and purified by flash chromatography (hexanes/EtOAc 10:1 → 8:1 → 5:1). After solvent removal and drying *in vacuo*, compound **296** was obtained as a colorless crystalline solid (2.15 g, 9.52 mmol, 93%). ^1H NMR (300 MHz, $CDCl_3$): δ = 7.66–7.53 (m, 2H), 7.47–7.34 (m, 3H), 5.27 (d, J = 14.2 Hz, 1H), 4.69 (d, J = 14.2 Hz, 1H), 3.91 (s, 2H) ppm; HRMS (ESI): *m/z* calcd for $C_{10}H_{11}N_1O_5Na$: 248.0529 $[M+Na]^+$; found: 248.0528.

Nitroacrylate 168b. A flame-dried flask (50 mL) was charged with compound **296** (2.13 g, 9.45 mmol, 1.00 eq), dry DMSO (30 mL), and acetic anhydride (2.70 mL, 28.6 mmol, 3.02 eq). The mixture was stirred at rt for 38 h under nitrogen atmosphere. Then, the mixture was diluted with water and CH_2Cl_2, the organic layer separated, and the aqueous layer extracted with CH_2Cl_2 (4x). The combined organic layers were washed with aqueous $NaHCO_3$ and dried over Na_2SO_4. The solvent was removed *in vacuo*, the crude product dissolved in CH_2Cl_2, adsorbed on silica gel (42 °C), and purified by flash chromatography (hexanes/EtOAc 20:1 → 15:1). After solvent removal and drying *in vacuo*, desired nitroacrylate **168b** was obtained as a yellow crystalline solid (1.22 g, 5.91 mmol, 63%). ^1H NMR (300 MHz, $CDCl_3$): δ = 7.59–7.41 (m, 5H), 7.36 (s, 1H), 4.00 (s, 3H) ppm; ^{13}C NMR (75 MHz, $CDCl_3$): δ = 165.4, 143.3, 134.8, 132.3, 129.7 (2C), 129.6, 127.7 (2C), 53.6 ppm; IR (film): $\tilde{\nu}$ = 1732, 1501, 1333, 1251, 1215, 1178, 965, 842, 770, 678, 663, 584, 464 cm^{-1}; HRMS (ESI): *m/z* calcd for $C_{10}H_9N_1O_4Na$: 230.0424 $[M+Na]^+$; found: 230.0423.

4.10 Asymmetric Reactions with Precatalyst Λ/Δ-T18 and Catalyst Λ/Δ-T18'

4.10.1 Steglich Rearrangements of *O*-Acylated Azlactones (13 → 14)

Absolute configurations of chiral *C*-acylated azlactones **14** were assigned by comparison of measured optical rotation values with literature reported values of products **14a**,[4,22a] **14b**,[22a] **14c**,[22a] and **14d**.[4] All other products **14** were assigned by analogy. Absolute stereochemical assignments from ref. 22a with respect to *C*-acylated azlactones **14** are based on X-ray structural analysis of a ring-opened derivative of *C*-acylated azlactone **14a**.[22a]

4.10.1.1 General Procedures E1)–E3)

General Procedure E1). Steglich rearrangements of *O*-acylated azlactones.

Table 10, entries 1–9: Standard-scale reactions (approx. 90 µmol substrate) with precatalyst **Λ/Δ-T18** and Cs_2CO_3.

An amber glass vial (2 mL)[154] was charged with the indicated amount of the respective *O*-acylated azlactone (**13**; 1.00 eq), Cs_2CO_3 (3 mol%), and a micro stir bar. The vial bottom was precooled for 5 s by immersion cooling at the indicated reaction temperature, which was directly followed by addition of a solution of precatalyst **Λ-T18** or **Δ-T18** (1 mol% or 0.5 mol%) in EtOAc (reactions at 0 °C: conc = 0.5 M; reactions at −30 °C: conc = 0.65 M). The vial was then immediately sealed with a PTFE screw cap[154] and the mixture stirred at the indicated temperature for the indicated time. In all cases, reaction completion was verified by TLC analysis. The solvent was removed *in vacuo*, the resulting residue taken up in a small amount of CH_2Cl_2, and purified by short-column chromatography with the indicated eluent. After drying *in vacuo*, the desired *C*-acylated azlactone (**14**) was obtained.

General Procedure E2). Steglich rearrangements of *O*-acylated azlactones.

Table 10, entries 11, 13, and 14: Standard-scale reactions (approx. 90 µmol substrate) with catalyst **Λ/Δ-T18'** (without Cs_2CO_3).

Same procedure as general procedure E1) except that *no* Cs_2CO_3 is added and that catalyst **Λ/Δ-T18'** is used instead of precatalyst **Λ/Δ-T18**.

General Procedure E3). Steglich rearrangements of *O*-acylated azlactones.

Table 10, entries 10 and 12: Scaled-up reactions reactions (approx. 1 mmol substrate) with catalyst **Λ/Δ-T18'** (without Cs_2CO_3).

Same procedure as general procedure E2) except that a larger threaded round-bottom glas vial (5 mL volume) with a PTFE screw cap was used as reaction vessel.

4.10.1.2 Synthetic Procedures and Characterizations

Benzyl (*R*)-4-benzyl-2-(4-methoxyphenyl)-5-oxo-4,5-dihydrooxazole-4-carboxylate (14a)[4,22a]

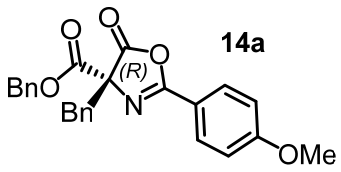

Table 10, entry 1: General procedure E1) was followed: *O*-Acylated azlactone **13a** (36.9 mg, 88.8 µmol); 0.5 mol% precatalyst **Λ-T18**; conc = 0.5 M, t = 0 °C, reaction time: 12 h; eluent: hexanes/MTBE 3:1; *C*-acylated azlactone **14a** was obtained as a viscous oil (35.8 mg, 86.2 µmol, 97%). Enantiomeric excess determined by chiral HPLC analysis: 88% ee (Chiralcel OD-H, 5 µm, 25 cm x 4.6 mm; *n*-hexane/*i*-PrOH 90:10, λ = 254 nm, 1.0 mL/min, t (column) = 25 °C; t_R (major) = 9.7 min, t_R (minor) = 11.6 min). ^{1}H NMR (300 MHz, $CDCl_3$): δ = 7.82 (d, J = 9.1 Hz, 2H), 7.42–7.27 (m, 5H), 7.23–7.08 (m, 5H), 6.91 (d, J = 8.9 Hz, 2H), 5.30 (d, J = 12.4 Hz, 1H), 5.24 (d, J = 12.4 Hz, 1H), 3.84 (s, 3H), 3.64 (d, J = 13.7 Hz, 1H), 3.50 (d, J = 13.7 Hz, 1H) ppm; ^{13}C NMR (75 MHz, $CDCl_3$): δ = 173.9, 165.9, 163.7, 162.9, 135.0, 133.1, 130.5 (2C), 130.3 (2C), 128.8 (2C), 128.6, 128.3 (2C), 128.1 (2C), 127.6, 117.5, 114.3 (2C), 77.7, 68.4, 55.6, 40.3 ppm; IR (film): $\tilde{\nu}$ = 1820, 1748, 1643, 1606, 1509, 1255, 1223, 1172, 1054, 975, 840, 734, 695, 602 cm^{-1}; HRMS (ESI): *m/z* calcd for $C_{25}H_{21}NO_5Na$: 438.1323 [M+Na]$^+$; found: 438.1311.

Table 10, entry 4: General procedure E1) was followed: *O*-Acylated azlactone **13a** (37.0 mg, 89.1 µmol); 0.5 mol% precatalyst **Λ-T18**; conc = 0.65 M, t = −30 °C, reaction time: 72 h; eluent: hexanes/MTBE 3:1; *C*-acylated azlactone **14a** was obtained as a viscous oil (35.3 mg, 85.0 µmol, 95%). Enantiomeric excess determined by chiral HPLC analysis: 93% ee; $[\alpha]_D^{23}$ = +128 (*c* 1.0, $CHCl_3$).

Table 10, entry 11: General procedure E2) was followed: *O*-Acylated azlactone **13a** (36.8 mg, 88.6 µmol); 1 mol% catalyst **Λ-T18'**; conc = 0.65 M, t = −30 °C, reaction time: 72 h; eluent: hexanes/MTBE 3:1; *C*-acylated azlactone **14a** was obtained as a viscous oil (35.8 mg, 86.2 µmol, 97%). Enantiomeric excess determined by chiral HPLC analysis: 93% ee.

Table 10, entry 12: General procedure E3) was followed: *O*-Acylated azlactone **13a** (381 mg, 917 µmol); 1 mol% catalyst **Λ-T18'**; conc = 0.65 M, t = −30 °C, reaction time: 72 h; eluent: hexanes/MTBE 3:1; *C*-acylated azlactone **14a** was obtained as a viscous oil (354 mg, 852 µmol, 93%). Enantiomeric excess determined by chiral HPLC analysis: 93% ee.

Benzyl (*R*)-4-isobutyl-2-(4-methoxyphenyl)-5-oxo-4,5-dihydrooxazole-4-carboxylate (14b)[22a]

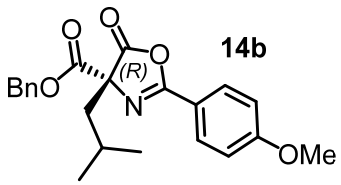

Table 10, entry 2: General procedure E1) was followed: *O*-Acylated azlactone **13b** (33.9 mg, 88.9 µmol); 0.5 mol% precatalyst **Λ-T18**; conc = 0.5 M, t = 0 °C, reaction time: 12 h; eluent: hexanes/MTBE 3:1; *C*-acylated azlactone **14b** was obtained as a viscous oil (30.8 mg, 80.7 µmol, 91%). Enantiomeric excess determined by chiral HPLC analysis: 70% ee (Chiralcel OD-H, 5 µm, 25 cm x 4.6 mm; *n*-hexane/*i*-PrOH 90:10, λ = 254 nm, 1.0 mL/min, t (column) = 25 °C; t_R (major) = 6.6 min, t_R (minor) = 7.8 min). $[\alpha]_D^{23}$ = +8 (*c* 1.0, $CHCl_3$); ^{1}H NMR (300 MHz, $CDCl_3$): δ = 7.98 (d, J = 8.9 Hz, 2H), 7.41–7.22 (m, 5H), 6.99 (d, J = 8.9 Hz, 2H), 5.30–5.14 (m, 2H), 3.88 (s, 3H), 2.39 (dd, J = 14.3 Hz, J = 5.8 Hz, 1H), 2.06 (dd, J = 14.4 Hz, J = 7.2 Hz, 1H), 1.79–1.63 (m, 1H), 0.92 (d, J = 6.6 Hz, 3H), 0.89 (d, J = 6.6 Hz, 3H) ppm; ^{13}C NMR (125 MHz, $CDCl_3$): δ = 175.1, 166.2, 163.8, 162.7, 135.0, 130.4 (2C), 128.7 (2C), 128.6, 128.0 (2C), 117.6, 114.5 (2C), 76.5, 68.2, 55.7, 42.8, 24.7, 24.9, 23.2 ppm; IR (film): $\tilde{\nu}$ = 1821, 1750, 1646, 1608, 1511, 1306, 1259, 1223, 1171, 1030, 971, 697 cm^{-1}; HRMS (APCI): *m/z* calcd for $C_{22}H_{23}NO_5H$: 382.1649 [M+H]$^+$; found: 382.1643.

Benzyl (*R*)-2-(4-methoxyphenyl)-4-methyl-5-oxo-4,5-dihydrooxazole-4-carboxylate (14c)[22a]

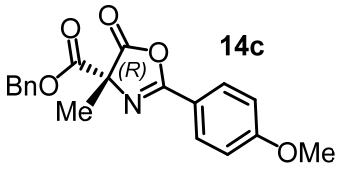

Table 10, entry 3: General procedure E1) was followed: *O*-Acylated azlactone **13c** (30.2 mg, 89.0 µmol); 0.5 mol% of precatalyst **Λ-T18**; conc = 0.5 M, t = 0 °C, reaction time: 12 h; eluent: hexanes/MTBE 3:1; *C*-acylated azlactone **14c** was obtained as a viscous oil (24.3 mg, 71.6 µmol, 80%). Enantiomeric excess determined by chiral HPLC analysis: 45% ee (Chiralcel OD-H, 5 µm, 25 cm x 4.6 mm; *n*-hexanes/*i*-PrOH 90:10, λ = 254 nm, 1.0 mL/min, t (column) = 25 °C; t_R (major) = 8.8 min, t_R (minor) = 12.3 min). $[\alpha]_D^{23}$ = +7 (*c* 0.4, $CHCl_3$); ^{1}H NMR (300 MHz, $CDCl_3$): δ = 7.96 (d, J = 8.9 Hz, 2H), 7.40–7.20 (m, 5H), 6.98 (d, J = 9.1 Hz, 2H), 5.26 (d, J = 12.4 Hz, 1H), 5.19 (d, J = 12.4 Hz, 1H), 3.88 (s, 3H), 1.78 (s, 3H) ppm; ^{13}C NMR (75 MHz, $CDCl_3$): δ = 175.3, 166.2, 163.9, 163.1, 135.0, 130.4 (2C), 128.7 (2C), 128.6, 127.9 (2C), 117.7, 114.5 (2C), 73.0, 68.3, 55.7, 20.7 ppm; IR (film): $\tilde{\nu}$ = 1823, 1751, 1644, 1607, 1510, 1304, 1258, 1163, 1121, 1091, 1020 cm^{-1}; HRMS (ESI): *m/z* calcd for $C_{19}H_{17}N_1O_5Na$: 362.0999 [M+Na]$^+$; found: 362.1003.

Methyl (*R*)-4-benzyl-2-(4-methoxyphenyl)-5-oxo-4,5-dihydrooxazole-4-carboxylate (14d)[4]

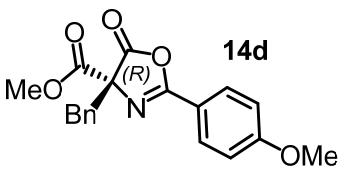

Table 10, entry 5: General procedure E1) was followed: *O*-Acylated azlactone **13d** (30.2 mg, 89.0 µmol); 1 mol% of precatalyst **Λ-T18**; conc = 0.65 M, t = −30 °C, reaction time: 72 h; eluent: hexanes/MTBE 3:1; *C*-acylated azlactone **14d** was obtained as a viscous oil (20.4 mg, 60.1 µmol, 68%). Enantiomeric excess determined by chiral HPLC analysis: 88% ee (Chiralcel OD-H, 5 µm, 25 cm x 4.6 mm; *n*-hexane/*i*-PrOH 90:10, λ = 254 nm, 1.0 mL/min, t (column) = 25 °C; t_R (major) = 8.2 min, t_R (minor) = 9.5 min). $[\alpha]_D^{23}$ = +184 (*c* 0.9, $CHCl_3$); ^{1}H NMR (300 MHz, $CDCl_3$): δ = 7.83 (d, J = 9.1 Hz, 2H), 7.24–7.11 (m, 5H), 6.92 (d, J = 8.9 Hz, 2H), 3.85 (s, 3H), 3.83 (s, 3H), 3.62 (d, J = 13.7 Hz, 1H), 3.49 (d, J = 13.7 Hz, 1H) ppm; ^{13}C NMR (125 MHz, $CDCl_3$): δ = 173.9, 166.5, 163.7, 162.8, 133.0, 130.6 (2C), 130.3 (2C), 128.4 (2C), 127.7, 117.3, 114.4 (2C), 77.5, 55.6, 53.8, 40.4 ppm; IR (film): $\tilde{\nu}$ = 1822, 1751, 1645, 1607, 1511, 1257, 1174, 1057, 981 cm^{-1}; HRMS (APCI): *m/z* calcd for $C_{19}H_{17}NO_5H$: 340.1179 $[M+H]^+$; found: 340.1179.

1,1,1-Trichloro-2-methylpropan-2-yl (*R*)-4-benzyl-2-(4-methoxyphenyl)-5-oxo-4,5-dihydrooxazole-4-carboxylate (14e)[143]

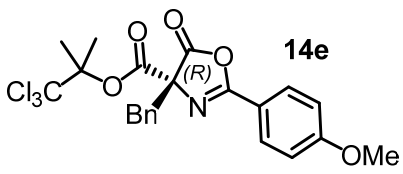

Table 10, entry 6: General procedure E1) was followed: *O*-Acylated azlactone **13e** (43.3 mg, 89.5 µmol); 1 mol% of precatalyst **Λ-T18**; conc = 0.65 M, t = −30 °C, reaction time: 72 h; eluent: hexanes/MTBE 3:1; *C*-acylated azlactone **14e** was obtained as an oil which crystallized on standing (43.2 mg, 89.3 µmol, >99%). Enantiomeric excess determined by chiral HPLC analysis: 90% ee (Chiralcel OD-H, 5 µm, 25 cm x 4.6 mm; *n*-hexane/*i*-PrOH 99.6:0.4, λ = 254 nm, 0.8 mL/min, t (column) = 25 °C; t_R (major) = 33.9 min, t_R (minor) = 38.7 min). $[\alpha]_D^{23}$ = +147 (*c* 1.0, $CHCl_3$); ^{1}H NMR (300 MHz, $CDCl_3$): δ = 7.80 (d, J = 8.9 Hz, 2H), 7.24–7.10 (m, 5H), 6.90 (d, J = 9.1 Hz, 2H), 3.84 (s, 3H), 3.60 (d, J = 13.8 Hz, 1H), 3.49 (d, J = 13.8 Hz, 1H), 1.95 (s, 3H), 1.92 (s, 3H) ppm; ^{13}C NMR (75 MHz, $CDCl_3$): δ = 173.8, 163.7, 163.6, 163.5, 133.2, 130.5 (2C), 130.2 (2C), 128.4 (2C), 127.6, 117.5, 114.3 (2C), 105.3, 91.1, 78.3, 55.6, 39.2, 21.3 (2C) ppm; IR (film): $\tilde{\nu}$ = 1821, 1757, 1645, 1607, 1511, 1256, 1151, 979, 796 cm^{-1}; HRMS (ESI): *m/z* calcd for $C_{22}H_{20}Cl_3N_1O_5Na$: 506.0299 $[M+Na]^+$; found: 506.0294.

Benzyl (*R*)-4-benzyl-2-(4-(*tert*-butyl)phenyl)-5-oxo-4,5-dihydrooxazole-4-carboxylate (14f)

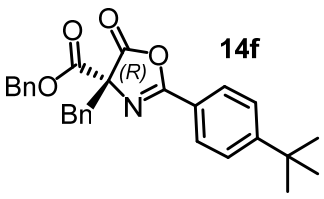

Table 10, entry 7: General procedure E1) was followed: *O*-Acylated azlactone **13f** (39.2 mg, 88.8 µmol); 1 mol% of precatalyst **Λ-T18**; conc = 0.65 M, $t = -30$ °C, reaction time: 72 h; eluent: hexanes/MTBE 3:1; *C*-acylated azlactone **14f** was obtained as a viscous oil (34.9 mg, 79.1 µmol, 89%). Enantiomeric excess determined by chiral HPLC analysis: 91% ee (Chiralcel OD-H, 5 µm, 25 cm x 4.6 mm; *n*-hexane/*i*-PrOH 90:10, λ = 254 nm, 1.0 mL/min, *t* (column) = 25 °C; t_R (major) = 5.8 min, t_R (minor) = 6.9 min). $[\alpha]_D^{23}$ = +131 (*c* 1.0, $CHCl_3$); ^{1}H NMR (300 MHz, $CDCl_3$): δ = 7.81 (d, *J* = 8.5 Hz, 2H), 7.45 (d, *J* = 8.5 Hz, 2H), 7.40–7.27 (m, 5H), 7.25–7.12 (m, 5H), 5.30 (d, *J* = 12.4 Hz, 1H), 5.23 (d, *J* = 12.4 Hz, 1H), 3.66 (d, *J* = 13.8 Hz, 1H), 3.52 (d, *J* = 13.8 Hz, 1H), 1.33 (s, 9H) ppm; ^{13}C NMR (125 MHz, $CDCl_3$): δ = 173.8, 165.7, 163.3, 157.2, 134.9, 133.0, 130.5 (2C), 128.8 (2C), 128.6, 128.4 (2C), 128.2 (2C), 128.1 (2C), 127.7, 125.9 (2C), 122.3, 77.7, 68.4, 40.2, 35.3, 31.2 (3C) ppm; IR (film): $\tilde{\nu}$ = 1823, 1751, 1646, 1225, 1093, 1055, 978, 698 cm^{-1}; HRMS (ESI): *m/z* calcd for $C_{28}H_{27}N_1O_4Na$: 464.1832 $[M+Na]^+$; found: 464.1830.

Benzyl (*R*)-4-benzyl-2-(naphthalen-1-yl)-5-oxo-4,5-dihydrooxazole-4-carboxylate (14g)

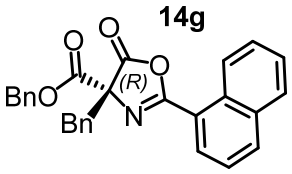

Table 10, entry 8: General procedure E1) was followed: *O*-Acylated azlactone **13g** (38.8 mg, 89.1 µmol); 1 mol% of precatalyst **Λ-T18**; conc = 0.65 M, $t = -30$ °C, reaction time: 72 h; eluent: hexanes/MTBE 3:1; *C*-acylated azlactone **14g** was obtained as a viscous oil (34.1 mg, 78.3 µmol, 88%). Enantiomeric excess determined by chiral HPLC analysis: 91% ee (Chiralpak AD-H, 5 µm, 25 cm x 4.6 mm; *n*-hexane/*i*-PrOH 98:2, λ = 254 nm, 1.0 mL/min, *t* (column) = 25 °C; t_R (minor) = 14.8 min, t_R (major) = 16.5 min). $[\alpha]_D^{23}$ = +120 (*c* 1.0, $CHCl_3$); ^{1}H NMR (300 MHz, $CDCl_3$): δ = 8.90–8.79 (m, 1H), 8.00 (d, *J* = 8.3 Hz, 1H), 7.93–7.84 (m, 1H), 7.81 (dd, *J* = 7.3 Hz, *J* = 1.2 Hz, 1H), 7.63–7.51 (m, 2H), 7.43 (dd, *J* = 8.2 Hz, *J* = 7.5 Hz, 1H), 7.39–7.29 (m, 5H), 7.29–7.11 (m, 5H), 5.37–5.25 (m, 2H), 3.74 (d, *J* = 13.6 Hz, 1H), 3.62 (d, *J* = 13.8 Hz, 1H) ppm; ^{13}C NMR (75 MHz, $CDCl_3$): δ = 173.6, 165.6, 163.4, 134.9, 133.9 (2C), 133.8, 133.1, 130.8, 130.6 (2C), 130.2, 128.8 (2C), 128.7, 128.5 (2C), 128.2, 128.1 (2C), 127.8, 126.7, 126.0, 124.7, 121.6, 78.4, 68.5, 40.1 ppm; IR (film): $\tilde{\nu}$ = 1819, 1749, 1641, 1250, 1225, 1095, 955, 776, 698 cm^{-1}; HRMS (ESI): *m/z* calcd for $C_{28}H_{21}N_1O_4H$: 436.1543 $[M+H]^+$; found: 436.1546.

Benzyl (*R*)-4-benzyl-2-(naphthalen-2-yl)-5-oxo-4,5-dihydrooxazole-4-carboxylate (14h)

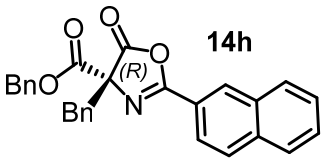

Table 10, entry 9: General procedure E1) was followed: *O*-Acylated azlactone **13h** (38.8 mg, 89.1 µmol); 1 mol% of precatalyst **Λ-T18**; conc = 0.65 M, t = −30 °C, reaction time: 72 h; eluent: hexanes/MTBE 3:1; *C*-acylated azlactone **14h** was obtained as an oil which crystallized on standing (35.0 mg, 80.4 µmol, 90%). Enantiomeric excess determined by chiral HPLC analysis: 95% ee (Chiralcel OD-H, 5 µm, 25 cm x 4.6 mm; *n*-hexane/*i*-PrOH 90:10, λ = 254 nm, 1.0 mL/min, t (column) = 25 °C; t_R (major) = 8.7 min, t_R (minor) = 10.7 min). $[\alpha]_D^{23}$ = +167 (*c* 1.0, $CHCl_3$); ^{1}H NMR (300 MHz, $CDCl_3$): δ = 8.33 (d, J = 0.9 Hz, 1H), 7.99 (dd, J = 8.7 Hz, J = 1.7 Hz, 1H), 7.93–7.82 (m, 3H), 7.65–7.49 (m, 2H), 7.40–7.28 (m, 5H), 7.26–7.20 (m, 2H), 7.20–7.09 (m, 3H), 5.33 (d, J = 12.5 Hz, 1H), 5.27 (d, J = 12.5 Hz, 1H), 3.71 (d, J = 13.6 Hz, 1H), 3.57 (d, J = 13.6 Hz, 1H) ppm; ^{13}C NMR (75 MHz, $CDCl_3$): δ = 173.7, 165.7, 163.4, 135.7, 134.9, 132.9, 132.6, 130.5 (2C), 129.9, 129.3, 128.9, 128.8 (2C), 128.7, 128.7, 128.4 (2C), 128.1 (2C), 128.0, 127.7, 127.2, 123.6, 122.3, 77.9, 68.5, 40.4 ppm; IR (film): $\tilde{\nu}$ = 1822, 1750, 1645, 1227, 1054, 988, 944, 902, 752, 699 cm^{-1}; HRMS (EI): *m/z* calcd for $C_{28}H_{21}NO_4$: 435.1471 $[M]^+$; found: 435.1462.

Table 10, entry 10: General procedure E3) was followed: *O*-Acylated azlactone **13h** (400 mg, 919 µmol); 1 mol% catalyst **Λ-T18'**; conc = 0.65 M, t = −30 °C, reaction time: 72 h; eluent: hexanes/MTBE 3:1; *C*-acylated azlactone **14a** was obtained as a viscous oil which crystallized on standing (375 mg, 861 µmol, 94%). Enantiomeric excess determined by chiral HPLC analysis: 94% ee.

Benzyl (*S*)-4-benzyl-2-(*tert*-butyl)-5-oxo-4,5-dihydrooxazole-4-carboxylate (*ent*-14i)

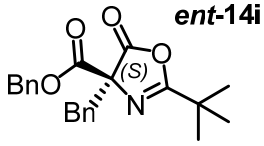

Table 10, entry 13: General procedure E2) was followed: *O*-Acylated azlactone **13i** (32.5 mg, 88.9 µmol); 1 mol% of catalyst **Δ-T18'**; conc = 0.65 M, t = −30 °C, reaction time: 72 h; eluent: hexanes/MTBE 3:1; *C*-acylated azlactone ***ent*-14i** was obtained as a viscous oil (29.5 mg, 80.7 µmol, 91%). Enantiomeric excess determined by chiral HPLC analysis: 96% ee (Chiralcel OD-H, 5 µm, 25 cm x 4.6 mm; *n*-hexane/*i*-PrOH 99:1, λ = 254 nm, 1.0 mL/min, t (column) = 10 °C; t_R (major) = 10.4 min, t_R (minor) = 11.8 min). $[\alpha]_D^{23}$ = −14 (*c* 1.0, $CHCl_3$); ^{1}H NMR (300 MHz, $CDCl_3$): δ = 7.42–7.28 (m, 5H), 7.28–7.18 (m, 3H), 7.18–7.08 (m, 2H), 5.30 (d, J = 12.5 Hz, 1H), 5.20 (d, J = 12.5 Hz, 1H), 3.53 (d, J = 13.8 Hz, 1H), 3.45 (d, J = 13.6 Hz, 1H), 0.99 (s, 9H) ppm; ^{13}C NMR (75 MHz, $CDCl_3$): δ = 174.7, 173.6, 165.6, 134.9, 133.0, 130.7 (2C), 128.8 (2C), 128.7, 128.3 (2C), 128.0 (2C), 127.7, 77.0, 68.3, 39.5, 34.1, 26.4 (3C) ppm; IR (film): $\tilde{\nu}$ = 1822, 1753, 1663, 1228, 1093, 1064, 993, 903,

736, 699 cm^{-1}; HRMS (APCI): *m/z* calcd for $C_{22}H_{23}N_1O_4H$: 366.1700 $[M+H]^+$; found: 366.1703.

Table 10, entry 14: General procedure E2) was followed: *O*-Acylated azlactone **13i** (32.5 mg, 88.9 µmol); 1 mol% catalyst **Δ-T18'** (*catalyst was left for 7 d in CD_2Cl_2 in an NMR tube at 25 °C before usage*), conc = 0.65 M, *t* = −30 °C, reaction time: 72 h; eluent: hexanes/MTBE 3:1; *C*-acylated azlactone ***ent*-14i** was obtained as a viscous oil (29.4 mg, 80.5 µmol, 90%). Enantiomeric excess determined by chiral HPLC analysis: 96% ee; $[\alpha]_D^{23} = -14$ (*c* 1.0, $CHCl_3$).

4.10.2 Black Rearrangements of *O*-Acylated Benzofuranones (142 → 143)

Absolute configurations of chiral *C*-acylated benzofuranones **143** were established by 1.) comparison of the measured optical rotation of product **143e** with the according literature reported value[22b] and 2.) by X-ray diffraction analysis of a crystal obtained from **143i** (grown from the batch from Table 13, entry 13 with 93% ee; see crystallographic section for further details). All other products **143** were assigned by analogy. Absolute stereochemical assignments from ref. 22b with respect to *C*-acylated benzofuranones **143** are based on X-ray structural analysis of the closely related *C*-acylated benzofuranone with R^1 = Ph and $R^2 = CMe_2CCl_3$ (**143e**: R^1 = Bn and $R^2 = CMe_2CCl_3$).[22b]

4.10.2.1 General Procedure F1)

Black rearrangements of *O*-acylated benzofuranones; Table 13.

An amber glass vial (2 mL)[154] was charged with the indicated amount of the respective *O*-acylated benzofuranone (**142**; 1.00 eq) and a micro stir bar. The vial bottom was precooled for 5 s by immersion cooling at the indicated reaction temperature, which was directly followed by addition of a solution of catalyst **Λ-Ir5'** or **Δ-Ir5'** (1 mol% or 2 mol%) in TAA or 2:1 TAA/CPME (reactions at 0 °C: TAA, conc = 0.3 M; reactions at −15 °C and −30 °C: 2:1 TAA/CPME, conc = 0.2 M). The vial was then immediately sealed with a PTFE screw cap[154] and the mixture stirred at the indicated temperature for the indicated time. Reaction completion was verified by TLC analysis. The solvent was removed *in vacuo* and the resulting residue taken up in a small amount of CH_2Cl_2 and purified by short-column chromatography with CH_2Cl_2 as eluent. After drying *in vacuo*, the desired *C*-acylated benzofuranone (**143**) was obtained.

4.10.2.2 Synthetic Procedures and Characterizations

Phenyl (*R*)-2-oxo-3-phenyl-2,3-dihydrobenzofuran-3-carboxylate (143a)[86b]

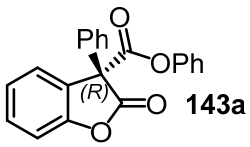

Table 13, entry 1: General procedure F1) was followed: *O*-Acylated benzofuranone **142a** (23.6 mg, 71.4 µmol); 1 mol% of catalyst **Λ-T18'**; solvent: TAA; conc = 0.3 M, t = 0 °C, reaction time: 18 h; TLC indicated sluggish conversion to **143a** (~50%) and the experiment was stopped, the experiment was not repeated, optimized, or worked up due to the low ee found for the crude product. Enantiomeric excess determined by chiral HPLC analysis: 30% ee (determined from crude mixture) (Chiralcel OJ-H, 5 µm, 25 cm x 4.6 mm; *n*-hexane/*i*-PrOH 90:10, λ = 254 nm, 0.7 mL/min, t (column) = 40 °C; t_R (major) = 36.9 min, t_R (minor) = 39.8 min); ^{1}H NMR (300 MHz, $CDCl_3$): δ = 7.60–6.89 (m, 14H) ppm; ^{13}C NMR (75 MHz, $CDCl_3$): δ = 171.2, 166.2, 154.0, 150.5, 134.3, 131.0, 129.6 (2C), 129.2 (2C), 128.4, 127.8 (2C), 126.3, 126.5, 125.3, 125.0, 121.0 (2C), 111.7, 62.8 ppm; IR (film): $\tilde{\nu}$ = 1812, 1758, 1486, 1467, 1181, 1126, 1060, 992, 955, 907, 875, 738, 685, 493 cm^{-1}; HRMS (ESI): *m/z* calcd for $C_{21}H_{14}O_4NH_4$: 348.1230 $[M+NH_4]^+$; found: 348.1230. Analytical data obtained from isolated racemic sample, identity with catalysis crude product verified by ^{1}H- and ^{13}C NMR spectra superposition.

Phenyl (*R*)-3-methyl-2-oxo-2,3-dihydrobenzofuran-3-carboxylate (143b)[23b]

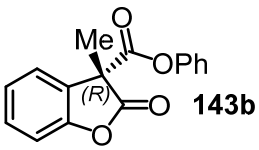

Table 13, entry 2: General procedure F1) was followed: *O*-Acylated benzofuranone **142b** (23.5 mg, 87.6 µmol); 1 mol% of catalyst **Λ-T18'**; solvent: TAA; conc = 0.3 M, t = 0 °C, reaction time: 10 h; *C*-acylated benzofuranone **143b** was obtained as a viscous oil (23.3 mg, 86.9 µmol, 99%). Enantiomeric excess determined by chiral HPLC analysis: 91% ee (Chiralcel OD-H, 5 µm, 25 cm x 4.6 mm; *n*-hexane/*i*-PrOH 97.5:2.5, λ = 254 nm, 1.0 mL/min, t (column) = 25 °C; t_R (minor) = 9.1 min, t_R (major) = 11.1 min); ^{1}H NMR (300 MHz, $CDCl_3$): δ = 7.39–7.29 (m, 2H), 7.29–7.20 (m, 2H), 7.20–7.09 (m, 3H), 6.94–6.85 (m, 2H), 1.81 (s, 3H) ppm; ^{13}C NMR (75 MHz, $CDCl_3$): δ = 173.8, 167.0, 153.5, 150.4, 130.4, 129.6 (2C), 128.4, 126.6, 125.0, 123.5, 121.1 (2C), 111.5, 54.1, 20.3 ppm; IR (film): $\tilde{\nu}$ = 2922, 1811, 1187, 1155, 1095, 1034, 746, 683 cm^{-1}; HRMS (ESI): *m/z* calcd for $C_{16}H_{12}O_4Na$: 291.0628 $[M+Na]^+$; found: 291.0635.

Table 13, entry 6: General procedure F1) was followed: *O*-Acylated benzofuranone **142b** (19.3 mg, 71.9 µmol); 1 mol% of catalyst **Λ-T18'**; solvent: 2:1 TAA/CPME; conc = 0.2 M, t = −15 °C, reaction time: 48 h; *C*-acylated benzofuranone **143b** was obtained as a viscous oil (18.9 mg, 70.4 µmol, 98%). Enantiomeric excess determined by chiral HPLC analysis: 92% ee.

Table 13, entry 9: General procedure F1) was followed: *O*-Acylated benzofuranone **142b** (19.5 mg, 72.7 µmol); 1 mol% of catalyst **Λ-T18'**; solvent: 2:1 TAA/CPME; conc = 0.2 M, *t* = −30 °C, reaction time: 48 h; *C*-acylated benzofuranone **143b** was obtained as a viscous oil (19.4 mg, 72.3 µmol, 99%). Enantiomeric excess determined by chiral HPLC analysis: 94% ee; $[\alpha]_D^{23}$ = +96 (*c* 1.0, $CHCl_3$).

Table 13, entry 14: A flask (25 mL) was charged with *O*-acylated benzofuranone **142b** (830 mg, 3.09 mmol) and 2:1 TAA/CPME (10.0 mL; final concentration: conc = 0.2 M). The flask was sealed with a septum, the mixture stirred until all of **142b** was dissolved, and the mixture cooled to −30 °C. Under stirring, catalyst **Λ-T18'** (45.2 mg, 32.4 µmol, 1.0 mol%) was added in 2:1 TAA/CPME (4.5 mL) at −30 °C via syringe. The mixture was stirred at −30 °C for 48 h under exclusion of light, after which TLC analysis indicated full conversion. All volatiles were removed *in vacuo* (40 °C), the residue dissolved in a small amount of the eluent CH_2Cl_2, and product **143b** isolated via short-column chromatography (CH_2Cl_2). After drying *in vacuo*, product **143b** was obtained as a colorless viscous oil which slowly crystallized on standing (822 mg, 3.06 mmol, 99%). Enantiomeric excess determined by chiral HPLC analysis: 92% ee; $[\alpha]_D^{23}$ = +92 (*c* 1.0, $CHCl_3$).

Reisolation of catalyst **Λ-T18'**.

Under the conditions mentioned above, the catalyst does not elute from the silica gel column and remains at the baseline. After complete elution of product **143b**, the yellow catalyst band was eluted by switching over from CH_2Cl_2 to 100:1:1 CH_2Cl_2/MeOH/Et_3N and the catalyst band was collected. All volatiles were removed *in vacuo* (40 °C), the remaining yellow residue dissolved in CH_2Cl_2 and washed with H_2O (2x), and the organic layer dried over Na_2SO_4. The CH_2Cl_2 layer was concentrated *in vacuo* (40 °C) and passed through a plug of piperidinomethylated polystyrene beads[83] (see synthesis of **Λ-** and **Δ-T18'** in chapter 4.7.2.18 for details; identical plug dimensions). After drying *in vacuo*, catalyst **Λ-T18'** was recovered in 94% yield (42.4 mg, 30.4 µmol) and indistinguishable from freshly prepared **Λ-T18'** according to ^{1}H NMR analysis and an enantiomeric excess of >99% was found (spectra comparison shown in chaper 4.13.2, chiral HPLC trace shown in chaper 5.2).

Recrystallization of product **143b** from methanol.

583 mg of product **143b** from Table 13, entry 14 with 92% ee were dissolved in MeOH (1.3 mL) at reflux. Upon cooling to rt, the product started to crystallize from the resulting solution. The mixture was then kept at −15 °C for 30 min and the supernatant carefully removed at −15 °C from crystallized **143b** with a syringe. The remaining crystalline preci-

pitate was washed with cold MeOH at −15 °C (2x 0.4 mL). Remaining crystalline **143b** was then fully dissolved in CH_2Cl_2 and an enantiomeric excess of 98% found via chiral HPLC analysis. After drying *in vacuo*, 430 mg of **143b** were obtained as a viscous oil which slowly crystallized on standing (combined yield for isolation and recrystallization: 73%).

Table 13, entry 15: General procedure F1) was followed: *O*-Acylated benzofuranone **142b** (22.3 mg, 83.1 µmol); 1 mol% of reisolated catalyst **Λ-T18'** (see procedure above belonging to *Table 13, entry 14*); solvent: 2:1 TAA/CPME; conc = 0.2 M, t = −30 °C, reaction time: 48 h; *C*-acylated benzofuranone **143b** was obtained as a viscous oil (22.0 mg, 82.0 µmol, 99%). Enantiomeric excess determined by chiral HPLC analysis: 93% ee; $[\alpha]_D^{23}$ = +95 (*c* 1.0, $CHCl_3$).

Phenyl (*S*)-3-methyl-2-oxo-2,3-dihydrobenzofuran-3-carboxylate (*ent*-143b)

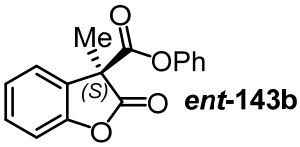

***ent*-143b**

Table 13, entry 10: General procedure F1) was followed: *O*-Acylated benzofuranone **142b** (21.2 mg, 79.0 µmol); 1 mol% of catalyst **Δ-T18'**; solvent: 2:1 TAA/CPME; conc = 0.2 M, t = −30 °C, reaction time: 48 h; *C*-acylated benzofuranone ***ent*-143b** was obtained as a viscous oil (21.0 mg, 78.3 µmol, 99%). Enantiomeric excess determined by chiral HPLC analysis: 94% ee; $[\alpha]_D^{23}$ = −97 (*c* 1.0, $CHCl_3$). See product **143b** above for further analytical data.

Benzyl (*R*)-3-methyl-2-oxo-2,3-dihydrobenzofuran-3-carboxylate (143c)[86b]

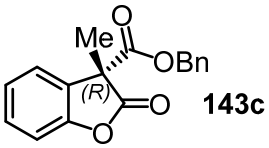

143c

Table 13, entry 3: General procedure F1) was followed: *O*-Acylated benzofuranone **142c** (20.1 mg, 71.2 µmol); 1 mol% of catalyst **Λ-T18'**; solvent: TAA; conc = 0.3 M, t = 0 °C, reaction time: 18 h; *C*-acylated benzofuranone **143c** was obtained as a viscous oil (19.8 mg, 70.1 µmol, 99%). Enantiomeric excess determined by chiral HPLC analysis: 80% ee (Chiralcel OJ-H, 5 µm, 25 cm x 4.6 mm; *n*-hexane/*i*-PrOH 85:15, λ = 254 nm, 1.0 mL/min, t (column) = 25 °C; t_R (major) = 18.3 min, t_R (minor) = 24.4 min); $[\alpha]_D^{23}$ = +55 (*c* 0.8, $CHCl_3$); ^{1}H NMR (300 MHz, $CDCl_3$): δ = 7.40–7.32 (m, 1H), 7.32–7.20 (m, 4H), 7.20–7.08 (m, 4H), 5.20–5.09 (m, 2H), 1.79 (s, 3H) ppm; ^{13}C NMR (75 MHz, $CDCl_3$): δ = 174.1, 168.1, 153.4, 135.0, 130.1, 128.7 (2C), 128.6, 128.5, 127.6 (2C), 124.7, 123.6, 111.3, 68.0, 54.0, 20.7 ppm; IR (film): $\tilde{\nu}$ = 1809, 1742, 1220, 1110, 1034, 892, 747, 696 cm^{-1}; HRMS (ESI): *m/z* calcd for $C_{17}H_{14}O_4Na$: 305.0784 [*M*+Na]$^+$; found: 305.0785.

Isopropyl (*R*)-3-methyl-2-oxo-2,3-dihydrobenzofuran-3-carboxylate (143d)

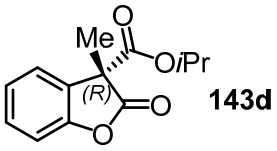

143d

Table 13, entry 4: General procedure F1) was followed: *O*-Acylated benzofuranone **142d** (19.6 mg, 83.7 µmol); 2 mol% of catalyst **Λ-T18'**; solvent: TAA; conc = 0.3 M, t = 0 °C, reaction time: 48 h; *C*-acylated benzofuranone **143d** was obtained as a viscous oil (19.3 mg, 82.4 µmol, 98%). Enantiomeric excess determined by chiral HPLC analysis: 82% ee (Chiralpak AD-H, 5 µm, 25 cm x 4.6 mm; *n*-hexane/*i*-PrOH 99.2:0.8, λ = 254 nm, 1.0 mL/min, t (column) = 25 °C; t_R (major) = 6.3 min, t_R (minor) = 6.6 min); $[\alpha]_D^{23}$ = +84 (*c* 0.8, $CHCl_3$); ^{1}H NMR (300 MHz, $CDCl_3$): δ = 7.35 (ddd, J = 7.7 Hz, J = 7.7 Hz, J = 1.4 Hz, 1H), 7.30–7.24 (m, 1H), 7.20–7.11 (m, 2H), 5.00 (sept, J = 6.3 Hz, 1H), 1.75 (s, 3H), 1.22 (d, J = 6.4 Hz, 3H), 1.08 (d, J = 6.2 Hz, 3H) ppm; ^{13}C NMR (75 MHz, $CDCl_3$): δ = 174.4, 167.8, 153.4, 129.9, 128.9, 124.7, 123.4, 111.2, 70.6, 54.2, 21.5, 21.4, 20.6 ppm; IR (film): $\tilde{\nu}$ = 1811, 1737, 1458, 1232, 1099, 1073, 1033, 894, 754 cm^{-1}; HRMS (ESI): *m/z* calcd for $C_{13}H_{14}O_4Na$: 257.0784 [M+Na]$^+$; found: 257.0784.

1,1,1-Trichloro-2-methylpropan-2-yl (*S*)-3-benzyl-2-oxo-2,3-dihydrobenzofuran-3-carboxylate (143e)[22b]

Note: Switching from R → S <u>not</u> caused by actual inversion of the stereocenter but by higher priority of the exocyclic acyl fragment according to CIP rules.[88]

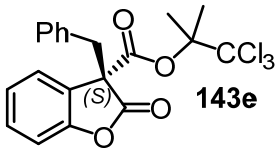

143e

Table 13, entry 5: General procedure F1) was followed: *O*-Acylated benzofuranone **142e** (38.8 mg, 90.7 µmol); 1 mol% of catalyst **Λ-T18'**; solvent: TAA; conc = 0.3 M, t = 0 °C, reaction time: 20 h; *C*-acylated benzofuranone **143e** was obtained as a colorless solid (38.2 mg, 89.3 µmol, 98%). Enantiomeric excess determined by chiral HPLC analysis: 89% ee (Chiralcel OD-H, 5 µm, 25 cm x 4.6 mm; *n*-hexane/*i*-PrOH 98:2, λ = 254 nm, 1.0 mL/min, t (column) = 25 °C; t_R (minor) = 6.6 min, t_R (major) = 7.6 min); $[\alpha]_D^{23}$ = +99 (*c* 0.9, CH_2Cl_2); ^{1}H NMR (300 MHz, $CDCl_3$): δ = 7.38 (dd, J = 7.5 Hz, J = 1.2 Hz, 1H), 7.31–7.22 (m, 1H), 7.18 (dd, J = 7.5 Hz, J = 1.0 Hz, 1H), 7.15–7.04 (m, 3H), 6.97–6.87 (m, 3H), 3.60 (s, 2H), 1.92 (s, 3H), 1.83 (s, 3H) ppm; ^{13}C NMR (75 MHz, $CDCl_3$): δ = 172.3, 165.4, 153.9, 133.6, 130.3, 130.2 (2C), 128.4 (2C), 127.5, 125.9, 124.4, 124.2, 111.1, 105.3, 90.9, 61.3, 39.6, 21.5, 21.2 ppm; IR (film): $\tilde{\nu}$ = 1796, 1749, 1459, 1232, 1206, 1148, 1070, 1022, 885, 794, 761, 732, 702, 585, 518 cm^{-1}; HRMS (ESI): *m/z* calcd for $C_{20}H_{17}Cl_3O_4Na$: 449.0085 [M+Na]$^+$; found: 449.0084.

Phenyl (*R*)-3-isobutyl-2-oxo-2,3-dihydrobenzofuran-3-carboxylate (143f)[23b]

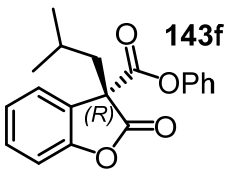

Table 13, entry 7: General procedure F1) was followed: *O*-Acylated benzofuranone **142f** (22.1 mg, 71.2 µmol); 1 mol% of catalyst **Λ-T18'**; solvent: 2:1 TAA/CPME; conc = 0.2 M, *t* = −15 °C, reaction time: 48 h; *C*-acylated benzofuranone **143f** was obtained as a viscous oil (21.9 mg, 70.6 µmol, 99%). Enantiomeric excess determined by chiral HPLC analysis: 90% ee (Chiralcel OJ-H, 5 µm, 25 cm x 4.6 mm; *n*-hexane/*i*-PrOH 90:10, λ = 254 nm, 1.0 mL/min, *t* (column) = 25 °C; t_R (major) = 12.2 min, t_R (minor) = 16.6 min); $[\alpha]_D^{23}$ = +83 (*c* 1.0, $CHCl_3$); ^{1}H NMR (300 MHz, $CDCl_3$): *δ* = 7.47–7.28 (m, 4H), 7.28–7.16 (m, 3H), 7.01–6.90 (m, 2H), 2.45 (dd, *J* = 14.4 Hz, *J* = 5.9 Hz, 1H), 2.36 (dd, *J* = 14.4 Hz, *J* = 7.7 Hz, 1H), 1.66–1.49 (m, 1H), 0.86 (d, *J* = 6.6 Hz, 3H), 0.78 (d, *J* = 6.8 Hz, 3H) ppm; ^{13}C NMR (75 MHz, $CDCl_3$): *δ* = 173.5, 166.9, 153.8, 150.4, 130.3, 129.6 (2C), 126.6, 126.5, 124.8, 124.3, 121.1 (2C), 111.4, 58.4, 42.5, 25.1, 23.9, 22.8 ppm; IR (film): $\tilde{\nu}$ = 1810, 1759, 1184, 1117, 1051, 986, 747, 683 cm^{-1}; HRMS (ESI): *m/z* calcd for $C_{19}H_{18}O_4Na$: 333.1097 [*M*+Na]$^+$; found: 333.1099.

Phenyl (*R*)-3-benzyl-2-oxo-2,3-dihydrobenzofuran-3-carboxylate (143g)[23b]

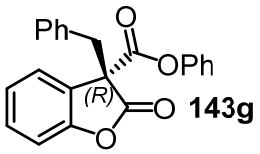

Table 13, entry 8: General procedure F1) was followed: *O*-Acylated benzofuranone **142g** (24.6 mg, 71.4 µmol); 1 mol% of catalyst **Λ-T18'**; solvent: 2:1 TAA/CPME; conc = 0.2 M, *t* = −15 °C, reaction time: 48 h; *C*-acylated benzofuranone **143g** was obtained as a viscous oil (24.4 mg, 70.9 µmol, 99%). Enantiomeric excess determined by chiral HPLC analysis: 91% ee (Chiralcel OJ-H, 5 µm, 25 cm x 4.6 mm; *n*-hexane/*i*-PrOH 90:10, λ = 254 nm, 1.0 mL/min, *t* (column) = 25 °C; t_R (minor) = 35.0 min, t_R (major) = 42.7 min); $[\alpha]_D^{23}$ = +116 (*c* 1.0, $CHCl_3$); ^{1}H NMR (300 MHz, $CDCl_3$): *δ* = 7.41 (dd, *J* = 7.4 Hz, *J* = 1.1 Hz, 1H), 7.37–7.24 (m, 3H), 7.24–7.17 (m, 2H), 7.15–7.03 (m, 3H), 7.02–6.86 (m, 5H), 3.67 (s, 2H) ppm; ^{13}C NMR (75 MHz, $CDCl_3$): *δ* = 172.5, 166.5, 153.8, 150.4, 133.4, 130.5, 130.2 (2C), 129.7 (2C), 128.4 (2C), 127.6, 126.6, 125.8, 124.6, 124.4, 121.2 (2C), 111.3, 60.4, 40.5 ppm; IR (film): $\tilde{\nu}$ = 1808, 1757, 1220, 1180, 1060, 992, 746, 689, 498 cm^{-1}; HRMS (ESI): *m/z* calcd for $C_{22}H_{16}O_4Na$: 367.0941 [*M*+Na]$^+$; found: 367.0942.

Methyl (*R*)-3-methyl-2-oxo-2,3-dihydrobenzofuran-3-carboxylate (143h)[23b]

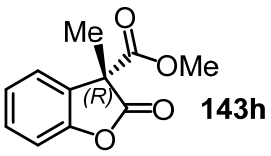

Table 13, entry 11: General procedure F1) was followed: *O*-Acylated benzofuranone **142h** (19.6 mg, 95.0 µmol); 1 mol% of catalyst **Λ-T18'**; solvent: 2:1 TAA/CPME; conc = 0.2 M, *t* = −30 °C, reaction time: 48 h; *C*-acylated benzofuranone **143h** was obtained as a viscous oil (18.2 mg, 88.3 µmol,

93%; *product volatile in vacuo*). Enantiomeric excess determined by chiral HPLC analysis: 70% ee (Chiralcel OJ-H, 5 µm, 25 cm x 4.6 mm; *n*-hexane/*i*-PrOH 90:10, λ = 254 nm, 1.0 mL/min, *t* (column) = 10 °C; t_R (major) = 17.6 min, t_R (minor) = 19.0 min); $[\alpha]_D^{23}$ = +88 (*c* 0.8, $CHCl_3$); ^{1}H NMR (300 MHz, $CDCl_3$): δ = 7.36 (ddd, *J* = 7.8 Hz, *J* = 7.8 Hz, *J* = 1.4 Hz, 1H), 7.32–7.25 (m, 1H), 7.21–7.11 (m, 2H), 3.71 (s, 3H), 1.78 (s, 3H) ppm; ^{13}C NMR (75 MHz, $CDCl_3$): δ = 174.1, 168.7, 153.2, 130.0, 128.5, 124.7, 123.5, 111.1, 53.6, 53.5, 20.7 ppm; IR (film): $\tilde{\nu}$ = 1808, 1741, 1229, 1112, 1034, 895, 753 cm^{-1}; HRMS (ESI): *m/z* calcd for $C_{11}H_{10}O_4Na$: 229.0471 $[M+Na]^+$; found: 229.0472.

1,1,1-Trichloro-2-methylpropan-2-yl (*S*)-3-methyl-2-oxo-2,3-dihydrobenzofuran-3-carboxylate (143i)

Note: Switching from R → S <u>not</u> caused by actual inversion of the stereocenter but by higher priority of the exocyclic acyl fragment according to CIP rules.[88]

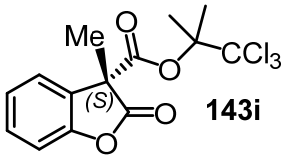

143i

Table 13, entry 12: General procedure F1) was followed: *O*-Acylated benzofuranone **142i** (25.2 mg, 71.7 µmol); 1 mol% of catalyst **Λ-T18'**; solvent: 2:1 TAA/CPME; conc = 0.2 M, *t* = −30 °C, reaction time: 48 h; *C*-acylated benzofuranone **143i** was obtained as colorless crystalline solid (25.0 mg, 71.1 µmol, 99%). Enantiomeric excess determined by chiral HPLC analysis: 93% ee (Chiralcel OD-H, 5 µm, 25 cm x 4.6 mm; *n*-hexane/*i*-PrOH 98.5:1.5, λ = 254 nm, 1.0 mL/min, *t* (column) = 25 °C; t_R (minor) = 5.3 min, t_R (major) = 5.7 min); $[\alpha]_D^{23}$ = +77 (*c* 1.0, $CHCl_3$); ^{1}H NMR (300 MHz, $CDCl_3$): δ = 7.35 (ddd, *J* = 7.8 Hz, *J* = 7.8 Hz, *J* = 1.5 Hz, 1H), 7.32–7.27 (m, 1H), 7.21–7.11 (m, 2H), 1.88 (s, 3H), 1.77 (s, 3H), 1.77 (s, 3H) ppm; ^{13}C NMR (75 MHz, $CDCl_3$): δ = 173.7, 165.9, 153.6, 130.2, 128.5, 124.7, 123.3, 111.3, 105.3, 90.6, 55.0, 21.4, 21.1, 19.8 ppm; IR (film): $\tilde{\nu}$ = 1811, 1749, 1233, 1215, 1153, 1118, 1036, 791, 752 cm^{-1}; HRMS (ESI): *m/z* calcd for $C_{14}H_{13}Cl_3O_4Na$: 372.9772 $[M+Na]^+$; found: 372.9773.

Table 13, entry 13: A flask (10 mL) was charged with *O*-Acylated benzofuranone **142i** (252 mg, 717 µmol) and 2:1 TAA/CPME (2.4 mL; final concentration: conc = 0.2 M). The flask was sealed with a septum, the mixture stirred until all of **142i** was dissolved, and the mixture then cooled to −30 °C. Under stirring, catalyst **Λ-T18'** (11.3 mg, 8.1 µmol, 1.1 mol%) in 2:1 TAA/CPME (1.0 mL) was added at −30 °C via syringe. The mixture was stirred at −30 °C for 48 h under exclusion of light, after which TLC analysis indicated full conversion. All volatiles were removed *in vacuo* (40 °C), the residue dissolved in a small amount of the eluent CH_2Cl_2, and product **143i** isolated by short-column chromatography (CH_2Cl_2). After drying *in vacuo*, product **143i** was obtained as colorless crystalline solid

(250 mg, 711 µmol, 99%). Enantiomeric excess determined by chiral HPLC analysis: 93% ee. XRD: X-ray quality crystals of **143i** were obtained by slow evaporation of the solvent from an Et_2O solution of **143i** at 4 °C (more details in the crystallographic data section).

4.10.3 Addition of 2-Cyanopyrrole to Aryl Alkyl Ketenes (153 + 162 → 163)

Absolute configurations of *α*-chiral *N*-acyl pyrroles (**163**) were assigned by comparison of measured optical rotation values with literature reported values of products **163a**,[26c] **163b**,[26c] and **163c**.[26c] All other products (**163**) were assigned by analogy. Absolute stereochemical assignments from ref. 26c with respect to *N*-acyl pyrroles (**163**) were established by reduction of enantioenriched *N*-acyl pyrroles (**163**) to the corresponding alcohols and trifluoroacetylation of those alcohols and comparison of their chiral GC retention times with the identical trifluoroacetylated products obtained from commercial enantiopure *α*-branched acids.[26c]

4.10.3.1 General Procedures G1) and G2)

General Procedure G1). Addition of 2-cyanopyrrole to aryl alkyl ketenes; Table 19, entries 1–6, 8, and 10: Standard-scale reactions (100−130 µmol ketene).

A flame-dried Schlenk tube (10 mL; threaded PTFE plug) equipped with a stir bar was charged with a solution of catalyst **Λ-T18'** (2 mol%) in CH_2Cl_2 (2 mL). Under stirring, the solvent was carefully removed *in vacuo* and the Schlenk tube with the solidified catalyst dried *in vacuo* for 1 h. Then, dry solvent (entries 1, 2: MTBE, entries 3–6, 8, 10: toluene; final concentration in both cases: conc = 12 mM; note that each ketene is added in a total volume of 0.5 mL of solvent) and 2-cyanopyrrole (**162**; 2.00 eq; addition via dry microliter syringe[155]) were added. Another flame-dried Schlenk tube (2 mL; threaded PTFE plug) was charged with the indicated amount of ketene (**153**; 1.00 eq; addition via dry microliter syringe;[155] amount of ketene was determined by weighting the syringe before and after the addition with a high precision analytical balance) and the ketene dissolved in dry solvent (0.25 mL). The Schlenk tube containing the solution of **Λ-T18'** and 2-cyanopyrrole (**162**) was cooled to 0 °C and the prepared ketene solution was added over 15 min with a well-sealed, dry microliter syringe.[155] The Schlenk tube which contained the ketene solution was rinsed with another 0.25 mL of dry solvent and the resulting solution added to the reaction's Schlenk tube with the same microliter syringe in order to transfer the ketene (**153**) as completely as possible. The reaction's Schlenk tube was then tightly sealed and stirred at 0 °C for 48 h under nitrogen atmosphere and under exclusion of light (*note that all operations until here were strictly performed under nitrogen atmosphere and under exclusion of moisture*). Then, all volatiles

were removed *in vacuo* and the crude product purified by short-column chromatography with the indicated eluent. After solvent removal and drying *in vacuo*, the desired *α*-chiral *N*-acyl pyrrole (**163**) was obtained.

General Procedure G2). Addition of 2-cyanopyrrole to aryl alkyl ketenes; Table 19, entries 7 and 9: Scaled-up reactions (approx. 1 mmol ketene).
In principle the same procedure as general procedure G1, some details had to be modified because of the increased reaction scale.
A flame-dried septum-sealed nitrogen flask (100 mL) equipped with a stir bar was charged with a solution of catalyst **Λ-T18'** (2 mol%) in CH_2Cl_2 (2 mL). Under stirring, the solvent was carefully removed *in vacuo* and the nitrogen flask with the solidified catalyst dried *in vacuo* for 1 h. Then, dry toluene (final reaction concentration: conc = 12 mM; note that each ketene is added in a total volume of 5.0 mL of toluene) and 2-cyanopyrrole (**162**; 2.00 eq; addition via dry microliter syringe[155]) were added. A flame-dried Schlenk tube (10 mL; threaded PTFE plug) was charged with the indicated amount of ketene (**153**; 1.00 eq; addition via dry microliter syringe;[155] amount of added ketene was determined by weighting the syringe before and after the addition with a high precision analytical balance) and the ketene dissolved in dry toluene (2.5 mL). The nitrogen flask containing the solution of **Λ-T18'** and 2-cyanopyrrole (**162**) was cooled to 0 °C and the prepared ketene solution was added through the flask's septum via canula with a well-sealed, dry microliter syringe over 15 min.[155] The Schlenk tube which contained the ketene solution was rinsed with another 2.5 mL of dry toluene and the resulting solution added to the reaction's flask with the same microliter syringe in order to transfer the ketene (**153**) as completely as possible. The resulting reaction mixture was then stirred at 0 °C for 48 h under nitrogen atmosphere and under exclusion of light (*note that all operations until here were strictly performed under nitrogen atmosphere and under exclusion of moisture*). Then, all solvents were removed *in vacuo* and the crude product purified by short-column chromatography with the indicated eluent. After solvent removal and drying *in vacuo*, the desired *α*-chiral *N*-acyl pyrrole (**163**) was obtained.

4.10.3.2 Synthetic Procedures and Characterizations

(*S*)-1-(2-Phenylbutanoyl)-1*H*-pyrrole-2-carbonitrile (163a)[26c]

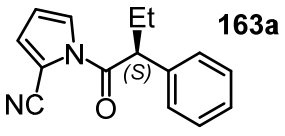

Table 19, entry 1: General procedure G1) was followed: Phenyl ethyl ketene (**153a**; 18.4 mg, 126 µmol); solvent: dry MTBE; conc = 12 mM, *t* = 0 °C, reaction time: 48 h; eluent: 2.5% acetone in toluene; *N*-acyl pyrrole **163a** was obtained as a viscous oil (28.9 mg, 121 µmol, 96%). Enantiomeric excess determined by chiral HPLC analysis: 89% ee (Chiralpak AD-H, 5 µm, 25 cm x

4.6 mm; *n*-hexane/*i*-PrOH 95:5, λ = 254 nm, 1.0 mL/min, *t* (column) = 25 °C; t_R (major) = 9.1 min, t_R (minor) = 10.2 min); $[\alpha]_D^{23}$ = +211 (*c* 1.0, $CHCl_3$); ^{1}H NMR (300 MHz, $CDCl_3$): δ = 7.37–7.14 (m, 6H), 6.88 (dd, *J* = 3.6 Hz, *J* = 1.3 Hz, 1H), 6.17 (t, *J* = 3.4 Hz, 1H), 4.07 (t, *J* = 7.3 Hz, 1H), 2.28–2.08 (m, 1H), 1.95–1.75 (m, 1H), 0.88 (t, *J* = 7.4 Hz, 3H) ppm; ^{13}C NMR (75 MHz, $CDCl_3$): δ = 170.1, 137.6, 129.5 (2C), 128.1, 127.9 (2C), 126.6, 124.8, 113.3, 113.1, 103.8, 53.2, 27.9, 12.1 ppm; IR (film): $\tilde{\nu}$ = 2223, 1728, 1450, 1354, 1276, 1247, 1226, 1121, 820, 733, 699, 586, 507 cm^{-1}; HRMS (ESI): *m/z* calcd for $C_{15}H_{14}N_2O_1Na$: 261.0998 $[M+Na]^+$; found: 261.1005.

(*S*)-1-(2-(*o*-Tolyl)butanoyl)-1*H*-pyrrole-2-carbonitrile (163b)[26c]

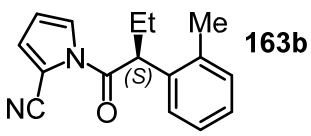

Table 19, entry 2: General procedure G1) was followed: *o*-Tolyl ethyl ketene (**153b**; 18.9 mg, 118 µmol); solvent: dry MTBE; conc = 12 mM, *t* = 0 °C, reaction time: 48 h; eluent: 2.5% acetone in toluene; *N*-acyl pyrrole **163b** was obtained as a viscous oil (29.6 mg, 117 µmol, 99%). Enantiomeric excess determined by chiral HPLC analysis: 84% ee (Chiralpak AD-H, 5 µm, 25 cm x 4.6 mm; *n*-hexane/*i*-PrOH 95:5, λ = 254 nm, 1.0 mL/min, *t* (column) = 40 °C; t_R (major) = 6.2 min, t_R (minor) = 7.4 min); $[\alpha]_D^{23}$ = +279 (*c* 1.0, $CHCl_3$); ^{1}H NMR (300 MHz, $CDCl_3$): δ = 7.21–7.03 (m, 4H), 7.00 (dd, *J* = 3.2 Hz, *J* = 1.3 Hz, 1H), 6.86 (dd, *J* = 3.5 Hz, *J* = 1.2 Hz, 1H), 6.13 (t, *J* = 3.4 Hz, 1H), 4.23 (dd, *J* = 8.1 Hz, *J* = 5.9 Hz, 1H), 2.40 (s, 3H), 2.27–2.06 (m, 1H), 1.84–1.65 (m, 1H), 0.94 (t, *J* = 7.4 Hz, 3H) ppm; ^{13}C NMR (75 MHz, $CDCl_3$): δ = 170.5, 136.6, 134.7, 131.4, 127.9, 127.3, 126.8, 126.3, 124.2, 113.2, 113.1, 103.9, 49.5, 27.3, 19.7, 12.4 ppm; IR (film): $\tilde{\nu}$ = 2224, 1731, 1451, 1352, 1275, 1250, 1226, 1113, 832, 754, 731 cm^{-1}; HRMS (ESI): *m/z* calcd for $C_{16}H_{16}N_2O_1Na$: 275.1155 $[M+Na]^+$; found: 275.1157.

(*S*)-1-(3-Methyl-2-phenylbutanoyl)-1*H*-pyrrole-2-carbonitrile (163c)[26c]

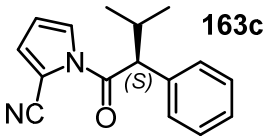

Table 19, entry 3: General procedure G1) was followed: Phenyl isopropyl ketene (**153c**; 18.9 mg, 118 µmol); solvent: dry toluene; conc = 12 mM, *t* = 0 °C, reaction time: 48 h; eluent: 2.5% acetone in toluene; *N*-acyl pyrrole **163c** was obtained as a viscous oil (29.5 mg, 117 µmol, 99%). Enantiomeric excess determined by chiral HPLC analysis: 93% ee (Chiralpak AD-H, 5 µm, 25 cm x 4.6 mm; *n*-hexane/*i*-PrOH 99:1, λ = 254 nm, 1.0 mL/min, *t* (column) = 40 °C; t_R (major) = 9.8 min, t_R (minor) = 10.8 min); $[\alpha]_D^{23}$ = +154 (*c* 1.0, $CHCl_3$); ^{1}H NMR (300 MHz, $CDCl_3$): δ = 7.36 (dd, *J* = 3.2 Hz, *J* = 1.3 Hz, 1H), 7.32–7.13 (m, 5H), 6.89 (dd, *J* = 3.5 Hz, *J* = 1.4 Hz, 1H), 6.19 (t, *J* = 3.4 Hz, 1H), 3.80 (d, *J* = 9.6 Hz, 1H), 2.50 (dsept, *J* = 9.8 Hz, *J* = 6.6 Hz, 1H), 1.03 (d, *J* = 6.6 Hz, 3H), 0.70 (d, *J* = 6.8 Hz, 3H) ppm; ^{13}C NMR

(75 MHz, $CDCl_3$): δ = 170.2, 136.6, 129.3 (2C), 128.5 (2C), 128.2, 126.8, 124.7, 113.4, 113.0, 103.8, 59.1, 32.6, 21.9, 20.2 ppm; IR (film): $\tilde{\nu}$ = 2223, 1728, 1450, 1351, 1298, 1248, 1225, 1110, 811, 740, 702 cm^{-1}; HRMS (ESI): *m/z* calcd for $C_{16}H_{16}N_2O_1Na$: 275.1155 $[M+Na]^+$; found: 275.1157.

(*S*)-1-(2-(4-Chlorophenyl)-3-methylbutanoyl)-1*H*-pyrrole-2-carbonitrile (163d)

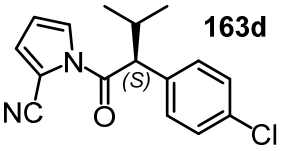

Table 19, entry 4: General procedure G1) was followed: *p*-Chlorophenyl isopropyl ketene (**153d**; 22.7 mg, 117 µmol); solvent: dry toluene; conc = 12 mM, *t* = 0 °C, reaction time: 48 h; eluent: 2.5% acetone in toluene; *N*-acyl pyrrole **163d** was obtained as a viscous oil (33.3 mg, 116 µmol, 99%). Enantiomeric excess determined by chiral HPLC analysis: 90% ee (Chiralcel OD-H, 5 µm, 25 cm x 4.6 mm; *n*-hexane/*i*-PrOH 95:5), λ = 254 nm, 1.0 mL/min, *t* (column) = 25 °C; t_R (major) = 7.2 min, t_R (minor) = 9.9 min); $[\alpha]_D^{23}$ = +138 (*c* 1.1, $CHCl_3$); ^1H NMR (300 MHz, $CDCl_3$): δ = 7.42 (dd, *J* = 3.3 Hz, *J* = 1.4 Hz, 1H), 7.37–7.24 (m, 4H), 6.99 (dd, *J* = 3.6 Hz, *J* = 1.3 Hz, 1H), 6.30 (t, *J* = 3.5 Hz, 1H), 3.90 (d, *J* = 9.8 Hz, 1H), 2.53 (dsept, *J* = 9.9 Hz, *J* = 6.6 Hz, 1H), 1.09 (d, *J* = 6.6 Hz, 3H), 0.77 (d, *J* = 6.8 Hz, 3H) ppm; ^{13}C NMR (75 MHz, $CDCl_3$): δ = 170.1, 135.0, 134.2, 129.8 (2C), 129.5 (2C), 127.1, 124.6, 113.3, 113.3, 103.8, 58.2, 32.8, 21.8, 20.1 ppm; IR (film): $\tilde{\nu}$ = 2224, 1728, 1450, 1345, 1297, 1247, 1226, 1098, 789, 731, 523 cm^{-1}; HRMS (ESI): *m/z* calcd for $C_{16}H_{15}Cl_1N_2O_1Na$: 309.0765 $[M+Na]^+$; found: 309.0769.

(*S*)-1-(2-(4-Methoxyphenyl)-3-methylbutanoyl)-1*H*-pyrrole-2-carbonitrile (163e)

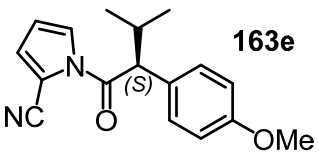

Table 19, entry 5: General procedure G1) was followed: *p*-Methoxyphenyl isopropyl ketene (**153e**; 21.3 mg, 112 µmol); solvent: dry toluene; conc = 12 mM, *t* = 0 °C, reaction time: 48 h; eluent: 2.5% acetone in toluene; *N*-acyl pyrrole **163e** was obtained as a viscous oil (31.5 mg, 112 µmol, >99%). Enantiomeric excess determined by chiral HPLC analysis: 91% ee (Chiralcel OD-H, 5 µm, 25 cm x 4.6 mm; *n*-hexane/*i*-PrOH 95:5, λ = 254 nm, 1.0 mL/min, *t* (column) = 25 °C; t_R (major) = 9.4 min), t_R (minor) = 12.5 min); $[\alpha]_D^{23}$ = +147 (*c* 1.0, $CHCl_3$); ^1H NMR (300 MHz, $CDCl_3$): δ = 7.43 (dd, *J* = 3.1 Hz, *J* = 1.2 Hz, 1H), 7.25 (d, *J* = 8.7 Hz, 2H), 6.96 (dd, *J* = 3.4 Hz, *J* = 1.3 Hz, 1H), 6.86 (d, *J* = 8.7 Hz, 2H), 6.26 (t, *J* = 3.5 Hz, 1H), 3.82 (d, *J* = 9.8 Hz, 1H), 3.77 (s, 3H), 2.52 (dsept, *J* = 9.8 Hz, *J* = 6.5 Hz, 1H), 1.08 (d, *J* = 6.4 Hz, 3H), 0.77 (d, *J* = 6.8 Hz, 3H) ppm; ^{13}C NMR (75 MHz, $CDCl_3$): δ = 170.5, 159.5, 129.5 (2C), 128.5, 126.7, 124.7, 114.7 (2C), 113.4, 113.0, 103.7, 58.2, 55.4, 32.5, 21.8, 20.1 ppm; IR (film): $\tilde{\nu}$ = 2223, 1728, 1510, 1449, 1346, 1298, 1249, 1226, 1179,

1107, 1031, 801, 774, 732 cm^{-1}; HRMS (ESI): *m/z* calcd for $C_{17}H_{18}N_2O_2Na$: 305.1260 $[M+Na]^+$; found: 305.1263.

(*S*)-1-(3-Methyl-2-(m-tolyl)butanoyl)-1*H*-pyrrole-2-carbonitrile (163f)

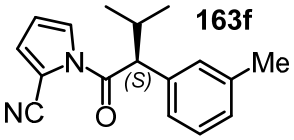

Table 19, entry 6: General procedure G1) was followed: *m*-Tolyl isopropyl ketene (**153f**; 19.5 mg, 112 µmol); solvent: dry toluene; conc = 12 mM, *t* = 0 °C, reaction time: 48 h; eluent: 2.5% acetone in toluene; *N*-acyl pyrrole **163f** was obtained as a viscous oil (29.8 mg, 112 µmol, >99%). Enantiomeric excess determined by chiral HPLC analysis: 95% ee (Chiralcel OD-H, 5 µm, 25 cm x 4.6 mm; *n*-hexane/*i*-PrOH 95:5, λ = 254 nm, 1.0 mL/min, *t* (column) = 25 °C; t_R (major) = 7.9 min, t_R (minor) = 14.9 min); $[\alpha]_D^{23}$ = +170 (*c* 1.0, $CHCl_3$); ^{1}H NMR (300 MHz, $CDCl_3$): δ = 7.44 (dd, *J* = 3.2 Hz, *J* = 1.3 Hz, 1H), 7.22 (t, *J* = 7.5 Hz, 1H), 7.18–7.04 (m, 3H), 6.96 (dd, *J* = 3.6 Hz, *J* = 1.3 Hz, 1H), 6.26 (t, *J* = 3.5 Hz, 1H), 3.82 (d, *J* = 9.8 Hz, 1H), 2.66–2.45 (m, 1H), 2.33 (s, 3H), 1.10 (d, *J* = 6.4 Hz, 3H), 0.77 (d, *J* = 6.8 Hz, 3H) ppm; ^{13}C NMR (75 MHz, $CDCl_3$): δ = 170.2, 139.1, 136.5, 129.1, 129.0, 128.9, 126.7, 125.7, 124.7, 113.4, 113.0, 103.8, 59.1, 32.6, 21.9, 21.6, 20.2 ppm; IR (film): $\tilde{\nu}$ = 2224, 1729, 1449, 1346, 1296, 1248, 1223, 1110, 828, 767, 735 cm^{-1}; HRMS (ESI): *m/z* calcd for $C_{17}H_{18}N_2O_1Na$: 289.1311 $[M+Na]^+$; found: 289.1313.

Table 19, entry 7: General procedure G2) was followed: *m*-Tolyl isopropyl ketene (**153f**; 194 mg, 1.11 mmol); solvent: dry toluene; conc = 12 mM, *t* = 0 °C, reaction time: 48 h; eluent: 2.5% acetone in toluene; *N*-acyl pyrrole **163f** was obtained as a viscous oil (292 mg, 1.10 mmol, 98%). Enantiomeric excess determined by chiral HPLC analysis: 95% ee.

(*S*)-1-(2-Cyclopentyl-2-phenylacetyl)-1*H*-pyrrole-2-carbonitrile (163g)

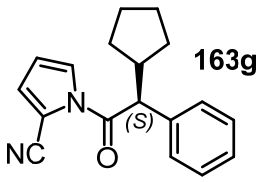

Table 19, entry 8: General procedure G1) was followed: Phenyl cyclopentyl ketene (**153g**; 20.8 mg, 112 µmol); solvent: dry toluene; conc = 12 mM, *t* = 0 °C, reaction time: 48 h; eluent: 2.5% acetone in toluene; *N*-acyl pyrrole **163g** was obtained as a viscous oil (30.9 mg, 111 µmol, 99%). Enantiomeric excess determined by chiral HPLC analysis: 93% ee (Chiralcel OD-H, 5 µm, 25 cm x 4.6 mm; *n*-hexane/*i*-PrOH 95:5, λ = 254 nm, 1.0 mL/min, *t* (column) = 25 °C; t_R (major) = 7.5 min, t_R (minor) = 12.5 min); $[\alpha]_D^{23}$ = +145 (*c* 1.0, $CHCl_3$); ^{1}H NMR (300 MHz, $CDCl_3$): δ = 7.34 (dd, *J* = 3.2 Hz, *J* = 1.3 Hz, 1H), 7.32–7.13 (m, 5H), 6.88 (dd, *J* = 3.6 Hz, *J* = 1.3 Hz, 1H), 6.18 (t, *J* = 3.4 Hz, 1H), 3.93 (d, *J* = 10.4 Hz, 1H), 2.76–2.54 (m, 1H), 2.09–1.89 (m, 1H), 1.69–0.92 (m, 7H) ppm; ^{13}C NMR (75 MHz, $CDCl_3$): δ = 170.2, 137.4, 129.3 (2C), 128.1 (2C), 128.1, 126.7, 124.7, 113.4, 113.0, 103.8, 57.3, 44.4,

32.0, 30.7, 25.2, 24.8 ppm; IR (film): $\tilde{\nu}$ = 2953, 2223, 1728, 1449, 1344, 1282, 1248, 1225, 1114, 811, 736, 701, 636 cm^{-1}; HRMS (ESI): *m/z* calcd for $C_{18}H_{18}N_2O_1Na$: 301.1311 [*M*+Na]$^+$; found: 301.1313.

Table 19, entry 9: General procedure G2) was followed: Phenyl cyclopentyl ketene (**153g**; 209 mg, 1.12 µmol); solvent: dry toluene; conc = 12 mM, *t* = 0 °C, reaction time: 48 h; eluent: 2.5% acetone in toluene; *N*-acyl pyrrole **163g** was obtained as a viscous oil (308 mg, 1.11 mmol, 99%). Enantiomeric excess determined by chiral HPLC analysis: 93% ee.

(*S*)-1-(2-Cyclohexyl-2-phenylacetyl)-1*H*-pyrrole-2-carbonitrile (163h)

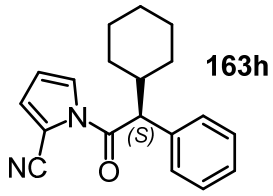

Table 19, entry 10: General procedure G1) was followed: Phenyl cyclohexyl ketene (**153h**; 21.1 mg, 105 µmol); solvent: dry toluene; conc = 12 mM, *t* = 0 °C, reaction time: 48 h; eluent: 2.5% acetone in toluene; *N*-acyl pyrrole **163h** was obtained as a viscous oil (30.7 mg, 105 µmol, >99%). Enantiomeric excess determined by chiral HPLC analysis: 93% ee (Chiralcel OD-H, 5 µm, 25 cm x 4.6 mm; *n*-hexane/*i*-PrOH 95:5, λ = 254 nm, 1.0 mL/min, *t* (column) = 25 °C; t_R (major) = 6.5 min, t_R (minor) = 10.3 min); $[\alpha]_D^{23}$ = +93 (*c* 1.0, $CHCl_3$); ^{1}H NMR (300 MHz, $CDCl_3$): δ = 7.37 (dd, *J* = 3.2 Hz, *J* = 1.3 Hz, 1H), 7.33–7.09 (m, 5H), 6.89 (dd, *J* = 3.5 Hz, *J* = 1.4 Hz, 1H), 6.19 (t, *J* = 3.4 Hz, 1H), 3.88 (d, *J* = 10.0 Hz, 1H), 2.27–2.09 (m, 1H), 1.94–1.79 (m, 1H), 1.74–1.45 (m, 3H), 1.39–0.64 (m, 6H) ppm; ^{13}C NMR (75 MHz, $CDCl_3$): δ = 170.2, 136.1, 129.2 (2C), 128.6 (2C), 128.1, 126.8, 124.7, 113.4, 113.0, 103.7, 57.9, 41.7, 32.5, 30.4, 26.3, 26.1 (2C) ppm; IR (film): $\tilde{\nu}$ = 2927, 2224, 1728, 1449, 1349, 1294, 1253, 1222, 1114, 818, 738, 702 cm^{-1}; HRMS (ESI): *m/z* calcd for $C_{19}H_{20}N_2O_1Na$: 315.1468 [*M*+Na]$^+$; found: 315.1470.

4.10.4 Intermolecular *C*-Acylations of Silyl Ketene Acetals (144 + 145 → 146)

The experiments from Table 14 with the best results in terms of enantioselectivity for each tested silyl ketene acetal (**145a–d**) are described in detail below, which are the experiments from entry 1 (**145a**), entry 2 (**145b**), entry 3 (**145c**), and entry 9 (**145d**). All other experiments from Table 14 were analogously performed.

Methyl 5,5-dimethyl-2-oxo-3-phenyltetrahydrofuran-3-carboxylate (146aa)[89]

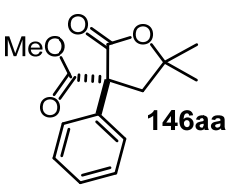

Table 14, entry 1: A flame-dried Schlenk tube (10 mL; threaded PTFE plug) was charged with silyl ketene acetal **145a** (24.0 mg, 91.5 µmol, 1.00 eq) and with a flame-dried stir bar. Another flame-dried Schlenk tube (2 mL; threaded PTFE plug) was charged with a solution of catalyst **Λ-T18'** (3.8 mg, 2.7 µmol, 3 mol%) in CH_2Cl_2, the CH_2Cl_2 subsequently carefully removed *in*

vacuo, and the Schlenk tube with the solidified catalyst dried *in vacuo* for 1 h. Then, the catalyst was dissolved in dry CH_2Cl_2 (1.1 mL) and this solution transferred to the Schlenk tube containing **145a**. Finally, acetic anhydride (**144a**; 11.2 µL, 118 µmol, 1.30 eq) was added via microliter syringe[155] and the resulting mixture stirred at rt for 36 h under nitrogen atmosphere. Full conversion was indicated by TLC analysis (hexanes/Et_2O 3:1). All volatiles were removed *in vacuo*, the crude product dissolved in CH_2Cl_2, adsorbed on silica gel, and purified by flash chromatography (hexanes/Et_2O 5:1). After solvent removal and drying *in vacuo*, product **146aa** was obtained as a colorless oil (19.3 mg, 83.1 µmol, 91%). Enantiomeric excess determined by chiral HPLC analysis: 17% ee (Chiralcel OD-H, 5 µm, 25 cm x 4.6 mm; *n*-hexane/*i*-PrOH 98.5:1.5, λ = 254 nm, 1.0 mL/min, *t* (column) = 25 °C; t_R (major) = 6.2 min, t_R (minor) = 7.2 min); ^{1}H NMR (300 MHz, $CDCl_3$): δ = 7.45–7.27 (m, 5H), 3.39 (d, J = 13.4 Hz, 1H), 2.25 (d, J = 13.6 Hz, 1H), 2.21 (s, 3H), 1.42 (s, 3H), 1.26 (s, 3H) ppm; ^{13}C NMR (75 MHz, $CDCl_3$): δ = 201.3, 172.8, 138.9, 129.6 (2C), 128.2, 126.7 (2C), 82.5, 68.6, 44.7, 29.1, 28.9, 26.4 ppm; IR (film): $\tilde{\nu}$ = 1753, 1714, 1271, 1180, 1135, 1100, 1034, 702 cm^{-1}; HRMS (ESI): *m/z* calcd for $C_{14}H_{16}O_3Na$: 255.1003 [M+Na]$^+$; found: 255.0990.

Methyl 3-(4-methoxyphenyl)-5,5-dimethyl-2-oxotetrahydrofuran-3-carboxylate (146ba)[89]

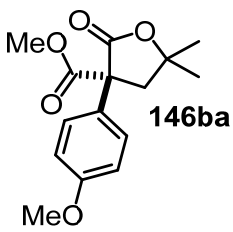

146ba

Table 14, entry 2: A flame-dried Schlenk tube (10 mL; threaded PTFE plug) was charged with silyl ketene acetal **145b** (39.4 mg, 135 µmol, 1.00 eq) and with a flame-dried stir bar. Another flame-dried Schlenk tube (2 mL; threaded PTFE plug) was charged with a solution of catalyst **Λ-T18'** (5.3 mg, 3.8 µmol, 3 mol%) in CH_2Cl_2, the CH_2Cl_2 subsequently carefully removed *in vacuo*, and the Schlenk tube with the solidified catalyst dried *in vacuo* for 1 h. Then, the catalyst was dissolved in dry CH_2Cl_2 (1.5 mL) and this solution transferred to the Schlenk tube containing **145b**. Finally, acetic anhydride (**144a**; 15.5 µL, 164 µmol, 1.21 eq) was added via microliter syringe[155] and the resulting mixture stirred at rt for 36 h under nitrogen atmosphere. Full conversion was indicated by TLC analysis (hexanes/Et_2O 3:1). All volatiles were removed *in vacuo*, the crude product dissolved in CH_2Cl_2, adsorbed on silica gel, and purified by flash chromatography (hexanes/Et_2O 5:1). After solvent removal and drying *in vacuo*, product **146ba** was obtained as a colorless crystalline solid (31.2 mg, 119 µmol, 88%). Enantiomeric excess determined by chiral HPLC analysis: 29% ee (Chiralcel OJ-H, 5 µm, 25 cm x 4.6 mm; *n*-hexane/*i*-PrOH 96:4, λ = 254 nm, 1.0 mL/min, *t* (column) = 25 °C; t_R (minor) = 20.9 min, t_R (major) = 23.0 min); ^{1}H NMR (300 MHz,

$CDCl_3$): δ = 7.27–7.16 (m, 2H), 6.88–6.75 (m, 2H), 3.74 (s, 3H), 3.28 (d, J = 13.4 Hz, 1H), 2.17 (d, J = 13.6 Hz, 1H), 2.14 (s, 3H), 1.34 (s, 3H), 1.19 (s, 3H) ppm; ^{13}C NMR (75 MHz, $CDCl_3$): δ = 201.6, 173.0, 159.5, 130.7, 127.9 (2C), 114.9 (2C), 82.4, 67.7, 55.4, 44.7, 29.0, 28.9, 26.2 ppm; IR (film): $\tilde{\nu}$ = 1752, 1713, 1510, 1252, 1180, 1138, 1031, 836, 597 cm^{-1}; HRMS (ESI): *m/z* calcd for $C_{15}H_{18}O_4Na$: 285.1097 [*M*+Na]$^+$; found: 285.1096.

Methyl 5,5-dimethyl-3-(naphthalen-1-yl)-2-oxotetrahydrofuran-3-carboxylate (146ca)[89]

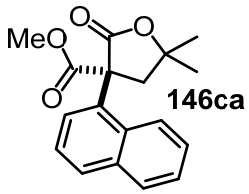

Table 14, entry 3: A flame-dried Schlenk tube (10 mL; threaded PTFE plug) was charged with silyl ketene acetal **145c** (30.1 mg, 96.3 µmol, 1.00 eq) and with a flame-dried stir bar. Another flame-dried Schlenk tube (2 mL; threaded PTFE plug) was charged with a solution of catalyst **Λ-T18'** (4.3 mg, 3.1 µmol, 3 mol%) in CH_2Cl_2, the CH_2Cl_2 subsequently carefully removed *in vacuo*, and the Schlenk tube with the solidified catalyst dried *in vacuo* for 1 h. Then, the catalyst was dissolved in dry CH_2Cl_2 (1.3 mL) and this solution transferred to the Schlenk tube containing **145c**. Finally, acetic anhydride (**144a**; 12.6 µL, 133 µmol, 1.38 eq) was added via microliter syringe[155] and the resulting mixture stirred at rt for 36 h under nitrogen atmosphere. Full conversion was indicated by TLC analysis (hexanes/Et_2O 3:1). All volatiles were removed *in vacuo*, the crude product dissolved in CH_2Cl_2, adsorbed on silica gel, and purified by flash chromatography (hexanes/Et_2O 5:1). After solvent removal and drying *in vacuo*, product **146ca** was obtained as a colorless oil (25.8 mg, 91.4 µmol, 95%). Enantiomeric excess determined by chiral HPLC analysis: 18% ee (Chiralcel OD-H, 5 µm, 25 cm x 4.6 mm; *n*-hexane/*i*-PrOH 99:1, λ = 254 nm, 1.0 mL/min, *t* (column) = 25 °C; t_R (major) = 7.7 min, t_R (minor) = 8.8 min); ^{1}H NMR (300 MHz, $CDCl_3$): δ = 7.98–7.80 (m, 2H), 7.75 (dd, J = 7.4 Hz, J = 1.1 Hz, 1H), 7.58–7.36 (m, 4H), 3.78 (d, J = 13.4 Hz, 1H), 2.33 (d, J = 13.4 Hz, 1H), 2.09 (s, 3H), 1.55 (s, 3H), 1.19 (s, 3H) ppm; ^{13}C NMR (75 MHz, $CDCl_3$): δ = 204.2, 173.1, 135.9, 134.9, 130.3, 129.8, 129.4, 127.3, 126.3 (2C), 125.7, 123.5, 83.3, 69.3, 44.2, 29.5, 29.4, 27.2 ppm; IR (film): $\tilde{\nu}$ = 1750, 1715, 1270, 1181, 1138, 780 cm^{-1}; HRMS (ESI): *m/z* calcd for $C_{18}H_{18}O_3Na$: 305.1148 [*M*+Na]$^+$; found: 305.1147.

Methyl 3-isobutyl-2-oxo-2,3-dihydrobenzofuran-3-carboxylate (146da)

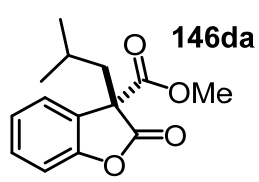

Table 14, entry 9: A flame-dried Schlenk tube (10 mL; threaded PTFE plug) was charged with silyl ketene acetal **145d** (27.7 mg, 106 µmol, 1.00 eq) and with a flame-dried stir bar. Another flame-dried Schlenk tube (2 mL; threaded PTFE plug) was charged with a solution of catalyst **Λ-T18'** (4.4 mg, 3.2 µmol, 3 mol%) in CH_2Cl_2, the CH_2Cl_2 subsequently carefully removed *in vacuo*, and the Schlenk tube with the solidified catalyst dried *in vacuo* for 1 h.

Then, the catalyst was dissolved in dry CH_2Cl_2 (1.3 mL) and this solution transferred to the Schlenk tube containing **145d**. Finally, acetic anhydride (**144a**; 13.0 µL, 138 µmol, 1.30 eq) was added via microliter syringe[155] and the resulting mixture stirred at rt for 43 h under nitrogen atmosphere. All volatiles were removed *in vacuo*, the crude product dissolved in CH_2Cl_2, adsorbed on silica gel, and purified by flash chromatography (hexanes/Et_2O 20:1). After solvent removal and drying *in vacuo*, 12 mg of a colorless oil were obtained which contained desired **146da** and **274**, which is the hydrolysis product of **145d**, in a 2.5:1 ratio. Accordingly, the oil contained calculated 9.1 mg of desired product **146da** (39.0 µmol, 37%). Apparently, the reaction was not yet complete when it was stopped. Enantiomeric excess determined by chiral HPLC analysis: 66% ee (Chiralcel OJ-H, 5 µm, 25 cm x 4.6 mm; *n*-hexane/*i*-PrOH 99.4:0.6, λ = 254 nm, 1.0 mL/min, *t* (column) = 15 °C; t_R (major) = 11.0 min, t_R (minor) = 13.3 min); ^{1}H NMR (300 MHz, $CDCl_3$): δ = 7.35–7.01 (m, 4H), 2.19 (dd, *J* = 14.3 Hz, *J* = 5.8 Hz, 1H), 2.09 (dd, *J* = 14.4 Hz, *J* = 7.6 Hz, 1H), 2.08 (s, 3H), 1.45–1.26 (m, 1H), 0.70 (d, *J* = 6.6 Hz, 3H), 0.64 (d, *J* = 6.6 Hz, 3H) ppm; ^{13}C NMR (75 MHz, $CDCl_3$): δ = 198.9, 175.3, 153.7, 130.1, 126.3, 125.0, 124.8, 111.2, 65.2, 42.3, 26.4, 25.3, 23.9, 22.8 ppm; HRMS (ESI): *m/z* calcd for $C_{14}H_{16}O_3Na$: 255.0992 $[M+Na]^+$; found: 255.0995.

4.10.5 Steglich-Type Rearrangements of *O*-Acylated Oxindoles

The Steglich-type rearrangements of *O*-acylated oxindoles from Table 15 where the desired *C*-acylated products could be isolated (entries 5–7) are described in detail below. All other experiments from Table 15 were analogously performed.

Gliocladin C Precursor 148b[90]

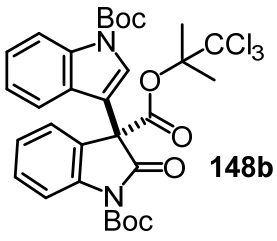

148b

Table 15, entry 5: An amber glas vial[154] with a micro stir bar was charged with gliocladin C precursor **147b**[90] (29.3 mg, 44.9 µmol, 1.00 eq), precatalyst **Λ-T18** (3.5 mg, 2.3 µmol, 5 mol%), Cs_2CO_3 (2.1 mg, 6.5 µmol, 15 mol%), and THF (55 µL). Then, the vial was capped with a PTFE-sealed screw cap[154] and the mixture stirred at 40 °C. After 48 h, TLC analysis (hexanes/Et_2O 6:1) indicated incomplete conversion (<50%). After a total of 130 h at 40 °C, TLC analysis indicated full although unclean conversion. All volatiles were removed *in vacuo*, the crude product dissolved in CH_2Cl_2, adsorbed on silica gel, and purified via flash chromatography (hexanes/Et_2O 6:1). After solvent removal and drying *in vacuo*, compound **148b** was obtained as a pale orange solid (4.8 mg, 7.4 µmol, 16%). Enantiomeric excess determined by chiral HPLC analysis: 28% ee (Chiralpak AD-H, 5 µm, 25 cm x 4.6 mm; *n*-hexane/*i*-PrOH 99.3:0.7, λ = 254 nm, 1.0 mL/min, *t* (column) =

25 °C; t_R (major) = 8.2 min, t_R (minor) = 9.9 min); ^{1}H NMR (300 MHz, DMSO-d_6): δ = 8.07 (d, J = 8.3 Hz, 1H), 7.93 (d, J = 8.3 Hz, 1H), 7.56 (ddd, J = 8.2 Hz, J = 7.6 Hz, J = 1.2 Hz, 1H), 7.46 (dd, J = 7.5 Hz, J = 1.6 Hz, 1H), 7.41 (s, 1H), 7.40–7.20 (m, 4H), 1.88 (s, 3H), 1.65 (s, 3H), 1.60 (s, 9H), 1.55 (s, 9H) ppm.

Diphenyl 3-methyl-2-oxoindoline-1,3-dicarboxylate (150a)[23f]

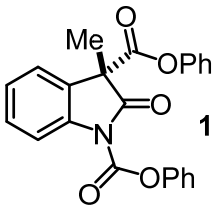

150a

Table 15, entry 6: An amber glas vial[154] with a micro stir bar was charged with substrate **149a** (20.0 mg, 51.6 µmol, 1.00 eq), catalyst **Λ-T18'** (1.5 mg, 1.1 µmol, 2 mol%), and THF (110 µL). The vial was capped with a PTFE-sealed screw cap[154] and the mixture stirred at rt. After 12 h, TLC indicated considerable conversion (~50%) and after 48 h TLC indicated full conversion. All volatiles were removed *in vacuo* and the crude product purified by short-column chromatography (CH_2Cl_2). After solvent removal and drying *in vacuo*, product **150a** was obtained as a colorless solid (19.6 mg, 50.6 µmol, 98%). Enantiomeric excess determined by chiral HPLC analysis: < 5% ee (Chiralpak AD-H, 5 µm, 25 cm x 4.6 mm; *n*-hexane/*i*-PrOH 97:3, λ = 254 nm, 1.0 mL/min, *t* (column) = 25 °C; t_{R1} = 24.4 min, t_{R2} = 36.7 min; ^{1}H NMR (300 MHz, $CDCl_3$): δ = 8.10–8.02 (m, 1H), 7.50–7.18 (m, 11H), 7.03–6.93 (m, 2H), 1.90 (s, 3H) ppm; ^{13}C NMR (75 MHz, $CDCl_3$): δ = 172.5, 167.7, 150.5, 150.3, 149.4, 139.3, 130.0, 129.8 (2C), 129.6 (2C), 126.7, 126.5, 125.8, 123.1, 121.6 (2C), 121.3 (2C), 121.1, 116.1, 56.1, 21.0 ppm; IR (film): $\tilde{\nu}$ = 1778, 1745, 1480, 1346, 1215, 1180, 1162, 1094, 743, 683, 498 cm^{-1}; HRMS (ESI): *m/z* calcd for $C_{23}H_{17}N_1O_5Na$: 410.0999 [M+Na]$^+$; found: 410.0998.

Diphenyl 3-benzyl-2-oxoindoline-1,3-dicarboxylate (150b)[23f]

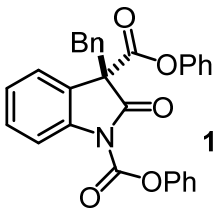

150b

Table 15, entry 7: An amber glas vial[154] with a micro stir bar was charged with substrate **149b** (23.8 mg, 51.3 µmol, 1.00 eq), catalyst **Λ-T18'** (1.5 mg, 1.1 µmol, 2 mol%), and THF (110 µL). The vial was capped with a PTFE-sealed screw cap[154] and the mixture stirred at rt. After 12 h, TLC indicated considerable conversion (80–90%) and after 48 h TLC indicated full conversion. All volatiles were removed *in vacuo* and the crude product purified by short-column chromatography (CH_2Cl_2). After solvent removal and drying *in vacuo*, product **150b** was obtained as a colorless solid (22.8 mg, 49.2 µmol, 96%). Enantiomeric excess determined by chiral HPLC analysis: 59% ee (Chiralpak AD-H, 5 µm, 25 cm x 4.6 mm; *n*-hexane/*i*-PrOH 97:3, λ = 254 nm, 1.0 mL/min, *t* (column) = 25 °C; t_R (major) = 29.2 min, t_R (minor) = 34.2 min; ^{1}H NMR (300 MHz, $CDCl_3$): δ = 7.81–7.72 (m, 1H), 7.55–7.47 (m, 1H), 7.46–7.05 (m, 13H), 7.05–6.98 (m, 2H), 6.96–6.88 (m, 2H), 3.78 (d, J = 13.3 Hz, 1H), 3.67 (d,

J = 13.3 Hz, 1H) ppm; ^{13}C NMR (75 MHz, $CDCl_3$): δ = 171.3, 167.3, 150.5, 150.2, 148.9, 140.0, 133.5, 130.2 (2C), 130.0, 129.7 (2C), 129.6 (2C), 128.2 (2C), 127.5, 126.6, 126.6, 126.3, 125.5, 123.8, 121.6 (2C), 121.3 (2C), 115.8, 61.8, 41.2 ppm; IR (film): $\tilde{\nu}$ = 1747, 1480, 1346, 1289, 1182, 1151, 1097, 1069, 1028, 739, 688, 499 cm^{-1}; HRMS (ESI): *m/z* calcd for $C_{29}H_{21}NO_5Na$: 486.1312 $[M+Na]^+$; found: 486.1315.

4.10.6 Asymmetric Reactions with Phenyl Ethyl Ketene (153a) as Substrate

The asymmetric reactions between phenyl ethyl ketene (**153a**) and various reaction partners from Table 16 where the desired products could be isolated (entries 1, 2, and 5) are described in detail below. All other experiments from Table 16 were analogously performed.

Remark: The reaction between phenyl ethyl ketene (**153a**) and 2-cyanopyrrole (**162**) from Table 16, entry 6 is described in chapter 4.10.3.

Diethyl 3-ethyl-4-oxo-3-phenyl-1,2-diazetidine-1,2-dicarboxylate 155a[26j]

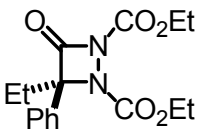

155a

Table 16, entry 1: A flame-dried Schlenk tube with a stir bar (10 mL; threaded PTFE plug) was charged with phenyl ethyl ketene (**153a**; 22.9 mg, 157 µmol, 1.00 eq) and dry CH_2Cl_2 (10 mL). Another flame-dried Schlenk tube (2 mL; threaded PTFE plug) was charged with a CH_2Cl_2 solution of catalyst **Λ-T18'** (6.5 mg, 4.7 µmol, 3 mol%), the CH_2Cl_2 subsequently carefully removed *in vacuo*, and the Schlenk tube with the solidified catalyst dried *in vacuo* for 1 h. Then, the catalyst was dissolved in dry CH_2Cl_2 (1.0 mL) and this solution transferred to the Schlenk tube containing ketene **153a**. Immediately, DEAD (**154**; 26.5 µL, 168 µmol, 1.07 eq) was added via microliter syringe[155] and the resulting mixture stirred at rt for 6 h under nitrogen atmosphere. After that, TLC analysis (hexanes/EtOAc 6:1) indicated full conversion. However, **155a** was not formed as major product (TLC comparison with a racemic sample of **155a**; one major unwanted spot which was not characterized). After a total of 25 h at rt, TLC analysis gave the same result. Then, all volatiles were removed *in vacuo*, the crude product dissolved in CH_2Cl_2, adsorbed on silica gel, and desired **155a** isolated via flash chromatography (hexanes/EtOAc 10:1). After solvent removal and drying *in vacuo*, **155a** was isolated as a colorless oil (5.9 mg, 18 µmol, 12%). Enantiomeric excess determined by chiral HPLC analysis: 64% ee (Chiralcel OD-H, 5 µm, 25 cm x 4.6 mm; *n*-hexane/*i*-PrOH 95:5, λ = 254 nm, 1.0 mL/min, *t* (column) = 25 °C; t_R (major) = 10.0 min, t_R (minor) = 13.8 min); ^{1}H NMR (300 MHz, $CDCl_3$): δ = 7.61–7.50 (m, 2H), 7.46–7.30 (m, 3H), 4.36 (q, J = 7.1 Hz, 2H), 4.30–4.12 (m, 2H), 2.50–2.35 (m, 1H), 2.35–2.17 (m, 1H), 1.37 (t, J = 7.2 Hz, 3H), 1.23 (t, J = 7.2 Hz, 3H), 1.08 (t, J = 7.4 Hz, 3H) ppm; HRMS (ESI): *m/z* calcd for $C_{16}H_{20}N_2O_5Na$: 343.1264 $[M+Na]^+$; found: 343.1266.

Perchloroprop-1-en-2-yl 2-chloro-2-phenylbutanoate 157a[26h,27c]

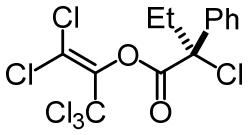

157a

Table 16, entry 2: A flame-dried Schlenk tube with a stir bar (10 mL; threaded PTFE plug) was charged with phenyl ethyl ketene (**153a**; 17.6 mg, 120 µmol, 1.00 eq) and dry toluene (6.0 mL). Another flame-dried Schlenk tube (2 mL; threaded PTFE plug) was charged with hexachloroacetone (**156**; 22.0 µL, 145 µmol, 1.20 eq) and dry toluene (0.7 mL). And another flame-dried Schlenk tube (2 mL; threaded PTFE plug) was charged with a CH_2Cl_2 solution of catalyst **Λ-T18'** (5.0 mg, 3.6 µmol, 3 mol%), the CH_2Cl_2 subsequently carefully removed *in vacuo*, and the Schlenk tube with the solidified catalyst dried *in vacuo* for 1 h and **Λ-T18'** redissolved in dry toluene (0.25 mL).

The ketene solution (**153a**) was then cooled to –78 °C and the hexachloroacetone solution (**156**) added, which was immediately followed by the catalyst solution (**Λ-T18'**). The resulting mixture was then stirred at –78 °C for 1 h under nitrogen atmosphere after which TLC analysis (hexanes/EtOAc 20:1) indicated full conversion. The mixture was allowed to warm to rt, all volatiles removed *in vacuo*, the crude product dissolved in CH_2Cl_2, adsorbed on silica gel, and purified by flash chromatography (hexanes/EtOAc 40:1). After solvent removal and drying *in vacuo*, desired product **157a** was obtained as a colorless oil (46.3 mg, 113 µmol, 94%). Enantiomeric excess determined by chiral HPLC analysis: 9% ee (Chiralcel OJ-H, 5 µm, 25 cm x 4.6 mm; *n*-hexane/*i*-PrOH 98.7:1.3, λ = 254 nm, 0.7 mL/min, *t* (column) = 20 °C; t_R (minor) = 7.8 min, t_R (major) = 8.7 min); ^{1}H NMR (300 MHz, $CDCl_3$): δ = 7.75–7.53 (m, 2H), 7.48–7.28 (m, 3H), 2.75–2.42 (m, 2H), 1.03 (t, J = 7.2 Hz, 3H) ppm; ^{13}C NMR (75 MHz, $CDCl_3$): δ = 166.4, 142.7, 136.6, 129.0, 128.6 (2C), 127.2 (2C), 124.8, 90.7, 74.7, 34.6, 8.9 ppm; IR (film): $\tilde{\nu}$ = 1773, 1156, 1061, 994, 817, 759, 684 cm^{-1}; HRMS (CI): *m/z* calcd for $C_{13}H_{10}{}^{35}Cl_5{}^{37}Cl_1O_2H$: 410.8843 $[M+H]^+$; found: 410.8861.

2-(*tert*-Butyl)phenyl 2-phenylbutanoate (161a)[26e]

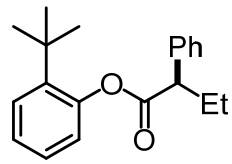

161a

Table 16, entry 5: A flame-dried Schlenk tube with a stir bar (10 mL; threaded PTFE plug) was charged with a CH_2Cl_2 solution of catalyst **Λ-T18'** (4.9 mg, 3.5 µmol, 3 mol%), the CH_2Cl_2 carefully removed under reduced pressure, and the Schlenk tube with the solidified catalyst dried *in vacuo* for 1 h. Then, dry toluene (9.5 mL) and 2-*tert*-butylphenol (**160**; 19.0 µL, 124 µmol, 1.05 eq) were added to this Schlenk tube. Another flame-dried Schlenk tube (2 mL; threaded PTFE plug) was charged with phenyl ethyl ketene (**153a**; 17.2 mg, 118 µmol, 1.00 eq) and dry toluene (0.25 mL). The ketene solution (**153a**) was then added to the other Schlenk tube via microliter syringe[155] and the ketene's Schlenk tube rinsed with dry toluene (0.25 mL) and

the resulting solution added to the reaction's Schlenk tube with the same microliter syringe in order to transfer the ketene as completely as possible. The reaction mixture was then stirred at rt for 2.5 h under nitrogen atmosphere after which TLC (hexanes/Et_2O 10:1) indicated full conversion. All volatiles were removed *in vacuo*, the crude product dissolved in CH_2Cl_2, adsorbed on silica gel, and purified by flash chromatography (hexanes/Et_2O 20:1). After solvent removal and drying *in vacuo*, desired **161a** was obtained as a colorless oil (22.0 mg, 74.2 µmol, 63%). Enantiomeric excess determined by chiral HPLC analysis: 13% ee (Chiralpak IC, 5 µm, 25 cm x 4.6 mm; *n*-hexane/*i*-PrOH 96:4, $\lambda = 254$ nm, 1.0 mL/min, *t* (column) = 25 °C; t_R (minor) = 4.0 min, t_R (major) = 4.5 min); ^{1}H NMR (300 MHz, $CDCl_3$): $\delta = 7.46–7.23$ (m, 6H), 7.21–7.06 (m, 2H), 6.84 (dd, $J = 7.6$ Hz, $J = 1.7$ Hz, 1H), 3.73 (t, $J = 7.7$ Hz, 1H), 2.39–2.19 (m, 1H), 2.06–1.86 (m, 1H), 8.90 (s, 9H), 1.01 (t, $J = 7.4$ Hz, 3H) ppm; ^{13}C NMR (75 MHz, $CDCl_3$): $\delta = 172.6$, 149.7, 141.2, 138.2, 128.9 (2C), 128.5 (2C), 127.6, 127.2, 126.9, 125.7, 123.7, 54.3, 34.5, 30.1 (3C), 26.5, 12.4 ppm; IR (film): $\tilde{\nu} = 1751$, 1185, 1137, 1107, 1090, 751, 697 cm^{-1}; HRMS (ESI): *m/z* calcd for $C_{20}H_{24}O_2Na$: 319.1679 [*M*+Na]$^+$; found: 319.1671.

4.10.7 Exemplary Michael Addition of Octanal (167b) to *trans-β*-Nitrostyrene (182)

The Michael addition of octanal (**167b**) to *trans-β*-nitrostyrene (**182**) to give Michael addition products **183b** and ***epi*-183b** with catalyst ***rac*-T29** from Table 23, entry 1 is described below. Other experiments from Table 23 were analogously performed.

Michael Addition Products 183b and *epi*-183b (Table 23, Entry 1)

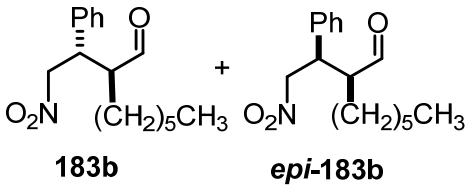

183b ***epi*-183b**

Table 23, entry 1: An amber glas vial[154] was charged with *trans-β*-nitrostyrene (**182**; 15.0 mg, 100 µmol, 1.00 eq), complex ***rac*-T29** (4.8 mg, 4.0 µmol, 4 mol%), and $NaBArF_{24}$ (5.3 mg, 6.0 µmol, 6 mol%). Then, dry toluene (100 µL) and freshly distilled octanal (**167b**; 23.5 µL, 150 µmol, 1.50 eq) were added, the vial capped with a PTFE-sealed screw cap[154] and the mixture stirred at rt for 30 h after which TLC indicated full conversion (hexanes/Et_2O 5:1). The solvent was removed *in vacuo*, the crude product dissolved in CH_2Cl_2, adsorbed on silica gel (42 °C), and purified by flash chromatography (hexanes/Et_2O 8:1 → 10:1). Diastereomers **183b** and ***epi*-183b** could be fully resolved and were obtained as colorless oils after solvent removal and drying *in vacuo* (first eluting diastereomer **183b**: 5.5 mg, 19.8 µmol, 20%; second eluting diastereomer ***epi*-183b**: 13.7 mg, 49.4 µmol, 49%; isolated d.r.: 2.5:1; total yield: 69%).

*Note: In a control experiment, the same reaction conditions gave no product when complex **rac-T29** was absent.*

I.) Analytical data for diastereomer **183b**:

^{1}H NMR (300 MHz, $CDCl_3$): δ = 9.41 (d, J = 3.0 Hz, 1H), 7.32–7.20 (m, 3H), 7.14–7.04 (m, 2H), 4.80–4.61 (m, 2H), 3.80–3.65 (m, 1H), 2.61–2.48 (m, 1H), 1.70–0.70 (m, 13) ppm; ^{13}C NMR (75 MHz, $CDCl_3$): δ = 203.5, 136.4, 129.3 (2C), 128.4 (2C), 128.4, 78.1, 53.7, 44.7, 31.6, 29.3, 27.7, 27.2, 22.7,14.1 ppm; IR (film): $\tilde{\nu}$ = 2954, 1722, 1552, 1378, 701 cm^{-1}; HRMS (ESI): *m/z* calcd for $C_{16}H_{23}N_1O_3Na$: 300.1570 [M+Na]$^+$; found: 300.1575.

II.) Analytical data for diastereomer ***ent*-183b**:

^{1}H NMR (300 MHz, $CDCl_3$): δ = 9.70 (d, J = 2.6 Hz, 1H), 7.41–7.25 (m, 3H), 7.23–7.12 (m, 2H), 4.79–4.56 (m, 2H), 3.77 (td, J = 9.5 Hz, J = 5.5 Hz, 1H), 2.76–2.60 (m, 1H), 1.66–0.71 (m, 13H) ppm; ^{13}C NMR (75 MHz, $CDCl_3$): δ = 203.3, 137.0, 129.3 (2C), 128.3, 128.2 (2C), 78.6, 54.1, 43.3, 31.5, 29.2, 27.5, 26.5, 22.5, 14.1 ppm; IR (film): $\tilde{\nu}$ = 2923, 2854, 1721, 1553, 1377, 700 cm^{-1}; HRMS (ESI): *m/z* calcd for $C_{16}H_{23}N_1O_3Na$ 300.1570 [M+Na]$^+$; found: 300.1570.

4.10.8 Preparation of Racemic References for Chiral HPLC Analysis

Racemic references for chiral HPLC analysis were obtained in case of the reactions from chapter 2. by relying on the procedures described in chapters 4.10.1–4.10.6 but by using 10–20 mol% of DMAP instead of the respective nucleophilic Ir(III) catalyst. In case of the reactions from chapter 3., racemic Ir(III) catalyst ***rac*-T29** was employed in the same way to obtain racemic references.

4.11 CD Spectra of Complexes Λ/Δ-(*S*)-T18, Λ/Δ-T18-(MeCN)$_2$, and Λ/Δ-T18

CD spectra were recorded of diastereomers **Λ-** and **Δ-(*S*)-T18**, bisacetonitrile intermediates **Λ-** and **Δ-T18-(MeCN)$_2$**, and precatalysts **Λ-** and **Δ-T18** in HPLC grade methanol or acetonitrile at 25.0 °C and conc = 0.20 mM using an actively thermostatted cell with a path length of d = 1.0 mm (Figures 40–42). Raw data obtained in millidegrees (θ [mdeg]) was converted into molar circular dichroism data (Δε [$M^{-1}\cdot cm^{-1}$]) with the aid of Eq. 3.[156]

$$\Delta\varepsilon\left[M^{-1}cm^{-1}\right] = \frac{\theta[\text{mdeg}]}{10 \cdot \text{conc}\left[\text{mol} \cdot L^{-1}\right] \cdot d[\text{cm}] \cdot 32980} \qquad \text{(Eq. 3)}$$

The absolute configurations of the iridium(III) complexes were assigned by comparison of the obtained CD spectra with literature reported CD spectra of closely related stereogenic-at-metal iridium(III) complexes.[38a,66,67,69] Importantly, absolute stereochemical assignments of the Ir(III) complexes from refs. 38a, 66, and 69 are based on X-ray structural analyses of enantiopure Ir(III) complex samples.

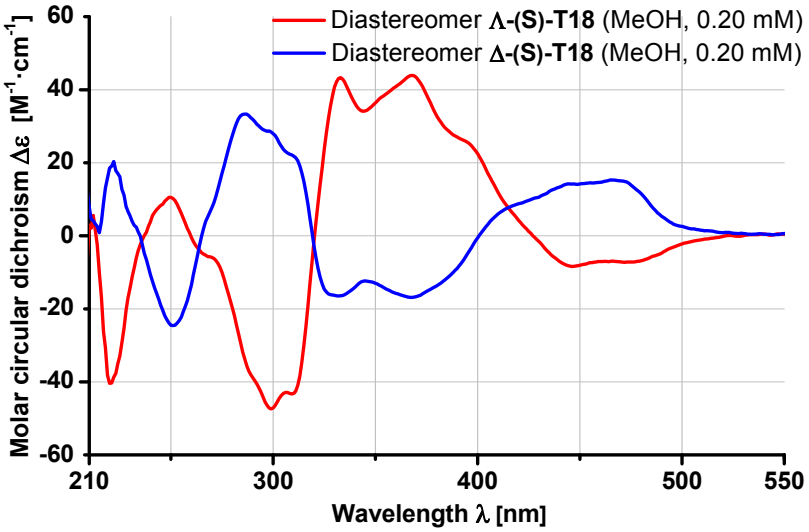

Figure 40. CD spectra of diastereomers **Λ-(*S*)-T18** and **Δ-(*S*)-T18**.

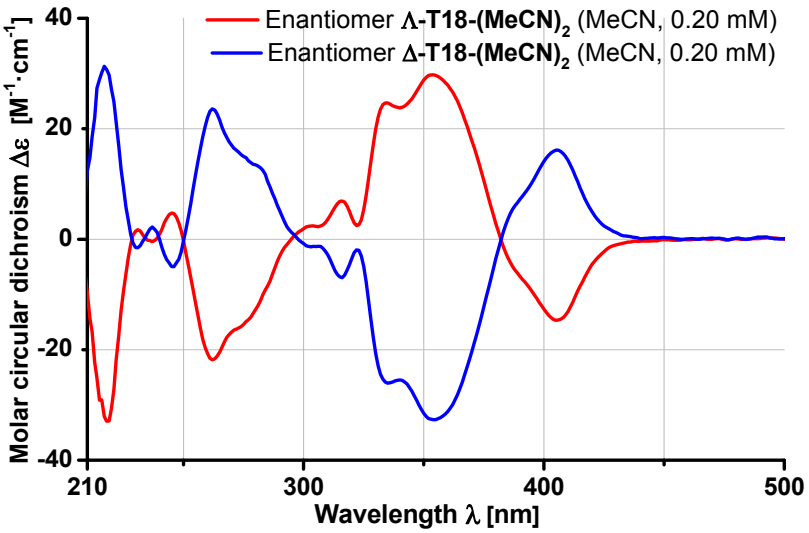

Figure 41. CD spectra of bisacetonitrile intermediates **Λ-T18-(MeCN)$_2$** and **Δ-T18-(MeCN)$_2$**.

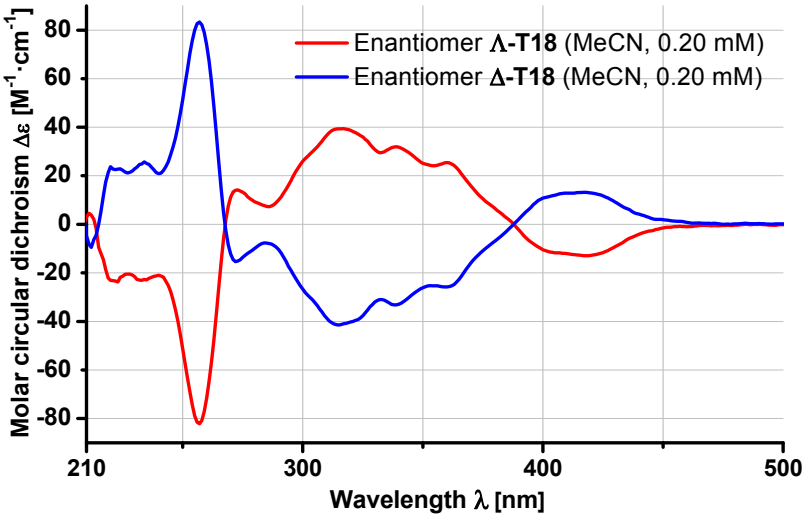

Figure 42. CD spectra of precatalysts **Λ-T18** and **Δ-T18**.

4.12 Preparation of Catalysis Intermediate Analog *rac*-T18-TfO

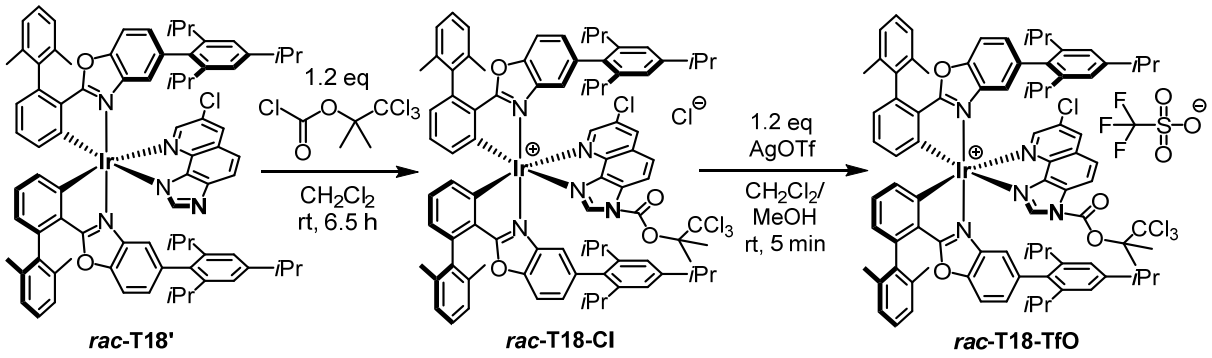

Scheme 97. Preparation of catalysis intermediate analog ***rac*-T18-TfO**.

A flask (10 mL) was charged with catalyst ***rac*-T18'** (310 mg, 222 µmol, 1.00 eq) and CH_2Cl_2 (1 mL). A solution of 2,2,2-trichloro-1,1-dimethylethyl chloroformate (62.8 mg, 262 µmol, 1.18 eq) in CH_2Cl_2 (3.5 mL) was added, the flask sealed with a septum, and the mixture stirred at rt for 6.5 h (formation of ***rac*-T18-Cl**). Then, a solution of AgOTf (67 mg, 261 µmol, 1.18 eq) in CH_2Cl_2/MeOH 1:1 (2 mL) was added and the mixture stirred at rt for 5 min. The mixture was subsequently diluted with CH_2Cl_2 and rapidly passed through a short plug of silica gel with CH_2Cl_2/MeOH 20:1. All volatiles were removed *in vacuo* at 32 °C (*higher temperatures lead to significant methanolysis of the product*), which yielded desired ***rac*-T18-TfO** as a yellow solid. ***Rac*-T18-TfO** was used without further purification and characterization to grow X-ray quality crystals as described in the crystallographic section.

Remarks:

- Prior to the synthesis of ***rac*-T18-TfO**, there had been attempts to crystallize primary chloride salt ***rac*-T18-Cl**. However, all crystal growing attempts with ***rac*-T18-Cl** had only provided tiny crystals unfeasible for X-ray diffraction analysis.

- When racemic catalyst ***rac*-T18'** (21 mg) was mixed with 3 eq of 2,2,2-trichloro-1,1-dimethylethyl chloroformate in a flame-dried NMR tube in dry CD_2Cl_2 (conc = 25 mM), full and clean conversion from ***rac*-T18'** to ***rac*-T18-Cl** took place in less than 10 min (formation of ***rac*-T18-Cl** confirmed by ^{1}H and ^{13}C NMR as well as by HRMS analysis).

4.13 ^{1}H NMR Spectra Comparisons

4.13.1 Comparison of Precatalyst Λ-T18 with Catalyst Λ-T18'

Figure 43 shows the ^{1}H NMR spectra of precatalyst **Λ-T18** (blue) and catalyst **Λ-T18'** (red). Both spectra are calibrated to the residual signal of CD_2Cl_2 (δ = 5.32 ppm).

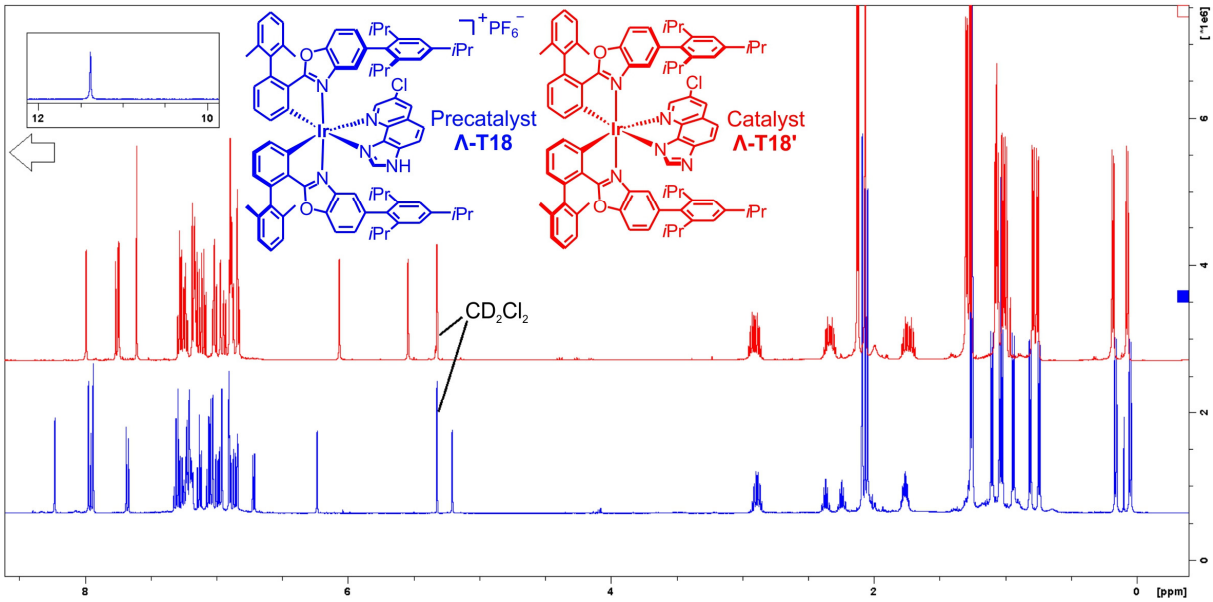

Figure 43. ^{1}H NMR spectra of precatalyst **Λ-T18** and catalyst **Λ-T18'** (500 MHz, CD_2Cl_2).

4.13.2 Comparison of Freshly Prepared Λ-T18' with Reisolated Λ-T18'

Figure 44 shows the ^{1}H NMR spectra of freshly prepared catalyst **Λ-T18'** (blue) and reisolated catalyst **Λ-T18'** (red; see chapter 2.3.3, Table 13, entries 14, 15 and the reisolation procedure from chapter 4.10.2.2). HPLC analysis revealed for both samples >99% ee (see chapter 5.2). Both spectra are calibrated to the residual signal of CD_2Cl_2 (δ = 5.32 ppm).

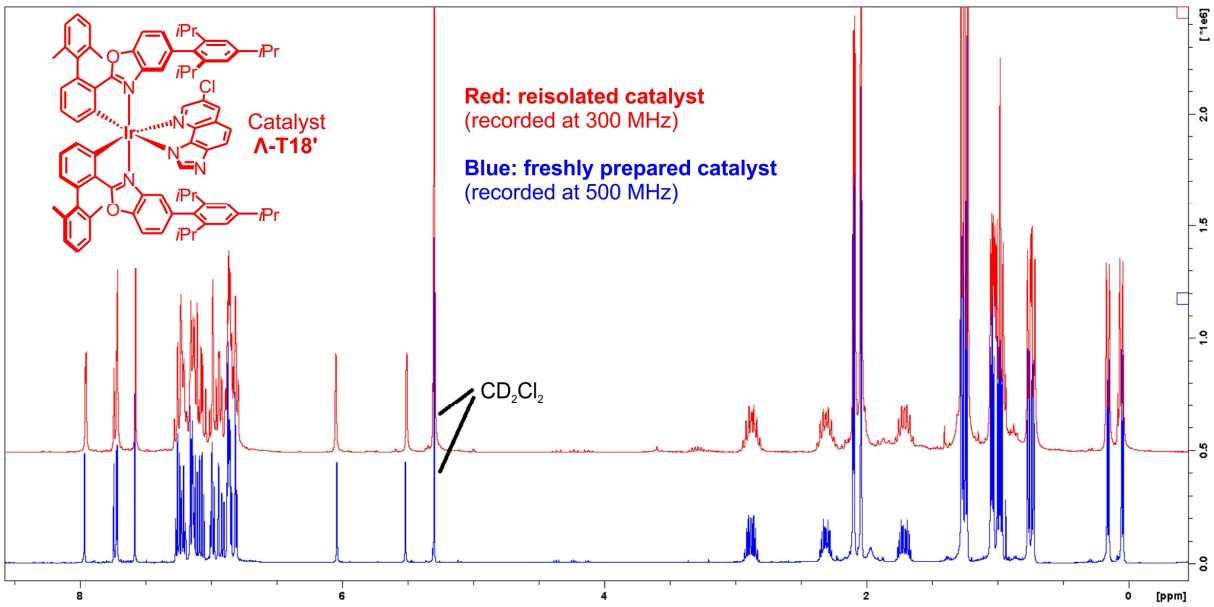

Figure 44. ^{1}H NMR spectra of freshly prepared and of reisolated catalyst **Λ-T18'** (CD_2Cl_2).

4.13.3 ^{1}H NMR Spectra of Enantiomeric Catalysts Λ-T18' and Δ-T18'

Figure 45 shows the ^{1}H NMR spectra of enantiomeric catalysts **Λ-T18** (blue) and **Δ-T18'** (red). Both spectra are calibrated to the residual signal of CD_2Cl_2 (δ = 5.32 ppm).

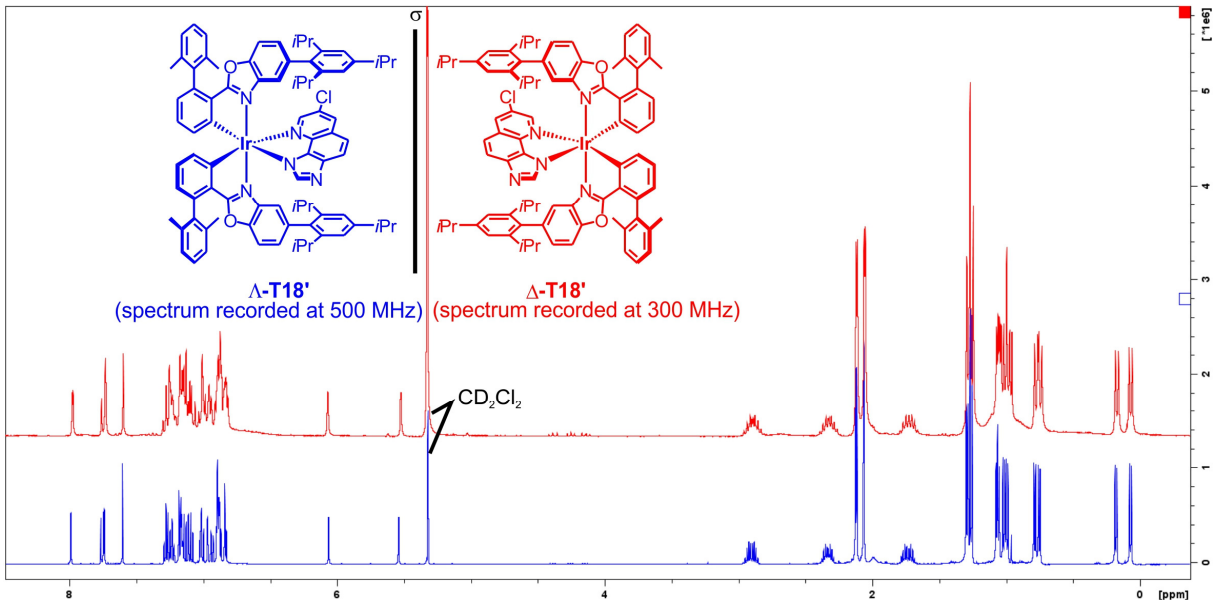

Figure 45. ^{1}H NMR spectra comparison of enantiomeric catalysts **Λ-T18'** and **Δ-T18'** (CD_2Cl_2).

4.14 Evaluation of the Stability of Catalyst Δ-T18' in Solution

Figure 46 shows the ^{1}H NMR spectra of freshly prepared catalyst **Δ-T18'** (green), catalyst **Δ-T18'** after one week in CD_2Cl_2 at 4 °C (blue), and catalyst **Δ-T18'** after one week in CD_2Cl_2 at 25 °C (red; for each experiment: 7 mg of catalyst **Δ-T18'** in 0.6 mL CD_2Cl_2). All spectra are calibrated to the residual signal of CD_2Cl_2 (δ = 5.32 ppm).

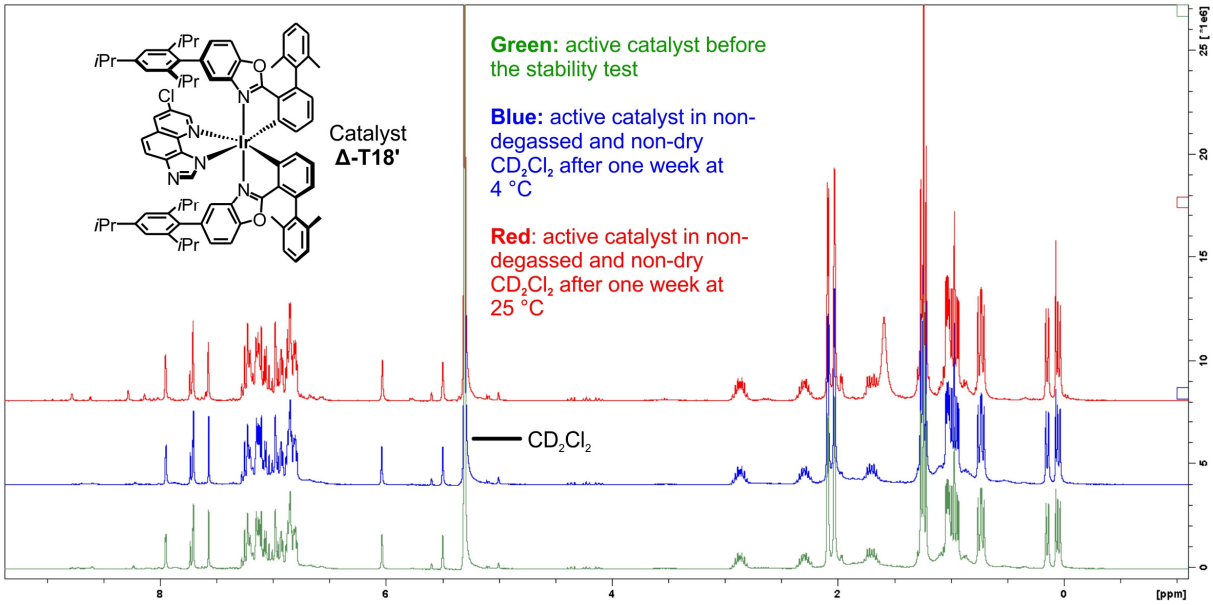

Figure 46. Catalyst **Δ-T18'** after one week in CD_2Cl_2 at 4 °C and at 25 °C (300 MHz, CD_2Cl_2).

While basically no decomposition is observable in case of the catalyst which was kept in CD_2Cl_2 for one week at 4 °C, traces of decomposition products are observable in case of the catalyst which was kept in CD_2Cl_2 for one week at 25 °C. However, when the latter catalyst sample was recovered and used without any purification in a catalysis experiment, exactly the same result was obtained as with freshly prepared catalyst (see chapter 2.3.2, Table 10, entries 11 and 12,). Furthermore, chiral HPLC analysis revealed for both samples >99% ee (see chapter 5.2). In this context, it is also worth mentioning that neither any decomposition nor any racemization of precatalyst **Λ/Δ-T18** or catalyst **Λ/Δ-T18'** were observed when they were stored as solids for about 6 months at 4 °C (refrigerator) under standard atmospheric conditions.

4.15 Mechanistic Experiments

4.15.1 Crossover Experiment with *O*-Acylated Benzofuranones

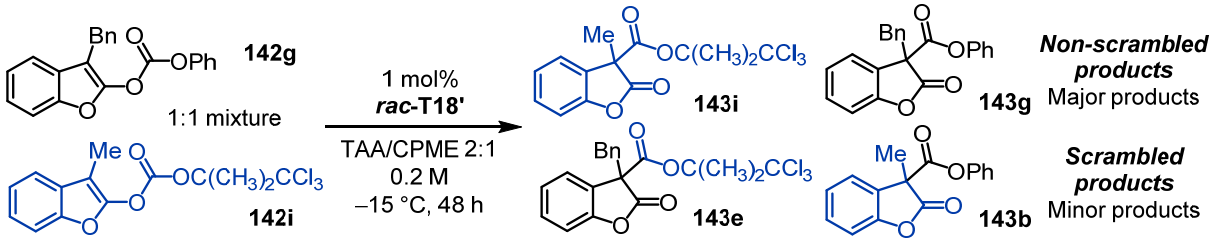

Scheme 98. Crossover experiment with *O*-acylated benzofuranones.

A flask was charged with substrate **142i** (50.9 mg, 145 µmol, 0.50 eq) and **142g** (49.7 mg, 144 µmol, 0.50 eq). Then, a solution of ***rac*-T18'** (4.1 mg, 2.94 µmol, 1.0 mol%) in 2:1 TAA/CPME (1.4 mL; conc = 0.2 M) was added at −15 °C and the mixture stirred for 48 h at −15 °C. All volatiles were removed *in vacuo* and the crude mixture analyzed by ^{1}H and ^{13}C NMR analysis (Figure 47). Both spectra confirmed the formation of scrambled **143b** and **143e** besides non-scrambled **143g** and **143i** (**143g**:**143i**:**143b**:**143e**; ratio approx. 4.5:4.5:1:1).

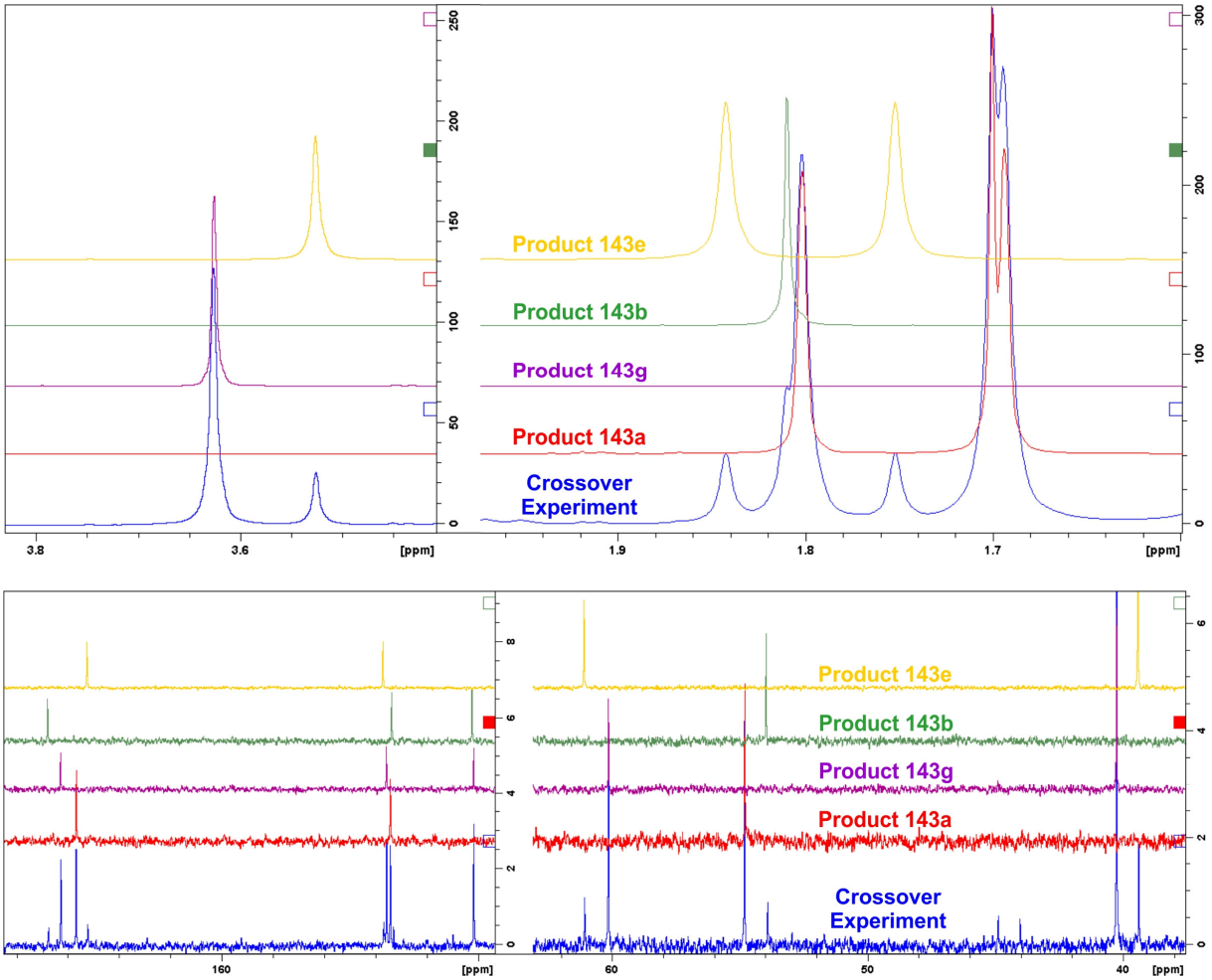

Figure 47. Excerpts from the ^{1}H NMR spectrum (top) and the ^{13}C NMR spectrum (bottom) of the crude mixture of the crossover experiment (blue) and the NMR spectra of the related pure products (300 MHz, $CDCl_3$).

4.15.2 Mixing of Catalyst *rac*-T18' with *p*-Chlorophenyl Isopropyl Ketene (153d)

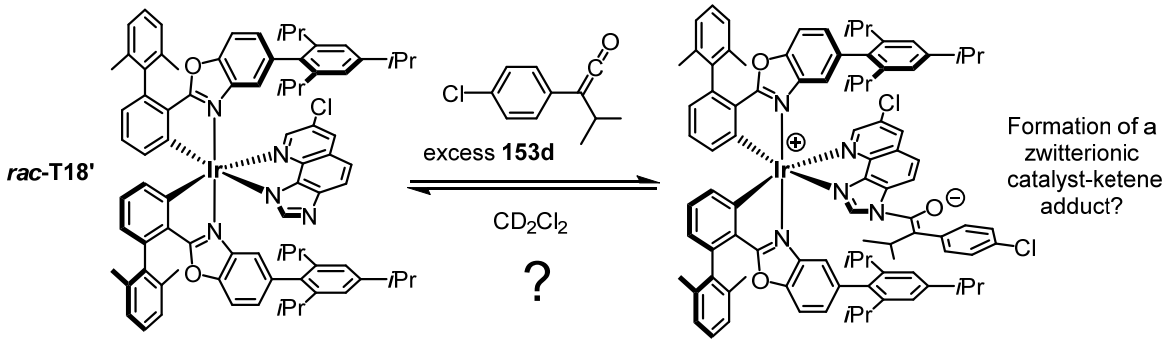

Scheme 99. Does mixing of catalyst ***rac*-T18'** with *p*-chlorophenyl isopropyl ketene (**153d**) lead to the formation of a zwitterionic ketene enolate species?

A flame-dried NMR-tube was charged with catalyst ***rac*-T18'** (33 mg, 23.6 µmol, 1.00 eq) and dry CD_2Cl_2 (0.65 mL) and an ^1H NMR spectrum was recorded. Then, 6 eq of *p*-chlorophenyl isopropyl ketene (**153d**) were added and again a spectrum recorded (15 min after initial mixing). Another 12 eq were added and a third spectrum was recorded (10 h after initial mixing). In addition, a spectrum of pure ketene **153d** was recorded.

Figure 48 shows all four spectra, each calibrated to the residual signal of CD_2Cl_2 (δ = 5.32 ppm). As it is apparent from Figure 48, the formation of a zwitterionic catalyst-ketene adduct, as depicted in Scheme 99, could not be observed with these NMR experiments.

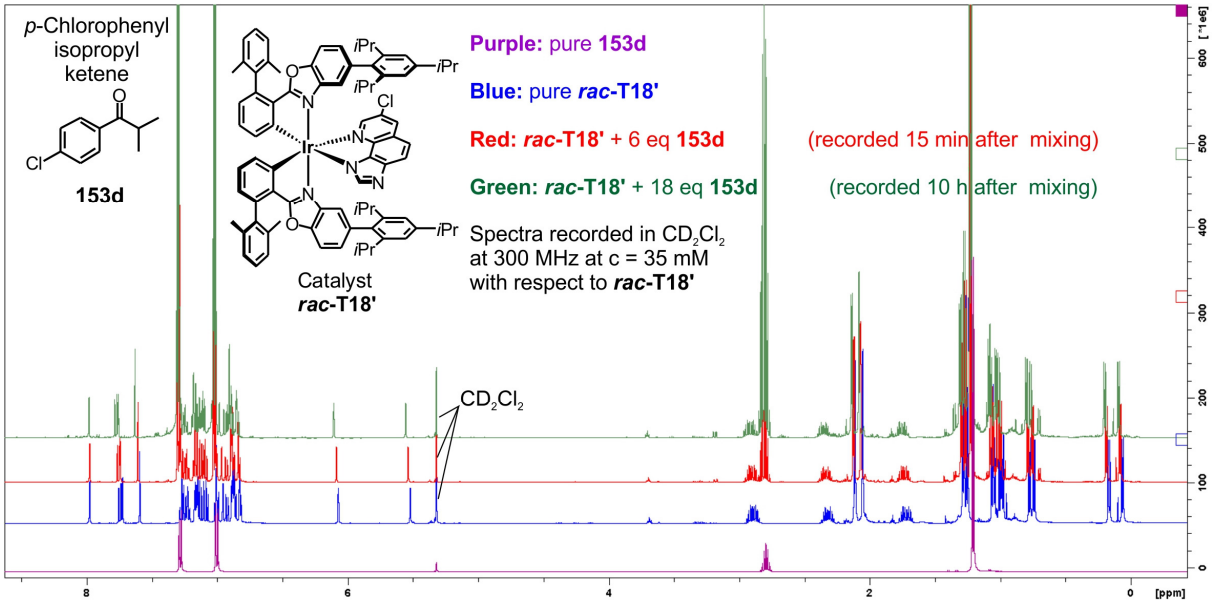

Figure 48. ^1H NMR spectra: Mixing of *p*-chlorophenyl isopropyl ketene (**153d**) with catalyst ***rac*-T18'** (300 MHz, CD_2Cl_2).

4.15.3 Mixing of Catalyst *rac*-T18' with 2-Cyanopyrrole (162)

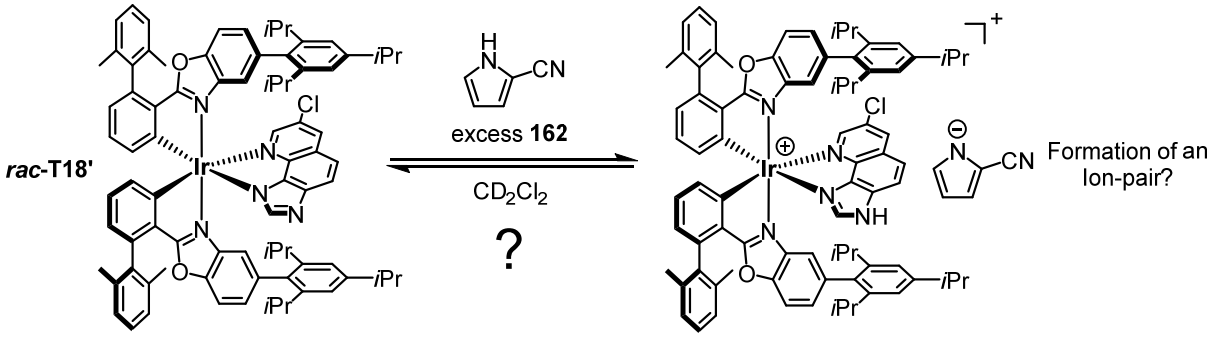

Scheme 100. Does Mixing of ***rac*-T18'** with 2-cyanopyrrole (**162**) lead to the formation of an ion-pair?

A flame-dried NMR-tube was charged with catalyst ***rac*-T18'** (15 mg, 10.7 µmol, 1.00 eq) and dry CD_2Cl_2 (0.65 mL) and an ^1H NMR spectrum was recorded. Then, 6 eq of 2-cyanopyrrole (**162**) were added and again a spectrum recorded (15 min after initial mixing). Another 12 eq were added and a third spectrum was recorded (2 h after initial mixing). In addition, two spectra were recorded of pure 2-cyanopyrrole (**162**) in CD_2Cl_2, one with 5 µL (6 eq) of **162** and one with 15 µL (18 eq) of **162**.

Figures 49–51 show all five spectra and additionally the spectrum of precatalyst ***rac*-T18** (spectrum on the top). The signals of catalyst ***rac*-T18'** and its HPF_6 salt ***rac*-T18** differ from each other in particular in the downfield region of their spectra. Excess of **162** with respect to ***rac*-T18'** causes these decisive signals of ***rac*-T18'** to shift downfield towards the δ-values of its corresponding HPF_6 salt ***rac*-T18**, which indicates an interaction between the acidic proton of 2-cyanopyrrole (**162**) and the basic nitrogen of the imidazoquinoline ligand of ***rac*-T18'**.

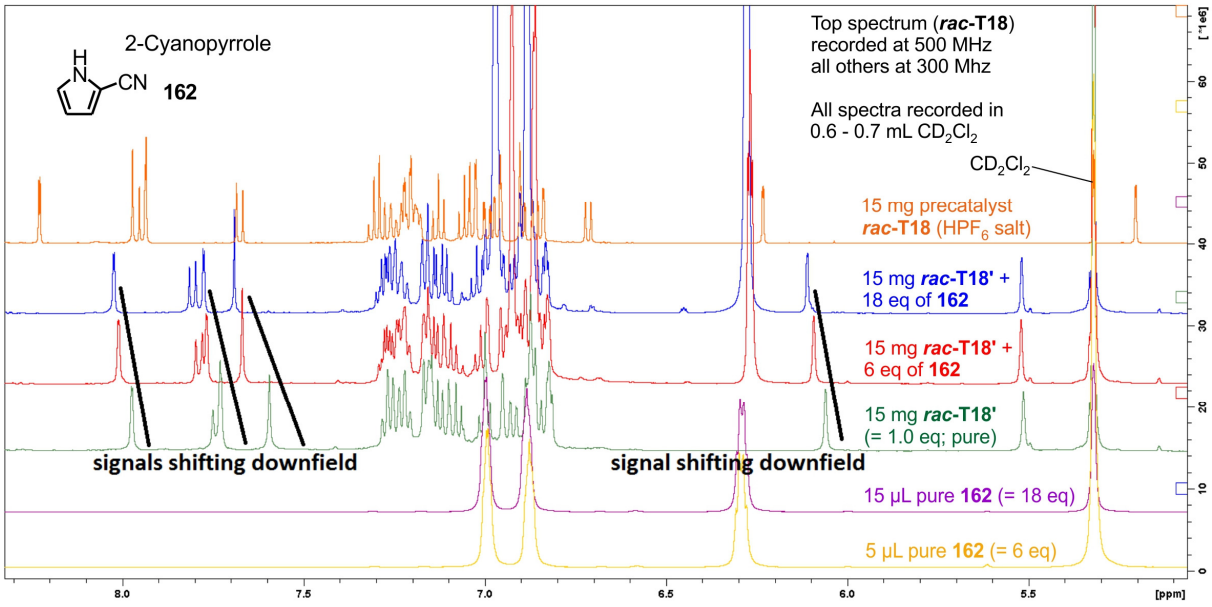

Figure 49. ^1H NMR spectra: Mixing of 2-cyanopyrrole (**162**) with catalyst ***rac*-T18'** (δ-range depicted from 8.5–5.0 ppm; recorded in CD_2Cl_2).

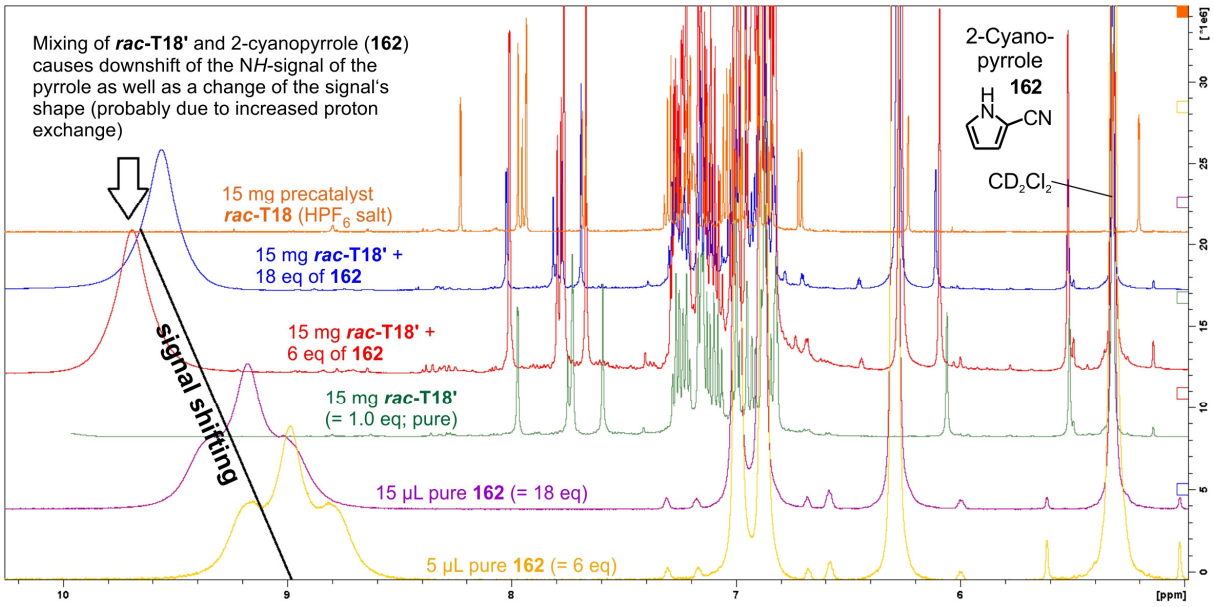

Figure 50. ^{1}H NMR spectra: Mixing of 2-cyanopyrrole (**162**) with catalyst ***rac*-T18'** (δ-range depicted from 10–5.0 ppm; recorded in CD_2Cl_2).

In addition, a change of the N*H*-signal's shape is observable (see Figure 50). This shape alteration can be explained with an increased proton exchange caused by the interaction of the acidic N*H* of **162** with Brønsted basic ***rac*-T18'**. This is further affirmed by the fact that the presence of ***rac*-T18'** in case of 6 eq of **162** leads to a downshift of the N*H*-signal of almost 1 ppm (see Figure 50). In this context, it should be noted that the N*H*-signal of HPF_6 salt ***rac*-T18** appears at about δ = 11–12 ppm (see Figure 51). The presence of 18 eq of **162** results in a smaller downshift than 6 eq of **162**, which is understandable taking into account that a smaller absolute fraction of **162** is then in interaction with ***rac*-T18'** (see Figure 50). Figure 51 shows the same spectra as Figures 49 and 50 but the entire ppm δ-range from 12–0 ppm.

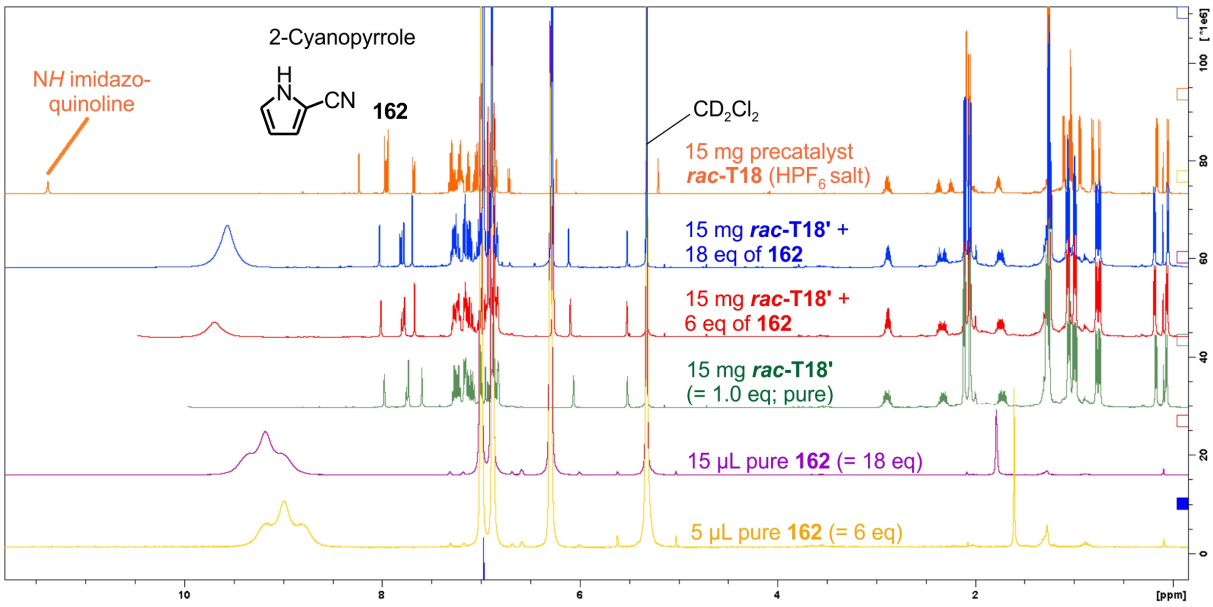

Figure 51. ^{1}H NMR spectra: Mixing of 2-cyanopyrrole (**162**) with catalyst ***rac*-T18'** (entire δ-range from from 12–0 ppm; recorded in CD_2Cl_2).

Apparently, ***rac*-T18'** and 2-cyanopyrrole (**162**) do not react under ion-pair formation as depicted in Scheme 100. However, it is apparent from Figures 49–51 that there are strong indications for a hydrogen-bonding interaction between the basic imidazoquinoline ligand of ***rac*-T18'** and the acidic proton of **162**.

4.15.4 Inactivity of *N*-Methylated Λ-T18-Me and Inactivity of Λ-T18 in Absence of Base

The experiments in Scheme 101 below show that precatalyst **Λ/Δ-T18** in not catalytically active in the absence of a Brønsted base and that *N*-methylated complex **Λ/Δ-T18-Me** is neither catalytically active in the absence nor in the presence of a Brønsted base.

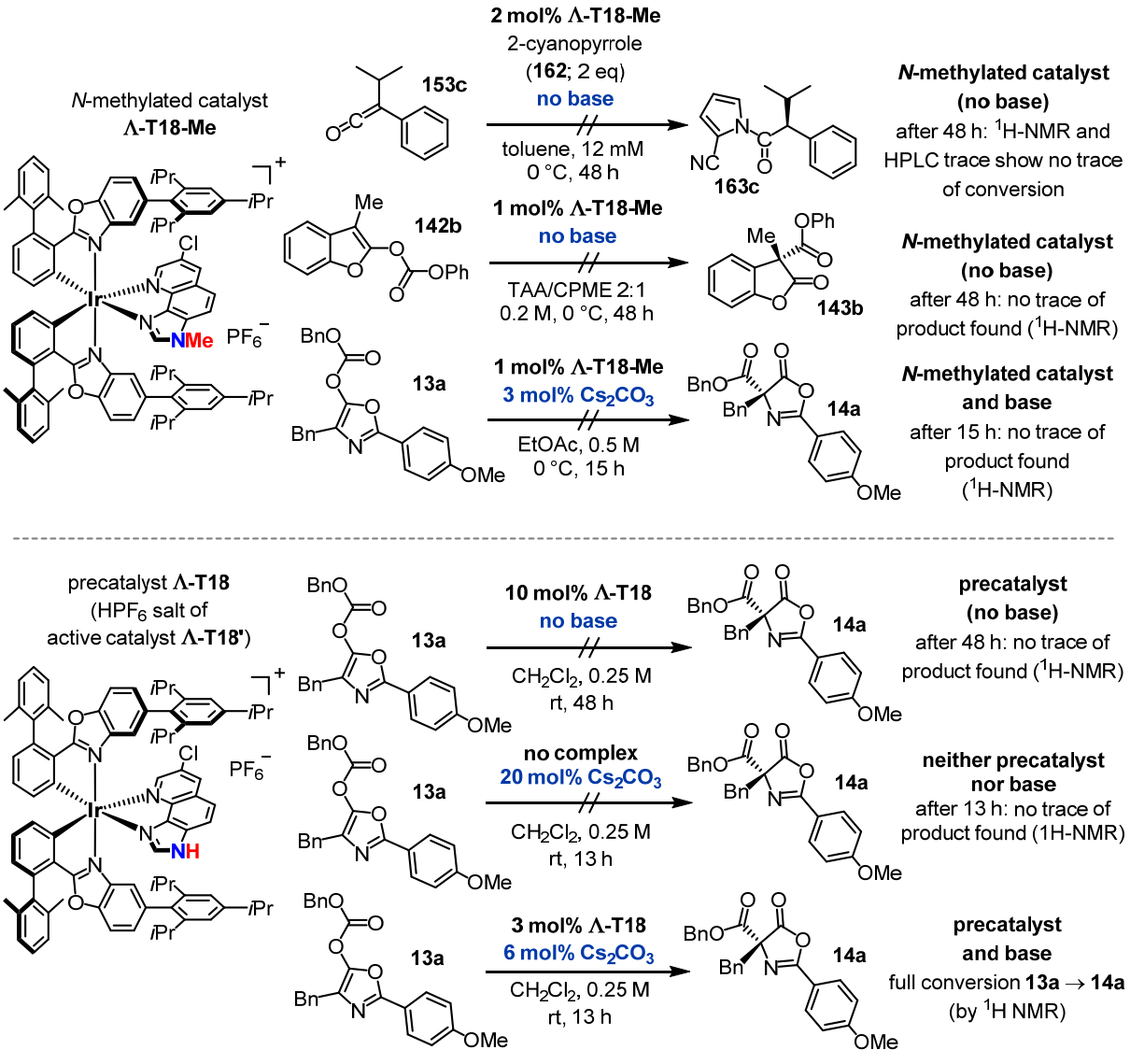

Scheme 101. *Top*: Catalytic activity experiments with *N*-methylated **Λ-T18-Me**.
Bottom: Catalytic activity experiments with precatalyst **Λ-T18**.

4.16 Quantum Chemical Calculations

The quantum chemical calculations included in the present thesis and described in detail in chapters 4.16.1 and 4.16.2 were planned in close collaboration with and designed and performed by cooperation partner Michael G. Medvedev, who was at the time of the calculations affiliated with the 'A. N. Nesmeyanov Institute of Organoelement Compounds RAS'[94] and with the 'N. D. Zelinsky Institute of Organic Chemistry RAS'[95] (ORCID M. G. M.: 0000-0001-7070-4052).

4.16.1 Quantum Chemical Modeling of the Conformations of *rac*-T18-TfO

The molecular geometries of the two conformers of the ***rac*-T18-TfO** complex cation – one with the carbonyl group oriented towards the quinoline subunit and one with it oriented otherwise (see chapter 2.3.8, Figure 22; conformers A and B) – were optimized at the PBE0[96]-D3[97]/IMCP-SR1[98,99]//PBE0-D3/SBKJC[100] SMD[101] (butanol) level of theory using the GAMESS-US[157] program package. The PBE0 functional was chosen because it is known to be accurate for organic chemistry calculations[96b] and has recently been shown to be well-grounded in theory.[96c] The IMCP-SR1 basis set was chosen as it incorporates scalar-relativistic effects, which are important for heavy elements, such as iridium in the studied case,[99] and belongs to model core potential basis sets which retain the correct nodal structures of atoms.[98]

The calculations revealed that the π-conjugated conformer which was also found in the crystal structure of ***rac*-T18-TfO** is about 5.3 kcal·mol^{-1} lower in energy than the alternative one.

4.16.2 Quantum Chemical Modeling of the Black Rearrangement's Stereogenic Step

The chirality-introducing step of the Black rearrangement is the nucleophilic attack of the benzofuranone enolate to the trigonal carbonyl atom of the corresponding *N*-acylated catalyst (see for example **Λ-T18-Int** in chapter 2.3.8, Scheme 36). The approaching routes available for the enolate are defined by two criteria: (1.) The two approaching carbons should have their bonds in staggered conformation and (2.) the benzene ring of the incoming enolate should not encounter with the closely disposed 2,6-dimethylphenyl group. These requirements led to the four possible transition states (TSs), which are depicted in chapter 2.3.8, Figure 25. The methods which led to their location are described in the following paragraphs.

To establish the true mechanism of the reaction, it was attempted to locate each of the corresponding TSs (see chapter 2.3.8, Figure 25). The reaction leading to product **143h** from substrate **142h** with $R_1 = R_2 =$ Me was modeled with model catalyst **Λ-T18'-QM** lacking the non-involved 2,6-dimethylphenyl group, the non-involved methyl group of the involved 2,6-dimethylphenyl group and two non-involved isopropyl groups of the involved 2,4,6-triiso-

propylphenyl group (**Λ-T18'-QM** is depicted in chapter 2.3.8, Figure 24). "Involved" ["non-involved"] means in this context that the said group is [not] part of the 'active center' and is [not] involved in the shaping of the mentioned 'molecular cavity'. Consequently, the shape of the catalyst's active center / molecular cavity remained entirely unchanged by these simplifications (compare Figures 23 and 26 from chapter 2.3.8 for an illustration).

The methodology applied to locate each of the four possible TSs is described in detail in ref. 158 and is an advanced version of the one recently applied by M. G. M. and co-workers to locate all 728 TSs feasible for an SpnF-catalyzed Diels–Alder cycloaddition.[107,158] At first, it was aimed to get as good transition state guesses as possible. Therefore, the geometries of four manually constructed initial TS guesses were optimized at the PBE0[96]-D3[97]/SBKJC[100] SMD[101](butanol) level of theory in GAMESS-US[157] with harmonic constraints on the forming C-C bonds (one constraint per TS), which held their lengths to be closely around 2.2 Å. The PBE0 functional was chosen because it is known to be accurate for organic chemistry calculations[96b] and has recently been shown to be well-grounded in theory.[96c]

After convergence of the preliminary geometry optimizations, the Hessians were computed for each conformation at the PBE[159]/SBKJC SG1 level of theory. Then, the actual searches for transition states were initiated at the PBE0-D3/SBKJC SMD(butanol) level of theory with QA[160] optimization algorithm (maximum step: 0.05 Bohr) using the calculated Hessians as initial guesses and updating them on each step using the POWELL[161] method.

After convergence of the transition state searches, single-point energy calculations were performed at the PBE0-D3/IMCP-SR1[98] SMD(butanol) level of theory. The IMCP-SR1 basis set was chosen for the final energy evaluations as it incorporates scalar-relativistic effects, which are important for heavy elements, such as iridium in the studied case,[99] and belongs to model core potential basis sets which retain the correct nodal structures of atoms.[98] Importantly, the performed calculations benefit from a favorable error cancellation, which rises from the fact that the studied TSs are very similar in nature, so systematic errors in them largely cancel out.[107,109]

In order to account for the interplay between the located transition states, the Curtin–Hammett principle[108] was finally invoked by M. G. M. to calculate the percentaged contribution (C) of each of the four transition states, which is described in detail in chapter 2.3.8. Based on the percentaged contributions (C), an enantiomeric excess of 48.4% (*R*) was calculated for product **143h**, which is, in consideration of the applied approximations, in a very good agreement with the experimentally found 70% ee (*R*) for product **143h** with actual catalyst **Λ-T18'** (see chapter 2.3.3, Table 13, entry 11).

4.17 Crystallographic Data

Single crystal X-ray diffraction data were collected at a temperature of 100 K (***rac*-T18-dimer**, ***rac*-T18'**, ***rac*-T18-TfO**) or 110 K (**(*S*)-143i**) on a Bruker D8 Quest diffractometer using Mo-Kα-radiation (Incoatec Microsource) and a PHOTON 100 CMOS area detector system. Scaling and absorption correction was performed by using the SADABS[162] software package from Bruker. Structures were solved using direct methods in SHELXT[163] and refined using the full-matrix least-squares procedure in SHELXL.[164] Hydrogen atoms were placed in calculated positions and refined as riding on their respective C atom and U_{iso}(H) was set at 1.2 $U_{eq}(C_{sp2})$ and 1.5 $U_{eq}(C_{sp3})$. Disorder was refined using restraints for both the geometry and the anisotropic displacement factors.

Structures of ***rac*-T18-dimer**, catalyst ***rac*-T18'**, catalysis intermediate analog ***rac*-T18-TfO**, and catalysis product **(*S*)-143i** are depicted in Figures 52–55. The corresponding crystal data and details of the structure determination are presented in Tables 24–27. The four structures have been deposited in the Cambridge Structural Database (http://www.ccdc.cam.ac.uk/) as CCDC 1536877 for ***rac*-T18-dimer**, CCDC 1536878 for ***rac*-T18'**, CCDC 1536879 for ***rac*-T18-TfO**, and CCDC 1545358 for **(*S*)-143i**.

Iridium(III) Dimer *rac*-T18-dimer. X-ray quality crystals of ***rac*-T18-dimer** were obtained by slow diffusion of MeOH into a concentrated acetone solution of ***rac*-T18-dimer** at rt (vapor diffusion technique).

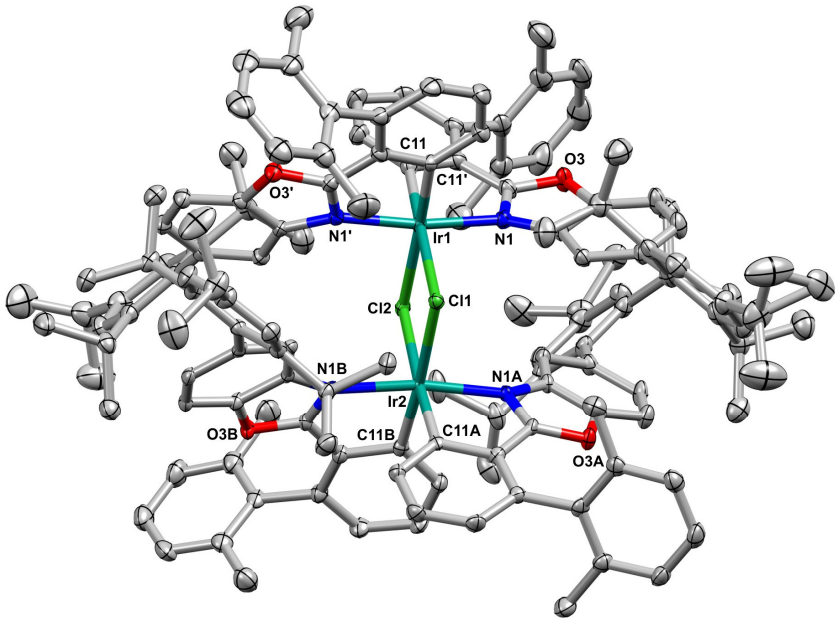

Figure 52. Crystal structure of iridium(III) dimer ***rac*-T18-dimer** with 50% probability of thermal ellipsoids. Cocrystallized solvent molecules and positional disorder are omitted for clarity (CCDC 1536877).[85]

Catalyst *rac*-T18'. X-ray quality crystals of catalyst ***rac*-T18'** were obtained by slow evaporation of CH_2Cl_2 out of a CH_2Cl_2/MeCN solution of ***rac*-T18'** at rt (low solubility of ***rac*-T18'** in MeCN; slow evaporation technique).

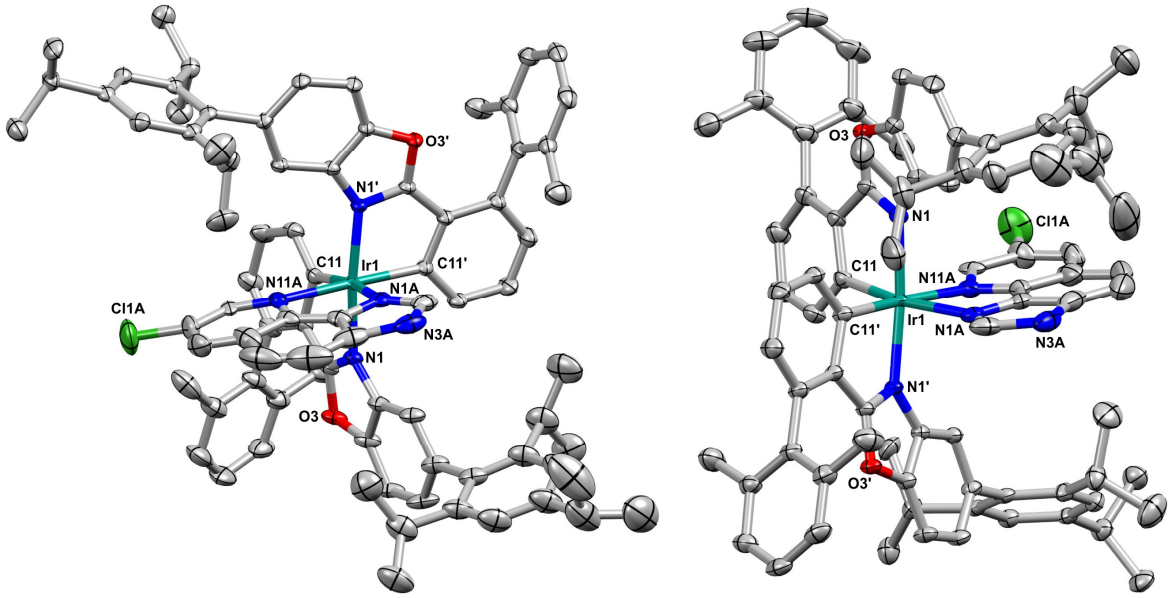

Figure 53. Structure of active catalyst **Λ-T18'** with 50% probability of thermal ellipsoids generated from the crystal structure obtained for ***rac*-T18'**. Cocrystallized solvent molecules and positional disorder are omitted for clarity.[85] **Λ-T18'** is shown from two different perspectives (CCDC 1536878).

Catalysis Intermediate Analog *rac*-T18-TfO. X-ray quality crystals of catalysis intermediate analog ***rac*-T18-TfO** were obtained by slow diffusion of *n*-hexane into a concentrated toluene solution of ***rac*-T18-TfO** at rt (vapor diffusion technique).

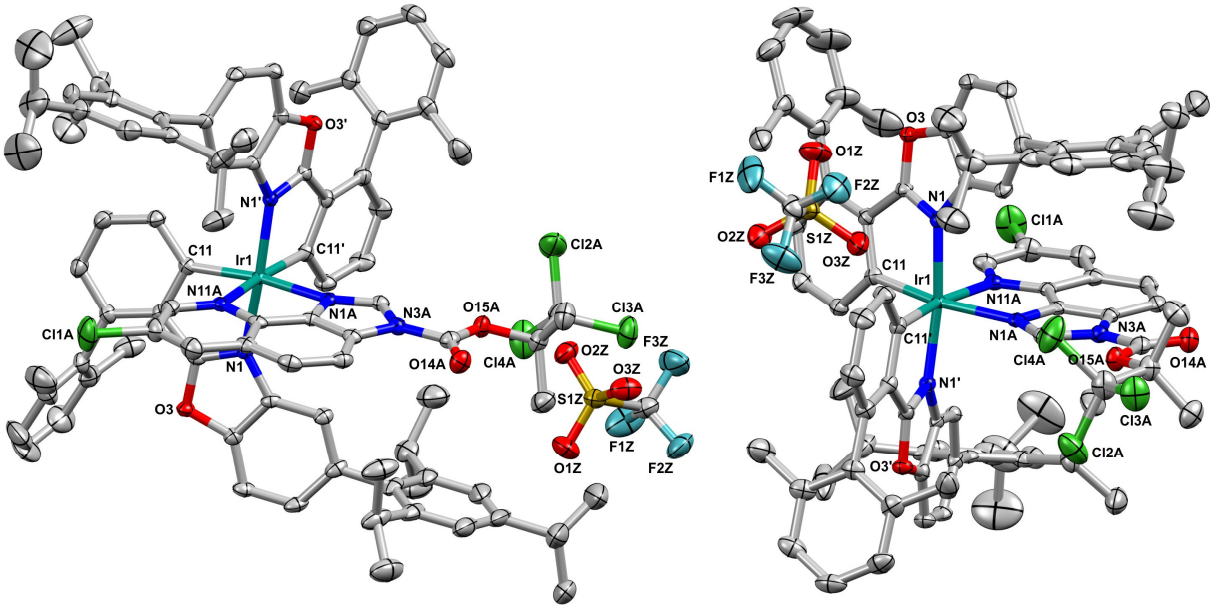

Figure 54. Structure of catalysis intermediate analog **Λ-T18-TfO** with 60% probability of thermal ellipsoids generated from the crystal structure obtained for ***rac*-T18-TfO**. Cocrystallized solvent molecules and positional disorder are omitted for clarity (CCDC 1536879).[85]

C-Acylated Benzofuranone (*S*)-143i

X-ray quality crystals of *C*-acylated benzofuranone **143i** were obtained by slow evaporation from a solution of **143i** in Et_2O at 4 °C (batch from Table 13, entry 13 with 93% ee). The absolute configuration of **143i** present in the measured crystal was determined as *S* using the anomalous dispersion method (Flack parameter: 0.012(12)).[165] This result is in accordance with the assignment for *C*-acylated benzofuranone **143e** based on the literature known optical rotation of **143e** (see chapter 4.10.2 for details) as well as in accordance with the calculated enantiomeric excess for *C*-acylated benzofuranone **143h** (see chapter 4.16 for details).

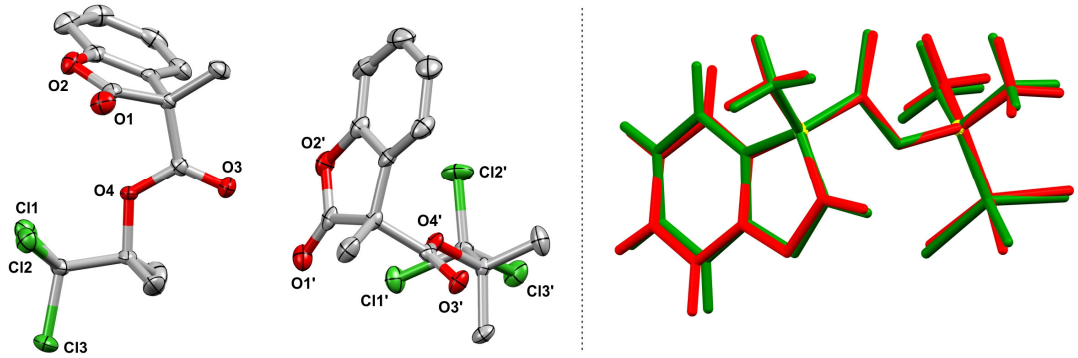

Figure 55. *Left:* Structure of both symmetry-independent molecules **(*S*)-143i** in the asymmetric unit with 60% probability of thermal ellipsoids (CCDC 1545358).[85] *Right*: Molecular overlay of the two symmetry-independent molecules.

Table 24. Crystal data and structure refinement for TCDimer_0m (= *rac*-T18-dimer).

Crystal data		
Identification code	TCDimer_0m	
Habitus, colour	prism, pale yellow	
Crystal size	0.51 x 0.42 x 0.20 mm^3	
Crystal system	Triclinic	
Space group	P-1	Z = 2
Unit cell dimensions	a = 16.2758(9) Å	α = 77.283(2)°.
	b = 16.4350(9) Å	β = 83.441(2)°.
	c = 27.5378(14) Å	γ = 65.571(2)°.
Volume	6540.0(6) $Å^3$	
Cell determination	9331 peaks with Theta 2.3 to 25.3°.	
Empirical formula	$C_{153}\,H_{170}\,Cl_2\,Ir_2\,N_4\,O_7$	
Moiety formula	$C_{144}\,H_{152}\,Cl_2\,Ir_2\,N_4\,O_4$, $3(C_3\,H_6\,O)$	
Formula weight	2632.22	
Density (calculated)	1.337 Mg/m^3	
Absorption coefficient	2.132 mm^{-1}	
F(000)	2720	
Data collection:		
Diffractometer type	Bruker D8 QUEST area detector	
Wavelength	0.71073 Å	
Temperature	100(2) K	
Theta range for data collection	2.242 to 25.325°.	
Index ranges	-19<=h<=19, -19<=k<=19, -33<=l<=33	
Data collection software	APEX3 (Bruker AXS Inc., 2015)[166]	
Cell refinement software	SAINT V8.35A (Bruker AXS Inc., 2015)[167]	
Data reduction software	SAINT V8.35A (Bruker AXS Inc., 2015)	
Solution and refinement:		
Reflections collected	139346	
Independent reflections	23847 [R(int) = 0.0410]	
Completeness to theta = 25.242°	99.9 %	
Observed reflections	20411[I > 2σ(I)]	
Reflections used for refinement	23847	
Absorption correction	Semi-empirical from equivalents[162]	
Max. and min. transmission	0.68 and 0.46	
Largest diff. peak and hole	1.330 and -1.228 e.$Å^{-3}$	
Solution	Direct methods	
Refinement	Full-matrix least-squares on F^2	
Treatment of hydrogen atoms	Calculated positions, constr. ref.	
Programs used	XT V2014/1 (Bruker AXS Inc., 2014)[163]	
	SHELXL-2014/7 (Sheldrick, 2014)[164]	
	DIAMOND (Crystal Impact)[168]	
	ShelXle (Hübschle, Sheldrick, Dittrich, 2011)[169]	
Data / restraints / parameters	23847 / 39 / 1562	
Goodness-of-fit on F^2	1.037	
R index (all data)	wR2 = 0.0559	
R index conventional [I > 2σ(I)]	R1 = 0.0254	

Table 25. Crystal data and structure refinement for TCracneu2_0m_sq (= *rac*-T18').

Crystal data

Identification code	TCracneu2_0m_sq	
Habitus, colour	plate, yellow	
Crystal size	0.26 x 0.21 x 0.11 mm^3	
Crystal system	Triclinic	
Space group	P-1	Z = 2
Unit cell dimensions	a = 13.1876(8) Å	α = 102.843(2)°.
	b = 14.7823(8) Å	β = 95.416(2)°.
	c = 20.8556(12) Å	γ = 106.648(2)°.
Volume	3743.0(4) $Å^3$	
Cell determination	9435 peaks with Theta 2.7 to 27.6°.	
Empirical formula	$C_{83.65}$ $H_{83.50}$ Cl Ir $N_{5.83}$ O_2	
Moiety formula	C_{82} H_{81} Cl Ir N_5 O_2, 0.826(C_2 H_3 N)	
Formula weight	1430.06	
Density (calculated)	1.269 Mg/m^3	
Absorption coefficient	1.869 mm^{-1}	
F(000)	1472	

Data collection:

Diffractometer type	Bruker D8 QUEST area detector
Wavelength	0.71073 Å
Temperature	100(2) K
Theta range for data collection	2.148 to 27.639°.
Index ranges	-17<=h<=17, -19<=k<=19, -27<=l<=27
Data collection software	APEX3 (Bruker AXS Inc., 2015)[166]
Cell refinement software	SAINT V8.35A (Bruker AXS Inc., 2015)[167]
Data reduction software	SAINT V8.35A (Bruker AXS Inc., 2015)

Solution and refinement:

Reflections collected	157290
Independent reflections	17277 [R(int) = 0.0452]
Completeness to theta = 25.242°	99.9 %
Observed reflections	15431[I > 2σ(I)]
Reflections used for refinement	17277
Absorption correction	Semi-empirical from equivalents[162]
Max. and min. transmission	0.82 and 0.66
Largest diff. peak and hole	2.986 and -1.566 e.$Å^{-3}$
Solution	Direct methods
Refinement	Full-matrix least-squares on F^2
Treatment of hydrogen atoms	Calculated positions, constr. ref.
Programs used	XT V2014/1 (Bruker AXS Inc., 2014)[163]
	SHELXL-2014/7 (Sheldrick, 2014)[164]
	DIAMOND (Crystal Impact)[168]
	ShelXle (Hübschle, Sheldrick, Dittrich, 2011)[169]
	PLATON ("SQUEEZE")[170]
Data / restraints / parameters	17277 / 316 / 961
Goodness-of-fit on F^2	1.057
R index (all data)	wR2 = 0.0810
R index conventional [I > 2σ(I)]	R1 = 0.0322

Table 26. Crystal data and structure refinement for TCZPOTf_0m (= *rac*-T18-TfO).

Crystal data

Identification code	TCZPOTf_0m	
Habitus, colour	plate, yellow	
Crystal size	0.37 x 0.17 x 0.08 mm^3	
Crystal system	Triclinic	
Space group	P-1	Z = 2
Unit cell dimensions	a = 16.3328(8) Å	α = 101.062(2)°.
	b = 18.4786(9) Å	β = 113.044(2)°.
	c = 19.2514(10) Å	γ = 91.864(2)°.
Volume	5209.8(5) $Å^3$	
Cell determination	9726 peaks with Theta 2.2 to 25.3°.	
Empirical formula	C_{115} H_{125} Cl_4 F_3Ir N_5 O_7 S	
Moiety formula	C_{87} H_{87} Cl_4Ir N_5 O_4, C F_3 O_3 S, 3(C_7 H_8), C_6 H_{14}	
Formula weight	2112.25	
Density (calculated)	1.346 Mg/m^3	
Absorption coefficient	1.467 mm^{-1}	
F(000)	2188	

Data collection:

Diffractometer type	Bruker D8 QUEST area detector
Wavelength	0.71073 Å
Temperature	100(2) K
Theta range for data collection	2.194 to 25.335°.
Index ranges	-19<=h<=19, -22<=k<=22, -23<=l<=23
Data collection software	APEX3 (Bruker AXS Inc., 2015)[166]
Cell refinement software	SAINT V8.35A (Bruker AXS Inc., 2015)[167]
Data reduction software	SAINT V8.35A (Bruker AXS Inc., 2015)

Solution and refinement:

Reflections collected	169407
Independent reflections	18983 [R(int) = 0.0425]
Completeness to theta = 25.242°	99.9 %
Observed reflections	17508[I > 2σ(I)]
Reflections used for refinement	18983
Absorption correction	Semi-empirical from equivalents[162]
Max. and min. transmission	0.89 and 0.75
Largest diff. peak and hole	1.140 and -0.837 e.$Å^{-3}$
Solution	Direct methods
Refinement	Full-matrix least-squares on F^2
Treatment of hydrogen atoms	Calculated positions, constr. ref.
Programs used	XT V2014/1 (Bruker AXS Inc., 2014)[163]
	SHELXL-2014/7 (Sheldrick, 2014)[164]
	DIAMOND (Crystal Impact)[168]
	ShelXle (Hübschle, Sheldrick, Dittrich, 2011)[169]
Data / restraints / parameters	18983 / 324 / 1316
Goodness-of-fit on F^2	1.065
R index (all data)	wR2 = 0.0733
R index conventional [I > 2σ(I)]	R1 = 0.0286

Table 27. Crystal data and structure refinement for TCEN1_0m (= (*S*)-143i).

Crystal data		
Identification code	TCEN1_0m	
Habitus, colour	needle, colourless	
Crystal size	0.511 x 0.059 x 0.042 mm^3	
Crystal system	Monoclinic	
Space group	$P2_1$	Z = 4
Unit cell dimensions	a = 7.1346(3) Å	α = 90°.
	b = 14.8376(6) Å	β = 98.492(2)°.
	c = 15.0064(6) Å	γ = 90°.
Volume	1571.17(11) $Å^3$	
Cell determination	9800 peaks with Theta 2.7 to 27.5°.	
Empirical formula	C_{14} H_{13} Cl_3 O_4	
Moiety formula	C_{14} H_{13} Cl_3 O_4	
Formula weight	351.59	
Density (calculated)	1.486 Mg/m^3	
Absorption coefficient	0.594 mm^{-1}	
F(000)	720	
Data collection:		
Diffractometer type	Bruker D8 QUEST area detector	
Wavelength	0.71073 Å	
Temperature	110(2) K	
Theta range for data collection	2.745 to 27.558°.	
Index ranges	-9<=h<=9, -19<=k<=19, -19<=l<=19	
Data collection software	APEX3 (Bruker AXS Inc., 2015)[166]	
Cell refinement software	SAINT V8.37A (Bruker AXS Inc., 2015)[167]	
Data reduction software	SAINT V8.37A (Bruker AXS Inc., 2015)	
Solution and refinement:		
Reflections collected	37928	
Independent reflections	7247 [R(int) = 0.0329]	
Completeness to theta = 25.242°	99.9 %	
Observed reflections	6771[I > 2σ(I)]	
Reflections used for refinement	7247	
Absorption correction	Semi-empirical from equivalents[162]	
Max. and min. transmission	0.97 and 0.91	
Flack parameter (absolute struct.)	0.012(12)[165]	
Largest diff. peak and hole	0.330 and -0.244 $e.Å^{-3}$	
Solution	Dual space algorithm	
Refinement	Full-matrix least-squares on F^2	
Treatment of hydrogen atoms	Calculated positions, constr. ref.	
Programs used	XT V2014/1 (Bruker AXS Inc., 2014)[163]	
	SHELXL-2016/6 (Sheldrick, 2016)[164]	
	DIAMOND (Crystal Impact)[168]	
	ShelXle (Hübschle, Sheldrick, Dittrich, 2011)[169]	
Data / restraints / parameters	7247 / 1 / 385	
Goodness-of-fit on F^2	1.036	
R index (all data)	wR2 = 0.0539	
R index conventional [I > 2σ(I)]	R1 = 0.0249	

5. Appendix

In chapter 5.1, the ^{1}H NMR and ^{13}C NMR spectra of the Ir(III) complexes are shown that are closely linked to catalyst **Λ-** and **Δ-T18'**, namely of diastereomeric auxiliary complexes **Λ-** and **Δ-(*S*)-T18**, of bisacetonitrile intermediate **Λ-T18-(MeCN)$_2$**, of precatalyst **Λ-T18**, of active catalyst **Λ-T18'** itself, and of *N*-methylated complex **Λ-T18-Me**.

In chapter 5.2, the chiral HPLC traces of catalysts ***rac*-**, **Λ-**, and **Δ-T18'** are shown. Moreover, the chiral HPLC trace of reisolated catalyst **Λ-T18'** from chapter 2.3.3, Table 13, entry 14 is shown there as well as the chiral HPLC trace of the sample of catalyst **Δ-T18'** which had been kept in CD_2Cl_2 for one week at 25 °C before HPLC analysis and use in a catalysis experiment (see chapter 2.3.2, Table 10, entry 14).

In chapter 5.3, the ^{1}H and ^{13}C NMR spectra of catalysis products **14a–i** (chapter 2.3.2, Table 10), **143b–i** (chapter 2.3.3, Table 13), and **163a–h** (chapter 2.3.7, Table 19) are shown.

In chapter 5.4, the chiral HPLC traces of catalysis products **14a–i** (chapter 2.3.2, Table 10), **143a–i** (chapter 2.3.3, Table 13), and **163a–h** (chapter 2.3.7, Table 19) are shown.

5.1 ^{1}H and ^{13}C NMR Spectra of Iridium(III) Complexes that are Linked to Λ/Δ-T18'

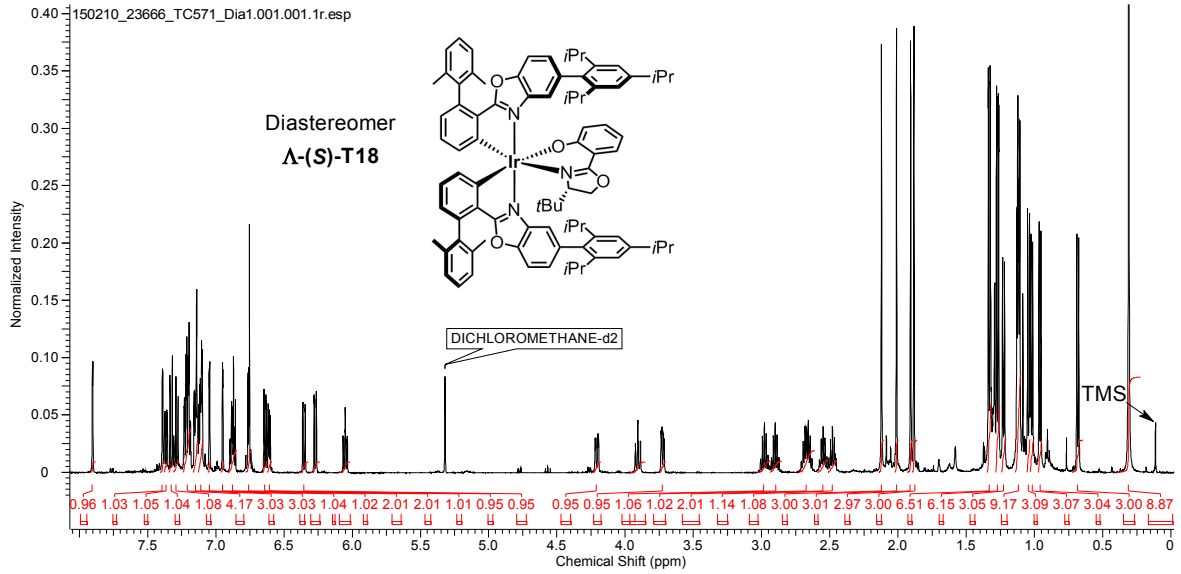

Figure 56. ^{1}H NMR spectrum of auxiliary complex **Λ-(*S*)-T18**.

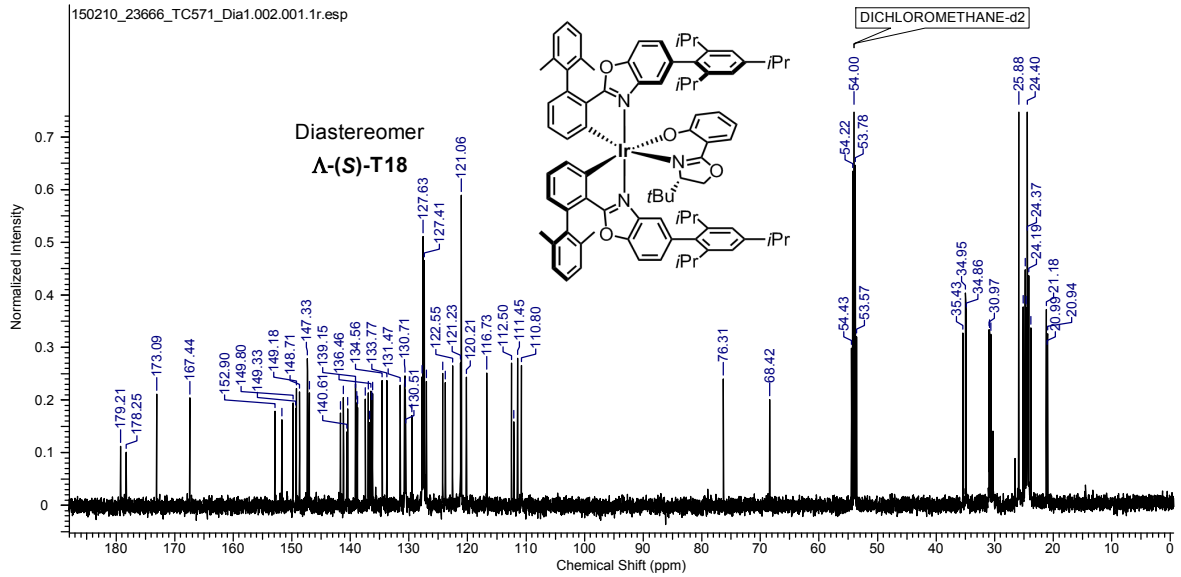

Figure 57. ^{13}C NMR spectrum of auxiliary complex **Λ-(*S*)-T18**.

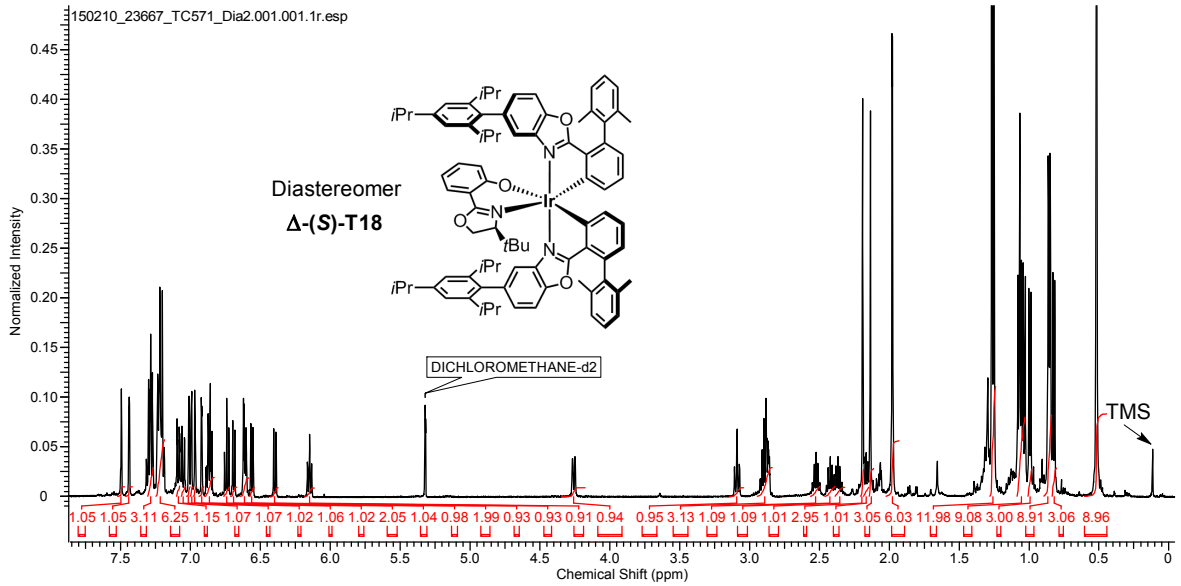

Figure 58. ^{1}H NMR spectrum of auxiliary complex **Δ-(*S*)-T18**.

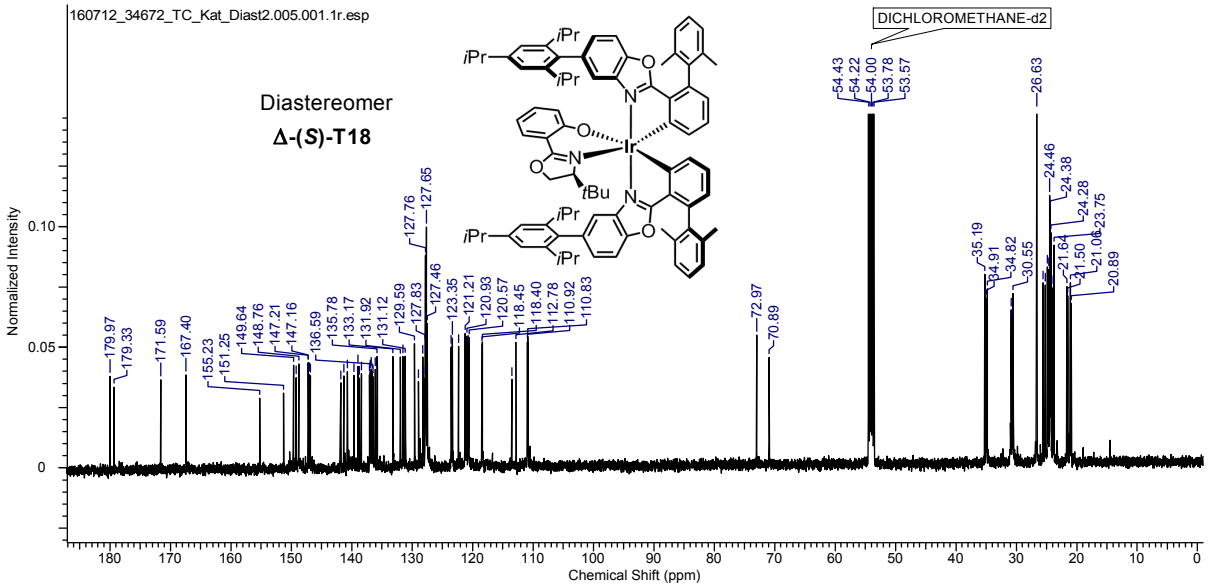

Figure 59. ^{13}C NMR spectrum of auxiliary complex **Δ-(*S*)-T18**.

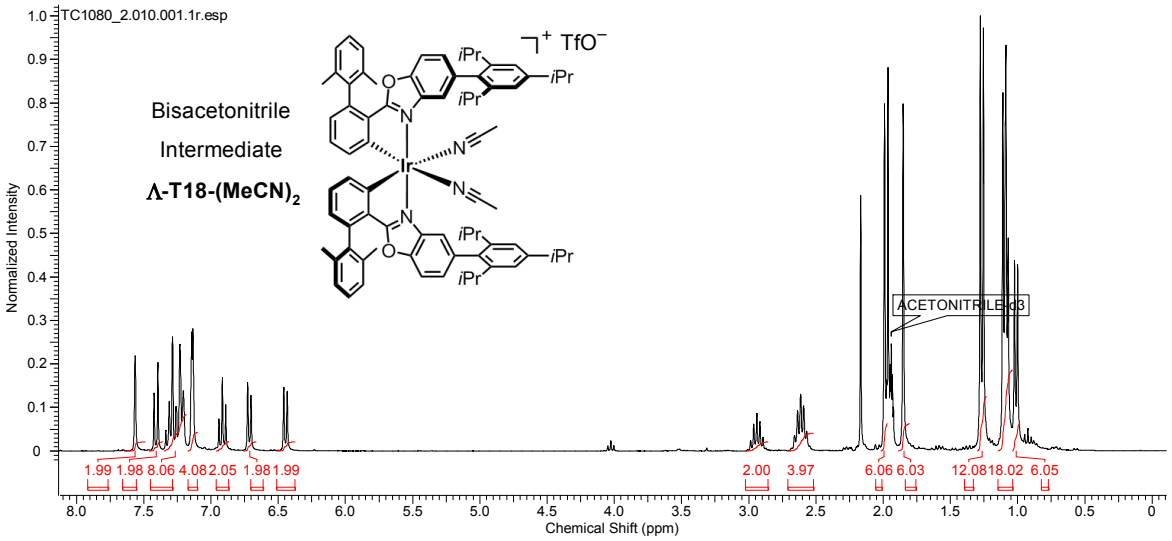

Figure 60. ^{1}H NMR spectrum of bisacetonitrile intermediate **Λ-T18-(MeCN)$_2$**.

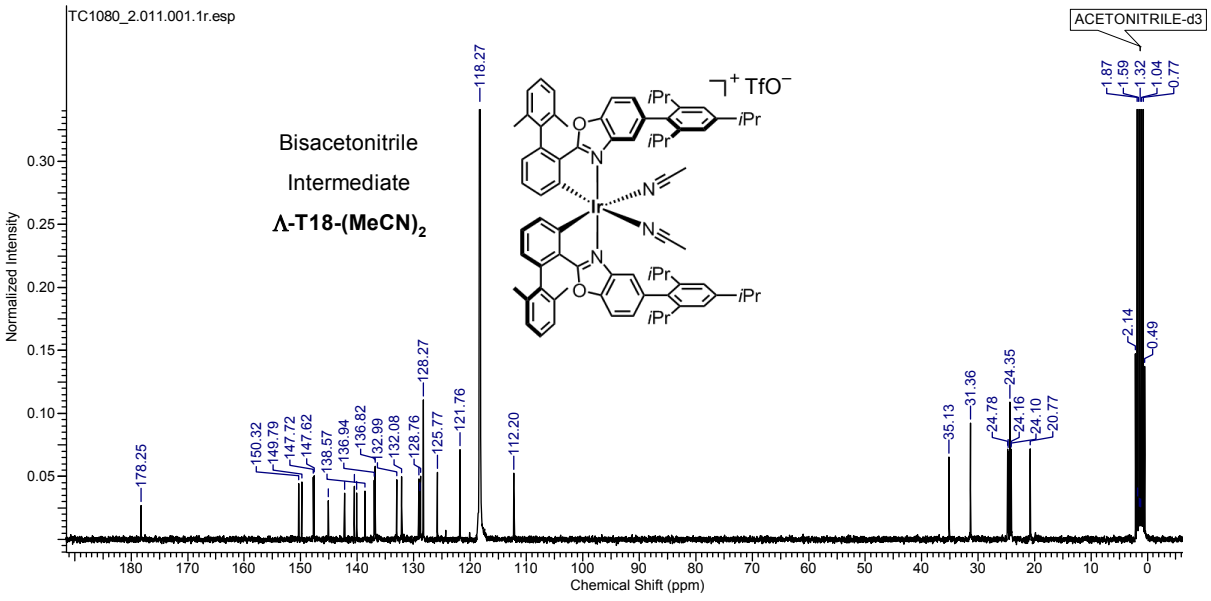

Figure 61. ^{13}C NMR spectrum of bisacetonitrile intermediate **Λ-T18-(MeCN)$_2$**.

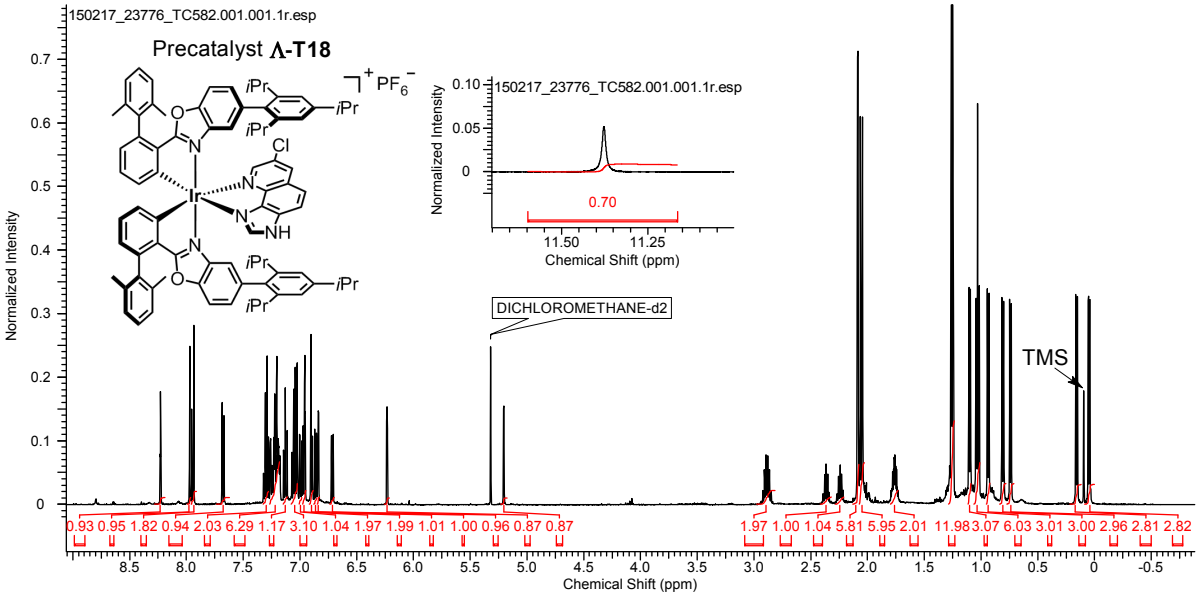

Figure 62. ^{1}H NMR spectrum of precatalyst complex **Λ-T18**.

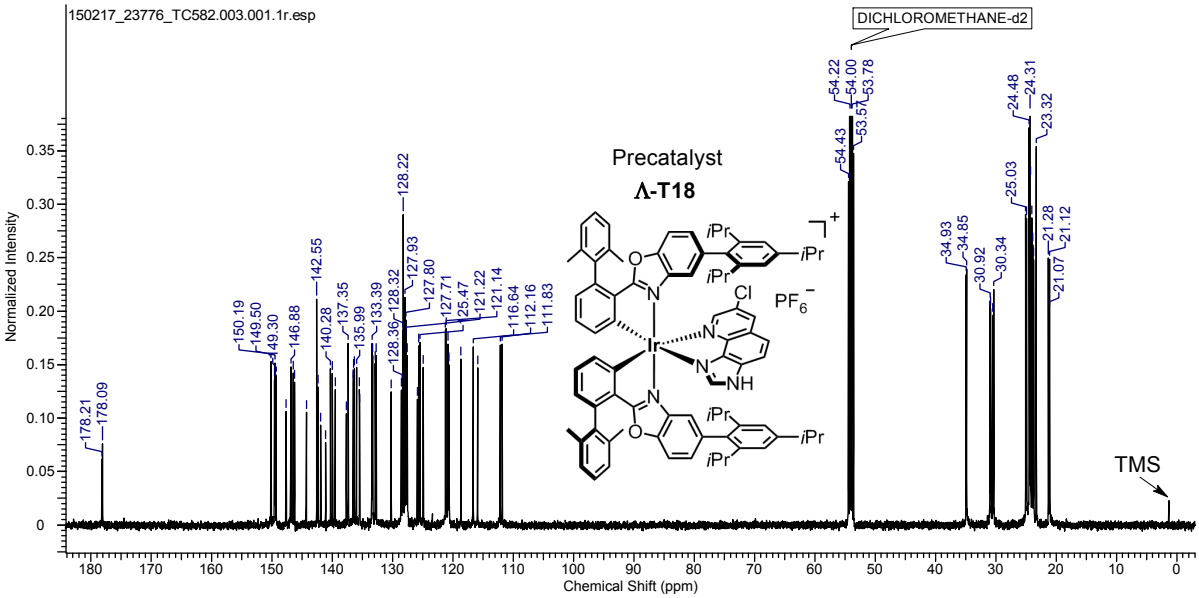

Figure 63. ^{13}C NMR spectrum of precatalyst complex **Λ-T18**.

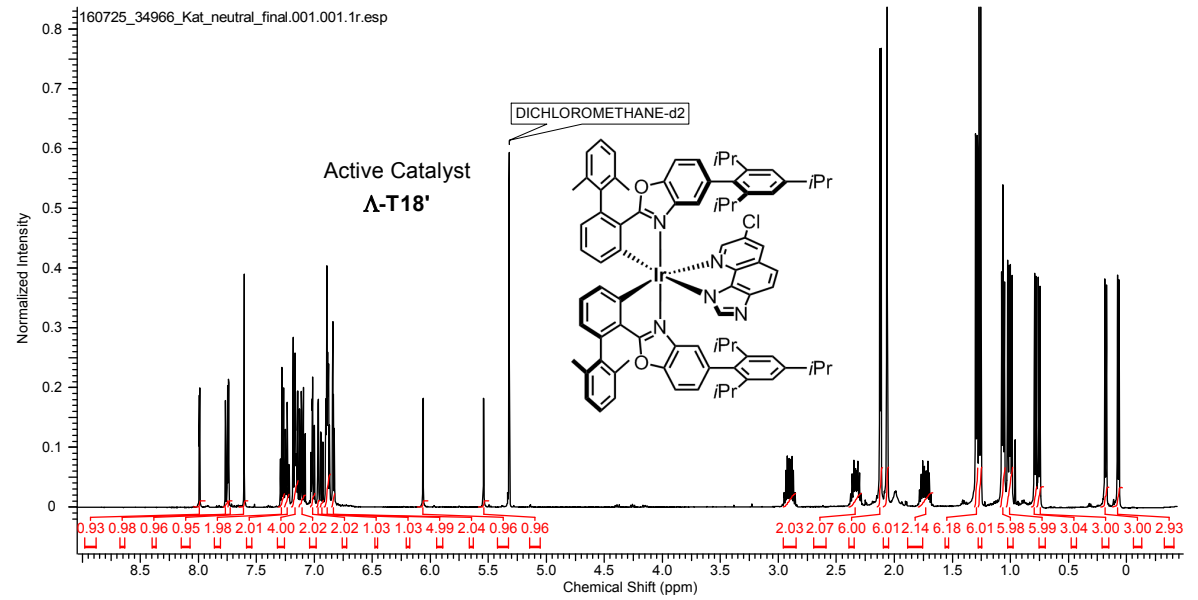

Figure 64. ^{1}H NMR spectrum of active catalyst **Λ-T18'**.

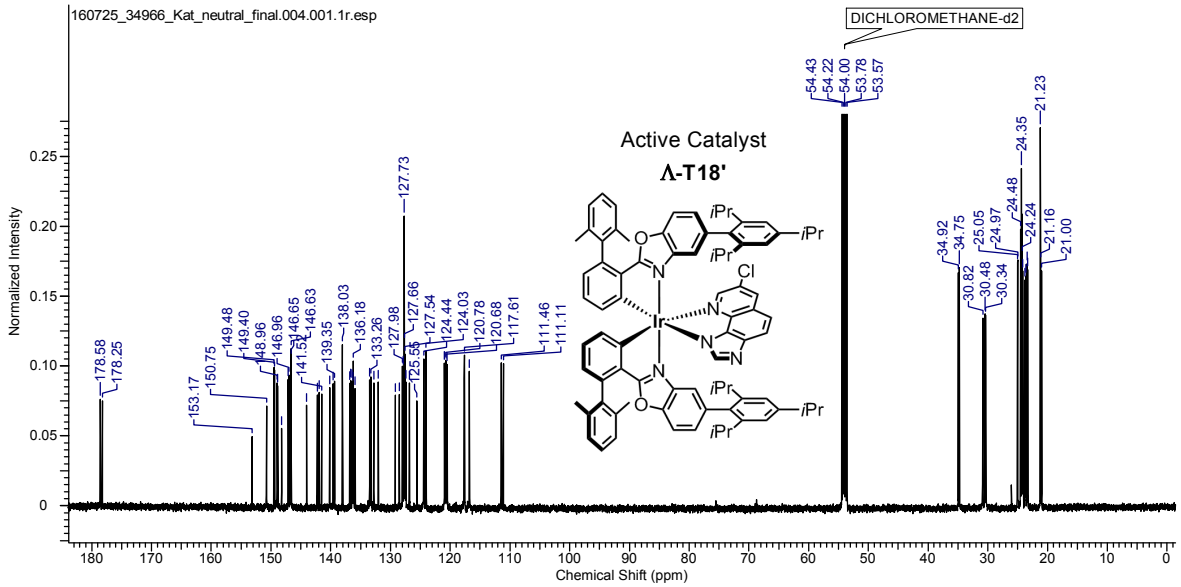

Figure 65. ^{13}C NMR spectrum of active catalyst **Λ-T18'**.

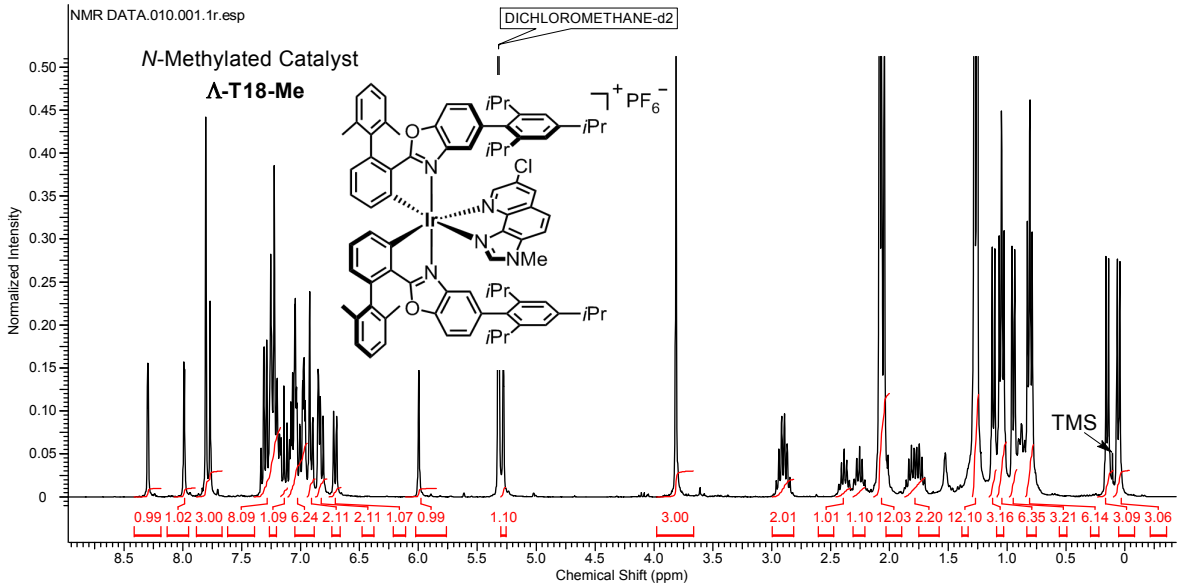

Figure 66. ^{1}H NMR spectrum of *N*-methylated catalyst **Λ-T18-Me**.

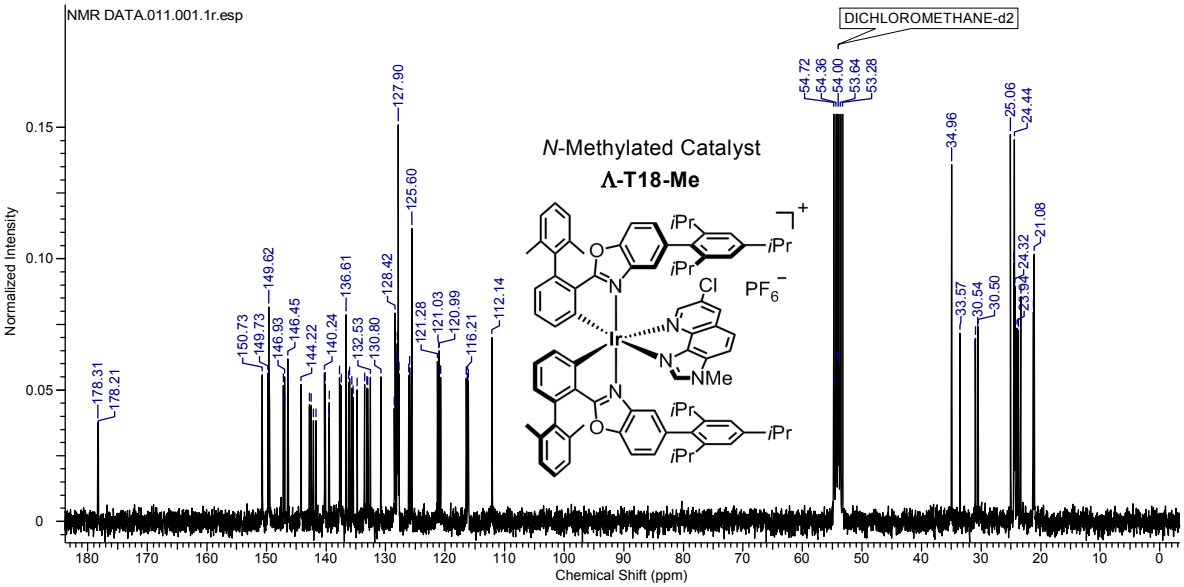

Figure 67. ^{13}C NMR spectrum of *N*-methylated catalyst **Λ-T18-Me**.

5.2 Chiral HPLC Traces of Iridium(III) Complexes *rac*-, Λ-, and Δ-T18'

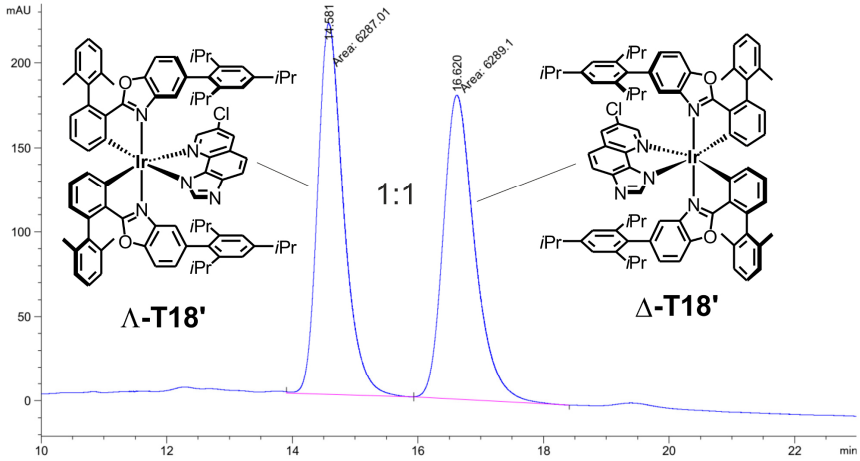

Peak #	RetTime [min]	Type	Width [min]	Area [mAU*s]	Height [mAU]	Area %
1	14.581	FM	0.4772	6287.01025	219.57513	49.9917
2	16.620	MM	0.5820	6289.10449	180.11317	50.0083

Figure 68. Chiral HPLC trace of racemic catalyst ***rac*-T18'**.

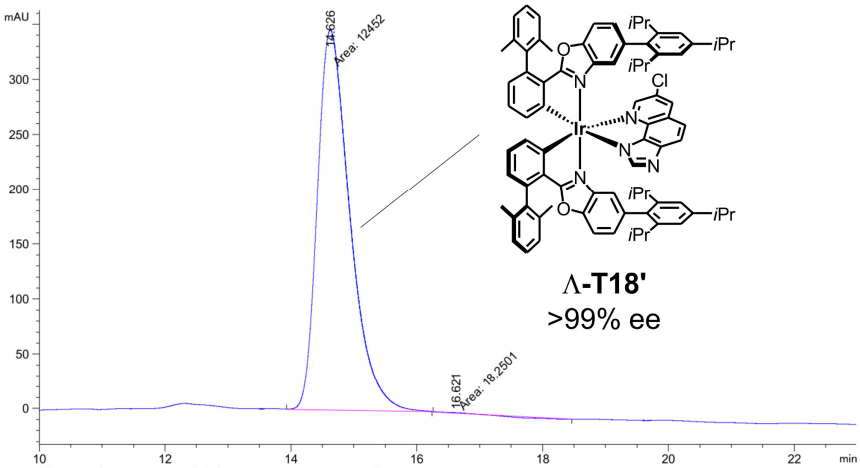

Peak #	RetTime [min]	Type	Width [min]	Area [mAU*s]	Height [mAU]	Area %
1	14.626	MM	0.5995	1.24520e4	346.15314	99.8537
2	16.621	MM	0.5305	18.25009	5.73374e-1	0.1463

Figure 69. Chiral HPLC trace of enantiopure catalyst **Λ-T18'**.

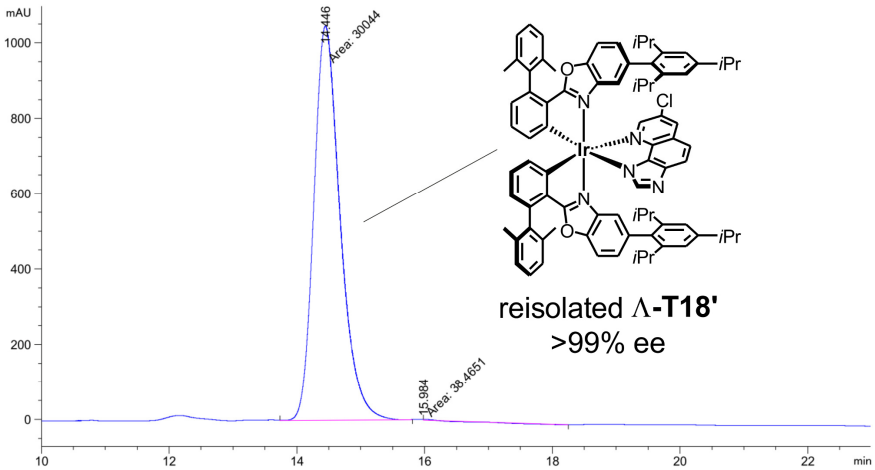

Peak #	RetTime [min]	Type	Width [min]	Area [mAU*s]	Height [mAU]	Area %
1	14.446	MM	0.4783	3.00440e4	1046.84229	99.8721
2	15.984	MM	0.2222	38.46510	2.88477	0.1279

Figure 70. Chiral HPLC trace of reisolated catalyst **Λ-T18'** (Table 13, entries 14 and 15).

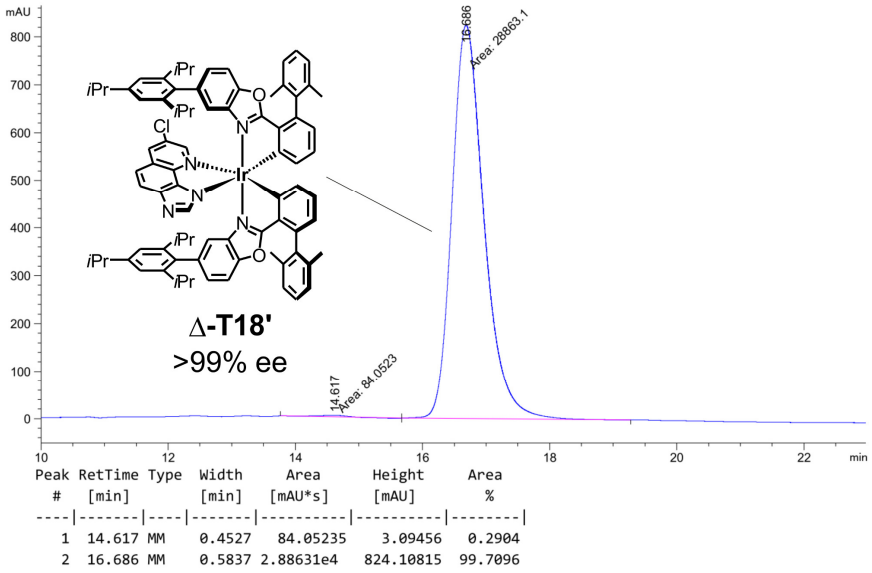

Peak #	RetTime [min]	Type	Width [min]	Area [mAU*s]	Height [mAU]	Area %
1	14.617	MM	0.4527	84.05235	3.09456	0.2904
2	16.686	MM	0.5837	2.88631e4	824.10815	99.7096

Figure 71. Chiral HPLC trace of enantiopure catalyst **Δ-T18'**.

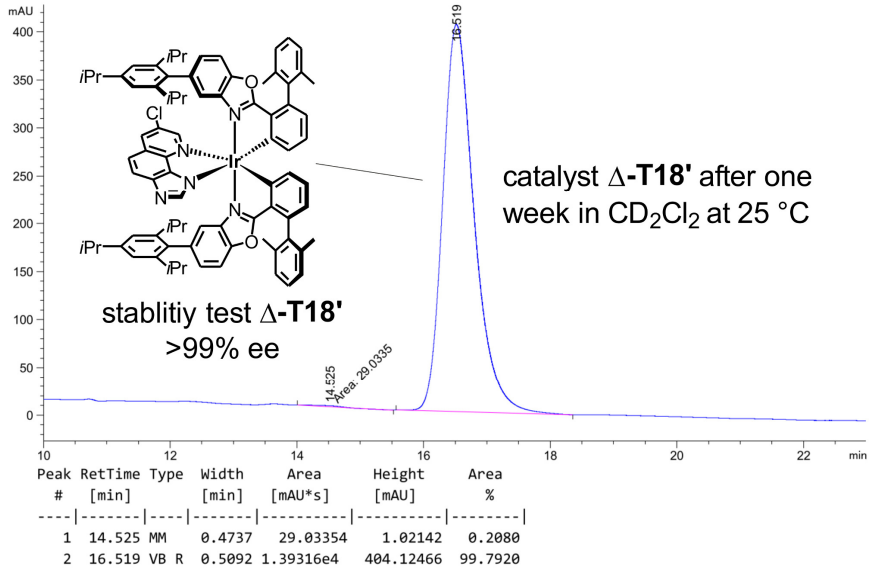

Peak #	RetTime [min]	Type	Width [min]	Area [mAU*s]	Height [mAU]	Area %
1	14.525	MM	0.4737	29.03354	1.02142	0.2080
2	16.519	VB R	0.5092	1.39316e4	404.12466	99.7920

Figure 72. Chiral HPLC trace of enantiopure catalyst **Δ-T18'** after one week in CD_2Cl_2 at 25 °C (Table 10, entry 14).

5.3 ^{1}H and ^{13}C NMR Spectra of Products 14 (Table 10), 143 (Table 13), 163 (Table 19)

5.3.1 ^{1}H and ^{13}C NMR Spectra of *C*-Acylated Azlactones 14 (Table 10)

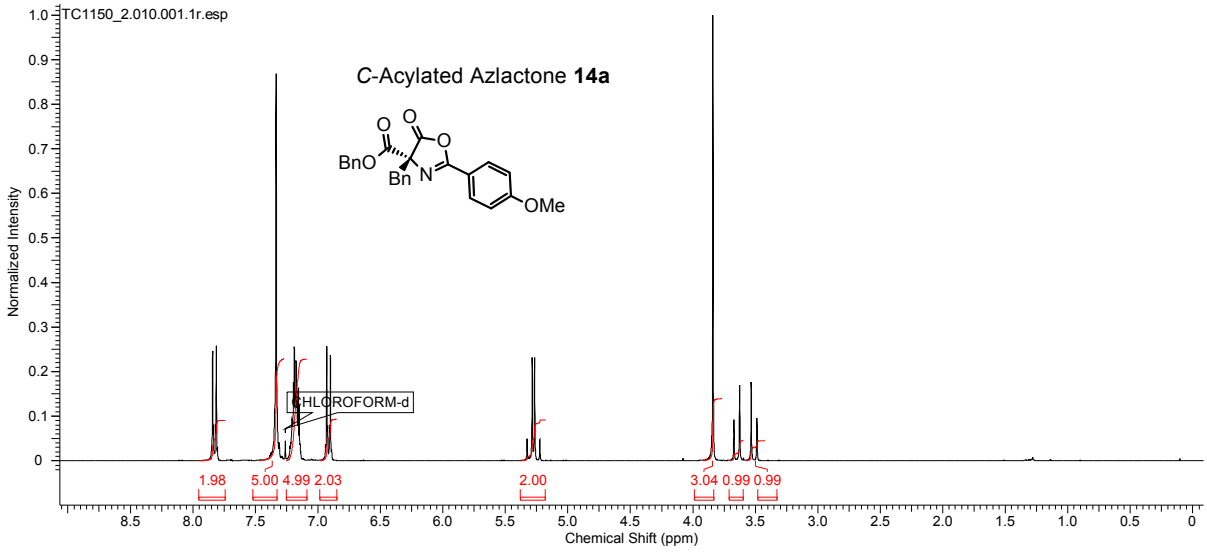

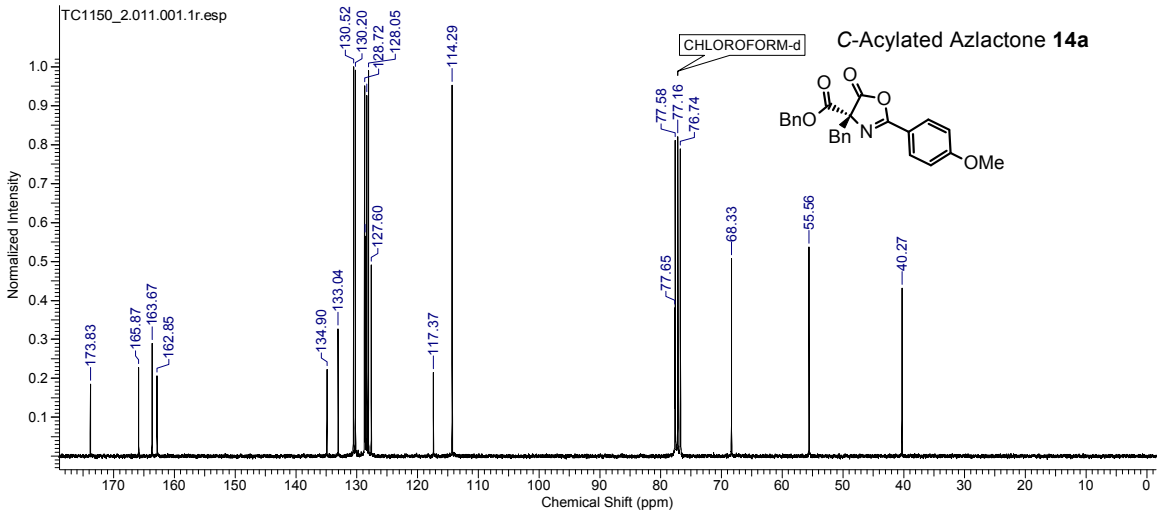

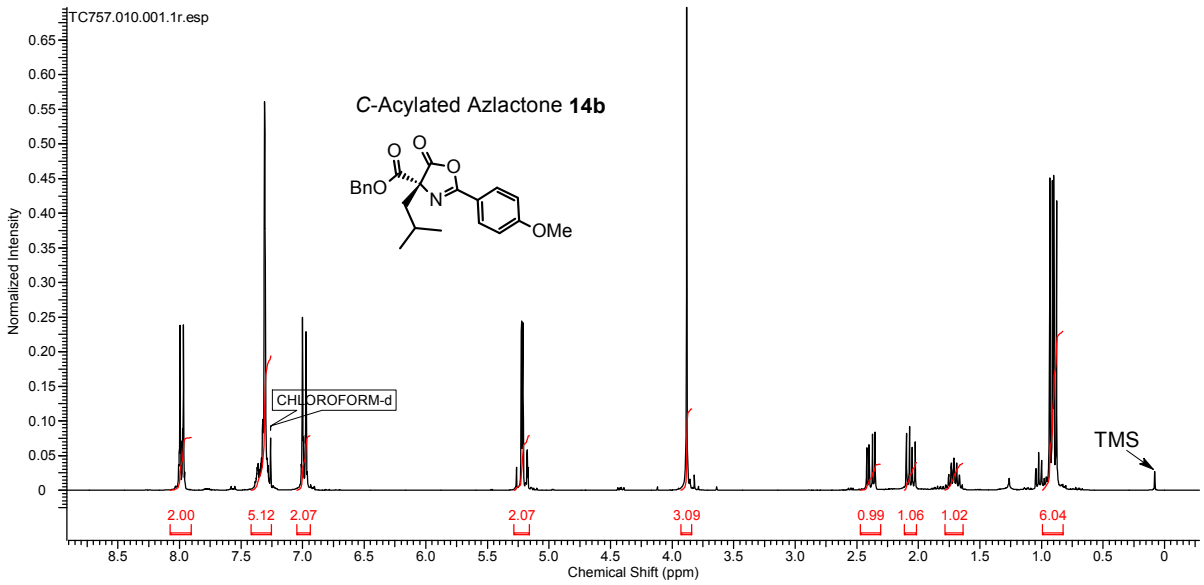

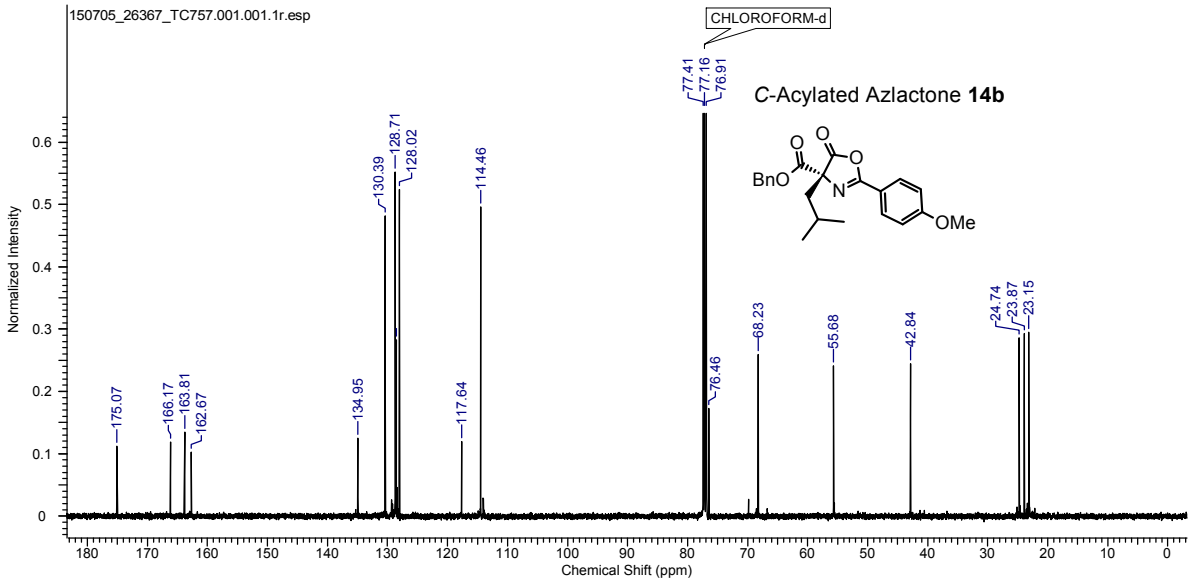
150705_26367_TC757.001.001.1r.esp
CHLOROFORM-d
77.41
77.16
76.91
C-Acylated Azlactone 14b
BnO
OMe
130.39
128.71
128.02
114.46
68.23
55.68
42.84
24.74
23.87
23.15
76.46
175.07
166.17
163.81
162.67
134.95
117.64
Normalized Intensity
Chemical Shift (ppm)

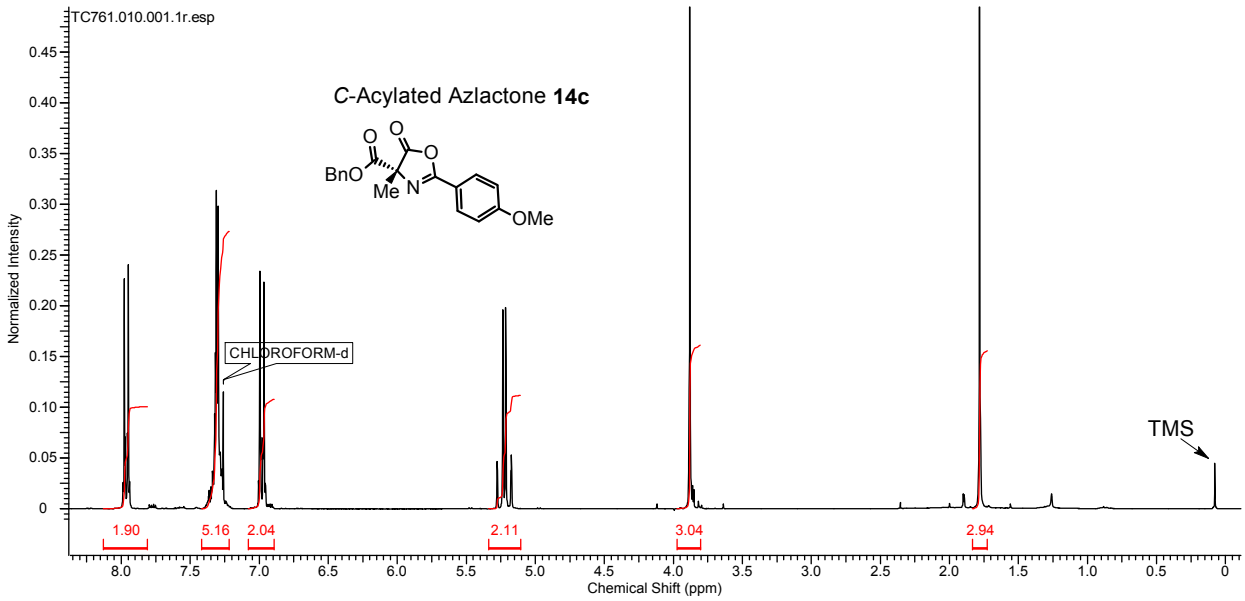
TC761.010.001.1r.esp
C-Acylated Azlactone 14c
BnO
Me
OMe
CHLOROFORM-d
TMS
1.90
5.16
2.04
2.11
3.04
2.94
Normalized Intensity
Chemical Shift (ppm)

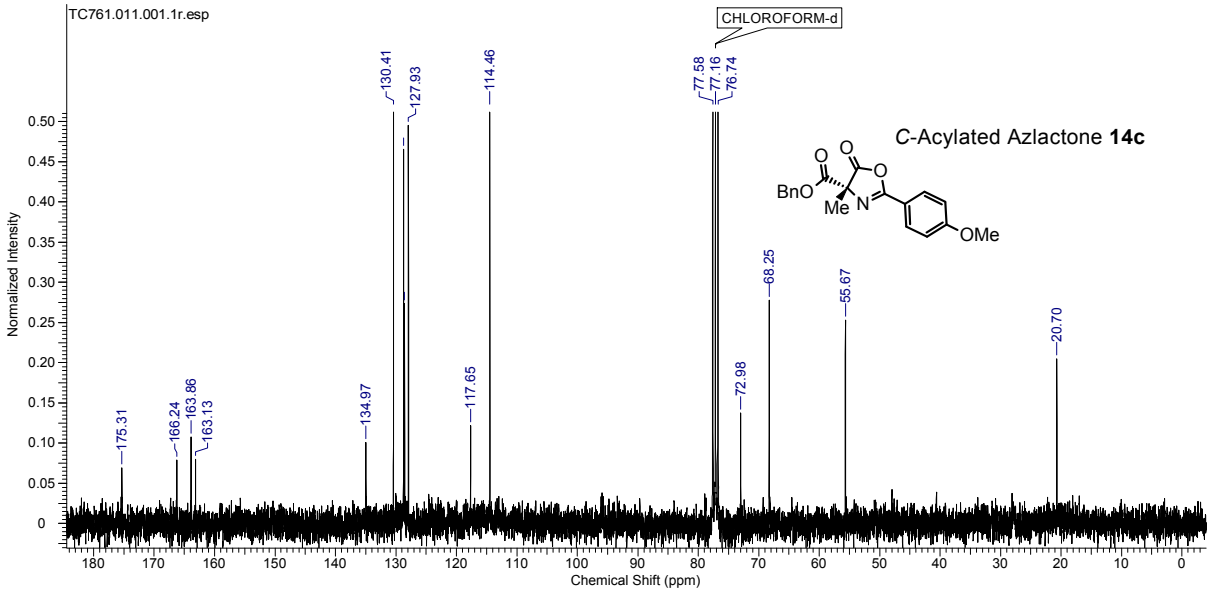
TC761.011.001.1r.esp
CHLOROFORM-d
77.58
77.16
76.74
130.41
127.93
114.46
C-Acylated Azlactone 14c
BnO
Me
OMe
68.25
55.67
20.70
72.98
175.31
166.24
163.86
163.13
134.97
117.65
Normalized Intensity
Chemical Shift (ppm)

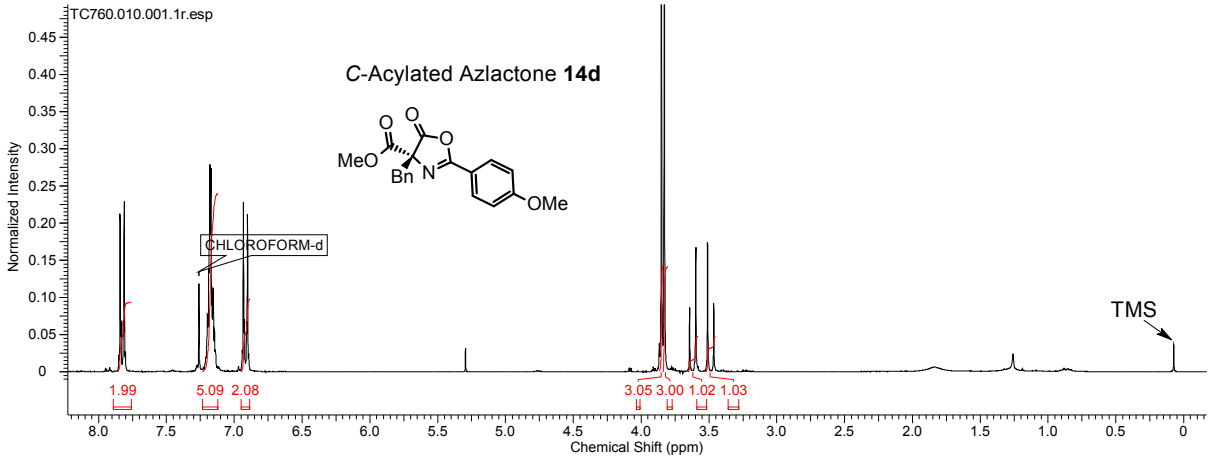
TC760.010.001.1r.esp
C-Acylated Azlactone 14d
MeO
Bn
OMe
CHLOROFORM-d
TMS
Normalized Intensity
1.99
5.09
2.08
3.05
3.00
1.02
1.03
Chemical Shift (ppm)

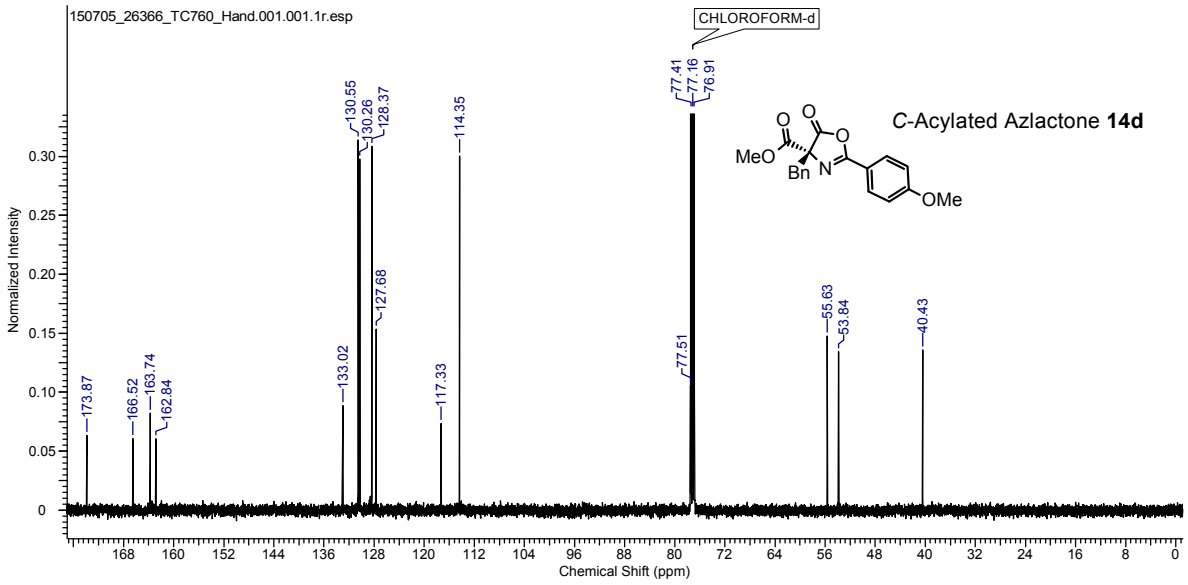
150705_26366_TC760_Hand.001.001.1r.esp
CHLOROFORM-d
C-Acylated Azlactone 14d
MeO
Bn
OMe
130.55
130.26
128.37
114.35
77.41
77.16
76.91
127.68
173.87
166.52
163.74
162.84
133.02
117.33
77.51
55.63
53.84
40.43
Normalized Intensity
Chemical Shift (ppm)

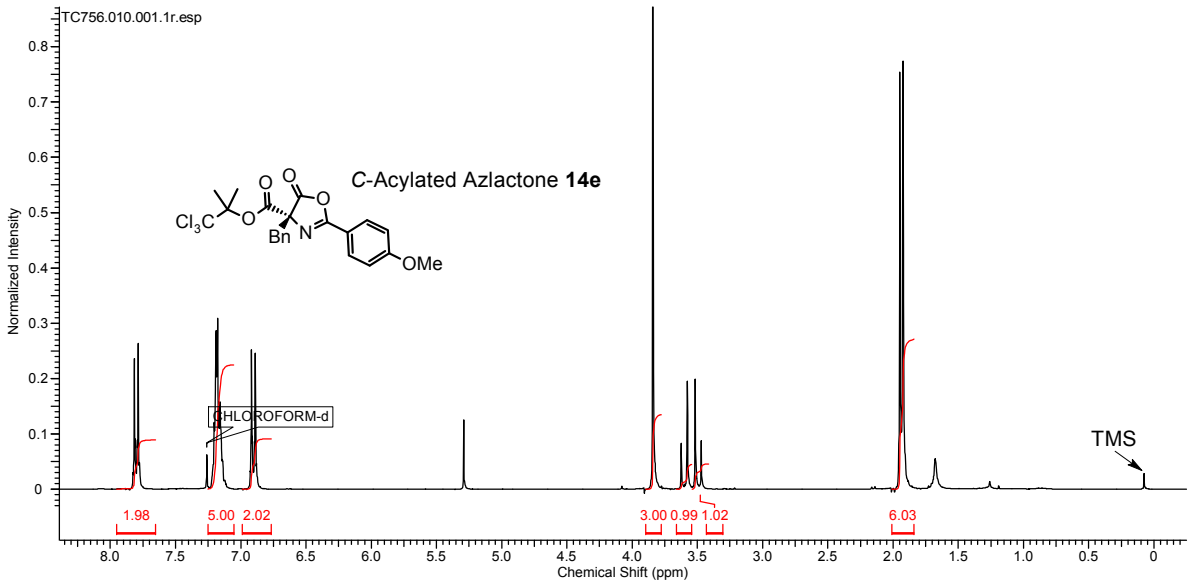
TC756.010.001.1r.esp
C-Acylated Azlactone 14e
Cl3C
Bn
OMe
CHLOROFORM-d
TMS
Normalized Intensity
1.98
5.00
2.02
3.00
0.99
1.02
6.03
Chemical Shift (ppm)

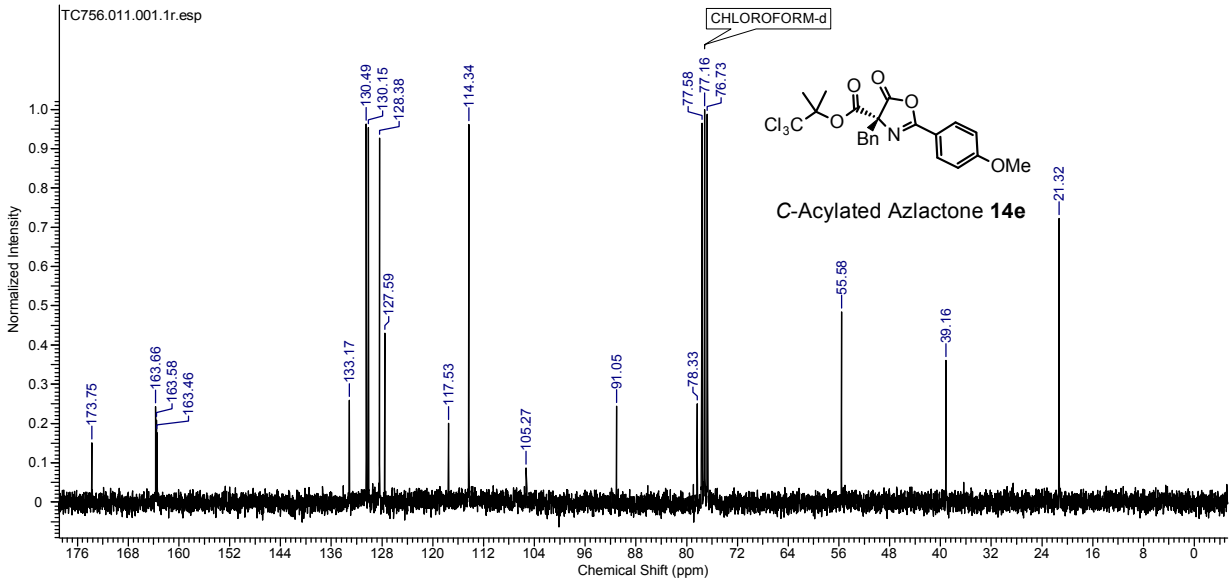
TC756.011.001.1r.esp
CHLOROFORM-d
130.49
130.15
128.38
114.34
77.58
77.16
76.73
21.32
55.58
39.16
127.59
133.17
117.53
105.27
91.05
78.33
173.75
163.66
163.58
163.46
Cl3C
Bn
OMe
C-Acylated Azlactone 14e
Normalized Intensity
Chemical Shift (ppm)

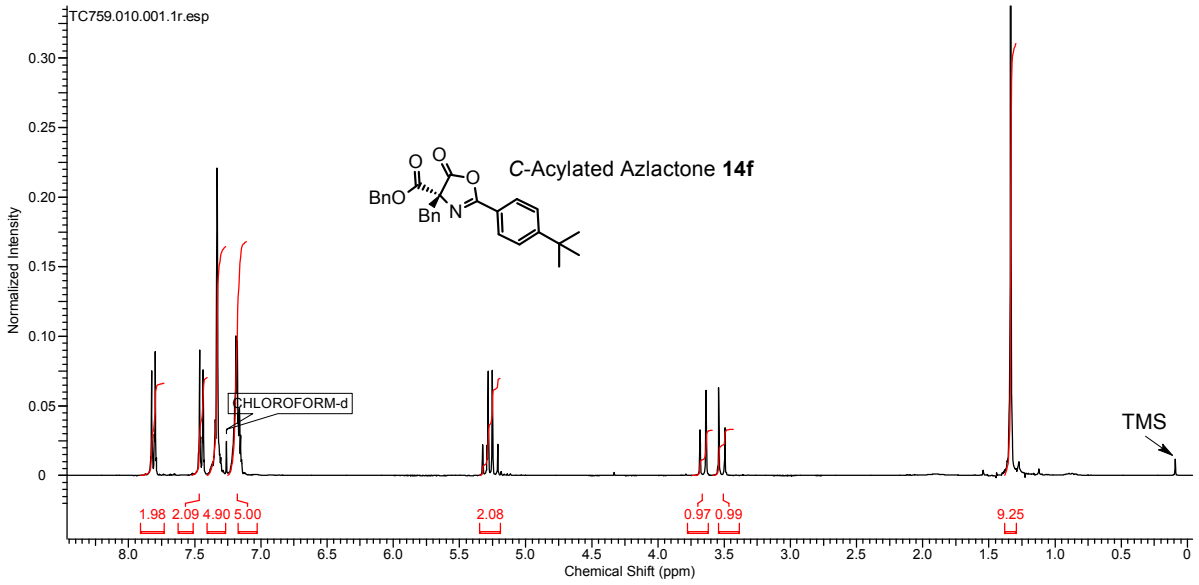
TC759.010.001.1r.esp
C-Acylated Azlactone 14f
BnO
Bn
CHLOROFORM-d
TMS
1.98
2.09
4.90
5.00
2.08
0.97
0.99
9.25
Normalized Intensity
Chemical Shift (ppm)

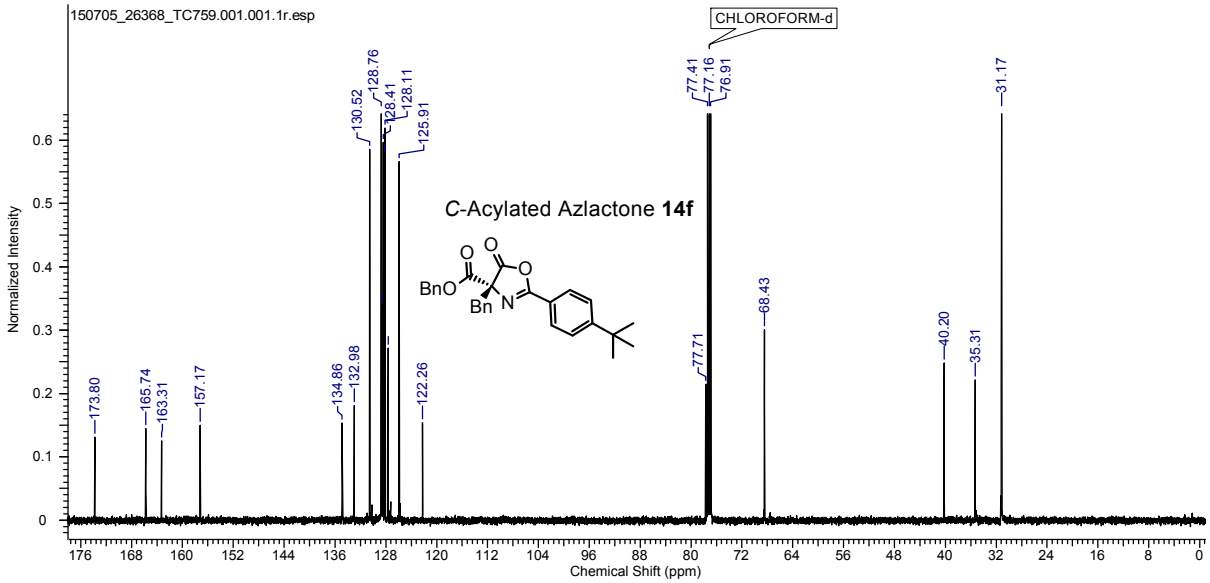
150705_26368_TC759.001.001.1r.esp
CHLOROFORM-d
130.52
128.76
128.41
128.11
125.91
77.41
77.16
76.91
31.17
68.43
40.20
35.31
77.71
134.86
132.98
122.26
173.80
165.74
163.31
157.17
C-Acylated Azlactone 14f
BnO
Bn
Normalized Intensity
Chemical Shift (ppm)

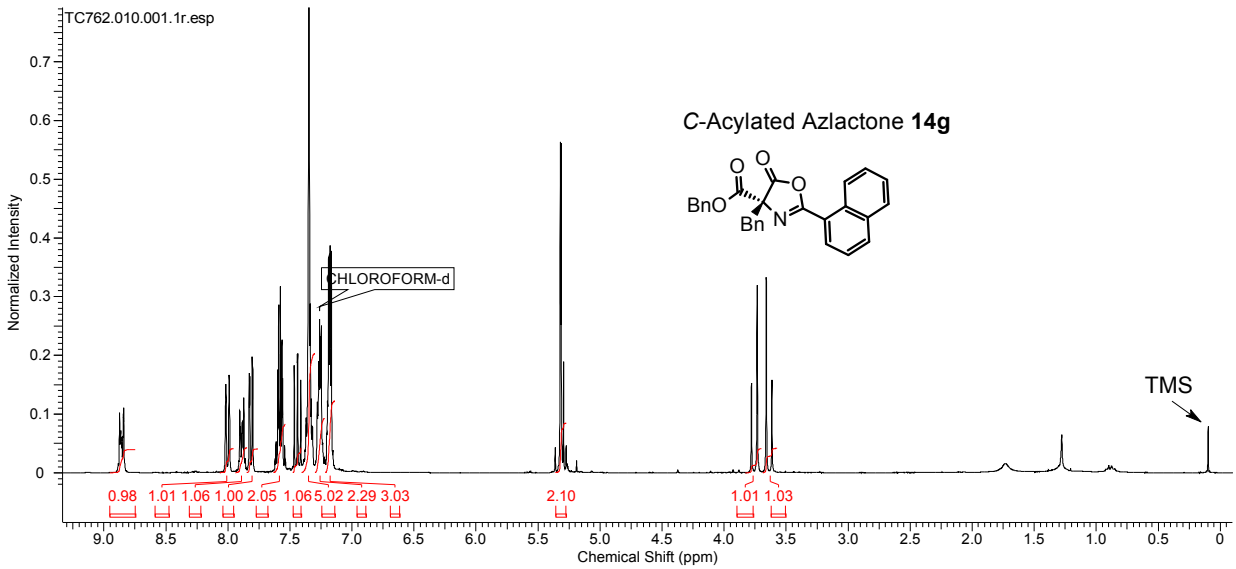
TC762.010.001.1r.esp
C-Acylated Azlactone 14g
CHLOROFORM-d
TMS
Normalized Intensity
Chemical Shift (ppm)
0.98 1.01 1.06 1.00 2.05 1.06 5.02 2.29 3.03
2.10
1.01 1.03

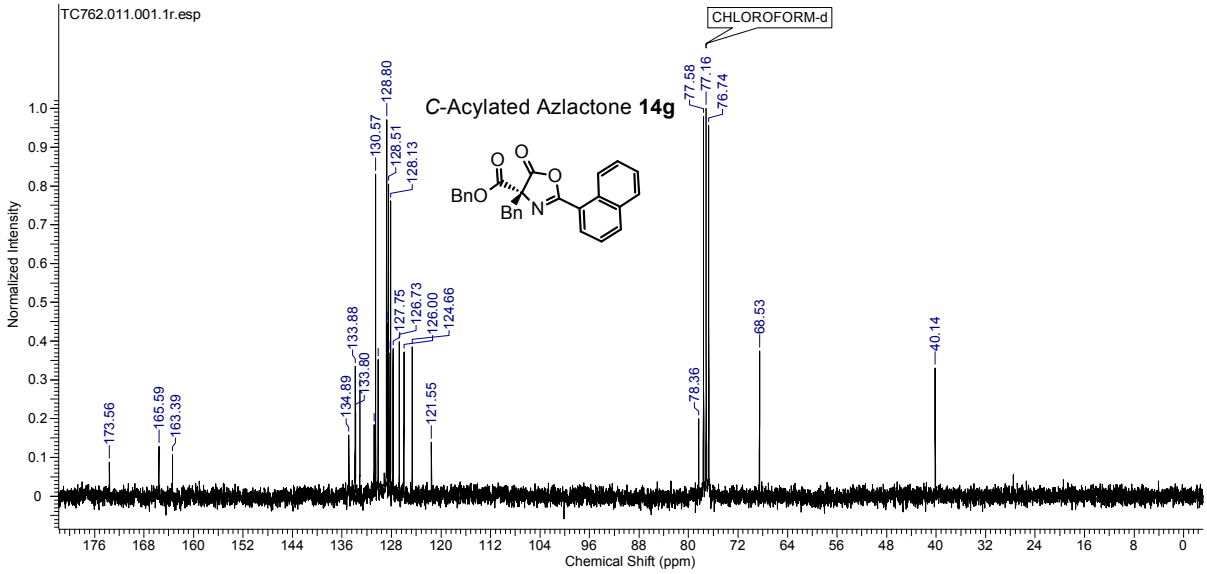
TC762.011.001.1r.esp
C-Acylated Azlactone 14g
CHLOROFORM-d
Normalized Intensity
Chemical Shift (ppm)
173.56
165.59
163.39
134.89
133.88
133.80
130.57
128.80
128.51
128.13
127.75
126.73
126.00
124.66
121.55
78.36
77.58
77.16
76.74
68.53
40.14

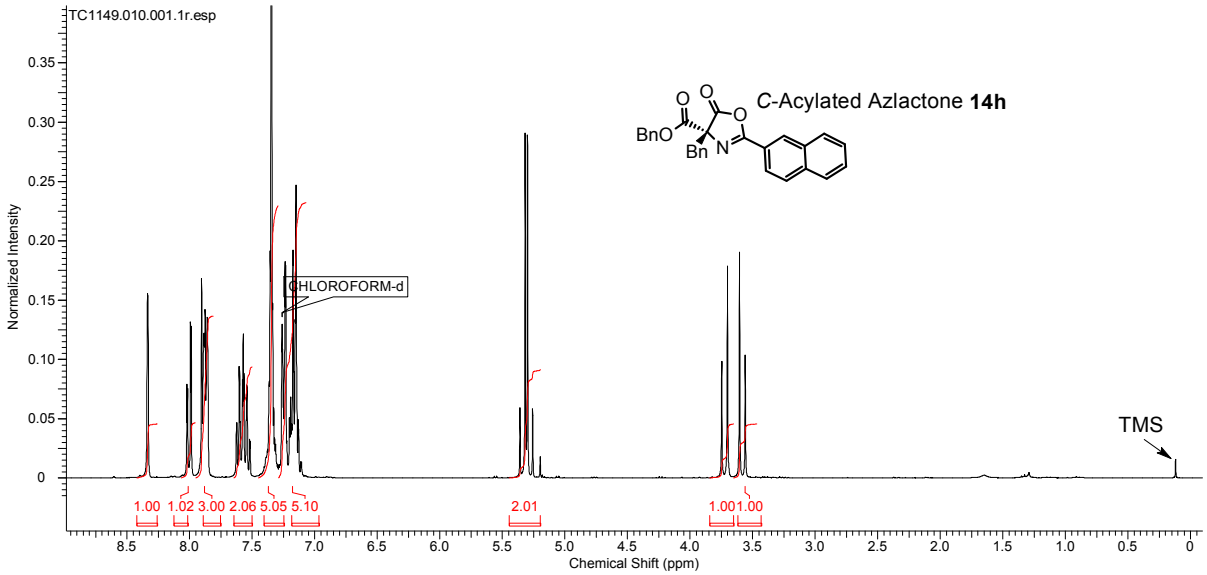
TC1149.010.001.1r.esp
C-Acylated Azlactone 14h
CHLOROFORM-d
TMS
Normalized Intensity
Chemical Shift (ppm)
1.00 1.02 3.00 2.06 5.05 5.10
2.01
1.00 1.00

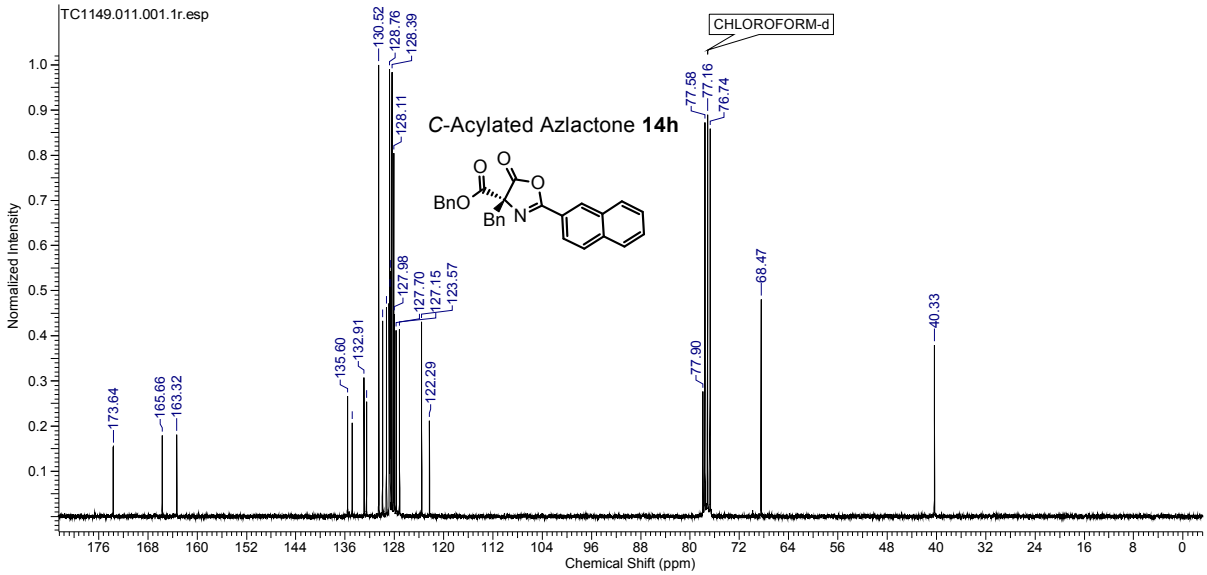
TC1149.011.001.1r.esp
C-Acylated Azlactone 14h
CHLOROFORM-d
130.52
128.76
128.39
128.11
127.98
127.70
127.15
123.57
135.60
132.91
122.29
173.64
165.66
163.32
77.58
77.16
76.74
77.90
68.47
40.33
Normalized Intensity
Chemical Shift (ppm)

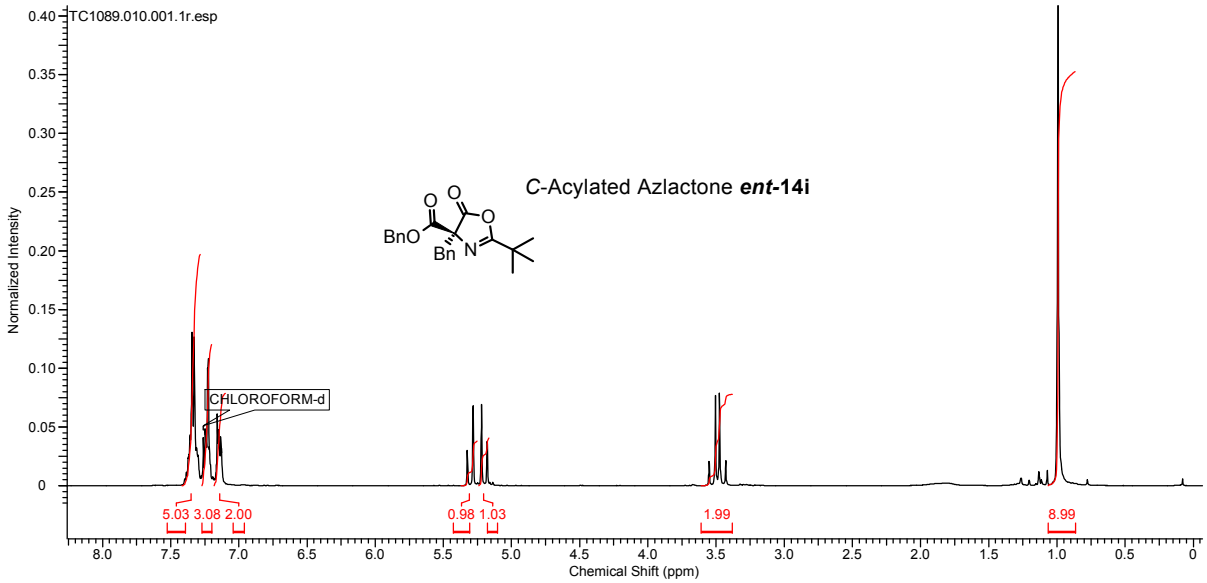
TC1089.010.001.1r.esp
C-Acylated Azlactone ent-14i
CHLOROFORM-d
5.03 3.08 2.00
0.98 1.03
1.99
8.99
Normalized Intensity
Chemical Shift (ppm)

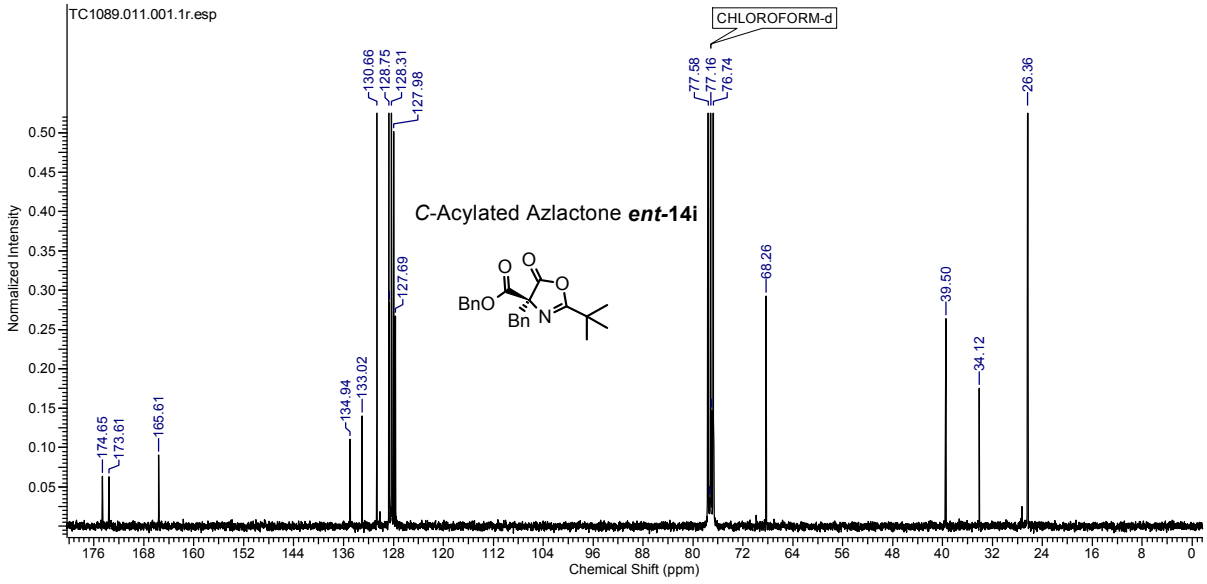
TC1089.011.001.1r.esp
C-Acylated Azlactone ent-14i
CHLOROFORM-d
130.66
128.75
128.31
127.98
127.69
134.94
133.02
174.65
173.61
165.61
77.58
77.16
76.74
68.26
39.50
34.12
26.36
Normalized Intensity
Chemical Shift (ppm)

5.3.2 ^{1}H and ^{13}C NMR Spectra of *C*-Acylated Benzofuranones 143 (Table 13)

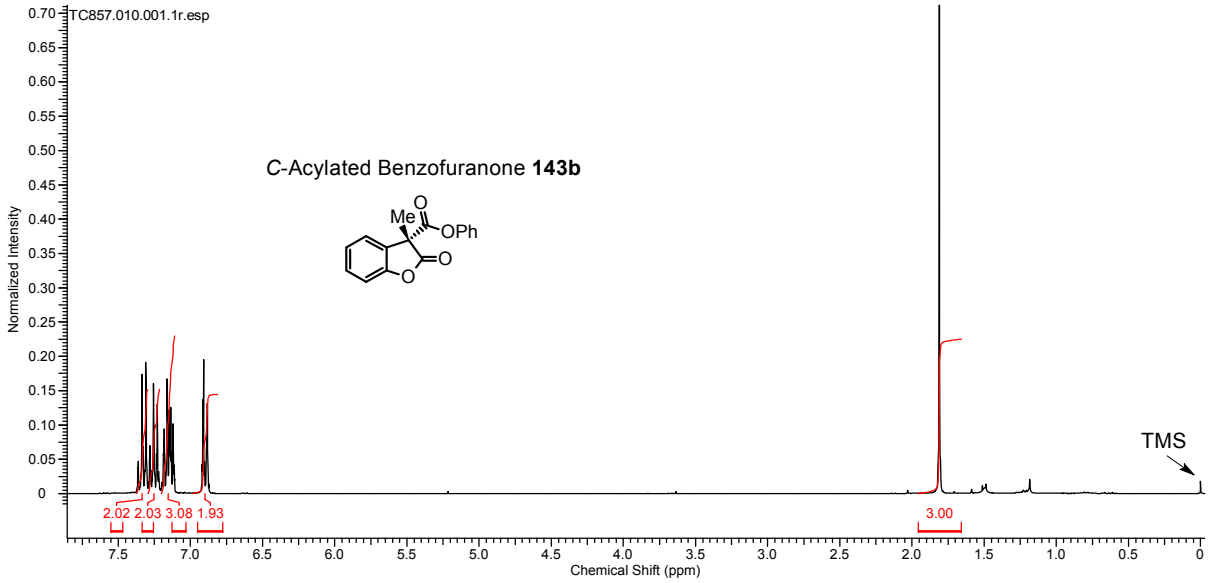

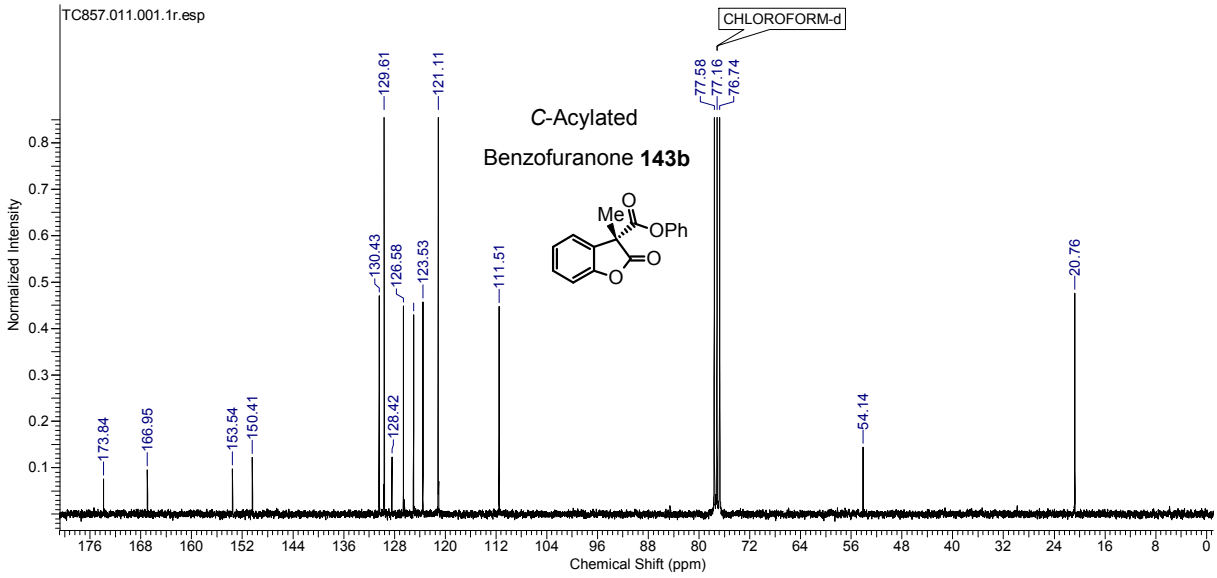

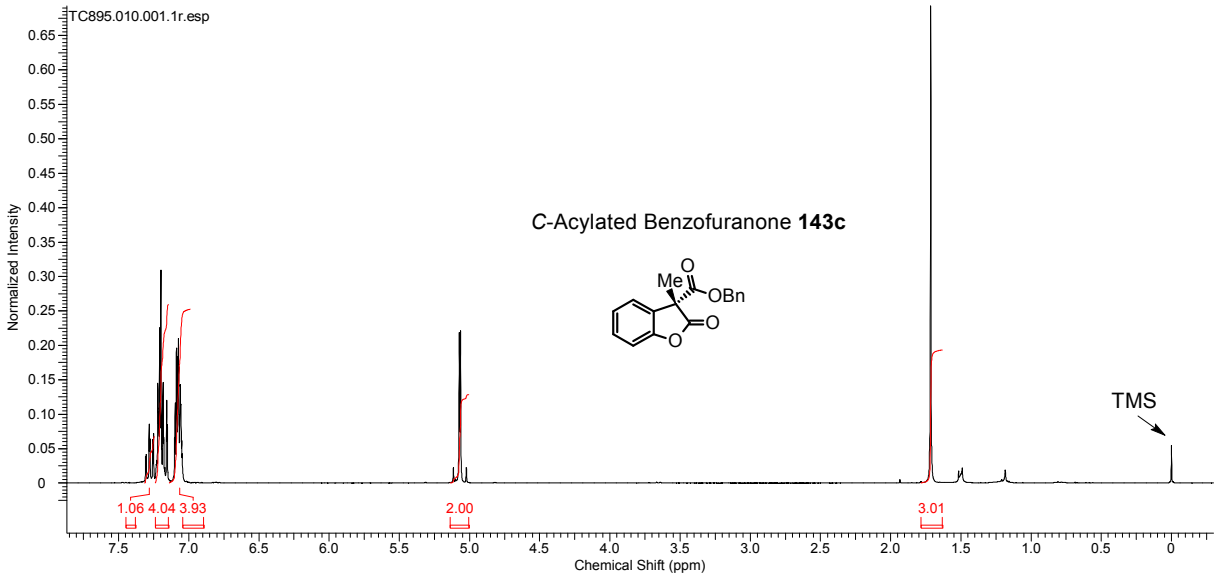

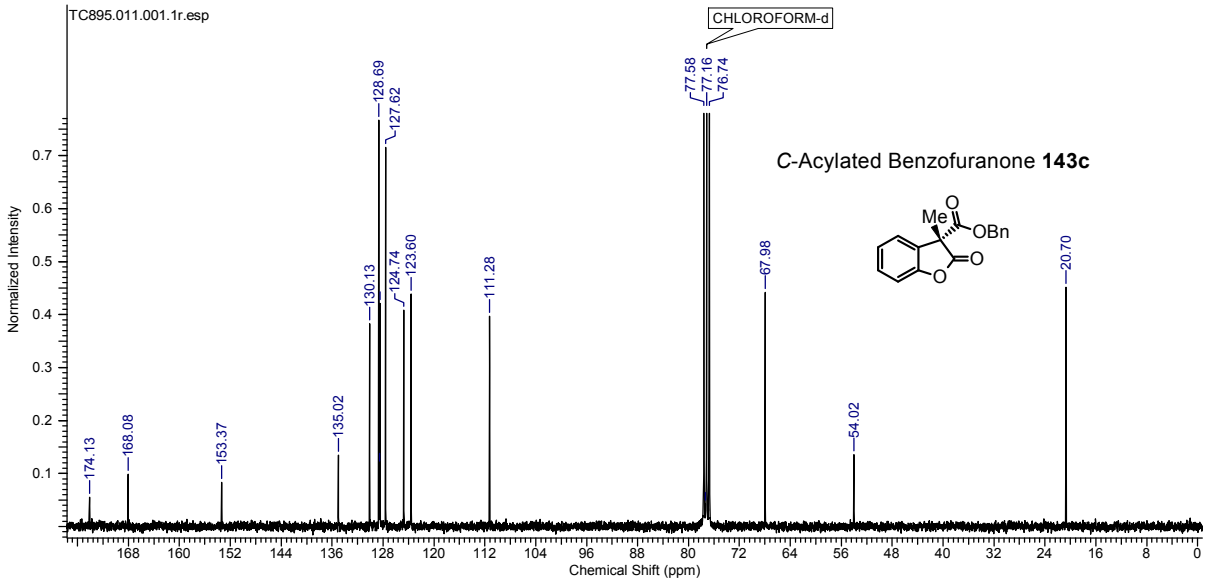
TC895.011.001.1r.esp
CHLOROFORM-d
77.58
77.16
76.74
128.69
127.62
130.13
124.74
123.60
111.28
67.98
20.70
135.02
54.02
174.13
168.08
153.37
C-Acylated Benzofuranone 143c
Me
OBn
O
Normalized Intensity
Chemical Shift (ppm)

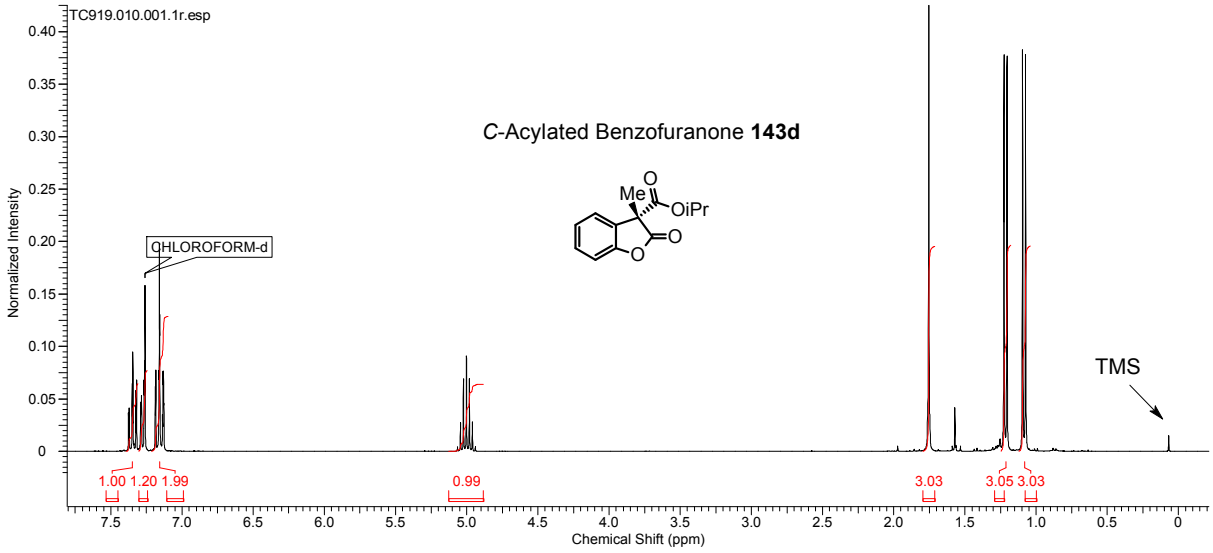
TC919.010.001.1r.esp
C-Acylated Benzofuranone 143d
Me
OiPr
O
CHLOROFORM-d
TMS
1.00 1.20 1.99
0.99
3.03
3.05 3.03
Normalized Intensity
Chemical Shift (ppm)

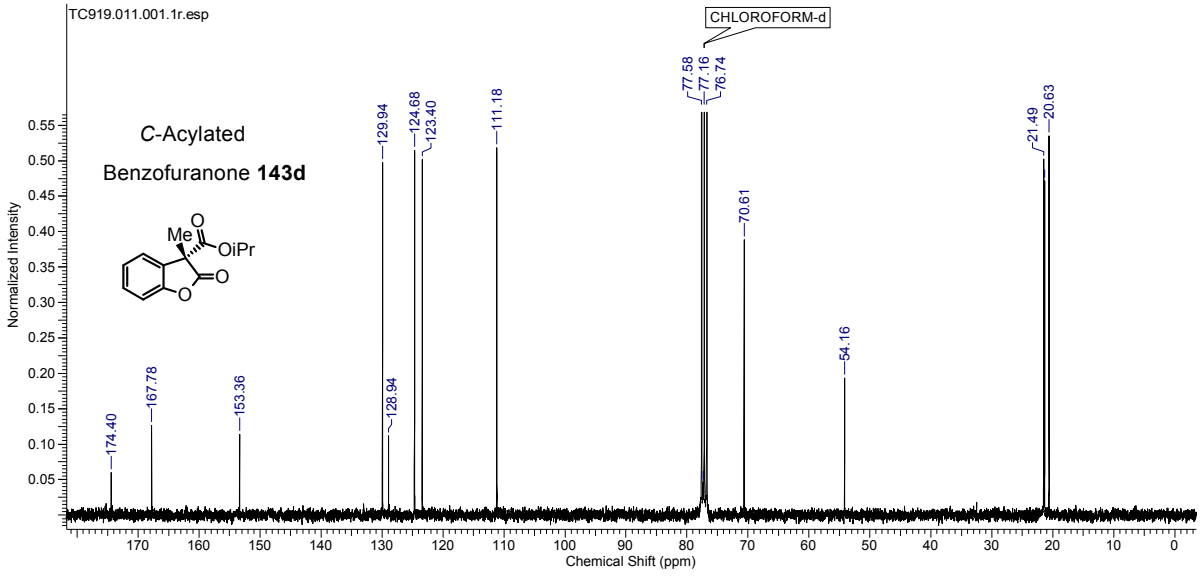
TC919.011.001.1r.esp
CHLOROFORM-d
77.58
77.16
76.74
129.94
124.68
123.40
111.18
70.61
54.16
21.49
20.63
128.94
174.40
167.78
153.36
C-Acylated
Benzofuranone 143d
Me
OiPr
O
Normalized Intensity
Chemical Shift (ppm)

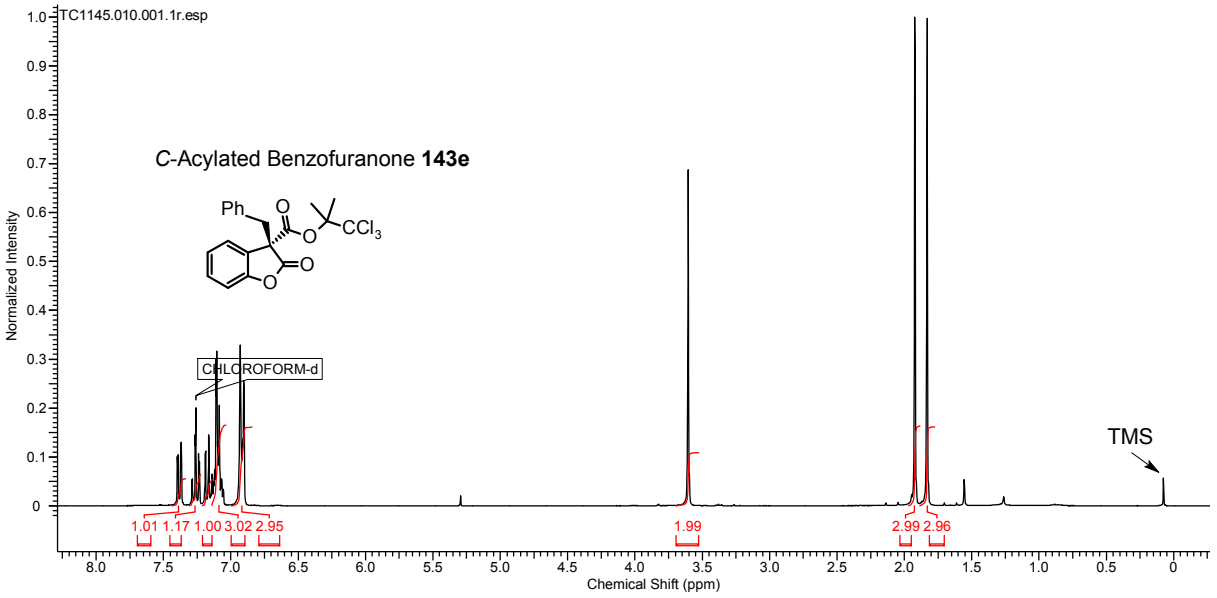
TC1145.010.001.1r.esp
C-Acylated Benzofuranone 143e
Ph
O
O
CCl3
O
O
CHLOROFORM-d
TMS
1.01 1.17 1.00 3.02 2.95
1.99
2.99 2.96
Normalized Intensity
Chemical Shift (ppm)

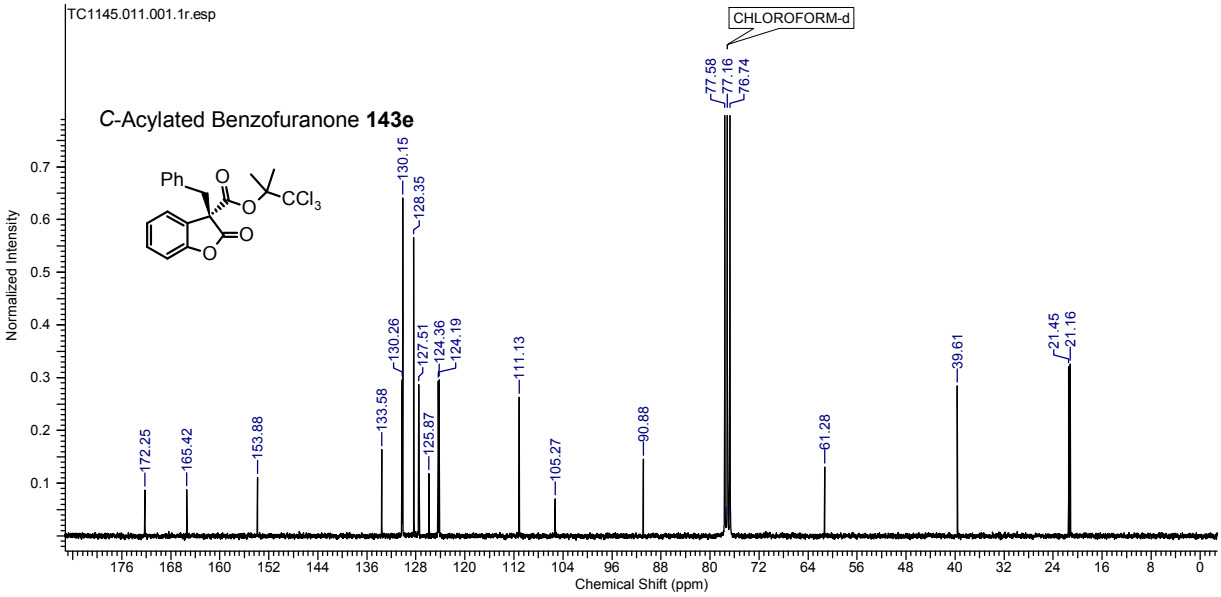
TC1145.011.001.1r.esp
C-Acylated Benzofuranone 143e
Ph
O
O
CCl3
O
O
CHLOROFORM-d
77.58
77.16
76.74
130.15
128.35
130.26
127.51
124.36
124.19
111.13
133.58
125.87
105.27
90.88
61.28
39.61
21.45
21.16
172.25
165.42
153.88
Normalized Intensity
Chemical Shift (ppm)

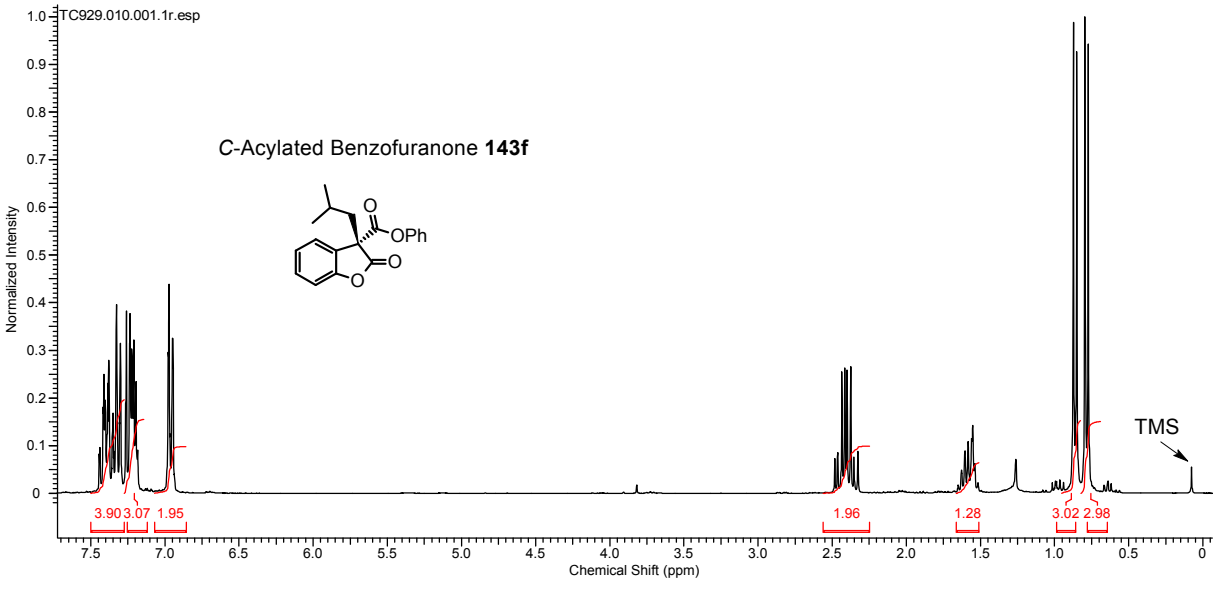
TC929.010.001.1r.esp
C-Acylated Benzofuranone 143f
O
OPh
O
TMS
3.90 3.07 1.95
1.96
1.28
3.02 2.98
Normalized Intensity
Chemical Shift (ppm)

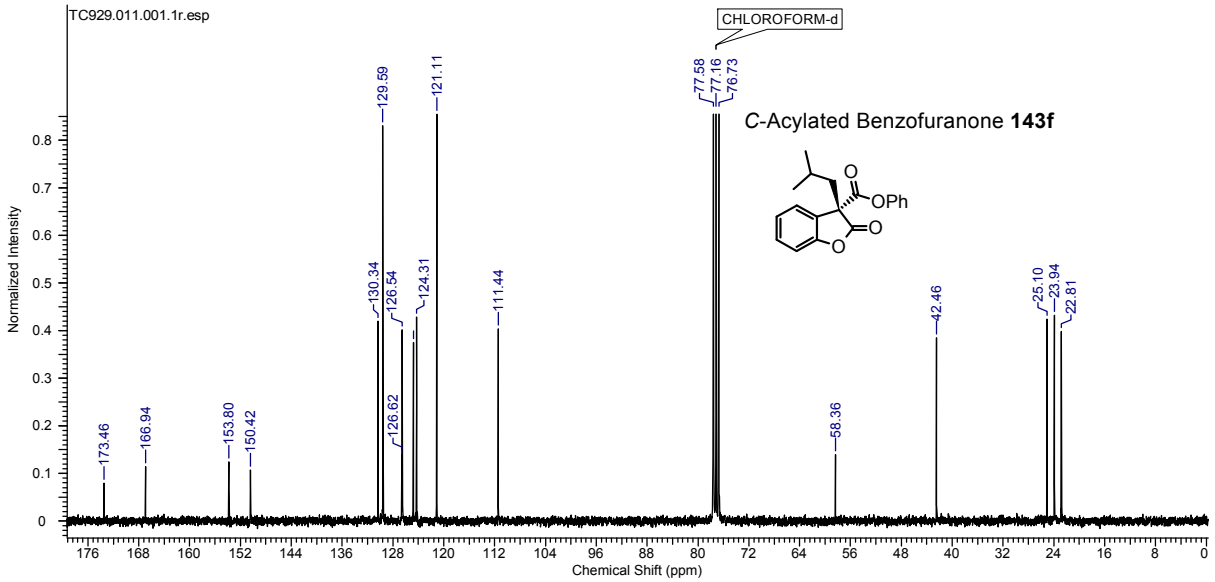
TC929.011.001.1r.esp
CHLOROFORM-d
77.58
77.16
76.73
129.59
121.11
130.34
126.54
124.31
111.44
126.62
173.46
166.94
153.80
150.42
58.36
42.46
25.10
23.94
22.81
C-Acylated Benzofuranone 143f
OPh
Normalized Intensity
Chemical Shift (ppm)

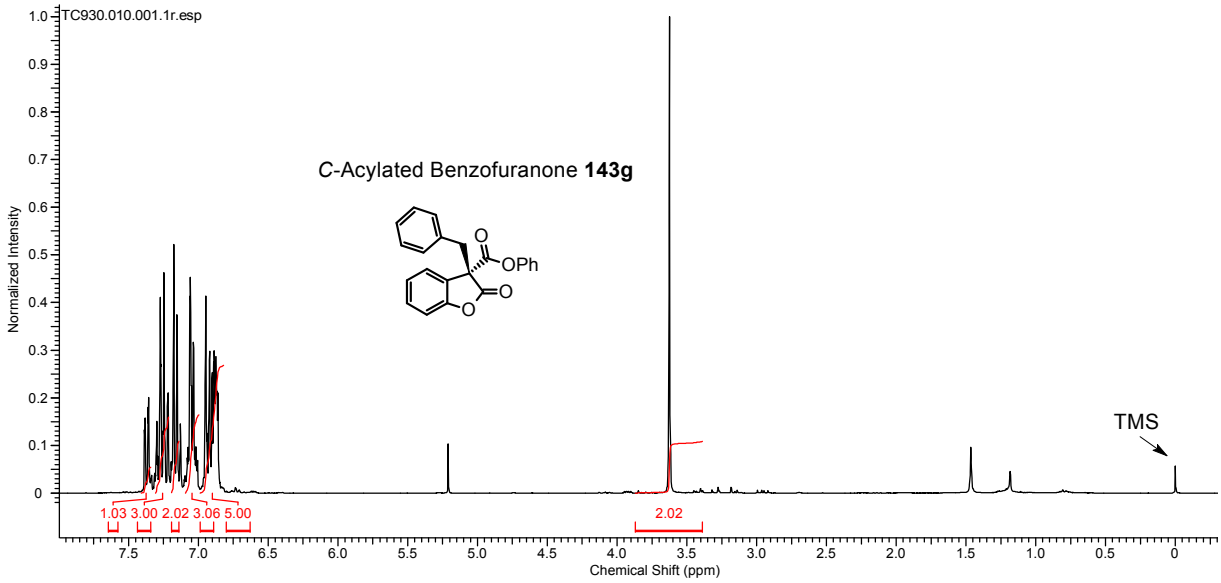
TC930.010.001.1r.esp
C-Acylated Benzofuranone 143g
OPh
TMS
1.03 3.00 2.02 3.06 5.00
2.02
Normalized Intensity
Chemical Shift (ppm)

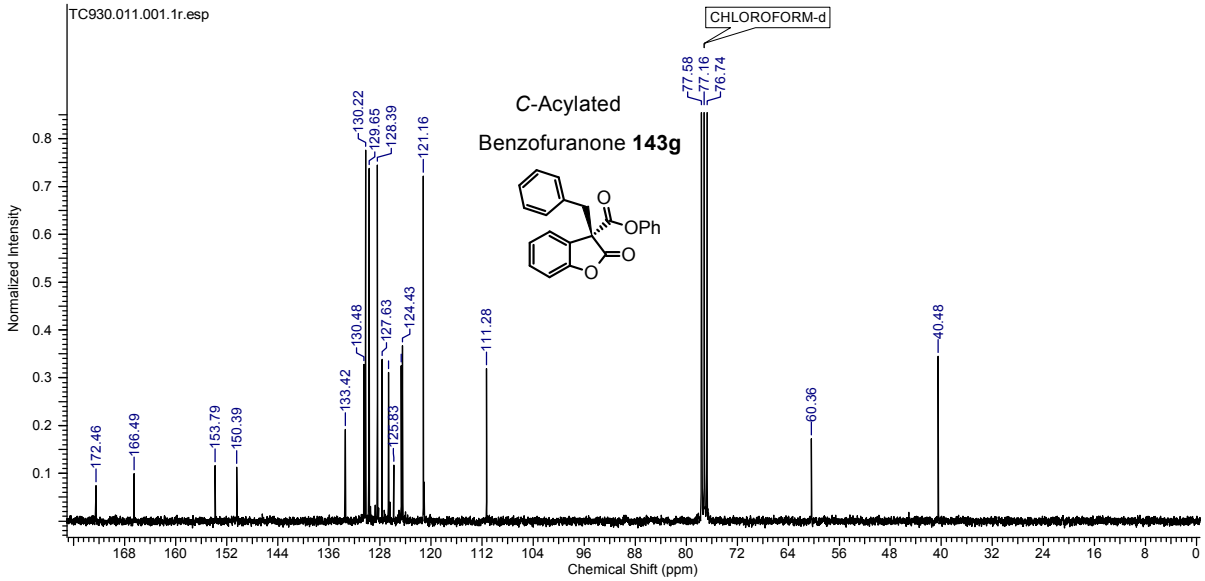
TC930.011.001.1r.esp
CHLOROFORM-d
77.58
77.16
76.74
C-Acylated
Benzofuranone 143g
OPh
130.22
129.65
128.39
121.16
130.48
127.63
124.43
111.28
133.42
125.83
172.46
166.49
153.79
150.39
60.36
40.48
Normalized Intensity
Chemical Shift (ppm)

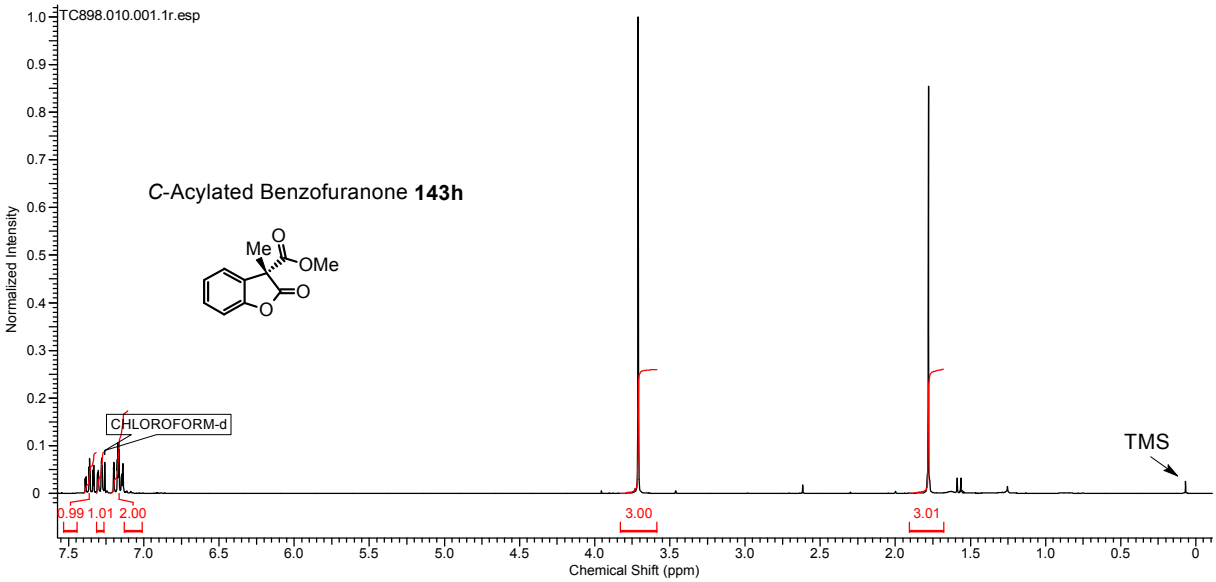
TC898.010.001.1r.esp
C-Acylated Benzofuranone 143h
Me
O
OMe
O
O
CHLOROFORM-d
TMS
0.99 1.01 2.00
3.00
3.01
Normalized Intensity
Chemical Shift (ppm)

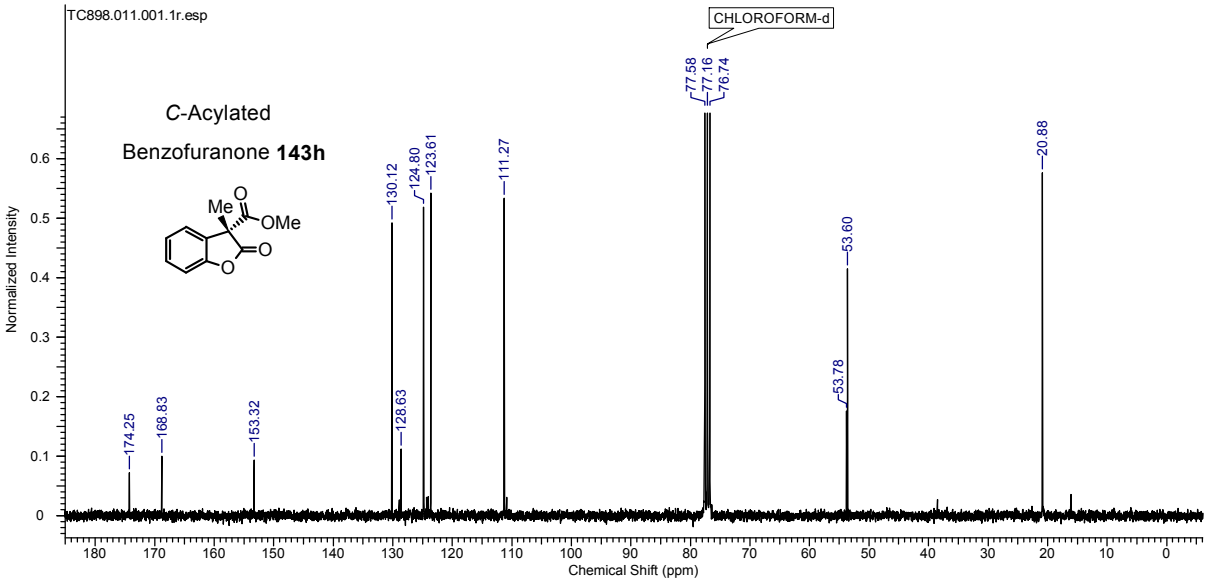
TC898.011.001.1r.esp
C-Acylated
Benzofuranone 143h
Me
O
OMe
O
O
CHLOROFORM-d
77.58
77.16
76.74
130.12
124.80
123.61
111.27
53.60
53.78
20.88
174.25
168.83
153.32
128.63
Normalized Intensity
Chemical Shift (ppm)

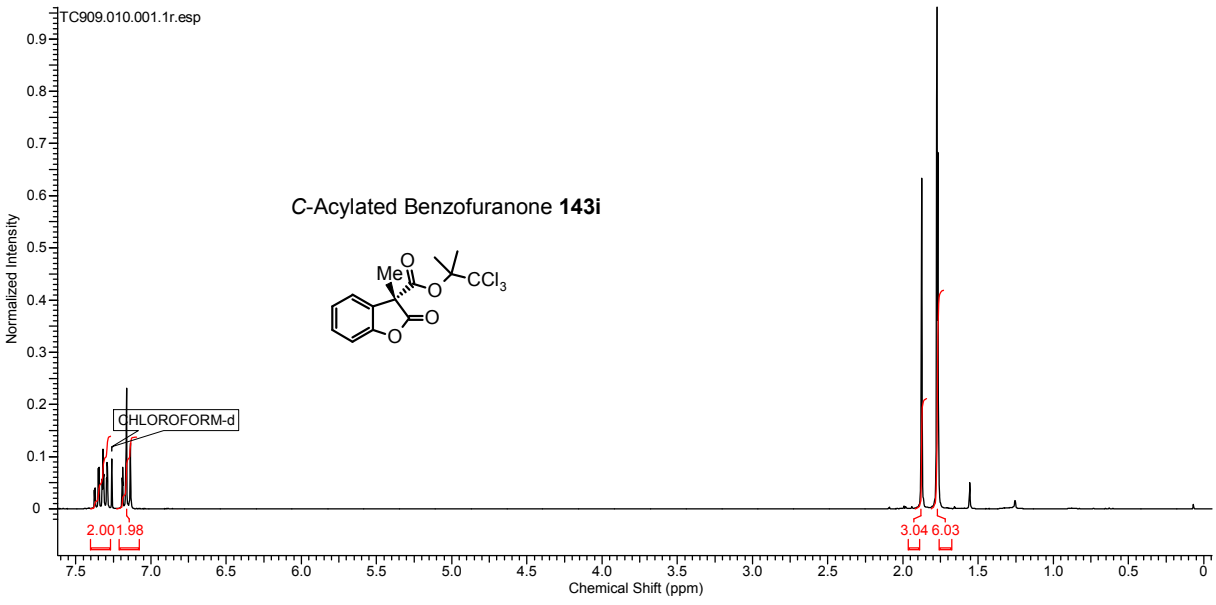
TC909.010.001.1r.esp
C-Acylated Benzofuranone 143i
Me
O
O
CCl3
O
O
CHLOROFORM-d
2.00 1.98
3.04 6.03
Normalized Intensity
Chemical Shift (ppm)

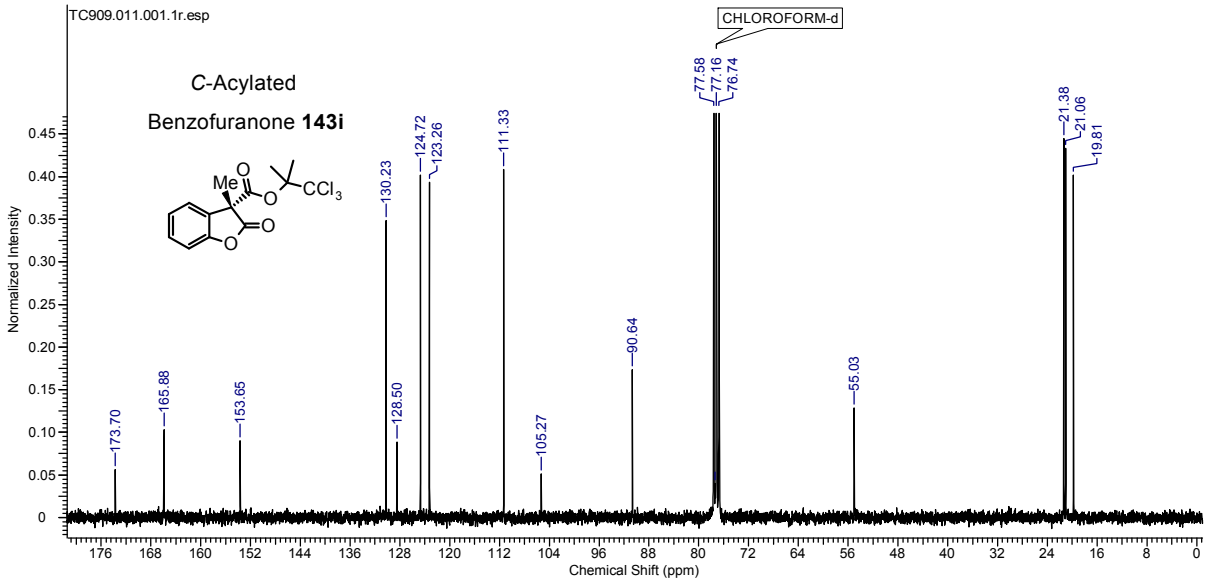
TC909.011.001.1r.esp
CHLOROFORM-d
C-Acylated
Benzofuranone 143i
Me
O
O
CCl3
O
O
77.58
77.16
76.74
130.23
124.72
123.26
111.33
21.38
21.06
19.81
90.64
55.03
173.70
165.88
153.65
128.50
105.27
Normalized Intensity
Chemical Shift (ppm)

5.3.3 ^{1}H and ^{13}C NMR Spectra of *α*-Chiral *N*-Acyl Pyrroles 163 (Table 19)

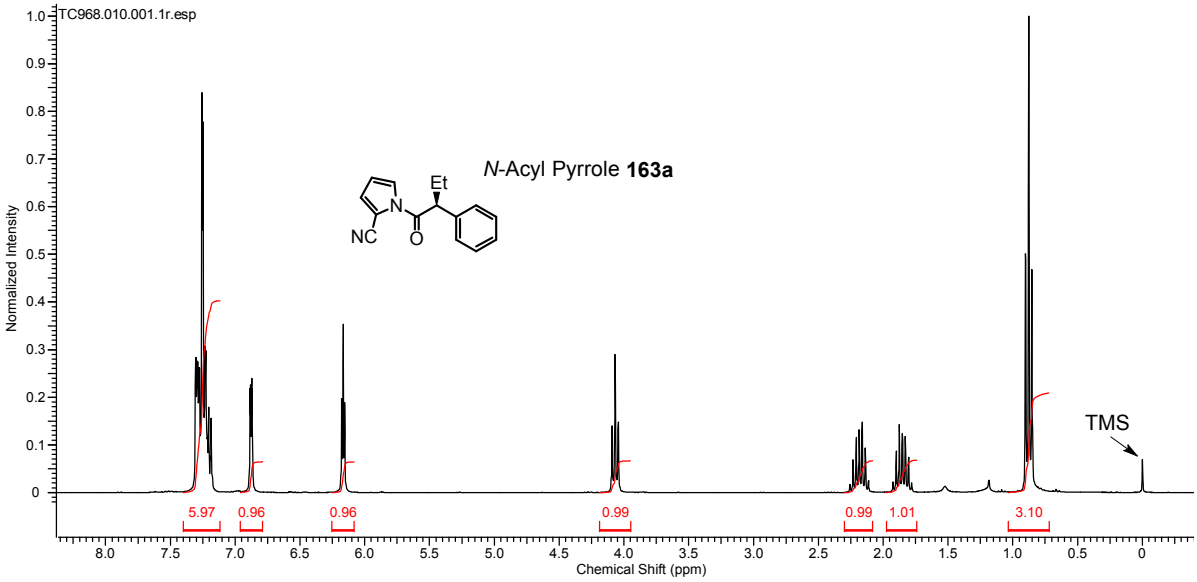

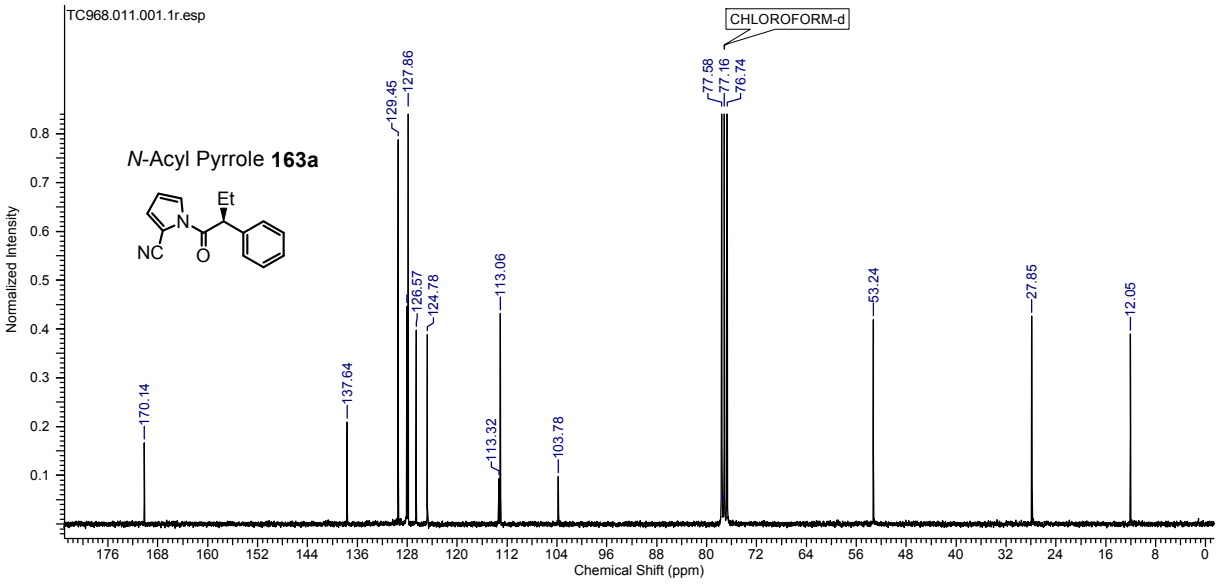

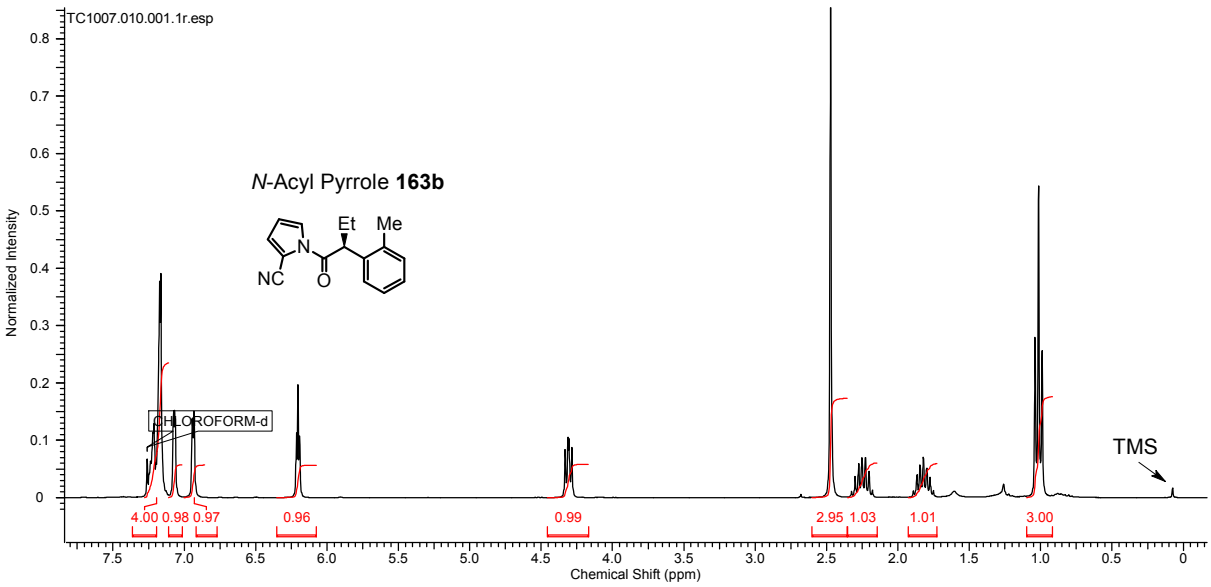

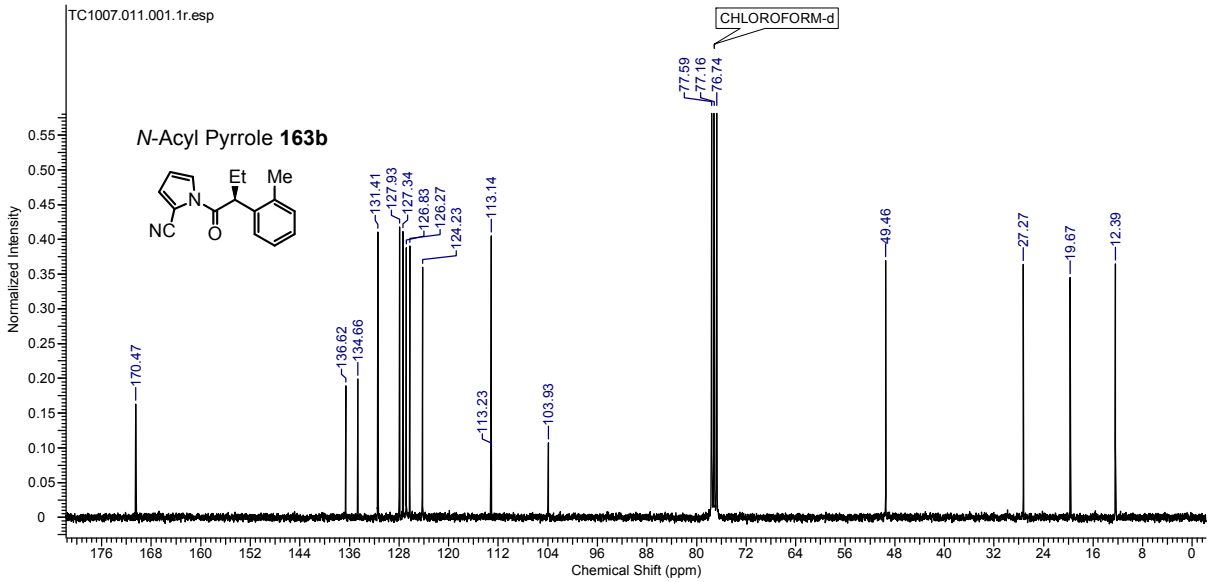
TC1007.011.001.1r.esp
CHLOROFORM-d
77.59
77.16
76.74
N-Acyl Pyrrole 163b
Et
Me
NC
O
131.41
127.93
127.34
126.83
126.27
124.23
113.14
49.46
27.27
19.67
12.39
170.47
136.62
134.66
113.23
103.93
Normalized Intensity
Chemical Shift (ppm)

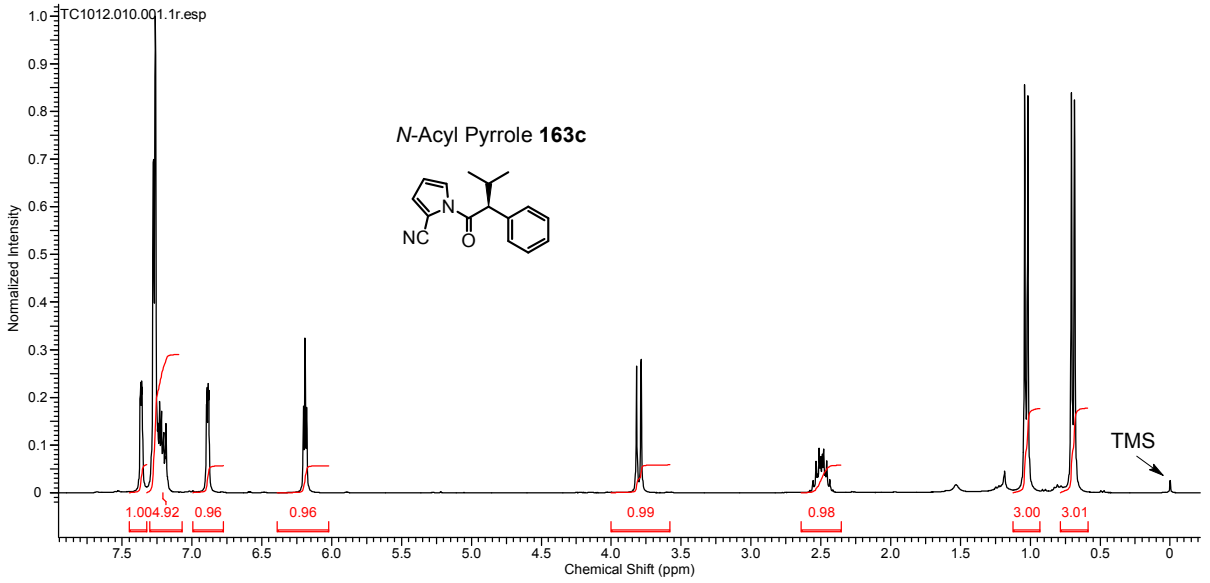
TC1012.010.001.1r.esp
N-Acyl Pyrrole 163c
NC
O
TMS
1.00
4.92
0.96
0.96
0.99
0.98
3.00
3.01
Normalized Intensity
Chemical Shift (ppm)

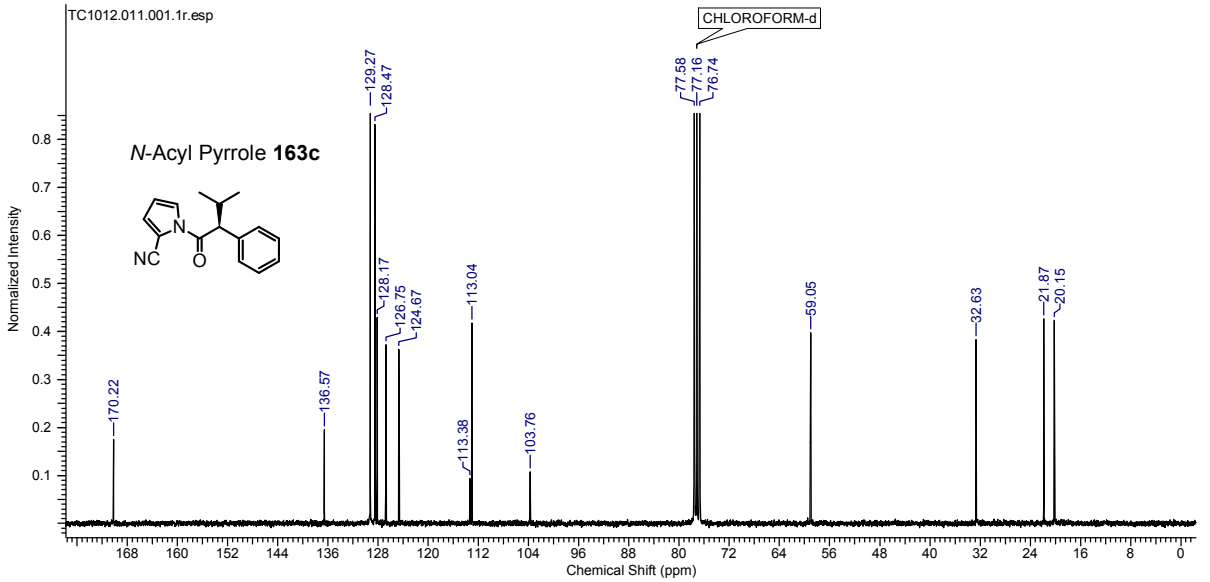
TC1012.011.001.1r.esp
CHLOROFORM-d
77.58
77.16
76.74
N-Acyl Pyrrole 163c
NC
O
129.27
128.47
128.17
126.75
124.67
113.04
59.05
32.63
21.87
20.15
170.22
136.57
113.38
103.76
Normalized Intensity
Chemical Shift (ppm)

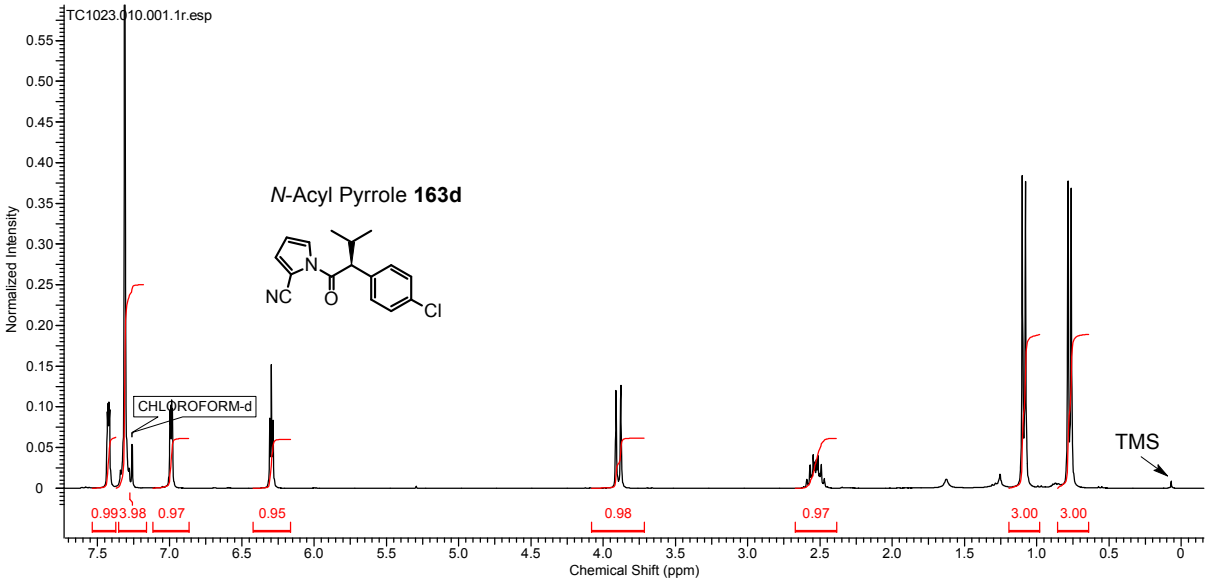
TC1023.010.001.1r.esp
Normalized Intensity
N-Acyl Pyrrole 163d
NC
O
Cl
CHLOROFORM-d
TMS
0.99 3.98 0.97 0.95 0.98 0.97 3.00 3.00
Chemical Shift (ppm)

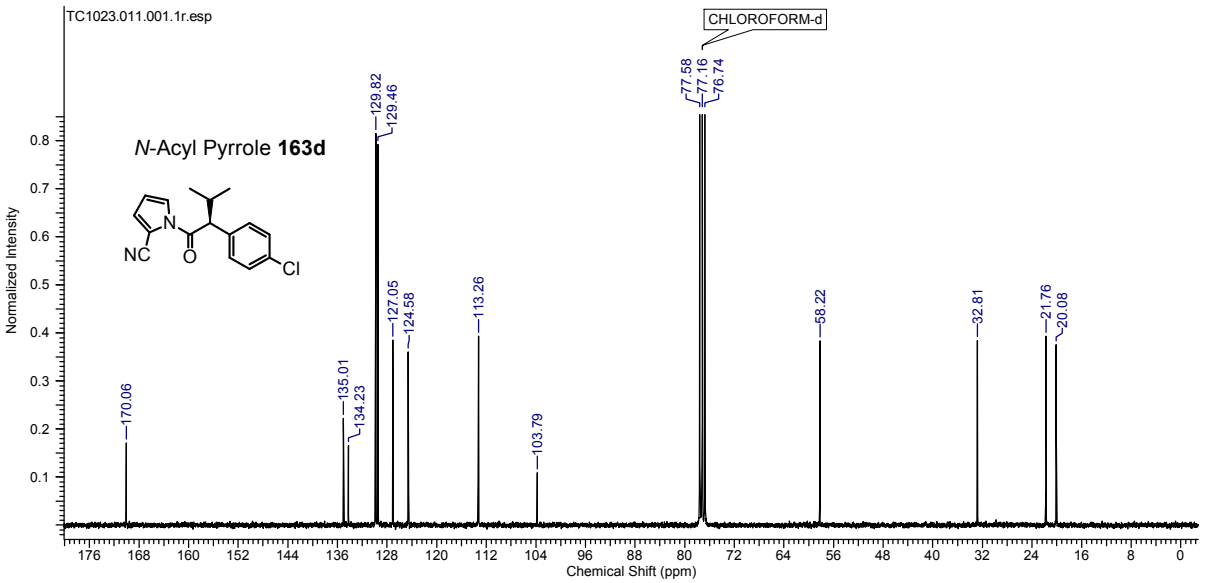
TC1023.011.001.1r.esp
Normalized Intensity
N-Acyl Pyrrole 163d
NC
O
Cl
CHLOROFORM-d
77.58
77.16
76.74
129.82
129.46
127.05
124.58
135.01
134.23
113.26
170.06
103.79
58.22
32.81
21.76
20.08
Chemical Shift (ppm)

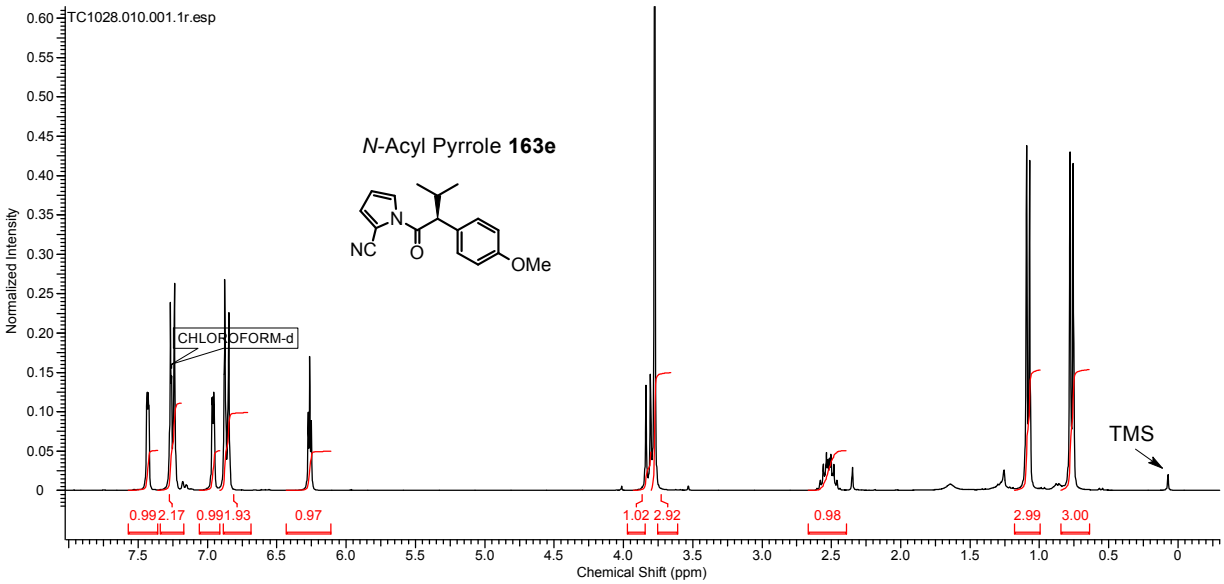
TC1028.010.001.1r.esp
Normalized Intensity
N-Acyl Pyrrole 163e
NC
O
OMe
CHLOROFORM-d
TMS
0.99 2.17 0.99 1.93 0.97 1.02 2.92 0.98 2.99 3.00
Chemical Shift (ppm)

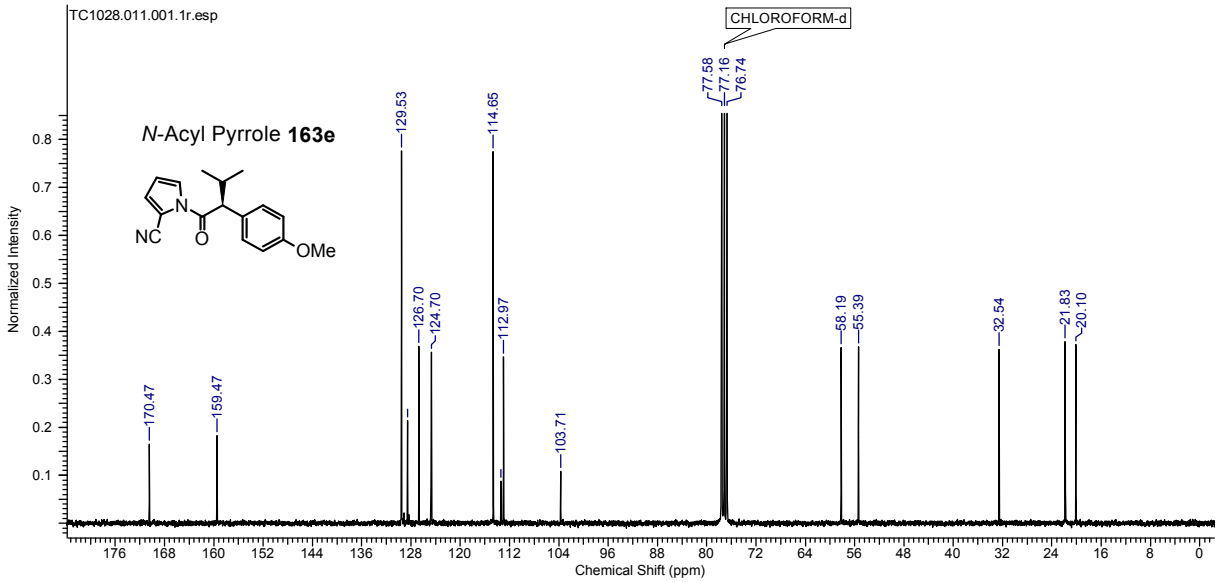
TC1028.011.001.1r.esp
CHLOROFORM-d
77.58
77.16
76.74
129.53
114.65
126.70
124.70
112.97
103.71
170.47
159.47
58.19
55.39
32.54
21.83
20.10
N-Acyl Pyrrole 163e
NC
O
OMe
Normalized Intensity
Chemical Shift (ppm)

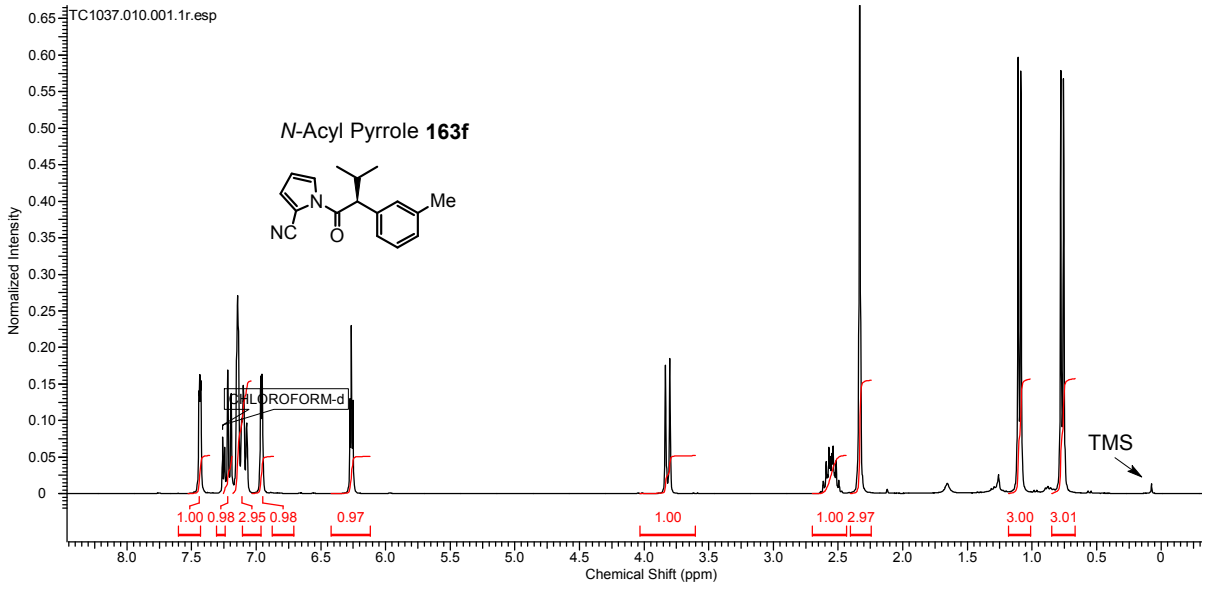
TC1037.010.001.1r.esp
N-Acyl Pyrrole 163f
NC
O
Me
CHLOROFORM-d
TMS
1.00 0.98 2.95 0.98
0.97
1.00
1.00 2.97
3.00 3.01
Normalized Intensity
Chemical Shift (ppm)

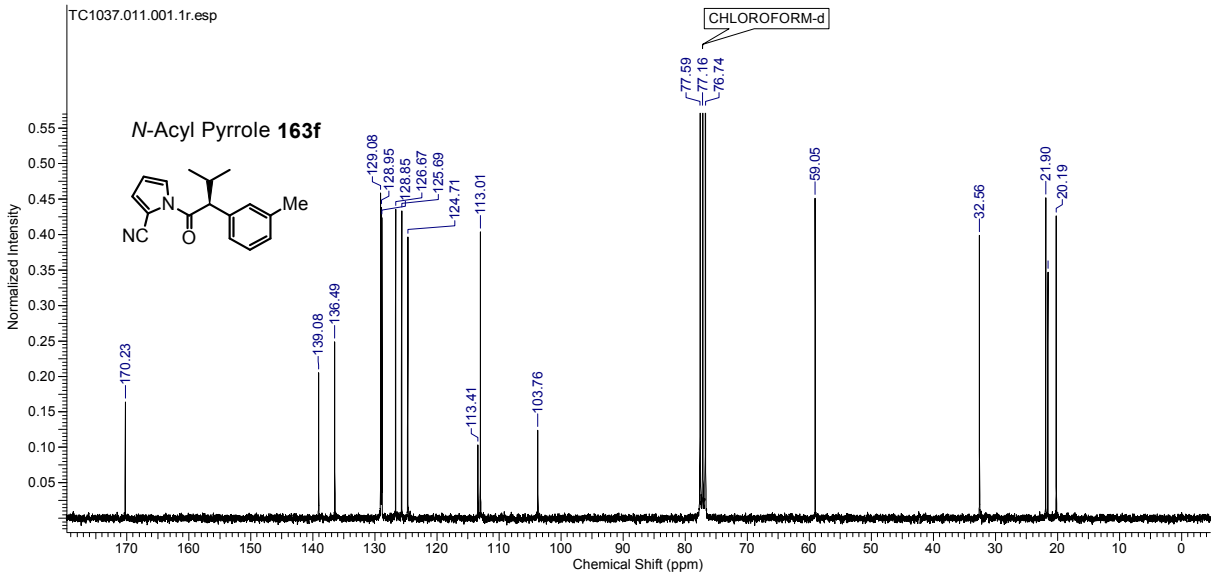
TC1037.011.001.1r.esp
CHLOROFORM-d
77.59
77.16
76.74
129.08
128.95
128.85
126.67
125.69
124.71
113.01
59.05
32.56
21.90
20.19
170.23
139.08
136.49
113.41
103.76
N-Acyl Pyrrole 163f
NC
O
Me
Normalized Intensity
Chemical Shift (ppm)

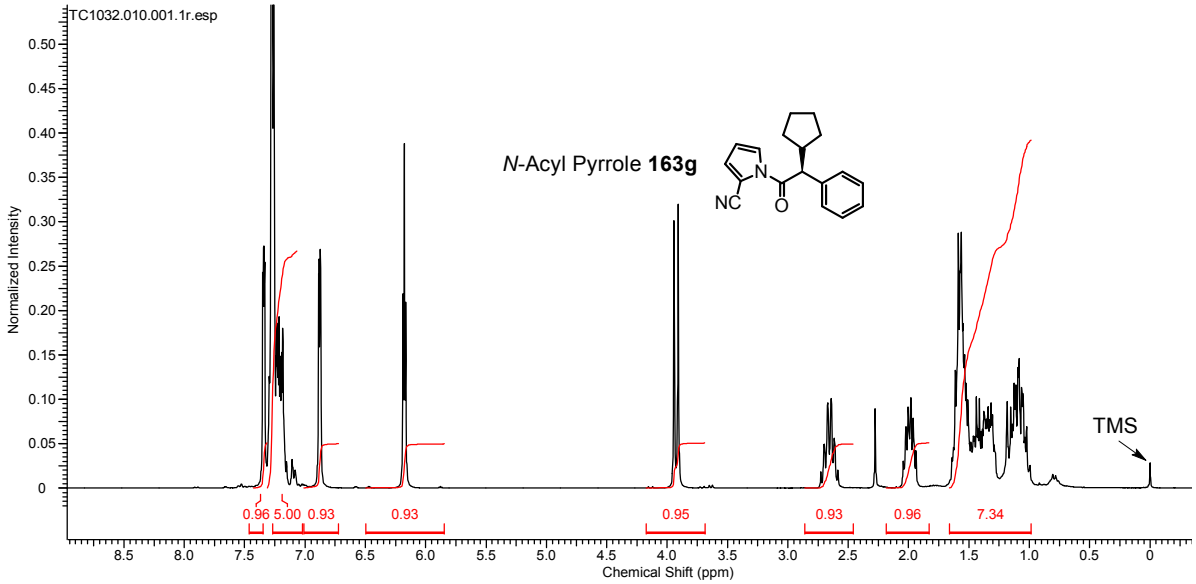
TC1032.010.001.1r.esp
Normalized Intensity
N-Acyl Pyrrole 163g
NC
O
TMS
0.96
5.00
0.93
0.93
0.95
0.93
0.96
7.34
Chemical Shift (ppm)

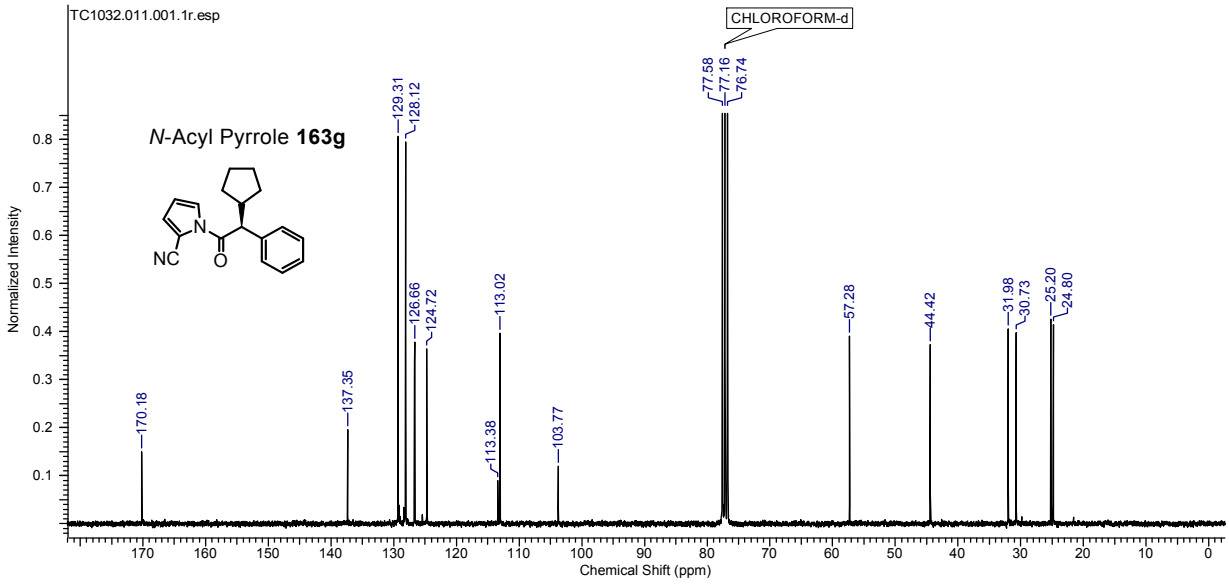
TC1032.011.001.1r.esp
CHLOROFORM-d
77.58
77.16
76.74
129.31
128.12
126.66
124.72
113.02
113.38
103.77
137.35
170.18
57.28
44.42
31.98
30.73
25.20
24.80
N-Acyl Pyrrole 163g
NC
O
Normalized Intensity
Chemical Shift (ppm)

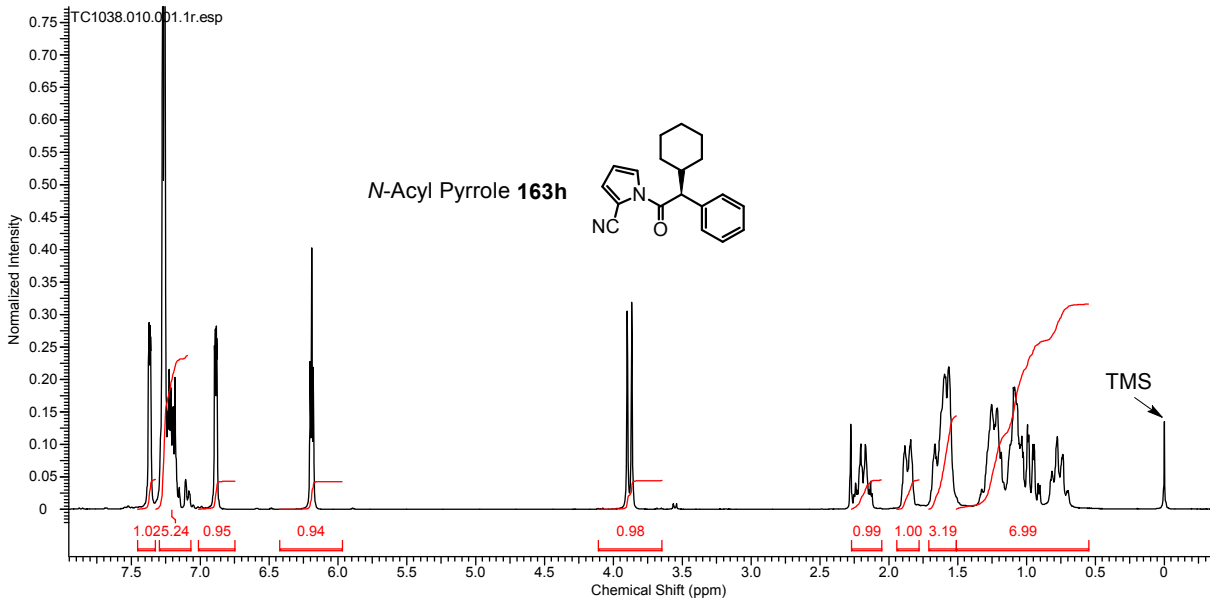
TC1038.010.001.1r.esp
N-Acyl Pyrrole 163h
NC
O
TMS
1.02
5.24
0.95
0.94
0.98
0.99
1.00
3.19
6.99
Normalized Intensity
Chemical Shift (ppm)

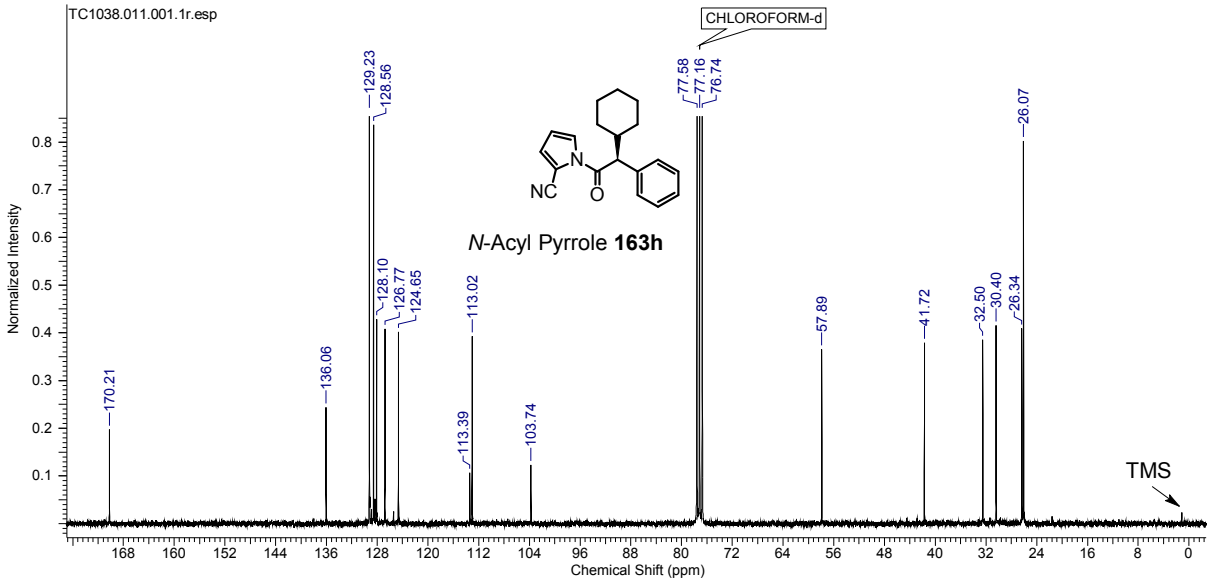
TC1038.011.001.1r.esp
CHLOROFORM-d
129.23
128.56
77.58
77.16
76.74
26.07
128.10
126.77
124.65
113.02
57.89
41.72
32.50
30.40
26.34
170.21
136.06
113.39
103.74
TMS
Normalized Intensity
Chemical Shift (ppm)
N
NC
O
N-Acyl Pyrrole **163h**

5.4 HPLC Traces of Products 14 (Table 10), 143 (Table 13), 163 (Table 19)

5.4.1 HPLC Traces of *C*-Acylated Azlactones 14 (Table 10)

Product **14a** from Table 10:

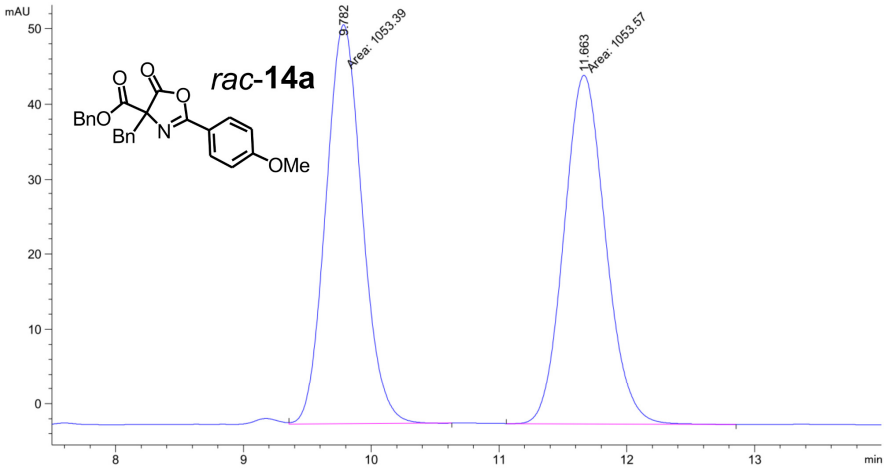

Peak #	RetTime [min]	Type	Width [min]	Area mAU *s	Height [mAU]	Area %
1	9.782	FM	0.3300	1053.38940	53.19519	49.9957
2	11.663	MM	0.3774	1053.56921	46.52334	50.0043

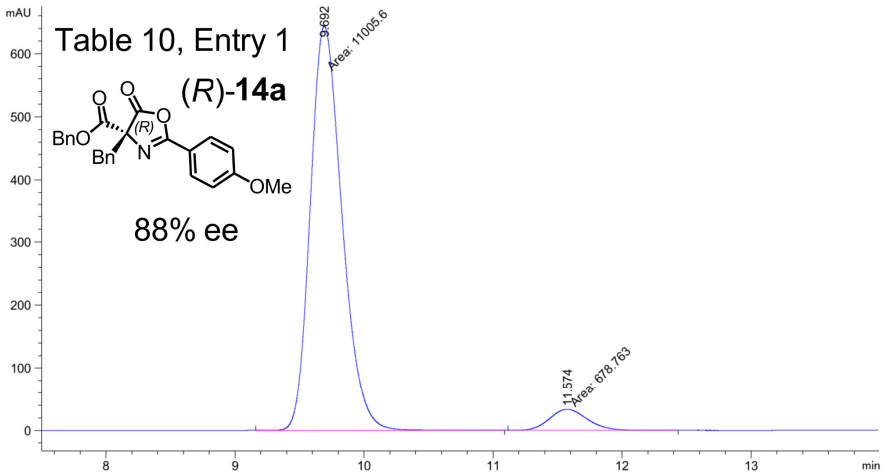

Peak #	RetTime [min]	Type	Width [min]	Area [mAU*s]	Height [mAU]	Area %
1	9.692	FM	0.2850	1.10056e4	643.54675	94.1908
2	11.574	MM	0.3388	678.76318	33.39364	5.8092

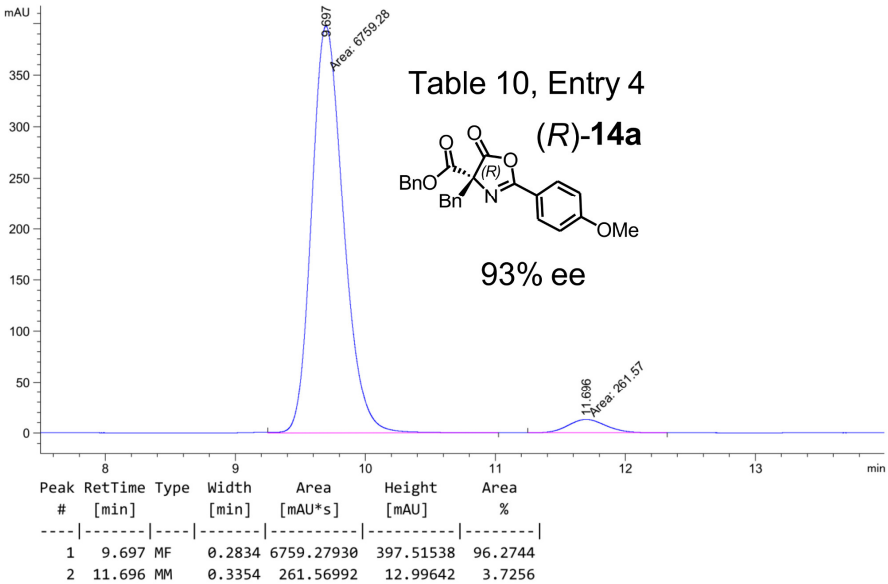

Peak #	RetTime [min]	Type	Width [min]	Area [mAU*s]	Height [mAU]	Area %
1	9.697	MF	0.2834	6759.27930	397.51538	96.2744
2	11.696	MM	0.3354	261.56992	12.99642	3.7256

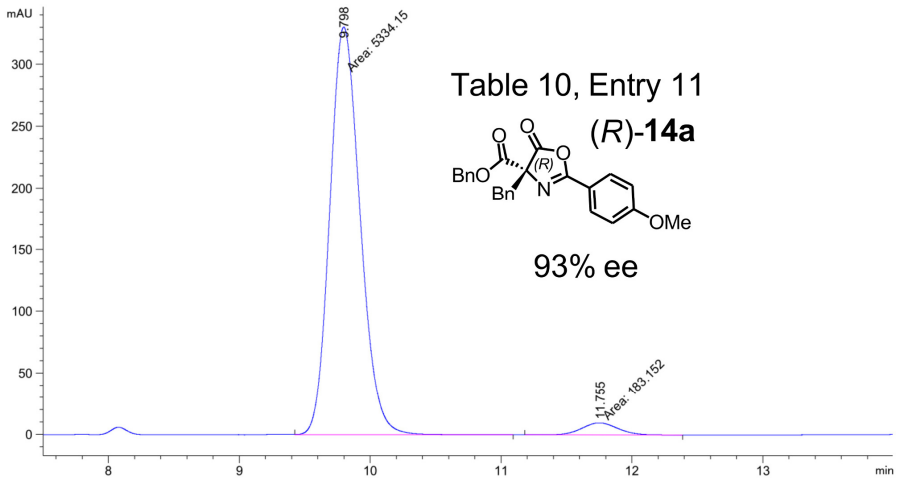

Peak #	RetTime [min]	Type	Width [min]	Area [mAU*s]	Height [mAU]	Area %
1	9.798	FM	0.2690	5334.15234	330.54672	96.6804
2	11.755	MM	0.3153	183.15207	9.68142	3.3196

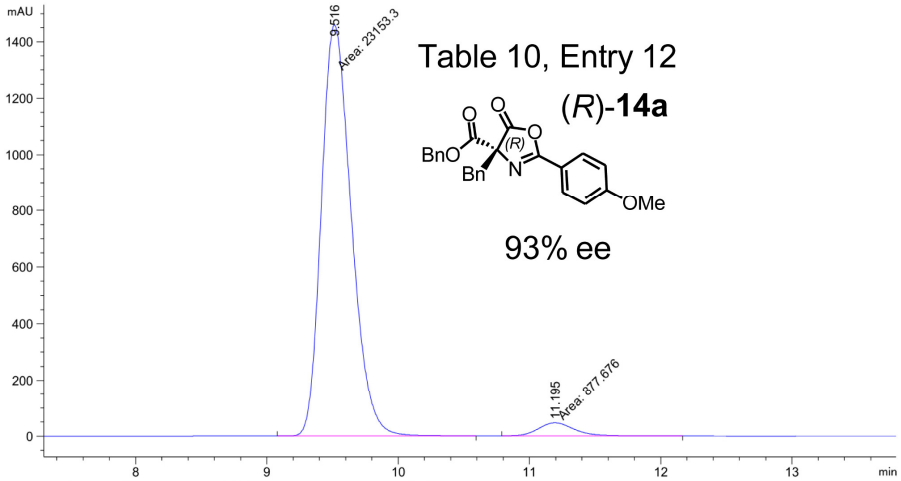

Peak #	RetTime [min]	Type	Width [min]	Area [mAU*s]	Height [mAU]	Area %
1	9.516	MM	0.2645	2.31533e4	1458.76880	96.3477
2	11.195	MM	0.3147	877.67596	46.47856	3.6523

Product **14b** from Table 10:

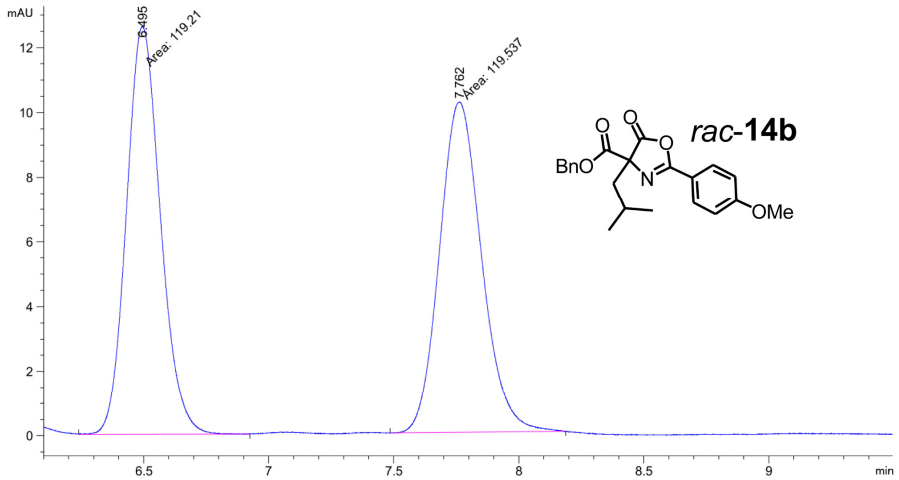

Peak #	RetTime [min]	Type	Width [min]	Area [mAU*s]	Height [mAU]	Area %
1	6.495	MM	0.1576	119.20994	12.60525	49.9314
2	7.762	MM	0.1950	119.53735	10.21900	50.0686

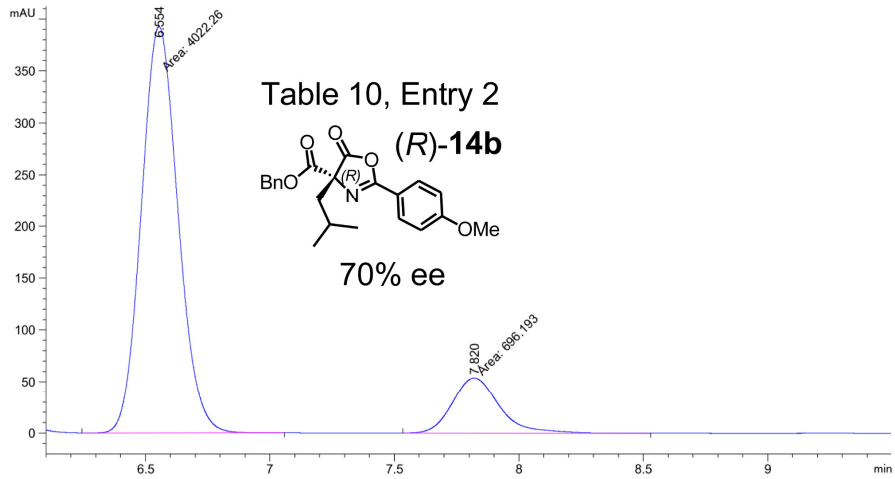

Peak #	RetTime [min]	Type	Width [min]	Area [mAU*s]	Height [mAU]	Area %
1	6.554	MM	0.1708	4022.26001	392.58298	85.2453
2	7.820	MM	0.2168	696.19293	53.52462	14.7547

Product **14c** from Table 10:

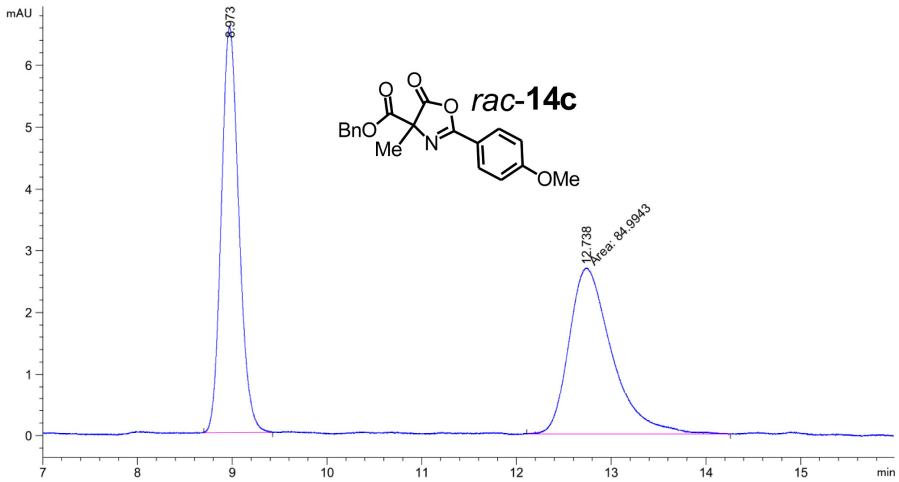

Peak #	RetTime [min]	Type	Width [min]	Area [mAU*s]	Height [mAU]	Area %
1	8.973	BB	0.1608	84.91059	6.56990	49.9754
2	12.738	MM	0.5266	84.99435	2.69020	50.0246

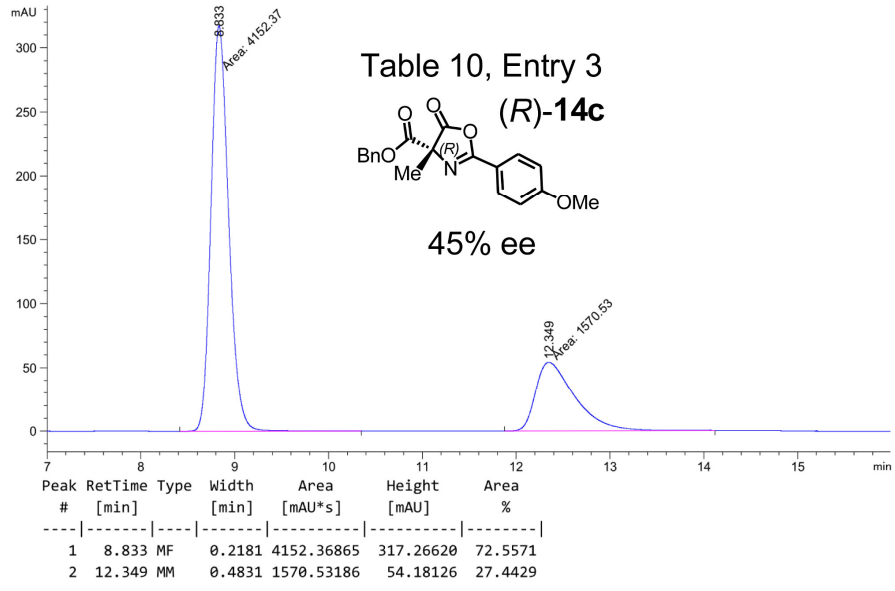

Peak #	RetTime [min]	Type	Width [min]	Area [mAU*s]	Height [mAU]	Area %
1	8.833	MF	0.2181	4152.36865	317.26620	72.5571
2	12.349	MM	0.4831	1570.53186	54.18126	27.4429

Product **14d** from Table 10:

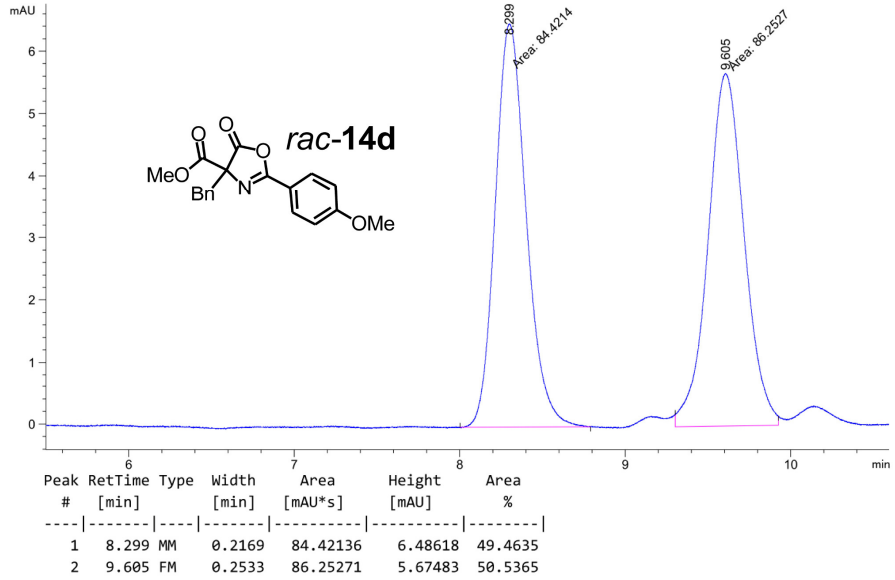

Peak #	RetTime [min]	Type	Width [min]	Area [mAU*s]	Height [mAU]	Area %
1	8.299	MM	0.2169	84.42136	6.48618	49.4635
2	9.605	FM	0.2533	86.25271	5.67483	50.5365

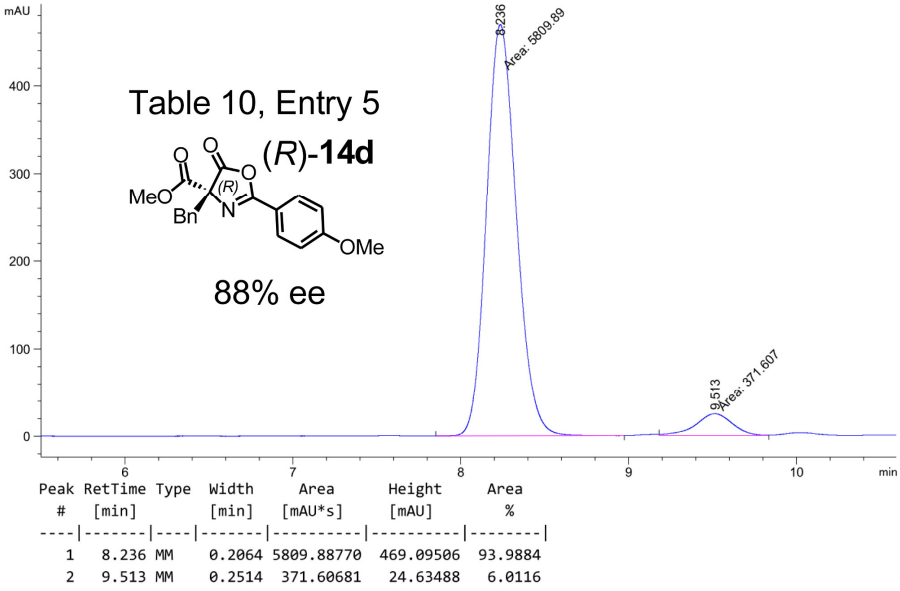

Peak #	RetTime [min]	Type	Width [min]	Area [mAU*s]	Height [mAU]	Area %
1	8.236	MM	0.2064	5809.88770	469.09506	93.9884
2	9.513	MM	0.2514	371.60681	24.63488	6.0116

Product **14e** from Table 10:

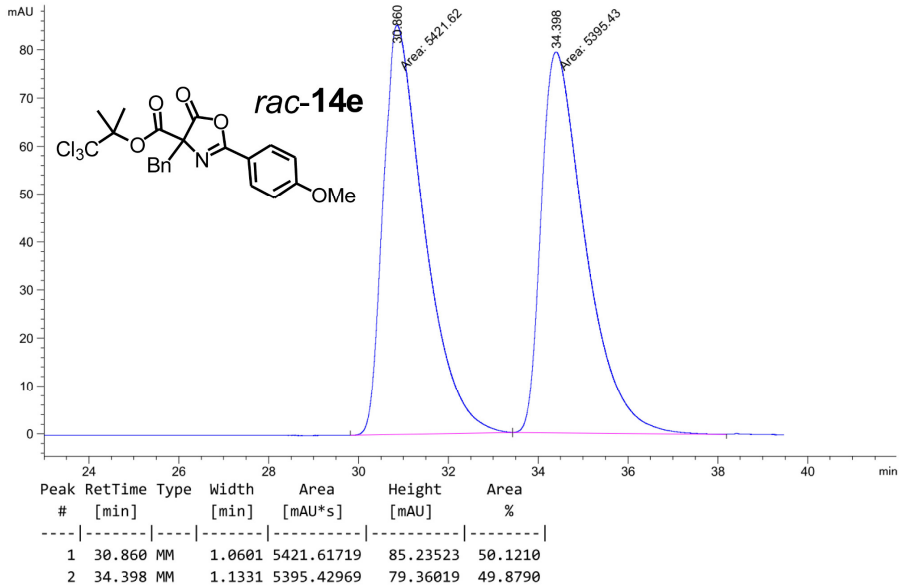

Peak #	RetTime [min]	Type	Width [min]	Area [mAU*s]	Height [mAU]	Area %
1	30.860	MM	1.0601	5421.61719	85.23523	50.1210
2	34.398	MM	1.1331	5395.42969	79.36019	49.8790

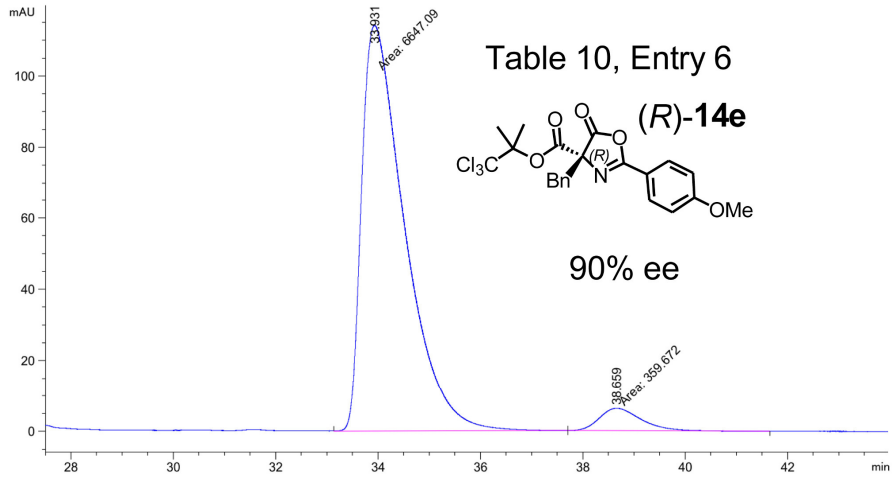

Peak #	RetTime [min]	Type	Width [min]	Area [mAU*s]	Height [mAU]	Area %
1	33.931	MM	0.9717	6647.08545	114.00632	94.8668
2	38.659	MF	0.9529	359.67212	6.29116	5.1332

Product **14f** from Table 10:

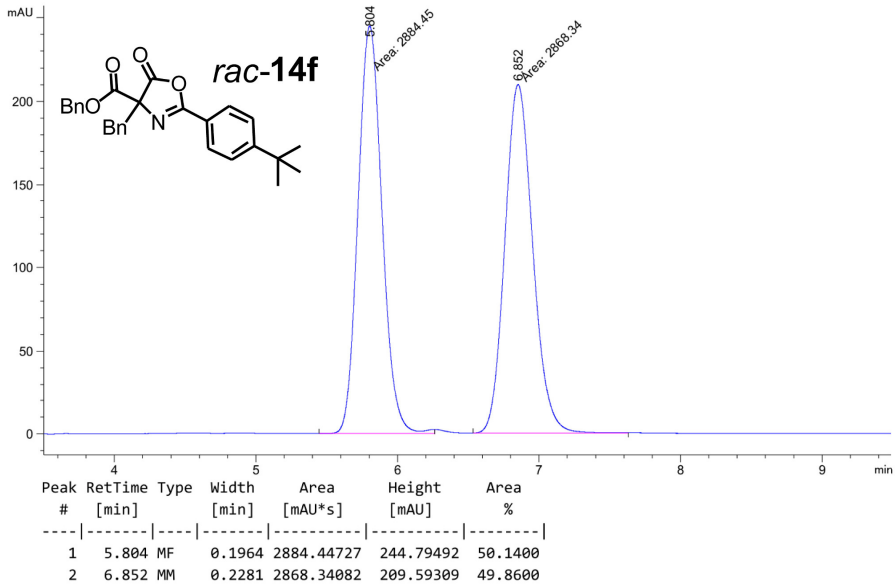

Peak #	RetTime [min]	Type	Width [min]	Area [mAU*s]	Height [mAU]	Area %
1	5.804	MF	0.1964	2884.44727	244.79492	50.1400
2	6.852	MM	0.2281	2868.34082	209.59309	49.8600

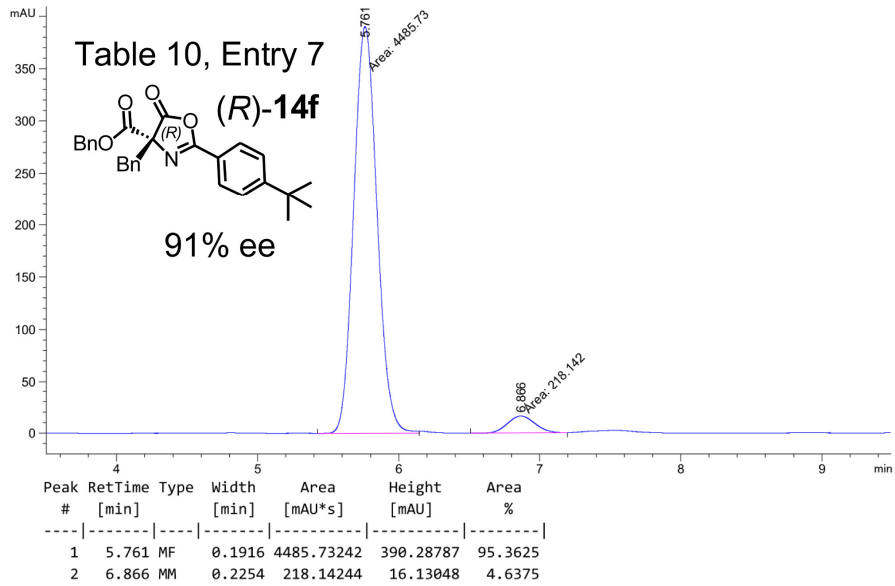

Peak #	RetTime [min]	Type	Width [min]	Area [mAU*s]	Height [mAU]	Area %
1	5.761	MF	0.1916	4485.73242	390.28787	95.3625
2	6.866	MM	0.2254	218.14244	16.13048	4.6375

Product **14g** from Table 10:

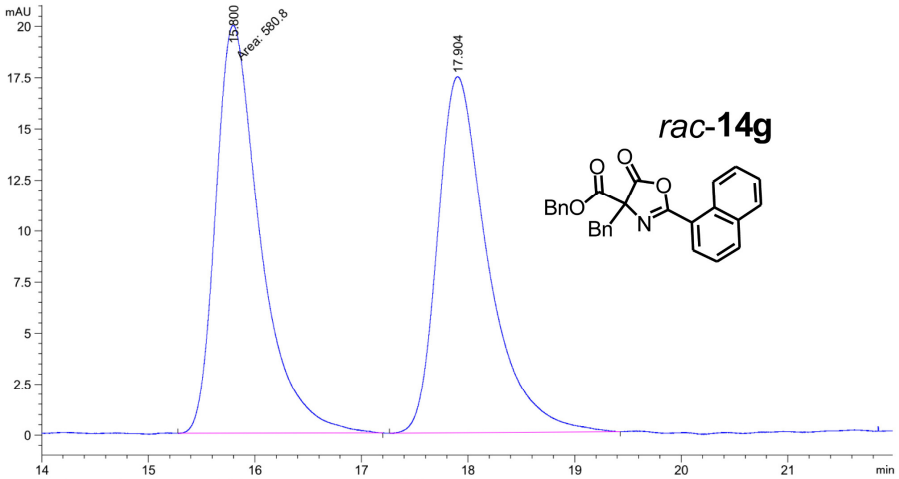

Peak #	RetTime [min]	Type	Width [min]	Area [mAU*s]	Height [mAU]	Area %
1	15.800	MM	0.4848	580.80017	19.96791	50.1846
2	17.904	BB	0.3908	576.52820	17.45533	49.8154

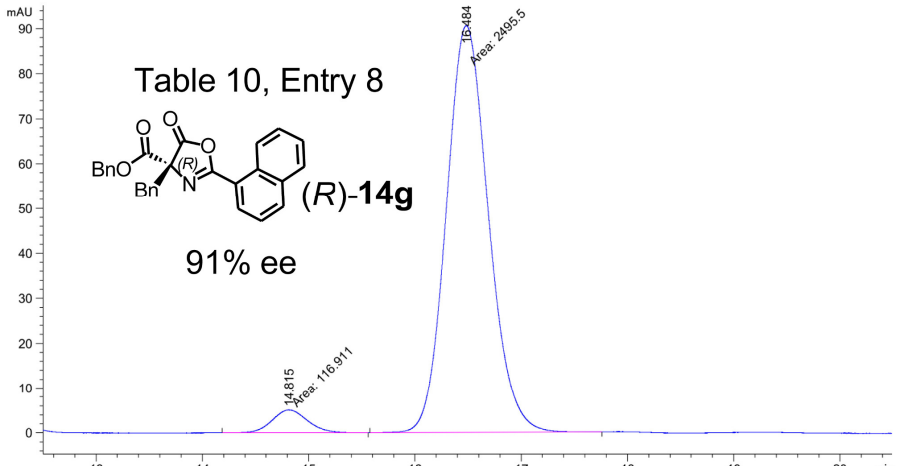

Peak #	RetTime [min]	Type	Width [min]	Area [mAU*s]	Height [mAU]	Area %
1	14.815	MM	0.3850	116.91068	5.06150	4.4752
2	16.484	MM	0.4592	2495.49634	90.57895	95.5248

Product **14h** from Table 10:

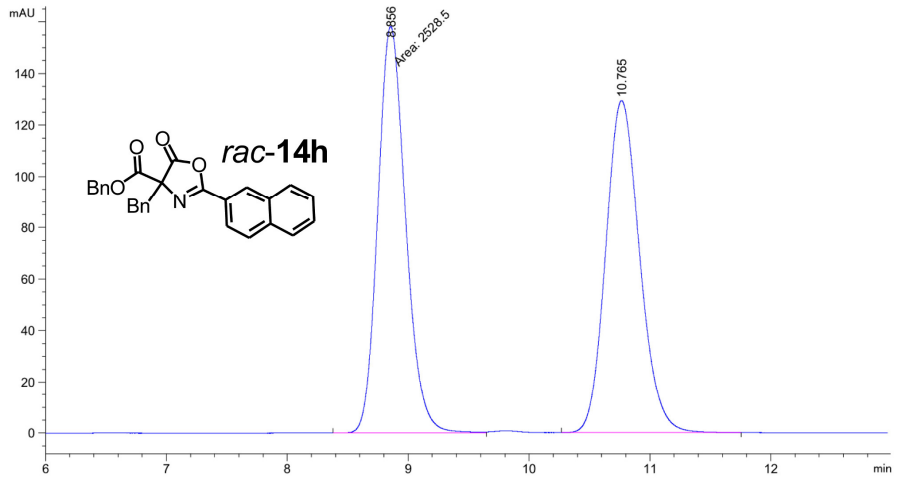

Peak #	RetTime [min]	Type	Width [min]	Area [mAU*s]	Height [mAU]	Area %
1	8.856	MF	0.2665	2528.49609	158.13303	50.0154
2	10.765	VB R	0.3009	2526.93433	129.33772	49.9846

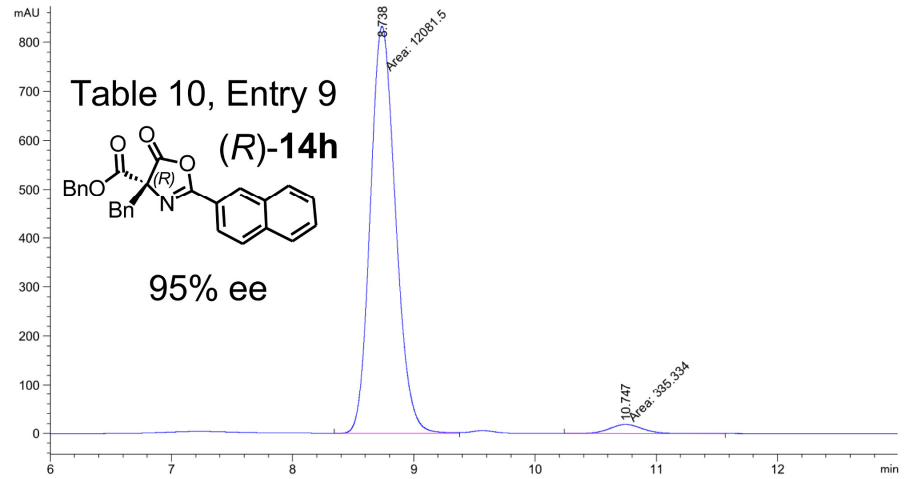

Peak #	RetTime [min]	Type	Width [min]	Area [mAU*s]	Height [mAU]	Area %
1	8.738	MF	0.2419	1.20815e4	832.49597	97.2994
2	10.747	MM	0.3078	335.33426	18.15687	2.7006

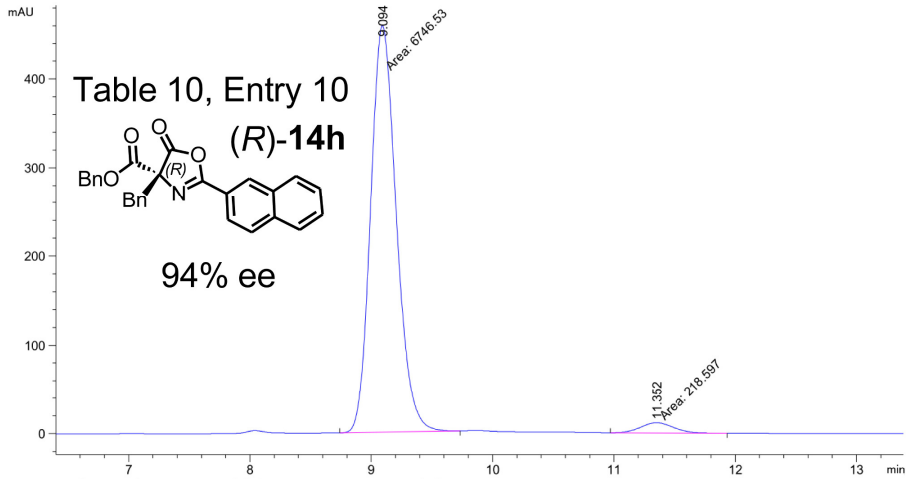

Peak #	RetTime [min]	Type	Width [min]	Area mAU *s	Height [mAU]	Area %
1	9.094	MM	0.2451	6746.53174	458.71774	96.8616
2	11.352	MM	0.3158	218.59657	11.53743	3.1384

Product **14i** from Table 10

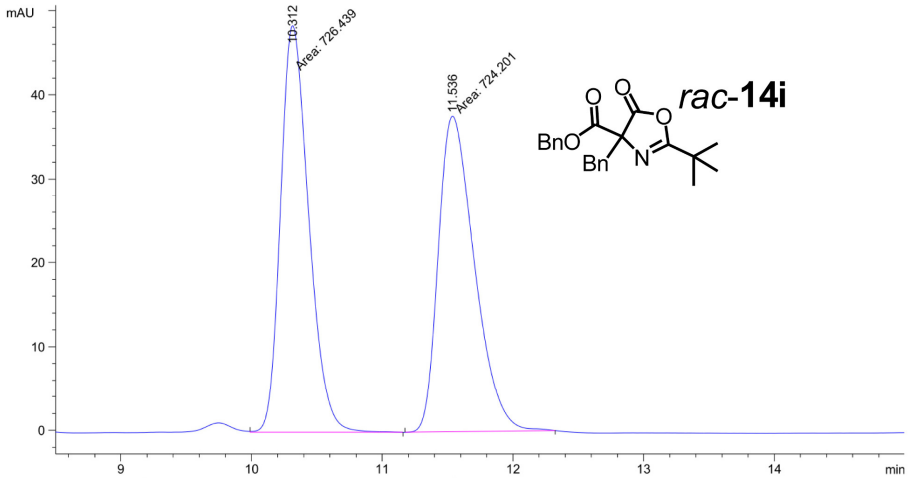

Peak #	RetTime [min]	Type	Width [min]	Area mAU *s	Height [mAU]	Area %
1	10.312	FM	0.2500	726.43921	48.43255	50.0771
2	11.536	MM	0.3206	724.20099	37.64690	49.9229

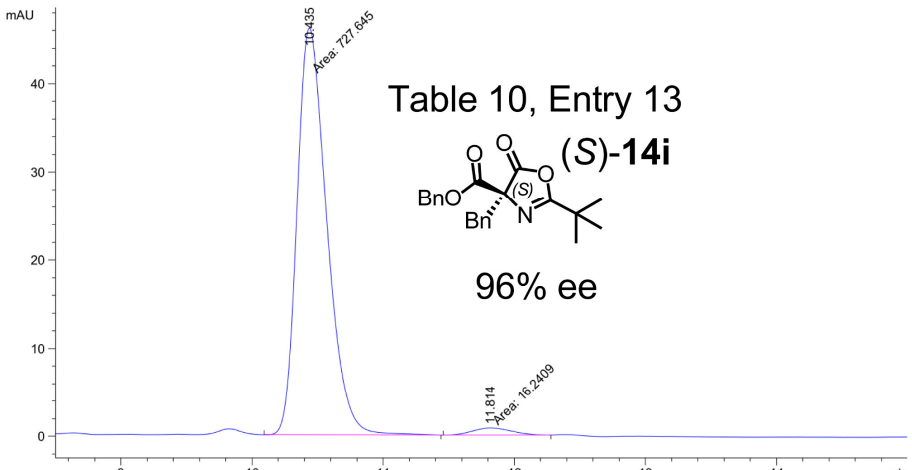

Peak #	RetTime [min]	Type	Width [min]	Area mAU *s	Height [mAU]	Area %
1	10.435	FM	0.2629	727.64453	46.12171	97.8167
2	11.814	MM	0.3371	16.24090	8.02915e-1	2.1833

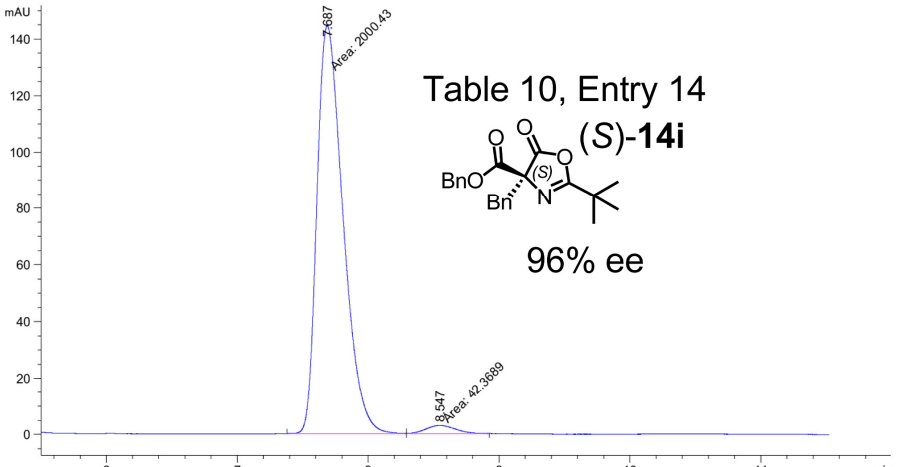

Peak #	RetTime [min]	Type	Width [min]	Area [mAU*s]	Height [mAU]	Area %
1	7.687	MM	0.2310	2000.43079	144.36105	97.9259
2	8.547	MM	0.2512	42.36893	2.81068	2.0741

5.4.2 HPLC Traces of *C*-Acylated Benzofuranones 143 (Table 13)

Product **143a** from Table 13 (*not isolated; determined from crude product mixture*):

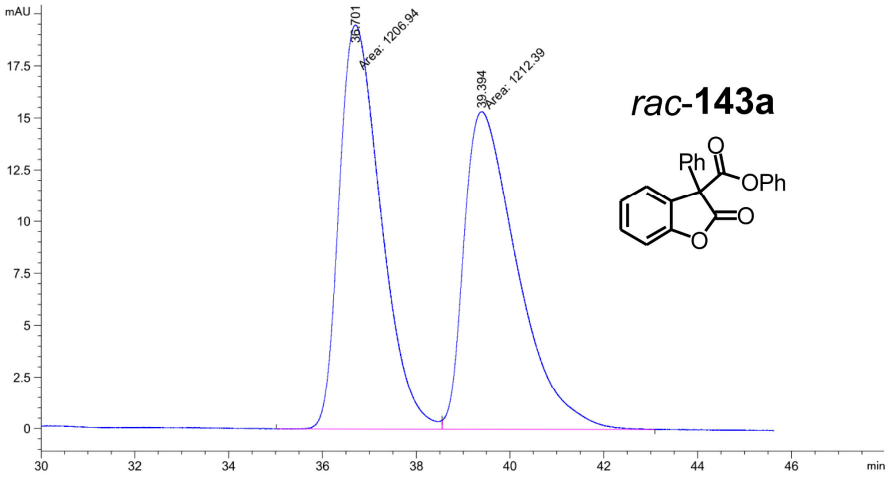

Peak #	RetTime [min]	Type	Width [min]	Area [mAU*s]	Height [mAU]	Area %
1	36.701	MF	1.0327	1206.94348	19.47822	49.8874
2	39.394	FM	1.3173	1212.39270	15.33905	50.1126

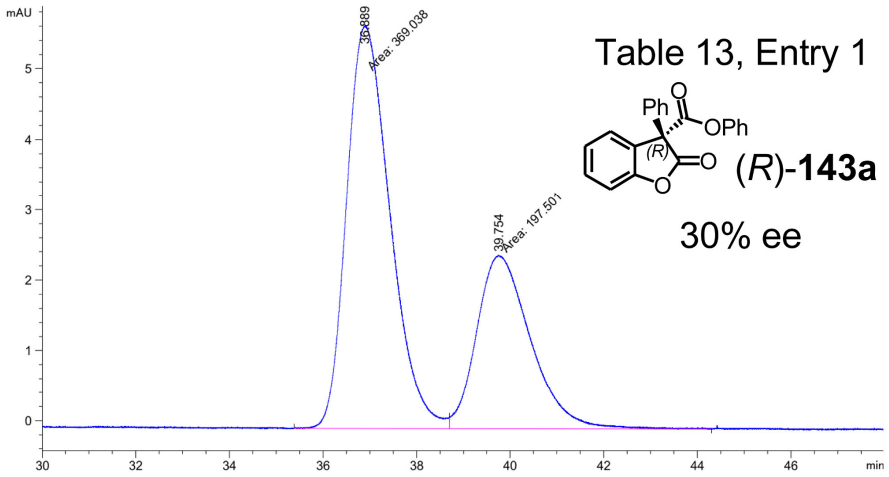

Peak #	RetTime [min]	Type	Width [min]	Area [mAU*s]	Height [mAU]	Area %
1	36.889	MF	1.0772	369.03806	5.70963	65.1390
2	39.754	FM	1.3337	197.50124	2.46808	34.8610

Product **143b** from Table 13:

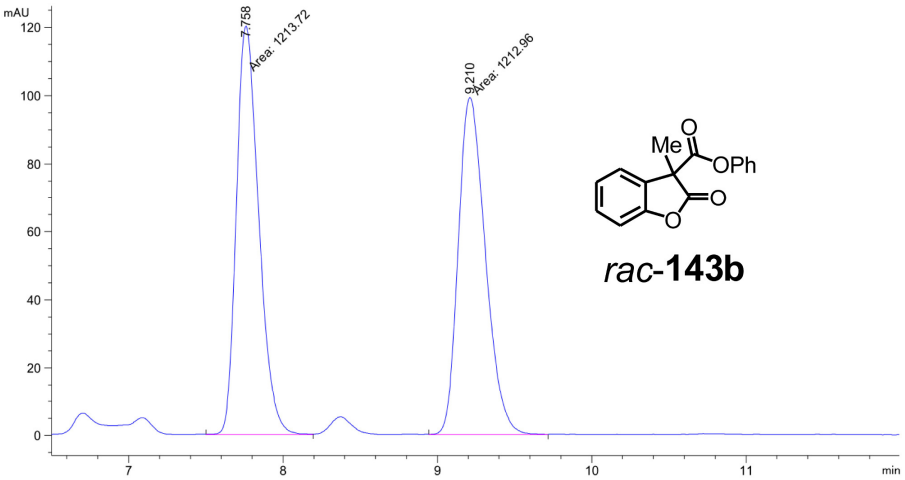

Peak #	RetTime [min]	Type	Width [min]	Area mAU *s	Height [mAU]	Area %
1	7.758	MM	0.1684	1213.71558	120.10494	50.0157
2	9.210	MM	0.2038	1212.95569	99.17461	49.9843

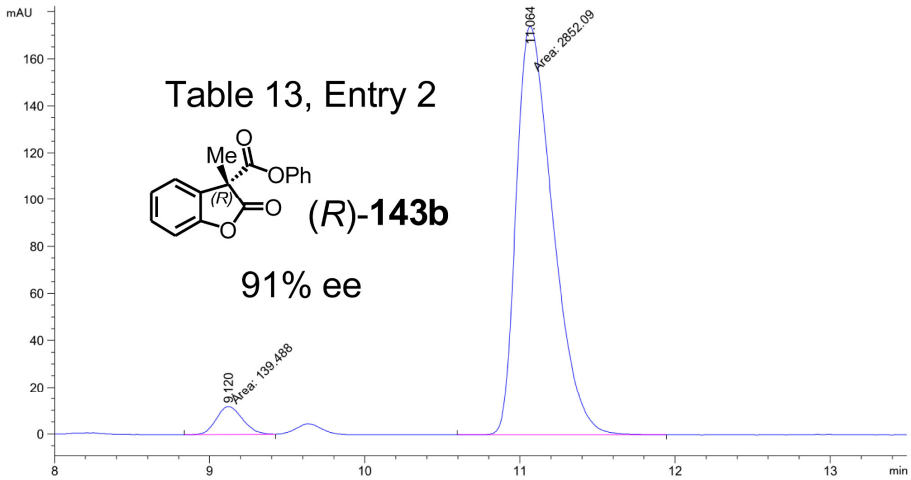

Peak #	RetTime [min]	Type	Width [min]	Area mAU *s	Height [mAU]	Area %
1	9.120	MM	0.1959	139.48756	11.86848	4.6627
2	11.064	MM	0.2729	2852.08667	174.19150	95.3373

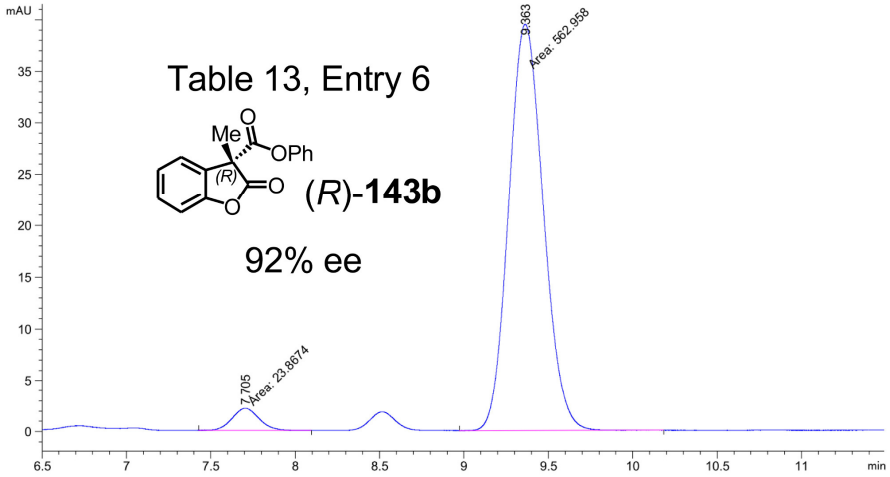

Peak #	RetTime [min]	Type	Width [min]	Area [mAU*s]	Height [mAU]	Area %
1	7.705	FM	0.1849	23.86740	2.15093	4.0672
2	9.363	MM	0.2377	562.95764	39.47039	95.9328

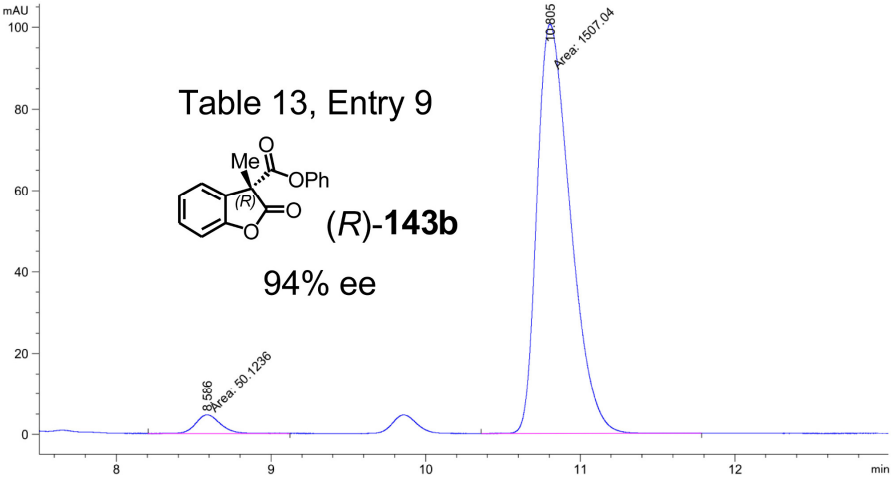

Peak #	RetTime [min]	Type	Width [min]	Area [mAU*s]	Height [mAU]	Area %
1	8.586	MM	0.1833	50.12360	4.55636	3.2189
2	10.805	MM	0.2499	1507.04041	100.51971	96.7811

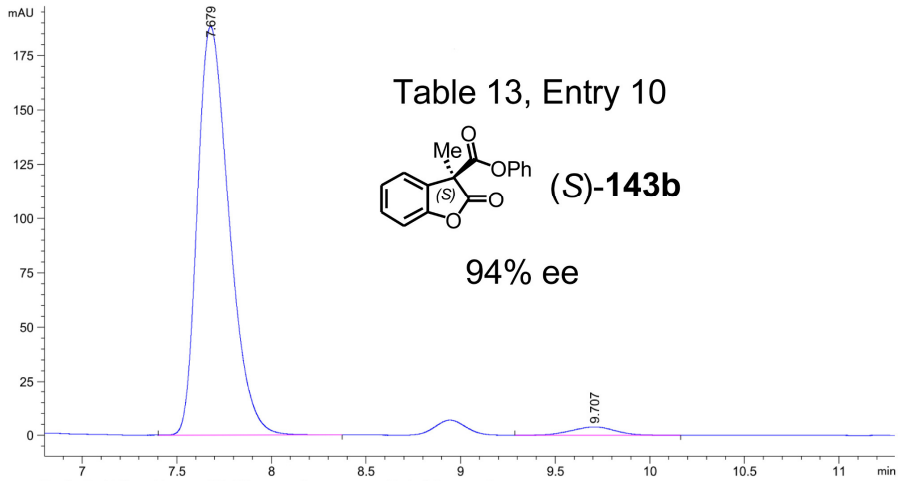

Peak #	RetTime [min]	Type	Width [min]	Area [mAU*s]	Height [mAU]	Area %
1	7.679	VB	0.1794	2192.90601	188.27101	97.2089
2	9.707	BB	0.1924	62.96354	3.85748	2.7911

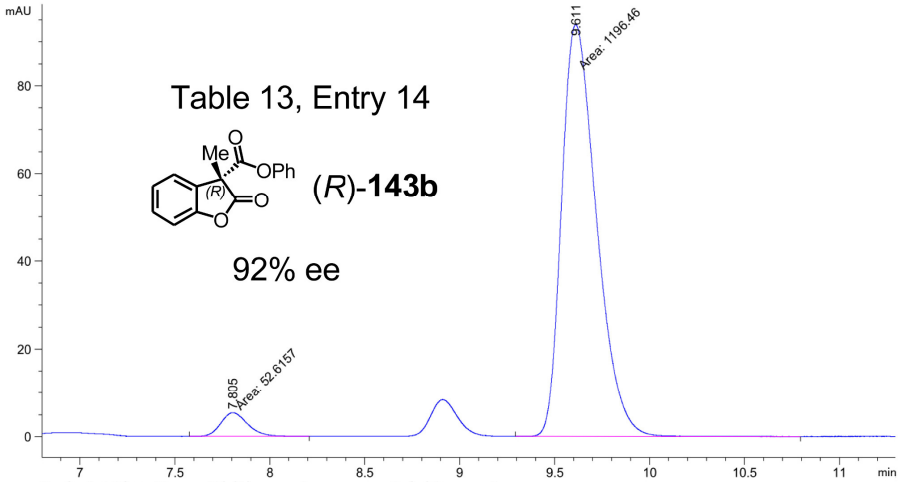

Peak #	RetTime [min]	Type	Width [min]	Area [mAU*s]	Height [mAU]	Area %
1	7.805	MM	0.1630	52.61570	5.38017	4.2124
2	9.611	MM	0.2124	1196.46399	93.88931	95.7876

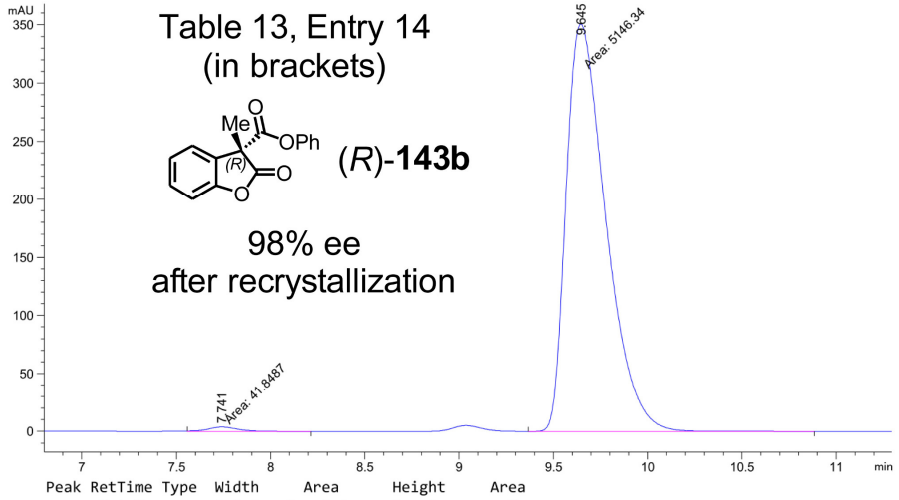

Peak #	RetTime [min]	Type	Width [min]	Area [mAU*s]	Height [mAU]	Area %
1	7.741	FM	0.1852	41.84869	3.76616	0.8066
2	9.645	MF	0.2445	5146.34180	350.83856	99.1934

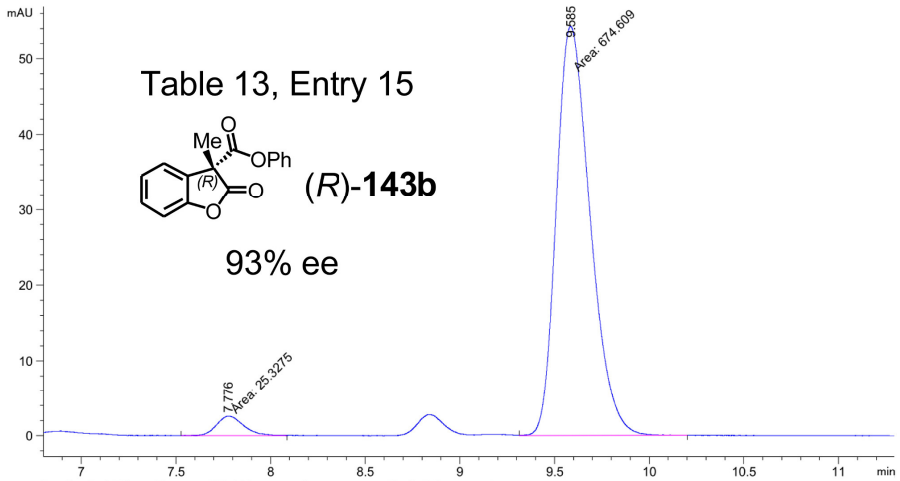

Peak #	RetTime [min]	Type	Width [min]	Area [mAU*s]	Height [mAU]	Area %
1	7.776	MM	0.1635	25.32750	2.58162	3.6185
2	9.585	FM	0.2073	674.60950	54.24463	96.3815

Product **143c** from Table 13:

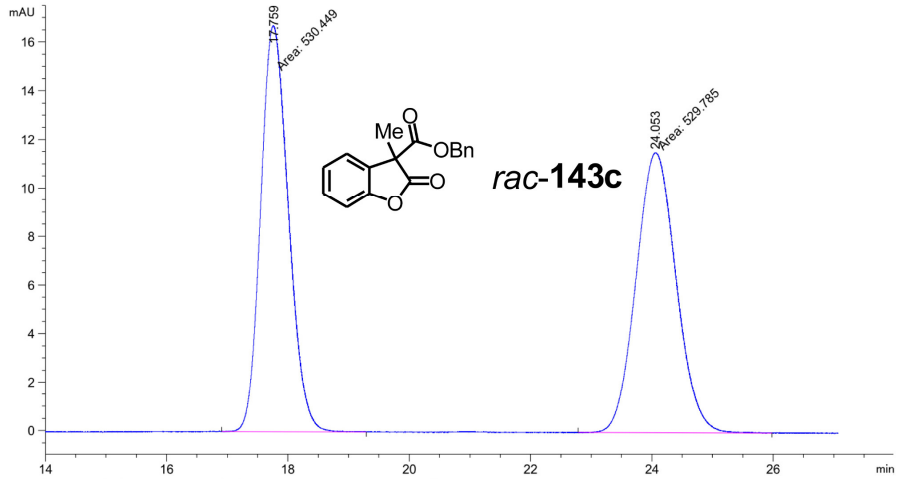

Peak #	RetTime [min]	Type	Width [min]	Area [mAU*s]	Height [mAU]	Area %
1	17.759	MM	0.5290	530.44873	16.71270	50.0313
2	24.053	MM	0.7644	529.78461	11.55053	49.9687

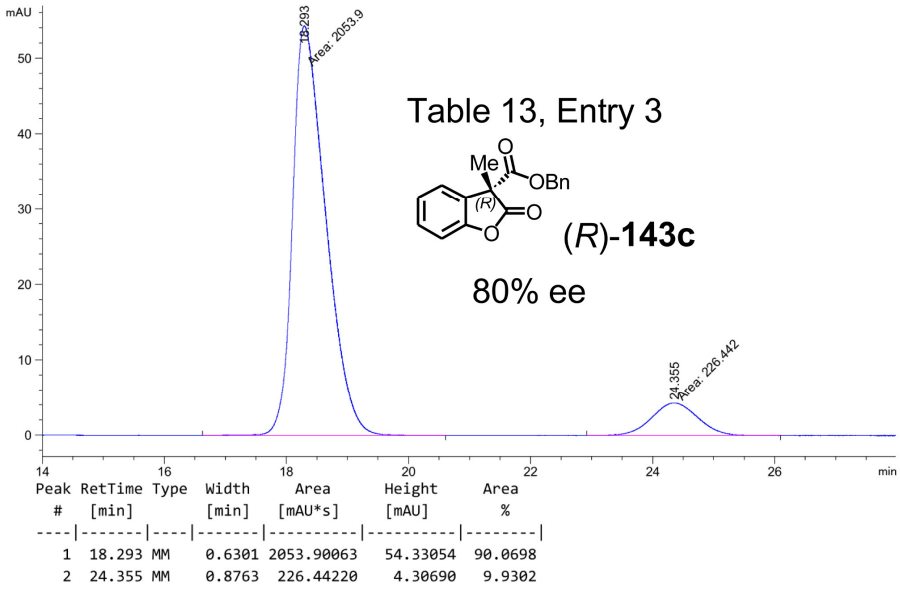

Peak #	RetTime [min]	Type	Width [min]	Area [mAU*s]	Height [mAU]	Area %
1	18.293	MM	0.6301	2053.90063	54.33054	90.0698
2	24.355	MM	0.8763	226.44220	4.30690	9.9302

Product **143d** from Table 13:

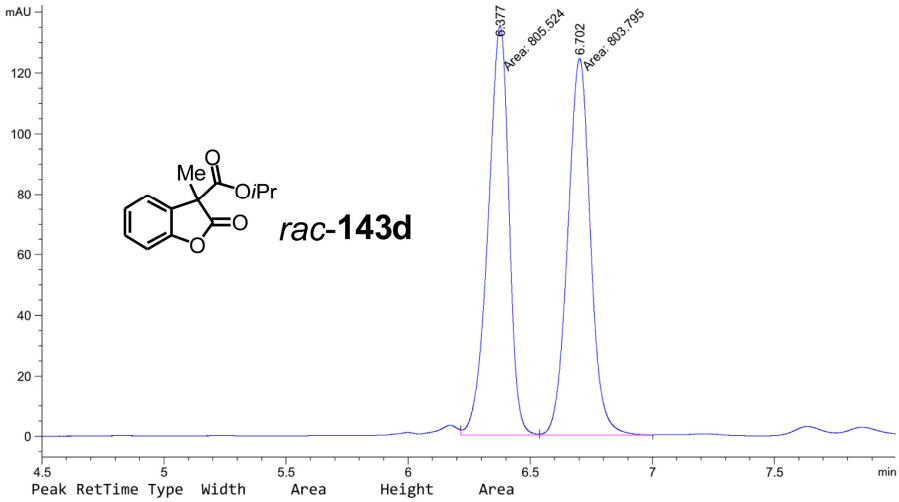

Peak #	RetTime [min]	Type	Width [min]	Area [mAU*s]	Height [mAU]	Area %
1	6.377	FM	0.0992	805.52429	135.26930	50.0537
2	6.702	FM	0.1077	803.79510	124.40717	49.9463

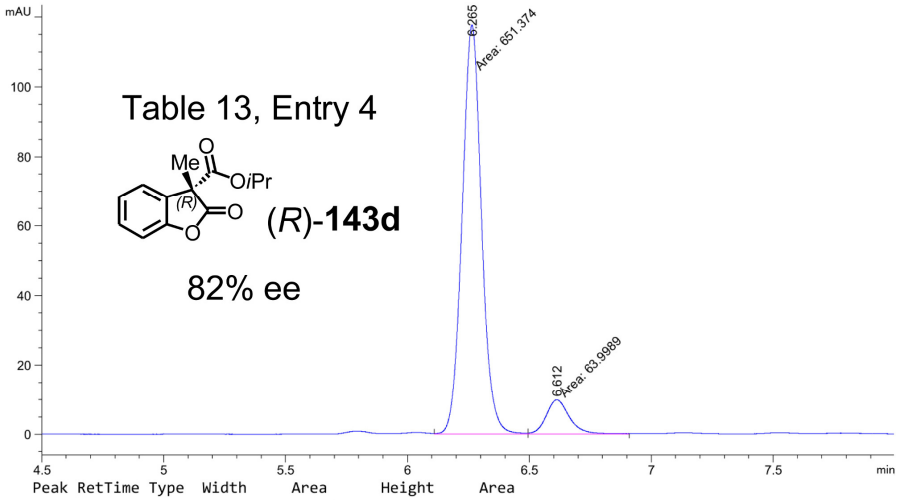

Peak #	RetTime [min]	Type	Width [min]	Area [mAU*s]	Height [mAU]	Area %
1	6.265	MF	0.0923	651.37445	117.61534	91.0538
2	6.612	FM	0.1087	63.99892	9.81629	8.9462

Product **143e** from Table 13:

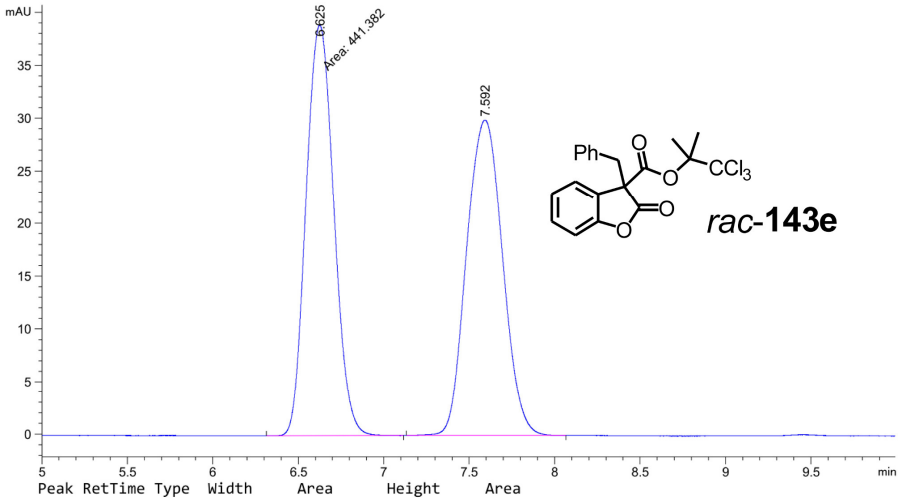

Peak #	RetTime [min]	Type	Width [min]	Area [mAU*s]	Height [mAU]	Area %
1	6.625	MM	0.1889	441.38239	38.94049	50.1222
2	7.592	BB	0.2300	439.22971	29.96670	49.8778

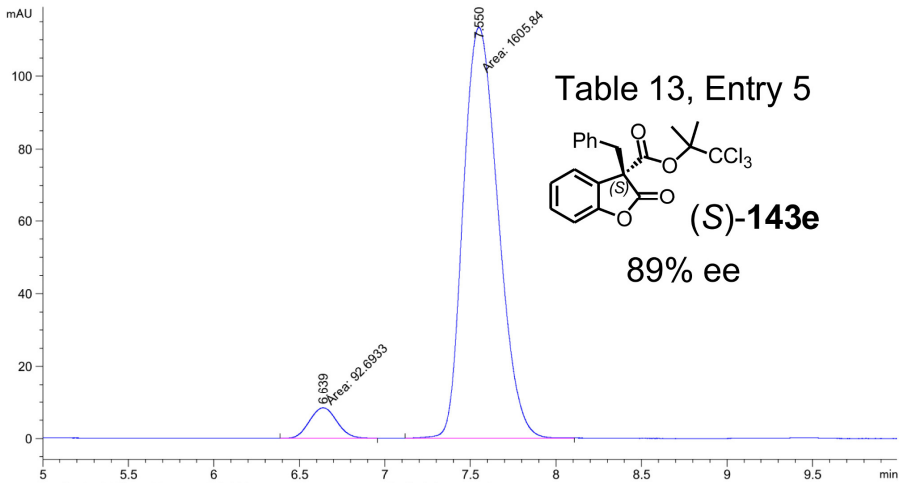

Peak #	RetTime [min]	Type	Width [min]	Area [mAU*s]	Height [mAU]	Area %
1	6.639	MM	0.1848	92.69329	8.35987	5.4573
2	7.550	MM	0.2362	1605.83716	113.33454	94.5427

Product **143f** from Table 13:

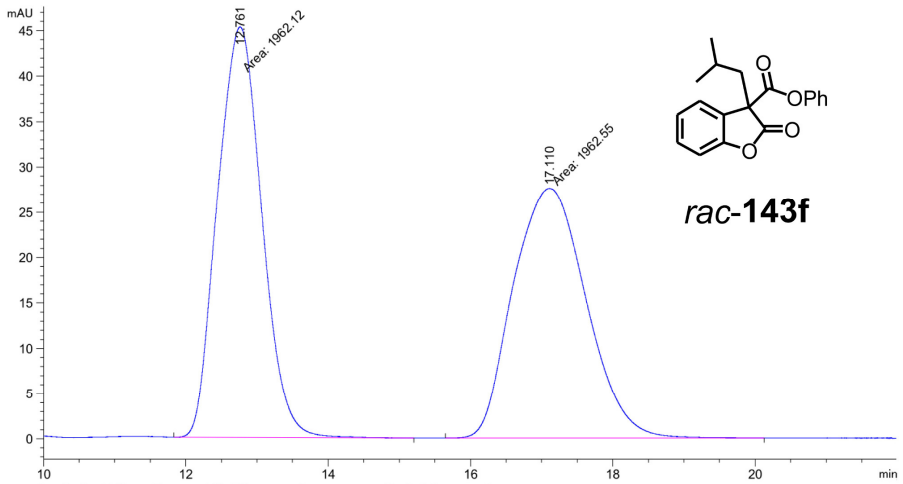

Peak #	RetTime [min]	Type	Width [min]	Area [mAU*s]	Height [mAU]	Area %
1	12.761	MM	0.7222	1962.11975	45.27796	49.9945
2	17.110	MM	1.1852	1962.55017	27.59839	50.0055

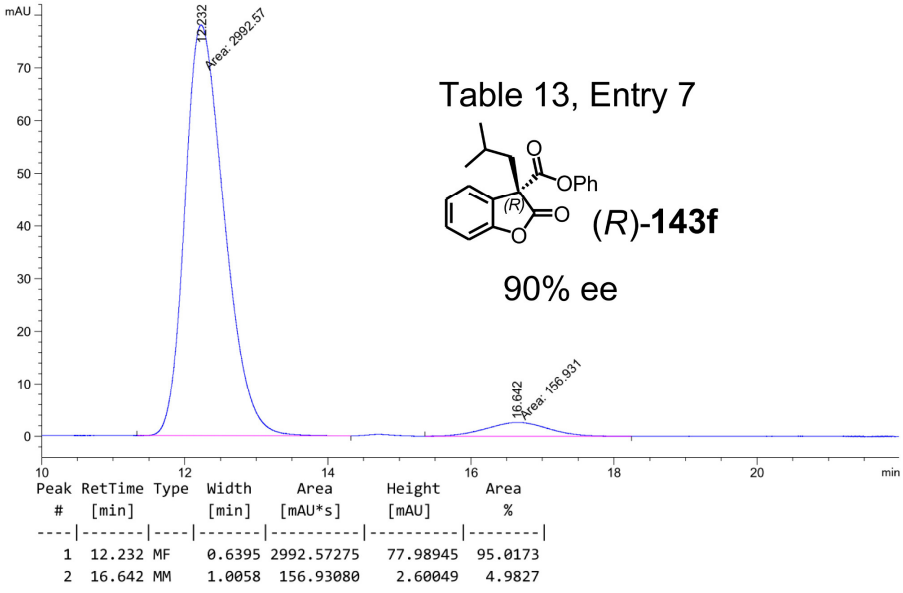

Peak #	RetTime [min]	Type	Width [min]	Area [mAU*s]	Height [mAU]	Area %
1	12.232	MF	0.6395	2992.57275	77.98945	95.0173
2	16.642	MM	1.0058	156.93080	2.60049	4.9827

Product **143g** from Table 13:

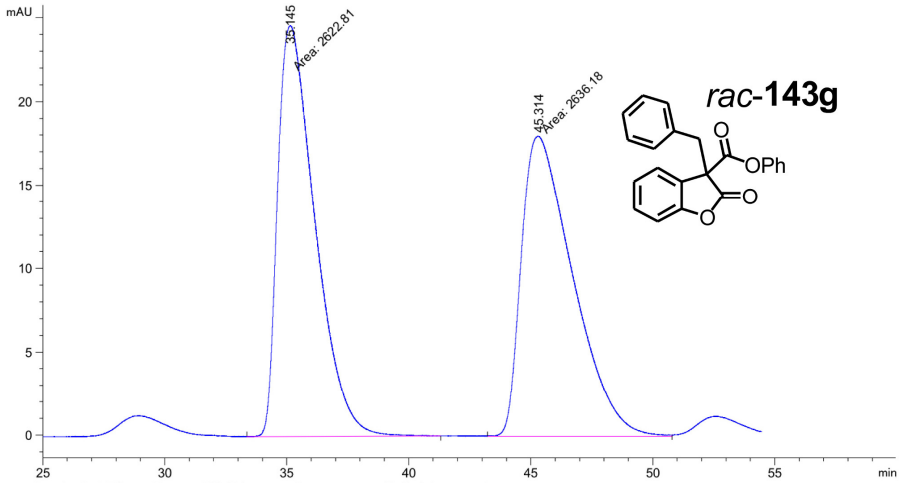

Peak #	RetTime [min]	Type	Width [min]	Area [mAU*s]	Height [mAU]	Area %
1	35.145	MM	1.7753	2622.81445	24.62327	49.8729
2	45.314	MM	2.4399	2636.17969	18.00712	50.1271

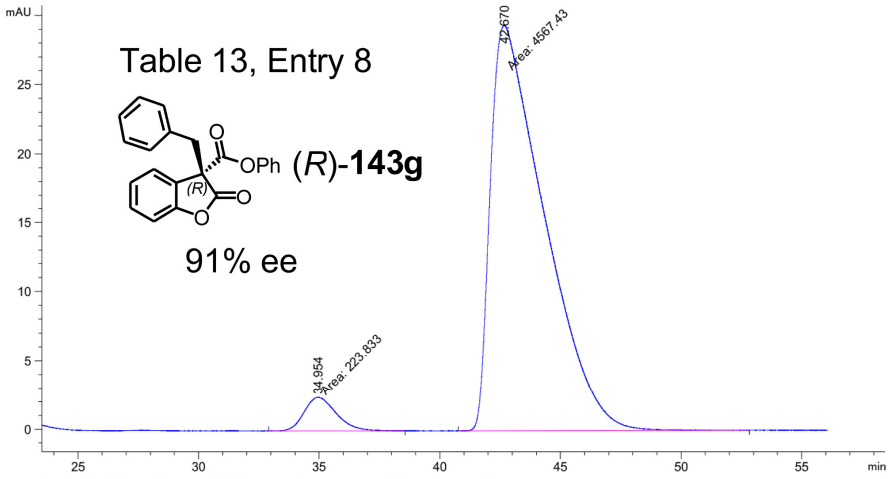

Peak #	RetTime [min]	Type	Width [min]	Area [mAU*s]	Height [mAU]	Area %
1	34.954	MM	1.5363	223.83299	2.42830	4.6717
2	42.670	MM	2.5917	4567.42920	29.37164	95.3283

Product **143h** from Table 13:

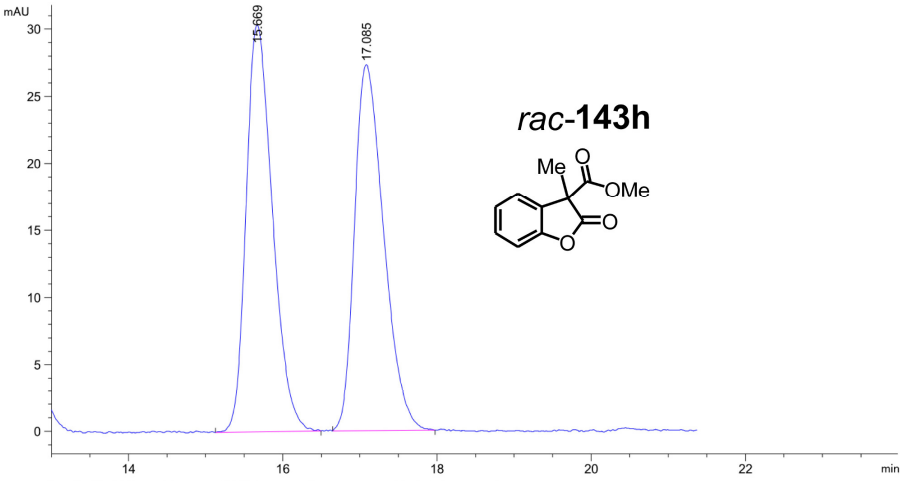

Peak #	RetTime [min]	Type	Width [min]	Area mAU *s	Height [mAU]	Area %
1	15.669	BV R	0.3716	723.74396	30.33132	50.1080
2	17.085	BV R	0.3952	720.62415	27.30927	49.8920

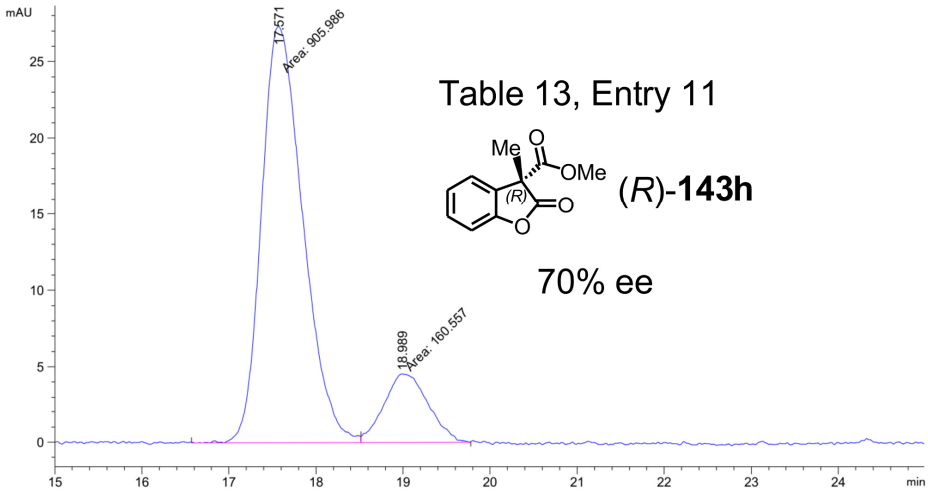

Peak #	RetTime [min]	Type	Width [min]	Area mAU *s	Height [mAU]	Area %
1	17.571	MF	0.5524	905.98572	27.33324	84.9461
2	18.989	FM	0.5882	160.55672	4.54921	15.0539

Product **143i** from Table 13:

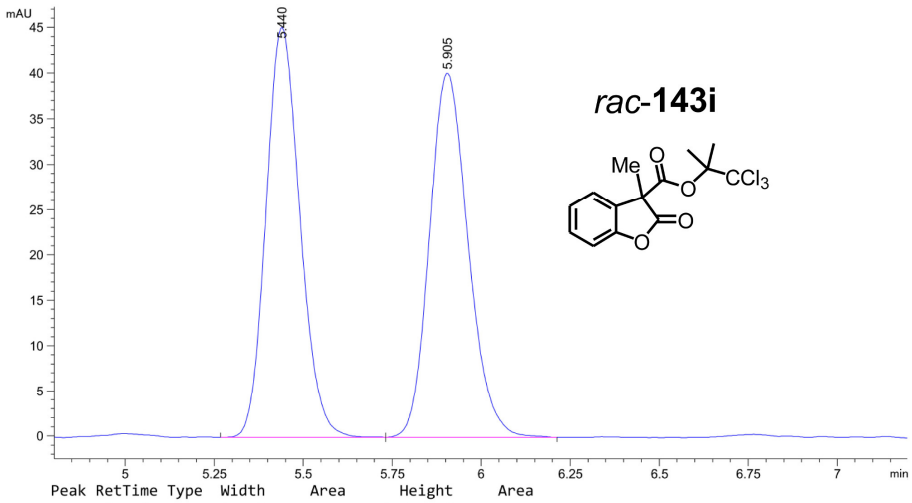

Peak #	RetTime [min]	Type	Width [min]	Area mAU *s	Height [mAU]	Area %
1	5.440	BB	0.1039	300.55234	45.16108	49.7156
2	5.905	BB	0.1174	303.99060	40.15825	50.2844

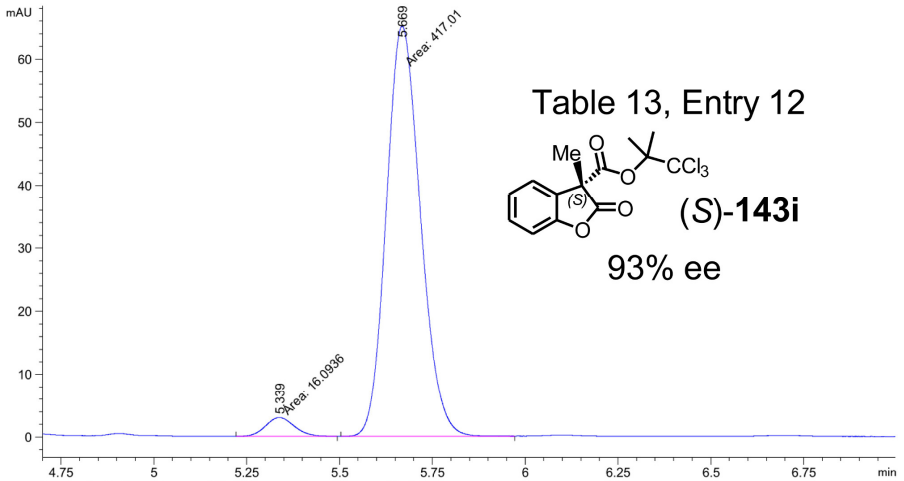

Peak #	RetTime [min]	Type	Width [min]	Area [mAU*s]	Height [mAU]	Area %
1	5.339	MM	0.0897	16.09363	2.98868	3.7159
2	5.669	MF	0.1067	417.00992	65.11306	96.2841

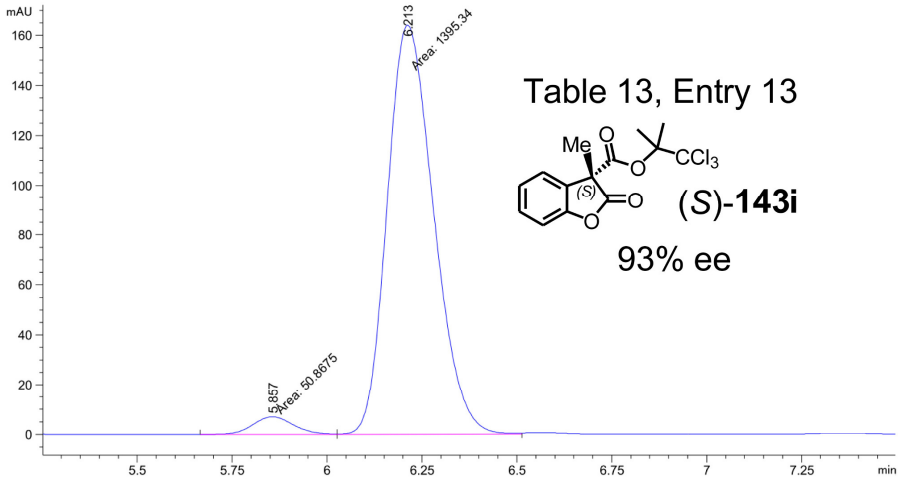

Peak #	RetTime [min]	Type	Width [min]	Area [mAU*s]	Height [mAU]	Area %
1	5.857	MF	0.1218	50.86752	6.96295	3.5173
2	6.213	FM	0.1418	1395.33789	163.99466	96.4827

5.4.3 HPLC Traces of *N*-Acyl Pyrroles 163 (Table 19)

Product **163a** from Table 19:

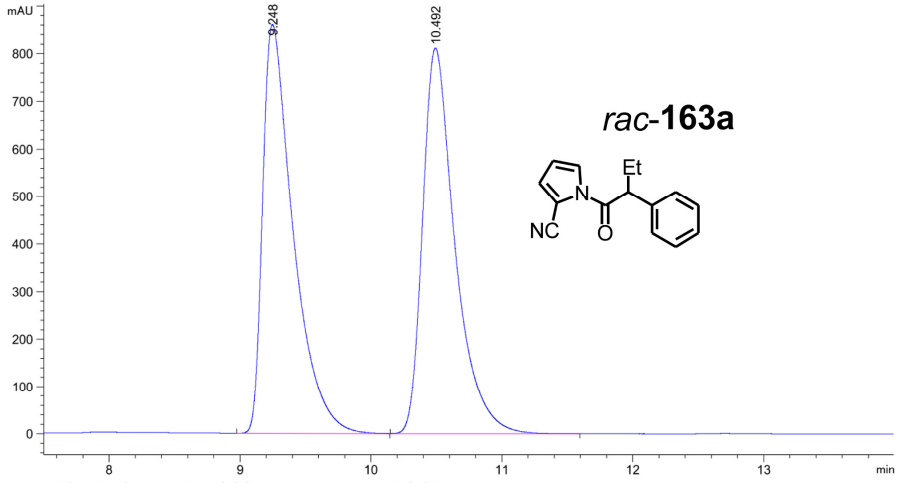

Peak #	RetTime [min]	Type	Width [min]	Area [mAU*s]	Height [mAU]	Area %
1	9.248	BB	0.2393	1.39567e4	860.12463	49.9906
2	10.492	BB	0.2563	1.39619e4	811.32257	50.0094

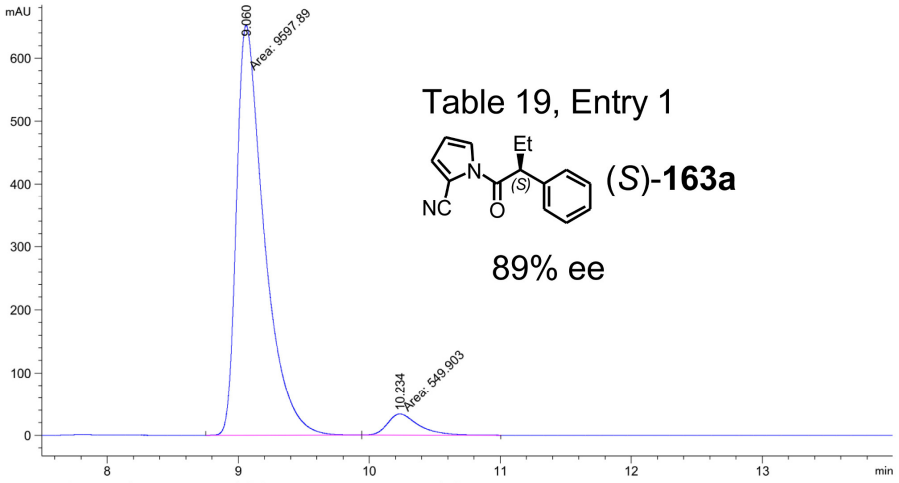

Peak #	RetTime [min]	Type	Width [min]	Area [mAU*s]	Height [mAU]	Area %
1	9.060	MM	0.2453	9597.89063	652.16077	94.5811
2	10.234	MM	0.2724	549.90295	33.64526	5.4189

Product **163b** from Table 19:

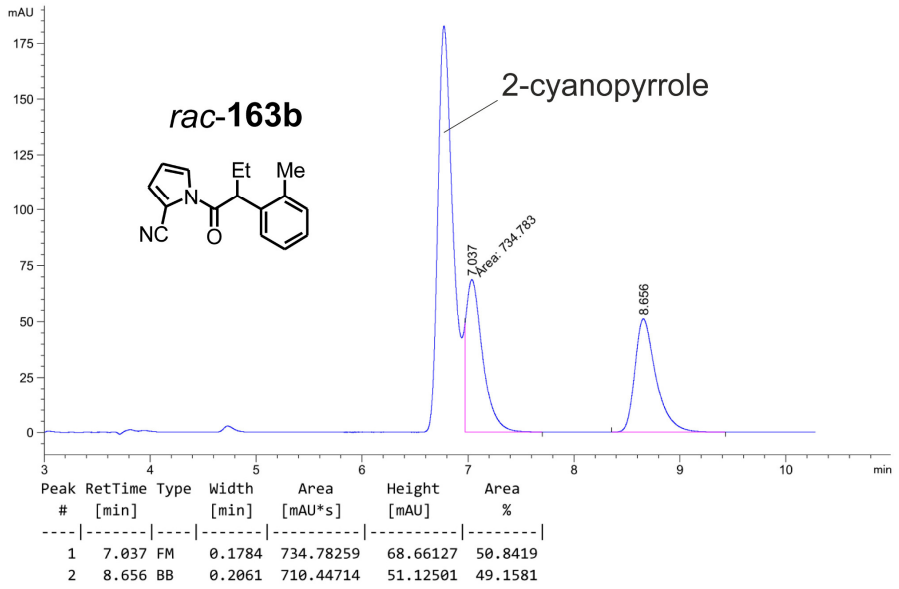

Peak #	RetTime [min]	Type	Width [min]	Area [mAU*s]	Height [mAU]	Area %
1	7.037	FM	0.1784	734.78259	68.66127	50.8419
2	8.656	BB	0.2061	710.44714	51.12501	49.1581

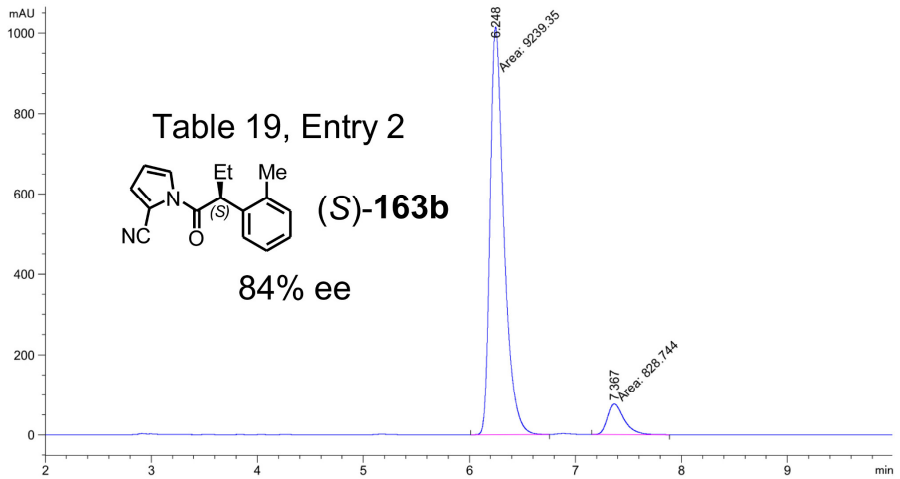

Peak #	RetTime [min]	Type	Width [min]	Area [mAU*s]	Height [mAU]	Area %
1	6.248	MF	0.1517	9239.34961	1014.99469	91.7686
2	7.367	MM	0.1810	828.74359	76.30655	8.2314

Product **163c** from Table 19:

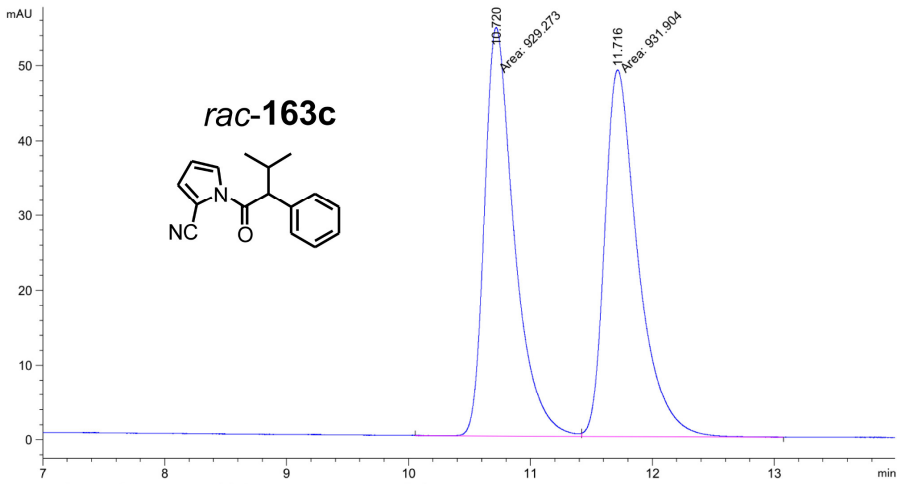

Peak #	RetTime [min]	Type	Width [min]	Area [mAU*s]	Height [mAU]	Area %
1	10.720	MF	0.2838	929.27319	54.57103	49.9293
2	11.716	FM	0.3170	931.90381	48.99731	50.0707

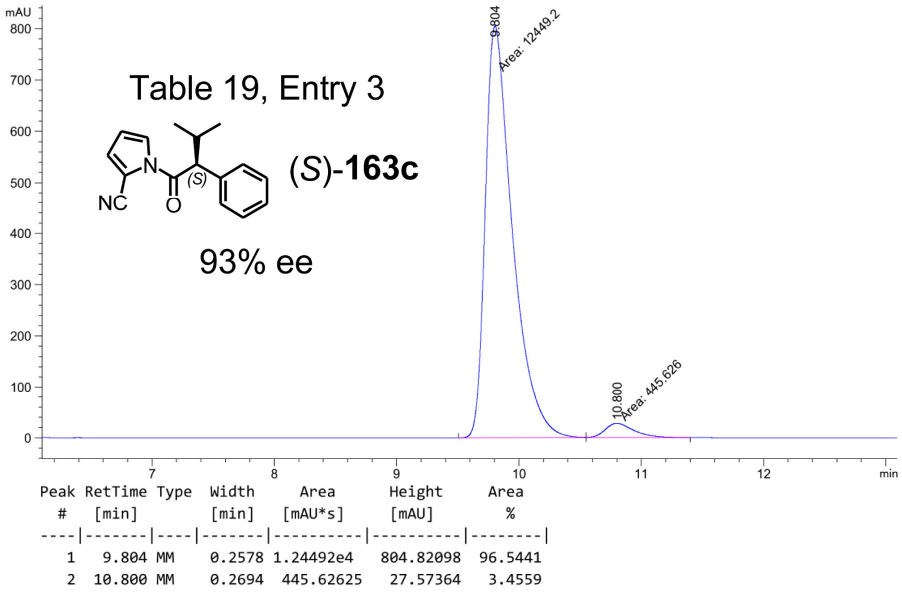

Peak #	RetTime [min]	Type	Width [min]	Area [mAU*s]	Height [mAU]	Area %
1	9.804	MM	0.2578	1.24492e4	804.82098	96.5441
2	10.800	MM	0.2694	445.62625	27.57364	3.4559

Product **163d** from Table 19:

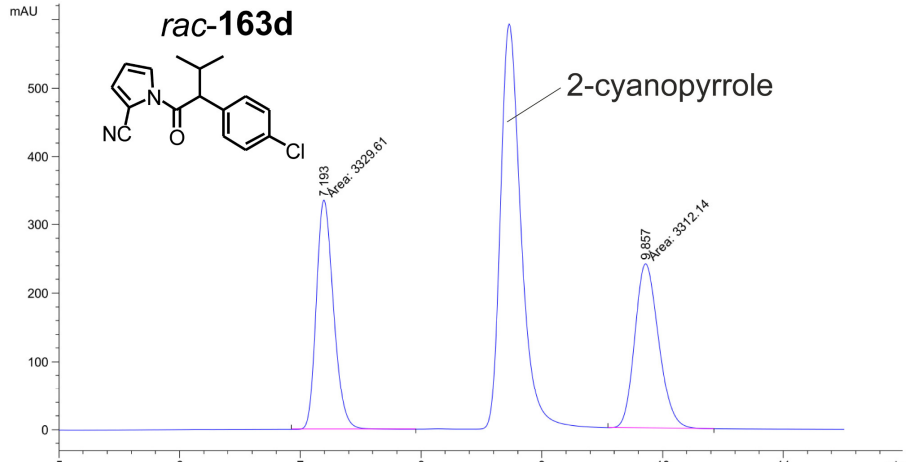

Peak #	RetTime [min]	Type	Width [min]	Area mAU *s	Height [mAU]	Area %
1	7.193	MM	0.1656	3329.60864	335.10242	50.1315
2	9.857	MM	0.2295	3312.14185	240.49414	49.8685

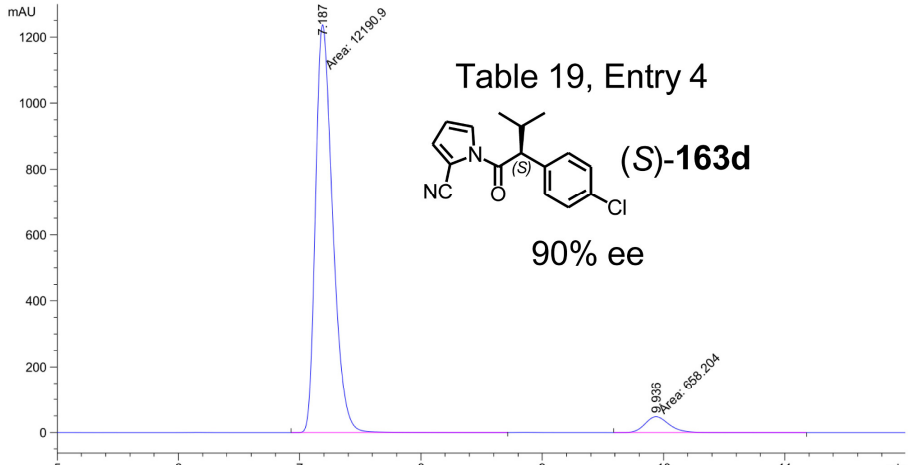

Peak #	RetTime [min]	Type	Width [min]	Area mAU *s	Height [mAU]	Area %
1	7.187	MF	0.1641	1.21909e4	1238.24255	94.8774
2	9.936	MM	0.2296	658.20410	47.78635	5.1226

Product **163e** from Table 19:

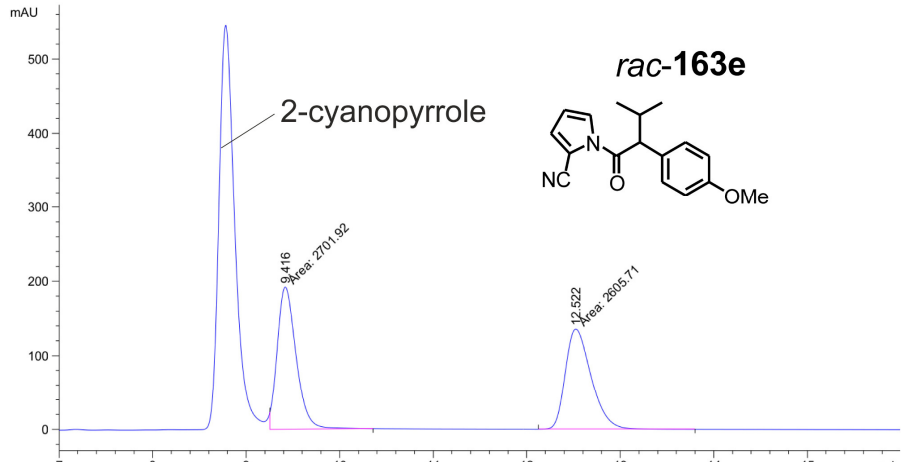

Peak #	RetTime [min]	Type	Width [min]	Area mAU *s	Height [mAU]	Area %
1	9.416	FM	0.2342	2701.91504	192.25436	50.9063
2	12.522	MM	0.3199	2605.70850	135.75185	49.0937

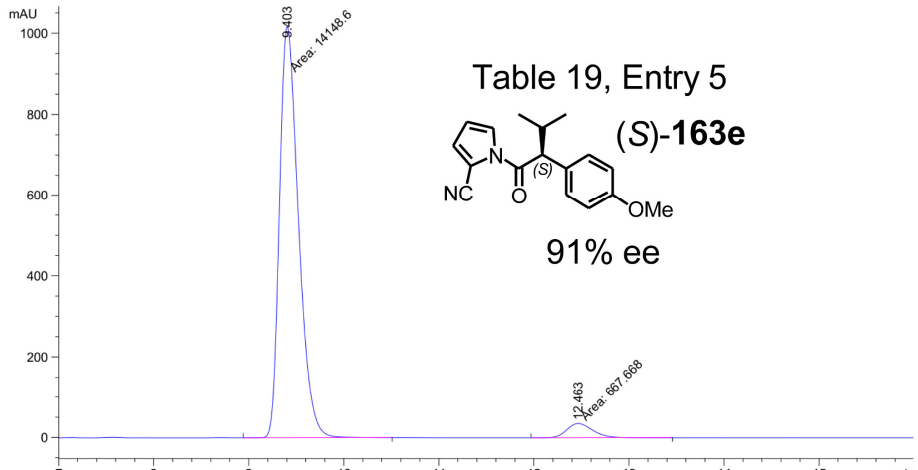

Peak #	RetTime [min]	Type	Width [min]	Area mAU *s	Height [mAU]	Area %
1	9.403	MF	0.2320	1.41486e4	1016.25854	95.4937
2	12.463	MM	0.3164	667.66791	35.17172	4.5063

Product **163f** from Table 19:

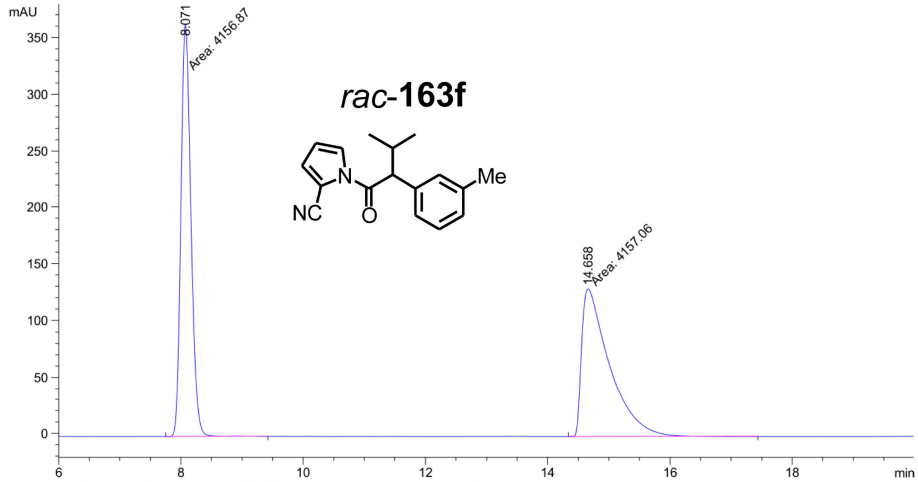

Peak #	RetTime [min]	Type	Width [min]	Area mAU *s	Height [mAU]	Area %
1	8.071	MM	0.1903	4156.87158	364.06601	49.9988
2	14.658	MM	0.5298	4157.06299	130.77002	50.0012

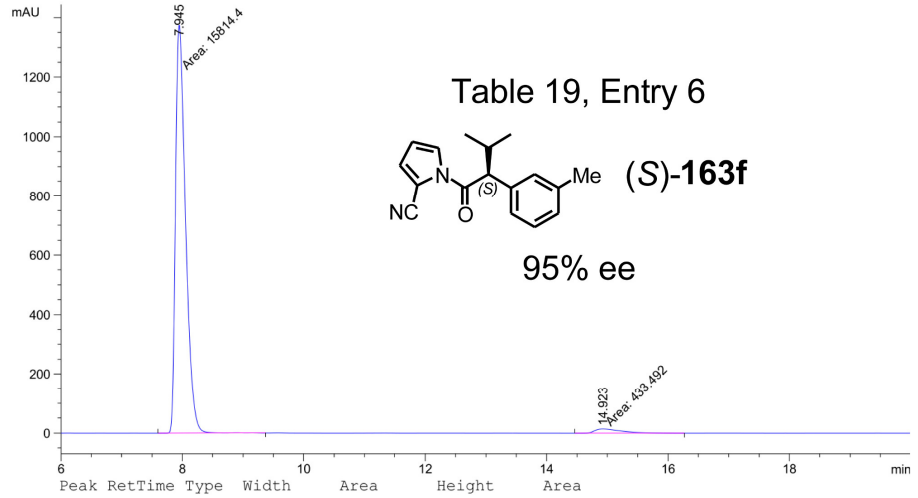

Peak #	RetTime [min]	Type	Width [min]	Area mAU *s	Height [mAU]	Area %
1	7.945	MM	0.1915	1.58144e4	1376.24377	97.3320
2	14.923	MM	0.5095	433.49237	14.17967	2.6680

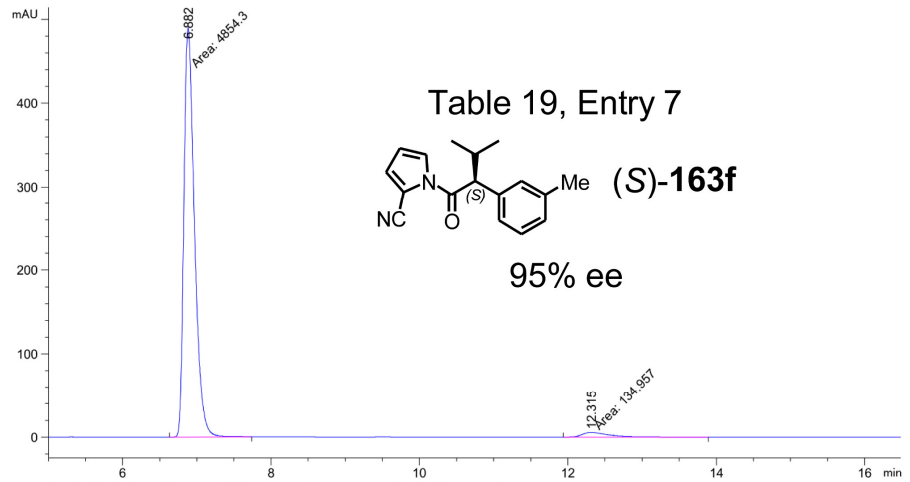

Peak #	RetTime [min]	Type	Width [min]	Area [mAU*s]	Height [mAU]	Area %
1	6.882	MM	0.1651	4854.29590	490.12518	97.2951
2	12.315	MF	0.4114	134.95677	5.46703	2.7049

Product **163g** from Table 19:

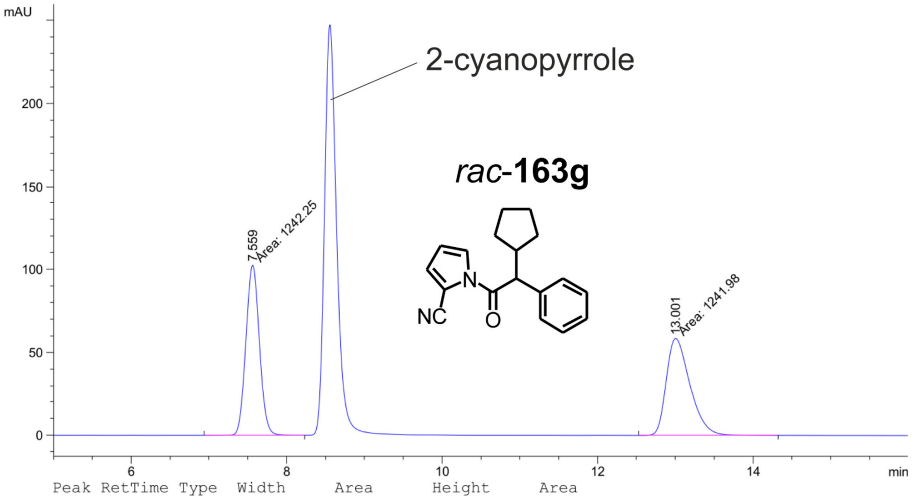

Peak #	RetTime [min]	Type	Width [min]	Area mAU *s	Height [mAU]	Area %
1	7.559	MM	0.2018	1242.25195	102.58724	50.0055
2	13.001	MM	0.3526	1241.97986	58.70325	49.9945

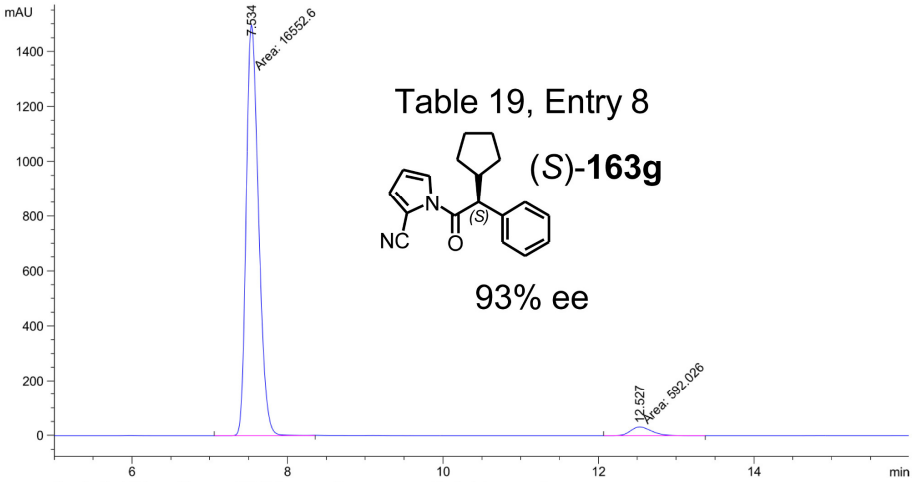

Peak #	RetTime [min]	Type	Width [min]	Area mAU *s	Height [mAU]	Area %
1	7.534	MF	0.1842	1.65526e4	1497.38599	96.5469
2	12.527	MM	0.3137	592.02643	31.45015	3.4531

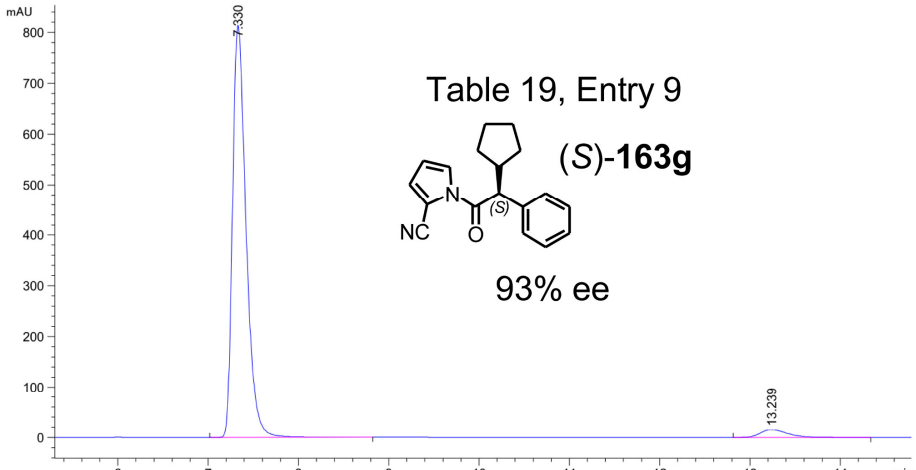

Peak #	RetTime [min]	Type	Width [min]	Area mAU *s	Height [mAU]	Area %
1	7.330	BB	0.1594	8479.46094	814.01276	96.3533
2	13.239	BB	0.3173	320.91995	15.49826	3.6467

Product **163h** from Table 19:

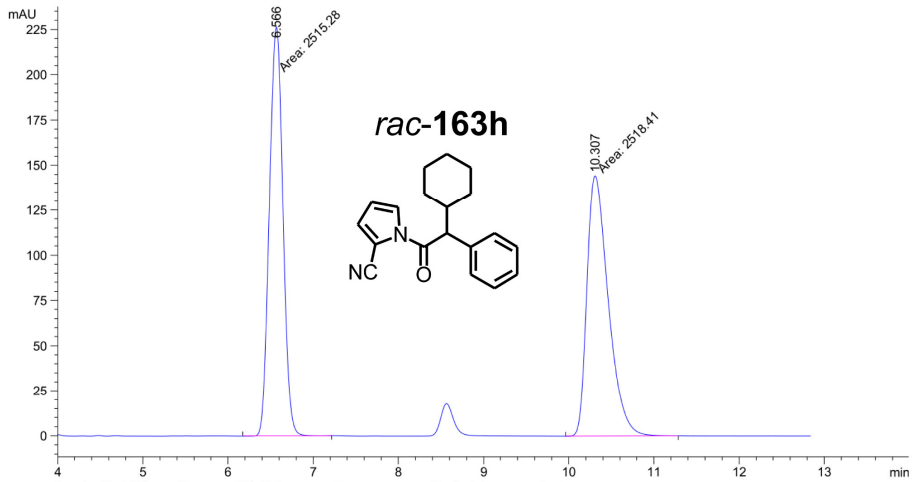

Peak #	RetTime [min]	Type	Width [min]	Area mAU *s	Height [mAU]	Area %
1	6.566	MF	0.1851	2515.27563	226.52173	49.9689
2	10.307	MF	0.2906	2518.41138	144.43420	50.0311

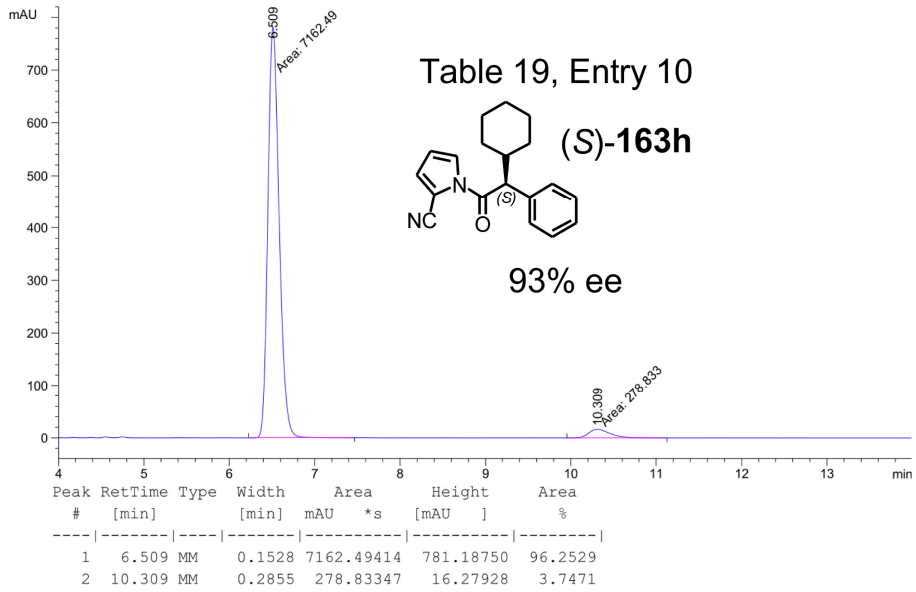

Peak #	RetTime [min]	Type	Width [min]	Area mAU *s	Height [mAU]	Area %
1	6.509	MM	0.1528	7162.49414	781.18750	96.2529
2	10.309	MM	0.2855	278.83347	16.27928	3.7471

6. List of Synthesized Compounds

6.1 Synthesized Iridium(III) Complexes (without their Precursor Complexes)

The syntheses of the following iridium(III) complexes are described in detail in chapter 4.7. Their corresponding precursor complexes, i.e., their corresponding iridium(III) dimers and auxiliary complexes, are *not* listed here. Nevertheless, the syntheses and characterizations of their precursor complexes are included in chapter 4.7.

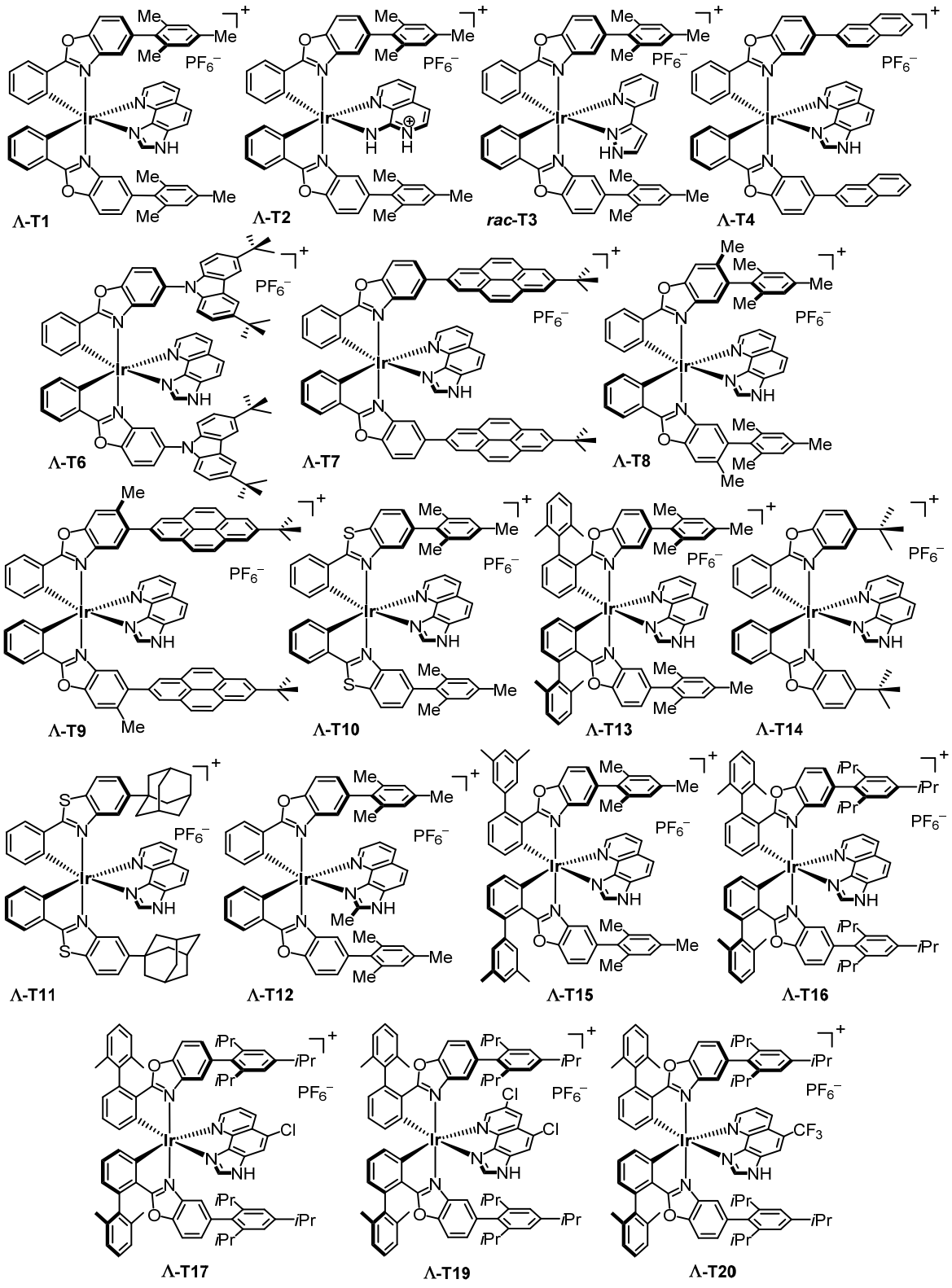

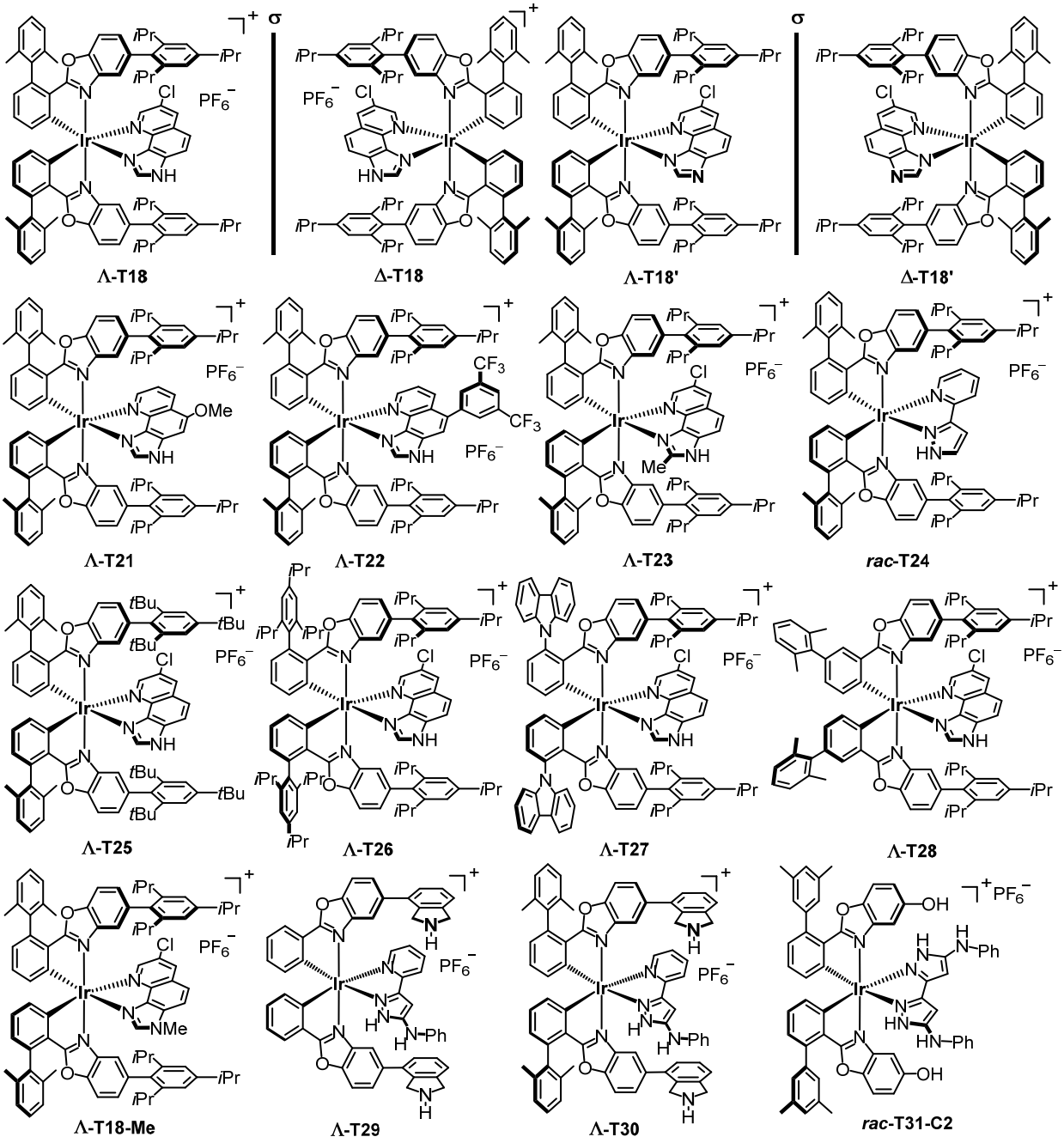

6.2 Synthesized Cyclometalating Ligands (with their Precursor Molecules)

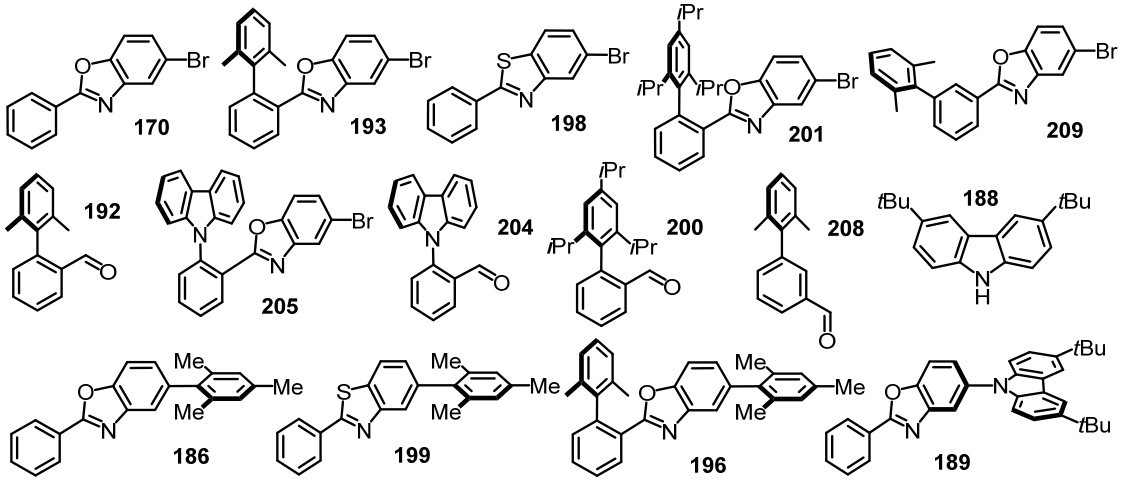

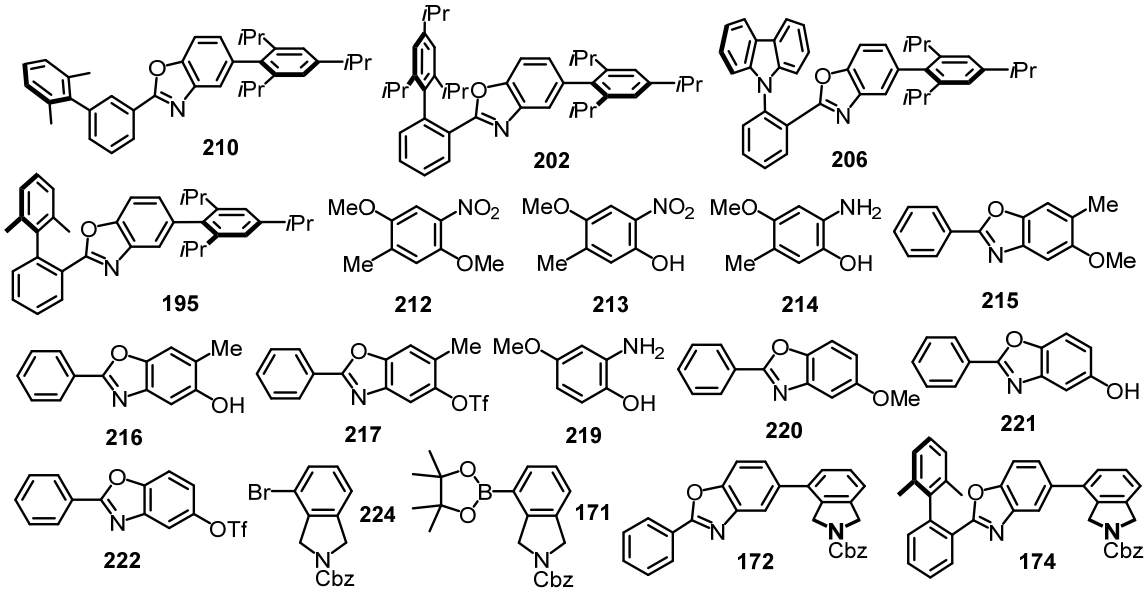

6.3 Synthesized Non-Cyclometalating Ligands (with their Precursor Molecules)

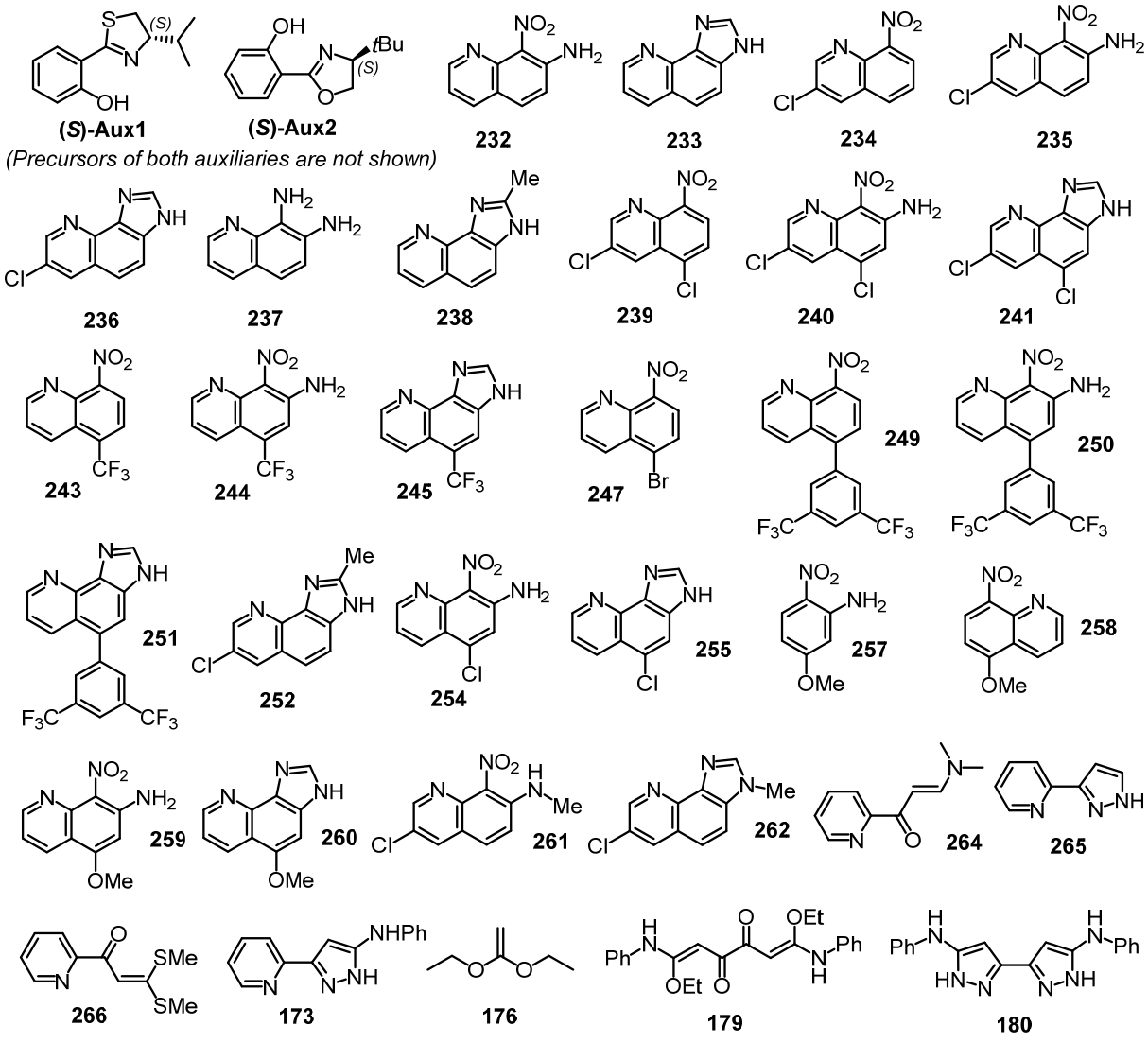

6.4 Synthesized Substrates for Catalysis Experiments (without their Precursors)

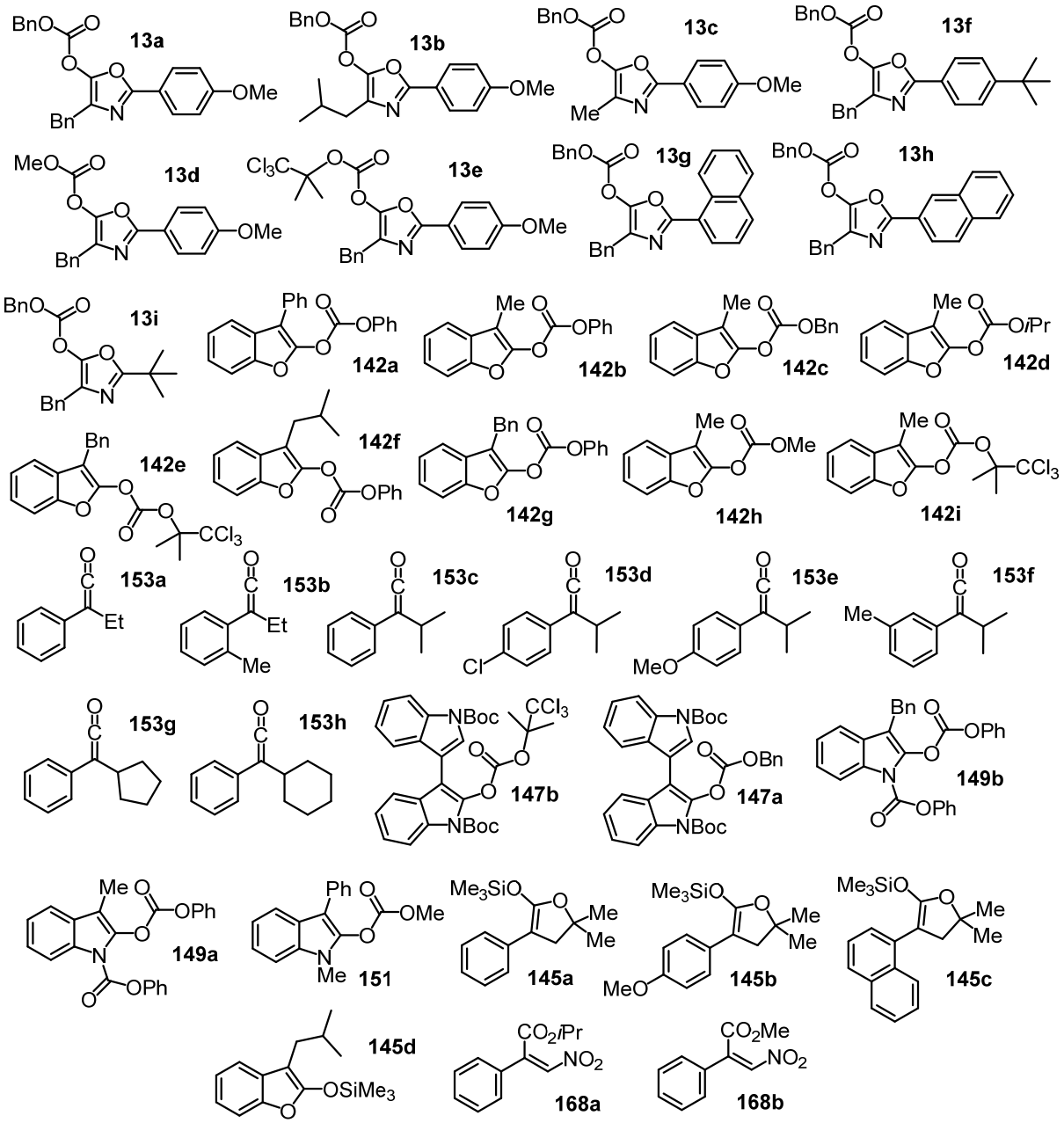

6.5 Isolated Catalysis Products (Each with the Best Achieved Enantiomeric Excess)

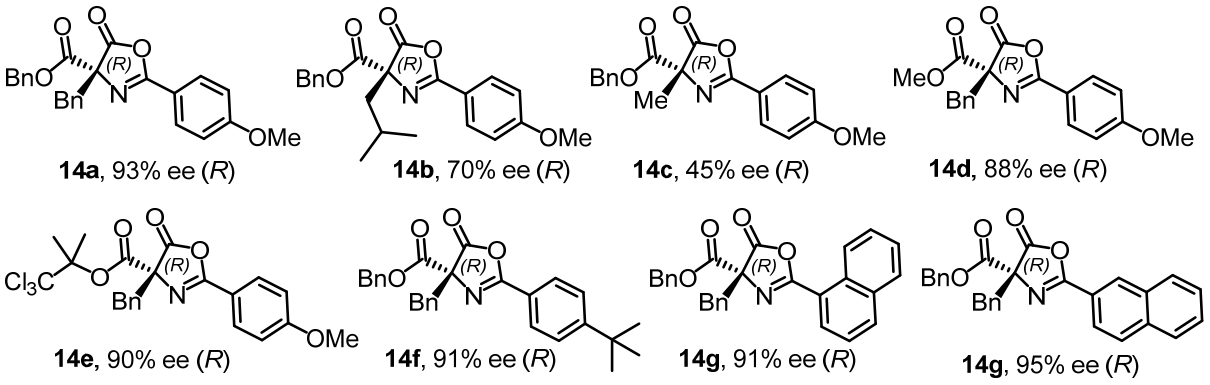

14a, 93% ee (*R*)

14b, 70% ee (*R*)

14c, 45% ee (*R*)

14d, 88% ee (*R*)

14e, 90% ee (*R*)

14f, 91% ee (*R*)

14g, 91% ee (*R*)

14g, 95% ee (*R*)

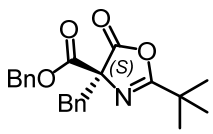

ent-**14i,** 96% ee (*S*)

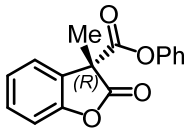

143b, 94% ee (*R*)

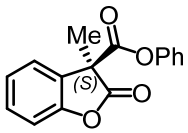

ent-**143b,** 94% ee (*S*)

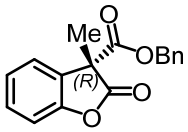

143c, 80% ee (*R*)

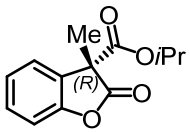

143d, 82% ee (*R*)

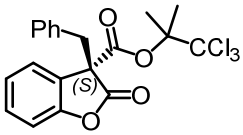

143e, 89% ee (*S*)

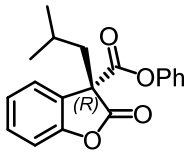

143f, 90% ee (*R*)

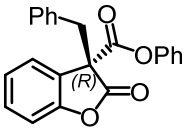

143g, 91% ee (*R*)

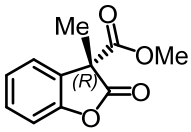

143h, 70% ee (*R*)

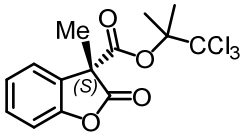

143i, 93% ee (*S*)

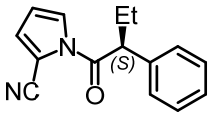

163a, 89% ee (*S*)

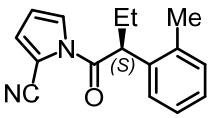

163b, 84% ee (*S*)

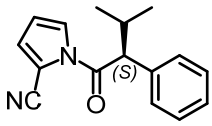

163c, 93% ee (*S*)

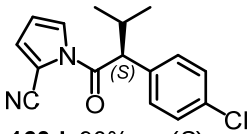

163d, 90% ee (*S*)

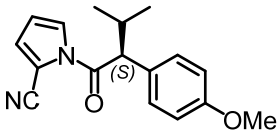

163e, 91% ee (*S*)

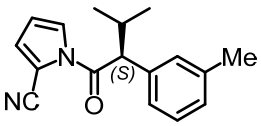

163f, 95% ee (*S*)

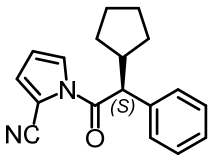

163g, 93% ee (*S*)

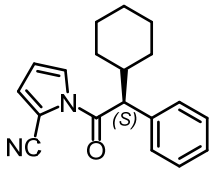

163h, 93% ee (*S*)

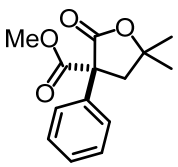

146aa, 17% ee

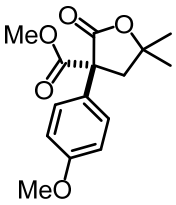

146ba, 29% ee

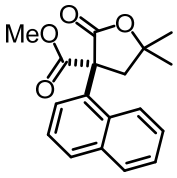

146ca, 18% ee

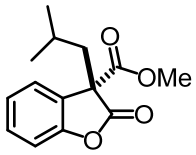

146da, 66% ee

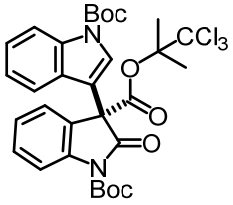

148b, 16% ee

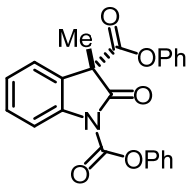

150a, <5% ee

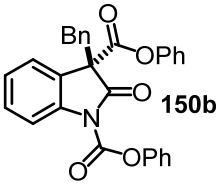

150b

150a, 59% ee

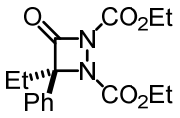

155a, 64% ee

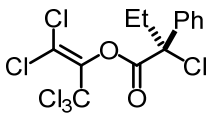

157a, 9% ee

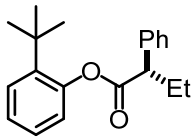

161a, 13% ee

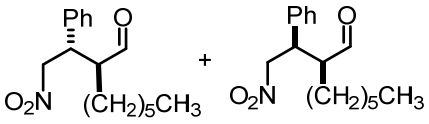

183b + ***epi*-183b** (only racemic)

7. Abbreviations and Symbols

$[\alpha]_D^{23}$	specific rotation α in degrees at the sodium D line (λ = 589 nm) at 23 °C
1x, 2x, 3x...	one time, two times, three times...
3D	three-dimensional
Å	ångström (unit of length; 1Å = 10^{-10} m)
acc.	according
AK	Arbeitskreis
APCI	atmospheric pressure chemical ionization
approx.	approximately
aq	aqueous
arom	aromatic
atm	atmosphere (unit of pressure; 1 atm = 101.3 kPa = 1013 mbar)
ATR	attenuated total reflection
$BArF_{24}$	tetrakis(3,5-bis(trifluoromethyl)phenyl)borate
BINAP	2,2'-bis(diphenylphosphino)-1,1'-binaphthyl
BINOL	1,1'-bi-2-naphthol
Bn	benzyl
Boc	*tert*-butyloxycarbonyl
$BrCamSulf^-$	3-bromo-camphor-8-sulfonate anion
Bz	benzoyl
C	conversion (see chapter 1.2, Eq. 1)
C	contribution (see chapter 2.3.8, Eq. 2)
C_q	quaternary carbon, carbon atom without attached hydrogen(s) (NMR)
c	concentration in g/100 mL (only used for specific rotation values)
C^N	*C*,*N*-coordinating bidentate ligand
C_n	n-fold rotational axis of symmetry
calcd	calculated
cat.	catalyst *or* catalytic
Cbz	carboxybenzyl
CCDC	Cambridge Crystallographic Data Centre
CD	circular dichroism
CI	chemical ionization
CIP rules	Cahn–Ingold–Prelog priority rules (see ref. 88)
cis / *trans*	*cis-trans* isomerism of a) organic compounds *or* b) of complexes
cod	cyclooctadiene
coe	cyclooctene
conc	concentration *or* concentrated
conv	conversion
CPME	cyclopentyl methyl ether
δ	chemical shift in ppm (NMR)
Δ / Λ	absolute stereochemical descriptors: left- (Λ), right- (Δ) handed propeller
Δε	molar circular dichroism in $M^{-1}cm^{-1}$ (see chapter 4.11, Eq. 3)
d, s, t, q, sept, m	doublet, singlet, triplet, quartet, septet, multiplet (NMR)
d	length, thickness of a layer
d.r.	diastereomeric ratio
DBU	1,8-diazabicyclo[5.4.0]undec-7-ene
DCC	dicyclohexylcarbodiimide
DEAD	diethyl azodicarboxylate
decomp.	decomposition
DFT	density functional theory
DIPA	diisopropylamine

DKR	dynamic kinetic resolution
DMAP	4-(dimethylamino)pyridine
DME	1,2-dimethoxyethane
DMF	*N*,*N*-dimethylformamide
DMF-DMA	*N*,*N*-dimethylformamide-dimethylacetal
dmp	2,9-dimethyl-1,10-phenanthroline
DMPU	1,3-dimethyl-3,4,5,6-tetrahydro-2(1*H*)-pyrimidinone
DMSO	dimethyl sulfoxide
dppf	1,1'-bis(diphenylphosphino)ferrocene
dtbpy	4,4'-di-*tert*-butyl-2,2'-dipyridyl
e.g.	for example (*Latin: exempli gratia*)
ee	enantiomeric excess
EI	electron (impact) ionization
en	ethylenediamine
eq	equivalent(s)
Eq.	equation
ESI	electrospray ionization
et al.	and others (*Latin: et alii*)
EWG	electron-withdrawing group
exp	natural exponential function
ex situ	opposite of *in situ* (see below)
f	extent of labeling / degree of functionalization (resin)
f. c.	flash chromatography
FD	field desorption ionization
flow	flow rate (HPLC)
GAMESS	General Atomic and Molecular Electronic Structure System
GDCh	Gesellschaft Deutscher Chemiker
h	hour(s)
HOMO	highest occupied molecular orbital
HPLC	high-performance liquid chromatography
HRMS	high-resolution mass spectrometry
i-	*iso*- (compound prefix)
i.e.	that is to say / namely (*Latin: id est*)
in silico	performed on computer / via computer simulation
in situ	in the reaction mixture / in the course of the reaction
in vacuo	in a vacuum / within a vacuum
in vitro	in glass / reaction vessel; meant as opposite of *in silico* (see above)
incomp.	incomplete
IR	infrared
ISC	intersystem crossing
J	coupling constant in Hz (NMR)
k	reaction rate constant
KIE	kinetic isotope effect
KR	kinetic resolution
λ	wavelength
LED	light-emitting diode
ln	natural logarithm
LUMO	lowest unoccupied molecular orbital
M	molecule / compound of interest (HRMS)
M	molar concentration, molarity
m-	*meta*- (compound prefix)
M. G. M.	Michael Gennadiyevich Medvedev

m/*z*	mass-to-charge ratio (HRMS)
min	minute(s)
mol%	molar percentage
mp	melting point
MS	molecular sieves *or* mass spectrometry
MTBE	methyl *tert*-butyl ether
n-	*normal*- (compound prefix)
n.d.	not determined
n.c.	no conversion
N^N	*N*,*N*-coordinating bidentate ligand
NCS	*N*-chlorosuccinimide
NHC	*N*-heterocyclic carbene
NMM	*N*-methylmorpholine
NMP	*N*-methyl-2-pyrrolidone
NMR	nuclear magnetic resonance
M / *P*	absolute stereochemical descriptors *M* and *P* for helical-chiral compounds
NRC	National Research Center
o-	*ortho*- (compound prefix)
OC-FPR	Organisch-chemisches Fortgeschrittenenpraktikum
OC-MPR	Organisch-chemisches Masterpraktikum
ORCID	Open Researcher and Contributor ID (https://orcid.org)
p-	*para*- (compound prefix)
p. / pp.	page (p.) / pages (pp.)
PCET	proton-coupled electron transfer
Pd/C	palladium metal finely dispersed on charcoal
phgly	phenylglycinate
pH	$pH = -\log_{10} a(H^+)$; $a(H^+)$: activity of hydrogen ions in solution
Piv	pivaloyl
ppm	parts per million
PPY	4-pyrrolidinopyridine
PS	photosensitizer *or* polystyrene
PTFE	polytetrafluoroethylene
quant.	quantitative
R	ideal gas constant (8.314 $J \cdot mol^{-1}K^{-1}$; see chapter 4.11, Eq. 3)
R / *S*	absolute stereochemical descriptors *R* and *S*
r	radius
rac	racemic *or* racemate
RAS	Russian Academy of Sciences
RDS	rate determining step
ref. / refs.	reference (ref.) / references (refs.)
rt	room temperature (~25 °C, no active thermostatization)
σ	mirror plane
s	second(s)
S	selectivity factor (see chapter 1.2, Eq. 1)
S_1	lowest excited singlet state
sat.	saturated
SET	single-electron transfer
SPhos	2-dicyclohexylphosphino-2',6'-dimethoxybiphenyl
SpnF	enzyme SpnF
t	temperature (in °C)
t-	*tert*- (compound prefix)
T	temperature (in K)

T. C.	Thomas Cruchter
T_1	lowest excited triplet state
TAA	*tert*-amyl alcohol
TEMPO	(2,2,6,6-tetramethylpiperidin-1-yl)oxyl, free radical
TES	triethylsilane
Tf	triflyl, trifuoromethanesulfonyl
TfO^-	triflate anion
TFA	trifluoroacetic acid
THF	tetrahydrofurane
TLC	thin-layer chromatography
TMHI	1,1,1-trimethylhydrazinium iodide
Tol	tolyl
TON	turnover number
t_R	retention time
TRIS(PHAT)	tris(tetrachloro-1,2-benzenediolato)phosphate(V)
TS	transition state
UV	ultraviolet
$\tilde{\nu}$	wavenumbers in cm^{-1}
vol%	percentage by volume
w	week(s)
wt%	percentage by weight
X. S.	Xiaodong Shen
XRD	X-ray diffraction
Z. L.	Zhijie Lin

8. References and Remarks

[1] Fu, G. C. *Acc. Chem. Res.* **2000**, *33*, 412–420.

[2] Fu, G. C. *Acc. Chem. Res.* **2004**, *37*, 542–547.

[3] Uraguchi, D.; Koshimoto, K.; Miyake, S.; Ooi, T. *Angew. Chem., Int. Ed.* **2010**, *49*, 5567–5569.

[4] Joannesse, C.; Johnston, C. P.; Concellón, C.; Simal, C.; Philp, D.; Smith, A. D. *Angew. Chem., Int. Ed.* **2009**, *48*, 8914–8918.

[5] Denmark, S. E.; Beutner, G. L. *Angew. Chem., Int. Ed.* **2008**, *47*, 1560–1638.

[6] *Lewis Base Catalysis in Organic Synthesis*, 1st ed.; Vedejs, E., Denmark, S. E., Eds.; Wiley-VCH: Weinheim, 2016.

[7] Mukherjee, S.; Yang, J. W.; Hoffmann, S.; List, B. *Chem. Rev.* **2007**, *107*, 5471–5569.

[8] Erkkilä, A.; Majander, I.; Pihko, P. M. *Chem. Rev.* **2007**, *107*, 5416–5470.

[9] Patra, A.; Mukherjee, S.; Das, T. K.; Jain, S.; Gonnade, R. G.; Biju, A. T. *Angew. Chem., Int. Ed.* **2017**, *56*, 2730–2734.

[10] France, S.; Guerin, D. J.; Miller, S. J.; Lectka, T. *Chem. Rev.* **2003**, *103*, 2985–3012.

[11] Articles which focus on the high catalytic activity of DMAP and its derivatives:
(a) Litvinenko, L. M.; Kirichenko, A. I. *Dokl. Chem.* **1967**, 763–766; *Dokl. Akad. Nauk SSSR, Ser. Khim.* **1967***, 176,* 97–100. (b) Steglich, W.; Höfle, G. *Angew. Chem., Int. Ed.* **1969**, *8*, 981. (c) Grondal, C. *Synlett* **2003**, *10*, 1568–1569. (d) Spivey, A. C.; Arseniyadis, S. *Angew. Chem., Int. Ed.* **2004**, *43*, 5436–5441.

[12] Vedejs, E.; Chen, X. *J. Am. Chem. Soc.* **1996**, *118*, 1809–1810.

[13] Kinetic resolutions with Fu's planar-chiral DMAP-derived catalysts:
(a) Ruble, J. C.; Fu, G. C. *J. Org. Chem.* **1996**, *61*, 7230–7231. (b) Ruble, J. C.; Latham, H. A.; Fu, G. C. *J. Am. Chem. Soc.* **1997**, *119*, 1492–1493. (c) Liang, J.; Ruble, J. C.; Fu, G. C. *J. Org. Chem.* **1998**, *63*, 3154–3155. (d) Tao, B.; Ruble, J. C.; Hoic, D. A.; Fu, G. C. *J. Am. Chem. Soc.* **1999**, *121*, 5091–5092. (e) Lee, S. Y.; Murphy, J. M; Ukai, A.; Fu, G. C. *J. Am. Chem. Soc.* **2012**, *134*, 15149–15153. (f) Díaz-Álvarez, A. E.; Mesas-Sánchez, L.; Dinér, P. *Angew. Chem., Int. Ed.* **2013**, *52*, 502–504.

[14] Kinetic resolutions with other DMAP-derived catalysts:
(a) Kawabata; T.; Nagato, M.; Takasu, K.; Fuji, K. *J. Am. Chem. Soc.* **1997**, *119*, 3169–3170. (b) Spivey, A. C.; Fekner, T.; Spey, S. E. *J. Org. Chem.* **2000**, *65*, 3154–3159. (c) Spivey, A. C.; Zhu, F.; Mitchell, M. B.; Davey, S. G.; Jarvest, R. L. *J. Org. Chem.* **2003**, *68*, 7379–7385. (d) Priem, G.; Pelotier, B.; Macdonald, S. J. F.; Anson,

M. S.; Campbell, I. B. *J. Org. Chem.* **2003**, *68*, 3844–3848. (e) Spivey, A. C.; Leese, D. P.; Zhu, F.; Davey, S. G.; Jarvest, R. L. *Tetrahedron* **2004**, *60*, 4513–4525. (f) Spivey, A. C.; Arseniyadis, S.; Fekner, T.; Maddaford, A.; Leese, D. P. *Tetrahedron* **2006**, *62*, 295–301. (g) Nguyen, H. V.; Motevalli, M.; Richards, C. J. *Synlett* **2007**, 725–728. (h) Crittall, M. R.; Rzepa, H. S.; Carbery, D. R. *Org. Lett.* **2011**, *13*, 1250–1253. (i) Crittall, M. R.; Fairhurst, N. W. G.; Carbery, D. R. *Chem. Commun.* **2012**, *48*, 11181–11183.

[15] Kinetic resolutions with amidine-derived catalysts:
(a) Birman, V. B.; Uffman, E. W.; Jiang, H.; Li, X.; Kilbane, C. J. *J. Am. Chem. Soc.* **2004**, *126*, 12226–12227. (b) Birman, V. B.; Jiang, H. *Org. Lett.* **2005**, *7*, 3445–3447. (c) Birman, V. B.; Li, X.; Jiang, H.; Uffman, E. W. *Tetrahedron* **2006**, *62*, 285–294. (d) Hu, B.; Meng, M.; Wang, Z.; Du, W.; Fossey, J. S.; Hu, X.; Deng, W.-P. *J. Am. Chem. Soc*. **2010**, *132*, 17041–17044. (e) Li, X.; Jiang, H.; Uffman, E. W.; Guo, L.; Zhang, Y.; Yang, X.; Birman, V. B. *J. Org. Chem.* **2012**, *77*, 1722–1737. (f) Jiang, S.-S.; Xu, Q.-C.; Zhu, M.-Y.; Yu, X.; Deng, W.-P. *J. Org. Chem.* **2015**, *80*, 3159–3169. (g) Jiang, S.-S.; Gu, B.-Q.; Zhu, M.-Y.; Yu, X.; Deng, W.-P. *Tetrahedron* **2015**, *71*, 1187–1191.

[16] Kinetic resolutions with isothiourea-derived catalysts:
(a) Birman, V. B.; Li, X. *Org. Lett.* **2006**, *8*, 1351–1354. (b) Birman, V. B.; Jiang, H.; Li, X.; Guo, L.; Uffman, E. W. *J. Am. Chem. Soc.* **2006**, *128*, 6536–6537. (c) Birman, V. B.; Guo, L. *Org. Lett.* **2006**, *8*, 4859–4861. (d) Yang, X.; Birman, V. B. *Adv. Synth. Catal.* **2009**, *351*, 2301–2304. (e) Bumbu, V. D.; Birman, V. B. *J. Am. Chem. Soc.* **2011**, *133*, 13902–13905. (f) Yang, X.; Bumbu, V. D.; Liu, P.; Li, X.; Jiang, H.; Uffman, E. W.; Guo, L.; Zhang, W.; Jiang, X.; Houk, K. N.; Birman, V. D. *J. Am. Chem. Soc.* **2012**, *134*, 17605–17612. (g) Bumbu, V. D.; Yang, X.; Birman, V. B. *Org. Lett.* **2013**, *15*, 2790–2793.

[17] Examples for kinetic resolutions with imidazole-derived catalysts:
(a) Miller, S. J.; Copeland G. T.; Papaioannou, N.; Horstmann, T. E.; Ruel, E. M. *J. Am. Chem. Soc.* **1998**, *120*, 1629–1630. (b) Jarvo, E. R.; Copeland, G. T.; Papaioannou, N.; Bonitatebus, P. J. Jr.; Miller, S. J. *J. Am. Chem. Soc.* **1999**, *121*, 11638–11643. (c) Ishihara, K.; Kosugi, Y.; Akakura, M. *J. Am. Chem. Soc.* **2004**, *126*, 12212–12213. (d) Müller, C. E.; Wanka, L.; Jewell, K.; Schreiner, P. R. *Angew. Chem., Int. Ed.* **2008**, *47*, 6180–6183.

[18] Example for a kinetic resolution with an *O*-nucleophilic catalyst:
Notte, G. T.; Sammakia, T. *J. Am. Chem. Soc.* **2006**, *128*, 4230–4231.

[19] Examples for chiral nucleophilic catalysis with phosphine-based catalysts:
(a) Vedejs, E.; Daugulis, O.; Diver, S. T. *J. Org. Chem.* **1996**, *61*, 430–431. (b) Vedejs, E.; Daugulis, O. *J. Am. Chem. Soc.* **1999**, *121*, 5813–5814. (c) Vedejs, E.; Daugulis, O.; MacKay, J. A.; Rozners, E. *Synlett* **2001**, 1499–1505. (d) Vedejs, E.; Daugulis, O. *J. Am. Chem. Soc.* **2003**, *125*, 4166–4173. (e) Xiao, Y.; Guo, H.; Kwon, O. *Aldrichimica Acta* **2016**, *49*, 2–13. (f) Fujiwara, Y.; Fu, G. C. *J. Am. Chem. Soc.* **2011**, *133*, 12293–12297.

[20] Recent review articles about chiral amidine- and isothiourea-derived catalysts:
(a) Merad, J.; Pons, J.-M.; Chuzel, O.; Bressy, C. *Eur. J. Org. Chem.* **2016**, 5589–5610. (b) Birman, V. B. *Aldrichimica Acta* **2016**, *49*, 23–33.

[21] (a) Steglich, W.; Höfle, G. *Angew. Chem., Int. Ed.* **1968**, *7*, 61. (b) Steglich, W.; Höfle, G. *Chem. Ber.* **1969**, *102*, 883–898. (c) Steglich, W.; Höfle; G. *Chem. Ber.* **1969**, *102*, 899–903. (d) Steglich, W.; Höfle, G. *Tetrahedron Lett.* **1970**, *11*, 4727–4730.

[22] Steglich-type rearrangements with Fu's planar-chiral DMAP-derived catalysts:
(a) Ruble, J. C.; Fu, G. C. *J. Am. Chem. Soc.* **1998**, *120*, 11532–11533. (b) Hills, I. D.; Fu, G. C. *Angew. Chem., Int. Ed.* **2003**, *42*, 3921–3924.

[23] Steglich-type rearrangements with other DMAP-derived catalysts:
(a) Shaw, S. A.; Aleman, P.; Vedejs, E. *J. Am. Chem. Soc.* **2003**, *125*, 13368–13369. (b) Shaw, S. A.; Aleman, P.; Christy, J.; Kampf, J. W.; Va, P.; Vedejs, E. *J. Am. Chem. Soc.* **2006**, *128*, 925–934. (c) Nguyen, H. V.; Butler, D. C. D.; Richards, C. J. *Org. Lett.* **2006**, *8*, 769–772. (d) De, C. K.; Mittal, N.; Seidel, D. *J. Am. Chem. Soc.* **2011**, *133*, 16802–16805. (e) Poisson, T.; Oudeyer, S.; Levacher, V. *Tetrahedron Lett.* **2012**, *53*, 3284–3287. (f) Mandai, H.; Fujiwara, T.; Noda, K.; Fujii, K.; Mitsudo, K.; Korenaga, T.; Suga, S. *Org. Lett.* **2015**, *17*, 4436–4439. (g) Mandai, H.; Fuji, K.; Yasuhara, H.; Abe, K.; Mitsudo, K.; Korenaga, T.; Suga, S. *Nat. Commun.* **2016**, *7*, 11297. (h) Chen, C.-T.; Tsai, C.-C.; Tsou, P.-K.; Huang, G.-T.; Yu; C.-H. *Chem. Sci.* **2017**, *8*, 524–529. (i) Duffey, T. A.; Shaw, S. A.; Vedejs, E. *J. Am. Chem. Soc.* **2009**, *131*, 14–15.

[24] Steglich-type rearrangements with isothiourea-derived catalysts (in addition to ref. 4):
Viswambharan, B.; Okimura, T.; Suzuki, S.; Okamoto, S. *J. Org. Chem.* **2011**, *76*, 6678–6685.

[25] Steglich-type rearrangements with imidazole-derived catalysts:
(a) Zhang, Z.; Xie, F.; Jia, J.; Zhang, W. *J. Am. Chem. Soc.* **2010**, *132*, 15939–15941. (b) Wang, M.; Zhang, Z.; Liu, S.; Xie, F.; Zhang, W. *Chem. Commun.* **2014**, *50*, 1227–1230.

[26] Ketene reactions catalyzed by Fu's planar-chiral DMAP-type catalysts:
(a) Hodous, B. L.; Ruble, J. C.; Fu, G. C. *J. Am. Chem. Soc.* **1999**, *121*, 2637–2638. (b) Hodous, B. L.; Fu, G. C. *J. Am. Chem. Soc.* **2002**, *124*, 1578–1579. (c) Hodous, B. L.; Fu, G. C. *J. Am. Chem. Soc.* **2002**, *124*, 10006–10007. (d) Wilson, J. E.; Fu, G. C. *Angew. Chem., Int. Ed.* **2004,** *43*, 6358–6360. (e) Wiskur, S. L.; Fu, G. C. *J. Am. Chem. Soc.* **2005**, *127*, 6176–6177. (f) Lee, E. C.; Hodous, B. L.; Bergin, E.; Shih, C.; Fu, G. C. *J. Am. Chem. Soc.* **2005**, *127*, 11586–11587. (g) Schaefer, C.; Fu, G. C. *Angew. Chem., Int. Ed.* **2005**, *44*, 4606–4608. (h) Lee, E. C.; McCauley, K. M.; Fu, G. C. *Angew. Chem., Int. Ed.* **2007**, *46*, 977–979. (i) Dai, X.; Nakai, T.; Romero, J. A. C.; Fu, G. C. *Angew. Chem., Int. Ed.* **2007**, *46*, 4367–4369. (j) Berlin, J. M.; Fu, G. C. *Angew. Chem., Int. Ed.* **2008**, *47*, 7048–7050.

[27] Ketene reactions catalyzed by chiral NHC-derived catalysts:
(a) Zhang, Y.-R.; He, L.; Wu, X.; Shao, P.-L.; Ye, S. *Org. Lett.* **2008**, *10*, 277–280. (b) Wang, X.-N.; Lv, H.; Huang, X.-L.; Ye, S. *Org. Biomol. Chem.* **2009**, *7*, 346–350. (c) Douglas, J.; Ling, K. B.; Concellón, C.; Churchill, G.; Slawin, A. M. Z.; Smith, A. D. *Eur. J. Org. Chem.* **2010**, 5863–5869. (d) Jian, T.-Y.; Shao, P.-L.; Ye, S. *Chem. Commun.* **2011**, *47*, 2381–2383. (e) Kano, T.; Maruoka, K. *Org. Lett.* **2005**, *7*, 1347–1349.

[28] Review articles dealing with nucleophilic catalysis / Lewis base catalysis (in addition to refs. 5, 6, 10 and 11d; also in a broader sense):
(a) Methot, J. L.; Roush, W. R. *Adv. Synth. Catal.* **2004**, *346*, 1035–1050. (b) Wurz, R. P. *Chem. Rev.* **2007**, *107*, 5570–5595. (c) Gaunt, M. J.; Johansson, C. C. C. *Chem. Rev.* **2007**, *107*, 5596–5605. (d) Spivey, A. C.; Arseniyadis, S. *Top. Curr. Chem.* **2010**, *291*, 233–280. (e) Müller, C. E.; Schreiner, P. R. *Angew. Chem., Int. Ed.* **2011**, *50*, 6012–6042.

[29] Mártin-Matute, B.; Edin, M.; Bogár, K.; Kaynak, F. B.; Bäckvall, J.-E. *J. Am. Chem. Soc.* **2005**, *127*, 8817–8825.

[30] Kagan, H. B.; Fiaud, J. C. *Top. Stereochem.* **1988**, *18*, 249–330.

[31] Garrett, C. E.; Fu, G. C. *J. Am. Chem. Soc.* **1998**, *120*, 7479–7483.

[32] Oriyama, T.; Imai, K.; Sano, T.; Hosoya, T. *Tetrahedron Lett.* **1998**, *39*, 3529–353.

[33] Iwabuchi, Y.; Nakatani, M.; Yokoyama, N.; Hatakeyama, S. *J. Am. Chem. Soc.* **1999**, *121*, 10219–10220.

[34] (a) Pattawong, O.; Mustard, T. J. L.; Johnston, R. C.; Cheong, P. H.-Y. *Angew. Chem., Int. Ed.* **2013**, *52*, 1420–1423. (b) Walden, D. M.; Ogba, O. M.; Johnston, R. C.; Cheong, P. H.-Y. *Acc. Chem. Res.* **2016**, *49*, 1279–1291.

[35] Check, C. T.; Jang, K. P.; Schwamb, C. B.; Wong, A. S.; Wang, M. H.; Scheidt, K. A. *Angew. Chem., Int. Ed.* **2015**, *54*, 4264–4268.

[36] Yamamoto, T.; Murakami, R.; Suginome, M. *J. Am. Chem. Soc.* **2017**, *139*, 2557–2560.

[37] (a) Chavarot, M.; Ménage, S.; Hamelin, O.; Charnay, F.; Pécaut, J.; Fontecave, M. *Inorg. Chem.* **2003**, *42*, 4810–4816. (b) Hamelin, O.; Rimboud, M.; Pécaut, J.; Fontecave, M. *Inorg. Chem.* **2007**, *46*, 5354–5360.

[38] (a) Chen, L.-A.; Xu, W.; Huang, B.; Ma, J.; Wang, L.; Xi, J.; Harms, K.; Gong, L.; Meggers, E. *J. Am. Chem. Soc.* **2013**, *135*, 10598–10601. (b) Chen, L.-A.; Tang, X.; Xi, J.; Xu, W.; Gong, L.; Meggers, E. *Angew. Chem., Int. Ed.* **2013**, 52, 14021–14025.

[39] Cao, Z.-Y.; Brittain, W. D. G.; Fossey, J. S.; Zhou, F. *Catal. Sci. Technol.* **2015**, *5*, 3441–3451.

[40] Zhang, L.; Meggers, E. *Acc. Chem. Res.* **2017**, *50*, 320–330.

[41] Werner, A.; Vilmos, A. *Z. Anorg. Chem.* **1899**, *21*, 145–158.

[42] Constable, E. C. *Chem. Soc. Rev.* **2013**, *42*, 1637–1651.

[43] Werner, A.; King, V. L. *Ber. Dtsch. Chem. Ges.* **1911**, *44*, 1887–1898.

[44] Excerpt from ref. 41:

"Es scheint aber doch nicht ausgeschlossen zu sein, dafs sich solche Isomere durch Enantiomorphie an ihren Krystallen charakterisieren könnten und dadurch der Weg zur Trennung derselben geboten würde. Die untersuchen Oxalatodiäthylendiaminsalze haben in der angedeuteten Richtung kein positives Resultat ergeben; da sich die gewonnenen Krystalle jedoch nur schlecht zur Beobachtung eigneten (sie wurden in der Regel nur sehr klein und in wenig geeigneter Form erhalten), so kann dem negativen Resultat nur eine beschränkte Bedeutung zukommen."

[45] King, V. L. *J. Chem. Educ.* **1942**, *19*, 345.

[46] Belokon, Y. N.; Bulychev, A. G.; Maleev, V. I.; North, M.; Malfanov, I. L.; Ikonnikov, N. S. *Mendeleev Commun.* **2004**, *14*, 249–250.

[47] Zheng, Y.; Harms, K.; Zhang, L.; Meggers, E. *Chem. - Eur. J.* **2016**, *22*, 11977–11981.

[48] Kurono, N.; Arai, K.; Uemura, M.; Ohkuma, T. *Angew. Chem., Int. Ed.* **2008**, *47*, 6643–6646.

[49] Ganzmann, C.; Gladysz, J. A. *Chem. - Eur. J.* **2008**, *14*, 5397–5400.

[50] Werner, A. *Ber. Dtsch. Chem. Ges.* **1912**, *45*, 121–130.

[51] Nishida, H.; Takada, N.; Yoshimura, M.; Sonoda, T.; Kobayashi, H. *Bull. Chem. Soc. Jpn.* **1984**, *57*, 2600–2604.

[52] Lewis, K. G.; Ghosh, S. K.; Bhuvanesh, N.; Gladysz, J. A. *ACS Cent. Sci.* **2015**, *1*, 50–56.

[53] Kumar, A.; Ghosh, S. K.; Gladysz, J. A. *Org. Lett.* **2016**, *18*, 760–763.

[54] Ghosh, S. K.; Ganzmann, C.; Bhuvanesh, N.; Gladyzs, J. A. *Angew. Chem., Int. Ed.* **2016**, *55*, 4356–4360.

[55] Ref. 48, 3rd paragraph, last sentence:
*"The $^{31}P\{^{1}H\}$ NMR spectrum of (S,S,S)-**3** in $CDCl_3$ shows a singlet at δ = 52.3 ppm, which indicates a trans-Ru(OCOR)$_2$ geometry."*

[56] Kurono, N.; Yoshikawa, T.; Yamasaki, M.; Ohkuma, T. *Org. Lett.* **2011**, *13*, 1254–1257.

[57] Kurono, N.; Nii, N.; Sakaguchi, Y.; Uemura, M.; Ohkuma, T. *Angew. Chem., Int. Ed.* **2011**, *50*, 5541–5544.

[58] Sakaguchi, Y.; Kurono, N.; Yamauchi, K.; Ohkuma, T. *Org. Lett.* **2014**, *16*, 808–811.

[59] Belokon, Y. N.; Maleev, V. I.; North, M.; Larionov, V. A.; Savel'yeva, T. F.; Nijland, A.; Nelyubina, Y. V. *ACS Catal.* **2013**, *3*, 1951–1955.

[60] Donnell, M. J. *Aldrichimica Acta* **2001**, *34*, 3–15.

[61] Maleev, V. I.; North, M.; Larionov, V. A.; Fedyanin, I. V.; Savel'yeva, T. F.; Moscalenko, M. A.; Smolyakov, A. F.; Belokon, Y. N. *Adv. Synth. Catal.* **2014**, *356*, 1803–1810.

[62] (a) Zhang, Z.; Schreiner, P. R. *Chem. Soc. Rev.* **2009**, *38*, 1187−1198. (b) Connon, S. J. *Chem. - Eur. J.* **2006**, *12*, 5418–5427.

[63] Xu, W.; Arieno, M.; Löw, H.; Huang, K.; Xie, X.; Cruchter, T.; Ma, Q.; Xi, J.; Huang, B.; Wiest, O.; Gong, L.; Meggers, E. *J. Am. Chem. Soc.* **2016**, *138*, 8774–8780.

[64] Xu, W.; Shen, X.; Ma, Q.; Gong, L.; Meggers, E. *ACS Catal.* **2016**, *6*, 7641–7646.

[65] Palomo, C.; Oiarbide, M.; López, R. *Chem. Soc. Rev.* **2009**, *38*, 632–653.

[66] Ma, J.; Ding, X.; Hu, Y.; Huang, Y.; Gong, L.; Meggers, E. *Nat. Commun.* **2014**, *5*, 4531.

[67] Huo, H.; Fu, C.; Wang, C.; Harms, K.; Meggers, E. *Chem. Commun.* **2014**, *50*, 10409–10411.

[68] Konishi, H.; Lam, T. Y.; Malerich, J. P.; Rawal, V. H. *Org. Lett.* **2010**, *12*, 2028–2031.

[69] Huo, H.; Fu, C.; Harms, K.; Meggers, E. *J. Am. Chem. Soc.* **2014**, *136*, 2990–2993.

[70] Larionov, V. A.; Cruchter, T.; Mietke, T.; Meggers, E. *Organometallics* **2017**, *36*, 1457–1460.

[71] (a) Huo, H.; Shen, X.; Wang, C.; Zhang, L.; Röse, P.; Chen, L.-A.; Harms, K.; Marsch, M.; Hilt, G.; Meggers, E. *Nature* **2014**, *515*, 100–103. (b) Wang, C.; Chen, L.-A.; Huo, H.; Shen, X.; Harms, K.; Gong, L.; Meggers E. *Chem. Sci.* **2015**, *6*, 1094–1100. (c) Wang, C.; Zheng, Y.; Huo, H.; Röse, P.; Zhang, L.; Harms, K.; Hilt, G.; Meggers, E. *Chem. - Eur. J.* **2015**, *21*, 7355–7359. (d) Shen, X.; Huo, H.; Wang, C.; Zhang, B.; Harms, K.; Meggers, E. *Chem. - Eur. J.* **2015**, *21*, 9720–9726. (e) Huang, Y.; Song, L.; Gong, L.; Meggers, E. *Chem. - Asian J.* **2015**, *10*, 2738–2743. (f) Huo, H.; Wang, C.; Harms, K.; Meggers, E. *J. Am. Chem. Soc.* **2015**, *137*, 9551–9556. (g) Tan, Y.; Yuan, W.; Gong, L.; Meggers, E. *Angew. Chem., Int. Ed.* **2015**, *54*, 13045–13048. (h) Wang, C.; Qin, J.; Shen, X.; Riedel, R.; Harms, K.; Meggers, E. *Angew. Chem., Int. Ed.* **2016**, *55*, 685–688. (i) Huo, H.; Huang, X.; Shen, X.; Harms, K.; Meggers, E. *Synlett* **2016**, *27*, 749–753. (j) Tian, C.; Gong, L.; Meggers, E. *Chem. Commun.* **2016**, *52*, 4207–4210. (k) Huo, H.; Harms K.; Meggers, E. *J. Am. Chem. Soc.* **2016**, *138*, 6936–6939. (l) Song, L.; Gong, L.; Meggers, E. *Chem. Commun.* **2016**, *52*, 7699–7702. (m) Ma, J.; Shen, X.; Harms, K.; Meggers, E. *Dalton Trans.* **2016**, *45*, 8320–8323. (n) Shen, X.; Harms, K.; Marsch, M.; Meggers, E. *Chem. - Eur. J.* **2016**, *22*, 9102–9105. (o) Ma, J.; Harms, K.; Meggers, E. *Chem. Commun.* **2016**, *52*, 10183–10186. (p) Huang, X.; Webster, R. D.; Harms, K.; Meggers, E. *J. Am. Chem. Soc.* **2016**, *138*, 12636–12642. (q) Wang, C.; Harms, K.; Meggers, E. *Angew. Chem., Int. Ed.* **2016**, *55*, 13495–13498. (r) Zhou, Z.; Li, Y.; Gong, L.; Meggers, E. *Org. Lett.* **2017**, 19, 222–225. (s) Feng, L.; Dai, X.; Meggers, E.; Gong, L. *Chem. - Asian J.* **2017**, *12*, 963–967. (t) Lin, H.; Zhou, Z.; Cai, J.; Han, B.; Gong, L.; Meggers, E. *J. Org. Chem.* **2017**, *82*, 6457–6467. (u) Tutkowski, B.; Meggers, E.; Wiest, O. *J. Am. Chem. Soc.* **2017**, *139*, 8062–8065. (v) Zhou, Z.; Li, Y.; Han B.; Gong, L.; Meggers, E. *Chem. Sci.* **2017**, *8*, 5757–5763. (w) Huang, X.; Quinn, T. R.; Harms, K.; Webster, R. D.; Zhang, L.; Wiest O.; Meggers, E. *J. Am. Chem. Soc.* **2017**, *139*, 9120–9123. (x) Li, Y.; Lei, M.; Yuan, W.; Meggers, E.; Gong, L. *Chem.*

Commun. **2017**, *53*, 8089–8092. (y) Luo, S.; Zhang, X.; Zheng, Y.; Harms, K.; Zhang, L. *J. Org. Chem.* **2017**, *82*, 8995−9005. (z) Yuan, W.; Zhou, Z.; Gong, L.; Meggers, E. *Chem. Commun.* **2017**, *53*, 8964–8967. (a2) Huang, X.; Luo, S.; Burghaus, O.; Webster, R. D.; Harms, K.; Meggers, E. *Chem. Sci.* **2017**, *8*, 7126–7131. (b2) Zheng, Y.; Tan Y.; Harms, K.; Marsch, M.; Riedel, R.; Zhang, L.; Meggers, E. *J. Am. Chem. Soc.* **2017**, *139*, 4322–4325. (c2) Zhang, X.; Qin, J.; Huang, X.; Meggers, E. *Org. Chem. Front.* **2018**, *5*, 166–170. (d2) Chen, S.; Huang, X.; Meggers, E.; Houk, K. N. *J. Am. Chem. Soc.* **2017**, *139*, 17245–17248. (e2) Ma, J.; Rosales, A. R.; Huang, X.; Harms, K.; Riedel, R.; Wiest, O.; Meggers, E. *J. Am. Chem. Soc.* **2017**, *139*, 17245–17248.

[72] Review articles about catalysis with (photoactive) Lewis acidic stereogenic-at-metal catalysts developed in the Meggers group (in addition to ref. 40):
(a) Zhang, L; Meggers, E. *Chem. - Asian J.* **2017**, *12*, 2335–2342. (b) Meggers E. *Angew. Chem., Int. Ed.* **2017**, *56*, 5668–5675.

[73] Prier, C. K..; Rankic, D. A.; MacMillan, D. W. C. *Chem. Rev.* **2013**, *113*, 5322–5363.

[74] Wilsey, S.; González, L.; Robb, M. A.; Houk, K. N. *J. Am. Chem. Soc.* **2000**, *122*, 5866–5876.

[75] (a) Lin, Z. *Asymmetric synthesis and applications of octahedral metal complexes*. PhD Thesis, Philipps-Universität Marburg, 2013; pp. 70–101 (doi: 10.17192/z2013.0234).
(b) In the present thesis, the terms 'cyclometalated' and 'non-cyclometalated' and according terms are used with regard to a definition of 'cyclometalation reactions' provided by M. I. Bruce in *Angew. Chem., Int. Ed.* **1977**, *16*, 73–86:
"Reactions of transition metal complexes in which an organic ligand undergoes intramolecular metalation with formation of a metal-carbon σ bond are termed cyclometalation reactions."

[76] Unpublished preliminary research results from the Meggers laboratory from former PhD student Xiaodong Shen. Philipps-Universität Marburg, 2014.

[77] (a) Nonoyama, M. *Bull. Chem. Soc. Jpn.* **1974**, *47*, 767–768. (b) You, Y.; Nam, W. *Chem. Soc. Rev.* **2012**, *41*, 7061–7084.

[78] Mietke, T.; Cruchter, T.; Winterling, E.; Tripp, M.; Harms, K.; Meggers, E. *Chem. - Eur. J.* **2017**, *23*, 12363–12371.

[79] Helms, M.; Lin, Z.; Gong, L.; Harms, K.; Meggers, E. *Eur. J. Inorg. Chem.* **2013**, 4164–4172.

[80] (a) Bolm, C.; Weickhardt, K.; Zehnder, M.; Ranff, T. *Chem. Ber.* **1991**, *124*, 1173−1180. (b) Takemoto, Y.; Kuraoka, S.; Hamaue, N.; Aoe, K.; Hiramatsu, H.; Iwata, C. *Tetrahedron* **1996**, *52*, 14177–14188.

[81] In principle, the bidentate auxiliary ligands can be replaced with more strongly coordinating bidentate ligands, such as 3*H*-imidazo[4,5-*h*]quinolines, in a one-pot procedure in MeCN with NH_4PF_6 as weak acid (see ref. 38 for experimental details). However, lower yields and purification problems were experienced with this procedure. Thus, the according intermediate bisacetonitrile complexes were formed at first, purified via short-column chromatography, and both acetonitrile ligands then replaced in a separate step with the desired final bidentate ligand.

[82] It is worth noting that the desired complexes were initially formed as TfO^- salts (Scheme 30 / 79, C1, I and II). However, chromatographic purification of the corresponding PF_6^- salts was found to be considerably easier (the TfO^- salts displayed strong tailing during flash chromatography). For this reason, the TfO^- counteranions were usually exchanged for PF_6^- counteranions (Scheme 30 / 79, C1, III).

[83] *Piperidine, polymer-bound (200-400 mesh; extent of labeling: 3.0-4.0 mmol/g loading; 1% cross-linked with divinylbenzene)*. Sigma-Aldrich product number: 494615.

[84] Cruchter, T.; Medvedev, M. G.; Shen, X.; Mietke, T.; Harms, K.; Marsch, M.; Meggers, E. *ACS Catal.* **2017**, *7*, 5152–5162.

[85] (a) 3D model generated with: *Mercury, version 3.7 RC1*; The Cambridge Crystallographic Data Centre: Cambridge, UK, 2015. (b) Rendered with: *POV-Ray for Windows*, version3.7.0.mscv10.win64; Persistance of Vision Pty. Ltd.: Williamstown, Victoria, Australia, 2013.

[86] (a) Black, T. H.; Arrivo, S. M.; Schumm, J. S.; Knobeloch, J. M. *J. Chem. Soc., Chem. Commun.* **1986**, 1524–1525. (b) Black, T. H.; Arrivo, S. M.; Schumm, J. S.; Knobeloch; J. M. *J. Org. Chem.* **1987**, *52*, 5425–5430.

[87] *2-Methyl-2-butanol (tert-amyl alcohol)*. Sigma-Aldrich product number: 721123.

[88] Cahn, R. S.; Ingold, C.; Prelog, V. *Angew. Chem., Int. Ed.* **1966**, *5*, 385–415.

[89] Mermerian, A. H.; Fu, G. C. *J. Am. Chem. Soc.* **2003**, *125*, 4050–4051.

[90] DeLorbe, J. E.; Jabri, S. Y.; Mennen, S. M.; Overman L. E.; Zhang, F.-L. *J. Am. Chem. Soc.* **2011**, *133*, 6549–6552.

[91] Staudaher, N. D.; Lovelace, J.; Johnson, M. P.; Louie, J. *Org. Synth.* **2017**, *94*, 1–15.

[92] Tidwell, T. T. *Angew. Chem., Int. Ed.* **2005**, *44*, 5778–5785.

[93] In a thorough literature search with CAS SciFinder and Elsevier Reaxys, only the mentioned publication (ref. 26c) from Fu et al. was found (it was searched for asymmetric reactions between NH-heterocycles and ketenes yielding the corresponding addition products).

[94] A. N. Nesmeyanov Institute of Organoelement Compounds of the Russian Academy of Sciences (INEOS RAS); Vavilova St. 28, 119991 Moscow, Russian Federation (https://ineos.ac.ru/en/).

[95] N. D. Zelinsky Institute of Organic Chemistry of the Russian Academy of Sciences (ZIOC RAS); Leninsky Prospect 47, 119991 Moscow, Russian Federation (http://zioc.ru/?lang=en).

[96] (a) Adamo, C.; Barone, V. *J. Chem. Phys.* **1999**, *110*, 6158–6170. (b) Peverati, R.; Truhlar, D. G. *Philos. Trans. R. Soc., A* **2014**, *372*, 20120476. (c) Medvedev, M. G.; Bushmarinov, I. S.; Sun, J.; Perdew, J. P.; Lyssenko, K. A. *Science* **2017**, *355*, 49–52.

[97] Grimme, S.; Antony, J.; Ehrlich, S.; Krieg, H. *J. Chem. Phys.* **2010**, *132*, 154104.

[98] (a) Lovallo, C. C.; Klobukowski, M. *J. Comput. Chem.* **2003**, *24*, 1009–1015. (b) Lovallo, C. C.; Klobukowski, M. *J. Comput. Chem.* **2004**, *25*, 1206–1213.

[99] Smith, A. R. G.; Riley, M. J.; Lo, S.-C.; Burn, P. L.; Gentle, I. R.; Powell, B. J. *Phys. Rev. B* **2011**, *83*, 041105.

[100] (a) Stevens, W. J.; Basch, H.; Krauss, M. *J. Chem. Phys.* **1984**, *81*, 6026–6033. (b) Stevens, W. J.; Krauss, M.; Basch, H.; Jasien, P. G. *Can. J. Chem.* **1992**, *70*, 612–630.

[101] Marenich, A. V.; Cramer, C. J.; Truhlar, D. G. *J. Phys. Chem. B* **2009**, *113*, 6378–6396.

[102] A similar conformational preference has been observed in related systems, see refs. 4, 13d, 22b, 31, 34 and: Velázquez-Ponce, M.; Salgado-Zamora, H.; Jiménez-Vázquez, H. A.; Campos-Aldrete, M. E.; Jiménez, R.; Cervantes, H.; Hadda, T. B. *Chem. Cent. J.* **2013**, *7*, 20.

[103] (a) Connolly, M. L. *Science* **1983**, *221*, 709–713. (b) Connolly, M. L. *J. Appl. Cryst.* **1983**, *16*, 548–558. (c) Connolly, M. L. *J. Am. Chem. Soc.* **1985**, *107*, 1118–1124.

[104] Düren, T.; Millange, F.; Férey, G.; Walton, K. S.; Snurr, R. Q. *J. Phys. Chem. C* **2007**, *111*, 15350–15356.

[105] 3D model (and Connolly surface, if depicted) generated and rendered with: *PyMOL*, version 0.99rc6; DeLano Scientific LLC: Palo Alto, CA, USA, 2006.

[106] (a) Neel, A. J.; Hilton, M. J.; Sigman, M. S.; Toste, F. D. *Nature* **2017**, *543*, 637–646. (b) Knowles, R. R.; Jacobsen, E. N. *Proc. Natl. Acad. Sci. USA* **2010**, *107*, 20678–20685.

[107] Medvedev, M. G.; Zeifman, A. A.; Novikov, F. N.; Bushmarinov, I. S.; Stroganov, O. V.; Titov, I. Y.; Chilov, G. G.; Svitanko, I. V. *J. Am. Chem. Soc.* **2017**, *139*, 3942–3945.

[108] (a) Seeman, J. I. *J. Chem. Educ.* **1986**, *63*, 42–48. For a deeper discussion, see: (b) Seeman, J. I. *Chem. Rev.* **1983**, *83*, 83–134.

[109] Mardirossian, N.; Head-Gordon, M. *Mol. Phys.* **2017**, *115*, 2315–2372.

[110] Medford, A. J.; Wellendorff, J.; Vojvodic, A.; Studt, F.; Abild-Pedersen, F.; Jacobsen, K. W.; Bligaard, T.; Nørskov, J. K. *Science* **2014**, *345*, 197–200.

[111] Recently, the Meggers group has demonstrated for hydrogen-bonding catalysts that such rigid octahedral metal-templated catalysts are well-suited for rational improvements due to their constrained geometries (see refs. 63 and 64 for further details).

[112] Lautens, M.; Franzoni, I. *Synfacts* **2017**, *13*, 0945.

[113] Unpublished research results. The resulting reaction mixtures turn dark under these conditions and the amino-functionalized ligands to be cyclometalated decompose. Philipps-Universität Marburg, 2014.

[114] Birkofer, L.; Bierwirth, E.; Ritter, A. *Chem. Ber.* **1961**, *94*, 821–824.

[115] Baranoff, E.; Curchod, B. F. E.; Frey, J.; Scopelliti, R.; Kessler, F.; Tavernelli, I.; Rothlisberger, U.; Grätzel, M.; Nazeeruddin, M. K. *Inorg. Chem.* **2012**, *51*, 215–224.

[116] Böttcher, H.-C.; Graf, M.; Sünkel, K.; Mayer, P.; Krüger, H. *Inorg. Chim. Acta* **2011**, *365*, 103–107.

[117] Wuts, P. G. M.; Greene, T. W.: *Greene's Protective Groups in Organic Synthesis*, 4th ed.; John Wiley & Sons: Hoboken, NJ (US), 2007; pp. 748–753.

[118] (a) Stachel, H.-D. *Chem. Ber.* **1960**, *93*, 756–757. (b) Stachel, H.-D. *Chem. Ber.* **1960**, *93*, 1059–1063. (c) Stachel, H.-D. *Chem. Ber.* **1962**, *95*, 2166–2171.

[119] Fitzi, R.; Seebach, D. *Tetrahedron* **1988**, *44*, 5277–5292.

[120] Chen, Y.-X.; Quian, L.-F.; Zhang, W.; Han, B. *Angew. Chem., Int. Ed.* **2008**, *47*, 9330–9333.

[121] Von Wantoch Rekowski, M.; Pyriochou, A.; Papapetropoulos, N.; Stößel, A.; Papapetropoulos, A.; Giannis, A. *Bioorg. Med. Chem.* **2010**, *18*, 1288–1296.

[122] Y. Liu, M. Nishiura, Y. Wang, Z. Hou, *J. Am. Chem. Soc.* **2006**, *128*, 5592–5593.

[123] Jiang, W.; Duan, L.; Qiao, J.; Dong, G.; Zhang, D.; Wang, L.; Qiu, Y. *J. Mater. Chem.* **2011**, *21*, 4918–4926.

[124] Barder, T. E.; Walker, S. D.; Martinelli, J. R.; Buchwald, S. L. *J. Am. Chem. Soc.* **2005**, *127*, 4685–4696.

[125] Nguyen, T. B.; Ermolenko, L.; Retailleau, P.; Al-Mourabit, A. *Angew. Chem., Int. Ed.* **2014**, *53*, 13808–13812.

[126] Neeb, M. J.; Sehon, C. A.; Viet, A. Q.; Goodman, K. B.; Wang, G. Z. *Morpholinyl and pyrrolidinyl analogs* (Smithkline Beecham Corp.). WO Patent 2008011551 A1, Jan. 24, 2008; pp. 111–113.

[127] Aitken, R. A.; Armstrong, D. P.; Galt, R. H. B.; Mesher, S. T. E. *J. Chem. Soc., Perkin Trans. 1* **1997**, *1*, 935–943.

[128] McKennon, M. J.; Meyers, A. I.; Drauz, K; Schwarm, M. *J. Org. Chem.* **1993**, *58*, 3568–3571.

[129] Grzegożek, M. *J. Heterocycl. Chem.* **2008**, *45*, 1879–1882.

[130] Pagoria, P. F.; Mitchell, A. R.; Schmidt, R. D. *J. Org. Chem.* **1996**, *61*, 2934–2935.

[131] Flash chromatography: Heavy tailing with eluent mixtures of hexanes/EtOAc.

[132] Zhang, Z.-H.; Li, J.-J.; Gao, Y.-Z.; Liu, Y.-H. *J. Heterocycl. Chem.* **2007**, *44*, 1509–1512.

[133] Gershon, H.; Clarke, D. D. *Monatsh. Chem.* **1991**, *122*, 935–941.

[134] Kubo, T.; Aihara, Y.; Chatani, N. *Chem. Lett.* **2015**, *44*, 1365–1367.

[135] Huynh, T. H. V.; Mantel, M. L. H.; Mikkelsen, K.; Lindhardt, A. T.; Nielsen, N. C.; Otzen, D.; Skrydstrup, T. *Org. Lett.* **2009**, *11*, 999–1002.

[136] D'Amora, A.; Fanfoni, L; Cozzula, D.; Guidolin, N.; Zangrando, E.; Felluga, F.; Gladiali, S.; Benedetti, F.; Milani, B. *Organometallics* **2010**, *29*, 4472–4485.

[137] Pleier, A.-K.; Glas, H.; Grosche, M.; Sirsch, P.; Thiel, W. R. *Synthesis* **2001**, 55–62.

[138] Kumar, S.; Ila, H.; Junjappa, H. *J. Org. Chem.* **2009**, *74*, 7046–7051.

[139] DeHaven-Hudkins, D. L.; Earley, W. G.; Kumar, V.; Miller, M. S.; Mallomo, J. P. *12-Hetero-substituted 6,11-ethano-6,11-dihydrobenzo[b] quinolizium salts and compositions and method of use thereof* (Sterling Winthrop Inc.). EP Patent 0648769 A1, April 19, 1995; p. 24.

[140] Usually, the purified intermediate bisacetonitrile complexes **Λ-** and **Δ-T#-(MeCN)$_2$** were used in the next step without any characterization as they eluted as single neat bands. However, in case of **Λ-** and **Δ-T18-(MeCN)$_2$** they were fully characterized and

their CD spectra recorded in order to obtain more data for the assignment of the absolute configuration of the chiral iridium(III) complexes.

[141] Crawford, A. G.; Liu, Z.; Mkhalid, I. A. I.; Thibault, M.-H.; Schwarz, N.; Alcaraz, G.; Steffen, A.; Collings, J. C.; Batsanov, A. S.; Howard, J. A. K.; Marder, T. B. *Chem. - Eur. J.* **2012**, *18*, 5022–5035.

[142] Thompson, J. E.; Campbell, C. D.; Concellón, C.; Duguet, N.; Rix, K.; Slawin, A. M. Z.; Smith, A. D. *J. Org. Chem.* **2008**, *73*, 2784–2791.

[143] Joannesse, C.; Simal, C.; Concellón, C.; Thomson, J. E.; Campbell, C. D.; Slawin, A. M. Z.; Smith, A. D. *Org. Biomol. Chem.* **2008**, *6*, 2900–2907.

[144] Padwa, A.; Dehm, D.; Oine, T.; Lee, G. A. *J. Am. Chem. Soc.* **1975**, *97*, 1837–1845.

[145] (a) Citterio, A.; Gandolfi, M.; Piccolo, O.; Filippini, L.; Tinucci, L.; Valoti, E. *Synthesis* **1984**, 760–763. (b) Piccolo, O.; Filippini, L.; Tinucci, L.; Valoti, E.; Citterio, A. *J. Chem. Res., Synop.* **1985**, 258–259.

[146] Schultz, A. G.; Kirincich, S. J. *J. Org. Chem.* **1996**, *61*, 5631–5634.

[147] Baigrie, L. M.; Seiklay, H. R.; Tidwell, T. T. *J. Am. Chem. Soc.* **1985**, *107*, 5391–5396.

[148] Allen, A. D.; Baigrie, L. M.; Gong, L.; Tidwell, T. T. *Can. J. Chem.* **1991**, *69*, 138–145.

[149] Aaron, C.; Dull, D. L.; Schmiegel, J. L.; Jaeger, D.; Ohashi, Y.; Mosher, H. S. *J. Org. Chem.* **1967**, *32*, 2797–2803.

[150] Bergman, J. *Acta Chem. Scand.* **1971**, *25*, 1277–1280.

[151] Galzerano, P.; Bencivenni, G.; Pesciaioli, F.; Mazzanti, A.; Giannichi, B.; Sambri, L.; Bartoli, G.; Melchiorre, P. *Chem. - Eur. J.* **2009**, *15*, 7846–7849.

[152] Trost, B. M.; Xie, J.; Sieber, J. D. *J. Am. Chem. Soc.* **2011**, *133*, 20611–20622.

[153] Martin, N. J. A.; Cheng, X.; List, B. *J. Am. Chem. Soc.* **2008**, *130*, 13862–13863.

[154] Amber glas vial: Agilent part no. 5182-0716; PTFE screw cap: Agilent part no. 5182-0717.

[155] All used microliter syringes were vacuum-dried overnight and equipped with well-sealed PTFE-tipped plungers.

[156] Rodger, A.; Nordén, B.: *Circular Dichroism and Linear Dichroism*; Oxford University Press: Oxford, England (UK), 1997; pp. 6–8.

[157] Schmidt, M. W.; Baldridge, K. K.; Boatz, J. A.; Elbert, S. T.; Gordon, M. S.; Jensen, J. H.; Koseki, S.; Matsunaga, N.; Nguyen, K. A.; Su, S.; Windus, T. L.; Dupuis, M.; Montgomery Jr, J. A. *J. Comput. Chem.* **1993**, *14*, 1347–1363.

[158] Medvedev, M. G.; Panova, M. V.; Chilov, G. G.; Bushmarinov, I. S.; Novikov, F. N.; Stroganov, O. V.; Zeifman, A. A.; Svitanko, I. V. *Mendeleev Commun.* **2017**, *27*, 224–227.

[159] Perdew, J. P.; Burke, K.; Ernzerhof, M. *Phys. Rev. Lett.* **1996**, *77*, 3865–3868.

[160] Culot, P.; Dive, G.; Nguyen, V. H.; Ghuysen, J. M. *Theor. Chim. Acta* **1992**, *82*, 189–205.

[161] Powell, M. J. D. *Math. Program., Ser. A* **1971**, *1*, 26–57.

[162] *SADABS. Bruker AXS area detector scaling and absorption correction*; Bruker AXS Inc.: Madison, Wisconsin, USA, 2014.

[163] Sheldrick, G. M. *Acta Crystallogr.* **2015**, *A71*, 3–8.

[164] Sheldrick, G. M. *Acta Crystallogr.* **2015**, *C71*, 3–8.

[165] Parsons, S.; Flack, H. D.; Wagner, T. *Acta Crystallogr.* **2013**, *B69*, 249–259.

[166] *APEX3*; Bruker AXS Inc.: Madison, Wisconsin, USA, 2015.

[167] *SAINT*; Bruker AXS Inc.: Madison, Wisconsin, USA, 2015.

[168] *Diamond - Crystal and Molecular Structure Visualization*; Crystal Impact - Dr. H. Putz & Dr. K. Brandenburg GbR: Bonn, Germany, 2014.

[169] Hübschle, C. B.; Sheldrick, G. M.; Dittrich, B. *J. Appl. Crystallogr.* **2011**, *44*, 1281–1284.

[170] Spek, A. L. *Acta Crystallogr.* **2015**, *C71*, 9–18.

9. Erklärung

gemäß § 10, Absatz 1 der Promotionsordnung der Mathematisch-Naturwissenschaftlichen Fachbereiche und des Medizinischen Fachbereichs für seine mathematisch-naturwissenschaftlichen Fächer der Philipps-Universität Marburg vom 15.07.2009:

Ich, Thomas Josef Cruchter, versichere hiermit, dass ich noch keine Promotion an einer anderen Hochschule als der Philipps-Universität Marburg versucht habe und dass ich die vorliegende Dissertation mit dem Titel:

"Design, Synthesis, and Application
of a Nucleophilic Octahedral
Stereogenic-Only-at-Metal
Iridium(III) Catalyst"

selbst und ohne fremde Hilfe verfasst habe und dass ich keine anderen Quellen und Hilfsmittel als die angegebenen verwendet habe. Alle vollständigen oder sinngemäß übernommenen Zitate wurden als solche kenntlich gemacht. Ich versichere außerdem hiermit, dass ich die Dissertation in der vorliegenden oder einer ähnlichen Form noch bei keiner anderen in- oder ausländischen Hochschule anlässlich eines Promotionsgesuchs oder zu anderen Prüfungszwecken eingereicht habe.

Marburg, den 15.02.2018

.....

(Thomas Cruchter)

10. Publikationsliste (Peer-Review-Artikel)

[7] *Asymmetric Nazarov Cyclizations Catalyzed by Chiral-at-Metal Complexes*
T. Mietke, T. Cruchter, V. A. Larionov, T. Faber, K. Harms, E. Meggers.

- Eingereicht als *Communication* bei *Adv. Synth. Catal*., Manuskript in Revision zum Zeitpunkt der Abgabe der vorliegenden Dissertation.

[6] *Asymmetric Nucleophilic Catalysis with an Octahedral Chiral-at-Metal Iridium(III) Complex*
T. Cruchter, M. G. Medvedev, X. Shen, T. Mietke, K. Harms, M. Marsch, E. Meggers
ACS Catal. **2017**, *7*, 5152–5162 (*Research Article*).

- Highlight in *Synfacts* (M. Lautens, I. Franzoni, *Synfacts* **2017**, *13*, 0945).
- Hauptpublikation zur vorliegenden Dissertation.

[5] *Suzuki Cross-Coupling for Post-Complexation Derivatization of Non-Racemic Bis-Cyclometalated Iridium(III) Complexes*
T. Mietke, T. Cruchter, E. Winterling, M. Tripp, K. Harms, E. Meggers
Chem. Eur. J. **2017**, *23*, 12363–12371 (*Full Paper*).

- Artikel als Teil einer Sonderausgabe von *Chem. Eur. J.* anlässlich des 150-jährigen Bestehens der GDCh.

[4] *Polymer-Supported Chiral-at-Metal Lewis Acid Catalysts*
V. A. Larionov, T. Cruchter, T. Mietke, E. Meggers
Organometallics **2017**, *36*, 1457–1460 (*Communication*).

[3] *Metal-Templated Design: Enantioselective Hydrogen-Bond-Driven Catalysis Requiring Only Parts-per-Million Catalyst Loading*
W. Xu, M. Arieno, H. Löw, K. Huang, X. Xie, T. Cruchter, Q. Ma, J. Xi, B. Huang, O. Wiest, L. Gong, E. Meggers
J. Am. Chem. Soc. **2016**, *138*, 8774–8780 (*Article*).

[2] *Strain-Promoted Azide-Alkyne Cycloaddition with Ruthenium(II) Azido Complexes*
T. Cruchter, K. Harms, E. Meggers
Chem. Eur. J. **2013**, *19*, 16682–16689 (*Full Paper*).

[1] *Organometallic Pyridylnaphthalimide Complexes as Protein Kinase Inhibitors*
S. Blanck, T. Cruchter, A. Vultur, R. Riedel, K. Harms, M. Herlyn, E. Meggers
Organometallics **2011**, *30*, 4598–4606 (*Article*).

- Coverartikel der betreffenden Ausgabe von *Organometallics*.